A Global and Targeted Proteomic Investigation of *Aspergillus fumigatus*

Rebecca Owens BSc

Thesis submitted to the

National University of Ireland

for the degree of

Doctor of Philosophy

September 2012

Supervisor:
Prof. Sean Doyle,
Biotechnology Laboratory,
Department of Biology,
National University of Ireland Maynooth
Co. Kildare.

Head of Department:
Prof. Paul Moynagh

Table of Contents

Declaration of Authorship

This thesis has not previously been submitted in whole or in part to this or any other University for any other degree. This thesis is the sole work of the author, with the exception of the generation of the *A. fumigatus gliK* mutant, which was generated by Dr. Lorna Gallagher.

_____

Rebecca Owens BSc.

Acknowledgements

I would like to sincerely thank my supervisor Prof. Sean Doyle for the unlimited support, guidance and encouragement provided throughout the course of my PhD. I have really appreciated all of your time and help over the years. I would also like to thank Drs Luke O' Shaughnessy and Stephen Carberry for answering endless questions with great patience. Additionally, sincere thanks to Caroline Batchelor for assistance and training on the Ion Trap (LC-MS), and to Michelle and all of the technicians for your help along the way. I would like to acknowledge and thank the Irish Research Council (IRCSET), Kildare County Council and the biology department, for funding this PhD and providing this opportunity. In addition, I would like to thank the HEA for providing equipment funding for the HPLC and LC-MS, both of which facilitated this work.

To all the members of the Biotech lab, I couldn't have asked for a better place to spend the last few years. Grainne, Cindy, Carol, Lorna, Karen, Natasha, Lara, Stephen H and the honorary members, John and Karen T, thank you all for the help, chats and the 'odd' tea break. Also thank you, to all the students in the lab over the years. Thanks also to everyone in the biology department for helping out with advice, reagents or just a chat when needed.

A special thanks to my better half, Ro, I would not have come through this without you. For your unwavering support, patience and belief in me, I am eternally grateful. Thank you for always knowing how to pick me up, make me laugh, and encourage me to keep going when it got tough. (I promise I won't do another thesis)

I would like to thank my sisters, Liz (and brother-in-law Denis), Kelley and Hannah. Thank you for always being there (or a phonecall, text or skype away) when I needed a break and a chat. To my gorgeous nieces and nephew, Ash, Cait, Shay and Molly, I hope at least one of you thinks science is 'cool' now because of your aunty.

Finally, I wish to thank my parents, who have always believed in me and made me the person I am today. Mum, your encouragement and support have always made me strive to do my best and I could not have started this journey without you. I miss you every day and I hope I have made you proud. Dad, I can never thank you enough for being so strong and keeping us all going. I dedicate this thesis to you both.

Publications and Presentations

Research Publications:

Gallagher, L., **Owens, R.A**., O' Keeffe, G., Dolan, S.K., Schrettl, M., Kavanagh, K., Jones, G. and Doyle, S. (2012). The *Aspergillus fumigatus* Protein GliK Protects Against Oxidative Stress and is Essential for Gliotoxin Biosynthesis. *Eukaryotic Cell*, **11**(10): 1226-1238.

Owens, R.A., O' Keeffe, G., Jones, G. and Doyle, S. (2012). Gliotoxin: Defender and Attacker. In preparation.

Owens, R.A., Moore, M. and Doyle, S. (2012). Large-scale proteomic and immunoproteomic analysis of *Aspergillus fumigatus*. In preparation.

Owens, R.A., O' Keeffe, G., and Doyle, S. (2013). Virulence of Human Fungal Pathogens: *Aspergillus*. In Human Pathogenic Fungi: New technologies and new insights. D. Sullivan and G. Moran, ed. (Horizon Scientific Press). In preparation.

Oral Presentations:

Large-scale investigation of the *Aspergillus fumigatus* proteome and identification of novel immunoreactive antigens in mycelia. *Irish Fungal Society Inaugural Meeting*. Trinity College Dublin 16-17th June 2011. Awarded 1st prize.

Proteomic and Immunoproteomic investigation of *Aspergillus fumigatus*. *British Society for Medical Mycology Annual Meeting*. Glasgow, Scotland 17-19th April 2011.

Poster Presentations:

Mechanisms involved in gliotoxin relief of oxidative stress in *A. fumigatus*. *Biology Research Day*. NUI Maynooth, 20th July 2012.

Mechanisms involved in gliotoxin relief of oxidative stress in *A. fumigatus*. *Irish Fungal Society Meeting*. Belfast City Hospital, 21-22th June 2012.

Abbreviations

2D-PAGE	Two-dimensional polyacrylamide gel electrophoresis
2PF	2-Pentylfuran
4-HCCA	α-cyano-4-hydroxycinnamic acid
5'-IAF	5'-iodoacetamidofluorescein
A4	Aldrithiol-4
aa-tRNA	Aminoacyl-tRNA
ABC	ATP-binding cassette
ABPA	Allergic bronchopulmonary aspergillosis
AICAR	5-aminoimidazole-4-carboxamide ribonucleotide
AIF	Apoptosis-inducing factor
AmB	Amphotericin B
AMM	*Aspergillus* minimal media
APS	Ammonium persulfate
AspGD	*Aspergillus* Genome Database
AuNP	Gold nanoparticle
BAL	Bronchoalveolar lavage
bFGF	Basic fibroblast growth factor
bmGT	Bis-methylated gliotoxin
BSA	Bovine serum albumin
bZIP	Basic leucine zipper
CADRE	Central *Aspergillus* Data Repository
CF	Cystic fibrosis
CFTR	Cystic fibrosis transmembrane conductance regulator
CGD	Chronic granulomatous disease
COPD	Chronic obstructive pulmonary disease
CSF	Colony stimulating factor

CTL	Cytotoxic T lymphocytes
DAB	3, 3’-diaminobenzidine tetrachloride hydrate
DC	Dendritic cell
DIC	Differential interference contrast
DMAT	Dimethylallyl tryptophan synthetases
DMSO	Dimethyl sulfoxide
DNA	Deoxyribonucleic acid
DTT	Dithiothreitol
EF	Elongation factor
EGT	Ergothioneine
EIA	Enzyme-immunoassay
ELISA	Enzyme-linked immunosorbent assay
EORTC/MSG	European Organisation for Research and Treatment of Cancer/Invasive Fungal Infections Cooperative Group and the National Institute of Allergy and Infectious Diseases Mycoses Study Group
ER	Endoplasmic reticulum
ERG-AF	Acetamidofluorescein ergothioneine
ESI	Electrospray ionisation
ETC	Electron transport chain
ETP	Epipolythiodioxopiperazine
ETT	Ergothioneine transporter
FDA	Food and drug administration
FunCat	Functional Catalogue
G-CSF	Granulocyte-CSF
GDC	Glycine decarboxylase complex
GGCT	Gamma-glutamyl cyclotransferase
GM	Galactomannan
GM-SCF	Granulocyte-macrophage CSF

GO	Gene ontology
GRAVY	Grand average of hydropathy
GS-AF	Acetamidofluorescein glutathione
GSH	Glutathione
GST	Glutathione-S-transferase
GT	Gliotoxin
GT-$(AF)_2$	Di-acetamidofluorescein gliotoxin
H_2O_2	Hydrogen peroxide
HIV	Human immunodeficiency virus
HRP	Horseradish peroxidase
HSCT	Hematopoietic stem cell transplant
HUVEC	Human umbilical vein endothelial cell
IA	Invasive aspergillosis
IEF	Isoelectric focusing
IFI	Invasive fungal infection
IgG	Immunoglobulin G
IL	Interleukin
IMP	Inosine 5'-monophosphate
IPA	Invasive pulmonary aspergillosis
IPG	Immobilised pH gradient
iTRAQ	Isobaric tags for relative and absolute quantitation
kDa	Kilodalton
KEGG	Kyoto Encyclopedia of Genes and Genomes
LC-MS/MS	Liquid chromatography, tandem mass spectrometry
m/z	Mass to charge ratio
MAb	Monoclonal antibody
MALDI-ToF	Matrix assisted laser desorption/ionisation-time of flight

MAPK	Mitogen-activated protein kinase
MBL	Mannose-binding lectin
MFS	Major facilitator superfamily
MPO	Myeloperoxidase
M_r	Molecular mass
mRNA	Messanger RNA
MS	Mass spectrometry
MS^2	Tandem mass spectrometry
MS^n	Tandem mass spectrometry
MTHFR	Methylenetetrahydrofolate reductase
MudPIT	Multi-dimensional protein identification technology
$NaBH_4$	Sodium borohydride
NCP	Nitrocellulose paper
NET	Neutrophil extracellular trap
nm	Nanometer
NOX	NADPH-oxidase
NRP	Non-ribosomal peptide
NRPS	Non ribosomal peptide synthetase
ns	Not significant
O_2^-	Superoxide anion
O_2^{2-}	Peroxide
OPT	Oligopeptide transporter
PBS	Phosphate buffered saline
PBST	PBS-Tween
PCNA	Proliferating cell nuclear antigen
PCR	Polymerase chain reaction
PDI	Protein disulphide isomerase

PET	Positron emission tomography
PFF	Pattern recognition receptor
p*I*	Isoelectric point
PKS	Polyketide synthase
PLP	Pyridoxal-phosphate
PMN	Polymorphonuclear
PMNL	Polymorphonuclear leucocytes
PP2A	Protein phosphatase 2a
Prx	Peroxiredoxin
PTM	Post-translational modification
qPCR	Quantitative PCR
RIA	Reductive iron assimilation
RNA	Ribonucleic acid
RNAi	RNA interference
RNS	Reactive nitrogen species
ROS	Reactive oxygen species
RP-HPLC	Reversed phase-high performance liquid chromatography
rpm	Revolutions per minute
R_T	Retention time
RT-PCR	Reverse transcription-polymerase chain reaction
SAM	S-adenosylmethionine
SCX	Ion exchange chromatography
SDS	Sodium dodecyl sulfate
SDS-PAGE	Sodium dodecyl sulfate-Poylacrylamide gel electrophoresis
SILAC	Stable-isotope labelling by amino acids in cell culture
SM	Secondary metabolite
SMURF	Secondary Metabolite Unknown Region Finder

SNP	Single nucleotide polymorphism
SOD	Superoxide dismutase
TB	Tuberculosis
TCA	Trichloroacetic Acid
TCA cycle	Tricarboxylic acid cycle
THF	Tetrahydrofolate
TIC	Total ion chromatograph
TLC	Thin-layer chromatography
TLR	Toll-like receptor
TM	Transmembrane
tM_r	Theoretical molecular mass
TNF-α	Tumor necrosis factor alpha
tp*I*	Theoretical isoelectric point
tRNA	transfer RNA
Trx	Thioredoxin
TrxR	Thioredoxin reductase
UFP	Unknown function protein
UPR	Unfolded protein response
UV	Ultraviolet
v/v	Volume per volume
V_e	Elution volume
VEGF	Vascular endothelial growth factor
VOC	Volatile organic compound
w/v	Weight per volume

Summary

Aspergillus fumigatus is an opportunistic pathogen that can cause invasive disease in immunocompromised individuals and, less frequently, in immunocompetent hosts. Proteomic investigation of *A. fumigatus* has the potential to enable global analysis of protein expression, identify potential targets for vaccine or diagnostic tool development, and characterise system-wide responses to external stimuli. Implementation of a large-scale proteomic strategy lead to the identification of non-redundant proteins from mycelia (n = 390) and culture supernatants (n = 42) of *A. fumigatus*. Utilisation of MS-based proteomics facilitated the identification of proteins typically under-represented in 2D-PAGE proteome maps, including proteins with multiple transmembrane regions, hydrophobic proteins and proteins with extremes of molecular mass and p*I*. Pre-fractionation of complex protein samples, by gel-filtration or gold nanoparticle pre-incubation, demonstrated potential for reduction of sample complexity. Indirect identification of secondary metabolite cluster expression was achieved using a global MS-based proteomic approach, with proteins (n = 20) from LaeA-regulated clusters detected. Targeted immunoproteomics resulted in the identification of antigenic proteins (n = 25) from *A. fumigatus*, reactive with sera from healthy individuals, and characterisation of these proteins may shed light on the pathobiology of *A. fumigatus*. Mechanisms involved in the interaction of *A. fumigatus* with gliotoxin were also examined, using phenotypic analysis, comparative proteomics and metabolomics. Gliotoxin was observed to relieve H_2O_2-induced stress, in a dose-dependent manner (0 - 10 µg/ml) and this correlated with a significant increase in expression of the gliotoxin oxidoreductase GliT ($p < 0.05$). This indicates a role for gliotoxin, and potentially GliT, in relief of oxidative stress in *A. fumigatus*. Correspondingly, proteins associated with response to stress were observed to significantly decrease in expression in the co-addition condition, relative to H_2O_2 alone ($p < 0.05$). Comparative proteomic profiling of the gliotoxin-sensitive mutant, *A. fumigatus* Δ*gliK*, revealed perturbation of translation, the methyl cycle and the endoplasmic reticulum in response to gliotoxin. This informs on the mechanisms involved in gliotoxin-mediated toxicity and may apply to other gliotoxin-sensitive species. Loss of gliotoxin production in *A. fumigatus* Δ*gliK* correlated with significant elevation in intracellular ergothioneine levels ($p < 0.001$). This study describes the first identification of ergothioneine in *A. fumigatus* and represents a target for future redox investigations.

CHAPTER 1

Introduction

1 Chapter 1. Introduction

1.1 General Characteristics of *Aspergillus fumigatus*

The saprophytic fungus *Aspergillus fumigatus* is a member of the class Ascomycota, with over 200 species of the genus *Aspergillus* identified to date (Anzai *et al.*, 2008). This soil-associated fungus plays an important role in recycling carbon and nitrogen, and is prevalent in the environment (Latge, 1999). In a laboratory setting, *A. fumigatus* can grow on minimal agar containing a simple carbon source (e.g. glucose), a nitrogen source (e.g. ammonium tartrate) and trace elements (Brakhage and Langfelder, 2002). The ability of *A. fumigatus* to thrive at 37 °C enables the pathogenicity of the fungus. The relative thermo-tolerance of *A. fumigatus* allows it to grow at temperatures up to 55 °C, reflective of the presence of an ecological niche in compost heaps, and the conidia can withstand temperatures up to 70 °C (Latge, 1999; Bhabhra and Askew, 2005). *A. fumigatus* produces hydrophobic conidia (spores) that are aerially dispersed and only 2.5-3 μm in diameter (Brakhage and Langfelder, 2002). These conidia are ubiquitous to the environment and hundreds are inhaled every day (Latge, 1999). The small size and buoyant nature of these conidia enables them to reach the alveoli of the lungs, where they are generally cleared in healthy individuals (Dagenais and Keller, 2009). A relatively small proportion of *Aspergillus* species are associated with human disease, with *A. fumigatus* demonstrating the highest pathogenicity (Kradin and Mark, 2008). *A. fumigatus* is an opportunistic pathogen, which causes disease in immuno-compromised individuals (Ben-Ami *et al.*, 2010). A markedly high mortality rate is observed with invasive *Aspergillus*-related disease, ranging from 40% to 95% (Abad *et al.*, 2010).

A. fumigatus reproduction is predominantly asexual and is mediated by the dispersion of haploid conidia. The asexual life cycle of *A. fumigatus* is initiated by

germination of conidia into septate hyphae which form a network of mycelia (Ward *et al.*, 2005). Conidiophores form on hyphal extensions from the mycelial mass, and produce chains of grey-green conidia for dispersion (Figure 1.1). Genes regulating sexual development in *A. fumigatus* were identified following the sequencing of the genome, in addition to pheromone-associated genes (Nierman *et al.*, 2005; Paoletti *et al.*, 2005). Subsequently, the presence of a sexual cycle in *A. fumigatus* was experimentally verified (O'Gorman *et al.*, 2009).

Sequencing of the genome of the *A. fumigatus* clinical isolate Af293 revealed the presence of 9,926 putative protein-coding genes along eight chromosomes, in a 29.4 megabase genome (Nierman *et al.*, 2005). Subsequently, a second strain of *A. fumigatus*, A1163, was sequenced, and demonstrated the presence of a set of core, highly conserved genes common to both sequenced strains (Fedorova *et al.*, 2008). Comparison of the *A. fumigatus*, *Neosartorya fischeri* and *Aspergillus clavatus* genome sequences revealed a number of genes that are unique to *A. fumigatus*. These include genes involved in secondary metabolism and detoxification, which may contribute to pathogenicity (Nierman *et al.*, 2005; Fedorova *et al.*, 2008). Data from genome sequencing and annotation is available from a number of online warehouses including the Central *Aspergillus* Data Repository (CADRE) (http://www.cadre-genomes.org.uk/) and the *Aspergillus* Genome Database (AspGD) (http://www.aspgd.org/). These resources combine *in silico* computational gene annotation with manually curated information obtained from experimentation to provide extensive profiling of the genome. CADRE provides a unique identifier for each gene with the nomenclature indicating the respective strain (e.g. AFUA_ indicates *A. fumigatus* Af293, AFUB_ indicates *A. fumigatus* A1163).

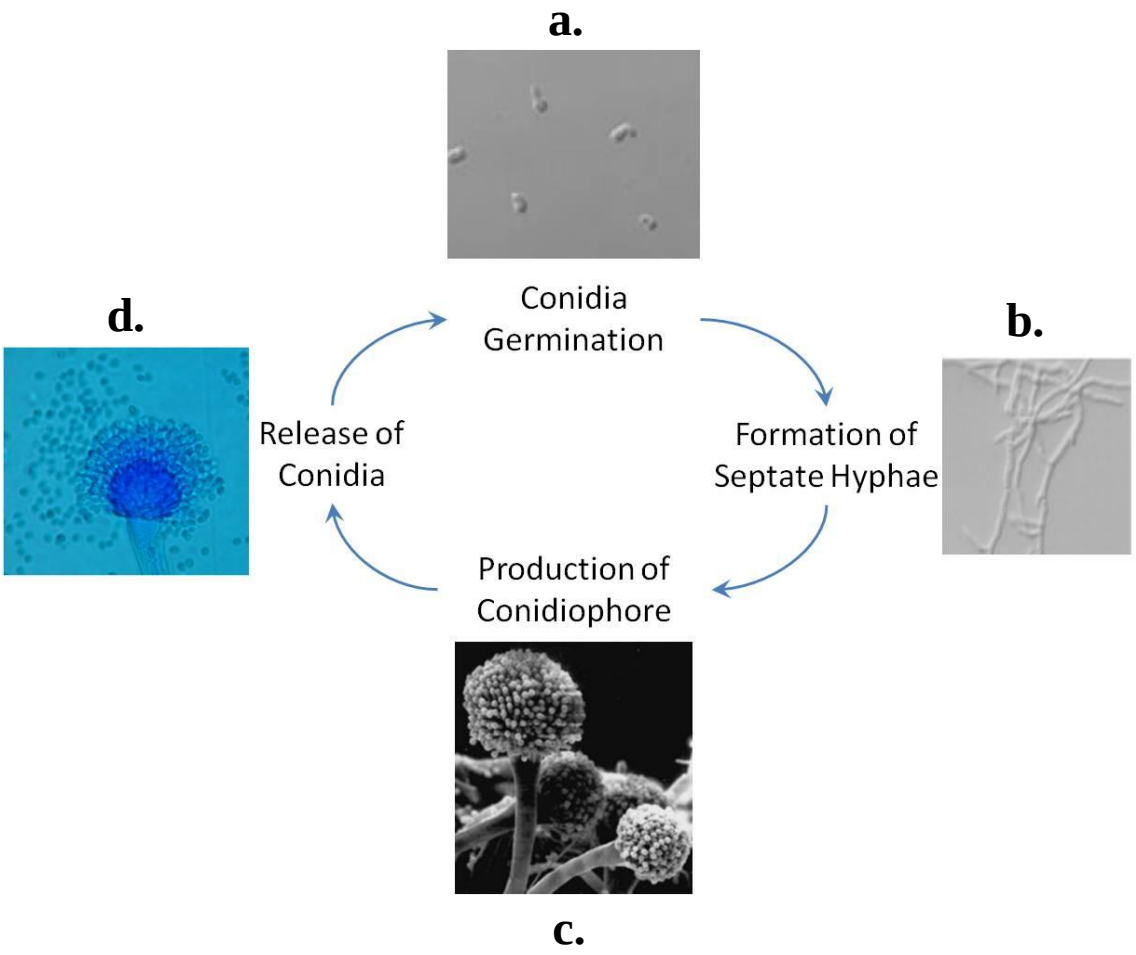

Figure 1.1: Overview of asexual life cycle of *A. fumigatus*. Differential interference contrast (DIC) microscopy of (a) germinating conidia and (b) septate hyphae of *A. fumigatus* (Images from Suh *et al.* (2012)). (c) Scanning electron microscopy of *A. fumigatus* conidiophores (Image from Hannover Medical School). (d) Light microscopy of conidia release from conidiophore (Image from www.*Aspergillus*.org.uk).

In the case of *A. fumigatus* Af293 the chromosome number and relative gene locus are also included in the identifier (e.g. AFUA_6G09740 indicates the gene is at locus number 9740 along chromosome 6 in *A. fumigatus* Af293).

1.2 Fungal Systems Biology

The field of systems biology aims to provide a global model of the mechanisms and interactions taking place in a biological system, through integration of data from multiple tiers of the 'omics' platforms (Rochfort, 2005). Combination of transcriptomic, proteomic and metabolomic information enables the multi-dimensional interpretation of data generated from experimental investigations. From the perspective of fungal systems biology, a large emphasis has been placed on the use of this approach to elucidate the mechanisms of fungal pathogenicity and related disease (Albrecht *et al.*, 2011; Rizzetto and Cavalieri, 2011; Santamaría *et al.*, 2011; Horn *et al.*, 2012). While this approach is still in its infancy in filamentous fungi, advances in global modelling have been made in unicellular microorganisms such as *Escherichia coli*, *Saccharomyces cerevisiae* and *Candida albicans* (Guthke *et al.*, 2005; Costanzo *et al.*, 2010; Stincone *et al.*, 2011; Tierney *et al.*, 2012).

In a dual-transcriptional investigation, Tierney *et al.* (2012) investigated the network of interactions between *S. cerevisiae* and cells of the innate immune system (dendritic cells and macrophages). This was achieved by simultaneous analysis of the yeast and mammalian transcriptomes following co-incubation using RNA-seq. The mechanisms of pathogenicity and conditions experienced *in vivo* during infection have also been investigated. Following recovery of fungal material from a murine model of IA, the transcriptome of *A. fumigatus* during initiation of infection was characterised (McDonagh *et al.*, 2008). Analysis of transcript abundance revealed the various stresses (e.g. oxidative stress, iron-limitation) imposed on *A. fumigatus* in the neutropenic

murine lung, in addition to identifying the increase in expression of various secondary metabolite clusters. Systems biology has also been applied for the amalgamation of data generated from distinct sources, demonstrating added value through retrospective analysis of targeted studies. Using this approach, an exhaustive metabolic map of *A. niger* was constructed based on modelling of curated data from published sources (Andersen *et al.*, 2008). Biochemical reactions, totalling 2240, were mapped to create a gapless metabolic network, providing a useful tool for future analysis of transcriptomic or proteomic data, in the context of metabolism (Andersen *et al.*, 2008).

Discrepancies have been observed when combining proteomic and transcriptomic data and no strict linear relationship exists between these two platforms (Albrecht *et al.*, 2011). Poor correlation between transcripts and their relative proteins can be indicative of regulatory mechanisms at either the transcriptional or translational level (Albrecht *et al.*, 2011). Furthermore, as translation occurs after transcription, a lag can exist between the appearance of the transcript and the respective protein. Results from a proteomic investigation of the heat shock response in *A. fumigatus* were related to a previous transcriptomic analysis, across a time-course (Nierman *et al.*, 2005; Albrecht *et al.*, 2010). Low correlation was initially observed between the data sets, but allowing for a time-shift resulted in improved agreement between the transcriptomic and proteomic data (Albrecht *et al.*, 2010). This demonstrates that an integrative approach to global profiling provides a more comprehensive and accurate overview of the systems involved in response to the applied stimulus.

1.3 Functional and Comparative Proteomics in Aspergilli

Large scale analyses of the proteomes of the genus *Aspergillus* have been emerging following the sequencing and annotation of multiple genomes from these species (Galagan *et al.*, 2005; Machida *et al.*, 2005; Nierman *et al.*, 2005; Pel *et al.*, 2007; Fedorova *et al.*, 2008). Methods for fungal proteomic investigations are summarised in Figure 1.2, and can typically be divided into two categories, gel-based and gel-free. Techniques utilised in proteomics, included MS-based proteomics and 2D-PAGE, will be outlined in detail in Chapters 3 and 5.

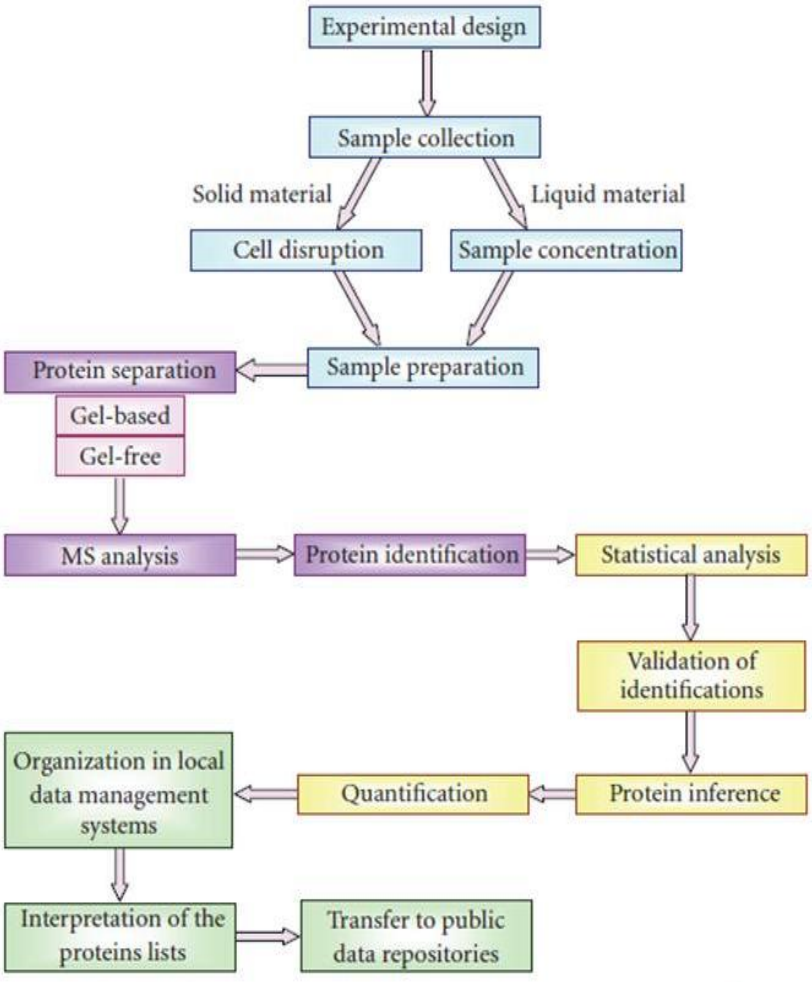

Figure 1.2: Outline of general workflow of proteomic approach in fungal studies. From González-Fernández *et al.* (2010).

While *A. nidulans* has represented a model organism of filamentous fungi in terms of genetics and cell biology research, the majority of proteomic investigations carried out to date have focused on *A. fumigatus* (Kniemeyer, 2011). This may be due to the status of *A. fumigatus* as the major pathogen of the *Aspergillus* genus. The focus of proteomic studies carried out with *A. niger* is predominately related to the characterisation of the secreted and intracellular enzymes produced by this fungus, reflective of the biotechnological associations of *A. niger* (Adav *et al.*, 2010; Lu *et al.*, 2010; Ferreira de Oliveira *et al.*, 2011). Changes in the proteome of *A. fumigatus* have been studied in response to various stimuli, in an attempt to further elucidate the stress-response pathways and mechanisms utilised by this opportunistic pathogen to colonise susceptible hosts. Further understanding of the factors contributing to the ability of *A. fumigatus* to grow and persist in the human host may aid in the directed development of anti-fungal therapies or improved diagnostic tools (Abad *et al.*, 2010).

The robust nature of filamentous fungal cells, due to the presence of a cell wall, meant that initial proteomic investigations required optimisation of more vigorous techniques for optimal protein extraction, than those required for eukaryotic cells of animal origin (Kim *et al.*, 2007). Development of reproducible extraction and purification methodologies lead the way for future use of 2D-PAGE in comparative analyses of *A. fumigatus* (Carberry *et al.*, 2006; Kniemeyer *et al.*, 2006). Production of proteome maps for the mycelia, mitochondria and conidia of *A. fumigatus* established large-scale identification of translation products, identified cellular localisations of proteins and could be used to validate genomic annotations of ‘hypothetical’ proteins (Asif *et al.*, 2006; Carberry *et al.*, 2006; Kniemeyer *et al.*, 2006; Vödisch *et al.*, 2009; Teutschbein *et al.*, 2010; Doyle, 2011b). Identification of so-called ‘hypothetical’ or ‘predicted’ proteins by MS, allows re-annotation as ‘unknown function proteins’ (UFPs)

due to confirmation of their existence (Doyle, 2011b). A large number of immunoproteomic studies have also emerged, detecting allergenic and antigenic proteins from intracellular and extracellular fractions (Asif *et al.*, 2010; Singh *et al.*, 2010a, 2010b; Shi *et al.*, 2012a). These studies will be described in more detail in Chapter 4. More recently, a move towards mass spectrometry-based proteomics is evident and represents the next generation in the proteome research (Cagas *et al.*, 2011b; Suh *et al.*, 2012). Advances in mass spectrometry technology, coupled with software development for enhanced analysis capabilities, is paving the way for proteomics to match the high genome coverage attained in transcriptomics (Gstaiger and Aebersold, 2009).

Comparative proteomic investigations have expanded the understanding of the molecular response of *Aspergillus* species to stress, whether physical (e.g. heat shock), chemical (e.g. antifungals) or due to nutrient limitation (e.g. iron-depletion) (Hortschansky *et al.*, 2007; Gautam *et al.*, 2008; Albrecht *et al.*, 2010). The oxidative stress response has been investigated in both *A. fumigatus* and *A. nidulans* using two distinct triggers of reactive oxygen stress. Addition of H_2O_2, leading to a rise in intracellular peroxide (O_2^{2-}) levels, resulted in fold increases in the putative thioredoxin peroxidase Aspf3 and peroxiredoxin Prx1 (Lessing *et al.*, 2007). Paradoxically, extended use of menadione to induce oxidative stress in *A. nidulans* lead to the significant repression of peroxiredoxin and peroxidase translation (Pusztahelyi *et al.*, 2011). Menadione generates oxidative stress through the production of superoxide and hydroxyl radicals, and this variance in the type of ROS produced may explain the differentiation in regulation. Alternatively, the exposure of *A. fumigatus* to H_2O_2 (45 min) compared to the incubation of *A. nidulans* with menadione (6 h) may suggest different short- and long-term adaptations to oxidative stress (Kniemeyer *et al.*, 2011).

Comparative analysis of exposure to hypoxia has also been independently investigated in *A. fumigatus* and *A. nidulans* using 2D-PAGE (Shimizu *et al.*, 2009; Vödisch *et al.*, 2011; Barker *et al.*, 2012). Vödisch *et al.* (2011) examined the response to low oxygen over 30 h, following initial cultivation of *A. fumigatus* in normoxia, and observed an increase in the levels of respiratory proteins and reactive nitrogen species (RNS)-detoxifying protein. Additionally, expression of the secondary metabolite pseurotin A biosynthesis cluster was up-regulated at the transcriptional and translational level following prolonged exposure to hypoxia. Short-term adaptation to hypoxia in *A. fumigatus* revealed a decrease in proteins constituting the TCA cycle, along with a decrease in purine metabolism and ribosome biogenesis (Barker *et al.*, 2012). Cultivation of *A. nidulans* in hypoxic conditions, followed by a time-course proteomic investigation indicated the increase in pentose and nucleotide metabolism, with a corresponding rise in the expression of thiamine biosynthesis enzymes. These apparent differences may again arise from time-dependent adaptation to hypoxia or alternatively demonstrate distinct mechanisms of hypoxia response between the species (Kniemeyer *et al.*, 2011). Comparative 2D-PAGE analysis in *A. fumigatus* will be discussed in more detail in Chapter 5.

Comparative proteomics can also be employed to deduce changes to the proteome of the organism following deletion of a specific gene. In combination with phenotypic analysis, this approach can provide insight into the role of the respective protein through monitoring of the processes altered in the deletion strain relative to the parent strain (Doyle, 2011b). This methodology has been used for the functional investigation of a number of proteins from the *Aspergillus* species (Bruneau *et al.*, 2001; Hortschansky *et al.*, 2007; Lessing *et al.*, 2007; Sato *et al.*, 2009; Zhang *et al.*, 2009; O'Hanlon *et al.*, 2012). The production of non-ribosomal peptides (NRPs) is carried out

by large modular enzymes, referred to as NRP synthetases (NRPSs). The respective peptide products of these NRPSs can be difficult to identify, and gene deletion studies can facilitate matching of the enzyme to the respective product, in addition to elucidating the biochemical role of the NRP in the cell (Balibar and Walsh, 2006; Cramer *et al.*, 2006; Kupfahl *et al.*, 2006; Maiya *et al.*, 2006; Reeves *et al.*, 2006; O'Hanlon *et al.*, 2011, 2012). Deletion of the gene encoding the largest NRPS, *pes3*, from *A. fumigatus* resulted in the generation of a strain with impaired germ tube formation, increased sensitivity to voriconazole and demonstrating enhanced virulence in a corticosteroid mouse model of IA (O'Hanlon *et al.*, 2011). Reduced immunogenicity of the Δ*pes3* strain was also observed and evasion of the immune reaction may attribute to the increase in virulence noted in this mutant. Comparative 2D-PAGE was used to analyse the relative changes to the proteome of *A. fumigatus* germlings following deletion of the *pes3* gene. O'Hanlon *et al.* (2011) detected an increase in the protein Rab11, with a predicted role in the regulation of plasma membrane-endosome trafficking. Disruption of this mechanism may account for the enhance sensitivity to voriconazole associated with Δ*pes3*. Down-regulation of actin, spermidine synthase and the petafunctional AroM protein are reflective of the observed morphological differences and germination deficiency of Δ*pes3*. The differential characterisation of the proteomes of Δ*pes3* and the parent strain, provided confirmatory data for phenotypic analyses and indicated a structural role for the Pes3-encoded peptide (O'Hanlon *et al.*, 2011). This demonstrates the capacity for proteomics to contribute to the functional elucidation of genes and their down-stream products, through characterising the effects of gene deletion (Doyle, 2011b).

1.4 Pathogenesis of *A. fumigatus*

1.4.1 *A. fumigatus*-related disease

The opportunistic pathogen, *A. fumigatus*, is responsible for a range of diseases, with host susceptibility closely linked to the immune status of the individual (Latge, 1999). *A. fumigatus*-associated disease can be classified into three general groups; (a) allergic reactions, (b) colonisation with limited invasiveness and (c) invasive infections (Brakhage and Langfelder, 2002). The latter category tends to be observed in immunocompromised individuals, demonstrative of the classification of *A. fumigatus* as an opportunistic pathogen (Abad *et al.*, 2010).

Allergic airway diseases, associated with *A. fumigatus*, include allergic bronchopulmonary aspergillosis (ABPA) and related conditions. ABPA is a hypersensitivity disorder that predominantly affects individuals with cystic fibrosis (CF) and asthma (Knutsen and Slavin, 2011). ABPA can lead to chronic lung damage and deterioration of lung function in this cohort of patients (Kraemer *et al.*, 2006; Chaudhary and Marr, 2011). The major predisposing factor for development of ABPA is the ineffective clearance of inhaled conidia from the lung (Pihet *et al.*, 2009; Patterson and Strek, 2010). Structural abnormalities associated with chronic lung disease can contribute to the conidial evasion of the host mucociliary clearance mechanism (Thomas *et al.*, 2010; Chaudhary and Marr, 2011). CF is characterised by mutations in the CF transmembrane conductance regulator (CFTR), leading to disruption of chloride channels in many epithelial cells. This results in the development of thick, viscous mucous in the lung, which can impede the clearance of inhaled microorganisms (Pihet *et al.*, 2009). In the absence of ABPA, lung function is not affected by *A. fumigatus* colonisation, which is observed frequently in CF patients (De Vrankrijker *et al.*, 2011). Conidia evading extrusion from the lung must germinate

before allergy can be established, as dormant conidia are immunologically inert due to presence of an external hydrophobic rodlet layer (Aimanianda *et al.*, 2009). Damage to pulmonary epithelium following germination permits exposure of *A. fumigatus* antigens to host dendritic cells (DCs). Pulmonary DCs subsequently elicit a Th2-type response with secretion of cytokines and B-cell isotype switching to IgE production (Chaudhary and Marr, 2011). Elevation of total IgE levels and secretion of proinflammatory cytokines is indicative of the allergic response associated with ABPA (Knutsen, 2006; Patterson and Strek, 2010). Diagnostic guidelines for ABPA include presence of pre-disposing conditions (e.g. CF), elevation in total IgE, elevation in anti-*A. fumigatus* antibodies and a number of other criteria (Agarwal, 2011).

Aspergilloma is an example of the second category of *A. fumigatus*-related disease, characterised by colonisation in the absence of extensive invasiveness. *A. fumigatus* colonisation of pre-existing cavities in the lung can result in the formation of an aspergilloma (fungus-ball). Tuberculosis (TB) is the most common cause of cavitation leading to aspergilloma formation, with 11 % of individuals possessing cavities showing radiographical signs of aspergilloma (Kawamura *et al.*, 2000; Zmeili and Soubani, 2007). The aspergilloma consists of a mass of fungal hyphae, inflammatory cells, fibrin mucous and cell debris and the condition is usually non-invasive (Latge, 1999; Zmeili and Soubani, 2007). Detection and diagnosis of aspergilloma is usually through routine radiography, as the condition is often asymptomatic (Zmeili and Soubani, 2007; Kradin and Mark, 2008). Sporulation of conidia, is postulated to occur in addition to mycelial growth, as multiple isogenic, azole-resistant strains were isolated from an aspergilloma during a course of anti-fungal therapy (Camps *et al.*, 2012). Surgical intervention is utilised for removal of the

aspergilloma, and the use of anti-fungals as an adjunct has been found to be ineffective (Brik *et al.*, 2008; Sagan and Goździuk, 2010).

The third sub-category of disease associated with *A. fumigatus* is classified by invasive disease, which may disseminate and result in systemic infection. Invasive aspergillosis (IA) is a term used to describe clinical presentations that fall into this group. IA is the most detrimental *Aspergillus*-related disease, with associated mortality rates ranging from 40 to 95 % (Nivoix *et al.*, 2008; Abad *et al.*, 2010). Various factors including the immune status of the patient, site of infection and treatment affect these mortality rates (Maertens *et al.*, 2002). Individuals at risk for the development of IA include patients with haematological malignancies (e.g. leukaemia), chronic obstructive pulmonary disease (COPD), solid organ and hematopoietic stem cell transplant (HSCT) recipients, extended corticosteroid use and HIV-positive individuals (Dagenais and Keller, 2009; Gangneux *et al.*, 2010). COPD has been identified as a risk factor for development of *Aspergillus*-related hypersensitivity and ABPA (Agarwal *et al.*, 2010). Genetic factors also influence the susceptibility of individuals to IA, and individuals with single nucleotide polymorphisms (SNPs) in genes such as plasminogen, IL-10 and mannose-binding lectin (MBL) are pre-disposed to develop IA (Crosdale *et al.*, 2001; Brouard *et al.*, 2005; Sainz *et al.*, 2007; Zaas *et al.*, 2008). Two distinct risk factors exist for the development of IA, neutropenia and corticosteroid-induced immunosuppression (Figure 1.3). Prolonged neutropenia represents the dominant risk for development of pulmonary IA and the associated disease is characterised by angioinvasion and disseminated fungal growth (Kradin and Mark, 2008; Ben-Ami *et al.*, 2010). Additionally, disruption in neutrophil function (e.g. chronic granulomatous disease (CGD) can result in a similar clinical presentation of IA, although angioinvasion is generally not observed in this sub-set of patients (Segal and Romani, 2009). A different

pathology is observed in IA associated with corticosteroid-induced immunosuppression. Non-neutropenic or corticosteroid-related IA is generally non-angioinvasive, with limited fungal development or dissemination. Instead, the condition is characterised by excessive inflammation resulting in damage to tissues due to an aggressive host response (Balloy *et al.*, 2005). Inhaled conidia that evade mucociliary clearance, are generally phagocytosed by macrophages in the lung (Bhatia *et al.*, 2011). In addition to their function as phagocytes, alveolar macrophages modulate the immune response, and elicit the migration of other immune effector cells through the release of chemo- and cytokines. Engulfed conidia are killed in macrophages through the action of reactive oxygen species (ROS) and acidification in the phagolysosome (Ibrahim-Granet *et al.*, 2003; Philippe *et al.*, 2003). While corticosteroids do not affect phagocytosis of conidia by alveolar macrophages, ROS-mediated killing is inhibited. This can lead to germination of phagocytosed conidia in individuals undergoing corticosteroid treatment (Philippe *et al.*, 2003). Circulating neutrophils are recruited to the lung and are important in defence against fungal hyphae. Neutrophils mediate killing of hyphae by oxidative mechanisms following attachment to hyphal surfaces and de-granulation (Levitz and Farrell, 1990; Feldmesser, 2006). Tissue damage resulting from corticosteroid-associated IA is through an excessive influx of neutrophils and associated inflammation (Balloy *et al.*, 2005). Conversely, in neutropenia-associated IA, hyphal growth and extensive fungal development occurs due to the absence of neutrophils (Balloy *et al.*, 2005; Feldmesser, 2006). Diagnosis of IA is often delayed due to the non-specificity of the associated symptoms and limited sensitivity of diagnostic tests, which can contribute to delayed treatment (Segal and Walsh, 2006; Trof *et al.*, 2007). Treatment of IA involves the use of anti-fungal therapy, which includes the azole, echinocandin and polyene classes of drugs (Kontoyiannis, 2012).

1.4.2 Detection and diagnostic strategies for IA

Diagnosis of IA has been hampered by the presence of a multi-factorial disease, coupled with a wide-range of pre-disposing host factors. Together with the limited array of validated laboratory diagnostic methods, late diagnosis of IA contributes to delayed treatment and correspondingly high mortality rates (Maertens *et al.*, 2007). This phenomenon is exemplified by the high disparity between post-mortem detection and ante-mortem diagnosis of invasive fungal infections (IFIs), and specifically IA (Chamilos *et al.*, 2006; Antinori *et al.*, 2009). The current criteria for diagnosis of IFIs have been outlined by the consensus group of the European Organisation for Research and Treatment of Cancer/Invasive Fungal Infections Cooperative Group and the National Institute of Allergy and Infectious Diseases Mycoses Study Group (EORTC/MSG) (De Pauw *et al.*, 2008). Following the revised EORTC/MSG guidelines diagnoses of IFIs can be delineated into proven, probable or possible categories of disease. Classification is dependent on the presence of host factors (e.g. recent neutropenia or prolonged corticosteroid use), observation of clinical indications (e.g. radiographic findings) and mycological criteria (e.g. direct microscopy or detection of antigens). Mycological evidence of IFI involves the direct or indirect detection of the causative fungal agent. Direct methods of detection include culture of the fungus from patient specimens, including sputum or bronchoalveolar lavage (BAL) fluid, or observation of fungal elements by microscopy. Indirect mycological detection methods currently approved for use in EORTC/MSG guidelines are typically only applicable to aspergillosis and candidiasis due to the selectivity of these tests (De Pauw *et al.*, 2008).

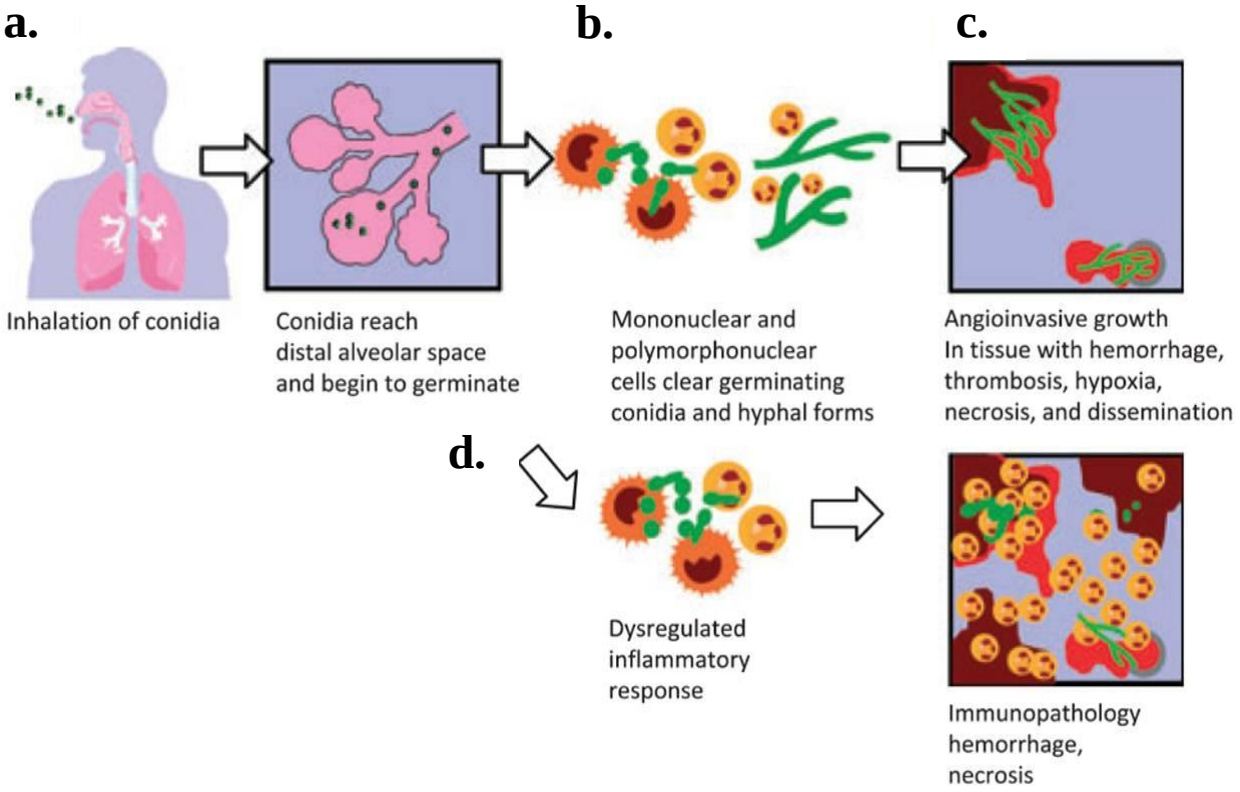

Figure 1.3: Pathogenesis of IA based on immune status of the host. (a) *A. fumigatus* conidia are inhaled and reach the alveoli of the lungs, where germination occurs. (b) Conidia are cleared by cells of the immune system, including alveolar macrophages and PMN cells. (c) Germination and tissue invasion occurs in individuals with reduced quantity or efficacy of PMN cells. (d) Non-neutropenic hosts (e.g. long-term corticosteroid use) develop tissue damage as a result of excessive PMN cell recruitment. From Ben-Ami *et al.* (2010).

Detection of circulating antigens using the enzyme-immunoassay (EIA) format has contributed to the detection and monitoring of *Aspergillus* infections. Galactomannan is a heat-stable polysaccharide component of the cell walls of *Aspergillus* and *Penicillium spp*, which is secreted during fungal growth (Latgé *et al.*, 1994). The FDA-approved Platelia© sandwich EIA, for the detection of *Aspergillus* galactomannan, is routinely used as an adjunct diagnostic tool for IA (Maertens *et al.*, 2007). Levels of circulating galactomannan (GM) have been considered to be proportional to the relative fungal load, with absence of GM subsidence an indicator of prognosis (Boutboul *et al.*, 2002). An additional cell wall constituent, β-glucan, is another diagnostic target for IFIs. Since β-glucan is present on cell walls from most pathogenic fungi, excluding Cryptococcus and Zygomycetes, it does not specifically indicate IA but instead is a 'pan-fungal' detection strategy (Hope *et al.*, 2005; Maertens *et al.*, 2007; Thornton, 2010). Investigation of the specificity and sensitivity of these indirect detection strategies, currently in routine use for IFI diagnosis, has resulted in widely varying results. Host-factors appear to influence the performance of these antigen assays, with accuracy of GM detection differing between patients with haematological disorders and immunosuppressed individuals (Pfeiffer *et al.*, 2006; Ku *et al.*, 2012). Furthermore, anti-fungal therapy can also reduce the sensitivity of these antigen immunoassays, highlighting the need for further validated tests for IA diagnosis (Marr *et al.*, 2005). Polymerase chain reaction (PCR)-based detection strategies, for use in IA diagnosis, are undergoing development, with further validation required before they can be included in the EORTC/MSG guidelines for IFI diagnosis (De Pauw *et al.*, 2008). Efforts have been undertaken to standardise procedures used in PCR-based detection of IA, in addition to reduction in the incidence of false-positives (White *et al.*, 2010, 2011). Emerging real-time quantitative PCR (qPCR) strategies for detection of *Aspergillus* are compliant with stringent guidelines for reporting and may signal the

shift towards inclusion of these molecular tests in the IA diagnostic tool-belt (Johnson *et al.*, 2012).

Several novel strategies are under investigation for the diagnosis of IA, including immuno-based methods and detection of *Aspergillus*-specific low molecular mass metabolites. The use of monoclonal antibodies (MAbs) for detection of alternative targets to previously described (i.e. GM, β-glucan) has been examined by a number of groups with the potential for enhanced selectivity and sensitivity of detection. The development of an *Aspergillus* antigen capture ELISA has been described, using two distinct MAbs for the enhanced capture and detection of an *Aspergillus* antigen (Hao *et al.*, 2008). Combination of an antigen-assay with detection of anti-*Aspergillus* antibodies has also been explored, for the overall improvement in diagnostic capabilities. The gliotoxin oxidoreductase, GliT, has demonstrated immunoreactivity and has been identified both intracellularly and extracellularly in *A. fumigatus* (Schrettl *et al.*, 2010; Kumar *et al.*, 2011). Measurement of anti-GliT antibody levels, has been examined as a putative tool for IA diagnosis in non-neutropenic patients, although coupling of this assay with GM detection was suggested for optimal results (Shi *et al.*, 2012b). A lateral flow device has been developed for the detection of an *Aspergillus*-specific antigen, utilising a MAb directed against an undisclosed external component of *Aspergillus*, which is secreted during active growth (Thornton, 2008). Due to the ease of use, this device represents a significant development in IA diagnostics (Thornton *et al.*, 2012).

Additional studies have been carried out to investigate the potential of low molecular mass fungal metabolites in diagnosis. A novel metabolite-based detection strategy, under preliminary investigation, comprises a breath test for IA, and is based on the detection of an *Aspergillus*-specific volatile organic compound (VOC) (Chambers *et*

al., 2011). The premise of this test is the use of 2-Pentylfuran (2PF) as a biomarker of IA, however technical apparatus required to characterise these samples make this technology incompatible with a clinical setting in its current form (Chambers *et al.*, 2011). MS-based detection of cyclic non-ribosomal peptides has been proposed as a way by which to detect fungal infection and distinguish between fungal strains, based on distinct cyclic peptide profiles (Jegorov *et al.*, 2006). Additionally, detection of the bis-methylated derivative of gliotoxin (bmGT), was achieved using thin layer chromatography (TLC) and high performance liquid chromatography (HPLC), and was put forward as a more reliable diagnostic candidate than native gliotoxin (Domingo *et al.*, 2012). Further to their potential for use as biomarkers of infection, fungal metabolites can also be employed for detection of fungal growth *in vivo*. Petrik *et al.* (2010) exploited the iron scavenging activity of *A. fumigatus*, by using modified siderophores as a reporting mechanism. Radio-labelled siderophores were selectively taken up by *A. fumigatus in vivo* and accumulation allowed the detection of *A. fumigatus* infection using positron emission tomography (PET). Again this strategy hinged on the principle of using fungal-specific molecules or mechanisms for detection, to eliminate false positives from host interference. Further development of indirect detection methods for IA is of paramount importance, as sensitive and selective techniques would preclude the need for invasive diagnostic procedures.

1.5 Anti-fungal therapy for IA

Therapeutic goals in the treatment of invasive fungal infections (IFI) include the restoration of immune function, if applicable, and the reduction of the fungal burden (Traunmüller *et al.*, 2011). Anti-fungal agents are utilised to achieve the latter, and include polyenes, triazoles and echinocandins for the treatment of IA (Thompson and Patterson, 2008). Due to relatively close phylogenetic relationship between fungi and

humans, unique targets for anti-fungal therapeutics are limited and the identification of differential mechanisms may expand this base (Denning and Hope, 2010). One such target for anti-fungal agents is the cell wall, which represents a fungal-specific entity, distinct from the host background (Vandeputte *et al.*, 2012). Additionally ergosterol, a component of the fungal cell membrane, is not found in human cell membranes, with particular classes of drugs targeting these molecules (Beauvais and Latgé, 2001). The polyene class of anti-fungals, including amphotericin B (AmB) deoxycholate, exploit this unique fungal target to elicit their function. AmB binds to ergosterol in the fungal cell membrane and forms pores, which lead to leakage of potassium ions. The resultant proton gradient ultimately results in fungal cell death (Lemke *et al.*, 2005). AmB was classically the primary anti-fungal used for the treatment of IA, however substantial side effects, including nephrotoxicity, have lead to the development and use of lipid formulations with reduced toxicity (Wingard *et al.*, 1999; Kleinberg, 2006; Ullmann *et al.*, 2006).

Voriconazole, itraconazole and posaconazole are member of the triazole class of anti-fungals used to treat invasive fungal infection. Triazoles inhibit the cytochrome P450 enzyme resulting in disruption of ergosterol biosynthesis and consequently cell membrane dysfunction and cell death (Thompson and Patterson, 2008). Voriconazole inhibits the action of 14α-lanosterol demethylase, a key step in the production of ergosterol which is required for normal cell membrane function (Denning and Hope, 2010). Some hepatic-related side effects are associated with voriconazole use, principally due to metabolism via host cytochrome P450 enzymes (Johnson and Kauffman, 2003). Despite this, voriconazole has emerged as the primary therapy for IA due to the reduced toxicity profile and enhanced efficacy, relative to AmB (Herbrecht *et al.*, 2002; Azie *et al.*, 2012). Emergence of resistance to azoles has been noted in some

cases and this represents a potential concern for long-term use of these therapeutics (Howard *et al.*, 2006; Trof *et al.*, 2007; Camps *et al.*, 2012).

Caspofungin is a member of the echinocandin class of anti-fungal agents, which function by disrupting cell wall synthesis. Caspofungin is currently recommended for use as a second line or salvage therapy for IA (Maertens *et al.*, 2004; Kartsonis *et al.*, 2005). Recent studies have also indicated the effectiveness of this agent in the primary treatment of IA, with efficacy and favourable toxicity profiles shown in patients with haematological disorders and HSCT recipients (Herbrecht *et al.*, 2010; Jarque *et al.*, 2012). The mechanism of action of caspofungin is the targeted disruption of β(1,3)-D-glucan biosynthesis, through non-competitive inhibition of β(1,3)-D-glucan synthase. Inhibition of β(1,3)-D-glucan biosynthesis, a principle cell wall component, results in destabilisation of fungal cell walls and limits fungal growth (Letscher-Bru, 2003). Caspofungin is utilised as a monotherapy for IFIs, in addition to inclusion in combination therapy (Maertens *et al.*, 2010). Combination therapy for the treatment of IA offers a number of theoretical advantages, including reduced risk of resistance, wider target area, and more rapid effect, however preliminary studies have not conclusively demonstrated the effectiveness of this approach over monotherapy (Trof *et al.*, 2007; Tunger *et al.*, 2008; Garbati *et al.*, 2012). *In vitro* studies suggest positive outcomes upon combinations of azoles with echinocandins, possibly due to differential targets associated with these agents (Jeans *et al.*, 2012).

Immunotherapy represents another strategy for the treatment of IA, focusing on modulation of immune function for enhanced anti-fungal activity (Carvalho *et al.*, 2012). Administration of recombinant colony stimulating factors (CSFs), including granulocyte-CSF (G-CSF) and granulocyte-macrophage CSF (GM-CSF), has been investigated for potential in the treatment of invasive fungal infections. G-CSF

stimulates the proliferation and survival of neutrophils and their precursors, and is used in the prevention of chemotherapy-associated febrile neutropenia (Silvestris *et al.*, 2012). GM-CSF promotes neutrophil survival and stimulates neutrophil effector function, in addition to stimulation of macrophage proliferation and activity (Hercus *et al.*, 2012). Therapeutic use of these CSFs in treatment of IFI was expected to restore immune function and consequently enhance fungal clearance, however results from various *in vitro* studies and clinical reports were contradictory (Lehrnbecher *et al.*, 2011). Post-transplant administration of G-CSF has also been demonstrated to impair immune recovery due to the induction of an inflammatory Th2 response (Volpi *et al.*, 2001). GM-CSF represents a more appropriate agent for use against *Aspergillus*-associated infection due to stimulation of both neutrophils and macrophage activity. Additionally GM-CSF, unlike G-CSF, does not dramatically increase total leukocytes counts, resulting in reduced tissue injury from the inflammatory neutrophil response (Graybill *et al.*, 1998). Use of G-CSF has been shown to shorten recovery times and length of hospitalisation when used in the treatment of IA, however no effect was noted regarding mortality rates (Pagano *et al.*, 2010). The most beneficial use of CSFs appears to be in prophylactic treatment for the prevention of infection in high-risk patient cohorts (Falagas *et al.*, 2008). Therefore this immunotherapy represents a promising preventative or adjunct therapy for IA.

1.6 Factors contributing to *A. fumigatus* pathogenicity

A. fumigatus has been postulated to be an accidental pathogen, lacking sophisticated virulence factors (McCormick *et al.*, 2010). Many of the traits of *A. fumigatus*, which contribute to its pathogenicity under opportune conditions, have developed to enable survival in the primary ecological niche of this fungus, the soil. Through functional genomics investigations a number of genes connected to thermo-

tolerance in *A. fumigatus* were identified, including *afpmt1* (AFUA_3G06450), *afmnt1* (AFUA_5G10760), *cgrA* (AFUA_8G02750), *thtA* (AFUA_1G03992) and *midA* (AFUA_3G10960) (Bhabhra *et al.*, 2004; Chang *et al.*, 2004; Zhou *et al.*, 2007; Wagener *et al.*, 2008; Dichtl *et al.*, 2012). The genes *afmnt1, cgrA*, *thtA* and *midA* are essential for growth at 48 °C, while conidiation at 50 °C is inhibited upon deletion of *afpmt1*. A range of distinctive mechanisms contribute to attenuation of thermo-tolerance in these deletion strains. CprA has a role in ribosomal synthesis, and is required for conidial germination at higher temperatures. *Afpmt1* and *afmnt1* code for an α-1,2-mannosyltransferase and an O-mannosyltransferase respectively, with deletion of these genes resulting in loss of cell wall integrity (Zhou *et al.*, 2007; Wagener *et al.*, 2008). This implicates the cell wall as an integral component in resistance to thermal stress. Comparative proteomics has also identified mechanisms that are differentially regulated upon exposure to heat shock. Protein chaperones, proteins involved in carbon and nitrogen metabolism, translation, and proteins involved in defence against oxidative and nitrosative stress, were all significantly up-regulated upon temperature shift from 30 to 48 °C (Albrecht *et al.*, 2010). Proteins involved in cell wall and cytoskeleton assembly were also observed to increase in expression following thermal stress, further demonstrating the importance of cell wall integrity in resistance to stress.

The cell wall provides a physical barrier between the fungal cell and the external environment, affording structural integrity to the hyphae and conidia in addition to physical protection from exogenous stresses. The cell wall of *A. fumigatus* is composed primarily of polysaccharides, and is a dynamic structure embedded with proteins, that can change in response to environmental stimuli (Abad *et al.*, 2010). The constituents of the cell wall include α(1,3)-glucans, β(1,3)-glucans, chitins and galactomannans (Figure 1.4). Disruption of the cell wall integrity increases the sensitivity of *A. fumigatus* to

external stresses, and additionally can enhance the susceptibility to antifungal agents. Deletion of *afmnt1* and *afpmt1*, involved in cell wall component biosynthesis, increases the sensitivity of the mutants to azoles and hygromycin respectively (Zhou *et al.*, 2007; Wagener *et al.*, 2008). Additionally, *wsc1* mutants lacking a protein involved in cell wall integrity signalling, are significantly more sensitive to echinocandin treatment (Dichtl *et al.*, 2012). The cell wall constituent, β-glucan is recognised by the host immune system and is a ligand for the Dectin-1 receptor, which activates the inflammatory immune response (Steele *et al.*, 2005). β-glucan is not exposed on the surface of resting conidia, but becomes available for Dectin-1 binding following the initiation of conidia swelling and germination (Hohl *et al.*, 2005). Components of the cell wall also exhibit immunomodulatory mechanisms, which can result in attenuation of the innate immune response. Specifically, α-glucan reduces toll-like receptor (TLR)-2 and TLR4-mediated production of interleukin (IL)-6, while β-glucan decreases IL6 production via TLR4 (Chai *et al.*, 2011b). These effects were dose-dependent and more pronounced IL6 attenuation was observed using extracts from germinating conidia compared to resting conidia (Chai *et al.*, 2011b). TLRs recognise specific non-self molecules and trigger immune responses through signalling mechanisms. IL6 triggers the innate immune response and modulation of the production of this molecule demonstrates an immunoevasion mechanism elicited by the cell wall of *A. fumigatus*.

As described earlier, the innate immune response directed against *A. fumigatus* involves alveolar macrophages and dendritic cells, resident in the lung, as a first-line of defence. Additionally, recruitment and activation of other leukocytes is required to fend off infiltrating fungal infection. As *A. fumigatus* is an opportunistic pathogen, virulence is associated with impairment in the host defence system.

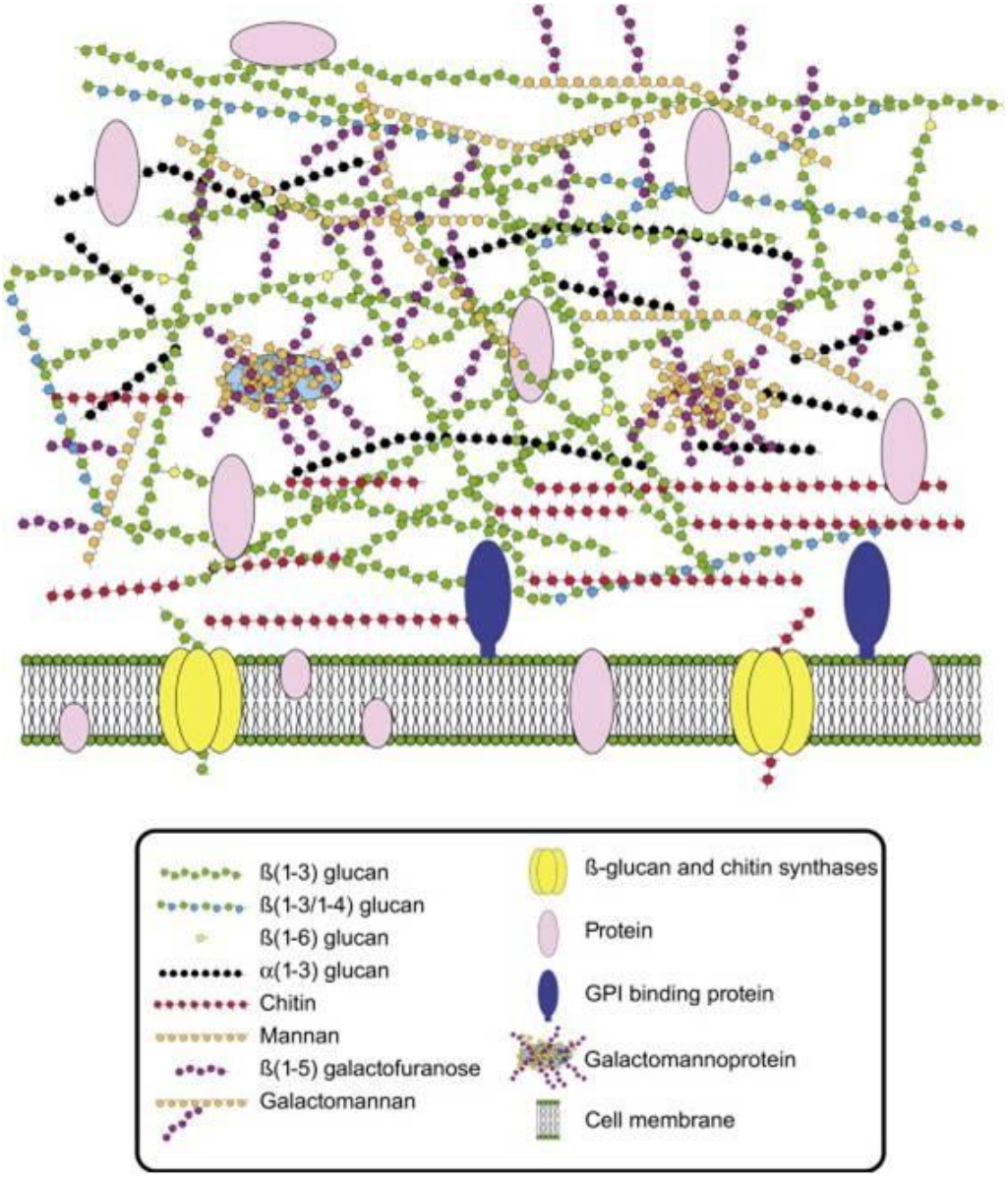

Figure 1.4: Schematic of *A. fumigatus* cell wall. From Abad *et al.* (2010).

Moreover, *A. fumigatus* has a number of characteristics that enhance immune evasion and enable resistance to components of the host immune response. In addition to the cell wall components discussed previously, *A. fumigatus* possesses exterior features that impart protection against external stresses. Melanin is located on the external surface of conidia and is responsible for the dark pigment associated with *A. fumigatus* conidia (Tsai *et al.*, 1999; Schmaler-Ripcke *et al.*, 2009). Melanin has been demonstrated to play a protective role in *A. fumigatus* conidia through a number of mechanisms: (i) protection against UV light, (ii) down-regulation of the complement cascade, (iii) ROS scavenging and (iv) masking cell surface ligands of the innate immune system (e.g. β-glucan) (Tsai *et al.*, 1998, 1999; Brakhage and Liebmann, 2005; Nosanchuk and Casadevall, 2006; Chai *et al.*, 2011a). Furthermore, following phagocytosis of conidia by macrophages, melanin inhibits phagolysosome acidification and apoptosis, thus prolonging the survival of infected macrophages (Thywißen *et al.*, 2011; Volling *et al.*, 2011). An additional hydrophobic layer, encases the surface of conidia, and is composed of RodA protein covalently bound to the cell wall. This rodlet or hydrophobin layer aids in the dispersion of conidia, through the associated hydrophobicity, and also decreases the immunogenicity of resting conidia. Conidia from mutants deficient in the RodA protein activated dendritic cells and alveolar macrophages, with associated release of cytokines, while wild-type resting conidia were immunologically silent (Aimanianda *et al.*, 2009; Dagenais *et al.*, 2010). An additional mechanism employed by neutrophils in the defence against *A. fumigatus* is the production of neutrophil extracellular traps (NETs), consisting of secreted DNA complexes with anti-microbial granular proteins, which surround the fungal cells (Wartha *et al.*, 2007; Bruns *et al.*, 2010a). RodA is responsible for reduced NET formation, with reduced levels or absence correlating with enhanced secretion of NETs by neutrophils (Bruns *et al.*, 2010a). As with melanin, the hydrophobin layer provides a

mask for immunogenic cell surface ligands in dormant conidia, allowing spores to evade host defences prior to germination.

An integral component of *A. fumigatus*, in resistance to effector functions of the host defences, is the plethora of enzymes for detoxification of ROS. Macrophage and neutrophil-mediated killing of conidia and hyphae is achieved in part through the generation of ROS. NADPH-oxidase (NOX) is responsible for release of ROS and is essential for defence against fungal infection (Brown *et al.*, 2009a). Correspondingly, defects in the NOX enzyme, associated with CGD, results in impaired capacity of neutrophils to kill fungi and leads to increased susceptibility to infections (Segal and Romani, 2009). The mitogen-activated protein kinase (MAPK) family of enzymes play a role in cell signalling and regulate intracellular responses to stress. In *A. fumigatus*, MpkA and SakA are two MAPKs associated with response to ROS and mediate their function through signal transduction cascades (Du *et al.*, 2006; Valiante *et al.*, 2008). MpkA is involved in the regulation of a number of genes encoding anti-oxidant proteins, including catalases and superoxide dismutase (SOD) (Jain *et al.*, 2011). In *A. nidulans*, the interaction of SakA with the transcription factor AtfA facilitates stress signalling and is involved in the regulation of catalase and peroxiredoxin expression (Lara-Rojas *et al.*, 2011). The transcription factor, Yap1, plays an integral role in the regulation of antioxidant genes in *A. fumigatus* (Aguirre *et al.*, 2006). Upon exposure to oxidative stress, Yap1 accumulates in the nucleus and induces the transcription of genes involved in protecting the cell from stress-induced damage (Kuge *et al.*, 1997). Yap1 targets, identified by comparative proteomics using a *yap1* deletion strain, included catalases, chaperones, peroxidases and a mitochondrial peroxiredoxin (Lessing *et al.*, 2007). While Δ*yap1* displayed no change in pathogenicity relative to the wild-type in a mouse model of invasive pulmonary aspergillosis (IPA), Yap1 was essential for

virulence in an ocular keratitis infection model (Lessing *et al.*, 2007; Sixto *et al.*, 2012). This may result from the use of a neutropenic mouse model for IPA infection, as Yap1 is crucial in the defence against neutrophil-mediated killing (Lessing *et al.*, 2007; Sixto *et al.*, 2012). A zinc finger transcription factor, SebA, has recently been identified in *A. fumigatus*, with a role in protection against various forms of stress, including oxidative and heat shock stress (Dinamarco *et al.*, 2012). The deletion strain of *sebA*, demonstrated increased sensitivity to H_2O_2 and paraquat treatments, and *sebA*-dependent regulation of anti-oxidant enzymes was observed in response to these stimuli (Dinamarco *et al.*, 2012). The fungal response to oxidative stress therefore plays an integral role in the ability to function as a human pathogen (Brown *et al.*, 2009a) and further characterisation of this response is necessary for the understanding of pathogenicity.

The exposure to hypoxia represents a further physiological stress imposed on *A. fumigatus* during pathogenesis (Vödisch *et al.*, 2011). The sterol-regulatory element binding protein, SrbA, regulates ergosterol biosynthesis, maintains cell polarity and is essential for growth in hypoxic conditions (Willger *et al.*, 2008). Furthermore deletion of *srbA* results in attenuated virulence in both neutropenic and corticosteroid models of IA, underpinning the role of hypoxia adaptation in the pathogenicity of *A. fumigatus* (Willger *et al.*, 2008, 2009). Large-scale proteomic and transcriptomic investigations have been carried out to identify mechanisms differentially regulated in *A. fumigatus* in response to both short-term and long-term hypoxia (Vödisch *et al.*, 2011; Barker *et al.*, 2012). Long-term exposure to low oxygen conditions correlated with the increase in expression of proteins involved in glycolysis, respiration and secondary metabolite production. The transcription factor SrbA was activated in response to a requirement for ergosterol biosynthesis, and additionally NO-detoxifying flavohemoprotein was up-

regulated, indicating the production of reactive nitrogen species (RNS) may be associated with hypoxia (Vödisch *et al.*, 2011). Similarly, following short-term exposure to hypoxia, ergosterol biosynthesis and flavohemoprotein were also up-regulated, indicating the requirement for these components in the adaption to, and the maintenance of growth in, hypoxic conditions (Barker *et al.*, 2012).

As *A. fumigatus* is a saprophytic fungus, the ability to extract nutrients from the host plays an integral part in the ability of the fungus to survive and persist in the lung. Secreted enzymes, including proteases, hydrolases and lipases, allow acquisition of nutrients, in addition to destruction of host barriers to enable invasive growth. A transcriptional regulator of proteases, PrtT, was detected in *A. fumigatus* following the identification of homologs in *A. niger* and *A. oryzae* (Bergmann *et al.*, 2009; Sharon *et al.*, 2009). While PrtT-regulated proteases were essential for the utilisation of protein as a nutrient source, these enzymes did not contribute to virulence in a neutropenic or corticosteroid mouse models of IA (Bergmann *et al.*, 2009; Sharon *et al.*, 2009). Another prerequisite for the survival of *A. fumigatus* in the host is the ability to obtain and store iron, an essential nutrient and cofactor for a number of enzymes (Haas, 2012). Conditions encountered by *A. fumigatus* in the lung are iron-limited and the capacity to acquire iron is crucial for growth (Schrettl *et al.*, 2007; Haas, 2012). Two distinct routes exist by which *A. fumigatus* can obtain iron, reductive iron assimilation (RIA) and siderophore-assisted iron uptake, both of which are induced in iron-limiting conditions (Schrettl *et al.*, 2007). The latter of these systems involves the production of siderophores, which specifically chelate ferric iron and can be used to sequester iron from the host environment or store iron internally (Schrettl *et al.*, 2004). Abrogation of siderophore biosynthesis, by disruption of the *sidA*, resulted in complete attenuation of

virulence in a neutropenic mouse model of IA, demonstrating the essential role of the siderophore system in *A. fumigatus* pathogenicity (Schrettl *et al.*, 2004, 2007).

A. fumigatus is capable of producing a range of toxic molecules which may attribute to its success as an opportunistic pathogen. Many of these molecules are secondary metabolites in *A. fumigatus* and those implicated in pathogenicity are listed in Table 1.1. Over 200 secondary metabolites are secreted by *A. fumigatus* and include melanins and ergosterols discussed earlier (Frisvad *et al.*, 2009). Gliotoxin represents the most characterised secondary metabolite of *A. fumigatus*, with relevance to virulence. The mechanism of action of gliotoxin will be discussed in detail later in the Chapter, in addition to the effect of gliotoxin on the host defences. Briefly, gliotoxin is a redox-active metabolite, which exerts numerous immunomodulatory mechanisms, contributing to the success of *A. fumigatus* as an opportunistic pathogen (Figure 1.5) (Abad *et al.*, 2010). Helvolic acid is a triterpene which demonstrates ciliostatic activity, albeit with lower activity than gliotoxin and fumagillin (Amitani *et al.*, 1995). A putative cluster involved in helvolic acid biosynthesis has been identified on Chromosome 4 in *A. fumigatus*, however the biosynthetic pathway has not been elucidated to date (Lodeiro *et al.*, 2009; Mitsuguchi *et al.*, 2009). Ergot alkaloids are conidia-associated toxins that interact with monoamine receptors and can affect the nervous and reproductive systems through this antagonism (Coyle *et al.*, 2007). Recently, the non-ribosomal peptide synthetases (NRPS), Pes1 and PesL, have been implicated in the production of the ergot alkaloid, fumigaclavine C (Figure 1.5) (O'Hanlon *et al.*, 2012). Fumigaclavine C has been shown to inhibit the proliferation and activation of T lymphocytes in addition to reducing the production of TNFα *in vivo* and *in vitro* (Zhao *et al.*, 2004). Other mycotoxins associated with conidia have been identified following sporulation and include fumiquinazoline C, tryptoquivaline F,

trypacidin, monomethylsulochrin and questin (Figure 1.5). Of these, trypacidin was observed to have toxic characteristics, and significantly and substantially reduced the cell viability of a human alveolar carcinoma cell line (A549) (Gauthier *et al.*, 2012). Trypacidin triggered cell death through necrosis in both primary and immortal lung cells, with oxidative stress induction implicated in the irreversible death process (Gauthier *et al.*, 2012). Fumagillin produced by *A. fumigatus* has been suggested to have genotoxic effects on mammalian cells *in vivo*, in addition to anti-angiogenic activity (Figure 1.5) (Stanimirovic *et al.*, 2007). Moreover, fumagillin has recently been identified as an inhibitor of neutrophil function through interruption of the NAPDH oxidase complex assembly (Fallon *et al.*, 2010). Degranulation of neutrophils was also reduced in fumagillin treated cells, which could contribute to the persistence of *A. fumigatus* in the host (Fallon *et al.*, 2010). Pseurotin A and related analogues have demonstrated suppression of IgE production *in vitro* (Figure 1.5) (Ishikawa *et al.*, 2009). Pseurotin A biosynthesis is encoded by a portion of a secondary metabolite 'supercluster' on Chromosome 8, with the sole hybrid polyketide synthase/non-ribosomal peptide synthetase (PKS/NRPS) in *A. fumigatus* essential for pseurotin A production (Maiya *et al.*, 2007; Perrin *et al.*, 2007). The pseurotin precursor molecules, propionyl-coenzyme A, phenylalanine and malonyl-coenzyme A, are utilised to produce a PKS-NRPS bound intermediate, with the remaining genes in the cluster putatively responsible for further modification of this intermediate (Maiya *et al.*, 2007).

No single factor appears to be responsible for virulence of *A. fumigatus* and the associated disease is multi-faceted (Abad *et al.*, 2010). Collectively, all of the features described contribute to the pathogenicity of *A. fumigatus* in the immunocompromised host. Further exploration into these mechanisms of tolerance and resistance to host induced stresses may expand our understanding of the pathogenicity of *A. fumigatus*.

1.7 Secondary Metabolism in Fungi

1.7.1 Identification of Secondary Metabolite Clusters

Secondary metabolites are predominantly low molecular mass molecules, produced by a range of organisms, which are dispensable for primary growth (Keller *et al.*, 2005). The production of SMs can often be associated with specific morphological stages and SMs may confer selective advantages in the presence of competing organisms (Calvo *et al.*, 2002; Losada *et al.*, 2009). Secondary metabolites can be broadly categorised based on the enzyme classes responsible for their biosynthesis, and include (i) polyketides, (ii) non-ribosomal peptides (iii) terpenes and (iv) indole alkaloids. Biosynthesis of these SMs is carried out by polyketide synthetases (PKSs), NRPSs, terpene cyclases and dimethylallyl tryptophan synthetases (DMATS), respectively. These enzymes catalyse the first step in the biosynthesis of SMs and are referred to as 'backbone enzymes' (Khaldi *et al.*, 2010). Enzymes involved in the biosynthesis of SMs are usually grouped in contiguous clusters in the genome with a proclivity towards telomeric localisation (Keller *et al.*, 2005; Nierman *et al.*, 2005). This phenomenon is not observed in primary metabolite biosynthetic pathways, nor in secondary metabolism genes from other kingdoms. The sequencing of the genome of *A. fumigatus* Af293, revealed the presence of 26 SM clusters, including a number of clusters not identified in *A. oryzae* or *A. nidulans* (Nierman *et al.*, 2005). The number of SM gene clusters was subsequently revised to 22 by Perrin *et al.* (2007).

Recent developments in automated web-based tools, including Secondary Metabolite Unknown Region Finder (SMURF), have aided in locating SM clusters in fungi (Khaldi *et al.*, 2010). Additionally, the inclusion of a second sequenced strain of *A. fumigatus*, A1163, has resulted in the total number of SMs in *A. fumigatus* being adjusted to 36 (Table 1.2) (Fedorova *et al.*, 2008; Sanchez *et al.*, 2012).

Table 1.1: Secondary metabolites of *A. fumigatus* implicated in virulence. Adapted from Dagenais and Keller (2009).

Secondary Metabolite	Fungal Association(s)	Potential function *in vivo*
Gliotoxin	Hyphae	Induction of host cell apoptosis
		Epithelial cell damage and slowed ciliary beating
		Inhibition of phagocytosis and oxidative burst
		Inhibition of T-cell responses
Restrictocin	Hyphae	Inhibition of neutrophil-mediated hyphal damage
Verruculogen	Hyphae, Conidia	Affects transepithelial resistance and induces hyperpolarization, cytoplasmic vacuolization of epithelial cells
Fumagillin	Hyphae	Epithelial cell damage and slowed ciliary beating; angiogenesis inhibitor
Helvolic acid	Hyphae	Epithelial cell damage and slowed ciliary beating
Ergot alkaloids	Hyphae, Conidia	Unknown
Fumitremorgin	Unknown	Unknown

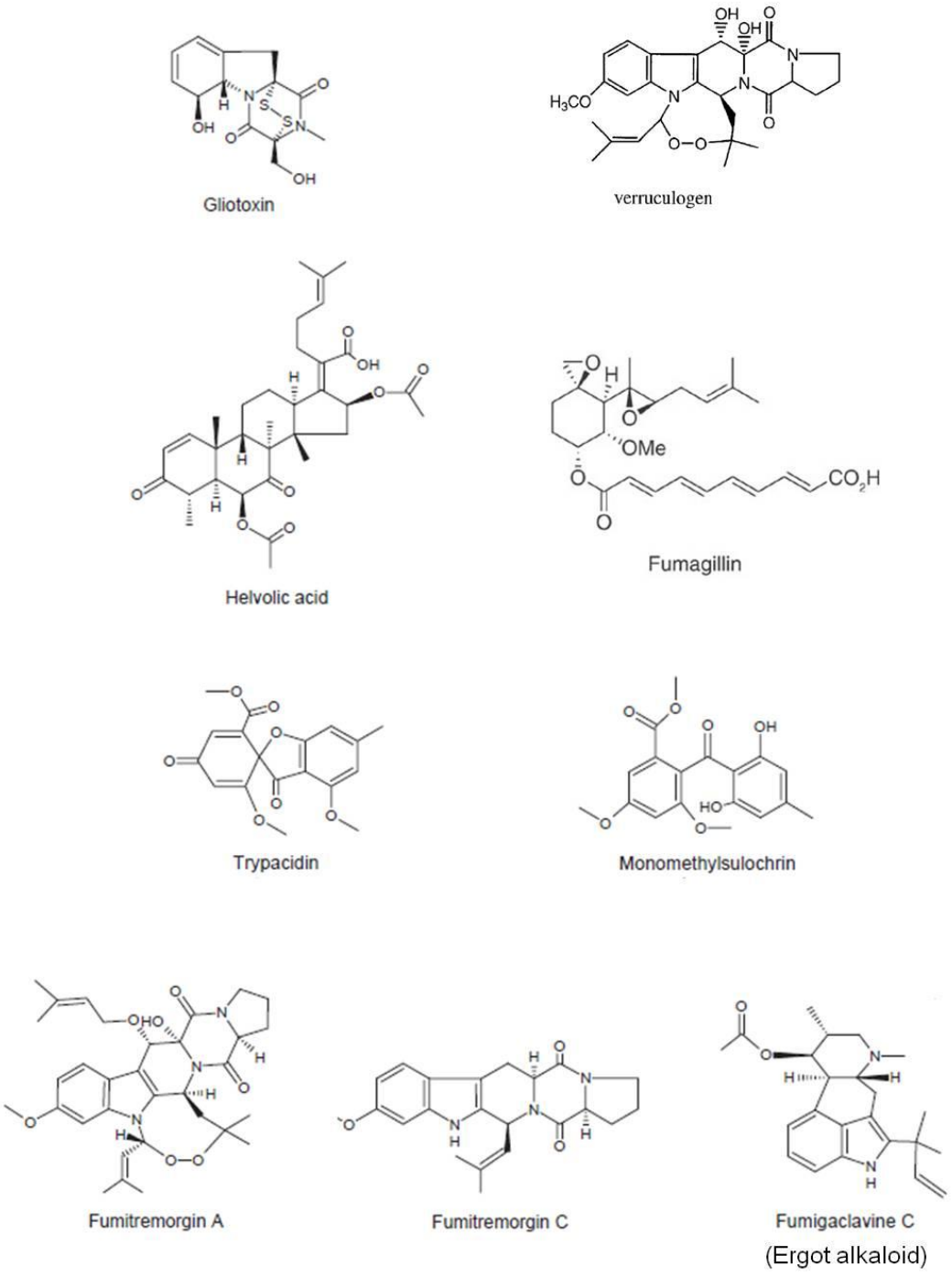

Figure 1.5: Structures of several secondary metabolites produced by *A. fumigatus*. Images from Rundberget and Wilkins (2002); Kikuchi and Kakeya (2006); Frisvad *et al.* (2009).

Characterisation of mechanisms required for the production of specific classes of secondary metabolites has enabled the identification of similar clusters in disparate species. The identification of the gliotoxin biosynthetic cluster in *A. fumigatus* was facilitated by comparison with another previously characterised epipolythiodioxopiperazine (ETP), sirodesmin, from *Leptosphaeria maculans* (Gardiner and Howlett, 2005). Subsequently, both of these biosynthetic clusters were used to identify other ETP clusters from across a range of fungi, and resulted in the detection of a second smaller ETP cluster in *A. fumigatus* (Patron *et al.*, 2007). Techniques routinely used to identify and characterise secondary metabolites from fungi include organic extraction, TLC, reversed-phase HPLC (RP-HPLC), LC-MS/MS and NMR. These methodologies will be elaborated upon in Chapter 6.

1.7.2 Secondary Metabolite Cluster Regulation

Various factors can influence the production of secondary metabolites and regulation of SM gene cluster expression is controlled by transcription factors. 'Broad'-domain transcription factors can co-regulate the expression of multiple gene clusters, resulting in an integrated response to external stimuli (Keller *et al.*, 2005). Conversely, 'narrow' range transcription factors, are often located within gene clusters and specifically regulate expression of the respective SM pathway. Secondary metabolism is influenced by external environmental factors, including pH, temperature, light and nutrient source, in addition to morphological development (Calvo *et al.*, 2002; Reverberi *et al.*, 2010). In *A. terreus* the production of the poyketide lovastatin, is influenced by the carbon:nitrogen ratio, while the biosynthesis of aflatoxin in *A. flavus* is dependent on temperature (Casas López *et al.*, 2003; O'Brian *et al.*, 2007).

Table 1.2: Secondary metabolism gene clusters in *A. fumigatus*, with central enzymes (e.g. NRPS, DMATS, PKS) listed. Adapted from Sanchez *et al.* (2012).

No	Af293 gene	A1163 gene	Gene Name	Actual or predicted product
1	AFUA_1G01010	No homolog		
2	AFUA_1G10380	AFUB_009800	*pesB* (*pes1*)	
3	AFUA_1G17200	AFUB_016590	*sidC*	ferricrocin, hydroxyferricrocin
4	AFUA_1G17740	AFUB_045790		
5	AFUA_2G01290	AFUB_018370		
6	AFUA_2G05760	AFUB_022790		
7	AFUA_2G17600	AFUB_033290	*alb1*(*pksP*)	YWA1
8	AFUA_3G01410	AFUB_046990		
9	AFUA_3G02530	No homolog		
10	AFUA_3G02570	No homolog		
11	AFUA_3G02670	AFUB_045610		
12	AFUA_3G03350	AFUB_044900	*sidE*	
13	AFUA_3G03420	AFUB_044830	*sidD*	fusarinine C, triacetylfusarinine C
14	AFUA_3G12920	AFUB_036270	*pesF*	putative ETP
15	AFUA_3G13730	AFUB_035460	*pesG*	
16	AFUA_3G14700	AFUB_034520		
17	AFUA_3G15270	AFUB_033950	*pesH*	

No	Af293 gene	A1163 gene	Gene Name	Actual or predicted product
18	AFUA_4G00210	AFUB_100730		
19	AFUA_4G14560	AFUB_071800		
20	AFUA_5G10120	AFUB_057720		
21	AFUA_5G12730	AFUB_060400	*pesI*	
22	AFUA_6G03480	AFUB_094810		
23	AFUA_6G08560	AFUB_074520		
24	AFUA_6G09610	AFUB_075660	*pesJ*	
25	AFUA_6G09660	AFUB_075710	*gliP*	gliotoxin
26	AFUA_6G12050	AFUB_078040		fumiquinazolines
27	AFUA_6G12080	AFUB_078070		fumiquinazolines
28	AFUA_6G13930	AFUB_000820	*pyr2*	pyripyropene A
29	AFUA_7G00160	AFUB_086700		
30	AFUA_8G00170	AFUB_086360	*ftmA*	fumitremorgins
31	AFUA_8G00370	AFUB_086200		
32	AFUA_8G00540	AFUB_086030	*psoA*	pseurotin A
33	AFUA_8G01640	AFUB_084950		
34	AFUA_8G02350	AFUB_084240		
35	No homolog	AFUB_07971		
36	No homolog	AFUB_045640		

A methyltransferase domain protein, LaeA, is a global regulator of secondary metabolism and development in *Aspergillus* species (Bok and Keller, 2004; Sarikaya Bayram *et al.*, 2010). The function of LaeA is putatively executed via methyltransferase activity and regulation of chromatin remodelling (Bok and Keller, 2004; Bok *et al.*, 2005; Keller *et al.*, 2006; Perrin *et al.*, 2007). LaeA was originally identified as a SM regulator following complementation of the loss of sterigmatocystin biosynthesis from *A. nidulans*, and was subsequently recognised as essential for the production of penicillin and conidial pigments (Bok and Keller, 2004). In *A. nidulans*, two of the velvet family of proteins, VeA and VelB, were shown to form a trimeric complex with LaeA and subsequently up-regulate asexual development and secondary metabolism (e.g. sterigmatocystin biosynthesis) (Bayram *et al.*, 2008). Translocation of VeA, and consequently VelB, to the nucleus is inhibited by light and thus interaction with LaeA occurs in the absence of light (Bayram *et al.*, 2008; Sarikaya Bayram *et al.*, 2010). While a similar trimeric interaction (VelB-VeA-LaeA) is noted in *A. fumigatus*, absence of VeA and VelB did not affect biosynthesis of gliotoxin in *A. fumigatus* (Park *et al.*, 2012). A large-scale transcriptional investigation identified multiple SM gene clusters under full or partial LaeA-regulation in *A. fumigatus*, including those involved in ergot alkaloid biosynthesis and the gliotoxin biosynthetic cluster (Perrin *et al.*, 2007). The contribution of secondary metabolites to the pathogenicity of *A. fumigatus* was evidenced by the reduction in virulence, in a neutropenic model of pulmonary aspergillosis, upon deletion of the *laeA* gene (Bok *et al.*, 2005). An increase in macrophage-mediated conidial phagocytosis of Δ*laeA*, was caused by a reduction in the hydrophobic rodlet layer due to delayed expression of *rodA* (Bok *et al.*, 2005; Dagenais *et al.*, 2010). Moreover, reduced killing of polymorphonuclear neutrophils (PMNs) by Δ*laeA* hyphae was due to reduction in secreted SMs, causing reduction in the PMN-respiratory burst (Bok *et al.*, 2005; Sugui *et al.*, 2007a). During the onset of IA, a

significant number of the SM genes regulated by LaeA were increased in expression, including member of the pseurotin and gliotoxin gene clusters (McDonagh *et al.*, 2008).

1.8 Gliotoxin

1.8.1 General Information

Gliotoxin is classified as an epipolythiodioxopiperazine (ETP) toxin, and is produced by a range of fungal species including *A. fumigatus*, *A. terreus*, *A. flavus*, *A. oryzae*, *Trichoderma virens* and some *Penicillium* species (Patron *et al.*, 2007). ETPs are characterised by the presence of an internal disulphide bridge across a dioxopiperazine ring, formed from a modified cyclic dipeptide (Gardiner *et al.*, 2005b; Fox and Howlett, 2008). The toxicity and reactivity of gliotoxin is mediated by the disulphide bridge, which can cross-link proteins through reaction with thiol-containing cysteine residues (Patron *et al.*, 2007). Additionally, gliotoxin is a redox-active metabolite, generating ROS as it cycles between its oxidised (disulphide) and reduced (dithiol) forms (Figure 1.6) (Gardiner and Howlett, 2005). Gliotoxin ($C_{13}H_{14}N_2O_4S_2$) is a 326 Da metabolite, and through radiolabelled isotope feeding experiments the precursor molecules for the diketopiperazine core were found to be phenylalanine and serine (Suhadolnik and Chenowath, 1958; Winstead and Suhadolnik, 1960). Gliotoxin has been extensively studied for its toxicity properties towards mammalian cells, with anti-microbial activity also attributed to this molecule (Pardo *et al.*, 2006; Carberry *et al.*, 2012).

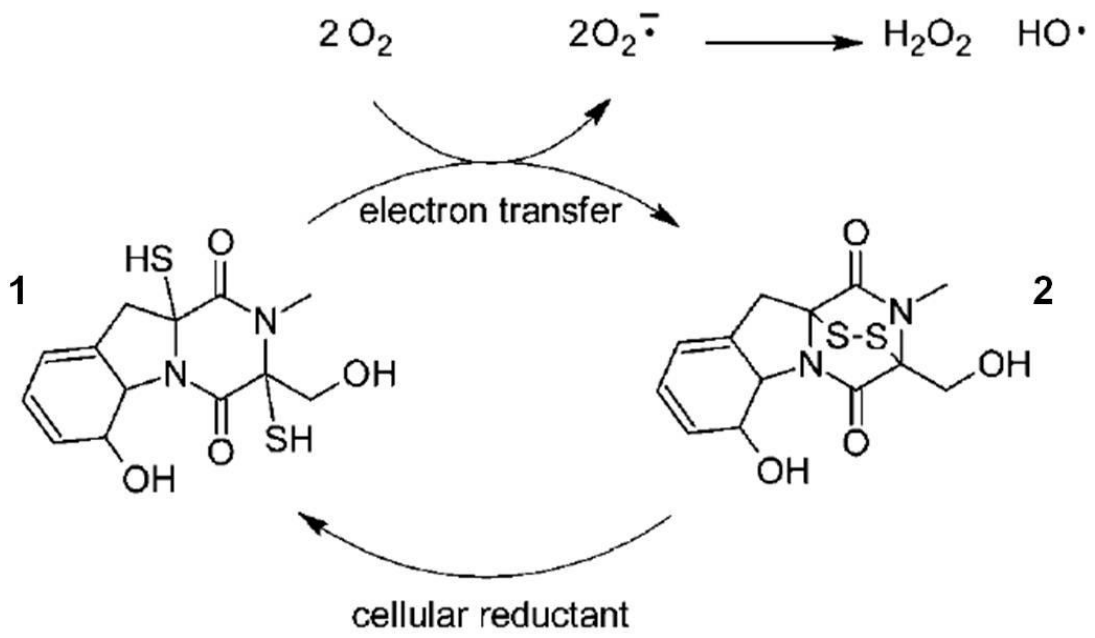

Figure 1.6: Redox cycling between the reduced (**1**) and oxidised (**2**) forms of gliotoxin, with the oxidation of gliotoxin producing ROS. From Gardiner and Howlett (2005).

1.8.2 Gliotoxin Biosynthesis

As mentioned previously, the genes for gliotoxin biosynthesis are clustered together, and the *gli* cluster is comprised of thirteen genes (Figure 1.7a) (Gardiner and Howlett, 2005; Schrettl *et al.*, 2010). Functional genomics demonstrated that the NRPS, GliP, is essential for the production of gliotoxin (Cramer *et al.*, 2006; Kupfahl *et al.*, 2006; Spikes *et al.*, 2008). The initial step in the biosynthesis of gliotoxin was subsequently elucidated, through heterologous expression and purification of GliP from *Escherichia coli* (Balibar and Walsh, 2006). GliP was observed to catalyse a condensation reaction between L-phenylalanine and L-serine, resulting in the formation of a dipeptide (Balibar and Walsh, 2006). GliP is the 'backbone' enzyme of the *gli* cluster and is multi-modular, a feature of NRPSs. Release of the dipeptide from the GliP enzyme occurs non-enzymatically, due to the absence of a thioesterase domain on the NRPS, and results in a cyclic diketopiperazine molecule (Figure 1.7b) (Balibar and Walsh, 2006; Davis *et al.*, 2011a).

An integral stage in the formation of gliotoxin is the introduction of the sulphur atoms that confer the signature redox activity to gliotoxin. Since neither phenylalanine nor serine are sulphur-containing amino acids, other molecular species were proposed as potential sulphur donors, including cysteine, methionine and sodium sulphate (Suhadolnik and Chenowath, 1958; Gardiner *et al.*, 2005b). A putative glutathione-S-transferase gene, *gliG*, is situated within the cluster, and presented a potential route for sulphur incorporation into the gliotoxin precursor (Gardiner *et al.*, 2005b). This hypothesis was confirmed through functional genomics whereby the *gliG* was deleted, resulting in abrogation of gliotoxin biosynthesis and accumulation of an off-pathway shunt metabolite (Molecule 4; Figure 1.7b) (Davis *et al.*, 2011a; Scharf *et al.*, 2011). Davis *et al.* (2011a) validated the glutathione-S-transferase (GST) activity of the

enzyme using recombinant GliG and demonstrated that GliG does not confer auto-protection against exogenous gliotoxin. Scharf *et al.* (2011) demonstrated the activity of the P450 monooxygenase, GliC,which is required for a hydroxylation reaction prior to the GliG-mediated conjugation of glutathione (GSH) to the gliotoxin precursor. The function of a number of GSTs relates to detoxification of non-polar compounds (i.e. xenobiotics) through conjugation of GSH, allowing subsequent metabolism of the glutathionylated molecule. While the proposed gliotoxin biosynthetic pathway partially resembles this mechanism, GliG is phylogenetically distinct from these detoxification enzymes (Davis *et al.*, 2011a; Scharf *et al.*, 2011).

Exposure of the thiol groups of gliotoxin was predicted to be catalysed by GliI utilising pyridoxyl-5'-phophate (PLP) as a co-factor (Figure 1.5) (Fox and Howlett, 2008; Davis *et al.*, 2011a; Scharf *et al.*, 2011). Recently, the activity of GliI as a C-S lyase was experimentally verified, and was demonstrated to perform concurrent cleavage for the formation of both thiols in the ETP (Scharf *et al.*, 2012a). Identification of a cytosolic, water-soluble intermediate, exclusive to the *gliI* mutant (Δ*gliI*), enabled elucidation of the mechanism of action of this enzyme in gliotoxin biosynthesis (Scharf *et al.*, 2012a).

The final step in gliotoxin biosynthesis has also been elucidated and involves the oxidation of the dithiol form of gliotoxin to form the disulphide bridge (Figure 1.7) (Scharf *et al.*, 2010; Schrettl *et al.*, 2010). This action is mediated by the enzyme, GliT, which was initially annotated as a thioredoxin reductase. While dithiol to disulphide oxidation is required to complete the biosynthesis of gliotoxin, GliT also exhibits NADPH-dependant gliotoxin reductase activity (Schrettl *et al.*, 2010). This mechanism is key in the auto-protection of *A. fumigatus* from the toxic effects exerted by gliotoxin through the disulphide bond. Indeed deletion of *gliT* resulted in a phenotype that was

hypersensitive to exogenous gliotoxin, confirming the role of GliT in self-protection against gliotoxin (Scharf *et al.*, 2010; Schrettl *et al.*, 2010). Additionally, transformation of *gliT* into *A. nidulans* and *S. cerevisiae* conferred gliotoxin resistance to these typically sensitive species. Hlm1, a functionally homologous enzyme to GliT was recently identified in *Streptomyces clavuligerus* and is associated with the production of the antibiotic, holomycin. As with GliT, Hlm1 is responsible for the oxidation of the dithiol in the final step of holomycin biosynthesis, and also confers protection against the toxic effects of this molecule (Li and Walsh, 2011).

The *gli* cluster also contains a selection of genes that are not directly involved in the gliotoxin biosynthetic process, namely the transporter, *gliA*, and the transcriptional regulator, *gliZ*. The *gliA* gene encodes a transporter of the major facilitator superfamily (MFS), while the homologous gene in the sirodesmin cluster of *L. maculans*, *sirA*, encodes an ATP binding cassette (ABC) transporter (Gardiner and Howlett, 2005). MFS transporters are more commonly found in fungal toxin biosynthetic clusters (e.g. aflatoxin) than ABC transporters (Gardiner *et al.*, 2005a). Disruption of the *gliA* homolog, *sirA*, in *L. maculans* resulted in increased secretion of sirodesmin, indicating that SirA is not solely responsible for efflux of sirodesmin from the cell. Despite this observation, Δ*sirA* demonstrated enhanced sensitivity to exogenous sirodesmin and gliotoxin, relative to the parent strain (Gardiner *et al.*, 2005a). Furthermore, complementation of Δ*sirA* with *gliA* resulted in acquired tolerance to gliotoxin but not sirodesmin. This indicates that the MFS transporter, GliA, specifically imparts auto-protection against the gliotoxin through its action as an efflux pump.

Regulation of the *gli* cluster expression is controlled by the global transcription factor, LaeA (Bok and Keller, 2004). Additionally, a narrow range transcriptional regulator, GliZ, is present within the cluster and regulates the expression of the cluster

genes in response to various stimuli (Bok *et al.*, 2006; Schrettl *et al.*, 2010). GliZ is a Zn_2Cys_6 transcription factor and deletion of *gliZ* gene results in abolition of gliotoxin biosynthesis due to loss of expression of a number of *gli* cluster genes, including *gliA*, *gliG* and *gliI* (Bok *et al.*, 2006; Schrettl *et al.*, 2010). Exogenous gliotoxin induces *gli* cluster expression, a process mediated by GliZ (Schrettl *et al.*, 2010). In the absence of *gliZ*, gliotoxin is unable to induce expression of cluster components such as *gliG* or *gliA*, however *gliT* expression is regulated independently of *gliZ* (Schrettl *et al.*, 2010). While deletion of *gliZ* resulted in reduced virulence of *A. fumigatus* in an insect model of infection, Δ*gliZ* demonstrated no significant change in pathogenicity in a murine IA infection model relative to the parent strain (Bok *et al.*, 2006; Schrettl *et al.*, 2010). This is in contrast to deletion of the global SM regulator, *laeA*, which resulted in reduced virulence owing to the disruption of SM biosynthesis (Bok *et al.*, 2005, 2006). Furthermore, supernatants from both Δ*laeA* and Δ*gliZ* triggered significantly less apoptosis of PMN *in vitro*, relative to the respective parent strains (Bok *et al.*, 2006). Recently, differential metabolomic analysis has resulted in the identification of a number of *gliZ*-dependent metabolites (Forseth *et al.*, 2011). While many of these molecules represent shunt metabolites of the gliotoxin biosynthesis pathway, they may elaborate on the mechanisms involved in gliotoxin biosynthesis (Forseth *et al.*, 2011). Several of the sulphurised *gliZ*-dependent metabolites identified were S-methylated, including the previously characterised bisdethiobis(methylthio)gliotoxin, with a methyl group bound to each of the thiol groups on the piperazine ring (Forseth *et al.*, 2011). While the significance of this thiol methylation is not yet understood, this may represent a mechanism by which to reduce the toxicity of gliotoxin and associated intermediates in *A. fumigatus*, through capping of the reactive moieties.

To date, the putative functions of the other members of the *gli* cluster have not been experimentally validated. While both *gliC* and *gliF* genes are predicted to encode cytochrome P450 monooxygenases, the hydroxylation of the diketopiperazine, prior to C-S bond formation, does not appear to involve GliF (Scharf *et al.*, 2011). GliM and GliN have putative assigned functions as an O-methyltransferase and a methyltransferase, respectively, and both genes have homologs in the sirodesmin biosynthetic cluster (Gardiner and Howlett, 2005). Transfer of methyl groups to gliotoxin precursors is likely mediated through the methyl donor S-adenosylmethionine (SAM) (Davis *et al.*, 2011a). Additionally, a GliM homolog is also found in a second smaller putative ETP biosynthetic cluster in *A. fumigatus* (Kremer *et al.*, 2007; Patron *et al.*, 2007). A putative dipeptidase, GliJ, may act by cleavage of L-glutamate groups from the bis-glutathionylated intermediate (Molecule 8; Figure 1.7) or alternatively may release the cyclic peptide, tethered to the GliP enzyme (Fox and Howlett, 2008; Davis *et al.*, 2011a; Scharf *et al.*, 2011). Finally, two unknown function proteins, GliK and GliH are included in the *gli* cluster. GliH (AFUA_6G09745) was recently recognised as a member of the gliotoxin biosynthetic cluster and is not involved in self-protection against gliotoxin (Schrettl *et al.*, 2010). Prior to the work carried out in this thesis, the function of GliK had not been investigated. No GliK homolog is present in the sirodesmin biosynthetic cluster in *L. maculans*, indicating that the function of GliK may be specific to gliotoxin biosynthesis as opposed to broad ETP synthetic activity (Gardiner and Howlett, 2005; Gardiner *et al.*, 2005b). Indeed, *gliK*-like genes are only found in gliotoxin-producing species such as *A. oryzae*, *A. terreus* and *T. virens* (Patron *et al.*, 2007). Additionally, the presence of *gliK* in fungal ETP clusters coincides with the presence of a MFS transporter as opposed to an ABC transporter in that cluster (Patron *et al.*, 2007). Elucidation of the contribution of GliK to *A. fumigatus*

biochemistry and gliotoxin production could aid in the characterisation of this protein in other organisms.

a.

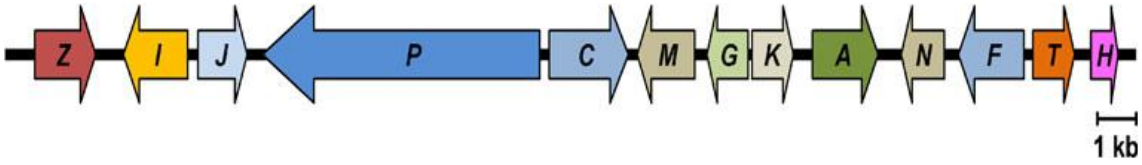

b.

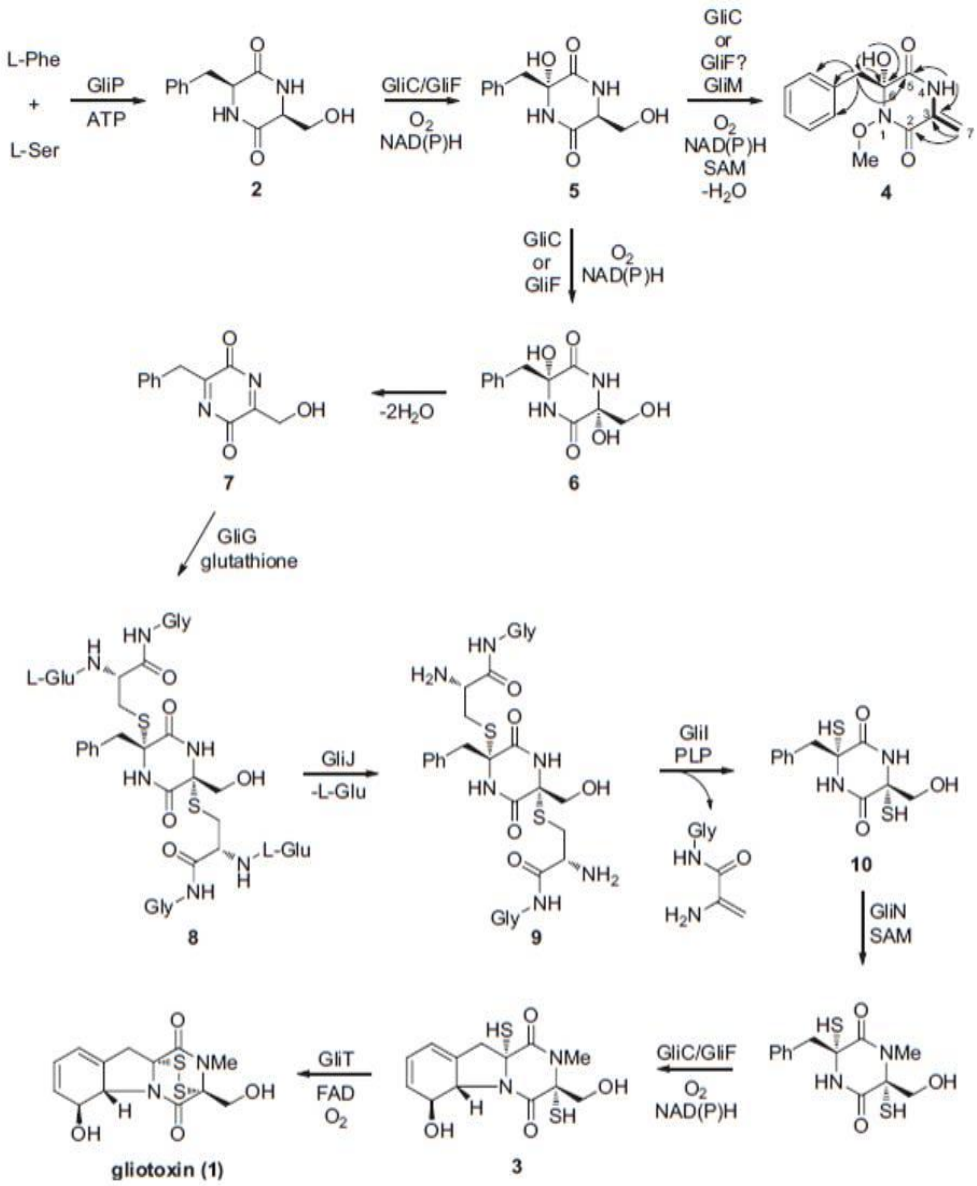

Figure 1.7: (a) Gliotoxin biosynthetic cluster and (b) proposed biosynthetic pathway. GliP-mediated conjugation of L-Phe and L-Ser lead to the formation of an acyl imine intermediate (7), which undergoes glutathionylation via GliG. Subsequent reactions, putatively catalysed by GliJ and GliI de-protect the thiol groups on the gliotoxin precursor. From Scharf *et al.* (2012) and Davis *et al.* (2011), respectively.

1.8.3 Gliotoxin: Effects on host cells

Gliotoxin has been shown to elicit a range of modulatory mechanisms on immune and non-immune cells, both *in vitro* and *in vivo* (Pardo *et al.*, 2006; Kwon-Chung and Sugui, 2009). Induction of mammalian cell apoptosis has been associated with gliotoxin, and this effect has been demonstrated in a range of cells from the immune system. Polymorphonuclear (PMN) cells undergo apoptosis following incubation with purified gliotoxin *in vitro*, in both hypoxic and normoxic conditions (Dyugovskaya *et al.*, 2011). Apoptosis of monocytes, the precursors of macrophages, was also induced by gliotoxin (Stanzani *et al.*, 2005; Orciuolo *et al.*, 2007). Culture supernatants from *A. fumigatus* mutants, deficient in gliotoxin production (e.g. Δ*gliP*, Δ*gliZ*), induced significantly less apoptosis in PMN and macrophage-like cells (Bok *et al.*, 2006; Kupfahl *et al.*, 2006; Sugui *et al.*, 2007b). Gliotoxin-induced apoptosis is mediated by a member of the proapoptotic Bcl-2 family, Bak (Pardo *et al.*, 2006). The Bak protein is localised in the mitochondria of mammalian cells and elicits initiation of apoptosis following a conformational change in response to cell-damage stimuli (Figure 1.8) (Griffiths *et al.*, 1999). Subsequent oligomerisation of the Bak protein occurs and creates a pore in the mitochondrial membrane resulting in membrane permeability (Dewson *et al.*, 2009). Gliotoxin interacts with the Bak protein to cause a conformational change and consequently leads to ROS production and disruption of the mitochondrial membrane (Figure 1.8) (Pardo *et al.*, 2006). Interestingly oligomerisation of the Bak protein involves cysteine linkages (Dewson *et al.*, 2009) and may represent the mode of action for gliotoxin activation of this process. Following activation of Bak, release of other proapoptotic factors, including cytochrome c and apoptosis-inducing factor (AIF), from the mitochondria ultimately results in cell death (Figure 1.8). This

mechanism contributes to the virulence of the fungus, with mice deficient in Bak exhibiting reduced mortality in a corticosteroid model of IA (Pardo *et al.*, 2006).

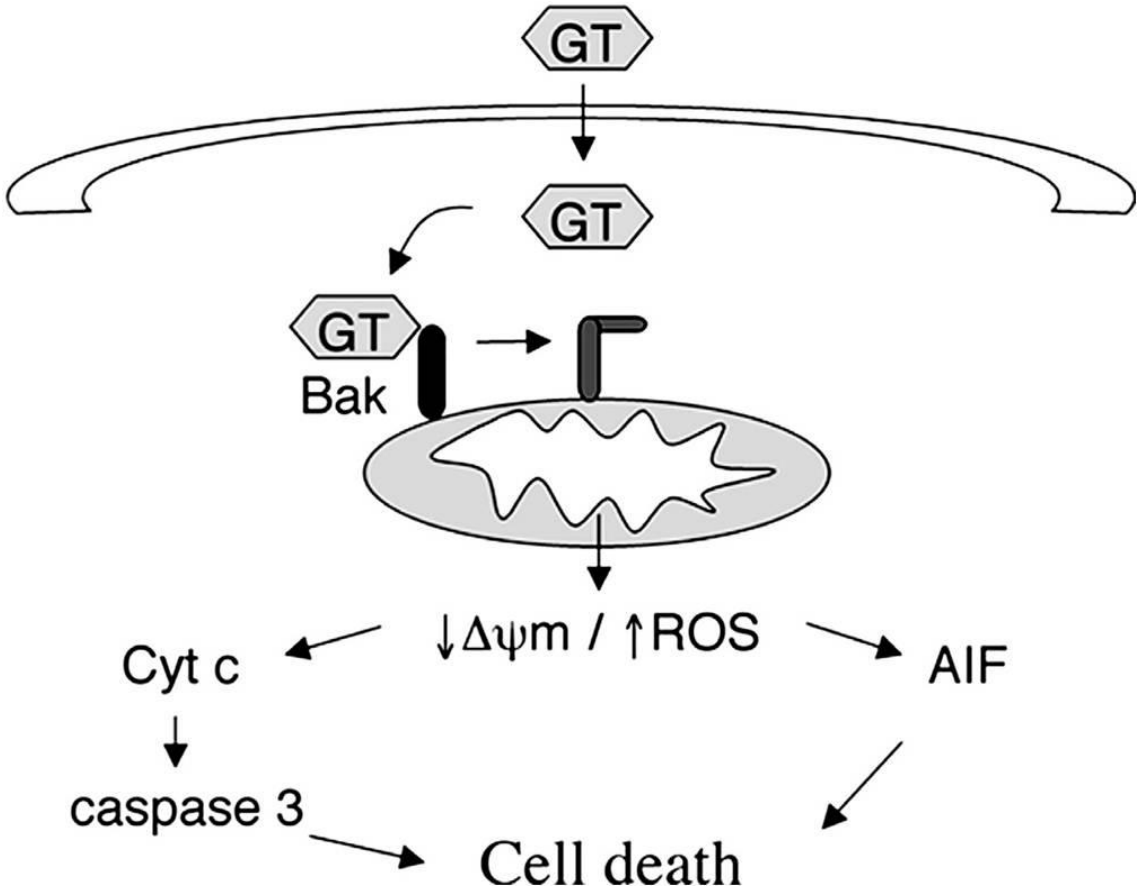

Figure 1.8: Proposed mechanism of gliotoxin (GT)-induced apoptosis. Gliotoxin produced by *A. fumigatus* enters mammalian cells and causes a conformational change in the mitochondrial Bak protein. This results in mitochondrial membrane disruption, depolarisation (↓Δψm) and ROS production, leading to release of pro-apoptotic proteins and cell death. AIF, apoptosis-inducing factor; Cyt c, cytochrome C. Adapted from Pardo *et al.* (2006).

Another mechanism employed by gliotoxin, to suppress the immune response to *A. fumigatus*, is the inhibition of the NADPH-dependent oxidative burst from PMN cells such as neutrophils. Culture supernatants from gliotoxin-producing strains of *A. fumigatus* inhibited the oxidative burst of human neutrophils, while gliotoxin-deficient mutants had no inhibitory effects (Sugui *et al.*, 2007b). ROS generation is achieved through the NADPH oxidase enzyme, which generates O_2^- from molecular oxygen (Figure 1.9). Release of ROS from immune effector cells contributes to the killing of invading microorganisms, and defects in NADPH oxidase (e.g. CGD) result in increased incidence of invasive fungal infections (IFIs) (Henriet *et al.*, 2012). The components of NADPH oxidase are dispersed between the cytosol and the membrane in resting cells. Upon stimulation the cytosolic elements ($p47^{phox}$, $p67^{phox}$, $p40^{phox}$ and Rac2) translocate to the membrane and assemble with flavocytochrome b_{558} (Figure 1.9). Gliotoxin inhibits the assembly and activation of the NADPH oxidase enzyme through disruption of the translocation of $p47^{phox}$, $p67^{phox}$ and $p40^{phox}$ to the membrane (Tsunawaki *et al.*, 2004). Furthermore, gliotoxin directly interacts with flavocytochrome b_{558}, inhibiting electron transport capabilities prior to assembly of the oxidase enzyme (Nishida *et al.*, 2005). These authors postulated that the mechanism of inhibition of flavocytochrome activity was through the reaction of gliotoxin with available cysteines on the protein. In this way gliotoxin prevents the activation of NADPH oxidase but it not effective in inhibiting the activity of the assembled enzyme (Tsunawaki *et al.*, 2004). The action of gliotoxin is mediated through the disulphide bridge on the ETP molecule, and blocking the thiol groups of gliotoxin negated the effect of the metabolite on NADPH activation (Tsunawaki *et al.*, 2004).

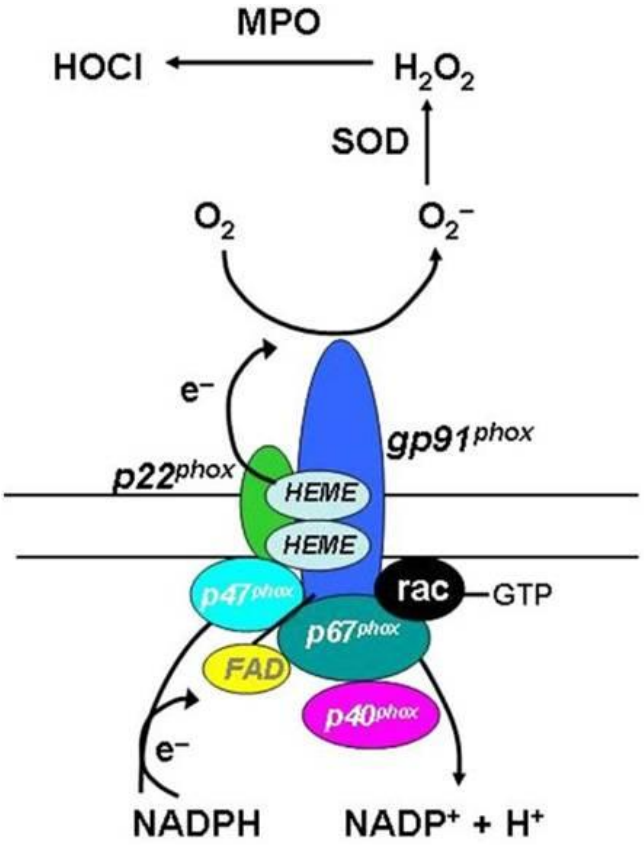

Figure 1.9: Model of assembled NADPH oxidase enzyme at cell membrane, and associated activities. SOD, superoxide dismutase; MPO, myeloperoxidase. From Segal and Romani (2009).

Angiogenesis, the formation of new blood vessels from existing ones, is a feature of IA and occurs possibly in response to tissue hypoxia associated with invasion of the pulmonary vasculature (Ben-Ami *et al.*, 2010). Following interaction with *A. fumigatus* hyphae, endothelial cells release proinflammatory cytokines, including TNFα and IL-8, and this event is not affected by the presence or absence of gliotoxin (Chiang *et al.*, 2008). The activation of pro-angiogenic signalling pathways is elicited by these cytokines, resulting in the induction of vascular endothelial growth factor (VEGF) and basic fibroblast growth factor (bFGF) (Yoshida *et al.*, 1997). Cytokine-mediated recruitment of PMN cells to the site of infection results in the release of ROS, and consequently, induction of NF-κB. Further up-regulation of pro-angiogenic molecules is induced by NF-κB (Figure 1.10). ROS, including H_2O_2, derived from NADPH oxidase, are important mediators of angiogenesis (Ushio-Fukai and Alexander, 2004). Gliotoxin performs an anti-angiogenic function through reduction of ROS generation by PMN cells and inhibition of NF-κB (Figure 1.10). Gliotoxin also has the potential to act as an antioxidant, reducing intracellular H_2O_2 to H_2O via the mammalian thioredoxin redox system, hence eliminating a potent inducer of NF-κB and angiogenesis (Choi *et al.*, 2007). By replacing the function of 2-cys peroxiredoxin, gliotoxin reduces H_2O_2 in a dose-dependent manner, thus preventing H_2O_2-induced angiogenesis (Choi *et al.*, 2007). Redox-cycling between the oxidised and reduced forms of gliotoxin is integral to this action and involves the transfer of electrons from NADPH to gliotoxin (Choi *et al.*, 2007). This suggests a dual-function for gliotoxin, in production and neutralisation of ROS, and further investigation of this dichotomy is required to understand the role of gliotoxin in *A. fumigatus* and pathogenesis. Despite the pro-angiogenic signals elicited by *A. fumigatus* infection, culture filtrates were demonstrated to have potent anti-angiogenic properties *in vitro* (Ben-Ami *et al.*, 2009).

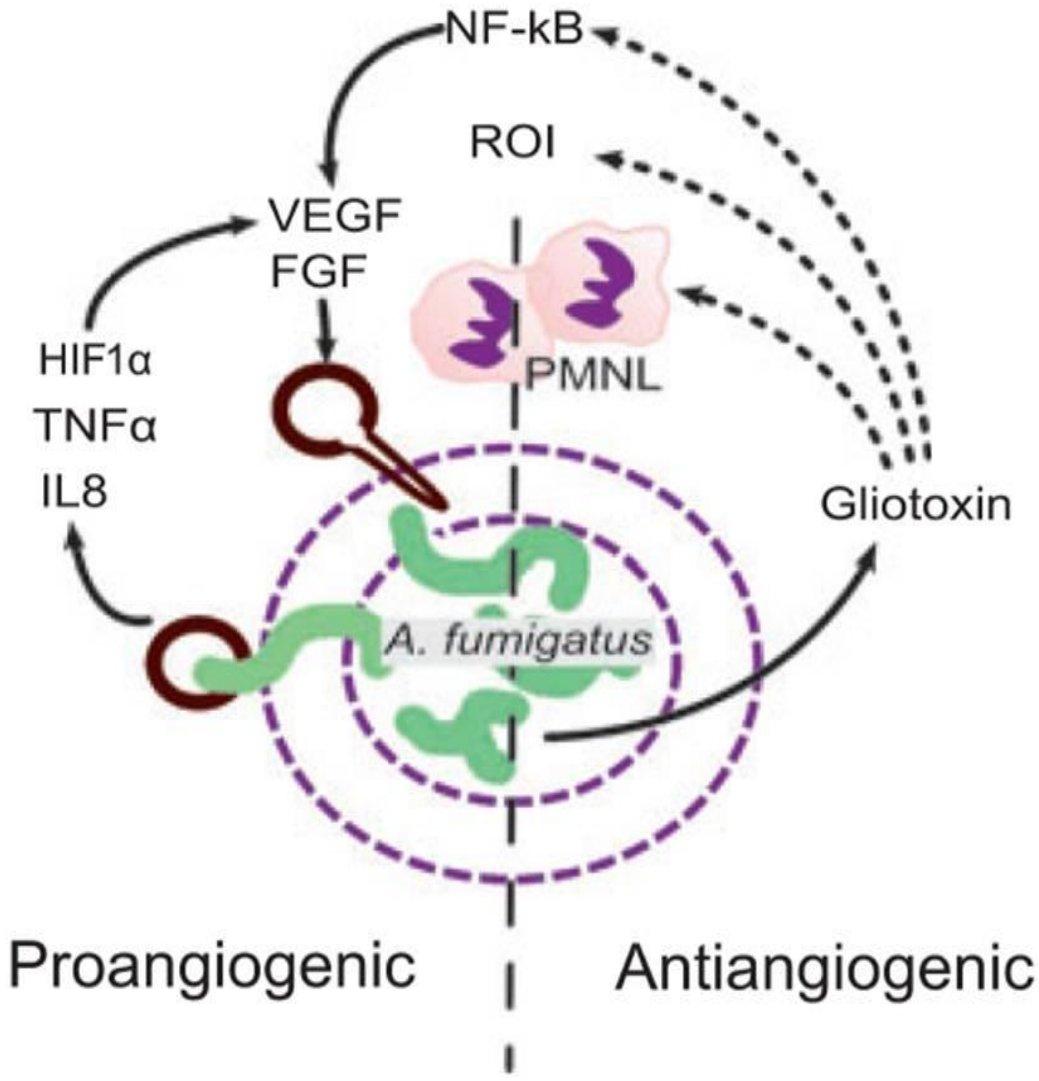

Figure 1.10: Pro- and anti-angiogenic signals in IA. Pro-angiogenic factors secreted from endothelial cells, macrophages and PMN cells are positioned on the left of the image. The anti-angiogenic activities elicited by gliotoxin are indicated on the right of the figure. From Ben-Ami *et al.* (2010).

This anti-angiogenic activity is attributable to secondary metabolites in *A. fumigatus*, as evidenced by the loss of this activity from the Δ*laeA* mutant. Using a gliotoxin-deficient mutant, Δ*gliP*, these authors verified that gliotoxin was responsible for approximately 40% of the LaeA-dependent anti-angiogenic activity of *A. fumigatus* (Ben-Ami *et al.*, 2009, 2010).

A number of other immunomodulatory effects are attributable to gliotoxin and may contribute to the virulence of *A. fumigatus in vivo*. These functions include inhibition of T-cell responses, impairment of phagocytosis and reduction in ciliary movement of epithelial cells (Abad *et al.*, 2010). Gliotoxin interferes with human T-cell activation, suppressing the response of these cells to antigens. This action is accomplished by inhibition of antigen presentation as opposed to directly impairing T-cell function (Stanzani *et al.*, 2005). Gliotoxin also impedes the activities of cytotoxic T lymphocytes (CTLs) through blocking the binding of CTLs to target cells (Yamada *et al.*, 2000). Again, the disulphide bridge of gliotoxin is indispensible for this process, as reduced gliotoxin (i.e. dithiol form) was unable to inhibit CTL-mediated cytotoxicity (Yamada *et al.*, 2000). The influence of gliotoxin on phagocytosis has also been highlighted, with low concentrations of gliotoxin significantly inhibiting the phagocytic capacity of human PMN cells (Coméra *et al.*, 2007; Orciuolo *et al.*, 2007). It was also noted that gliotoxin promoted cytoskeleton reorganisation, with F-actin collapse noted around nuclei of affected cells, however it was proposed that these events were independent (Coméra *et al.*, 2007). Through inhibition of phagocytosis, gliotoxin could contribute to the persistence of *A. fumigatus* in infected tissue. Additionally, reduction in the rate of ciliary movement, as caused by gliotoxin, could result in impaired clearance of inhaled conidia from the lung and reduced capacity to keep conidia from reaching the epithelium (Amitani *et al.*, 1995).

The variety of host mechanisms affected by gliotoxin is due to the disulphide bridge across the piperazine ring. This confers the ability to cross-link proteins or other molecules via thiol residues and can result in antagonism of active sites or induction of conformational changes, disrupting protein function (Waring *et al.*, 1995; Hurne *et al.*, 2000; Srinivasan *et al.*, 2006). Furthermore, redox cycling between the reduced (dithiol) and oxidised (disulphide) forms of gliotoxin can produce ROS, with deleterious effects (Bernardo *et al.*, 2003; Gardiner *et al.*, 2005b; Kwon-Chung and Sugui, 2009). As discussed in the previous section, ROS reducing activity is also possible through incorporation into the thioredoxin redox system (Choi *et al.*, 2007), contributing to the multi-faceted role of gliotoxin. An increase in the potency of gliotoxin is observed upon reduction of mammalian cell density, as a result of active concentration of the toxin within cells (Bernardo *et al.*, 2003). The oxidised (disulphide) form of gliotoxin can gain entry into cells while the reduced (dithiol) form cannot permeate cells (Bernardo *et al.*, 2003). This mechanism forms the basis of gliotoxin accumulation in cells and the consequent execution of toxic effects. Oxidised gliotoxin, is subsequently reduced by intracellular glutathione (GSH) leading to concentration of reduced gliotoxin within the cell (Figure 1.11). The ensuing depletion of glutathione leads to reversion of gliotoxin to the oxidised form and efflux is restored. Glutathione-dependent accumulation of gliotoxin correlated with an increase in mammalian cell apoptosis and hence defines a route by which this metabolite exerts its effects (Bernardo *et al.*, 2003). This process allows recycling of gliotoxin from apoptotic cells and increases the efficiency of cytotoxicity. These authors also postulated that the accrual of gliotoxin intracellularly could be caused by other cellular reductants, in addition to glutathione, indicating intracellular redox potential as a moderator of gliotoxin susceptibility.

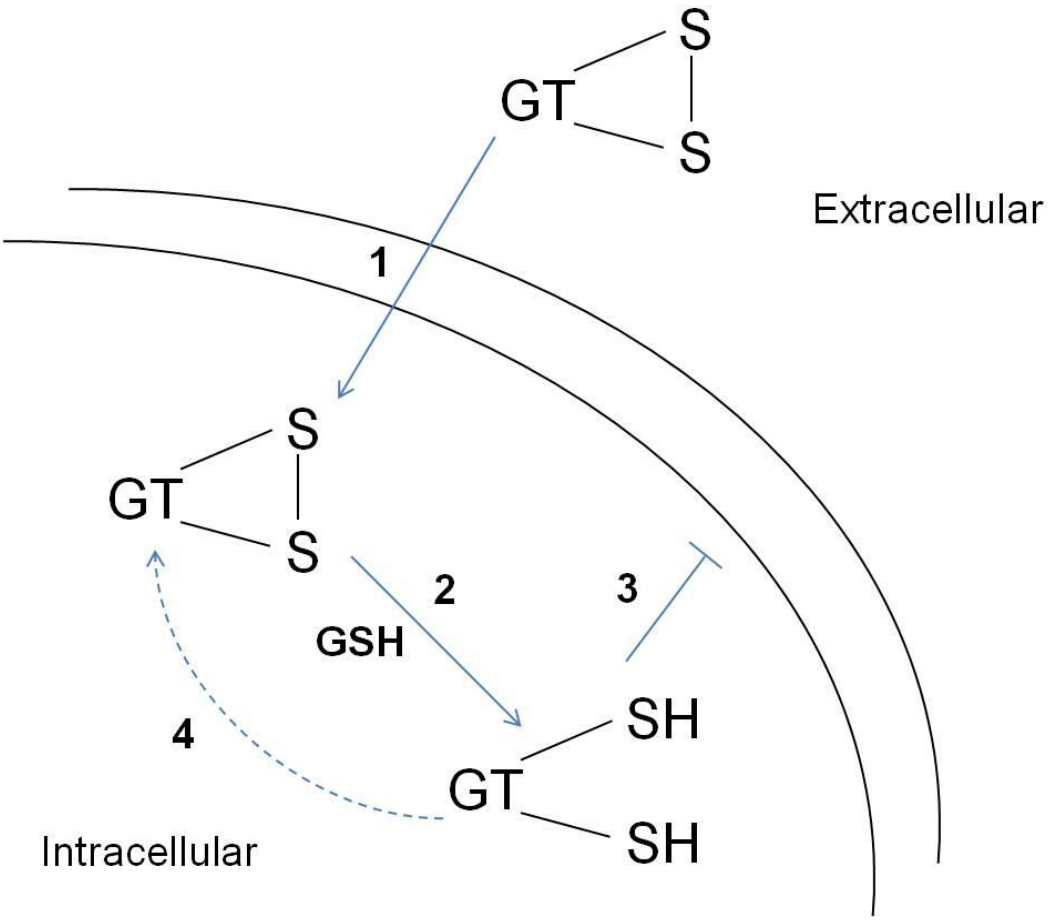

Figure 1.11: Schematic representation of glutathione-dependent accumulation of gliotoxin inside cells. (1) Oxidised gliotoxin passes into cells and (2) is reduced by intracellular glutathione (GSH). (3) Reduced gliotoxin is unable to permeate cells and so is concentrated intracellularly. (4) Depletion of intracellular GSH leads to spontaneous re-oxidation of gliotoxin (Bernardo *et al.*, 2003).

Despite the range of effects of gliotoxin on mammalian cells, the contribution of gliotoxin to the pathogenicity of *A. fumigatus* has been debated. Mouse models infected with gliotoxin-deficient strains of *A. fumigatus* displayed divergent results, making the definition of gliotoxin as a virulence factor tentative. The immunosuppression regime utilised for the IA infection model appears to be of paramount importance in assessing the effect of gliotoxin on the pathogenicity of *A. fumigatus*. Mice treated with cyclophosphamide (inducing neutropenia) coupled with corticosteroids demonstrated comparable mortality rates when infected with gliotoxin-deficient strains of *A. fumigatus* (Δ*gliP*, Δ*gliZ*), relative to the respective gliotoxin-producing parent strains (Bok *et al.*, 2006; Cramer *et al.*, 2006; Kupfahl *et al.*, 2006; Spikes *et al.*, 2008). These results appeared to indicate that gliotoxin did not contribute significantly to the development of IA in the absence of neutrophils. Conversely, when corticosteroids were used alone for immunosuppression, gliotoxin-deficient strains of *A. fumigatus* displayed significantly reduced pathogenicity compared to the wild-type strains (Sugui *et al.*, 2007b; Spikes *et al.*, 2008). This observation correlates with the effects of gliotoxin on neutrophils and suggests that gliotoxin contributes to virulence in a non-neutropenic setting but may be dispensable in a more severely immunocompromised host.

In addition to induction of toxicity in mammalian cells, gliotoxin also exhibits anti-fungal effects (Losada *et al.*, 2009; Schrettl *et al.*, 2010; Coleman *et al.*, 2011; Carberry *et al.*, 2012). Metabolite extracts from *A. fumigatus*, containing gliotoxin, were demonstrated to induce moderate inhibition on a number of *Aspergillus* species, and this may have contributed to *A. fumigatus* out-competing *A. clavatus* in co-culture conditions at 37 °C (Losada *et al.*, 2009). Carberry *et al.* (2012) confirmed the activity of gliotoxin against a number of filamentous fungi, including *A. terreus*, *A. niger* and *Neurospora crassa*. The activity of gliotoxin against various species of yeast has also

been illustrated, with potent anti-fungal activity observed against *C. albicans*, *Cryptococcus neoformans* and *Saccharomyces cerevisiae* (Coleman *et al.*, 2011; Carberry *et al.*, 2012). This anti-fungal activity may confer a competitive advantage to *A. fumigatus* in its environmental niche or in the human host. Furthermore the sensitivity of fungal strains to gliotoxin was linked to glutathione levels, as observed in mammalian cells (Bernardo *et al.*, 2003; Carberry *et al.*, 2012). Deletion of a glutathione biosynthetic enzyme, *gsh1*, in *S. cerevisiae* correlated with reduced sensitivity to gliotoxin. Similarly, elevated GSH levels were present in the gliotoxin sensitive mutant *A. fumigatus* Δ*gliT*, which, in addition to GliT absence, may contribute to the potency of gliotoxin (Carberry *et al.*, 2012). The presence of mechanisms for gliotoxin resistance in *A. fumigatus*, including the gliotoxin oxidoreductase GliT and the putative gliotoxin transporter GliA, provide protection from the toxic effects of gliotoxin (Scharf *et al.*, 2010; Schrettl *et al.*, 2010; Coleman *et al.*, 2011). Additional uncharacterised protective mechanisms may exist in *A. fumigatus*, which confer resistance to gliotoxin. This allows *A. fumigatus* to remain tolerant to gliotoxin while benefiting from its activity against competitors or host cells.

1.9 Thesis Rationale and Objectives

A large proportion of fungal proteins are annotated as 'hypothetical' or 'conserved hypothetical' due to a lack of sequence homology to functionally characterised proteins (Brachat *et al.*, 2003; Nierman *et al.*, 2005). Many of these proteins currently represent *in silico* predicitions from nucleic acid sequences, and with no experimental detection, the existence of these proteins remains unconfirmed. Expansion of fungal proteomics through large-scale detection of proteins by MS, can aid in the corroboration of genome sequencing data. Furthermore, *de novo* elucidation of functions for 'hypothetical' proteins and validation of bioinformatically assigned functions, will greatly enhance the analysis and interpretation of data from future studies (Lubec *et al.*, 2005; Mazandu and Mulder, 2012). Determination of protein function can also facilitate the retrospective analysis of previously conducted studies. Strategies for the characterisation of proteins include identification of protein localisation, *in silico* analysis, comparative analysis and determination of immunogenicity of proteins of interest (Doyle, 2011b).

The GliK protein forms part of the gliotoxin biosynthesis cluster, but as of yet the function of this protein has not been investigated (Gardiner and Howlett, 2005). No role for GliK as part of the gliotoxin biosynthetic pathway has previously been proposed. Characterisation of an *A. fumigatus gliK* deletion mutant by comparative proteomic and metabolomic analysis should therefore aid in the elucidation of the role of GliK in *A. fumigatus* biochemistry.

Therefore, the overall objectives of this thesis were as follows:

(i) To expand the identification of *A. fumigatus* proteins, both intracellular and extracellular, through the use of MS-based proteomics.

(ii) To characterise the immunoreactivity of intracellular *A. fumigatus* mycelial proteins, with subsequent identification of antigenic proteins.

(iii) Phenotypic characterisation of *A. fumigatus* ATCC26933 and Δ*gliK* to combinatorial stresses of gliotoxin and H_2O_2, with subsequent use of comparative proteomics for the identification of mechanisms involved in observed phenotypic alterations.

(iv) To investigate the role of GliK in gliotoxin biosynthesis and overall *A. fumigatus* biochemistry through comparative metabolite profiling of *A. fumigatus* ATCC26933 and Δ*gliK*.

CHAPTER 2

Materials and Methods

2 Chapter 2. Materials and Methods

2.1 Materials

All chemicals were purchased from Sigma-Aldrich Chemical Co. Ltd. (U.K.), unless otherwise stated

2.1.1 Solutions for pH Adjustment

2.1.1.1 5 M Hydrochloric Acid (HCl)

Hydrochloric Acid (43.64 ml) was added slowly to deionised water (40 ml) in a glass graduated cylinder. The final volume was adjusted to 100 ml with deionised water. The solution was stored at room temperature.

2.1.1.2 5 M Sodium Hydroxide (NaOH)

NaOH pellets (20 g) were added to deionised water (80 ml) and dissolved using a magnetic stirrer. The final volume was adjusted to 100 ml with deionised water. The solution was stored at room temperature.

2.1.2 SDS-PAGE and Western Blotting Reagents

2.1.2.1 10 % (w/v) Sodium Dodecyl Sulfate (SDS)

SDS (10 g) was added to 80 ml of distilled water and dissolved. The solution was adjusted to 100 ml with distilled water and stored at room temperature.

2.1.2.2 1.5 M Tris-HCl pH 8.3

Trizma-hydrochloride (23.64 g) was dissolved in 60 ml distilled water. The pH was adjusted to 8.3 using 5 M NaOH (Section 2.1.1.2). The volume was adjusted to 100 ml with distilled water and stored at 4 °C.

2.1.2.3 0.5 M Tris-HCl pH 6.8

Trizma-hydrochloride (7.88 g) was dissolved in 60 ml distilled water. The pH was adjusted to 6.8 using 5 M NaOH (Section 2.1.1.2). The volume was adjusted to 100 ml with distilled water and stored at 4 °C.

2.1.2.4 10% (w/v) Ammonium Persulfate (APS)

Ammonium persulfate (0.1 g) was added to 1 ml distilled water. The solution was stored at 4 °C and used within 8 h.

2.1.2.5 1% (w/v) Bromophenol blue

Bromophenol blue (0.2 g) was added to distilled water (20 ml). The solution was stored at 4 °C.

2.1.2.6 0.5% (w/v) Bromophenol blue

Bromophenol blue (0.1 g) was added to distilled water (20 ml). The solution was stored at 4 °C.

2.1.2.7 5 X Solubilisation buffer

Glycerol (8 ml) was added to distilled water (4 ml), containing 1.6 ml of 10 % (w/v) SDS (Section 2.1.2.1) and 1 ml of 0.5 M Tris-HCl, pH 6.8 (Section 2.1.2.3). 2-mercaptoethanol (0.4 ml) was added to the solution along with 0.2 ml of 0.5 % (w/v) bromophenol blue solution (Section 2.1.2.6). The solution was stored at -20 °C in aliquots.

2.1.2.8 5 X SDS Electrode running buffer

Trizma base (30 g), glycine (144 g) and SDS (10 g) were added to 1600 ml distilled water, and dissolved using a magnetic stirrer. The pH was adjusted to between 8.6 and 8.8. The final volume was adjusted to 2 L. The solution was stored at room temperature.

2.1.2.9 1 X SDS Electrode running buffer

5 X SDS Electrode running buffer (200 ml) (Section 2.1.2.8) was added to 800 ml distilled water.

2.1.2.10 Coomassie® Blue Stain Solution

Distilled water (600 ml), glacial acetic acid (100 ml) and methanol (300 ml) were added to a glass bottle containing 1 g Coomassie® Brilliant Blue R. The solution was stored at room temperature.

2.1.2.11 Destain Solution

Glacial acetic acid (100 ml) was added to distilled water (600 ml) and methanol (300 ml). The solution was stored at room temperature.

2.1.2.12 Gel Fixing Solution for Colloidal Coomassie® Stain

Phosphoric acid (30 ml) was added to ethanol (500 ml) and distilled water (470 ml). The solution was stored at room temperature.

2.1.2.13 Incubation Buffer for Colloidal Coomassie® Stain

Ammonium sulfate (170 g) was dissolved in a solution containing methanol (340 ml), phosphoric acid (30 ml) and brought to 1 L with distilled water.

2.1.2.14 Towbin Electrotransfer Buffer for Semi-Dry Transfer

Trizma base (6.06 g) and glycine (28.8 g) were added to distilled water (600 ml) and methanol (200 ml). The final volume was adjusted to 1 L with distilled water. The solution was stored at room temperature.

2.1.2.15 Wet Transfer Buffer

Trizma base (3.03 g) and glycine (14.4 g) were added to distilled water (600 ml) and methanol (200 ml). The final volume was adjusted to 1 L with distilled water. The solution was stored at 4 °C.

2.1.2.16 Blocking Solution

Marvel® (Powdered milk) (5 g) was added to 100 ml PBST (Section 2.1.2.21)

2.1.2.17 BSA Blocking Solution

Marvel® (Powdered milk) (5 g) and bovine serum albumin (1 g) (BSA) were added to 100 ml PBST (Section 2.1.2.21)

2.1.2.18 Antibody Buffer

Marvel® (Powdered milk) (1 g) was added to 100 ml PBST (Section 2.1.2.21)

2.1.2.19 BSA Antibody Buffer

Marvel® (Powdered milk) (1 g) and bovine serum albumin (1 g) (BSA) were added to 100 ml PBST (Section 2.1.2.21).

2.1.2.20 Phosphate Buffered Saline (PBS)

One PBS tablet (Oxoid) was dissolved in 100 ml distilled water. The solution was stored autoclaved at 121 °C for 15 min and stored at room temperature.

2.1.2.21 Phosphate Buffered Saline/ Tween-20 (PBST 0.05%)

Tween-20 (0.5 ml) was added to 1 L PBS (Section 2.1.2.20). The solution was stored at room temperature.

2.1.2.22 DAB Substrate Buffer

Trizma-HCl (15.76 g) was added to 700 ml distilled water and the pH was adjusted to 7.6 with 5 M NaOH (Section 2.1.1.2). The final volume was adjusted to 1 L.

2.1.2.23 Developing Solution

Developing Solution (Kodak, 200 ml) was added to 400 ml distilled water and stirred. The bottle was stored at room temperature, protected from light.

2.1.2.24 Fixing Solution

Fixing Solution (Kodak, 150 ml) was added to 450 ml distilled water and stirred. The bottle was stored at room temperature, protected from light.

2.1.2.25 8 M Urea

Urea (24 g) was dissolved in distilled water and brought to a final volume of 50 ml. The solution was stored at room temperature.

2.1.2.26 100 mM Borate Buffer pH 7.0

Borax (38.14 g) was dissolved in 800 ml distilled water and the pH was adjusted to 7.0. The solution was brought to 1 L and stored at room temperature.

2.1.2.27 2 mM Borate Buffer pH 8.0

100 mM Borate buffer pH 7.0 (Section 2.1.2.26) (20 ml) was added to 800 ml distilled water. The pH was adjusted to 8.0 and solution was brought to 1 L with distilled water.

2.1.3 Mass Spectrometry Reagents

2.1.3.1 100 mM Ammonium bicarbonate (NH_4HCO_3)

NH_4HCO_3 (395 mg) was dissolved in deionised water (50 ml). The solution was prepared fresh on day of use.

2.1.3.2 50 mM Ammonium bicarbonate (NH_4HCO_3)

100 mM ammonium bicarbonate (Section 2.1.3.1) (5 ml) was added to 5 ml of deionised water. The solution was prepared fresh on day of use.

2.1.3.3 10 mM Ammonium bicarbonate(NH_4HCO_3)

100 mM ammonium bicarbonate (Section 2.1.3.1) (1 ml) was added to 9 ml of deionised water. The solution was prepared fresh on day of use.

2.1.3.4 1 M Dithiotreitol (DTT)

DTT (154 mg) was dissolved in 100 mM ammonium bicarbonate (Section 2.1.3.1) (1 ml). The solution was prepared fresh on day of use.

2.1.3.5 1 M Iodoacetamide

Iodoacetamide (185 mg) was dissolved in 100 mM ammonium bicarbonate (Section 2.1.3.1) (1 ml). The solution was prepared fresh on day of use.

2.1.3.6 Whole Protein Lysate Fungal Extraction Buffer

Trizma hydrochloride (790 mg), Guanidine hydrochloride (114.6 g) and DTT (308 mg) were dissolved in distilled water (150 ml). The pH was adjusted to 8.6 using 5 M NaOH (Section 2.1.1.2) and the solution was brought to 200 ml. The solution was stored at 4 °C.

2.1.3.7 Trypsin diluent

100 mM ammonium bicarbonate (Section 2.1.3.1) (1 ml) and acetonitrile (1 ml) were brought to 10 ml with distilled water. The solution was prepared fresh on day of use.

2.1.3.8 0.1 % (v/v) Formic Acid

Formic Acid (1 ml) was added to LC-MS grade water (1 L).

2.1.3.9 10 % (v/v) Methanol in 0.1% (v/v) Formic Acid

HPLC-grade methanol (1 ml) was added to 0.1 % (v/v) formic acid (9 ml) (Section 2.1.3.8).

2.1.3.10 0.1 % (v/v) Trifluoroacetic acid (TFA)

Trifluoroacetic acid (TFA) (10 µl) was added to HPLC-grade water (9.99 ml). This solution was prepared immediately before use.

2.1.3.11 Matrix (α-cyano-4-hydroxycinnamic acid) (4-HCCA)

Trifluoroacetic acid (Section 2.1.3.10) (0.1 % (v/v); 350 µl) was added to 4-HCCA (5 mg) and vortexed for 30 s. Acetonitrile (350 µl) was added to the mixture and vortexed for an additional 30 s. The sample was centrifuged at 13000 rpm for 1 min in a

microfuge and 200 µl of the supernatant was retained. Internal calibrants, hATCH 19 - 39 and Angiotensin fragment III, were added in sufficient quantities for visualisation by MALDI-ToF analysis.

2.1.4 Reverse Phase-High Performance Liquid Chromatography (RP-HPLC) Reagents

2.1.4.1 Solvent A: 0.1 % (v/v) Trifluoroacetic Acid (TFA) in HPLC grade water

TFA (1 ml) was added to 1 L of HPLC grade water. Solution was prepared fresh on day of use.

2.1.4.2 Solvent B: 0.1 % (v/v) Trifluoroacetic Acid (TFA) in HPLC grade Acetonitrile

TFA (1 ml) was added to 1 L of HPLC grade acetonitrile. Solution was prepared fresh on day of use.

2.1.5 *Aspergillus* Media and Reagents

2.1.5.1 *Aspergillus* Trace Elements

$Na_2B_4O_7.7H_2O$ (0.04 g), $CuSO_4.5H_20$ (0.4 g), Fe (III) $SO_4.2H_2O$ (0.8 g), $Na_2MoO.2H_20$ (0.8 g), $ZnSO_4.7H_2O$ (8 g) were dissolved in deionised water (900 ml) in the order given. The solution was adjusted to a final volume of 1 L with deionised water. The solution was split into 50 ml aliquots and stored at - 20 °C

2.1.5.2 50 X *Aspergillus* Salt Solution

KCl (26 g), $MgSO_4.7H_20$ (26 g), KH_2PO_4 (76 g) and *Aspergillus* Trace elements (50 ml) (Section 2.1.5.1) were dissolved in 800 ml distilled water. The solution was

brought to 1 L with distilled water and autoclaved. Chloroform (2 ml) was added to the solution and it was stored at room temperature.

2.1.5.3 100 X Ammonium Tartrate

Ammonium tartrate (92 g) was dissolved in 1 L of distilled water and autoclaved. The solution was stored at room temperature.

2.1.5.4 0.3 M L-glutamine

L-glutamine (43.8 g) was dissolved in 800 ml distilled water, with 1-2 drops of 5 M HCl (Section 2.1.1.1) added to aid solubility. The pH was adjusted to 6.5 and brought to a final volume of 1 L with distilled water. The solution was filter sterilised (0.22 µm filter) and stored at room temperature.

2.1.5.5 *Aspergillus* Minimal Media (AMM)

100 X ammonium tartrate (10 ml) (Section 2.1.5.3), 50 X *Aspergillus* salt solution (20 ml) (Section 2.1.5.2) and glucose (10 g) were added to 800 ml distilled water and dissolved. The pH was adjusted to 6.8 and the solution was made up to 1 L with distilled water. The solution was autoclaved at 105 °C for 30 min and stored at room temperature.

2.1.5.6 *Aspergillus* Minimal Media (AMM) Agar

100 X ammonium tartrate (10 ml) (Section 2.1.5.3), 50 X *Aspergillus* salt solution (20 ml) (Section 2.1.5.2) and glucose (10 g) were added to 800 ml distilled water. The pH was adjusted to 6.8. Agar (18 g) (Scharlau Chemie S.A., Barcelona, Spain) was added to the solution and made up to 1 L with distilled water. The solution was autoclaved at 105 °C for 30 min and allowed to cool to ~50 °C before being poured

into 90 mm petri dishes under sterile conditions. The plates were allowed to set and were stored at 4 °C.

2.1.5.7 Malt Extract Agar (MEA)

Malt extract agar (50 g) (Oxoid Ltd, Hants., England) was dissolved in 1 L of distilled water. Agar solution was autoclaved at 115 °C for 10 min and allowed to cool to ~50 °C before being poured into 90 mm petri dishes under sterile conditions.

2.1.5.8 Sabouraud Dextrose Broth

Sabouraud dextrose powder (30 g) (Oxoid Ltd, Hants., England) was dissolved in 1 L of distilled water. Solution was autoclaved at 121 °C for 15 min.

2.1.5.9 Czapek-Dox Broth

Difco™ Czapek-Dox powder (35 g) (BD Biosciences) was dissolved in 1 L of distilled water and autoclaved at 121 °C for 15 min.

2.1.5.10 Czapek-Dox Agar

Agar (18 g) (Scharlau Chemie S.A., Barcelona, Spain) was added to 1L of Czapek-Dox broth (Section 2.1.5.9). The solution was autoclaved at 121 °C for 15 min and allowed to cool to ~50 °C before being poured into 90 mm petri dishes under sterile conditions. The plates were allowed to set and were stored at 4 °C.

2.1.5.11 YES broth

Yeast extract (20 g) and sucrose (40 g) were dissolved in 800 ml distilled water. The pH was adjusted to 5.8 and the solution was adjusted to a final volume of 1 L with distilled water. The solution was autoclaved at 121 °C for 15 min to sterilise.

2.1.5.12 RPMI media

Sucrose (10g) was dissolved in RPMI 1640 (400 ml) and the volume was adjusted to 465 ml with RPMI 1640. The solution was autoclaved at 121 °C 15 min to sterilise. L-glutamine (0.3 M; 35 ml) (Section 2.1.5.4) was added using sterile techniques once the media had cooled to 50 °C.

2.1.5.13 Phosphate Buffered Saline/ Tween-20 (PBST 0.1% (v/v))

Tween-20 (1 ml) was added to 1 L PBS (Section 2.1.2.20). The solution was autoclaved at 121 °C for 15 min and stored at room temperature.

2.1.5.14 100 mM Phenylmethylsulfonyl fluoride (PMSF)

PMSF (17.4 mg) was dissolved in 1 ml methanol. The solution was stored at room temperature.

2.1.5.15 Pepstatin A (1 mg/ml)

Pepstatin A (10 mg) was brought to 10 ml with distilled water. The solution was split into 1 ml aliquots and stored at -20 °C.

2.1.5.16 1M DTT

DTT (154 mg) was brought to 1 ml with distilled water. The solution was prepared fresh prior to use.

2.1.5.17 *Aspergillus* lysis buffer; reducing

Tris-HCl (15.7 g) and NaCl (2.9 g) were dissolved in 60 ml distilled water. Glycerol (10 ml) was added to the solution and 4 ml of 500 mM EDTA (Section 2.1.6.7) before adjusting the pH of the solution to 7.5. The solution was brought to a

final volume of 100 ml with distilled water and stored at 4 °C. Immediately prior to use, the solution was brought to 1 mM PMSF, 1 µg/ml Pepstatin A and 30 mM DTT by addition of appropriate amounts of the stock solutions (Section 2.1.5.14; 2.1.5.15, 2.1.5.16).

2.1.5.18 *Aspergillus* lysis buffer; non-reducing

Tris-HCl (15.7 g) and NaCl (2.9 g) were dissolved in 60 ml distilled water. Glycerol (10 ml) was added to the solution and 4 ml of 500 mM EDTA (Section 2.1.6.7) before adjusting the pH of the solution to 7.5. The solution was brought to a final volume of 100 ml with distilled water and stored at 4 °C. Immediately prior to use, the solution was brought to 1 mM PMSF and 1 µg/ml Pepstatin A by addition of appropriate amounts of the stock solutions (Section 2.1.5.14; 2.1.5.15).

2.1.5.19 100 % (w/v) TCA

Trichloroacetic acid (100 g) was added to 45.4 ml distilled water and dissolved. The solution was stored in the dark at 4 °C.

2.1.5.20 10 % (w/v) TCA

100 % (w/v) TCA (5 ml) (Section 2.1.5.19) was diluted in distilled water (45 ml) and stored in the dark at 4 °C.

2.1.5.21 Plate assays

A. fumigatus wild-type and mutant strains were grown on Czapek-Dox agar (Section 2.1.5.10) for 5 days at 37 °C after which conidia were harvested (Section 2.2.1.1). Conidia (5 µl; 5 x 10^3 conidia) were spotted in triplicate onto agar plates containing various additives (Table 2.1). Plates were incubated at 37 °C and growth was

monitored at specific time intervals by measuring the diameter of radial growth (cm) of each colony.

Table 2.1: Reagents and concentrations used in plate assays to test for phenotypic alterations in *A. fumigatus.*

Reagent	Stock Concentration	Concentration range used
Hydrogen peroxide	1 M in Czapek-Dox Broth (Section 2.1.5.9)	0 – 1 mM
Gliotoxin	1 mg/ml in Methanol	0 – 10 µg/ml

2.1.5.22 5'-Iodoacetamidofluorescein (IAF) (20 mg/ml)

5'-Iodoacetamidofluorescein (IAF) (20 mg) was dissolved in 1 ml dimethyl sulfoxide (DMSO). The solution was stored, protected from light, at -20 °C.

2.1.5.23 5'-IAF (3 mg/ml)

5'-IAF (20 mg/ml) (Section 2.1.5.22) was diluted in DMSO. The solution was prepared fresh on day of use and protected from light.

2.1.5.24 500 mM Sodium Borohydride

Sodium borohydride (1.89 g) was dissolved in 100 ml of distilled water. The solution was used within 30 min of preparation. Lid was not closed on bottle as hydrogen gas is liberated from solution.

2.1.6 2D-PAGE reagents

2.1.6.1 2M DTT

DTT (308 mg) was brought to 1 ml with IEF buffer (Section 2.1.6.2). The solution was prepared fresh prior to use.

2.1.6.2 2D-PAGE Isoelectric Focusing Buffer (IEF)

Urea (9.6 g), Thiourea (3.04 g), Trizma base (24 mg) Chaps (0.8 ml), Triton X-100 (0.2 ml) were brought to 20 ml with distilled water. The solution was split into 1 ml aliquots and stored at -20 °C. 2M DTT (Section 2.1.6.1) (32 µl) and appropriate ampholytes (GE Healthcare) (8 µl) were added to a 1 ml aliquot immediately prior to use.

2.1.6.3 IPG Strip Equilibration Buffer

Glycerol (150 ml), SDS (10 g), Urea (180 g) and Trizma base (3.03 g) were dissolved in 450 ml of distilled water. The pH was adjusted to 6.8 and the solution was brought to 500 ml. The solution was split into 50 ml aliquots and stored at -20 °C.

2.1.6.4 Equilibration Buffer A

DTT (200 mg) was added to IPG Strip Equilibration Buffer (Section 2.1.6.3) (10 ml). This volume was adequate for 1 strip. The solution was prepared immediately prior to use.

2.1.6.5 Equilibration Buffer B

Iodoacetamide (250 mg) was added to IPG Strip Equilibration Buffer (Section 2.1.6.3) (10 ml). This volume was adequate for 1 strip. Trace amounts of bromophenol blue was added to the solution. The solution was prepared immediately prior to use.

2.1.6.6 Agarose Sealing Solution

Trizma base (1.5 g), glycine (7.2 g) and SDS (0.5 g) were dissolved in 80 ml deionised water. Agarose (0.7g) and 1% (w/v) Bromophenol blue solution (200 µl) (Section 2.1.2.5) were added and the solution was adjusted to 100 ml with deionised water. The solution was heated to dissolve the agarose and stored at room temperature.

2.1.6.7 500 mM EDTA

Ethylenediaminetetraacetic acid dipotassium salt dehydrate (46.53 g) was added to 200 ml of distilled water. The pH was adjusted to 8.0 in order to dissolve the salt. The solution was brought to 250 ml with distilled water and stored at room temperature.

2.1.6.8 Aldrithiol-4 (A4)

Aldrithiol-4 (11 mg) was dissolved in absolute ethanol (1 ml). The solution was stored at -20 ℃.

2.1.6.9 Gel Fitration Calibrant Mixture

Thyroglobulin (25 mg/ml) (200 µl), Aldolase (25 mg/ml) (160 µl) and RNAse A (25 mg/ml) (160 µl) were brought to 1 ml with PBS (Section 2.1.2.20). The solution was stored at 4 ℃. All calibrants used were included in the HMW gel filtration calibration kit (GE Healthcare).

2.2 Methods

2.2.1 Microbiological culture methods

Fungal strains used in this study are listed in Table 2.2.

Table 2.2: List of fungal strains used in this study.

Species	Strain used	Genotype	Source/ Reference
Aspergillus fumigatus	ATCC 26933	Wild-type	ATCC collection
Aspergillus fumigatus	Δ*gliK*	Mutant	Gallagher *et al.* (2012)

2.2.1.1 *A. fumigatus* growth, maintenance and storage

A. fumigatus strains were maintained on MEA (Section 2.1.5.7) or AMM agar (Section 2.1.5.6). A sterile inoculation loop was used to seed conidia onto agar plates. The inoculated agar plates were incubated at 37 °C for 5-7 days. Conidia were harvested in a biological safety cabinet using sterile PBST (Section 2.1.5.13). Harvested conidia were centrifuged at 2000 g for 10 min and the conidia were washed twice with sterile PBS (Section 2.1.2.20) (10 ml). Centrifugation was repeated and the conidia were resuspended in sterile PBS (Section 2.1.2.20) (5 ml). Harvested conidia were stored at 4 °C. *A. fumigatus* mycelium was obtained by inoculation of sterile liquid media with relevant conidia. These cultures were incubated at 37 °C, with shaking at 200 rpm, for a time relevant to each experiment. Mycelia were harvested by filtering liquid culture through miracloth and PBS (Section 2.1.2.20) was used to wash media from the mycelium. Excess moisture was removed from mycelia by pressing between sheets of

absorbent paper. The mycelium was snap frozen in liquid nitrogen and stored at -80 °C until required.

2.2.1.2 Conidia counting using a haemocytometer

A haemocytometer was used to count conidia. Prior to use, the chamber and the coverslip were cleaned with alcohol and the coverslip was fixed in place. The conidia suspension was diluted 1/100 (i.e. 10 µl of conidia stock added to 990 µl of PBS (Section 2.1.2.20)). Diluted conidia suspension (10 µl) was placed on the grid of the haemocytometer. The slide was then viewed by a compound microscope under the 10X objective lens. The cells were counted in the large central gridded square (1 mm^2) (Figure 2.1). The conidia count was then multiplied by the dilution factor and also by 1 x 10^4 to estimate the number of conidia per ml. This count was performed on duplicate samples and the average was obtained.

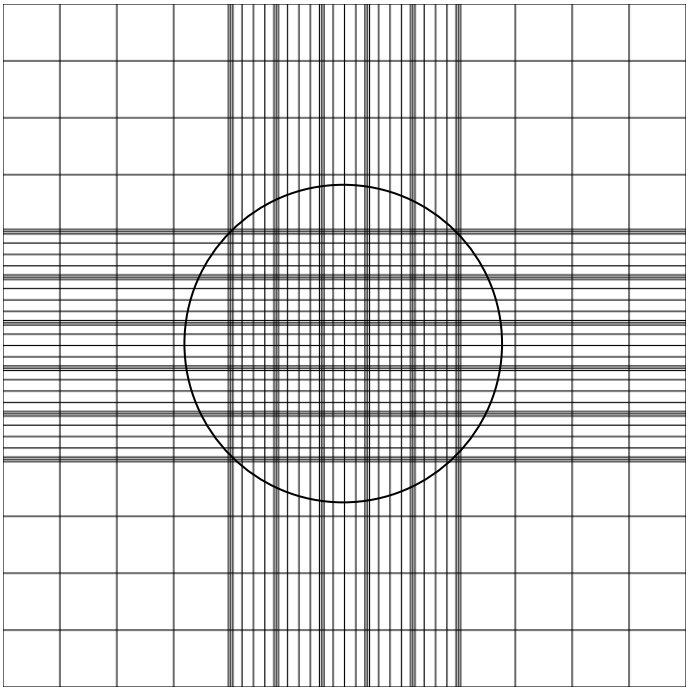

Figure 2.1 Diagram of haemocytometer. The circled region shows the large central grid used to count conidia.

2.2.2 Protein extraction methods

2.2.2.1 *A. fumigatus* whole protein extraction using bead-beating

Harvested mycelia (Section 2.2.1.1) was placed in a 50 ml tube, snap-frozen in liquid nitrogen and lyophilised overnight. 100 mg of lyophilised mycelium was placed in a 2 ml microfuge tube along with a tungsten bead. The mycelium was subjected to bead-beating at 30 Hz for 5 min in a bead beater (MM300, Retsch®). Ice-cold *A. fumigatus* lysis buffer, reducing (Section 2.1.5.17) or non-reducing (2.1.5.18) (0.5 ml), was added to the mycelium and the bead-beating step was repeated. An additional 0.1-0.5 ml of ice-cold *A. fumigatus* lysis buffer was added to the lysate and the suspension was incubated on ice for 1 h. The lysate was centrifuged at 12000 g for 5 min at 4 °C. The supernatant was placed in a sonication bath (Fisher Scientific) for 5 min and the centrifugation step was repeated. The supernatant was brought to 3 mM PMSF and 2 µg/ml Pepstatin A, final concentrations (Section 2.1.5.14; 2.1.5.15). Relative quality of extracted protein was analysed by SDS-PAGE (Section 2.2.4.2) and aliquots were stored at -20 °C until required for use.

2.2.2.2 *A. fumigatus* whole protein extraction for 2D-PAGE

Harvested mycelia (Section 2.2.1.1) was placed in a mortar and crushed into a fine powder using liquid nitrogen and a pestle. Mycelial powder was collected and stored immediately at -70 °C. Mycelial powder (250 mg) was weighed into a 15 ml tube. 10 % (w/v) TCA (Section 2.1.5.20) (1.5 ml) at 4 °C was added to the mycelia. The suspension was sonicated with a sonication probe (Bandelin Sonopuls, Bandelin electronic, Berlin) at 10% power, cycle 6 for 10 seconds. This was repeated twice more with the sample being cooled on ice between each sonication. The sample was incubated on ice for 15-30 min before being centrifuged at 10000 g for 10 min at 4 °C.

The supernatant was discarded and distilled water (60 µl) was added to the sample followed by vortexing. Ice-cold acetone (1 ml) was added to the sample and the pellet was resuspended as completely was possible by pipetting. The sample was vortexed and placed at -20 °C for 1 h, with vortexing at 10 min intervals. The sample was stored at -20 °C overnight. The sample was centrifuged at 10000 g for 10 min and the supernatant was removed. Ice-cold acetone (0.5 ml) was added to the sample and the centrifugation step was repeated. The supernatant was removed and the pellet was left to air-dry for a maximum of 5 min. The pellet was resuspended as completely as possible in IEF buffer (Section 2.1.6.2) (0.5 ml). The sample was left at room temperature for 1 h and then centrifuged at 13000 rpm for 1 min. The supernatant was removed to a clean 1.5 ml microfuge tube. Protein quantitation was carried out using the Bradford protein assay (Section 2.2.4.1)

2.2.2.3 *A. fumigatus* whole cell lysate extraction for shotgun mass spectrometry

Harvested mycelia (Section 2.2.1.1) was placed in a mortar and crushed into a fine powder using liquid nitrogen and a pestle. Mycelia powder was collected and stored immediately at -70 °C. Mycelia powder (1 g) was weighed into a 15 ml tube. Whole Protein Lysate Fungal Extraction Buffer (Section 2.1.3.6) (6 ml) was added gradually to disperse the mycelia. The suspension was sonicated at 10% power, cycle 6 for 10 seconds. This was repeated four more times with the sample being cooled on ice between each sonication. A small volume (0.1 ml) was retained for determination of protein concentration (Section 2.2.4.1). Following sonication, reduction was carried out using DTT, followed by alkylation using iodoacetamide. Briefly, 10 µl of 1 M DTT (Section 2.1.3.4) was added per ml of lysate and incubated at 56 °C for 30 min. The sample was allowed to cool to room temperature and 55 µl of 1 M iodoacetamide (Section 2.1.3.5) was added per ml of lysate. The sample was incubated in the dark for

20 min at room temperature. The whole cell lysate was dialysed (Section 2.2.4.9) against 100 mM ammonium bicarbonate (Section 2.1.3.1). The dialysed protein was stored at -20 °C until required for use.

2.2.3 Methods for Purification of Protein Samples

2.2.3.1 TCA/Acetone Precipitation

Solutions containing protein to be concentrated were brought to 10 % (w/v) TCA by addition to 1 volume of ice-cold 100 % (w/v) TCA (Section 2.1.5.19) to 9 volumes of protein solution at 4 °C. Samples were incubated on ice for 30 min followed by centrifugation at 12,000 g for 10 min at 4 °C. The supernatants were removed and the pellets were resuspended in ice-cold acetone (1 ml). The samples were incubated at – 20 °C for 1 h before centrifugation at 12,000 g for 10 min at 4 °C. The supernatants were removed and the pellets were washed once more with ice-cold acetone. After the supernatant was removed, the pellets were air-dried for 5 min. The pellets were resuspended in 8 M urea (Section 2.1.2.25).

2.2.3.2 Gel Filtration Chromatography

Gel filtration chromatography was carried out using an ÄKTA purifier coupled with (i) a Superose 6 10/300 GL column (GE Healthcare, Germany), used for analytical gel filtration, or (ii) a Sephacryl XK 16/S400 column, used for preparative gel filtration. Lines were purged prior to use and the column was equilibrated with PBS (Section 2.1.2.20). Samples were filtered through 0.22 µm filter or centrifuged at 10000 g for 10 min to remove particulates prior to injection onto column. A selection of molecular weight calibrants were applied to the column in order to prepare a standard curve based on molecular weight versus elution volume (V_e) (Section 2.1.6.9). The flow rate was set

to 0.2 ml/min, with absorbance monitored at 215, 254 and 280 nm. Fractions were collected if required for further analysis.

2.2.3.3 Gold nanoparticle (AuNP) co-incubation with *A. fumigatus* proteins

Colloidal gold (30 nm) (BB International, UK) (2 ml) was centrifuged at 10000 g for 10 min at 4 ℃ and the supernatant was removed. Pellet was resuspended in 2 mM borate pH 8.0 (Section 2.1.2.27) (1 ml). *A. fumigatus* protein lysates (Section 2.2.2.1) were diluted to 3 mg/ml using 2 mM borate pH 8.0 (Section 2.1.2.27). *A. fumigatus* lysates (100 µl) were incubated with colloidal gold (50 µl), with gentle mixing, for 30 min at room temperature. The gold:*A. fumigatus* protein solutions was centrifuged at 10000 g for 10 min at 4 °C and the supernatants were removed. The pellets were washed four times with PBST (Section 2.1.2.21) (40 µl) with centrifugation repeated each time. The final pellet was resuspended in 5X solubilisation buffer (Section 2.1.2.7) (40 µl) and boiled for 5 min. The *A. fumigatus* proteins that interact closely with the gold nanoparticles were analysed by SDS-PAGE (Section 2.2.4.2). Lanes containing this fraction was cut horizontally into 3 mm slices and subjected to trypsin digestion (Section 2.2.6.1) followed by LC-MS analysis (Section 2.2.6.3).

2.2.4 Protein Characterization Methods

2.2.4.1 Bradford Protein Assay

Bio-Rad protein assay dye was diluted 1/5 in sample buffer prior to use. The sample to be assayed was also diluted appropriately. 20 µl of the sample was added to 980 µl of the diluted Bio-Rad protein assay dye and mixed thoroughly. The final sample (1 ml) was transferred to a 1 ml plastic cuvette and incubated for 5 min at room temperature. The A_{595nm} was read relative to a blank and the protein concentration was

determined based on values obtained from a standard curve. All samples were prepared and analysed in duplicate.

2.2.4.2 Sodium Dodecyl Sulphate Polyacrylamide Gel Electrophoresis (SDS-PAGE)

SDS-PAGE gels, both stacking and resolving, were prepared according to Table 2.3 and Table 2.4, respectively. The gels were cast using the Mini-Protean II gel casting apparatus (BioRad, CA, USA) according to the manufacturer's guidelines. Samples were prepared by adding one volume of 5X solubilisation buffer (Section 2.1.2.7) to every 4 volumes of sample in a 1.5 ml microfuge tube. The samples were boiled for 5 min and centrifuged briefly to collect the sample to the bottom of the tube. An appropriate volume of sample was loaded onto the gel using a Hamilton syringe. A molecular mass marker was run alongside samples in order to estimate the relative size of observed proteins. The molecular mass marker used throughout this study ranged from 7-175 kDa (P7703, NEB). The electrophoresis tank was filled with 1X SDS electrode running buffer (Section 2.1.2.9). Electrophoresis was carried out initially at 80 V for 30 min, followed by electrophoresis at 120 V until the dye front reached the bottom of the gel.

Table 2.3: Reagents composition for SDS-PAGE Resolving Gels

% Acrylamide	*10%*	*10%*	*12%*	*12%*	*15%*
Number of Minigels	5	8	5	8	5
1.5 M Tris-HCl pH 8.3 (Section 2.1.2.2)	7.0 ml	10.5 ml	7.0 ml	10.5 ml	7.0 ml
10 % SDS (Section 2.1.2.1)	280 µl	420 µl	280 µl	420 µl	280 µl
30 % Acrylamide, 0.8 % Methylene bis Acrylamide	9.3 ml	13.9 ml	11.3 ml	16.9 ml	13.9 ml
Distilled water	12.3 ml	18.4 ml	9.3 ml	13.9 ml	6.3 ml
10 % Ammonium persulfate (Section 2.1.2.4)	100 µl	150 µl	100 µl	150 µl	100 µl
TEMED	23 µl	35 µl	23 µl	35 µl	23 µl

Table 2.4: Reagents composition for SDS-PAGE Stacking Gel

Number of Minigels	2	5	8
0.5 M Tris-HCl pH 6.8 (Section 2.1.2.3)	2.5 ml	4.0 ml	5.2 ml
10 % SDS (Section 2.1.2.1)	100 µl	160 µl	210 µl
30 % Acrylamide, 0.8 % Methylene bis Acrylamide	1.0 ml	1.5 ml	2.0 ml
Distilled water	6.4 ml	9.6 ml	12.8 ml
10 % Ammonium persulfate (Section 2.1.2.4)	100 µl	150 µl	200 µl
TEMED	10 µl	15 µl	20 µl

2.2.4.3 Isoelectric Focussing (IEF) and 2D-PAGE

Protein samples were prepared to the appropriate concentration and volume for the IPG strip size according to Table 2.5. Bromophenol blue was added to the protein samples, which were then centrifuged at 12,000 g for 5 min. Protein samples were loaded into the positive end of the ceramic IPG strip holders. The IPG strip was added, gel-side down, using a forceps, while the holder was tilted slightly to evenly distribute the sample along the holder. Care was taken to prevent the trapping of air bubbles underneath the strip. The strips were overlaid with Plus One Drystrip Coverfluid (Amersham) (1 - 1.5 ml) and subjected to IEF on an IPGphor II IEF Unit using the following programme;

Step	50 V	12 h
Step	250 V	0.15 h
Gradient	5000V	2 h
Step	5000 V	5 h
Gradient	8000 V	2 h
Step	8000 V	1 h
Step	250 V	1 h

Following IEF, the IPG strips were equilibrated in Reduction Buffer (Section 2.1.6.4) for 20 min, followed by equilibration in Alkylation Buffer (Section 2.1.6.5) for 20 min. The IPG strips were rinsed in 1 X Electrode Running Buffer (Section 2.1.2.9) and placed on top of 12 % SDS-PAGE gels (Table 2.6) using a forceps. The gels were overlaid with Agarose Sealing Solution (Section 2.1.6.6). Once set, the gels were placed in the PROTEAN Plus Dodeca Cell (BIO-RAD) as per manufacturer's instructions. The gels were electrophoresed in 1 X Electrode Running Buffer (Section 2.1.2.9) overnight

at 1.5 W per gel. In the morning, the voltage was increased to 5 W per gel until the dye-front was 2 cm from the end of the gels. The gels were stained with Colloidal Coomassie® Blue (Section 2.2.4.4).

Table 2.5: Protein amounts and volumes for different length IPG Strips

Strip Length	Protein amount	Volume of IEF Buffer
7 cm	125 µg	125 µl
13 cm	300 µg	250 µl

Table 2.6: Composition for large, 12 % acrylamide, SDS-PAGE Resolving Gels

No. of Gels	2	10
1.5 M Tris-HCl pH 8.3 (Section 2.1.2.2)	31.5 ml	157.5 ml
10 % SDS (Section 2.1.2.1)	1.21 ml	6.05 ml
30 % Acrylamide, 0.8 % Methylene bis Acrylamide	50.7 ml	253.5 ml
Distilled water	41.7 ml	208.5 ml
10 % Ammonium persulfate (Section 2.1.2.4)	405 µl	2.25 ml
TEMED	105 µl	525 µl

2.2.4.4 Colloidal Coomassie® Staining of SDS-PAGE gels

Following SDS-PAGE, gels were incubated for 3 h or overnight in fixing solution (Section 2.1.2.12). Following this period, the gels were washed 3 X 20 min with distilled water before being incubated for 1 h in Colloidal Coomassie® stain buffer (Section 2.1.2.13). A quantity of Colloidal Coomassie® Blue G-250 (Serva Electrophoresis, Germany) was scattered over each gel to attain a concentration of approximately 35 mg/ml. Gels were incubated, with stain, for 5 days and washed repeatedly with distilled water.

2.2.4.5 Semi-dry transfer of proteins to NCP

Nitrocellulose paper (NCP) and six sheets of filter paper were cut to the appropriate size of the gel and pre-soaked in Towbin Transfer Buffer (Section 2.1.2.14) for 15 min. The protein gels were removed carefully from the electrophoresis unit and assembled on the transfer unit in a NCP "sandwich" consisting of 3 sheets of saturated filter paper, soaked NCP, protein gel and an additional 3 sheets of saturated filter paper. Transfer was carried out at 18 V for 20 min using a semi-dry transfer unit. Ponceau S solution was applied to NCP to detect protein transfer with excess stain removed through washing with distilled water.

2.2.4.6 Wet transfer of proteins to NCP

Nitrocellulose paper (NCP) and two sheets of filter paper were cut to the appropriate size of the gel and pre-soaked in wet transfer buffer (Section 2.1.2.15) along with two transfer sponges. The protein gels were removed carefully from the electrophoresis unit and assembled as follows: sponge, filter paper, NCP, gel, filter paper, sponge. The layers were clamped together, ensuring no air bubbles are trapped. The clamped unit was submerged in wet transfer buffer (Section 2.1.2.15) in the transfer

tank with the NCP oriented next to the cathode and the gel oriented next to the anode. An ice pack was placed in the unit or alternatively the transfer unit was placed in a container of ice. Transfers were carried out at 100 V for 70 min for small gels or at 15 V overnight for large gels. Ponceau S solution was applied to NCP to detect protein transfer with excess stain removed through washing with distilled water.

2.2.4.7 Western Blot Analysis

Protein transferred to NCP using semi-dry transfer (Section 2.2.4.3) or wet transfer (Section 2.2.4.6) was used to carry out Western blot analysis. Blocking buffer (Section 2.1.2.16 or Section 2.1.2.17) was applied to the NCP and incubated for 1 h at room temperature with gentle rocking. The blocking buffer was poured off the blot and primary antibody, diluted in Antibody buffer (Section 2.1.2.18, 2.1.2.19), was added to the blot. This was incubated for 1 h at room temperature with gentle rocking. Three 10 min PBST (Section 2.1.2.21) washes were carried out on the blot. The secondary antibody was diluted in antibody buffer (Section 2.1.2.18, 2.1.2.19) and incubated with the blot for 1 h at room temperature with gentle rocking. Three 10 min PBST washes were carried out and the blot was developed using Supersignal West Pico enhanced chemiluminescent (ECL) substrate according to manufacturer's guidelines (Pierce Biotechnology). An alternative chromogenic development system was also employed. 3, 3'-diaminobenzidine tetrachloride hydrate (DAB) (10 mg) was dissolved in DAB Substrate buffer (Section 2.1.2.22) (15 ml). Hydrogen peroxide (7 µl) was added to the substrate solution which was then applied to blots. Blots were allowed to develop for 10 min and distilled water was applied to stop the reaction and reduce background staining.

2.2.4.8 Determination of Relative Immunoreactivity of *A. fumigatus* proteins

2D-PAGE Coomassie stained gels, Ponceau S stained 2D-PAGE blots and corresponding antisera probed immunoblots were aligned using Progenesis™ SameSpot Software (Nonlinear Dynamics Ltd, UK). Normalised volumes of aligned Coomassie stained spots were related to the normalised volumes of the corresponding spots on the antisera-probed immunoblots. The intensity of immunoreactivity relative to the amount of protein present was calculated as follows:

$$\frac{\text{Normalised Volume of Immunospot}}{\text{Normalised Volume of Coomassie Stained Spot}} = X$$

High immunoreactivity (H) was indicated if $X \geq 3.5$; Low immunoreactivity was indicated if $X \leq 0.02$; Medium immunoreactivity (M) was indicated if $0.02 < X < 3.5$.

2.2.4.9 Dialysis of protein samples

Dialysis tubing was pre-soaked in the appropriate buffer for 10 min. Protein sample was added to the dialysis tubing with an additional 50% free space included to allow for sample volume expansion. The sealed tubing, containing the sample, was dialysed against 50 volumes. Dialysis was carried out at 4 °C with stirring. A minimum of three buffer changes were carried out at 3 h intervals.

2.2.4.10 Analysis of Supernatant Proteins from *A. fumigatus*

A. fumigatus ATCC 26933 conidia (200 µl: 1 x 10^7 conidia) were inoculated into flasks containing AMM (Section 2.1.5.5) (200 ml) and cultured in static conditions at 37 °C for periods of 1, 2 and 3 weeks. Culture supernatants were harvested at each time point by filtering through miracloth and snap-frozen in liquid nitrogen. Lyophilisation of culture supernatants (40 ml) was carried out and resultant samples were stored at -70

°C. Samples were resuspended in 10 % (w/v) TCA (Section 2.1.5.20) (5 ml) and incubated on ice overnight. Solutions containing precipitated protein were centrifuged at 1700 g for 15 min at 4 °C, and the supernatant was discarded. Pellets were resuspended in ice-cold acetone (2 ml) and centrifuged at 10000 g for 15 min at 4 °C. This washing step was repeated twice more and the final pellet was resuspended in 8 M urea (Section 2.1.2.25). The sample was incubated on ice for 1 h before a final centrifugation step to remove insoluble material. Re-solubilised protein was quantified (Section 2.2.4.1) and analysed by SDS-PAGE (Section 2.2.4.2). The lane containing each sample was cut horizontally into slices and each one was subjected to trypsin digestion (Section 2.2.6.1). LC-MS analysis (Section 2.2.6.3) was subsequently carried out in order to perform a large-scale identification of secreted or external *A. fumigatus* proteins.

2.2.4.11 Organic Extraction of *A. fumigatus* Culture Supernatants

A. fumigatus culture supernatants (20 ml) were added to chloroform (20 ml) in a 50 ml tube and agitated vigorously for 3 min, with regular venting of the tube. The mixtures were centrifuged at 650 g for 10 min at room temperature to separate the organic layer from the aqueous layer. The lower organic layer was retained and stored at -20 °C until required.

2.2.4.12 Rotary evaporation of Organic Extraction Samples

Organic extracts (Section 2.2.4.11) (20 ml) were placed in a glass evaporation bulb. The chloroform was evaporated under vacuum whilst sitting in a water bath set to 37 ^{o}C (Heidolph Laborata 4001 efficient, Vacuubrand CVC 2000 II). The dried extract, retained in the bulb, was resuspended in HPLC grade methanol (200 µl). The resuspended extract was then transferred to clean glass vial and stored at – 20 ^{o}C.

2.2.5 Comparative Metabolite Profile Analysis by Reverse Phase - High Performance Liquid Chromatograhy (RP-HPLC)

2.2.5.1 RP-HPLC Analysis

Organic extracts from supernatants (Section 2.2.4.11, 2.2.4.12) or intracellular fractions (Section 2.2.5.3) were analysed by RP-HPLC with UV detection (Agilent 1200 system), using a C_{18} RP-HPLC column (Agilent Zorbax Eclipse XDB-C18; 5 mm particle size; 4.6 x 15 mm) at a flow rate of 1 ml/min. A mobile phase of water (Section 2.1.4.1) and acetonitrile (Section 2.1.4.2), with TFA, was used under various gradient conditions (Table 2.7, Table 2.8). Injection volume was set to 20 µl and fractions were collected if required.

Table 2.7: RP-HPLC Gradient 1

Time (min)	% B	% B / min
0	5	
5	5	95 % Δ B / 20 min
20	100	4.75 % Δ B / min
28	100	
30	5	

Table 2.8: RP-HPLC Gradient 2

Time (min)	% B	% B / min
0	35	
3	35	25 % Δ B / 6.25 min
9.25	60	4 % Δ B / min
10	100	
14	100	
16	35	

2.2.5.2 5'-IAF Labelling of Sulphydral groups of *A. fumigatus* metabolites

Sodium borohydride ($NaBH_4$) mediated reduction of disulfide bonds, and subsequent alkylation with 5'-Iodoacetamidofluorescein (5'-IAF) was carried out according to Davis *et al.* (2011). Briefly, organic extracts from *A. fumigatus* culture supernatants (Section 2.2.4.11; 2.2.4.12) (50 µl) or protein lysates (Section 2.2.5.3) (50 µl) were reduced by the addition of 500 mM $NaBH_4$ (Section 2.1.5.24) (1.25 µl; 625 nmoles) and incubation at room temperature for 1 h. Free sulphydral groups were then

alkylated by the addition of 5'-IAF (Section 2.1.5.23) (10 µl; 60 nmol) and samples were incubated at room temperature for 40 min in the dark. Control samples were prepared in-tandem, in which reduction was not carried out prior to 5'-IAF labelling. RP-HPLC analysis was carried out using Gradient 1 (Table 2.9) or Gradient 2 (Table 2.10). MALDI-ToF analysis (Section 2.2.7) was also carried out to ascertain the mass of the labelled compound.

2.2.5.3 Preparation of *A. fumigatus* Mycelial Lysates for Intracellular Metabolite Investigation

Mycelia, from *A. fumigatus* liquid cultures (ATCC 26933 and Δ*gliK*; 72 h; 37 °C) in Czapek-Dox (Section 2.1.5.9), were harvested by filtering through miracloth (Section 2.2.1.1). Protein was extracted from lyophilised mycelia (Section 2.2.2.1) using non-reducing lysis buffer (Section 2.1.5.18). Protein lysates (30 µl) were added to PBS (Section 2.1.2.20) (105 µl) along with HPLC-grade methanol (15 µl). These solutions were centrifuged at 10000 g for 10 min at 4 °C and the supernatants were retained. An aliquot (50 µl) of each supernatant was reduced and labelled with 5'-IAF (Section 2.2.5.2) followed by RP-HPLC analysis (Section 2.2.5.1).

2.2.5.4 Determination of Sulphydral Groups in *A. fumigatus* Mycelial Lysates

Mycelia, from *A. fumigatus* liquid cultures (ATCC26933 and Δ*gliK*; 72 h; 37 °C) in Czapek-Dox (Section 2.1.5.9), was harvested by filtering through miracloth (Section 2.2.1.1). Protein was extracted from lyophilised mycelia (Section 2.2.2.1) using non-reducing lysis buffer (Section 2.1.5.18). Protein lysates (100 µl) were diluted with PBS (400 µl) (Section 2.1.2.20). A control, consisting of non-reducing lysis buffer (100 µl) in PBS (400 µl) was also prepared. A volume of the control (100 µl) was transferred to a 0.1 ml quartz cuvette and this solution was used to blank at 280 nm on a

spectrophotometer. The A_{280nm} of the diluted mycelial lysate was measured (A_{280nm}(Sample)). A volume of the control (100 µl) was then used to blank at 324 nm. A4 (2 µl) (Section 2.1.6.8) was added and the A_{324nm} was measured after 1 min (A_{324nm}(Control)). The diluted mycelial lysates (100 µl) was used to blank at 324 nm and then A4 (2 µl) (Section 2.1.6.8) was added and the A_{324nm} was read after 1 min ($A_{324\ nm}$(Sample)). The concentration of free sulphydral groups ([SH]), relative to protein concentration ([Protein]), in the sample was determined using the following equations:

$$[\text{Protein}]\ \text{mg/ml} = A_{280nm} \times 5$$

$$[\text{SH}]\ \text{nMoles/ml} = \frac{A3_{24nm}(\text{Sample}) - A_{324nm}(\text{Control}) \times 5}{0.0198^*}$$

(*0.0198 is the A4 extinction coefficient)

$$\frac{[\text{SH}]\ \text{nMoles/ml}}{[\text{Protein}]\ \text{mg/ml}} = \text{nMoles SH/mg of protein.}$$

2.2.6 Mass Spectrometry Methods

2.2.6.1 In-gel Digestion of SDS-PAGE Samples

In-gel digestion of SDS-PAGE samples was carried out according to the protocol of Shevchenko *et al.* (2007). Briefly, selected bands or spots from SDS-PAGE gels were excised and placed in individual 1.5 ml microfuge tubes. Gel pieces were destained by addition of 100 µl of 100 mM ammonium bicarbonate (Section 2.1.3.1) : acetonitrile (1:1 v/v). Samples were vortexed periodically for 30 min. Acetonitrile (500 µl) was added to samples, followed by vortexing until the gel pieces became white and shrunk. Acetonitrile was removed and replaced with 50 µl of trypsin, diluted to 13 ng/µl

in trypsin buffer (Section 2.1.3.7). Samples were incubated at 4 °C for 2 h, with additional trypsin added to cover gel pieces if required. Samples were then incubated at 37 °C overnight. Gel pieces were subsequently placed in a sonication bath for 10 min followed by transfer of the digest supernatant to fresh microfuge tubes. Samples were dried to completion using a speedy vac (DNA Speedy Vac Concentrator, Thermo Scientific) and resuspended in 0.1% formic acid (Section 2.1.3.8) (20 µl). The samples were filtered through 0.22 µm Cellulose Spin-filters (Costar) before transfer to polypropylene vials. Care was taken to ensure there was no air trapped in the vials.

2.2.6.2 In-solution Digestion of Protein Samples

Solutions that had previously reduced and alkylated (Section 2.2.2.3) were subjected to trypsin digestion. Trypsin was diluted to 400 µg/ml in trypsin buffer (Section 2.1.3.7). Trypsin solution (5 µl; 2 µg) was added to protein samples (0.1 ml) and incubated at 37 °C overnight. Digested samples were diluted in 0.1 % formic acid (Section 2.1.3.8) prior to LC-MS analysis.

2.2.6.3 LC-MS/MS Analysis of Peptide Mixtures

Peptide mixtures generated from (i) in-gel digestion of protein spots or bands from SDS-PAGE (Section 2.2.6.1) or (ii) from in-solution digestion of protein samples (Section 2.2.6.2) were analysed using a 6340 Model Ion Trap LC-Mass Spectrometer (Agilent Technologies, Ireland) using electrospray ionisation. Samples (Sections 2.2.6.1, 2.2.6.2) (1 - 5 µl) were loaded onto a Zorbax 300 SB C-18 Nano-HPLC Chip (150 mm x 75 µm) with 0.1 % (v/v) formic acid (Section 2.1.3.8) at a flow rate of 4 µl/min. A high capacity HPLC chip with a 160 nL enrichment column (150 mm 300 Å C18) was employed for analysis of samples prepared by in-solution digestion (Section 2.2.6.2). Peptides were eluted using the appropriate gradient with a post run of 5 min.

The eluted peptides were ionised and analysed by the mass spectrometer. MS^n analysis was carried out on the 3 most abundant peptide precursor ions at each time point, as selected automatically by the mass spectrometer. Singly charged ions were excluded from analysis by the mass spectrometer.

2.2.6.4 LC-MS/MS Analysis of *A. fumigatus* Metabolites

Metabolites isolated by (i) organic extraction from culture supernatants of *A. fumigatus* (Section 2.2.4.11, 2.2.4.12) or (ii) fractionation following RP-HPLC analysis (Section 2.2.5.1) of intracellular metabolites, were analysed by LC-MS/MS. Samples were diluted in 0.1 % (v/v) formic acid (Section 2.1.3.8) prior to mass spectrometry and were loaded onto a Zorbax 300 SB C-18 Nano-HPLC Chip (150 mm x 75 µm) with 0.1 % (v/v) formic acid (Section 2.1.3.8) at a flow rate of 4 µl/min. Metabolites were eluted using the appropriate gradient with a post run of 5 min. MS^n was carried out on the 3 most abundant precursor ions at each timepoint, with *n* ranging from 2 to 5, depending on the analysis. Singly charged ions were not excluded from analysis, with the precursor range adjusted to include ions with *m/z* between 15 and 2200.

2.2.7 MALDI-ToF analysis

Aqueous samples were prepared for MALDI-ToF analysis by direct mixing of samples with prepared matrix (Section 2.1.3.11). Matrixed samples (0.5 µl) were deposited onto individual positions on the MALDI target slide and allowed to dry. Organic samples were applied using a layering technique, whereby matrix (Section 2.1.3.11) (0.5 µl) was deposited on the MALDI slide and allowed to dry, followed by addition of organic sample to the same position. All samples were subjected to delayed extraction reflectron MALDI-ToF analysis with a nitrogen laser (337 nm) at 20 kV using an Ettan™ MALDI-ToF Pro mass spectrometer (Amersham Biosciences). Each

MALDI target slide contained one spot of external calibration mix (LaserBio Labs, Proteomix C104) and these along with internal calibrants, Angiotensin III and ACTH fragment 18-39, were used to calibrate spectra.

2.2.7.1 Database Search

Database searches for identification of proteins were carried out using Spectrum Mill MS Proteomics Workbench (Revision A.03.03.084 SR4). Validation criteria were set to (i) maximum of two missed cleavages by trypsin, (ii) fixed modification: carboxymethylation of cysteines, (iii) variable modifications: oxidation of methionine, deamidation of asparagine, (iv) mass tolerance of precursor ions ± 2.5 Da and product ions ± 0.7 Da were employed and searches were carried out against a protein database of 8 *Aspergillus* species. Protein grouping was carried out based on the presence of ≥ 1 shared peptide. Protein identifications were manually verified based on the presence of ≥ 1 and a Spectrum Mill protein score ≥ 18.0.

Alternatively, MASCOT MS/MS Ion search, with interrogation of the NCBI (National Centre for Biotechnology Information, http://www.ncbi.nlm.nih.gov) database, was used for protein identification. Criterion for each search was set at (i) Taxonomy: Fungi, (ii) two missed cleavages by trypsin, (iii) fixed modification: carboxymethylation of cysteines, (iv) variable modification: oxidation of methionine, (v) mass tolerance of precursor ions ± 2Da and product ions ± 1Da.

2.2.7.2 Bioinformatic Analysis of Identified Proteins

Proteins identified from LC-MS analysis (Section 2.2.6.3) and database searches (Section 2.2.7.1) were managed using the BioEdit Sequence Alignment Editor V 7.0.9.0 (Hall, 1999) and proteins were characterised using a range of bioinformatics programs (Table 2.9).

Table 2.9: List of programs used to characterise proteins identified by LC-MS.

Program Name	***Protein charcterisation performed***	***Program link***
ExPASy Compute p*I*/Mw tool	Theoretical Mr and p*I* determination	http://web.expasy.org/compute_pi/
Phobius	Putative transmembrane regions (Kall *et al.*, 2004)	http://phobius.sbc.su.se/
SignalP	Putative signal peptide presence (Petersen *et al.*, 2011)	http://www.cbs.dtu.dk/services/SignalP/
GRAVY calculator	Relative hydrophobicity score calculated	http://www.gravy-calculator.de/
FungiFun	Functional annotation based on GO, FunCat and KEGG classification schemes (Priebe *et al.*, 2011)	https://www.omnifung.hki-jena.de/FungiFun/
BLAST2GO	Functional annotation based on BLAST and InterProScan searches (Conesa *et al.*, 2005)	http://www.blast2go.com/b2glaunch/start-blast2go

CHAPTER 3

Large-scale Proteomic Investigation of *A. fumigatus*

3 Chapter 3

3.1 Introduction

Following the publication of *A. fumigatus* Af293 (Nierman *et al.*, 2005) genomic sequence in 2005, and the more recent sequencing of a second *A. fumigatus* strain, A1163 (Fedorova *et al.*, 2008), numerous projects have been undertaken to characterise the proteome of this opportunistic pathogen (Asif *et al.*, 2006; Carberry *et al.*, 2006; Kniemeyer *et al.*, 2006; Vödisch *et al.*, 2009; Teutschbein *et al.*, 2010; Cagas *et al.*, 2011b; Wartenberg *et al.*, 2011; Suh *et al.*, 2012; Wiedner *et al.*, 2012). Traditional proteomic strategies have utilised 2D-PAGE separation with subsequent protein identification by mass spectrometry (MS). This approach involves the separation of complex protein mixtures based on their isoelectric point (p*I*) in the first dimension, followed by molecular mass (M_r) resolution using SDS-PAGE. Resolved proteins are subjected to in-gel digestion and resultant peptides are identified by MS coupled with database searching. However 2D-PAGE can be limiting for the identification of particular subsets of proteins, namely hydrophobic proteins, membrane proteins, and proteins with large molecular mass or extreme p*I* (Kniemeyer *et al.*, 2011). MS-based proteomics have developed more recently and provide an alternative method to 2D-PAGE for proteome profiling.

The premise of MS-based proteomics is the identification of peptides from complex mixtures by mass spectrometry (Aebersold and Mann, 2003). This is preceded by enzymatic digestion of protein extracts before fractionation of the resultant peptides. The first step involved in proteomics - based mass spectrometry is the imparting of charge to peptides, which can be achieved by electrospray ionisation (ESI) or matrix-assisted laser desorption ionisation (MALDI) (Karas and Hillenkamp, 1988; Fenn *et al.*, 1989). Electrospray ionisation is usually preceded by nano spray high performance

liquid chromatography (HPLC) which facilitates separation of peptides based on their relative hydrophobicity. This is typically achieved through the use of a reversed phase C_{18} column, and an appropriate solvent gradient (Finoulst *et al.*, 2011). ESI involves the reduction in size of small charged droplets of the analyte as they are directed towards the mass analyser via an electric field. Desolvation of droplets during flight results in further dispersion into smaller droplets based on electrostatic repulsions. Repetition of this cycle produces charged gas phase molecular ions that enter the mass analyser (Han *et al.*, 2005). MALDI provides an alternative method of sample ionisation, whereby desorption of molecular ions from a crystallised matrix is achieved by irradiation of the sample (Albrethsen, 2007). While ESI is capable of producing molecular ions with multiple charges, MALDI typically only produces singly charged ions (Karas *et al.*, 2000). Following ionisation, peptides are separated based on their mass to charge (*m/z*) ratio by the mass analyser. Tandem mass spectrometry (MS/MS) can be carried out using ion trap analysers allowing multi-stage fragmentations of selected precursor ions (Griffiths and Wang, 2009). MS/MS provides fragmentation patterns of analysed peptides in addition to the *m/z* of intact peptide.

The advent of shotgun or MS-based proteomics has expanded the range of studies in this field in recent years. Shotgun proteomics can take multiple forms including, (i) direct LC-MS/MS, (ii) indirect LC-MS/MS and (iii) 2D-LC-MS/MS (multidimensional protein identification technology, MudPIT) (Link *et al.*, 1999; Washburn *et al.*, 2001). Direct LC-MS/MS involves the on-line separation of complex peptide mixtures using a reversed phase nano column with an extended gradient. Indirect LC-MS/MS is where complex peptide or protein mixtures are pre-fractionated off-line (e.g. by 1D SDS PAGE) before LC-MS/MS analysis (Aebersold and Mann, 2003). Sample complexity can also be reduced using affinity pre-fractionation, whereby

abundant proteins can be removed or reduced in concentration (Pernemalm *et al.*, 2009). Affinity fractionation can be achieved through the use of beads possessing a library of ligands, facilitating differential binding to a range of proteins and subsequently the equalisation of protein concentration ranges (Thulasiraman *et al.*, 2005). Keidel *et al.* (2010) have shown that use of these ligand libraries may be redundant as the affinity of proteins for the solid phase beads themselves, based on hydrophobic binding, outweighs the specific protein-ligand affinity. Inorganic nanoparticles (e.g. gold nanoparticles (AuNPs) also exhibit adherent qualities, with proteins adsorbing to the nanoparticles surface and forming a protein shell or 'corona' (Casals *et al.*, 2010). Proteins adhering with high affinity to the nanoparticle surface form the hard corona (Lundqvist *et al.*, 2008). These qualities can be exploited to reduce sample complexity prior to MS. 2D-LC-MS/MS involves the on-line separation of peptides using two capillary columns arranged in a series, and fractionating based on two separate peptide attributes (e.g. acidity, hydrophobicity) before MS/MS (Link *et al.*, 1999; Washburn *et al.*, 2001). As with 2D-PAGE, MS-based proteomics can be used in either a quantitative or a qualitative manner. Quantitative methods involve isotope labelling of peptides using chemical tags (e.g. isobaric tags for relative and absolute quantification, iTRAQ) or through the metabolic introduction of isotopes (e.g. stable-isotope labelling by amino acids in cell culture, SILAC) (Ong *et al.*, 2002; Ross *et al.*, 2004). Label-free methods of MS-based quantitation, based on spectral counting and peak intensities, are also used (Old *et al.*, 2005).

2D-PAGE based proteomic maps of *A. fumigatus* have provided a global overview of the proteins from mycelia, conidia and the secretome (Asif *et al.*, 2006; Carberry *et al.*, 2006; Kniemeyer *et al.*, 2006; Vödisch *et al.*, 2009; Teutschbein *et al.*, 2010; Wartenberg *et al.*, 2011). Sub-proteome strategies have also been implemented to

investigate glutathione binding (Carberry *et al.*, 2006) and mitochondrial proteins (Vödisch *et al.*, 2009). The recent emergence of MS-based proteomics studies of *A. fumigatus* has been observed. A large-scale study of the *A. fumigatus* plasma membrane identified 530 associated proteins utilising a combination of 1D PAGE fractionation of total proteins followed by peptide separation and identification by 2D-LC-MS/MS (Ouyang *et al.*, 2010). This study could not have been undertaken using 2D-PAGE due to the incompatibility of hydrophobic proteins, and proteins with transmembrane (TM) regions with the detergents used in isoelectric focusing, the first separation stage of 2D-PAGE (Rabilloud, 2009). Quantitative MS-based proteomics, both label-free and using iTRAQ, have been used to comparatively profile the stages of *A. fumigatus* germination (Cagas *et al.*, 2011b; Suh *et al.*, 2012). In addition, a recent MS-based study has investigated the proteomic response of *A. fumigatus* to growth on human serum (Wiedner *et al.*, 2012).

The generation of large volumes of data from global proteomics investigations requires a 'systems biology' approach to data interpretation. This is aided by the availability of various bioinformatics tools, which allow semi-automation of data analysis (Conesa *et al.*, 2005; Priebe *et al.*, 2011). These tools include programs for the prediction of protein characteristics, such as protein molecular mass and p*I* based on primary structure, relative hydrophobicity, presence of transmembrane helices and signals for secretion (Bendtsen *et al.*, 2004; Kall *et al.*, 2004; Petersen *et al.*, 2011). Functional categorisation of proteins, detected in large-scale studies, can assist in the identification of pathways, processes or subsets of proteins that are active or targeted under particular experimental conditions. Functional classification schemes regularly used in *A. fumigatus* studies include Functional Catalogue (FunCat) (Ruepp *et al.*, 2004), Gene Ontology (GO) (Ashburner *et al.*, 2000) and Kyoto Encyclopedia of Genes

and Genomes (KEGG) (Kanehisa *et al.*, 2012). These classification schemes can be simultaneously accessed, for a range of fungal species, using the web-based FungiFun application (Priebe *et al.*, 2011; https://www.omnifung.hki-jena.de/FungiFun/). FunCat is an annotation scheme that provides a multilevel functional classification allowing proteins to be grouped into broad first level categories, with more specific categories branching from these (Ruepp *et al.*, 2004). GO provides a standardised terminology for the description of genes and their products across all organisms. It is divided into three sub-categories, describing biological process, molecular function and cellular localisation relevant to the gene product (Ashburner *et al.*, 2000). KEGG is unique in that it provides graphical representation of various metabolic pathways, displaying the relationship between a network of enzymes and metabolites.

The application of MS-based proteomics to dissect the proteome of *A. fumigatus* has the potential to provide a global overview of the pathways and biological processes active under a set of conditions. In addition, bioinformatic analysis can expand the characterisation of large datasets generated by MS-based proteomics. The aims of the work described in this Chapter were (i) to generate a global profile of the *A. fumigatus* mycelial proteome using MS-based proteomics, (ii) to investigate methods to reduce sample complexity prior to MS-based proteomics, (iii) to identify proteins in the secretome of *A. fumigatus* using direct and indirect methods of MS-based proteomics and (iv) to characterise the proteome of *A. fumigatus* using bioinformatic analysis.

3.2 Results

3.2.1 Identification of 370 proteins from *A. fumigatus* mycelia using shotgun mass spectrometry

Mycelia from *A. fumigatus* shaking cultures were harvested after 48 h in *Aspergillus* minimal media (AMM), and extracted protein was subjected to trypsin digestion as described in Sections 2.2.2.3 and 2.2.6.2. Tryptic peptide mixtures were separated on extended liquid chromatography gradients and subjected to tandem mass spectrometry using the Agilent 6340 Ion Trap LC-MS System (Agilent Technologies) (Section 2.2.6.3).

Utilising a direct shotgun proteomics approach a total of 1844 unique peptides were identified, corresponding to 511 unique *A. fumigatus* proteins. Proteins (n = 370) were manually verified, based on the presence of ≥ 2 peptides or a Spectrum Mill MS/MS search score ≥ 18.0 (Appendix I). The protein sequences of the entire *A. fumigatus* proteome were obtained from the *Aspergillus* comparative database provided by the Broad Institute (*Aspergillus* Comparative Sequencing Project, Broad Institute of Harvard and MIT (http://www.broadinstitute.org/). The sequences of the proteins identified in this study (n = 370) were extracted and the associated theoretical molecular mass (tM_r) and isoelectric point (tp*I*) were calculated using the Compute p*I*/MW tool from the ExPASy Proteomics Server. These proteins (n = 370) spanned a theoretical p*I* range of 3.9 to 11.8 and a M_r range of 9 to 434 kDa (Figure 3.1). All peptides identified contributed to a sequence coverage range of between 1 and 62 % of the relative proteins, with Spectrum Mill scores ranging between 18 and 1266.

.

In order to determine the relative hydrophobicity of identified proteins, the grand average of hydropathy (GRAVY) index was calculated using GRAVY calculator (www.gravy-calculator.de). The GRAVY index for identified proteins ranged from -1.632 to 0.483, with positive scores being indicative of hydrophobicity (Figure 3.2a). A number of hydrophobic proteins were identified (*n* = 28; 7.57 % of total identified proteins), based on positive GRAVY scores. Additionally, GRAVY scores were collected for the entire predicted proteome of *A. fumigatus* and it was observed that 15.6 % of the total proteome possess positive GRAVY scores (Figure 3.2). The majority of proteins identified by shotgun mass spectrometry (71.3 %) were slightly hydrophilic, with GRAVY scores ranging from -0.5 to 0. This is in-line with the total predicted proteome of *A. fumigatus*, where 55.1 % of all predicted proteins fall within this range. Using Phobius (phobius.cbr.su.se/), the number of putative transmembrane regions present in each identified protein was determined (Figure 3.2b). Proteins with transmembrane helices (*n* = 37; 10.0 % of total identified proteins) were detected. Several proteins were detected with 10 and more putative TM regions, including a plasma membrane H^+ - ATPase (AFUA_ 3G07640), an amino acid permease (Gap1) (AFUA_7G04290) and 2 ABC transporters (AFUA_1G14330 and AFUA_5G06070). One protein, a small oligopeptide transporter (OPT family) (AFUA_2G15240) was detected with 14 putative transmembrane regions and a GRAVY score of 0.276263.

Identified proteins were grouped into functional categories based on the FunCat (Functional Catalogue), GO (Gene Ontology) and KEGG (Kyoto Encyclopedia of Genes and Genomes) annotations, using the FungiFun application (https://www.omnifung.hki-jena.de/FungiFun/) (Priebe *et al.*, 2011). Annotations were available for 89.19 %, 86.76 % and 51.89 % of identified proteins using the FunCat, GO and KEGG schemes respectively (Figure 3.3). Based on the FunCat classification,

functional categories that were significantly overrepresented were protein synthesis (n = 77, p = 1.03 x 10^{-20}), energy (n = 86, p = 6.95 x 10^{-19}), protein with binding function or cofactor requirement (n = 227, p = 1.14 x 10^{-12}), transcription (n = 26, p = 1.97 x 10^{-9}) and cell cycle and DNA processing (n = 46, p = 0.028). Proteins (n = 21; 5.7 %) were identified which have no functional classifications using the aforementioned methods.

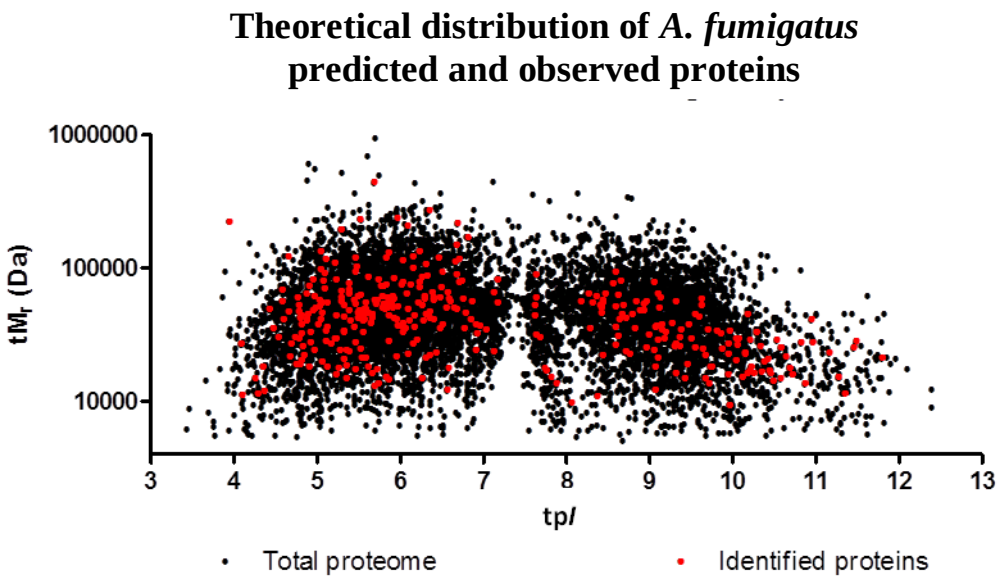

Figure 3.1: Proteome map showing distribution of *A. fumigatus* proteins based on theoretical M_r and p*I* Proteins identified by shotgun mass spectrometry (*n* = 370; red) are shown overlaid on the total *A. fumigatus* proteome (black). tM_r, theoretical molecular mass, axis drawn on logarithmic scale; tp*I*, theoretical isoelectric point, axis drawn on linear scale.

a.

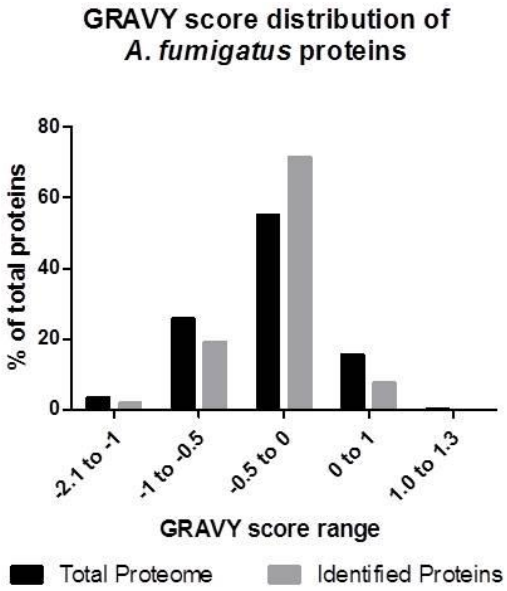

b.

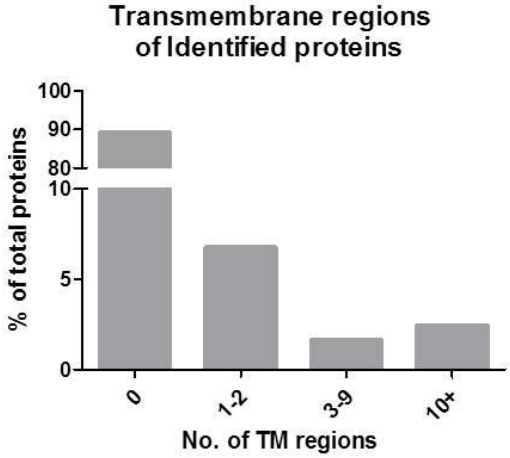

Figure 3.2: Distribution of proteins identified by shotgun mass spectrometry (MS) according to (a) their relative hydrophobicity and (b) the number of putative transmembrane regions per protein. Positive GRAVY scores are indicative of hydrophobic proteins and negative GRAVY scores represent hydrophillic proteins. (a) Relative distribution of GRAVY score across the entire proteome (black) is indicated alongside the proteins identified using shotgun MS (grey). (b) The number of putative transmembrane regions on each protein identified by shotgun MS is shown. GRAVY, grand average of hydropathy; TM, transmembrane; MS, mass spectrometry.

a.

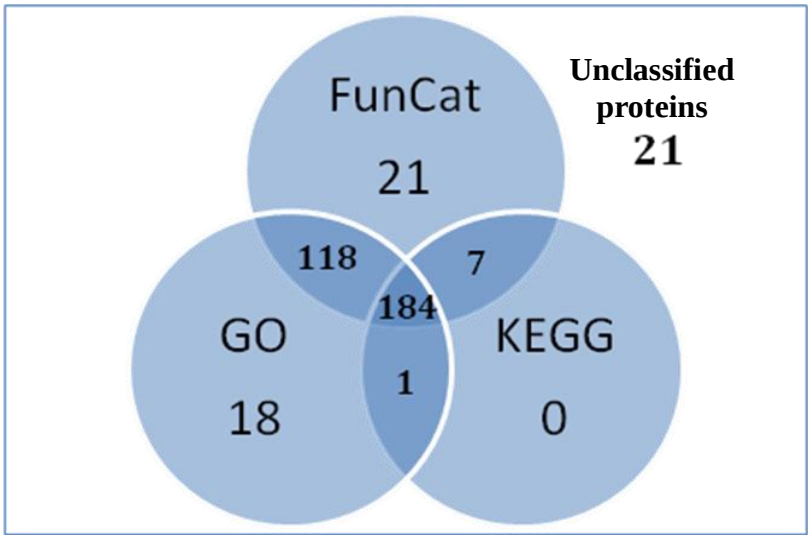

b.

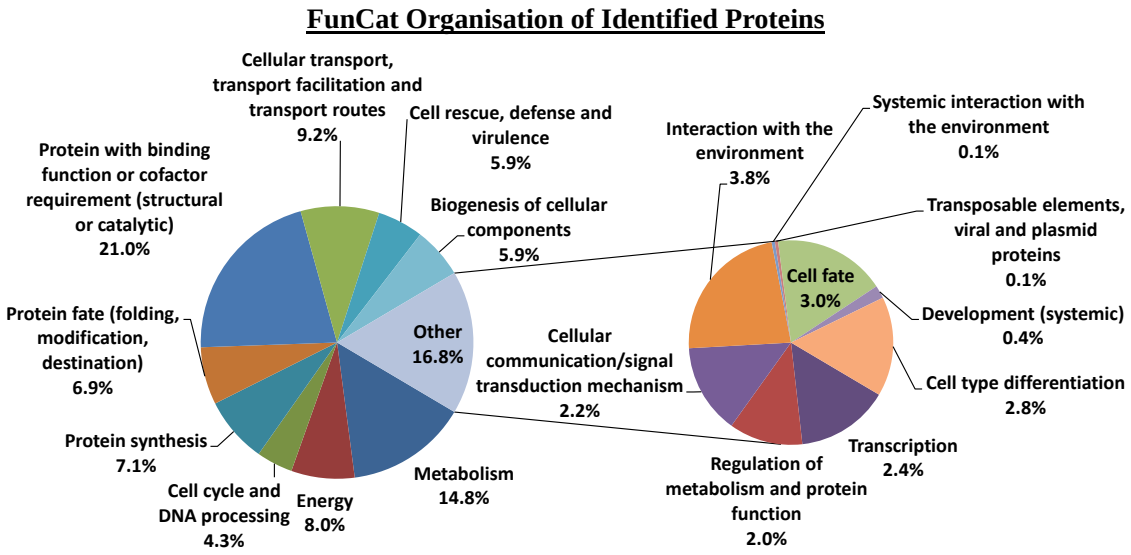

Figure 3.3: Distribution of functional annotations of *A. fumigatus* proteins identified using shotgun proteomics strategy. (a) GO (gene ontology), KEGG (Kyoto Encyclopedia of Genes and Genomes) and FunCat (Functional Catalogue) classification schemes were used for functional annotation utilizing the FungiFun application. A number of proteins (n = 21) were identified that possessed no functional classification using this system. (b) The functional categorization of the proteins identified here, based on the FunCat annotation scheme, are shown.

3.2.2 Identification of *A. fumigatus* secondary metabolite cluster expression at protein level

Proteins identified by shotgun mass spectrometry (n = 370) were mapped based on their relative loci on each of the eight *A. fumigatus* chromosomes, using their gene locus identifiers (Figure 3.4a). A number of proteins (n = 14) that comprise a secondary metabolite supercluster, involved in the production of pseurotin A and fumitremorgin B, were identified (Table 3.2) (Grundmann and Li, 2005; Maiya *et al.*, 2007; Perrin *et al.*, 2007). In addition, proteins were identified from the gliotoxin biosynthetic cluster on chromosome 6 (Gardiner and Howlett, 2005), a putative ETP cluster on chromosome 3 (Patron *et al.*, 2007) and two clusters responsible for the production of unknown metabolites on chromosomes 3 and 4 respectively (Table 3.2). A phosphoglycerate kinase PgkA protein (AFUA_1G10350) was also identified, which is predicted to be part of the *Afpes1* NRPS cluster on chromosome 1 (Nierman *et al.*, 2005). The identification of these proteins is indicative of the respective cluster activity under the growth conditions used. Interestingly, expression of all of the clusters identified here is partially or completely regulated by the transcription regulator LaeA (Figure 3.4b) (Perrin *et al.*, 2007).

a.

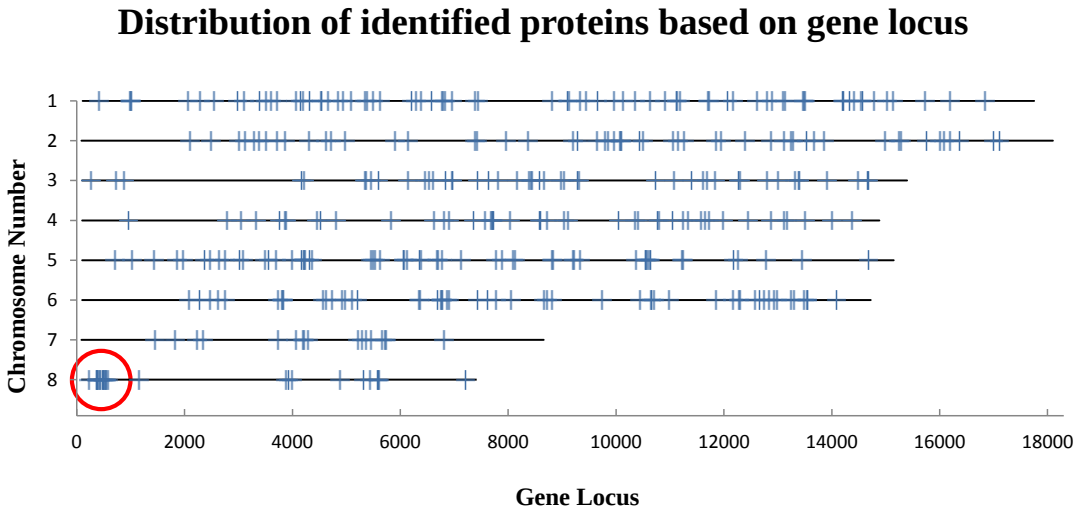

b.

Cluster Number	Chromosome	Location	Distance to Telomere (kb)	LaeA Regulation	Product(s)
1	1	Afu1g10360–Afu1g10390	2,300	Yes	Unknown product of Afpes1
2	1	Afu1g17640–Afu1g17740	100	No	Unknown
3	2	Afu2g17510–Afu2g17600	200	Yes	DHN-melanin
4	2	Afu2g17960–Afu2g18070	100	Yes	Ergot alkaloids: festuclavine, elymoclavine, fumigaclavines A, B, and C
5	3	Afu3g01290–Afu3g01600	400	Partial	Unknown
6	3	Afu3g02520–Afu3g02720	700	No	Unknown
7	3	Afu3g03190–Afu3g03370	900	No	Probably two compounds (a siderophore and a distinct toxin)[a]
8	3	Afu3g12870–Afu3g13010	700	Yes	Putative ETP
9	3	Afu3g13580– Afu3g13750	500	No	Unknown
10	3	Afu3g14560–Afu3g14760	200	Partial	Unknown
11	3	Afu3g15200–Afu3g15340	100	No	Unknown
12	4	Afu4g00110–Afu4g00280	100	Partial	Unknown
13	4	Afu4g14380–Afu4g14850	100	Partial	Unknown
14	5	Afu5g00110–Afu5g00160	100	No	Unknown
15	5	Afu5g00340–Afu5g00400	100	No	Unknown
16	5	Afu5g12700–Afu5g12740	700	No	Unknown
17	6	Afu6g03290–Afu6g03490	800	Yes	Unknown
18	6	Afu6g09580–Afu6g09770	1,500	Yes	Gliotoxin
19	6	Afu6g12040–Afu6g12080	800	Yes	Unknown
20	6	Afu6g13920–Afu6g14000	300	Yes	Unknown \
21	7	Afu7g00110–Afu7g00190	100	No	Unknown
22	8	Afu8g00100–Afu8g00720	100	Yes	Fumitremorgen B; supercluster probably producing more than one product

Figure 3.4: (a) Distribution of proteins identified using shotgun mass spectrometry (*n* = 370) based on gene locus (blue lines). Identification of proteins (*n* = 14) from a supercluster on chromosome 8, involved in the production of fumitremorgin B, pseurotin A and an unknown metabolite (red circle). (b) Summary of secondary metabolite gene cluster function and regulation by LaeA. A red box is used to indicate clusters from which protein expression was detected by shotgun mass spectrometry. From Perrin *et al.* (2007).

Table 3.2: *A. fumigatus* proteins, involved in secondary metabolism, and identified by shotgun mass spectrometry.

Cluster No[a]	CADRE ID. (AFUA_)	Protein name	Chromosome No	LaeA regulation[a]	Product(s)
1	**1G10350**	Phosphoglycerate kinase PgkA (EC 2.7.2.3)	1	Yes	Fumigaclavine C
8	**3G13010**	Zn-dependent hydrolase/oxidoreductase family protein, putative	3	Yes	Putative ETP
10	**3G14665**	Unknown function protein	3	Partial	Unknown
10	**3G14680**	Lysophospholipase 3 (EC 3.1.1.5) (Phospholipase B 3)	3	Partial	Unknown
13	**4G14380**	Glutathione S-transferase, putative	4	Partial	Unknown
18	**6G09740**	GliT (Thioredoxin reductase GliT) (EC 1.-.-.-)	6	Yes	Gliotoxin
22	**8G00230**	Phytanoyl-CoA dioxygenase family protein	8	Yes	‘Supercluster’ producing Fumitremorgin B, Pseurotin A and an unknown metabolite
22	**8G00370**	Polyketide synthase, putative	8	Yes	
22	**8G00380**	DltD N-terminal domain protein	8	Yes	
22	**8G00390**	O-methyltransferase, putative	8	Yes	
22	**8G00400**	Unknown function protein	8	Yes	
22	**8G00430**	Unknown function protein	8	Yes	
22	**8G00440**	Steroid monooxygenase, putative (EC 1.-.-.-)	8	Yes	

Cluster No[a]	CADRE ID. (AFUA_)	Protein name	Chromosome No	LaeA regulation[a]	Product(s)
22	**8G00480**	Phytanoyl-CoA dioxygenase family protein	8	Yes	
22	**8G00500**	Acetate-CoA ligase, putative (EC 6.2.1.1)	8	Yes	
22	**8G00510**	Cytochrome P450 oxidoreductase OrdA-like, putative	8	Yes	'Supercluster' producing Fumitremorgin B, Pseurotin A and an unknown metabolite
22	**8G00530**	Alpha/beta hydrolase, putative	8	Yes	
22	**8G00540**	Hybrid PKS-NRPS enzyme, putative	8	Yes	
22	**8G00550**	Methyltransferase SirN-like, putative	8	Yes	
22	**8G00580**	Glutathione S-transferase, putative	8	Yes	

CADRE ID., *A. fumigatus* gene annotation nomenclature according to Nierman *et al.* (2005) and Mabey *et al.* (2004). [a] Clusters numbers and LaeA regulation as denoted by Perrin *et al.* (2007).

3.2.3 Identification of 173 proteins from *A. fumigatus* mycelia using shotgun mass spectrometry coupled with gel filtration pre-fractionation

A. fumigatus mycelia from shaking cultures in AMM were harvested after 48 h. Protein was extracted and the soluble portion of the whole cell lysate was fractionated following gel filtration chromatography (Section 2.2.3.2). Fractionated proteins, along with the insoluble portion of the whole cell lysate, were trypsin digested using the in-solution method described in Section 2.2.6.2. LC-MS/MS was used to identify *A. fumigatus* proteins from each of the fractions (Section 2.2.6.3).

Pre-fractionation of the *A. fumigatus* mycelia proteome, followed by shotgun mass spectrometry, resulted in the identification of 768 unique peptides, corresponding to 227 unique *A. fumigatus* proteins. Proteins (n = 173) were manually verified, as before, based on the presence of ≥ 2 distinct peptides or a Spectrum Mill score ≥ 18.0. Proteins (n = 17) previously not identified by the exclusively shotgun mass spectrometry approach outlined in Section 3.2.1 are shown in Table 3.3. Proteins (n = 156) that were identified by both gel filtration coupled shotgun mass spectrometry and shotgun mass spectrometry alone are indicated in Appendix I.

The proteins identified by gel filtration coupled shotgun mass spectrometry (n = 173) spanned a theoretical pI range of 4.08 to 11.36 and a M_r range of 9 to 434 kDa. Proteins were identified by peptides attributing to between 1 and 65 % sequence coverage, with Spectrum Mill scores ranging from 18 to 404. The GRAVY index for proteins identified using this method ranges from -1.577 to 0.415, with 6.9 % of these proteins possessing a positive GRAVY score. The number of proteins containing putative transmembrane regions was determined using Phobius software (phobius.cbr.su.se/) and these accounted for 7.5 % of the proteins identified here. The

most hydrophobic protein identified using the approach described in this section was an amino acid permease (Gap1) (AFUA_7G04290), which possesses 12 putative TM regions and a GRAVY score of 0.415.

Table 3.3: *A. fumigatus* mycelia proteins (*n* = 17) identified by gel filtration coupled shotgun mass spectrometry, previously not identified by shotgun mass spectrometry alone. Proteins are arranged in order of increasing CADRE ID.

CADRE ID. (AFUA_)	Protein name	tp*I*	tM_r	GRAVY score	TM	Coverage (%)	Unique peptides	SM Score
1G06940	Chorismate synthase (EC 4.2.3.5)	6.12	44185.92	-0.3466	0	2	1	21.79
1G09550	Dynein light chain (Tctex1), putative	5.27	15325.41	0.076224	0	9	1	20.03
1G13780	Histone H4	11.36	11370.35	-0.53883	0	17	1	19.62
2G10600	NADH-ubiquinone oxidoreductase 299 kDa subunit, putative (EC 1.6.5.3)	5	27541.84	-0.73595	0	4	1	18.27
2G11340	Phosphatidylglycerol/phosphatidylinositol transfer protein (PG/PI-TP)	5.56	27290.30	-0.0125	0	14	4	54.95
2G15430	Sorbitol/xylulose reductase Sou1-like, putative (EC 1.-.-.-)	5.96	28220.04	-0.0688	0	12	2	33.85
3G07710	Nucleolin protein Nsr1, putative	4.68	58498.97	-1.37949	0	4	2	22.87
3G10920	Telomere and ribosome associated protein Stm1, putative	9.76	36892.45	-1.57734	0	5	2	27.41
4G10280	Phosphotransmitter protein Ypd1, putative	4.86	21367.02	-0.75393	0	14	2	27.75
4G11390	Ubiquinol-cytochrome c reductase complex 17 kDa protein	4.08	17895.00	-1.24684	0	12	2	36.6
4G12850	Calnexin homolog clxA	4.97	61853.81	-0.58295	1	5	3	35.32

CADRE ID. (AFUA_)	Protein name	tp*I*	tM_r	GRAVY score	TM	Coverage (%)	Unique peptides	SM Score
5G03540	Thioredoxin reductase	6.99	42850.34	-0.44482	0	8	3	46.83
5G05490	Seryl-tRNA synthetase (EC 6.1.1.11)	6.04	54190.19	-0.69494	0	3	1	21.45
5G11320	Thioredoxin (TrxA)	5.14	11975.72	-0.08182	0	32	2	36.47
7G01860	Heat shock protein (Sti1), putative	5.83	65031.41	-0.71863	0	8	2	34.43
7G05470	Electron transfer flavoprotein alpha subunit, putative	5.73	37630.02	0.042222	0	10	3	45.49
8G04120	Carboxypeptidase S1, putative (EC 3.4.16.6)	5.4	67672.79	-0.31098	0	11	5	81.77

CADRE ID., *A. fumigatus* gene annotation nomenclature according to Nierman *et al.* (2005) and Mabey *et al.* (2004); tp*I*, theoretical isoelectric point; tM_r, theoretical molecular mass; TM, number of transmembrane regions; GRAVY score, grand average of hydropathy; SM score, Spectrum Mill protein score.

3.2.4 Identification of *A. fumigatus* proteins adsorbing to gold nanoparticles

Mycelia from *A. fumigatus* ATCC26933 shaking cultures in AMM were harvested after 48 h. Protein was extracted as described in Section 2.2.2.1 and co-incubated with 30 nm colloidal gold nanoparticles (Section 2.2.3.3). Gold nanoparticles (AuNPs) were extensively washed to remove unbound or loosely bound proteins from the nanoparticles surface. Proteins interacting with the surface of the AuNPs were then analysed by SDS-PAGE and protein identification was achieved through in-gel trypsin digestion of the lanes and LC-MS/MS analysis (Section 2.2.6.1, 2.2.6.3).

A total of 43 *A. fumigatus* proteins that form the hard corona (Lundqvist *et al.*, 2008) of AuNPs (Figure 3.5), were identified by LC-MS/MS and verified based on a Spectrum Mill score ≥ 18.0 (Table 3.4). These proteins cover a p*I* range of 4.77 to 11.46 and a M_r range of 15 to 83 kDa. The GRAVY scores for the protein identified here extend from -1.016 to 0.247, with 3 proteins exhibiting positive GRAVY score, thus indicating hydrophobicity. Proteins were identified with up to 3 TM regions (n = 3) accounting for 7 % of the total number of proteins interacting with the AuNP surface.

Using the FungiFun application (https://www.omnifung.hki-jena.de/FungiFun/) (Priebe *et al.*, 2011), the proteins identified here were categorized based on their functional annotations. Annotations were available for 100 %, 90.7 % and 55.81 % of identified proteins using the FunCat, GO and KEGG schemes respectively. Based on the FunCat classification, functional categories that were significantly represented in this dataset included protein synthesis (n = 16, p = 3.25 x 10^{-8}), metabolism (n = 9, p = 2.206 x 10^{-5}) and energy (n = 13, p = 0.0002). Interestingly, a significant majority of the proteins identified (n =38/43, 88.4 %; p = 1.18 x 10^{-7}) were described as proteins with binding function or cofactor requirement, according to this system (Figure 3.5).

Table 3.3: *A. fumigatus* mycelia proteins (*n* = 43) interacting with AuNP surface, identified by 1D-SDS PAGE and LC-MS/MS. Proteins are arranged in order of increasing CADRE ID.

CADRE ID. (AFUA_)	Protein name	tp*I*	tM_r	GRAVY score	TM	Coverage (%)	Unique peptides	SM Score
1G03510	ATP synthase gamma chain	7.64	31546.83	-0.22276	0	7	1	19.61
1G04940	Small COPII coat GTPase sar1 (EC 3.6.5.-)	5.96	21431.73	-0.13333	0	15	2	27
1G05390	Mitochondrial ADP,ATP carrier protein (Ant), putative	9.97	33321.49	0.046429	2	20	5	74.33
1G06390	Elongation factor 1-alpha	9.12	50019.60	-0.29565	0	20	7	120.73
1G07440	Molecular chaperone Hsp70	5.08	69660.29	-0.4105	0	14	5	73.29
1G09100	60S ribosomal protein L9, putative	9.67	21843.17	-0.31875	0	6	1	18.35
1G11710	Ribosomal protein	9.88	24252.58	-0.31751	0	5	1	19.71
1G11730	ADP-ribosylation factor, putative (Adp-ribosylation factor, putative)	5.54	21003.07	-0.27596	0	9	2	29.12
1G12170	Elongation factor Tu	6.69	48285.99	-0.32227	0	7	2	33.57
1G14200	Mitochondrial processing peptidase beta subunit, putative (EC 3.4.24.64)	5.9	53269.94	-0.32401	0	4	2	44.14
1G14410	60S ribosomal protein L17	10.64	21666.02	-0.53041	0	4	1	20.78
2G03290	14-3-3 family protein ArtA, putative	4.77	29101.64	-0.43563	0	5	1	21.25

CADRE ID. (AFUA_)	Protein name	tp*I*	tM_r	GRAVY score	TM	Coverage (%)	Unique peptides	SM Score
2G03730	Ctr copper transporter family protein	8.08	28350.07	0.247082	3	6	1	23.49
2G07970	60S ribosomal protein L19	11.46	24785.90	-1.01611	0	5	2	26.76
2G09090	Prohibitin, putative	10.02	34280.16	-0.30643	0	8	1	19.12
2G09210	60S ribosomal protein L10	10.33	25586.74	-0.53722	0	4	1	19.9
2G09290	Antigenic mitochondrial protein HSP60, putative	5.53	61949.95	-0.09949	0	4	2	38.19
2G09850	Oxidoreductase, 2-nitropropane dioxygenase family, putative (EC 1.-.-.-)	6.52	37702.48	-0.02873	0	3	1	22.69
2G10600	NADH-ubiquinone oxidoreductase 299 kDa subunit, putative (EC 1.6.5.3)	5	27541.84	-0.73595	0	4	1	20.74
2G13530	Translation elongation factor EF-2 subunit, putative	6.51	93198.10	-0.23468	0	7	4	65.38
3G05350	Histone H2B	10.12	14955.22	-0.68	0	10	1	19.72
3G05600	60S ribosomal protein L27a, putative	10.44	16761.31	-0.6349	0	10	1	21.15
3G06970	40S ribosomal protein S9	9.95	26670.60	-0.54768	0	7	1	21.49
3G07810	Succinate dehydrogenase subunit Sdh1, putative	6.5	71148.03	-0.41314	0	2	1	19.86
3G08160	ATP-dependent RNA helicase eIF4A (EC 3.6.4.13) (Eukaryotic initiation factor 4A)	5.05	45778.53	-0.20222	0	5	2	28.15
3G10730	40S ribosomal protein S7e	10.15	22844.25	-0.54677	0	20	2	23.23

CADRE ID. (AFUA_)	Protein name	tp*I*	tM_r	GRAVY score	TM	Coverage (%)	Unique peptides	SM Score
3G13320	40S ribosomal protein S0	4.81	32122.23	-0.16498	0	7	2	27.53
4G03880	60S ribosomal protein L7	9.7	34252.62	-0.56869	0	10	2	32.69
4G06910	Outer mitochondrial membrane protein porin	9.47	36893.97	-0.14029	0	3	1	18.79
4G07210	Mitochondrial acetolactate synthase small subunit, putative (EC 2.2.1.6)	6.37	35573.55	-0.18012	0	3	1	19.84
4G10800	40S ribosomal protein S6	10.84	27279.81	-0.88819	0	7	1	25.49
4G11250	Carbonic anhydrase (EC 4.2.1.1)	8.62	30827.50	-0.04355	0	10	2	36.23
4G12850	Calnexin homolog clxA	4.97	61853.81	-0.58295	1	2	1	18.98
5G01970	Glyceraldehyde-3-phosphate dehydrogenase (EC 1.2.1.12)	6.96	36314.28	-0.11124	0	20	7	106.8
5G04210	Ubiquinol-cytochrome C reductase complex core protein 2, putative (EC 1.10.2.2)	8.89	48089.24	-0.02565	0	7	2	36.31
5G06360	60S ribosomal protein L8, putative	10.97	27485.65	-0.53976	0	13	2	28.52
5G10550	ATP synthase subunit beta (EC 3.6.3.14)	5.3	55620.38	-0.07881	0	10	4	70.17
6G04740	Actin Act1	5.87	43893.19	-0.20356	0	8	2	31.59
6G06340	Glucosamine-fructose-6-phosphate aminotransferase	6.24	77286.83	-0.14813	0	1	1	18.87
6G08810	NADH-ubiquinone oxidoreductase 304 kDa subunit (EC 1.6.5.3)	9.28	38191.46	-0.47395	0	1	1	20.4

CADRE ID. (AFUA_)	Protein name	tp*I*	tM_r	GRAVY score	TM	Coverage (%)	Unique peptides	SM Score
6G13300	GTP-binding nuclear protein Ran, putative	6.91	24077.71	-0.23721	0	3	2	22.8
8G04000	Acetyl-CoA acetyltransferase, putative (EC 2.3.1.9)	6.4	40908.96	0.067588	0	4	1	18.02
8G05320	ATP synthase subunit alpha	9.14	59932.73	-0.12824	0	13	5	67.27

CADRE ID., *A. fumigatus* gene annotation nomenclature according to Nierman *et al.* (2005) and Mabey *et al.* (2004); tp*I*, theoretical isoelectric point; tM_r, theoretical molecular mass; TM, number of transmembrane regions; GRAVY score, grand average of hydropathy; SM score, Spectrum Mill protein score.

a.

(i) 30 nm AuNP with hard corona

(ii) Unbound proteins

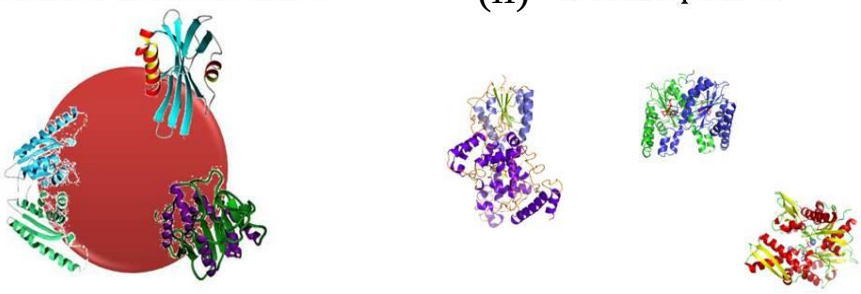

b.

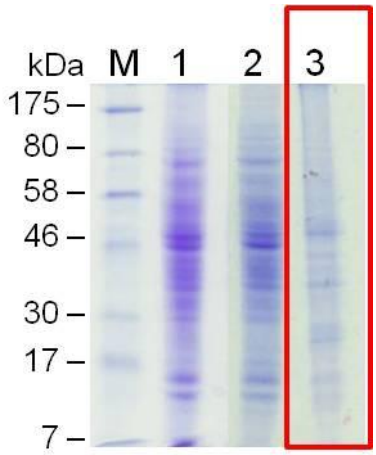

c.

FunCat Organisation of Proteins in Gold Nanoparticle Hard Corona

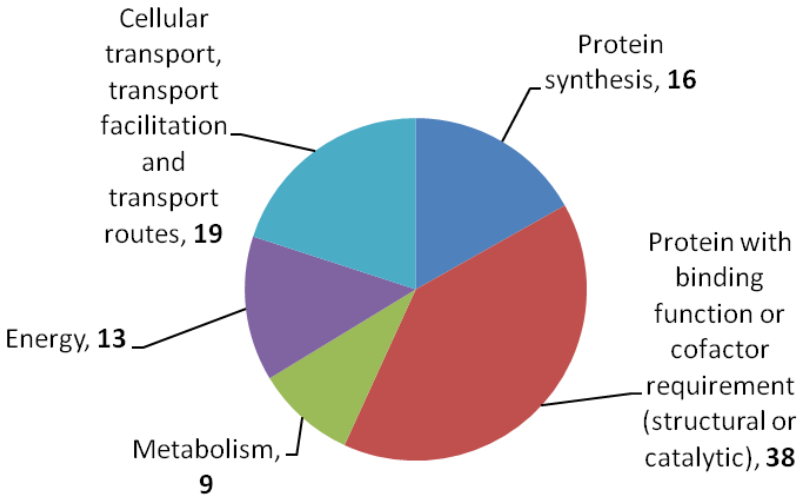

Figure 3.5: (a) Schematic representation of a (i) 30 nm colloidal AuNP (red sphere) with surrounding hard corona of adherent proteins and (ii) unbound proteins that do not adsorb to the nanoparticle surface. (b) SDS-PAGE of fractions from AuNP incubation with *A. fumigatus* mycelial proteins. M, protein marker; Lane 1, *A. fumigatus* lysate prior to AuNP incubation; Lane 2, Unbound *A. fumigatus* proteins following AuNP incubation; Lane 3, *A. fumigatus* proteins adhering to AuNP surface (hard corona). (c) The functional categorisation of *A. fumigatus* mycelial proteins (n = 43), comprising the hard corona of AuNPs, using the FunCat annoation scheme. Categories displaying a p value < 0.05, as determined by the FungiFun application (Priebe *et al.*, 2011), are shown and number of proteins with corresponding annotations are indicated in bold. Some proteins have multiple functional annotations.

3.2.5 Identification of 42 proteins from *A. fumigatus* supernatants using 1D-SDS PAGE and shotgun mass spectrometry

Supernatants from *A. fumigatus* static cultures were harvested after 1, 2 and 3 weeks of growth in AMM at 37 °C and lyophilized overnight. Dried supernatants were subjected to TCA/acetone precipitation (Section 2.2.4.10) and resultant precipitates were analysed by SDS-PAGE followed by in-gel trypsin digestion as described in Sections 2.2.4.2 and 2.2.6.1. Samples were also subjected to direct in-solution digestion, without prior SDS-PAGE, to enable shotgun mass spectrometric identification of culture supernatant proteins (Section 2.2.6.2). Tryptic peptide mixtures were analysed by LC-MS/MS and proteins were identified through database interrogation using the Spectrum Mill Workbench (Section 2.2.6.3, 2.2.7.1).

Utilising both direct (shotgun) and in-direct (SDS-PAGE) methods of sample processing, a total of 42 *A. fumigatus* proteins were identified from culture supernatants (Table 3.5). For the large scale investigation of secreted proteins, SDS-PAGE coupled with LC-MS/MS yielded more identifications (n = 39) than the shotgun mass spectrometry approach (n = 10). The culture supernatant proteins identified here spanned a theoretical pI range of 4.6 to 8.4 and a M_r range of 12 to 106 kDa. Peptides identified contributed to a sequence coverage range between 1 and 45 % of the relative proteins, with Spectrum Mill scores ranging between 18 and 300.

Functional annotations were determined for the identified supernatant proteins using the FungiFun application application (https://www.omnifung.hki-jena.de/FungiFun/) (Priebe *et al.*, 2011). Annotations were available for 76.19 %, 78.57 % and 28.57 % of identified proteins using the FunCat, GO and KEGG schemes respectively. Based on the GO classification, biological processes that were

significantly overrepresented included carbohydrate metabolic process (n = 13, p = 4.96 x 10^{-10}), proteolysis (n = 7, p = 1.45 x 10^{-6}), pathogenesis (n = 3, p = 0.0001) and polysaccharide catabolic process (n = 4, p = 0.0002). Molecular functions that were significantly represented in the sample set included hydrolase activity (n = 24, p = 4.19 x 10^{-13}) and peptidase activity (n = 4, p = 0.0016). Proteins were identified (n = 7; 16.7 %) were identified which have no functional classification using the aforementioned methods.

The relative hydrophobicity of the proteins identified was measured as outlined in Section 3.2.1. The GRAVY score was found to range from -0.6741 to 0.4203 with 9 proteins possessing positive scores (21.43 % of total supernatant proteins identified), thus indicating their hydrophobicity. Proteins with putative transmembrane regions were detected (n = 3; 7.14 %). One protein, a monosaccharide transporter (AFUA_6G03060) was detected with 12 putative TM regions and a GRAVY score of 0.4203. Interestingly, this highly hydrophobic protein was only detected using the shotgun mass spectrometry approach and not the SDS-PAGE coupled method.

An additional bioinformatics tool was utilized to characterise the proteins identified from *A. fumigatus* culture supernatants. SignalP (Petersen *et al.*, 2011) was utilized to determine that 34 (i.e. 79 %) of the proteins identified here possessed a signal peptide, that results in their secretion from the organism by classical pathways. SecretomeP (Bendtsen *et al.*, 2004) determined that an additional 5 (i.e. 12 %) of the proteins identified here are predicted to be secreted by non-classical pathways. Asp-hemolysin (Asp-HS) (AFUA_3G00590) and a unknown function protein (AFUA_6G00180) were not predicted to have a signal peptide or be secreted by a non-classical pathway, however these proteins have recently been identified in culture supernatants of *A. fumigatus* by Wartenberg *et al.* (2011) and Upadhyay *et al.* (2012),

respectively. This provides a positive validation of the techniques used here, from sample processing to verification of mass spectrometry data.

Table 3.5: *A. fumigatus* supernatant proteins (*n* = 42) identified by SDS-PAGE and shotgun mass spectrometry, arranged in order of increasing CADRE ID.

CADRE ID. (AFUA_)	Protein name	tp*I*	tM_r	GRAVY score	TM	Coverage (%)	Unique peptides	SM Score	SigP/ SecP
1G00980[a,b]	FAD-dependent oxidase, putative (EC 1.5.3.-)	6.76	53642.92	-0.0119	0	26	12	208.07	SigP
1G10790[a]	Alpha-1,2-mannosidase family protein, putative	5.97	92750.47	-0.36043	0	4	2	38.19	SigP
1G14560[a,b]	Probable mannosyl-oligosaccharide alpha-1,2-mannosidase 1B (EC 3.2.1.113) (Class I alpha-mannosidase 1B) (Man(9)-alpha-mannosidase 1B)	5.09	53840.28	-0.22495	0	37	16	299.83	SigP
1G16190[a]	Probable glycosidase crf1 (EC 3.2.-.-) (Crh-like protein 1) (allergen Asp f 9)	4.6	40283.87	-0.26076	0	6	2	33.67	SigP
1G16420[a]	GPI anchored protein	5.34	58557.10	-0.30918	0	6	2	35.71	SigP
1G17410[a]	Probable beta-glucosidase M (EC 3.2.1.21) (Beta-D-glucoside glucohydrolase M) (Cellobiase M)	5.14	82681.18	-0.2736	0	4	3	47.28	SigP
2G00690[a]	Glucoamylase (EC 3.2.1.3) (1,4-alpha-D-glucan glucohydrolase) (Glucan 1,4-alpha-glucosidase)	5.04	67100.35	-0.10301	0	27	11	178.22	SigP
2G03980[a]	Alpha-1,3-glucanase/mutanase, putative (EC 3.2.1.-)	4.98	54022.65	-0.2123	0	9	3	54.06	SigP
2G09030[a]	Dipeptidyl-peptidase 5 (EC 3.4.14.-) (Dipeptidyl-peptidase V) (DPP V) (DppV)	5.59	79744.94	-0.41956	0	4	3	44.37	SigP
2G11340[b]	Phosphatidylglycerol/phosphatidylinositol transfer protein (PG/PI-TP)	5.56	27290.30	-0.0125	0	4	1	18.8	SecP

CADRE ID. (AFUA_)	Protein name	tp*I*	tM_r	GRAVY score	TM	Coverage (%)	Unique peptides	SM Score	SigP/ SecP
2G12630[a,b]	Allergen Asp f 15 (Allergen Asp f 13) (allergen Asp f 15)	4.61	15943.84	-0.09408	0	15	2	38.33	SigP
2G16720[a]	DUF1237 domain protein	5.94	61508.47	-0.28444	0	14	5	85.7	SigP
3G00270[a]	Probable glucan endo-1,3-beta-glucosidase eglC (EC 3.2.1.39) (Endo-1,3-beta-glucanase eglC)	4.9	44651.21	0.064126	1	10	3	60.34	SigP
3G00320[a]	Endo-1,4-beta-xylanase xynf11a (Xylanase xynf11a) (EC 3.2.1.8) (1,4-beta-D-xylan xylanohydrolase xynf11a)	6.27	24493.69	-0.36096	0	11	2	30.86	SigP
3G00590[a,b]	Asp-hemolysin (Asp-HS)	5.29	15198.64	-0.6741	0	45	7	111.53	-
3G00840[a]	FAD-dependent oxygenase, putative	6.52	55026.25	-0.16785	0	26	10	182.58	SigP
3G01130[a,b]	Cell wall protein	4.8	19272.88	0.006667	0	10	2	33.27	SigP
3G02970[a]	Aspergillopepsin, putative (EC 3.4.23.-)	5.02	28013.98	-0.03717	0	10	2	31.69	SigP
3G03060[a]	Cell wall protein PhiA	5.2	19406.49	-0.19514	0	34	3	57.7	SigP
3G03080[a]	Endo-1,3(4)-beta-glucanase, putative (EC 3.2.1.6)	5.09	31087.62	-0.20456	0	27	7	135.29	SigP
4G03240[b]	Cell wall serine-threonine-rich galactomannoprotein Mp1	4.66	27361.21	0.178169	0	4	2	39.53	SigP
4G03490[a]	Tripeptidyl-peptidase sed2 (EC 3.4.14.-) (Sedolisin-B)	5.3	65838.74	-0.36777	0	1	1	20.59	SigP
4G03660[a]	Acid phosphatase, putative (EC 3.1.3.2)	5.94	46131.72	-0.34758	0	12	4	64.95	SigP
4G09030[a]	Aminopeptidase (EC 3.4.11.7)	6.31	106226.80	-0.27671	0	1	1	22.85	SecP

CADRE ID. (AFUA_)	Protein name	tp*I*	tM_r	GRAVY score	TM	Coverage (%)	Unique peptides	SM Score	SigP/ SecP
4G11800[a]	Oryzin (EC 3.4.21.63) (Alkaline proteinase) (ALP) (Elastase) (Elastinolytic serine proteinase)	6.31	42190.12	-0.1129	0	25	8	139.76	SigP
4G13750[a]	Penicillolysin/deuterolysin metalloprotease, putative (EC 3.4.-.-)	5.71	39404.88	-0.17297	0	11	3	63.45	SigP
4G13770[a]	Glycosyl hydrolase, putative (EC 3.-.-.-)	5.14	36755.60	0.085028	0	29	6	102.6	SigP
5G01200[a]	Carboxypeptidase S1, putative (EC 3.4.16.6)	4.84	54122.23	-0.33873	0	18	6	108.44	SigP
5G01990[a]	BYS1 domain protein, putative	4.8	16026.11	0.102564	0	11	1	21.46	SigP
5G02040[a]	Extracellular lipase, putative (EC 3.1.1.3)	5.59	31443.21	0.110368	0	13	4	84.65	SigP
5G02100[a,b]	Unknown function protein	5.13	29461.30	-0.65358	0	20	6	115.73	SecP
5G02130[a]	Probable alpha-galactosidase B (EC 3.2.1.22) (Melibiase B)	5.1	47214.90	-0.39296	0	15	4	68.46	SecP
5G03540[a]	Thioredoxin reductase, putative (EC 1.-.-.-)	6.99	42850.34	-0.44482	0	2	1	18.01	SigP
6G00180[a]	Unknown function protein	8.41	12131.63	-0.33578	1	31	2	38.96	-
6G00430[a]	IgE-binding protein	4.66	20487.89	0.0735	0	6	1	19.14	SecP
6G03060[b]	MFS monosaccharide transporter, putative	6.37	58272.82	0.420339	12	4	1	19.08	-
6G10130[a]	N,O-diacetyl muramidase, putative (EC 3.2.1.-)	6.02	24639.35	-0.16316	0	7	1	23.6	SigP
6G13270[a]	Exo-beta-1,3-glucanase, putative (EC 3.2.1.58)	5	84183.57	-0.01182	0	25	14	270.43	SigP

CADRE ID. (AFUA_)	Protein name	tp*I*	tM_r	GRAVY score	TM	Coverage (%)	Unique peptides	SM Score	SigP/ SecP
7G05140[a]	Class III chitinase, putative (EC 3.2.1.14)	4.89	46234.54	0.034152	0	7	2	36.78	SigP
7G06140[a]	Probable beta-glucosidase L (EC 3.2.1.21) (Beta-D-glucoside glucohydrolase L) (Cellobiase L)	5.65	78381.15	-0.16482	0	13	6	106.79	SigP
8G01410[a,b]	Chitinase (Class V chitinase ChiB1) (EC 3.2.1.14)	5.03	47622.12	-0.33418	0	41	11	218.09	SigP
8G07120[a]	Beta-1,6-glucanase Neg1, putative (EC 3.2.1.-)	5.51	51430.21	-0.17254	0	17	6	113.66	SigP

CADRE ID., *A. fumigatus* gene annotation nomenclature according to Nierman *et al.* (2005) and Mabey *et al.* (2004); tp*I*, theoretical isoelectric point; tM_r, theoretical molecular mass; TM, number of transmembrane regions; GRAVY score, grand average of hydropathy; SM score, Spectrum Mill protein score; SigP, presence of a signal peptide for secretion by classical pathways; SecP, indicates protein is secreted by non-classical pathways.

[a]Protein was identified following SDS-PAGE coupled with LC-MS/MS; [b]Protein was identified by shotgun mass spectrometry.

3.3 Discussion

An extensive investigation of the *A. fumigatus* intracellular and extracellular proteome was undertaken using a combination of SDS-PAGE, gel filtration and shotgun mass spectrometry. This Chapter outlines a global proteomics approach, which was carried out using alternative methods to those classically used for mapping the proteome of *A. fumigatus* mycelia, such as 2D-PAGE coupled with mass spectrometry (Carberry *et al.*, 2006; Kniemeyer *et al.*, 2006; Vödisch *et al.*, 2009; Teutschbein *et al.*, 2010). Utilising the methods outlined in this Chapter a total of 427 unique *A. fumigatus* mycelial and secreted proteins were identified. Proteins identified from the mycelia of *A. fumigatus* ATCC26933, after 48 h in AMM, totalled 390, while 42 proteins were identified from the culture supernatants of extended static cultures in AMM.

The utilisation of shotgun proteomics in this large scale investigation has enabled the identification of a number of proteins that are typically difficult to resolve using 2D-PAGE. High molecular mass proteins, hydrophobic proteins and proteins with transmembrane regions are generally under-represented in 2D-PAGE studies, due to their incompatibility with the isoelectric focusing stage or limited separation by SDS-PAGE (Harder *et al.*, 1999; Rabilloud, 2009). The standard molecular mass resolution of *A. fumigatus* mycelia proteins, using 2D-PAGE, ranges from 10 to 142 kDa (Carberry *et al.*, 2006; Kniemeyer *et al.*, 2006; Vödisch *et al.*, 2009). The constraint of large molecular mass did not apply to the shotgun proteomic approach used in this study, with the identification of 10 proteins possessing a molecular mass greater than 142 kDa. The largest protein detected was PesO, a hybrid polyketide synthase/ non-ribosomal peptide synthetase (PKS/NRPS) (AFUA_8G00540), with a theoretical molecular mass of 434 kDa. A total of 73 unique peptides were identified from this protein contributing to a sequence coverage of 28 %. *A. fumigatus pesO* has been

previously investigated in targeted and global transcriptomic studies (Da Silva Ferreira *et al.*, 2006; Lee *et al.*, 2009a; Vödisch *et al.*, 2011). PesO, the only hybrid PKS/NRPS in the *A. fumigatus* genome, is involved in the production of pseurotin A (Maiya *et al.*, 2007) and its identification provides evidence of expression of this secondary metabolite cluster. A 267 kDa polyketide synthase (AFUA_8G00370) was also identified by 10 unique peptides, contributing to 10% sequence coverage. These findings represent some of the largest *A. fumigatus* proteins to be identified by mass spectrometry to date. A study by Cagas *et al.* (2011b) utilised isobaric tagging for relative and absolute quantitation (iTRAQ) in order to profile the early development proteome of *A. fumigatus*. This gel-free method of large scale proteomic identification extended the molecular mass limits of detection to 9 to 255 kDa. More recently, Wiedner *et al.* (2012) introduced the use of chemical probes, to discern between active and inactive enzymes, coupled with quantitative MS. This study further expanded the identification of large molecular mass proteins in *A. fumigatus*, confirming the value of alternative methods for proteomic investigation.

Proteins with extended hydrophobic regions are difficult to analyse by 2D-PAGE due to their low water solubility and resulting incompatibility with the conditions used in isoelectric focusing (Rabilloud, 2009). This has resulted in the majority of recent *A. fumigatus* membrane investigations being carried out utilising SDS-PAGE coupled with mass spectrometry or gel-free iTRAQ (Ouyang *et al.*, 2010; Cagas *et al.*, 2011a). In contrast, proteomic analysis of *A. fumigatus* mycelia is dominated by the use of 2D-PAGE coupled with mass spectrometry (Carberry *et al.*, 2006; Kniemeyer *et al.*, 2006; Vödisch *et al.*, 2009). These studies have yielded large volumes of information on the mycelial proteome of *A. fumigatus*, however the limitations of 2D-PAGE have hindered the identification of hydrophobic proteins and proteins with multiple

transmembrane regions from these fractions. A comprehensive mycelial proteome reference map, produced by Vödisch *et al.* (2009), identified proteins with a GRAVY score up to 0.158 and fourteen proteins with 1-2 putative TM regions. This correlates to 4.2 %, of the total identified proteins, possessing TM regions. Here, in comparison, 37 proteins possessing predicted TM domains were identified from the mycelia of *A. fumigatus*, corresponding to 10 % of the total proteins identified using shotgun mass spectrometry alone (Figure 3.2). This represents a substantial increase (2.4 fold) in the identification of proteins with TM regions, compared to previous 2D-PAGE based studies with similar targets (Vödisch *et al.*, 2009). A small oligopeptide transporter, OPTB (AFUA_2G15240), was identified, which is predicted to contain 14 TM helices. While the differential regulation of the transcript of the *optB* gene has been reported previously (Da Silva Ferreira *et al.*, 2006; Hartmann *et al.*, 2011), this represents the first identification of the gene product at the protein level. Analysis of the entire *A. fumigatus* proteome predicts up to 24 % of total proteins with at least one TM helix (Vödisch *et al.*, 2009), and so under-identification of these proteins can result in disparity in the interpretation of the proteome under various conditions. This case is also mirrored in the identification of hydrophobic proteins, based on positive GRAVY scores. Using the shotgun proteomics approach 28 hydrophobic proteins, corresponding to 7.6 % of total identified proteins, were detected, including a protein transport protein SEC61 alpha subunit (AFUA_5G08130) with a GRAVY score of 0.4828. With 3.4 % of mycelia proteins, identified in the 2D-PAGE proteome map of Vödisch *et al.* (2009), possessing positive GRAVY scores, this too represents a significant improvement on the gel based methods of proteome investigation.

Functional classification of proteins identified by shotgun mass spectrometry revealed that categories describing (i) protein synthesis, (ii) energy, (iii) protein with

binding function or cofactor requirement, (iv) transcription and (v) cell cycle and DNA processing were significantly represented in the data set. Identification of a large number of ribosomal proteins (n = 48) (Figure 3.6) accounts for the high representation of the protein synthesis and the protein with binding or cofactor requirement functional categories. Despite their abundance in the cell (Warner, 1999), detection of ribosomal proteins by 2D-PAGE may be limited due the highly basic or acidic nature of these proteins and the relative low molecular mass of the subunits. Vödisch *et al.* (2009) identified 11 ribosomal proteins during the compilation of the mycelial proteome reference map of *A. fumigatus* while no ribosomal proteins were detected in earlier proteome maps (Carberry *et al.*, 2006; Kniemeyer *et al.*, 2006). Of the ribosomal proteins identified by shotgun mass spectrometry, 42 exhibited a p$I \geq 8.59$ and the remainder, described as acidic subunits displayed a p$I \leq 5.74$. All identified ribosomal proteins had a molecular mass ≤ 44 kDa, with 87.5 % having a M_r < 30 kDa. KEGG pathway mapping allows visualisation of the ribosomal proteins identified and their respective localisation in either the large (60S) or the small (40S) ribosomal subunits (Figure 3.6).

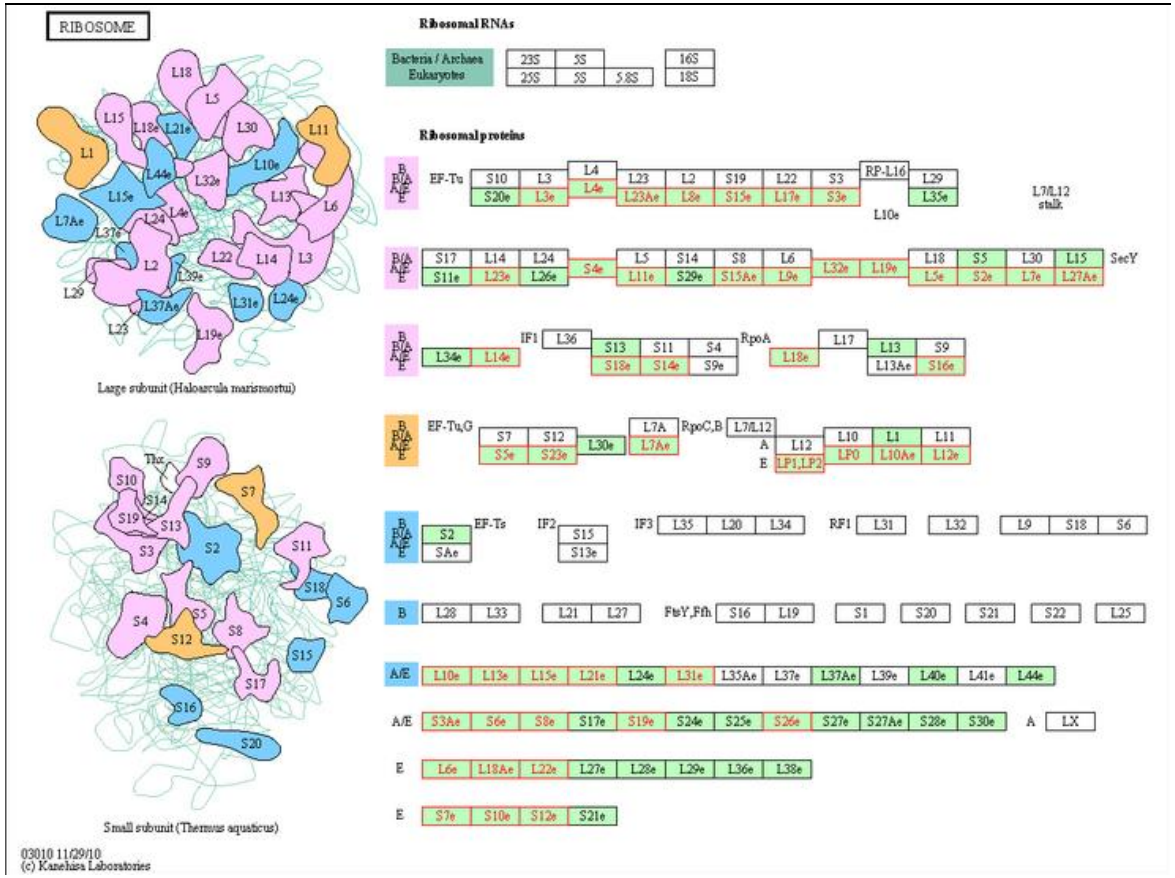

Figure: 3.6: *A. fumigatus* ribosomal proteins identified by shotgun mass spectrometry. Green boxes represent ribosomal proteins that have been annotated in *A. fumigatus* according to KEGG pathways (Kanehisa *et al.*, 2012). Boxes with red font and border represent proteins that were identified in this study.

The functional category describing proteins involved in energy metabolism or transfer was also significantly represented from the sample set of proteins identified by shotgun mass spectrometry (n = 86; p = 6.95e-18). The majority of the enzymes constituting the citrate cycle (TCA) were detected (Figure 3.7), in addition to proteins involved in electron transport and energy generation by ATP synthases. This observation reflects the growth on glucose as a sole carbon source, whereby glycolysis provides a substrate for the TCA cycle which in turn generates energy via the electron transport chain. Enzymes were also identified that are involved in the pentose phosphate pathway, an alternative route for glucose oxidation which can produce intermediate pentoses used in the biosynthesis of nucleic acids or aromatic amino acids. These enzymes included 6-phosphogluconate dehydrogenase (AFUA_6G08050) which is responsible for the metabolism of 6-phospho-D-gluconate, a derivative of glucose, to D-ribulose 5-P (Maaheimo *et al.*, 2001). Following the conversion of ribulose-5-P to D-xylulose 5-P, transketolase TktA (AFUA_1G13500) catalyses the production of sedoheptulose 7-P and fructose 6-P in separate reactions (Kleijn *et al.*, 2005). Sedoheptulose 7-P can then be metabolised to D-erythrose 4-P, an amino acid precursor, by transaldolase (AFUA_5G09120) (Schaaff *et al.*, 1990).

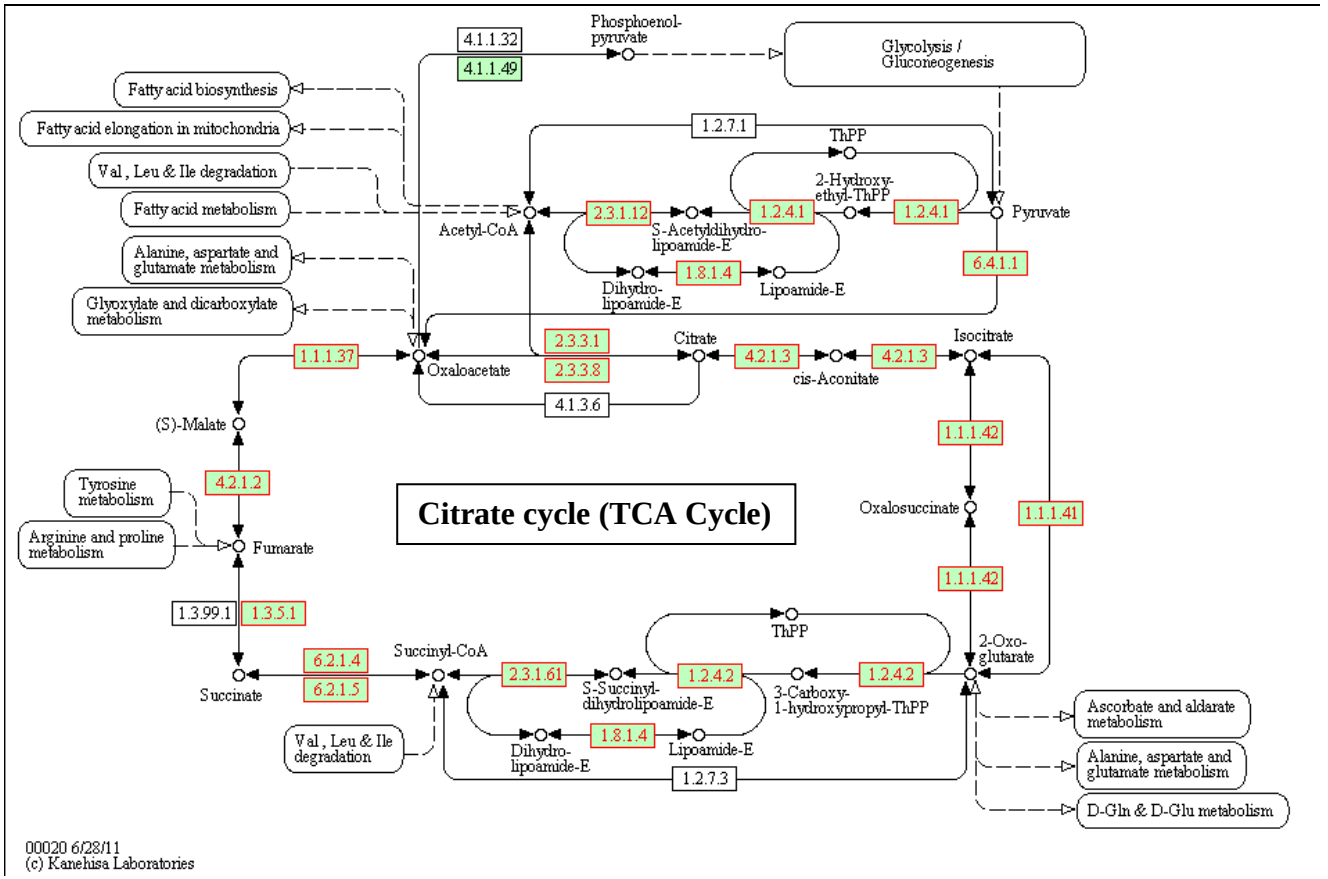

Figure 3.7: *A. fumigatus* proteins identified by shotgun mass spectrometry, involved in the TCA cycle. Green boxes represent proteins that have been annotated in *A. fumigatus* according to KEGG pathways (Kanehisa *et al.*, 2012). Boxes with red font and border represent proteins that were identified in this study.

A number of proteins (n = 21) were identified by shotgun proteomics with no functional annotation, based on FunCat, GO and KEGG annotation, using the FungiFun application (https://www.omnifung.hki-jena.de/FungiFun/) (Priebe *et al.*, 2011). Many of these proteins were annotated as hypothetical proteins (AFUA_1G02290, AFUA_1G09130, AFUA_2G02490, AFUA_3G00730, AFUA_3G06460, AFUA_3G08440, AFUA_3G14665, AFUA_5G14680, AFUA_6G10450, AFUA_8G00400, AFUA_8G00430, AFUA_8G04890, and AFUA_8G05600) and can now be reclassified as unknown function proteins (UFPs) as a result of the biochemical verification of their translation. Other proteins with unknown functions identified by shotgun mass spectrometry include high expression lethality protein (Hel10) (AFUA_1G06580), PT repeat family protein (AFUA_2G17000), conserved lysine-rich protein (AFUA_4G12450), DUF 89 domain protein (AFUA_5G06710), cipC-like antibiotic response protein (AFUA_5G09330), CFEM domain protein (AFUA_6G06690), M protein repeat protein (AFUA_6G08660) and dltD N-terminal domain protein (AFUA_8G00380).

Additional bioinformatics analysis, using the program BLAST2GO, enabled the putative functional annotation of some of these proteins based on sequence homology to proteins on the NCBI database (http://www.blast2go.com/b2glaunch/start-blast2go) (Conesa *et al.*, 2005). The unknown function protein (AFUA_2G02490) was re-annotated by this method as a putative glutamineamidotransferase subunit pdxT, with predicted nucleotide binding and transferase activities. Similarly the unknown function proteins (AFUA_1G109130, AFUA_1G02290 and AFUA_3G00730) were re-annotated as putative transcription factor Btf3, cyanovirin-n family protein and a glutathione s-transferase, respectively. The remaining proteins retained their original sequence descriptions, however GO identifications were assigned to a number of proteins based

on sequence homology. The unknown function protein (AFUA_8G00400) was predicted to have O-methyltransferase activity and this could allude to its function as part of the secondary metabolite cluster on Chromosome 8 (Perrin *et al.*, 2007). The M protein repeat protein was assigned GO identifications indicating its involvement in signal transduction and a localisation designating it as integral to the membrane. The DUF89 domain protein (AFUA_5G06710) was denoted putative molecular functions of protein serine/threonine phosphatase activity and metal ion binding. The conserved lysine-rich protein (AFUA_4G12450) was deemed to have protein and phospholipid binding activity, while the PT repeat family protein (AFUA_2G17000) was annotated with hydrolase and peptidase activity. This study is the first report to date on the unknown function proteins (AFUA_2G02490, AFUA_3G14665, AFUA_8G04890), PT repeat family protein and DUF 89 domain protein, with many others accounted for at the transcript level only (Sheppard *et al.*, 2005; da Silva Ferreira *et al.*, 2006; Twumasi-Boateng *et al.*, 2009). These proteins represent targets for future functional genomic or comparative proteomic projects to elucidate their role in the fungal cell (Doyle, 2011b).

Verification of the transcription and translation of genes found in secondary metabolite clusters was achieved in this study using shotgun mass spectrometry. Proteins identified are putatively found in six clusters, involved in the production of up to eight secondary metabolites (SM) (Perrin *et al.*, 2007). Products of these SM clusters include up to 4 unknown metabolites, fumitremorgin B (Grundmann and Li, 2005; Maiya *et al.*, 2006), pseurotin A (Maiya *et al.*, 2007), gliotoxin (Gardiner and Howlett, 2005) and a putative ETP (Patron *et al.*, 2007) (Figure 3.8). Perrin *et al.* (2007) annotated a ‘supercluster’ on Chromosome 8 (AFUA_8G00100-AFUA_8G00720) that is involved in the production of fumitremorgin B, pseurotin A and possibly an additional unknown metabolite (Grundmann and Li, 2005; Maiya *et al.*, 2007). Fourteen

proteins identified by shotgun mass spectrometry are annotated members of this 'supercluster', with one identified protein involved in fumitremorgin B production, four proteins involved in the pseurotin A biosynthetic portion of the cluster and the remaining nine proteins forming part of the cluster producing an unknown metabolite.

Phytanoyl-CoA dioxygenase family protein (FtmF) (AFUA_8G00230) was identified by 3 unique peptides and a sequence coverage of 14 %. FtmF, a non-heme Fe (II) and α-ketoglutarate-dependent dioxygenase, catalyses the conversion of fumitremorgin B to verruculogen via endoperoxide bond formation (Steffan *et al.*, 2009). This enzyme is also capable of conversion of fumitremorgin B to 12α, 13α-dihydroxyfumitremorgin C and 13-oxo-verruculogen, by deprenylation and oxidation mechanisms respectively (Kato *et al.*, 2011). Verruculogen, like fumitremorgin B, is a tremorgenic mycotoxin and has been shown to produce deleterious effects on respiratory epithelial cells (Khoufache *et al.*, 2007). The observation of the FtmF enzyme suggests the production of fumitremorgin B by *A. fumigatus* under the conditions of culture and its subsequent conversion to verrulculogen.

Pseurotin A is another metabolite produced by the 'supercluster' on Chromosome 8 (Figure 3.8) (Maiya *et al.*, 2007). Four enzymes, that form part of the pseurotin biosynthetic cluster, were detected here; an alpha/beta hydrolase (AFUA_8G00530), a hybrid PKS-NRPS enzyme PesO (AFUA_8G00540), a methyltransferase SirN-like (AFUA_8G00540) and a putative glutathione S-transferase (AFUA_8G00580) (Carberry *et al.*, 2006). This cluster has demonstrated increased expression at both the transcript and protein level under hypoxic conditions (Vödisch *et al.*, 2011). Furthermore, up-regulation of the methyltransferase and hybrid PKS-NRPS transcripts was also shown in the mouse lung during experimental aspergillosis (Vödisch *et al.*, 2011). As discussed earlier, the hybrid PKS-NRPS, a 434 kDa protein,

was identified and represents one of the largest proteins detected by MS in *A. fumigatus* to date.

The final section of the Chromosome 8 'supercluster' is hypothesised to produce a secondary metabolite, however this molecule has remained unidentified. Genes predicted to form this cluster span from AFUA_8G00300 to AFUA_8G00520 and nine of the corresponding proteins were identified by shotgun mass spectrometry, providing strong evidence of the production of this unknown metabolite under the conditions utilised here (i.e. minimal media, 37 °C, 200 rpm, dark, 48 h). Vödisch *et al.* (2011) identified two of these proteins, a steroid monooxygenase (AFUA_8G00440) and an unknown function protein (AFUA_8G00430), with significant upregulation under hypoxic growth conditions. This may suggest the uncharacterised metabolite could be a putative virulence factor, as cluster expression is up-regulated in conditions that reflect the hypoxic *in vivo* environment. Indeed, transcript expression of six of the proteins identified from this cluster was up-regulated in *A. fumigatus* Af293 during the initiation of murine infection (McDonagh *et al.*, 2008) (Table 3.6).

Table 3.6: Differential regulation of a secondary metabolite cluster on Chromosome 8 in *A. fumigatus* Af293 during initiation of murine infection

New Accessions	Protein Names	Expression ratio
AFUA_8G00360	NlpC/P60-like cell-wall peptidase, putative	5.6821133
AFUA_8G00370	polyketide synthase, putative	5.149378699
AFUA_8G00390	O-methyltransferase, putative	4.448825474
AFUA_8G00420	C6 finger transcription factor, putative	4.824826376
AFUA_8G00430	conserved hypothetical protein	4.777625406
AFUA_8G00440	steroid monooxygenase, putative	3.650200403
AFUA_8G00480	phytanoyl-CoA dioxygenase family protein	4.994227345
AFUA_8G00490	PKS-like enzyme, putative	4.744191198
AFUA_8G00500	acetate-CoA ligase, putative	7.309815039
AFUA_8G00520	integral membrane protein	8.686607449

Differential expression of genes during initiation of murine infection was depicted by a colour scale of red (up-) to green (down-regulation). Proteins identified by shotgun proteomics are surrounded by a red box. New Accessions., *A. fumigatus* gene annotation nomenclature according to Nierman *et al.* (2005) and Mabey *et al.* (2004). From McDonagh *et al.* (2008), supplementary table 6.

GliT (AFUA_6G09740), a member of the gliotoxin biosynthesis cluster located on Chromosome 6 (Gardiner and Howlett, 2005), is responsible for the oxidation and reduction of the disulphide bridge of gliotoxin. This provides a key component of the biosynthetic process and also mediates self-protection against the harmful effects of gliotoxin (Scharf *et al.,* 2010; Schrettl *et al.,* 2010). Gliotoxin belongs to the epipolythiodioxopiperazine (ETP) class of toxins, whose toxicity is mediated by an internal disulfide bridge (Patron *et al.*, 2007). Identification of GliT in mycelia extracts suggests this cluster is active and work carried out in Chapter 6 confirms the presence of gliotoxin in culture supernatants using the conditions described here.

Zn-dependent hydrolase/oxidoreductase family protein (AFUA_3G13010), identified here, belongs to a cluster that may putatively produce an additional ETP in *A.fumigatus* (Patron *et al.,* 2007; Perrin *et al.,* 2007). Patron *et al.* (2007) identified this second ETP cluster, which does not contain the full suite of genes found in the gliotoxin biosynthetic cluster (Figure 3.8). Crosstalk between the ETP clusters on Chromosomes 3 and 6 could potentially be required for the production of this second ETP from *A. fumigatus*. Three additional proteins were identified, that are associated with secondary metabolite clusters on Chromosomes 3 and 4. Phosphoglycerate kinase PgkA (AFUA_1G10350) was identified in this study and forms part of a cluster that includes the NRPS, Pes1 (AFUA_1G10380) (Nierman *et al.,* 2005). This NRP synthethase has recently been linked to the production of fumigaclavine C (O'Hanlon *et al.,* 2012), an ergot alkaloid, and PgkA could also be involved in the biosynthetic process of this metabolite. A putative glutathione S-transferase (AFUA_4G14380) was identified from a cluster on Chromosome 4 with an unknown product. Lysophospholipase 3 (AFUA_3G14680) and an unknown function protein (AFUA_3G14665) were also detected and form part of a cluster with an unidentified product.

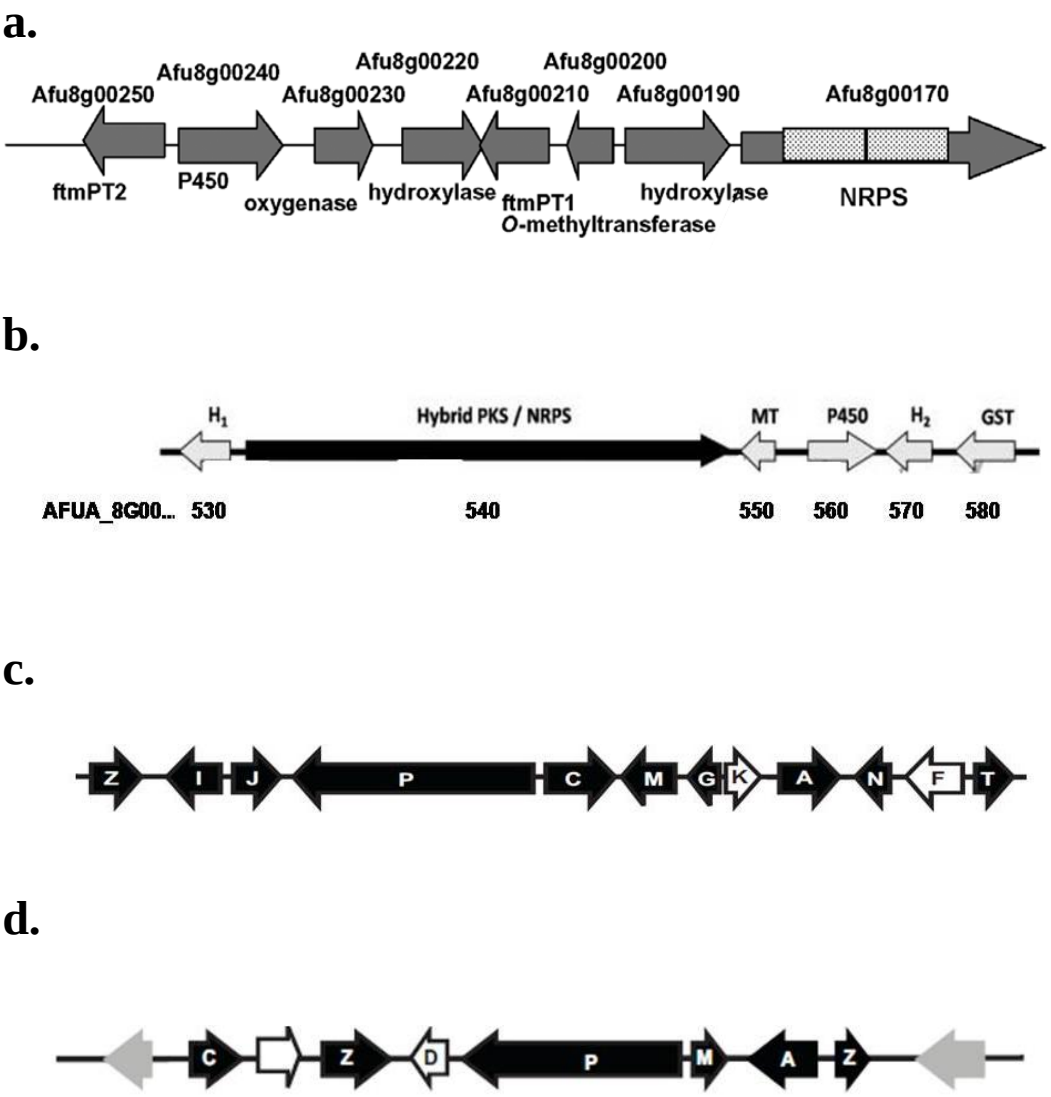

Figure 3.8: Arrangement of genes in *A. fumigatus* secondary metabolite clusters that produce (a) fumitremorgin B, (b) pseurotin A, (c) gliotoxin and (d) a putative ETP. *A. fumigatus* gene annotation nomenclature according to Nierman *et al.* (2005) and Mabey *et al.* (2004). Adapted from (a) Maiya *et al.* (2006), (b) Vödisch *et al.* (2011), (c) and (d) Patron *et al.* (2007).

A noteworthy observation is that expression of all of the clusters, identified here by mass spectrometry, is either partially or fully regulated by LaeA (Perrin *et al.*, 2007). LaeA (AFUA_ 1G14660) is a global transcriptional regulator of secondary metabolite clusters (Bok and Keller, 2004; Bok *et al.*, 2005; Perrin *et al.*, 2007) and its disruption results in reduced virulence. McDonagh *et al.* (2008) identified a number of LaeA regulated secondary metabolite genes that are induced during the initiation of murine invasive aspergillosis, including pseurotin A and gliotoxin. This highlights the importance of LaeA directed regulation to the success of *A. fumigatus* as a pathogen.

In an attempt to reduce the complexity of the *A. fumigatus* mycelial protein lysates, gel filtration chromatography was performed prior to in-solution digestion of size fractionated samples and shotgun mass spectrometry. While this pre-fractionation approach did not yield as many proteins identifications as shotgun proteomics alone (173 and 370 protein identifications, respectively), seventeen unique proteins were detected that had not be observed using the shotgun mass spectrometry method alone. The proteins identified using gel filtration coupled shotgun mass spectrometry spanned a similar range of molecular mass and p*I*, demonstrating that these factors were not limited by the addition of the pre-fractionation step. Similarly, hydrophobic proteins and proteins with up to 12 transmembrane regions were detected signifying that these attributes were compatible with the addition of the size exclusion step. Interestingly, five of the unique proteins, identified using gel filtration pre-fractionation, are involved in stress response as denoted by the FunCat classification scheme. Telomere and ribosome associated protein, Stm1 (AFUA_3G10920), is predicted to be involved in apoptosis-like cell death in response to oxidative stress, based on homology to the yeast Stm1 protein (Ligr *et al.*, 2001). The *A. nidulans* ortholog of the phosphotransmitter protein, Ypd1 (AFUA_4G10280), is part a signalling pathway that regulates osmotic

stress response (Furukawa *et al.*, 2005). The putative heat shock protein, Sti1 (AFUA_7g01860), was also identified and expression of this protein has been shown to be up-regulated following amphotericin B treatment of *A. fumigatus in vitro* (Gautam *et al.*, 2008). Thioredoxin, TrxA (AFUA_5G11320), is predicted to be involved in the oxidative stress response based on homology the *A. nidulans* TrxA protein (Thön *et al.*, 2007). Finally, a calnexin homolog, ClxA (AFUA_4G12850), is necessary for growth in thermal, nutrient and endoplasmic reticulum stress. Identification of protein expression from stress response pathways is valuable as these could present potential therapeutic targets. In order, to expand the number of proteins identified using this pre-fractionation technique a number of adjustments could be made. Possible improvements to this methodology include the use of a number of gel filtration columns arranged in a series for improved separation and resolution (Gordon *et al.*, 2010), or the use of extended gradients during liquid chromatography.

The *A. fumigatus* mycelial protein corona of gold nanoparticles was investigated using SDS-PAGE coupled with LC-MS/MS. A total of 43 proteins were found to interact strongly with the surfaces of the 30 nm colloidal gold nanoparticles (AuNPs) (Table 3.4). This 'affinity' purification enabled the identification of three additional mycelial proteins that were not detected by either shotgun proteomics alone or gel-filtration coupled shotgun mass spectrometry. One of these unique proteins was a mitochondrial acetolactate synthase small subunit (AFUA_4G07210) that shows induction during hypoxia (Vödisch *et al.*, 2011). A prohibitin (AFUA_2G09090) was identified, that has been detected in the germ-tubes of *A. fumigatus* (Suh *et al.*, 2012), and Ctr copper transporter family protein (AFUA_2G03730) has not been detected at the protein level previously. A note-worthy observation is that a significant majority of proteins identified (n = 38, 88.4 %, p = 1.18e-7) were classified as having a binding

function or co-factor requirement according to FunCat annotation. This demonstrates a potential method by which samples can be enriched for proteins from this functional category. A recent review by Kniemeyer *et al.* (2011) has collated all of the *A. fumigatus* proteomics data generated to that point and has reported that 18.5 % of all proteins identified, with FunCat annotations, fall into the category of protein with binding function or cofactor requirement. Taking this into account, this method could conversely be used to reduce the dynamic range of complex lysates by the removal of these proteins.

Several studies have been carried out to explore the *A. fumigatus* secretome using a variety of growth substrates and proteomic methodologies (Gautam *et al.*, 2008; Singh *et al.*, 2010a; Kumar *et al.*, 2011; Wartenberg *et al.*, 2011). Here, two proteomic strategies were utilised to obtain maximum characterisation of the *A. fumigatus* secretome; (i) SDS-PAGE coupled with mass spectrometry and (ii) in-solution digestion and shotgun mass spectrometry. The former approach yielded 39 *A. fumigatus* protein identifications while the latter detected 10 proteins (Table 3.5). Seven proteins were detected using both methods described, resulting in a total of 42 *A. fumigatus* extracellular proteins being identified. These proteins were analysed to determine whether they contained a signal peptide for secretion or whether they were part of a non-classical secretion pathway using the programs SignalP and SecretomeP respectively (Bendtsen *et al.*, 2005; Petersen *et al.*, 2011). This analysis revealed that 34 of the extracellular proteins identified possessed a signal peptide while 5 were predicted to be involved in a non-classical secretion pathway.

Functional characterisation of the extracellular proteins identified, based on FunCat annotation, revealed a significant representation of proteins involved in C-compound and carbohydrate metabolism (n = 19; p = 1.48 x 10^{-5}), as expected based on

its growth on glucose. Interestingly, despite growth on a minimal media with glucose as a sole carbon and energy source, a number of enzymes involved in protein/peptide degradation (n = 8, p = 7.5 x 10^{-4}) were present. Six proteins were detected, with no FunCat, GO or KEGG functional annotations and these proteins were analysed further to assign putative functions based on sequence homology using the BLAST2GO program (Conesa *et al.*, 2005). Only one of these proteins was assigned a GO annotation following this analysis, with methyltransferase activity predicted for the GPI anchored protein (AFUA_1G16420). With these limitations of systems-based functional predictions, molecular and biochemical methods will need to be implemented to elucidate the functions of these proteins and the biological processes in which they are involved.

A number of proteins, identified in the analysis of the secretome, have not been reported yet in the literature, including a FAD-dependent oxidase (AFUA_1G00980), alpha-1,2-mannosidase family protein (AFUA_1G10790), a GPI anchored protein (AFUA_1G16420), a cell wall protein (AFUA_3G01130) and a thioredoxin reductase (AFUA_5G03540). In addition several other proteins were described at the transcript level previously but no protein identification had been achieved until now. Consequently, analysis of the *A. fumigatus* secretome has verified both the translation of these gene products and also confirmed the localisation of the resultant proteins. This information may aid in future studies to confirm the functions of these extracellular proteins.

A number of proteins (n = 5) were identified from both mycelial and culture supernatant sources including the allergen Asp f9 (AFUA_1G16190), a phosphatidylglycerol/phosphatidylinositol transfer protein (PG/PI-TP) (AFUA_2G11340), an endo-1,3-beta-glucanase (EglC) (AFUA_3G00270), an

aminopeptidase (AFUA_4G09030) and a thioredoxin reductase (AFUA_5G03540). Aspf9, a well defined allergen, contains a signal peptide (Petersen *et al.*, 2011) and has been detected in culture supernatants (Singh *et al.*, 2010a; Wartenberg *et al.*, 2011), thus supporting its detection in the study of secreted proteins performed here. Asp f9 is also described as a GPI-anchored protein and is found in the cell membrane of *A. fumigatus* mycelia (Bruneau *et al.*, 2001), thus validating its identification in the mycelial fraction of this study. While there are no literature reports on the identification of the PG/PI-TP protein in *A. fumigatus*, its ortholog in *Saccharomyces cerevisiae*, NPC2, has been detected in both intracellular and supernatant fractions of transfected mammalian cells (Berger *et al.*, 2005). The EglC protein, a β (1-6)/β (1-3) glucan branching transglycosidase, has been identified from both *A. fumigatus* cell wall fraction (Gastebois *et al.*, 2010b) and culture supernatants (Singh *et al.*, 2010a). The aminopeptidase has similarly been identified in large scale proteomic studies of mycelia proteins (Albrecht *et al.*, 2010) and secreted proteins (Wartenberg *et al.*, 2011). Thioredoxin reductase (AFUA_5G03540) has not been reported in any literature to date and so this represents the first identification of this protein in *A. fumigatus*. An ortholog of thioredoxin reductase in *Aspergillus niger*, Sox1, has been identified in the extracellular or membrane fraction of *A. niger* cultures after growth on xylose and maltose (Lu *et al.*, 2010). These observations from previous studies validate the concurrent identification of proteins in both mycelia and secreted fractions and, in the case of EglC and thioredoxin reductase, provide the first evidence of protein localisation in *A. fumigatus*.

In summary, a MS-based proteomics strategy was applied to investigate the mycelial proteome and the secretome of *A. fumigatus* ATCC26933. Methods to reduce sample complexity, and subsequently allow greater proteome characterisation, were also

investigated. A total of 427 unique *A. fumigatus* proteins were identified from this study, including 390 mycelial proteins and 42 proteins from the secretome. Many of the proteins identified by this MS-based proteomics strategy are typically underrepresented in 2D-PAGE studies. Bioinformatic analysis of the resultant datasets identified proteins with extremes of molecular mass and p*I*, hydrophobic proteins and proteins with up to 14 transmembrane regions. Proteins of unknown function (n = 21) were also identified and this study represents the first report of the existence of many of these proteins. Additionally, large scale proteomic profiling of *A. fumigatus* mycelia revealed a number of proteins involved in secondary metabolite clusters, providing strong evidence for the activation of multiple clusters under the control the transcriptional regulator LaeA in the conditions tested. Overall, the findings of this Chapter demonstrate the importance of implementing MS-based proteomics, as an adjunct to gel based proteomics, in order to comprehensively analyse the biosystems active in *A. fumigatus*. While MS-based proteomics provides a global overview of genome-wide expression under set conditions, gel-based proteomics retains its importance in the proteomic tool-belt due to its well-defined compatibility with immunodetection and comparative analysis. In Chapter 4 2D-PAGE and immunoblotting will be utilised in an attempt to further characterise the immunoproteome of *A. fumigatus*, while Chapter 5 will rely on comparative 2D-PAGE analysis to discern the mechanism of action of gliotoxin relief of oxidative stress in *A. fumigatus*.

CHAPTER 4

Immunoproteomic analysis

of *A. fumigatus*

4 Chapter 4

4.1 Introduction

Immunoproteomics involves the identification and characterisation of antigenic proteins and provides valuable information on the potential involvement of these proteins in virulence (Doyle, 2011b). Identification of antigens can be exploited for the development of diagnostic tools, as the circulating antibodies directed against specific antigens can be utilised as biomarkers of disease (Tjalsma *et al.*, 2008). Identified antigens can also be utilised for the development of vaccines directed against the pathogen of interest (Kniemeyer, 2011). Current methodologies employed for the study of the immunoproteome can be classified as (i) gel-based or (ii) gel-free methods (Tjalsma *et al.*, 2008). Gel-free methods include the use of protein microarrays, which allow large-scale screening of immunoreactivity against semi-purified or recombinantly produced protein (Davies *et al.*, 2005; Tjalsma *et al.*, 2008). The majority of fungal immunoproteomics investigations implement gel-based methods for antigen identification (Kniemeyer, 2011). The coupling of 2D-PAGE and immunoblotting, with subsequent protein identification by mass spectrometry, enables the isolation, detection and identification of antigenic proteins (Tjalsma *et al.*, 2008; Doyle, 2011a).

2D-PAGE involves the separation of protein by p*I* in the first dimension, followed by separation by relative molecular mass in the second dimension by electrophoresis (Kniemeyer, 2011). Proteins resolved by 2D-PAGE can be transferred electrophoretically from the polyacrylamide gel to a membrane to produce a replication of the protein distribution pattern (Tjalsma *et al.*, 2008). Protein transfer from the gel to the membrane can be examined through the application of a reversible protein stain such as Ponceau S (Krah and Jungblut, 2004). These membranes are subsequently blocked to prevent non-specific binding of antibodies, followed by incubation with

purified antibodies or serum samples (Krah and Jungblut, 2004). Reactivity of antibodies with proteins on the membrane is detected through use of a secondary antibody conjugated to an enzyme (Figure 4.1) (Doyle, 2011a). Typical experimental design for 2D-PAGE coupled with immunoblotting involves the separation of protein extracts in duplicate by 2D-PAGE. Total proteins are visualised on gel 1 by staining, using Coomassie blue or silver staining. Gel 2 is transferred to membrane reversibly stained to obtain an image of the protein distribution pattern and subsequent immunoblotting is carried out (Figure 4.1) (Doyle, 2011a). Using the image of the reversibly stained blot as a reference, the immunoreactive proteins on the membrane can be aligned against the proteins from the stained gel (Figure 4.1). Following protein isolation, mass spectrometry can be utilised to identify the immunoreactive proteins. Comprehensive identification and characterisation of antigenic proteins from pathogenic organisms can aid in the development of diagnostic tools, in addition to providing information on the mechanisms of pathogenesis (Kumar *et al.*, 2011).

Due to the association of IA with neutropenia or immunosuppression, detection of elevated levels of anti-*Aspergillus* antibodies is often not possible, contributing to the difficulty in obtaining a diagnosis (Hope *et al.*, 2005). Instead, detection of circulating antigens has been investigated as a diagnostic tool for IA (Mennink-Kersten *et al.*, 2008). Another form of *A. fumigatus* related disease involves the colonisation of cavities in the lung, formed as a result of pre-existing conditions such as tuberculosis, resulting in a mass of hyphae termed an aspergilloma (Ma *et al.*, 2011). Aspergillomas occur in approximately 10 to 15 % of individuals with these pulmonary cavities and can be detected by radiography or elevated antibody levels (Latge, 1999). Allergic bronchopulmonary aspergillosis (ABPA) involves the colonisation of the airways by *A. fumigatus*, resulting in an allergy mediated inflammatory response.

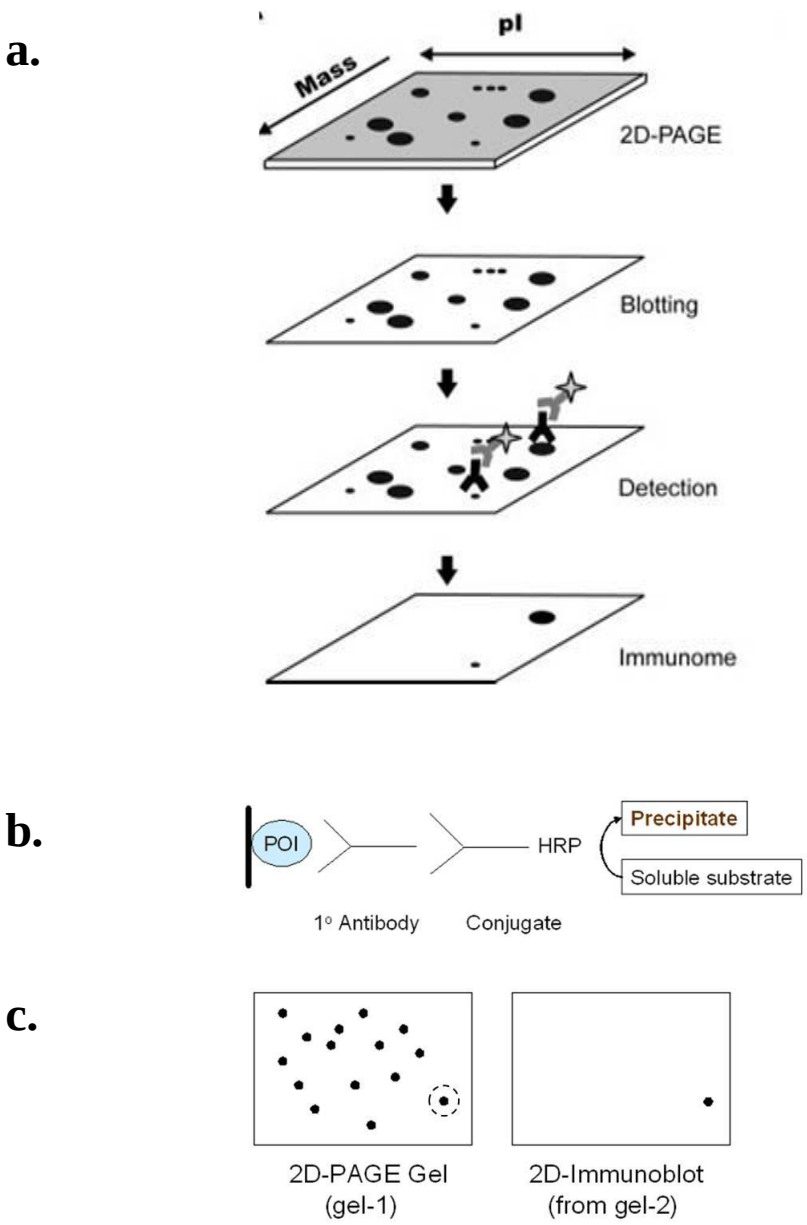

Figure 4.1: (a) Schematic representation of steps during gel-based immunoproteomics. 2D-PAGE involves protein separation by p*I*, followed by gel-based separation based on molecular mass. Next, proteins are transferred from the gel and immobilised on a membrane by blotting. (b) Antigenic proteins (immunome) can be detected by applying serum to the blot, after which bound antibodies can be visualised by secondary labelled antibodies. (c) Two gels are prepared in tandem, with total protein staining carried out on gel 1, and immunodetection carried out on gel 2. Detected antigens on gel 2 can be isolated from gel 1 for identification by MS. Adapted from Tjalsma *et al.* (2008) and Doyle (2011a).

ABPA affects mainly individuals with cystic fibrosis, and is exacerbated by the limited ability of CF patients to clear inhaled conidia effectively from the lungs (Pihet *et al.*, 2009). Due to the allergic nature of this disease, an elevation of IgE directed against *A. fumigatus* proteins is often associated with ABPA (Hafen *et al.*, 2009). The three *Aspergillus*-related diseases outlined involve the mycelial growth of *A. fumigatus* in the body and highlight the requirement for diagnostic tools for the detection of the fungus in this growth phase.

Following inhalation, *A. fumigatus* conidia encounter the mucous lining of the lungs along with a number of enclosed pattern recognition receptors (PRRs). These PRRs can bind to the surface of inhaled conidia and target them for phagocytosis and killing by alveolar macrophages (Reid *et al.*, 1997). Engulfed conidia swell inside the phagocyte and are subsequently destroyed through the action of reactive oxygen species (ROS) (Philippe *et al.*, 2003). Alveolar macrophages are resident in the lung, and primarily target conidia for phagocytosis. Conversely, neutrophils are recruited to the site of inflammation from the extensive pulmonary vascular system and are capable of arresting conidial growth, in addition to targeted killing of hyphae (Bonnett *et al.*, 2006; Feldmesser, 2006). Consequently, neutropenic individuals exhibit a high risk for developing invasive aspergillosis (Dagenais and Keller, 2009). Activation of PRRs also stimulates the maturation of dendritic cells, which function in antigen-presentation and prime the T-cell immune response. Th2-type responses can be detrimental to the host as they are related to allergy and may result in the development of asthma or allergic bronchopulmonary aspergillosis (ABPA). Helper T-cell activation of relevant B-cells, following antigen detection, results in the production of antibodies directed against *A. fumigatus* proteins. While these antibodies may not confer resistance to *A. fumigatus*,

their detection at elevated levels may be indicative of diseases such as aspergilloma and ABPA (Tillie-Leblond and Tonnel, 2005; Zmeili and Soubani, 2007).

Prior to the availability of the genomic sequence of *A. fumigatus* (Nierman *et al.*, 2005), numerous immunoproteomic studies had been carried out without definitive protein identification (Latge, 1999). Recent characterisation of the antigenic proteome of *A. fumigatus* has predominantly been achieved through a combination of 2D-PAGE, immunodetection and subsequent protein identification by mass spectrometry. Many studies have focused on the identification of *A. fumigatus* allergens based on the presence of reactive IgE in sera from patients with an allergy-based disease (Gautam *et al.*, 2007; Singh *et al.*, 2010a, 2010b). Others have expanded on this to incorporate identification of IgG reactive proteins from *A. fumigatus*, in addition to other antibody isoforms (IgA and IgM). This was achieved through immunoblotting with sera from both patients and animal models of *A. fumigatus* infection (Asif *et al.*, 2010; Singh *et al.*, 2010a, 2010b; Kumar *et al.*, 2011; Shi *et al.*, 2012a). Another distinguishing factor between various immunoproteomic studies is the cellular localisation of antigens, namely whether they are present intracellularly or extracellularly, and the developmental stage they are associated with (i.e. conidia or mycelia). The secretome of *A. fumigatus* presented an attractive target for many immunoproteomic studies, as these extracellular proteins were considered to come into direct contact with the host during pathogenesis (Kumar *et al.*, 2011). Investigation of culture filtrates has not only identified antigenic proteins but has also greatly contributed to the characterisation of the *A. fumigatus* secretome (Gautam *et al.*, 2007; Singh *et al.*, 2010a; Kumar *et al.*, 2011; Shi *et al.*, 2012a). The identification of antigens localised in germinating conidia has also been undertaken, with the identification of 66 proteins by immunoreactivity with pooled ABPA patients' sera (Singh *et al.*, 2010b) and 59 proteins displaying

reactivity with rabbit sera following invasive aspergillosis (Asif *et al.*, 2010). While all of these studies have utilised sera from sources with high anti-*Aspergillus* antibody titres, normal sera from healthy individuals also represents a source of these antibodies. Kurup *et al.* (2006) noted that sera from normal control subjects exhibited specific IgG_1 reactivity to crude extracts of *A. fumigatus* proteins and a number of controls showed strong IgA_2 reactivity. Additionally, Schrettl *et al.* (2010) noted the widespread presence of antibodies from normal sera, directed against the gliotoxin oxidoreductase GliT, and exploited this observation for the purification of anti-GliT antibodies using recombinant the antigen.

With the aim of expanding the characterisation of the immunoproteome of *A. fumigatus*, an investigation was carried out to identify proteins reactive with normal human sera. This was carried out using the 2D-PAGE, coupled with mass spectrometric identification of immunoreactive proteins from the mycelia of this opportunistic pathogen. A total of 25 unique proteins were identified, including 13 proteins which had previously not been characterised as antigenic. This novel approach, utilising (i) mycelia instead of conidia or secreted proteins, and (ii) sera from healthy donors in place of disease state sera, has demonstrated expansion of the currently described compilation of *A. fumigatus* antigens. The findings described in this Chapter may be relevant for advancing diagnostic tools or provide further elucidation of the mechanisms of disease.

4.2 Results

4.2.1 Detection of immunoreactivity to *A. fumigatus* mycelia proteins in normal human sera

Mycelia were harvested from *A. fumigatus* ATCC26933 shaking cultures in AMM after 48 h and proteins were extracted as outlined in Section 2.2.2.1. Protein extracts were separated using SDS-PAGE and gels were transferred to NCP (Section 2.2.4.5). Following transfer, NCP was cut vertically into strips which were then probed with pools of normal human sera (n = 135 serum samples, n = 29 serum pools; 5 serum samples/pool). Immunoreactivity directed against *A. fumigatus* proteins was detected using an anti-human IgG - HRP conjugate with a chromogenic substrate, DAB (Section 2.2.4.7). A section of the gel was stained with Coomassie blue as a reference (Figure 4.2).

Immunoreactivity against *A. fumigatus* mycelia proteins was observed in 93 % of sera pools tested (n = 27 pools). Sera pools displayed differential intensities and patterns of immunoreactivity, with high immunoreactivity observed from pools shown in lanes 6, 7 and 11 (Figure 4.2). Low immunoreactivity was observed in other samples, including sera pools in lanes 12 and 13 (Figure 4.2). Further separation of *A. fumigatus* mycelia proteins, using 2D-PAGE and subsequent Western blot analysis, was required in order to accurately isolate and identify the immunoreactive proteins. Serum pools 6, 7 and 11, identified with high relative immunoreactivity, were combined and subsequently used to probe 2D-PAGE immunoblots.

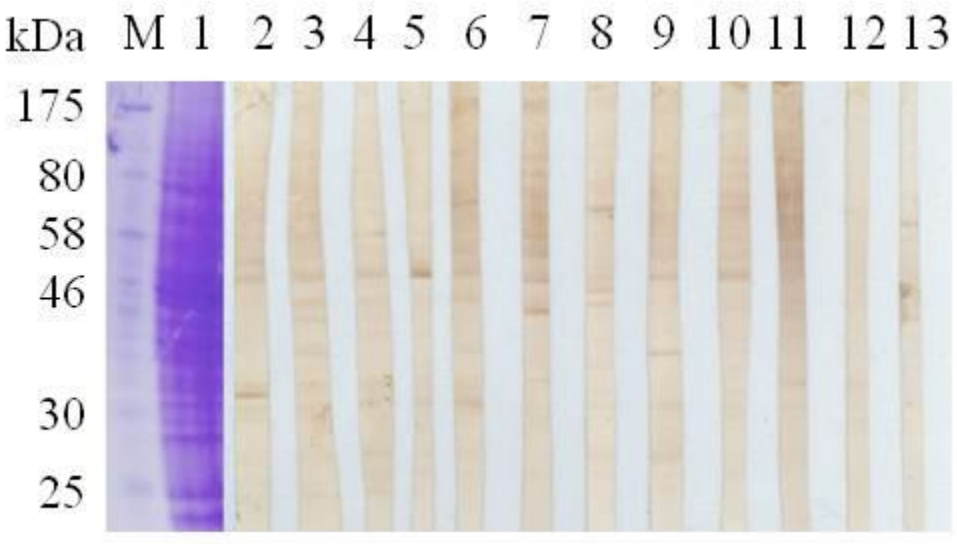

Figure 4.2: Screen of immunoreactivity of normal human sera samples against *A. fumigatus* mycelia proteins. SDS-PAGE of *A. fumigatus* ATCC26933 stained with Coomassie Blue (Lane 1) and transferred to NCP for western blot analysis (Lanes 2-13). NCP strips were probed with pools of normal human sera and immunoreactivity was detected using an anti-human IgG - HRP conjugate and DAB as a substrate. Differential levels of reactivity were observed, with high reactivity evident in lanes 6, 7 and 11, and low reactivity in lanes 12 and 13.

4.2.2 2D-PAGE of *A. fumigatus* ATCC26933 and Western Blot analysis using normal human sera

A. fumigatus ATCC26933 was grown in AMM for 48 h and protein was extracted from mycelia as described in Section 2.2.2.2. Protein lysates were TCA/acetone precipitated and resuspended in IEF buffer (Section 2.1.6.2) and quantitated (Section 2.2.4.1). Protein (300 µg) was separated by p*I* on pH 3 - 11 strips (Section 2.2.4.3) and subsequently by molecular mass by SDS-PAGE on 12 % gels. Proteins were transferred to NCP (Section 2.2.4.6) and protein transfer was visualised by Ponceau S staining. Western blot analysis was carried out using pools 6, 7 and 11 of normal human sera, identified in Section 4.2.1 as displaying immunoreactivity to *A. fumigatus* mycelia proteins. IgG reactivity to *A. fumigatus* proteins was detected as in Section 4.2.1. Additional reference gels were prepared simultaneously and were stained with Colloidal Coomassie (Section 2.2.4.4) in order to visualise total proteins and for use in the identification of proteins by mass spectrometry. Images of Colloidal Coomassie stained gels, Ponceau S stained and DAB developed blots were aligned using Progenesis™ SameSpot Software (Nonlinear Dynamics Ltd, UK) (Figure 4.3).

Following image alignments, 10 protein spots were detected that could be matched to distinct spots on the immunoblots. These spots were excised from the gels and subjected to in-gel trypsin digestion (Section 2.2.6.1) followed by LC-MS/MS analysis (Section 2.2.6.3).

a. pH 3 ——————————————— 11

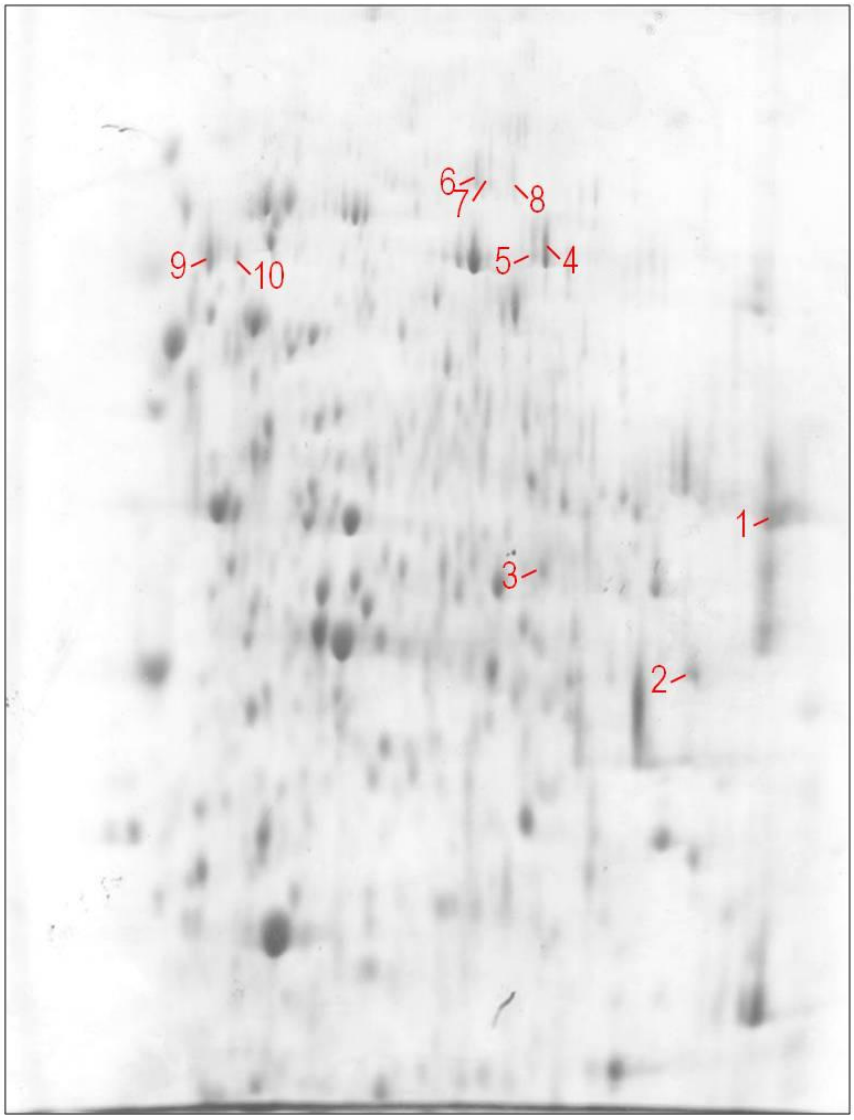

Colloidal Coomassie stained 2D-PAGE gel
of *A. fumigatus* mycelial proteins

b. pH 3 ——————————————— 11

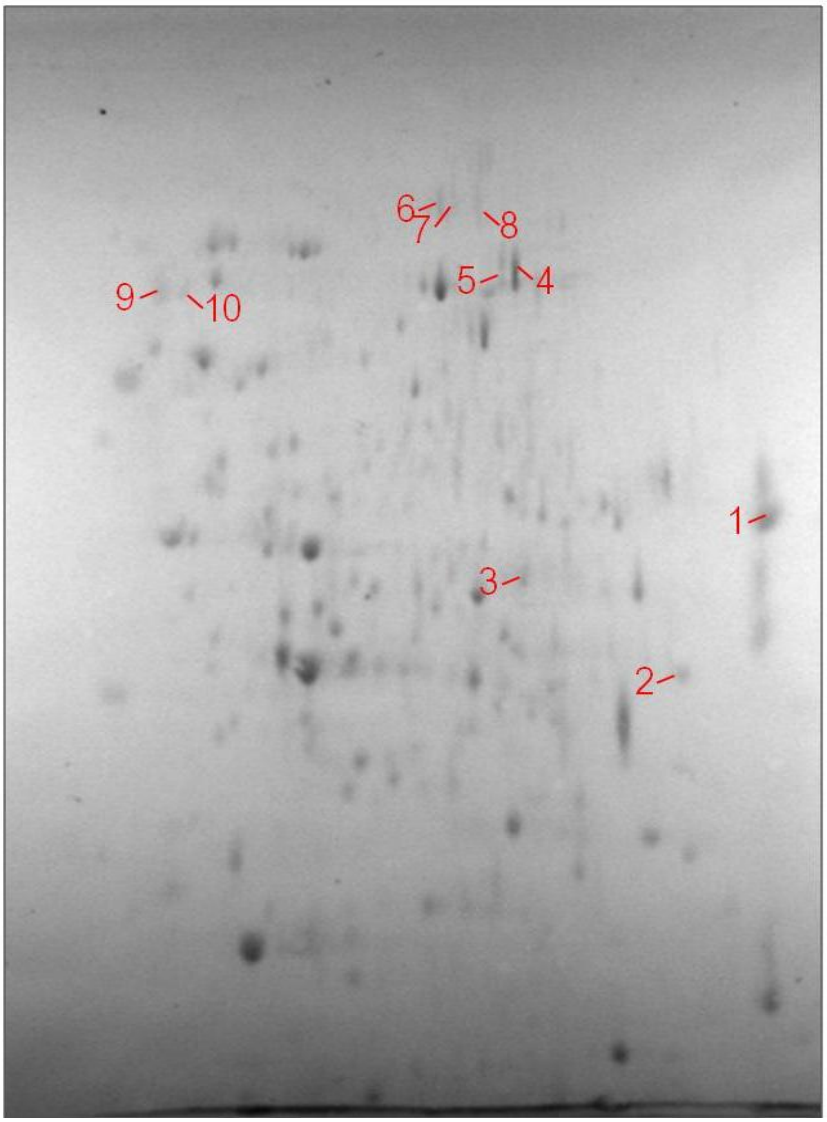

Ponceau S stained 2D-PAGE blot
of *A. fumigatus* mycelial proteins

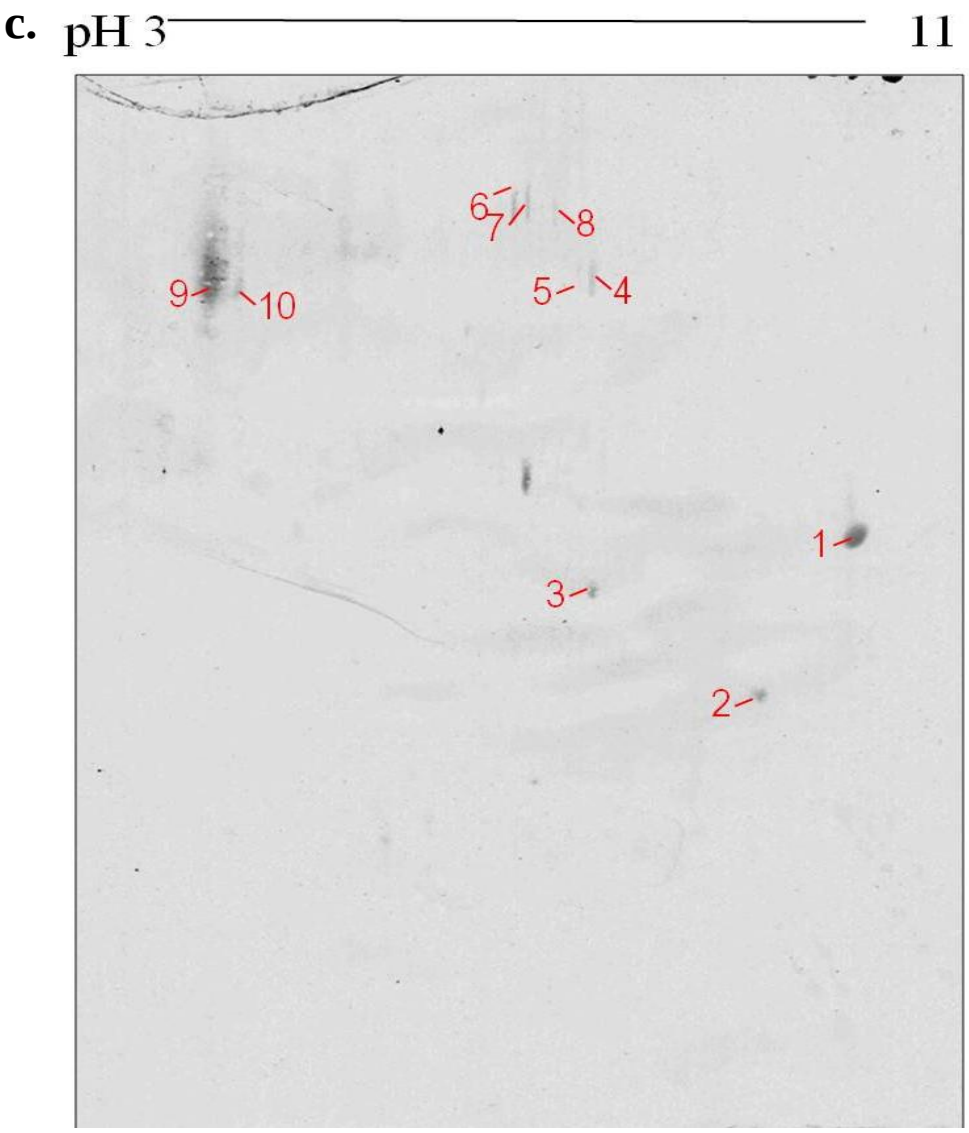

2D-PAGE immunoblot blot of *A. fumigatus*
mycelial proteins probed with antisera

Figure 4.3: Immunoblot analysis for the detection of *A. fumigatus* ATCC26933 proteins reactive with IgG in normal human sera. 2D-PAGE was carried out to separate mycelia proteins (300 µg) by p*I* in the pH range 3 – 11 and molecular mass using 12 % gels. (a) Colloidal Coomassie staining was used to visualise total proteins on gels. (b) Gels were transferred to NCP and Ponceau S staining was carried out. (c) Blots probed with normal human sera displayed some immunoreactivity when developed with DAB. Images were aligned using Progenesis™ SameSpot software and locations of immunoreactive spots are numbered on all images.

4.2.3 Mass spectrometry analysis of immunoreactive proteins

From the excised spots (n = 10), 7 distinct proteins were identified by LC-MS/MS (Table 4.1). The highest reactivity was observed from spot number 9 (Figure 4.3), identified as a carboxypeptidase S1 (AFUA_8G04120). A translation elongation factor EF-1 alpha subunit (AFUA_1G06390; Spot 1) also exhibited relatively high immunoreactivity.

A number of the identified proteins were observed in more than one spot, exhibiting different p*I* or molecular mass. This suggests the occurrence of post-translational modifications (PTMs) or protein degradation. A cobalamin-independent methionine synthase MetH/D (AFUA_4G07360; Spots 4 and 5) was detected in two individual spots with apparently differing p*I*s. Alpha-ketoglutarate dehydrogenase complex subunit Kgd1 (AFUA_4G11650; Spots 6, 7 and 8) was detected independently in three individual spots (Figure 4.3, Table 4.1). Again these spots displayed different apparent p*I*s but the same molecular mass, as deduced by their position on the gel. This is indicative of differential post-translational modification of these proteins.

In order to enhance the detection of immunoreactivity to *A. fumigatus* mycelial proteins, the amount of protein separated by 2D-PAGE was increased from 300 µg to 400 µg. The results obtained from this optimised protocol are described in Sections 4.2.4 and 4.2.5.

Table 4.1: *A. fumigatus* mycelia proteins, immunoreactive with normal human sera, identified by 2D-PAGE and LC-MS/MS.

Spot No	CADRE ID. (AFUA_)	Protein name	tp*I*	tM_r	Coverage (%)	Unique peptides	MASCOT Score
1	**1G06390**	Translation elongation factor EF-1 alpha subunit	9.12	50019.60	16	7	282
2	**4G10410**	Aspartate aminotransferase	8.94	47892.64	31	12	669
3	**6G02470**	Fumarate hydratase	9.1	63159.39	28	12	615
4	**4G07360**	Cobalamin-independent methionine synthase MetH/D	6.33	86894.57	49	33	1444
5	**4G07360**	Cobalamin-independent methionine synthase MetH/D	6.33	86894.57	29	18	842
6	**4G11650**	Alpha-ketoglutarate dehydrogenase complex subunit Kgd1, putative	6.47	118900.00	9	7	307
7	**4G11650**	Alpha-ketoglutarate dehydrogenase complex subunit Kgd1, putative	6.47	118900.00	7	5	230
8	**4G11650**	Alpha-ketoglutarate dehydrogenase complex subunit Kgd1, putative	6.47	118900.00	4	3	100
9	**8G04120**	Carboxypeptidase S1	5.4	67672.79	23	8	381
10	**5G04170**	Molecular chaperone and allergen Mod-E/Hsp90/Hsp1	4.95	80639.96	15	8	320

CADRE ID., *A. fumigatus* gene annotation nomenclature according to Nierman *et al.* (2005) and Mabey *et al.* (2004); tp*I*, theoretical isoelectric point; tM_r, theoretical molecular mass; MASCOT scores > 58 indicate identity or extensive homology ($p < 0.05$); Spot No. from Figure 4.3.

4.2.4 Optimised 2D-PAGE of *A. fumigatus* ATCC26933 and Western Blot analysis using normal human sera

A. fumigatus ATCC26933 mycelial protein lysates were prepared as in Section 4.2.2, with the exception of higher protein loading to enhance visualisation of immunoreactivity. Protein lysates in IEF buffer (400 µg) was separated initially on pH 3 - 11 strips (Section 2.2.4.3) and subsequently by SDS-PAGE on 12 % gels. Proteins were transferred to NCP (Section 2.2.4.6) and protein transfer was visualised by Ponceau S staining. Western blot analysis was carried out using pools 6, 7 and 11 of normal human sera, identified in Section 4.2.1 as displaying immunoreactivity to *A. fumigatus* mycelia proteins. IgG reactivity to *A. fumigatus* proteins was detected as in Section 4.2.1. Additional reference gels were prepared simultaneously and were stained with Colloidal Coomassie (Section 2.2.4.4) in order to visualise total proteins and for use in the identification of proteins by mass spectrometry. Images of Colloidal Coomassie stained gels, Ponceau S stained and DAB developed blots were aligned using Progenesis™ SameSpot Software (Nonlinear Dynamics Ltd, UK) (Figure 4.4).

Following image alignments, 28 protein spots were detected that could be matched to distinct spots on the immunoblots. Strong immunoreactivity was evident in the acidic region of the blot and appeared to be clustered near the top of the gel, indicating high molecular mass proteins. Enhanced levels of immunoreactivity were observed following optimisation of the method described in Section 4.2.2. The spots were excised from the gels and subjected to in-gel trypsin digestion (Section 2.2.6.1) followed by LC-MS/MS analysis (Section 2.2.6.3).

a.

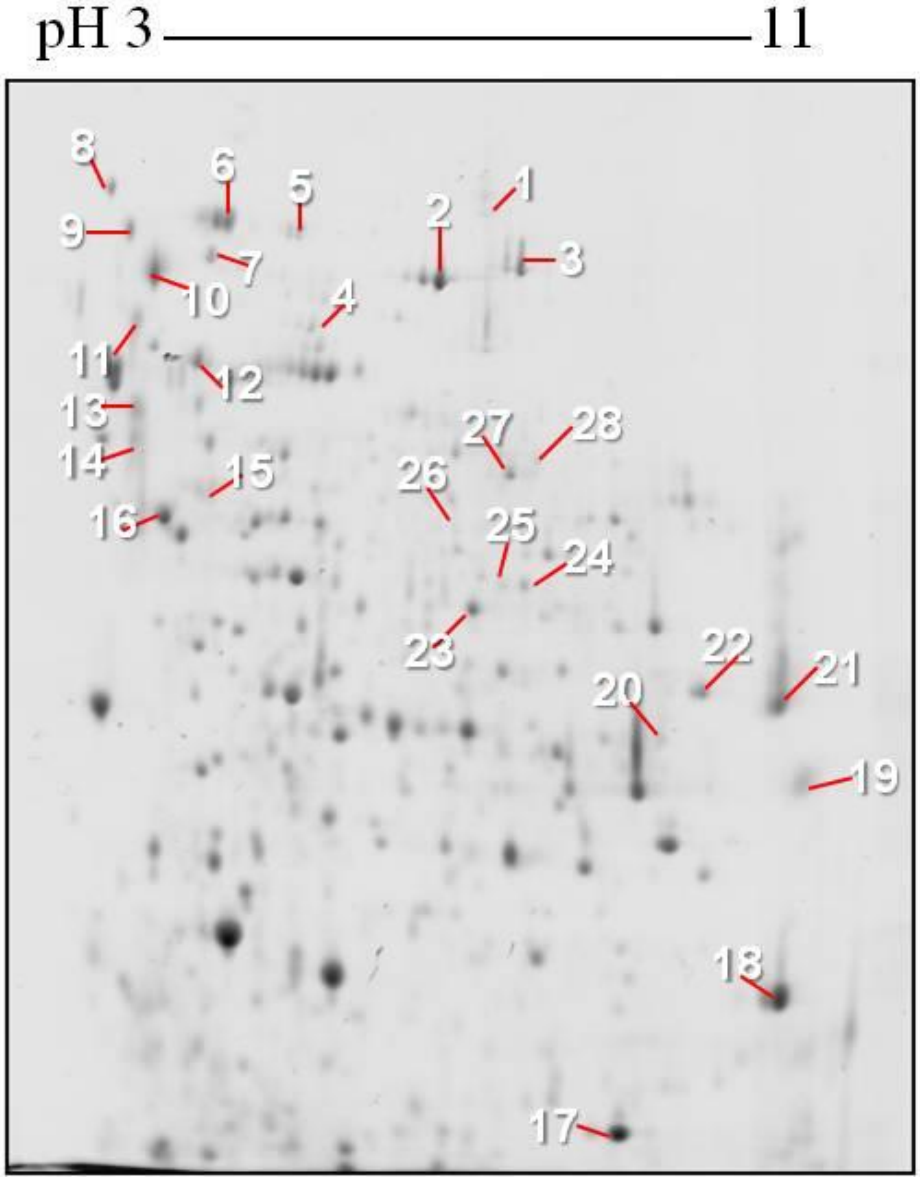

Colloidal Coomassie stained 2D-PAGE gel
of *A. fumigatus* mycelial proteins

b. pH 3 ——————————————— 11

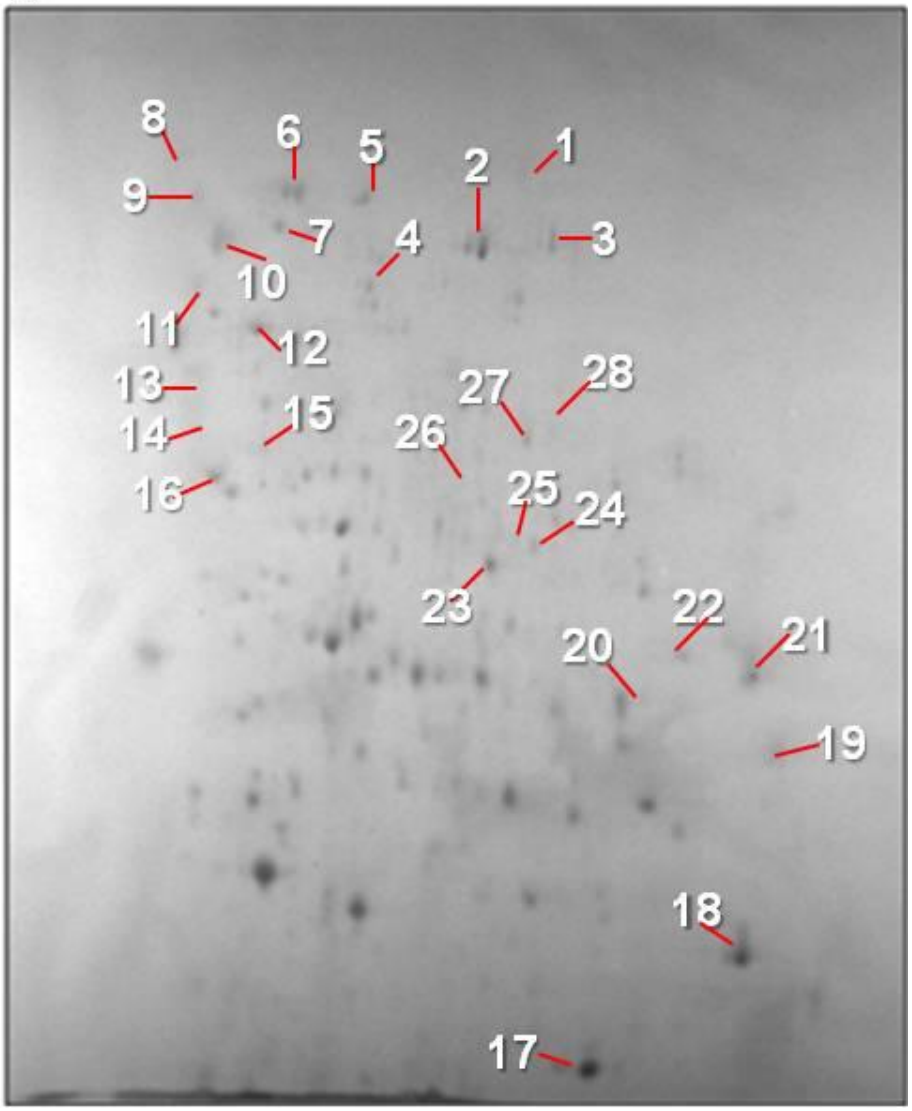

Ponceau S stained 2D-PAGE blot
of *A. fumigatus* mycelial proteins

c.

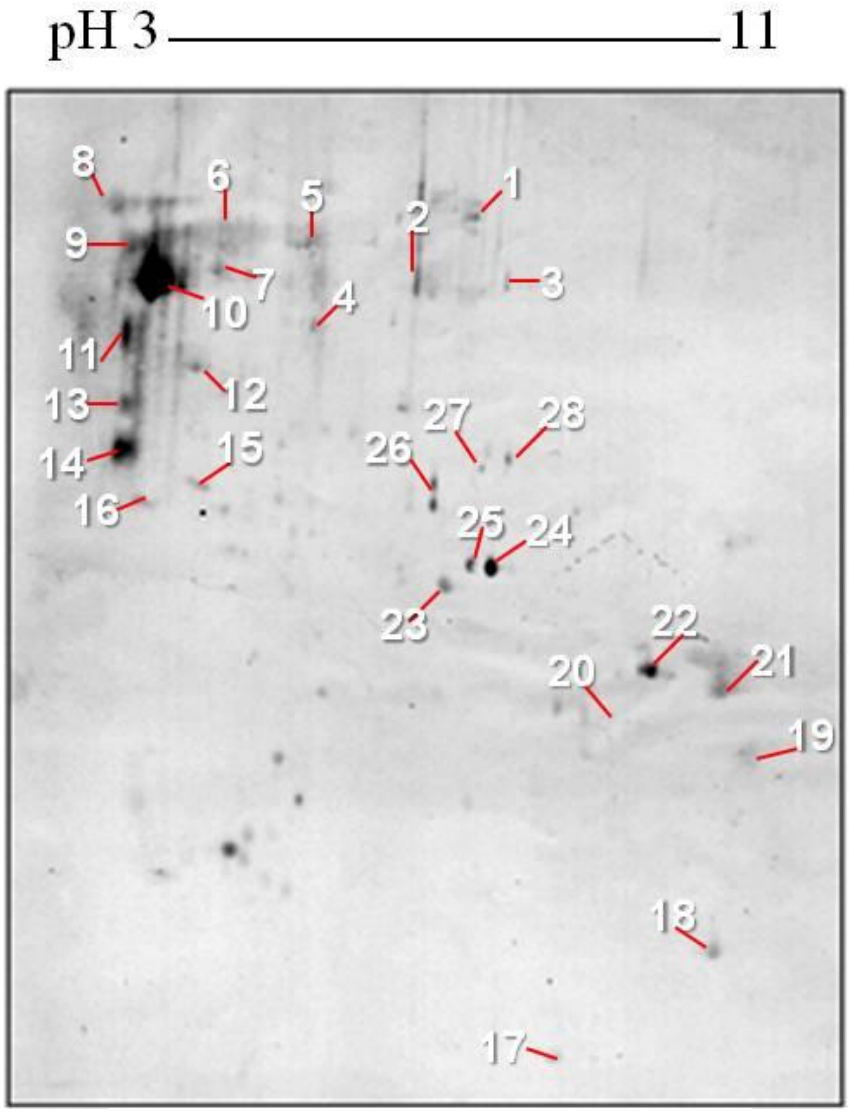

2D-PAGE immunoblot blot of *A. fumigatus* mycelial proteins probed with antisera

Figure 4.4: Optimised immunoblot analysis for the detection of *A. fumigatus* ATCC26933 proteins reactive with IgG in normal human sera. 2D-PAGE was carried out to separate mycelia proteins (400 µg) by p*I* in the pH range 3 – 11 and molecular mass using 12 % gels. (a) Colloidal Coomassie staining was used to visualise total proteins on gels. (b) Gels were transferred to NCP and Ponceau S staining was carried out. (c) Blots probed with normal human sera displayed some immunoreactivity when developed with DAB. Images were aligned using Progenesis™ SameSpot software and locations of immunoreactive spots are numbered on all images.

4.2.5 Mass spectrometry analysis of immunoreactive proteins

From the excised spots (n = 28), 24 distinct proteins were identified by LC-MS/MS (Table 4.2). The highest reactivity was observed from spot number 10 (Figure 4.3), identified as a carboxypeptidase S1 (AFUA_8G04120). An aminopeptidase (AFUA_2G00220; Spot 14), a 1, 3-β- glucosyltransferase (AFUA_2G05340; Spot 11), a fumarate hydratase (AFUA_6G02470; Spots 24 and 25) and an aspartate aminotransferase (AFUA_4G10410; Spot 22) also displayed relatively high immunoreactivity (Figure 4.4).

A number of the identified proteins were observed in more than one spot, exhibiting different pI or molecular mass. This suggests the occurrence of post-translational modifications or protein degradation. A woronin body protein HexA (AFUA_5G08830; Spots 17, 26 and 27), a fumarate hydratase (AFUA_6G02470; Spots 24 and 25) and a translation elongation factor EF-1 alpha subunit (AFUA_1G06390; Spots 19 and 21) were all detected in more than one spot (Figure 4.4, Table 4.2).

With the exception of the molecular chaperone and allergen Mod-E/Hsp90/Hsp1 (AFUA_5G04170; Spot 10; Figure 4.3), all of the antigens identified in Section 4.2.3, were also identified following optimisation of immunoprotein detection strategy. This demonstrates the improvement of the protocol used, with the identification of an additional 18 IgG-reactive proteins following method optimisation.

Table 4.2: *A. fumigatus* mycelia proteins, immunoreactive with normal human sera, identified following optimised 2D-PAGE and LC-MS/MS.

Spot No	CADRE ID. (AFUA_)	Protein name	tp*I*	tM_r	Coverage (%)	Unique peptides	MASCOT Score
1[1]	**4G11650**	Alpha-ketoglutarate dehydrogenase complex subunit Kgd1, putative	6.47	118900.00	9	7	307
2	**6G12930**	Mitochondrial aconitate hydratase	6.26	85529.08	38	23	974
3[1]	**4G07360**	Cobalamin-independent methionine synthase MetH/D	6.33	86894.57	32	21	1050
4	**6G10990**	NADPH cytochrome P450 reductase (CprA)	5.38	76782.85	11	6	296
5	**8G00440**	Steroid monooxygenase	5.48	101032.20	22	16	767
6	**3G14680**	Lysophospholipase Plb3	5.39	67416.54	27	16	824
7	**1G12610**	Hsp70 chaperone Hsp88	5.08	80044.81	20	13	477
8	**4G08720**	Lysophospholipase Plb1	4.59	68143.67	7	5	205
9	**5G07330**	Carboxypeptidase S1	4.74	68345.84	15	6	269
10[1]	**8G04120**	Carboxypeptidase S1	5.4	67672.79	24	8	371
11	**2G05340**	1,3-β-glucanosyltransferase Gel4	4.83	58872.59	6	2	100
12	**1G07440**	Molecular chaperone Hsp70	5.08	69660.29	44	19	758
13	**4G06820**	GPI-anchored cell wall organization protein Ecm33	4.8	41505.47	8	3	102
14	**2G00220**	Aminopeptidase	4.99	56702.95	7	2	91

Spot No	CADRE ID. (AFUA_)	Protein name	tp*I*	tM_r	Coverage (%)	Unique peptides	MASCOT Score
15	**2G05910**	Hexokinase Kxk	5.06	54209.22	16	4	300
16	**5G10550**	ATP synthase F1, beta subunit	5.3	55620.38	62	21	1117
17	**5G08830**	Woronin body protein HexA	6.56	49836.57	24	11	471
18	**4G06910**	Outer mitochondrial membrane protein porin	9.47	36893.97	60	17	812
19[1]	**1G06390**	Translation elongation factor EF-1 alpha subunit	9.12	50019.60	13	5	185
20	**6G06370**	NAD(+)-isocitrate dehydrogenase subunit I	8.42	49745.35	12	5	212
21[1]	**1G06390**	Translation elongation factor EF-1 alpha subunit	9.12	50019.60	17	5	267
22[1]	**4G10410**	Aspartate aminotransferase	8.94	47892.64	29	13	642
23	**1G10350**	Phosphoglycerate kinase PgkA	6.31	44761.47	60	22	867
24[1]	**6G02470**	Fumarate hydratase	9.1	63159.39	25	14	596
25[1]	**6G02470**	Fumarate hydratase	9.1	63159.39	4	3	102
26	**5G08830**	Woronin body protein HexA	6.56	49836.57	17	7	226
27	**5G08830**	Woronin body protein HexA	6.56	49836.57	31	12	512
28	**2G03610**	IMP dehydrogenase	6.25	57958.52	13	7	291

CADRE ID., *A. fumigatus* gene annotation nomenclature according to Nierman *et al.* (2005) and Mabey *et al.* (2004); tp*I*, theoretical isoelectric point; tM_r, theoretical molecular mass; MASCOT scores > 58 indicate identity or extensive homology ($p < 0.05$); Spot No. from Figure 4.4; [1]Protein also detected in Section 4.2.3, prior to method optimisation.

4.2.6 Putative location of immunogenic region on HexA protein

The woronin body protein HexA (AFUA_5G08830), identified in Section 4.2.5 was detected at three independent locations on the immunoblot, based on its reactivity with IgG in normal human sera. These locations indicated proteins of differing p*I* and molecular mass (Figure 4.4; Spot numbers 17, 26, 27). This protein has a theoretical molecular mass of 50 kDa and this correlates well with its identification from spots 26 and 27. However, spot number 17 represents a protein with a much lower molecular mass, indicated by its position at the bottom of the gel.

Examination of the sequence coverage, obtained from LC-MS/MS analysis of each of the independent protein spots, revealed that the peptides identified from the proteins in spots 26 and 27 are distributed throughout the entire sequence of the HexA protein (Figure 4.5). In contrast, the peptides identified from the protein in spot number 17 are localised exclusively in the C-terminus of the protein. (Figure 4.5) This observation, coupled with its position on the gel, indicate that the protein found in spot number 17 is a cleavage or breakdown product of the HexA protein. This low molecular mass C-terminal region of the HexA protein (Spot 17) displays a reduced level of immunoreactivity compared to that observed from the higher molecular mass HexA proteins (Spots 26 and 27). The reduction in immunoreactivity to the C-terminus section of the HexA protein (Spot 17) subsequently indicates the immunogenic epitope is predominantly located on the N-terminal region of this protein.

Spot 26

```
  1   MYSVESKFERDSRRDAQRTANLDFDARVPIPFSVFPSSYRSDAVPETTLT
 51   RVEGEVNLDRTSHVEREDTRTSAPLPDPRVYGREEVDIHISKDRLHAPSR
101   KGDDFQVIYEDRAHKDSRVPEVELSRERWKRSENNAKQNKNKNNTSTRRS
151   GDVLKAVSAKKVAPQAQTRADEKASYQLTQKARYRESTSRYEPLPPKPVY
201   DQALESQLDITEREYRRRTDPTYDVNLSYGRHQAPVDSYQAYQPQQTSDV
251   SLHRSKTEIDVSYDKAYTPKPLETRKGDSFSRSELTVESVPSRPSSASSI
301   SQVKVLKPYTAIDQPPARKMGYYDDDGNYHSFRRGVERAVDRITHPFHHH
351   HHHHDREEVVIADERGPVRYRDGVREDVRIVEPRASKTTAESVPIPCHFI
401   RIGDILILQGRPCQVIRISVSPQTGQHRYLGVDLFTRQLQEESSFVSNPS
451   PSVVVQTMLGPVYKTYRILDLHEDGTITAMTETGDVKQALPVVTQGQLFR
501   KIRDAFSEGRGSVRALVINDGGRELVVDYKVIHGSRL
```

Spot 27

```
  1   MYSVESKFERDSRRDAQRTANLDFDARVPIPFSVFPSSYRSDAVPETTLT
 51   RVEGEVNLDRTSHVEREDTRTSAPLPDPRVYGREEVDIHISKDRLHAPSR
101   KGDDFQVIYEDRAHKDSRVPEVELSRERWKRSENNAKQNKNKNNTSTRRS
151   GDVLKAVSAKKVAPQAQTRADEKASYQLTQKARYRESTSRYEPLPPKPVY
201   DQALESQLDITEREYRRRTDPTYDVNLSYGRHQAPVDSYQAYQPQQTSDV
251   SLHRSKTEIDVSYDKAYTPKPLETRKGDSFSRSELTVESVPSRPSSASSI
301   SQVKVLKPYTAIDQPPARKMGYYDDDGNYHSFRRGVERAVDRITHPFHHH
351   HHHHDREEVVIADERGPVRYRDGVREDVRIVEPRASKTTAESVPIPCHFI
401   RIGDILILQGRPCQVIRISVSPQTGQHRYLGVDLFTRQLQEESSFVSNPS
451   PSVVVQTMLGPVYKTYRILDLHEDGTITAMTETGDVKQALPVVTQGQLFR
501   KIRDAFSEGRGSVRALVINDGGRELVVDYKVIHGSRL
```

Spot 17

```
  1   MYSVESKFERDSRRDAQRTANLDFDARVPIPFSVFPSSYRSDAVPETTLT
 51   RVEGEVNLDRTSHVEREDTRTSAPLPDPRVYGREEVDIHISKDRLHAPSR
101   KGDDFQVIYEDRAHKDSRVPEVELSRERWKRSENNAKQNKNKNNTSTRRS
151   GDVLKAVSAKKVAPQAQTRADEKASYQLTQKARYRESTSRYEPLPPKPVY
201   DQALESQLDITEREYRRRTDPTYDVNLSYGRHQAPVDSYQAYQPQQTSDV
251   SLHRSKTEIDVSYDKAYTPKPLETRKGDSFSRSELTVESVPSRPSSASSI
300   SQVKVLKPYTAIDQPPARKMGYYDDDGNYHSFRRGVERAVDRITHPFHHH
351   HHHHDREEVVIADERGPVRYRDGVREDVRIVEPRASKTTAESVPIPCHFI
401   RIGDILILQGRPCQVIRISVSPQTGQHRYLGVDLFTRQLQEESSFVSNPS
451   PSVVVQTMLGPVYKTYRILDLHEDGTITAMTETGDVKQALPVVTQGQLFR
501   KIRDAFSEGRGSVRALVINDGGRELVVDYKVIHGSRL
```

Figure 4.5: Identification of the woronin body protein HexA in three independent spots and distribution of peptides detected from each. Peptides identified following trypsin digestion and LC-MS/MS analysis of each protein spot are shown in red. Peptides detected from spot 17 correspond exclusively to the C-terminal of the HexA protein.

4.3 Discussion

Immunoreactivity of proteins from mycelial lysates of *A. fumigatus* ATCC26933, with sera from healthy individuals, was investigated using SDS-PAGE and Western blot analysis. Positive reactivity was observed against 93 % of pooled sera samples tested (Figure 4.2), which reflects the constant exposure to environmental strains of *A. fumigatus*. Indeed, previous in-house studies investigating the antigenicity of recombinantly produced *A. fumigatus* proteins from the gliotoxin biosynthesis cluster noted a similarly high amount of healthy individuals that were seropositive for IgG directed against the respective antigens. Through ELISA screening, 63 % (n = 93) exhibited immunoreactivity against recombinantly produced GliG (AFUA_6G09690) (Prof. Sean Doyle, personal communication). The gliotoxin oxidoreductase, GliT, also demonstrated extensive immunoreactivity with normal serum samples and this was utilised for the purification of anti-GliT antibodies (Schrettl *et al.*, 2010). While this immunoreactivity would be relatively low compared to sera from patients with *A. fumigatus*-related infections (e.g. ABPA or aspergillosis), this nevertheless provides a way to expand the characterisation of *A. fumigatus* antigens. Differential levels of reactivity were observed between sera pools, and those displaying the highest immunoreactivity were used to identify IgG reactive *A. fumigatus* antigens. The method utilised in Section 4.2.1 describes an efficient way by which to screen large numbers of serum samples for the presence of immunoreactivity, for subsequent use in targeted immunoproteomics studies.

2D-PAGE was used to resolve the mycelial proteins, and subsequently, identify immunoreactive proteins with confidence. This initially yielded the identification of 7 unique IgG-reactive *A. fumigatus* proteins from 10 individual spots (Table 4.1). Subsequently, optimisation of the protocol was carried out in order to improve the

detection of immunoreactive *A. fumigatus* mycelial proteins. By increasing the amount of protein separated by 2D-PAGE from 300 µg (Section 4.2.2) to 400 µg (Section 4.2.4), a total of 24 unique proteins were identified from 28 individual protein spots displaying IgG-reactivity by Western blot analysis (Table 4.2). A substantial majority of the antigenic proteins detected in Section 4.2.2 (*n* = 6/7; 85.7 %), were also identified following optimisation of the immunodetection strategy (Section 4.2.4) demonstrating validation of the results through reproducibility. The molecular chaperone and allergen Mod-E/Hsp90/Hsp1 (AFUA_5G04170; Spot 10; Figure 4.3), was not detected following protocol optimisation and this may be accounted for by the substantial increase in the intensity of immunoreactivity observed from the carboxypeptidase S1 (AFUA_8G04120; Spot 10; Figure 4.4). This high level of immunoreactivity may have masked the detection of the molecular chaperone and allergen Mod-E/Hsp90/Hsp1, located adjacent to it (Figure 4.6). The optimisation of the immunodetection protocol resulted in the identification of an additional 18 IgG-reactive *A. fumigatus* proteins (Table 4.2), demonstrating a substantial improvement in the efficacy of the method, without significant loss in sensitivity. Collectively, this strategy resulted in the identification of 25 *A. fumigatus* proteins reactive with IgG from healthy individuals.

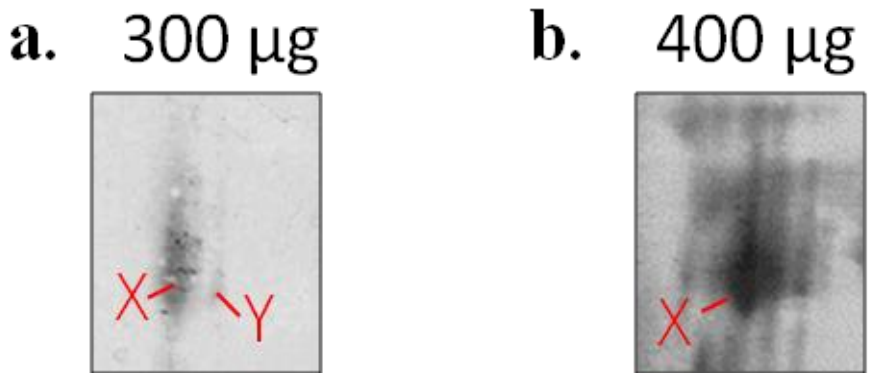

Figure 4.6: Increase in intensity of immunoreactivity following optimisation of immunodetection strategy. Carboxypeptidase S1 (X) masks the detection of the molecular chaperone and allergen Mod-E/Hsp90/Hsp1 (Y) following an increase in the amount of protein separated by 2D-PAGE, from (a) 300 µg to (b) 400 µg.

A number of proteins were detected that exhibited relatively high immunoreactivity with sera from healthy subjects. These proteins included a carboxypeptidase S1 (AFUA_8G04120), an aminopeptidase (AFUA_2G00220), a 1,3-β-glucosyltransferase (AFUA_2G05340), a fumarate hydratase (AFUA_6G02470) and an aspartate aminotransferase (AFUA_4G10410) (Figure 4.4). Several proteins were identified from multiple spots; woronin body protein HexA (AFUA_5G08830; Spots 17, 26 and 27; Figure 4.4) was identified from three individual spots, differing in both p*I* and molecular mass. HexA, identified from Spot 17, was positioned at the bottom of the gel, indicating a protein with a lower molecular mass than predicted and may be the result of protein degradation. Presence of multiple isoforms of the HexA protein has been demonstrated previously, with its identification from 12 individual spots in the mitochondrial proteome map of *A. fumigatus* (Vödisch *et al.*, 2009). This observation was confirmed by the detection of peptides exclusively from the C-terminal section of the HexA protein by LC-MS/MS (Figure 4.5) and further discussion of this protein will be undertaken later in the Chapter. Translation elongation factor EF-1 alpha subunit (AFUA_1G06390; Spots 19 and 21; Figure 4.4) was identified from two spots with apparent differing molecular masses. Fumarate hydratase (AFUA_6G02470; Spots 24 and 25; Figure 4.4) was identified from two spots which appeared to have the same molecular mass but differed slightly in p*I*, based on their positions side-by-side on the gel (Figure 4.4). This occurrence was also observed for cobalamin-independent methionine synthase MetH/D (AFUA_4G07360; Spots 4 and 5; Figure 4.3) and alpha-ketoglutarate dehydrogenase complex subunit, Kgd1 (AFUA_4G11650; Spots 6, 7 and 8; Figure 4.3). This indicates the presence of isoforms of these proteins, possibly as a result of post-translational modifications. Additionally, the detection of immunoreactivity against multiple protein isoforms provides validation of the results obtained, as it demonstrates binding of IgG to antigenic proteins is specific.

Thirteen proteins were identified, which had not been previously detected in *A. fumigatus* as antigens, representing a significant expansion of the currently established immunoproteome (Table 4.3). Among these, a hexokinase Kxk was identified, displaying 54 % sequence identity with the *Candida albicans* hexokinase Hxk2p (BLAST E-value = 0.0). An outer mitochondrial membrane protein porin (AFUA_4G06910) was also detected, with 42 % sequence identity to the outer membrane mitochondrial porin Por1p from *C. albicans* (BLAST E-value = 2 x 10^{-78}). These *C. albicans* proteins demonstrated IgG-reactivity following incubation of protein lysates with sera from patients with systemic candidiasis (Pitarch *et al.*, 2004). Immunoreactivity of these *A. fumigatus* orthologs demonstrates the antigenicity of these proteins and thus validates their identification as part of the immunoproteome. The remaining immunoreactive proteins identified here, have previously been characterised as antigenic and/or allergenic in *A. fumigatus*, based on their IgG or IgE reactivity respectively. Immunoproteomic studies carried out on *A. fumigatus* germlings and secretome have identified eleven of the antigens described here. Two lysophospholipases, Plb1 (AFUA_4G08720) and Plb3 (AFUA_2G03610), were identified, that have also been detected in the immunosecretome of *A. fumigatus* by Singh *et al.* (2010a). These proteins contain a signal peptide for secretion (Petersen *et al.*, 2011) and are involved in the degradation of phospholipids making them an important virulence factor (Abad *et al.*, 2010). The well characterised allergens, molecular chaperone and allergen Mod-E/Hsp90/Hsp1 (AFUA_5G04170), molecular chaperone Hsp70 (AFUA_1G07440), Hsp70 chaperone, Hsp88 (AFUA_1G12610) were identified, which have previously been detected in germlings based on their IgE reactivity (Singh *et al.*, 2010b). IgG-reactivity has previously been shown against inosine 5'-monophosphate (IMP) dehydrogenase (AFUA_2G03610), aspartate aminotransferase (AFUA_4G10410) and fumarate hydratase (AFUA_6G02470), using

sera from *A. fumigatus* immunised rabbits (Asif *et al.*, 2010). Phosphoglycerate kinase PgkA (AFUA_1G10350), cobalamin-independent methionine synthase MetH (AFUA_4G07360), ATP synthase F1 beta subunit (AFUA_5G10550) and mitochondrial aconitate hydratase (AFUA_6G12930) have been shown previously to exhibit IgG and IgE reactivity (Asif *et al.*, 2010; Singh *et al.*, 2010b). Detection of these previously characterised immunogens provides validation of the experimental process, despite the use on non-disease state sera.

Table 4.3: IgG-reactive proteins (*n* = 13) identified in this study, previously not classified as antigenic in *A. fumigatus*

Spot No	CADRE ID. (AFUA_)	Protein name	tp*I*	tM_r	Intensity of immunoreactivity[1]		
					L	M	H
1	**4G11650**	Alpha-ketoglutarate dehydrogenase complex subunit Kgd1	6.47	118900.00		✓	
4	**6G10990**	NADPH cytochrome P450 reductase (CprA)	5.38	76782.85		✓	
5	**8G00440**	Steroid monooxygenase	5.48	101032.20		✓	
9	**5G07330**	Carboxypeptidase S1	4.74	68345.84			✓
10	**8G04120**	Carboxypeptidase S1	5.4	67672.79			✓
11	**2G05340**	1,3-β-glucanosyltransferase Gel4	4.83	58872.59			✓
13	**4G06820**	GPI-anchored cell wall organization protein Ecm33	4.8	41505.47		✓	
14	**2G00220**	Aminopeptidase	4.99	56702.95			✓
15	**2G05910**	Hexokinase Kxk	5.06	54209.22		✓	
17	**5G08830**	Woronin body protein HexA	6.56	49836.57	✓		
18	**4G06910**	Outer mitochondrial membrane protein porin	9.47	36893.97	✓		
19	**1G06390**	Translation elongation factor EF-1 alpha subunit	9.12	50019.60		✓	
20	**6G06370**	NAD(+)-isocitrate dehydrogenase subunit I	8.42	49745.35		✓	
21	**1G06390**	Translation elongation factor EF-1 alpha subunit	9.12	50019.60		✓	

Spot No	CADRE ID. (AFUA_)	Protein name	tp*I*	tM_r	Intensity of immunoreactivity[1]		
					L	M	H
26	**5G08830**	Woronin body protein HexA	6.56	49836.57		✓	
27	**5G08830**	Woronin body protein HexA	6.56	49836.57		✓	

CADRE ID., *A. fumigatus* gene annotation nomenclature according to Nierman *et al.* (2005) and Mabey *et al.* (2004); tp*I*, theoretical isoelectric point; tM_r, theoretical molecular mass; Spot No. from Figure 4.4; [1]Iintensity of immunoreactivity on immunoblot relative to intensity of the corresponding spot on the Coomassie stained 2D-PAGE gel; L, low relative intensity; M, medium relative intensity; H, high relative intensity (Section 2.2.4.8).

In addition to identification in the mycelia, many of the IgG-reactive proteins identified here have also exhibited differential developmental or cellular localisation. The conidia proteome map of Teutschbein *et al.* (2010) identified five of these antigens as being enriched or abundant in the conidia of *A. fumigatus*; Hsp70 chaperone Hsp88 (AFUA_1G12610), translation elongation factor EF-1 alpha subunit (AFUA_1G06390), molecular chaperone Hsp70 (AFUA_1G07440), phosphoglycerate kinase PgkA (AFUA_10350) and mitochondrial aconitate hydratase (AFUA_6G12930). Additionally, an outer mitochondrial membrane protein porin (AFUA_4G06910), alpha-ketoglutarate dehydrogenase complex subunit Kgd1 (AFUA_4G11650), woronin body protein HexA (AFUA_5G08830), molecular chaperone and allergen Mod-E/Hsp90/Hsp1(AFUA_5G04170) and NAD(+)-isocitrate dehydrogenase subunit I (AFUA_6G06370) were found in the early development proteome of *A. fumigatus* germlings (Cagas *et al.*, 2011b; Suh *et al.*, 2012). Two glycosylphosphatidylinositol (GPI)-anchored proteins were detected, 1,3-β-glucanosyltransferase Gel4 (AFUA_2G05340) and GPI-anchored cell wall organization protein Ecm33 (AFUA_4G06820), with locations on the plasma membrane (Bruneau *et al.*, 2001), are involved in assembly of the cell wall (Chabane *et al.*, 2006; Gastebois *et al.*, 2010a). Proteins with signal peptides for secretion included an aminopeptidase (AFUA_2G00220), two separate carboxypeptidases (AFUA_5G07330, AFUA_8G04120) and NADPH cytochrome P450 reductase CprA (AFUA_6G10990) (Petersen *et al.*, 2011). The majority of the remaining proteins were detected in germinating conidia or the secretome based on their immunoreactivity as discussed earlier (Asif *et al.*, 2010; Singh *et al.*, 2010a, 2010b). The occurrence of these proteins extracellularly or in early developmental stages, in addition to intracellularly in the mycelia, may explain the development of immunoreactivity directed against these proteins. Routine environmental exposure to *A. fumigatus* involves inhalation of

conidia, followed predominantly by their clearance from the lungs before mycelia development (Murdock *et al.*, 2011). This would result in the host, in the absence of *A. fumigatus*-related disease, predominantly encountering proteins of the conidia, early germlings and secreted proteins.

Upon detailed review of the literature, on the proteomic response of *A. fumigatus* to stress, it was observed that the immunogenic proteins identified here have been shown to be up-regulated in response to heat shock, oxidative stress, hypoxia and interactions with host cells (Lessing *et al.*, 2007; Sugui *et al.*, 2008; Albrecht *et al.*, 2010; Fraczek *et al.*, 2010; Morton *et al.*, 2011; Vödisch *et al.*, 2011). Seven of the antigens herein detected have been found to be up-regulated in response to heat shock, brought about by a temperature shift from 30°C to 48°C (Albrecht *et al.*, 2010). The heat shock proteins, Hsp88, Hsp90 and Hsp70, were up-regulated, in addition to the translation elongation factor EF-1 alpha subunit, hexokinase Kxk, cobalamin-independent methionine synthase MetH/D and alpha-ketoglutarate dehydrogenase complex subunit Kgd1. This may reflect the temperature shift from ambient to 37°C, experienced by conidia upon entering of the pulmonary alveoli. We speculate that up-regulation of these proteins could account for their presentation to the adaptive immune system and the subsequent generation of an antibody response. Cobalamin-independent methionine synthase MetH/D and Hsp88 also showed Yap1 dependent induction in response to oxidative stress in the form of H_2O_2 (Lessing *et al.*, 2007). The molecular chaperone and allergen Mod-E/Hsp90/Hsp1, in addition to other *A. fumigatus* allergens, is also up-regulated in response to H_2O_2 (Fraczek *et al.*, 2010). Inhaled conidia are exposed to oxidative stress, in the form of reactive oxygen species (ROS) generated by alveolar macrophages and polymorphonuclear leucocytes (PMNLs). Another environmental condition that inhaled conidia encounter is a limited oxygen supply and

the inability of *A. fumigatus* to adapt a hypoxia response is coupled with its loss of virulence (Willger *et al.*, 2008). Vödisch *et al.* (2011) identified 59 proteins that were up-regulated in *A. fumigatus* ATCC46645 following cultivation in hypoxic compared to normoxic conditions, including 10 of the IgG-reactive proteins detected here. Comparative analysis of the entire mycelial proteome revealed up-regulation of phosphoglycerate kinase PgkA (AFUA_1G10350), asparate aminotransferase (AFUA_4G10410) and steroid monooxygenase (AFUA_8G00440) in response to hypoxia. A sub-proteomic investigation of the mitochondria also revealed significant up-regulation of 1,3-β-glucanosyltransferase Gel3 (AFUA_2G05340), lysophospholipases Plb1 and Plb3 (AFUA_4G08720 and AFUA_3G14680), GPI-anchored cell wall organisation protein Ecm33 (AFUA_4G06820), outer mitochondrial membrane protein porin (AFUA_4G06910), ATP synthase F1, beta subunit (AFUA_5G10550) and mitochondrial aconitate hydratase (AFUA_6G12930) in response to hypoxia. Conversely, an additional antigenic protein, woronin body protein HexA (AFUA_5G08830) was observed as being down-regulated in hypoxia (1.7 fold) in the whole mycelia proteome comparison. However a truncated version of this protein was significantly up-regulated in hypoxic conditions (5.68 fold) upon comparison of the mitochondrial fractions (Vödisch *et al.*, 2011). This differential regulation may be explained by the fact that many isoforms of the HexA protein are resolved by 2D-PAGE and these proteins have more relative abundance in the mitochondria (Vödisch *et al.*, 2009). These conditions of increased temperature, hypoxia and oxidative stress are similar to those encountered by conidia upon entering the alveoli of the lungs. We postulate that up-regulation of the immunoreactive proteins identified here, in response to stress, may allude to the development of an adaptive immune response directed towards them.

Numerous comparative transcriptomic and proteomic studies have been carried out previously to characterise the regulation of genes and proteins of *A. fumigatus* in response to host cells. These, in addition to experiments aiming to replicate environmental conditions within the host, provide valuable information on the mechanisms of *A. fumigatus* virulence. Upon exposure of *A. fumigatus* conidia to human neutrophils, three of the antigens identified here were found to be up-regulated at the transcript level (Sugui *et al.*, 2008). Phosphoglycerate kinase PgkA (AFUA_1G10350), aspartate aminotransferase (AFUA_4G10410) and mitochondrial aconitate hydratase (AFUA_6G12930) transcripts were all up-regulated following incubation of conidia with neutrophils for 1.5 h. These results were replicated when conidia were incubated with neutrophils from patients with chronic granulomatous disease (CGD), which are defective in the production of ROS, thus excluding the influence of ROS on the regulation of these genes (Sugui *et al.*, 2008). Aspartate aminotransferase (AFUA_4G10410) was also found to be up-regulated following incubation of *A. fumigatus* conidia with airway epithelial cells, in addition to the putative IMP dehydrogenase (AFUA_2G03610) (Oosthuizen *et al.*, 2011) also identified here. The transcripts of two lysophospholipases, Plb1 (AFUA_4G08720) and Plb3 (AFUA_2G03610), were observed to be up-regulated in the presence of lecithin, a constituent of human lung surfactant, in a directed study using quantitative PCR (Shen *et al.*, 2004). Additionally, the antigenic woronin body protein HexA (AFUA_5G08830) was up-regulated following 9 and 12 h incubation with immature human dendritic cells (Morton *et al.*, 2011) and the molecular chaperone and allergen Mod-E/Hsp90/Hsp1 (AFUA_5G04170) was up-regulated following co-incubation with macrophages (Fraczek *et al.*, 2010). We hypothesize that up-regulation of these genes, in the host-pathogen response, may increase the opportunity for presentation to the adaptive immune system and thus explain the development of their immunoreactivity.

The independent detection of the woronin body protein HexA (AFUA_5G08830) from three separate locations by 2D-PAGE provided an interesting observation on the putative position of antigenic epitope on the protein (Figure 4.3). As discussed above the occurrence of multiple isoforms of the HexA protein has been observed in previous 2D-PAGE studies, with its identification from 12 independent spots on the mitochondrial and 2 spots in the mycelia protein map (Vödisch *et al.*, 2009). This phenomenon indicates the presence of modified versions of the protein, with different p*I*s and molecular masses as deduced by the positions of the spots on the gel. Alterations of the isoelectric point of the protein, without a change in apparent molecular size could result from post-translational modifications such as phosphorylation. Identification of HexA from spots 26 and 27 (Figure 4.4), was in agreement with the theoretical molecular mass (tM_r = 50 kDa) and p*I* (6.56) of the protein. In contrast, the identification of HexA from spot 17 did not correlate to the tM_r, with its position on the gel indicative of a much smaller protein. Interrogation of the peptides identified from each of the HexA protein spots (Spot numbers: 17, 26 and 27; Figure 4.4) revealed that while broad sequence coverage of the proteins from spots 26 and 27 was achieved, peptides identified from spot 17 were confined exclusively to the C-terminal section (Figure 4.5). The level of immunoreactivity to the truncated HexA protein, observed in spot 17, is lower than that observed from the intact HexA proteins in spots 26 and 27, which indicates the antigenic epitope recognised by human IgG may predominantly be contained on the N-terminal section of the protein. Truncation of the protein may therefore result in loss of the IgG binding site or weaken the affinity of the IgG towards it.

In summary, the work described in this Chapter expands the characterisation of the *A. fumigatus* immunoproteome. Proteins (*n* = 25) were identified as IgG-reactive

antigens, through 2D-PAGE and Western blot analysis using sera from healthy individuals. This work represents the first classification of 13 of these proteins as immunogenic which signifies a substantial extension of the currently recognised collection of *A. fumigatus* antigens. Many of these IgG-reactive antigens, identified from the mycelia of *A. fumigatus*, were also detected previously in the secretome of *A. fumigatus* or additionally are associated with early developmental stages of growth. Additionally 19 of these immunogenic proteins have been described, in comparative proteomics studies, to be up-regulated in response to cellular stress or in response to interactions with host cells. These conditions of stress, including heat-shock, oxidative stress, hypoxia and exposure to host cells, may mimic the internal host environment encountered by the routinely inhaled conidia of *A. fumigatus*. We postulate that the up-regulation of these proteins may account for their presentation to the immune system and the subsequent generation of an antibody response to *A. fumigatus* in healthy individuals. In addition to the characterisation of the *A. fumigatus* immunoproteome, 2D-PAGE coupled with Western blot analysis enabled the putative location of the dominant immune-epitope on the HexA protein to be identified. The reduction in the relative intensity of immunoreactivity to the C-terminal fragment of the HexA protein indicates the antigenic epitope is located predominantly on the N-terminal section of the protein. Further work would be required to isolate the exact location of the antigenic epitope on the HexA protein however this work provides guidance for the direction of future investigations. The reactivity of disease-state sera with mycelial proteins in future studies could expand the field of *A. fumigatus* immunoproteomics further. However, the use of sera from healthy individuals represents a novel baseline method by which to characterise the immune response to *A. fumigatus* in the absence of disease. The global characterisation of the proteome of *A. fumigatus*, using MS-based proteomics as described in Chapter 3, and immunoproteomics, as described in this Chapter, provides a

comprehensive overview of the systems operating in this opportunistic pathogen, both *in vitro* and *in vivo*. In Chapter 5, phenotypic analysis of *A. fumigatus* will be carried out in response to a combination of stresses and comparative proteomics will be utilised in order to elucidate the cellular mechanisms differentially regulated in these conditions.

CHAPTER 5

Comparative proteomic profiling of gliotoxin-associated mechanisms in *A. fumigatus*

5 Chapter 5

5.1 Introduction

Large-scale MS-based proteomics studies, as described in Chapter 3, can provide a global overview of the many biochemical systems active in an organism under a given set of conditions. The traditional proteomics strategy, comprising 2D-PAGE coupled with MS for protein identification, has been utilised in countless comparative studies, for relative quantitation of changes in the proteome constituents, in addition to detection of post-translational modifications (PTMs) (Rabilloud *et al.*, 2010). Comparative 2D-PAGE has extended the understanding of pathways which respond to various forms of stress in *A. fumigatus* (Lessing *et al.*, 2007). Often, comparative 2D-PAGE studies are undertaken following observation of altered growth phenotypes, either due to exogenous stress and/or genetic mutations (Doyle, 2011b). 2D-PAGE has been carried out to elucidate the mechanisms involved in response to hypoxia (Vödisch *et al.*, 2011; Barker *et al.*, 2012), oxidative stress (Lessing *et al.*, 2007), heat shock (Albrecht *et al.*, 2010), gliotoxin (Schrettl *et al.*, 2010; Carberry *et al.*, 2012) and anti-fungal agents (Gautam *et al.*, 2008, 2011; Singh *et al.*, 2012) in *A. fumigatus*. Additionally, 2D-PAGE-based proteomics can identify putative targets of specific genes, through comparative analysis of the proteome changes following gene disruption. For example, investigation of the bZIP-like transcription factors AfYap1 (Lessing *et al.*, 2007) and HapX (Hortschansky *et al.*, 2007), the nonribosomal peptide synthetase Pes3 (O'Hanlon *et al.*, 2011), the glucosidase 1 AfCwh41 (Zhang *et al.*, 2009) and cell wall biosynthesis proteins (Bruneau *et al.*, 2001) employed this approach.

Lessing *et al.* (2007) investigated the proteomic response of *A. fumigatus* to exogenous H_2O_2, and identified differential expression of 28 proteins, with functions

ranging from stress-response and antioxidant properties to amino acid metabolism. Many of these proteins represented putative targets of the transcriptional regulator AfYap1, based on inference from similar studies in yeast. Accordingly, disruption of the Af*yap1* gene, resulted in H_2O_2- and menadione-sensitive phenotypes. Comparative 2D-PAGE analysis of wild-type and the Af*yap1* mutant, following exposure to H_2O_2, revealed altered expression of 29 proteins that could putatively be controlled by AfYap1. This revealed the Af*yap1*-dependent expression of a number of catalases, heat shock proteins and factors involved in protein synthesis in response to H_2O_2, and highlighted the importance of this transcriptional regulator in the response to oxidative stress.

A study carried out by Carberry *et al.* (2012) charted the proteomic response of *A. fumigatus* to gliotoxin and observed the differential regulation of 27 unique proteins. These included the down-regulation of a catalase and a peroxiredoxin, proteins involved in the relief of oxidative stress. A member of the gliotoxin biosynthetic cluster, *gliT*, encodes a gliotoxin oxidoreductase, which imparts protection to exogenous gliotoxin (Scharf *et al.*, 2010; Schrettl *et al.*, 2010). GliT has been demonstrated to catalyse gliotoxin reduction, with the concurrent oxidation of NADPH to $NADP^+$ and transcription and translation of GliT are induced by exogenous gliotoxin (Schrettl *et al.*, 2010). Additionally Scharf *et al.* (2010) characterised the FAD-dependent oxidation of reduced gliotoxin, in a reaction that generates ROS. In the absence of the GliT protein, significant sensitivity to exogenous gliotoxin is observed in *A. fumigatus* and transformation of the *gliT* gene into other gliotoxin-sensitive fungi resulted in acquired resistance to the metabolite (Schrettl *et al.*, 2010).

Another member of the gliotoxin biosynthetic cluster is *gliK* (Gardiner and Howlett, 2005), which encodes a protein with a putative gamma-glutamyl

cyclotransferase (GGCT) domain (Gallagher *et al.*, 2012). As described in Chapter 1, the GliK protein has remained experimentally uncharacterised until recently. Work presented in Chapter 6, demonstrates that the GliK protein is essential for the biosynthesis of gliotoxin and absence of this protein results in increased sensitivity to exogenous gliotoxin and to H_2O_2 (Gallagher, 2010; Gallagher *et al.*, 2012). GliK also appears to be involved in gliotoxin efflux, with increased accumulation of exogenously added gliotoxin observed in the deletion strain, Δ*gliK* (Gallagher, 2010; Gallagher *et al.*, 2012). Characterisation of the systems involved in the interaction of gliotoxin with *A. fumigatus* Δ*gliK* could facilitate a greater understanding of both the role of GliK in the cell and the influence of gliotoxin-imposed stress on *A. fumigatus*.

The effect of combinatorial stresses is emerging as a new focus of investigation, due to the simultaneous exposure of organisms to distinct stresses in their environment. As discussed in Chapter 1, *A. fumigatus* is exposed to an array of physical, chemical and host-associated stresses as a human pathogen, including heat shock, hypoxia and oxidative stress. Kaloriti *et al.* (2012) have demonstrated the influence of combinatorial stresses on *C. albicans* and *C. glabrata.* These authors noted that coupling of oxidative stress to either osmotic or nitrosative stress significantly decreases growth or viability of the yeast cells, relative to either stress applied in isolation. The molecular response of fungi to a combination of stresses has largely gone uncharacterised, with limited large-scale transcriptomic or proteomic analyses performed in this area to date (Kaloriti *et al.*, 2012). Comparative proteomics of *A. fumigatus*, examining the response to stresses, applied singularly or in tandem, could elaborate on the mechanisms influenced by the exposure to combinatorial stresses.

The work presented in this Chapter stemmed from the hypothesis that, based on the observed increase in sensitivity of *A. fumigatus* Δ*gliK* to gliotoxin and H_2O_2 individually (Gallagher, 2010), an additive or synergistic effect may be observed by combining the stresses. In light of any alteration of phenotype, comparative 2D-PAGE would identify alterations to the proteome in response to a combination of challenges. These proteomic profiles may reveal the pathways and molecular mechanisms affected by exposure to a combination of gliotoxin and H_2O_2. Additionally, analysis of the proteome of *A. fumigatus* Δ*gliK* in response to gliotoxin may further elucidate a possible function for the yet unclassified, GliK protein. Thus, the aims of the work carried out in this Chapter were; (i) to carry out phenotypic analysis of *A. fumigatus* ATCC26933 and Δ*gliK* in response to simultaneous challenge with gliotoxin and H_2O_2, (ii) to investigate changes to the proteome of *A. fumigatus* in response to co-addition of gliotoxin and H_2O_2 and (iii) to investigate the proteome of *A. fumigatus* Δ*gliK* in response to exogenous gliotoxin.

5.2 Results

5.2.1 Phenotypic analysis of *A. fumigatus* ATCC26933 and Δ*gliK* in response to a combination of gliotoxin and H_2O_2

Following the observation that growth of *A. fumigatus* Δ*gliK* is significantly inhibited relative to the wild-type in the presence of gliotoxin (≥ 1 µg/ml; $p < 0.001$) or H_2O_2 (≥ 1 mM; $p < 0.001$) individually (Gallagher, 2010; Gallagher *et al.*, 2012), the effect of combining these stresses was investigated. Plate assays were carried out in order to determine the combined phenotypic response of *A. fumigatus*, ATCC26933 and Δ*gliK*, to gliotoxin plus H_2O_2 (Section 2.1.5.21). *A. fumigatus*, ATCC26933 and Δ*gliK*, were exposed to gliotoxin (1 - 10 µg/ml) and H_2O_2 (0 - 1 mM) in Czapek-Dox agar (Section 2.1.5.10), individually and in combination. Equivalent volumes of methanol were added to appropriate plates as a solvent control for gliotoxin, and the radial growth of replicate colonies was measured at 72 h.

The radial growth of *A. fumigatus* ATCC26933 (wild-type) was significantly attenuated in the presence of 10 µg/ml gliotoxin ($p < 0.001$), whereas lower gliotoxin concentrations (≥ 1 µg/ml) were sufficient to significantly inhibit growth of Δ*gliK* ($p < 0.01$) (Figure 5.1a and Figure 5.2a). Similarly, *A. fumigatus* Δ*gliK* demonstrated significantly higher sensitivity to H_2O_2, with $p < 0.05$ at 0.5 mM and $p < 0.001$ at 1 mM H_2O_2 (Figure 5.1b and Figure 5.2b). No growth of *A. fumigatus* Δ*gliK* was visible in Czapek-Dox agar plates supplemented with 1 mM H_2O_2 at 72 h. Unexpectedly, co-addition of gliotoxin and H_2O_2 resulted in reduced H_2O_2 sensitivity in both *A. fumigatus* wild-type and Δ*gliK* (Figure 5.1c, Figure 5.2c and d). This relief of H_2O_2-induced growth inhibition was achieved in a dose-dependent manner, where 10 µg/ml gliotoxin was sufficient to restore radial growth to the same level as observed for gliotoxin alone.

Gliotoxin-mediated relief of H_2O_2-induced growth inhibition was observed for both wild-type and Δ*gliK* strains of *A. fumigatus*.

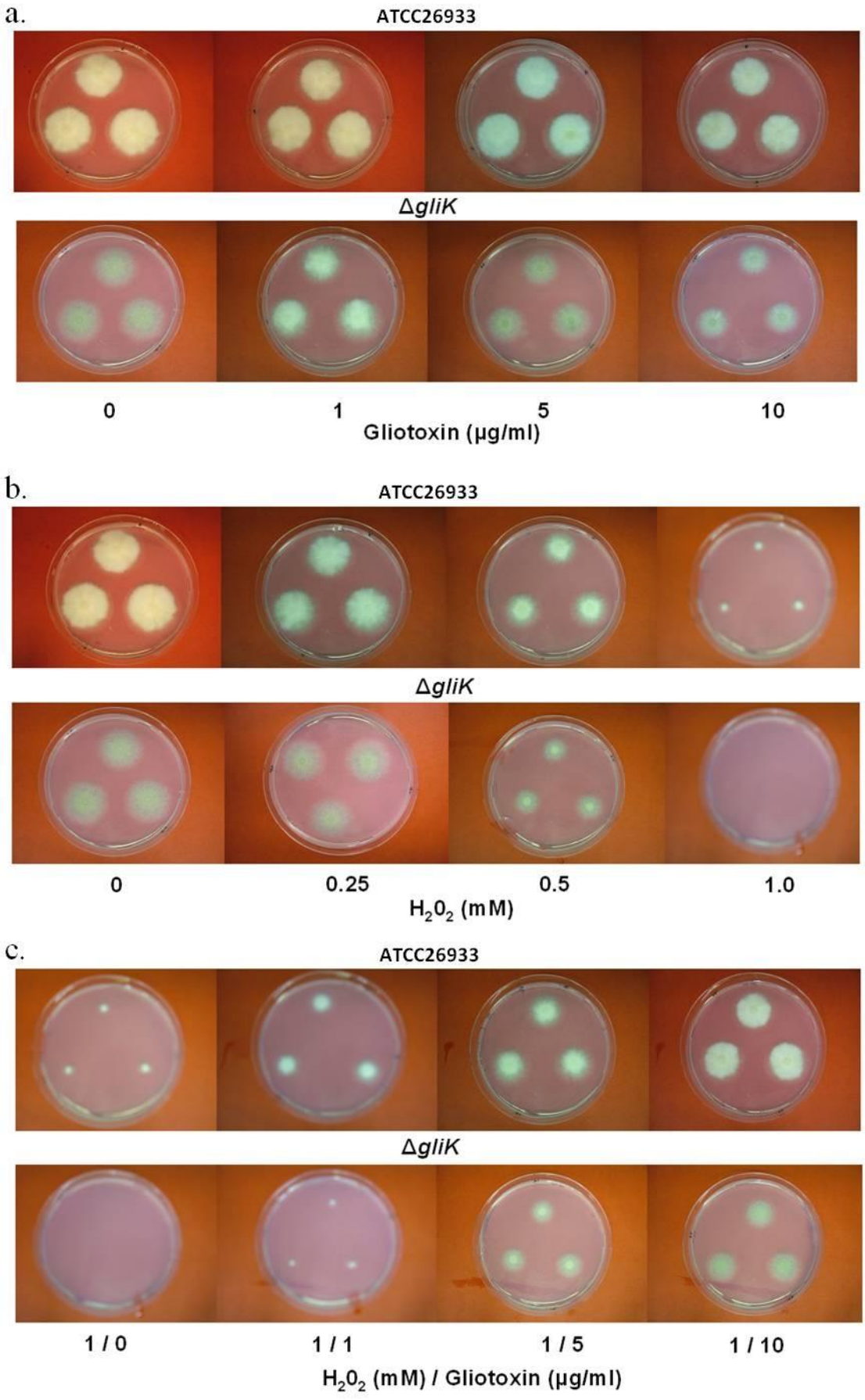
a.
ATCC26933
ΔgliK
0
1
5
10
Gliotoxin (μg/ml)
b.
ATCC26933
ΔgliK
0
0.25
0.5
1.0
H2O2 (mM)
c.
ATCC26933
ΔgliK
1 / 0
1 / 1
1 / 5
1 / 10
H2O2 (mM) / Gliotoxin (μg/ml)

Figure 5.1: Phenotypic analysis demonstrating the individual and combined effects of gliotoxin (0-10 μg/ml) and H_2O_2 on *A. fumigatus* ATCC26933 and Δ*gliK*. (a) Gliotoxin (10 μg/ml) significantly inhibits *A. fumigatus* Δ*gliK* growth, relative to ATCC26933. (b) H_2O_2 (1 mM) completely inhibits *A. fumigatus* Δ*gliK* growth, compared to ATCC26933. (c) Gliotoxin (1-10 μg/ml) relieves H_2O_2–mediated growth inhibition of both *A. fumigatus* ATCC26933 and Δ*gliK* in a dose dependent manner.

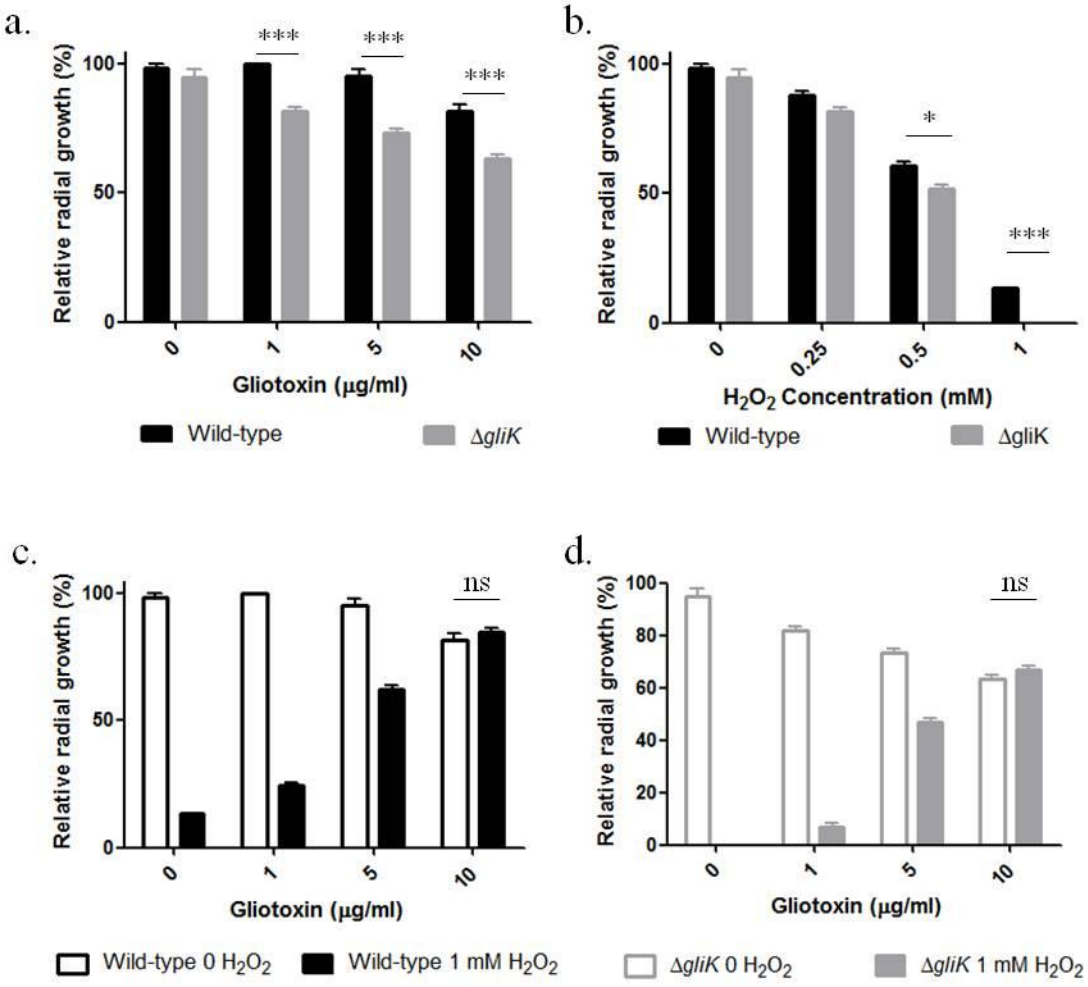

Figure 5.2: Graphical representation of phenotypic analysis shown in Figure 5.1. Individual and combined effects of gliotoxin (0-10 µg/ml) and H_2O_2 on *A. fumigatus* ATCC26933 (wild-type) and Δ*gliK*. (a) Gliotoxin (10 µg/ml) significantly inhibits *A. fumigatus* Δ*gliK* growth, compared to wild-type. (b) H_2O_2 (1 mM) completely inhibits *A. fumigatus* Δ*gliK* growth, relative to wild-type. (c and d) Gliotoxin (1-10 µg/ml) relieves H_2O_2–mediated growth inhibition of both *A. fumigatus* ATCC26933 (wild-type) and Δ*gliK* in a dose dependent manner. Co-addition of gliotoxin (10 µg/ml) and H_2O_2 (1 mM) recovered growth to the same level as the gliotoxin control (10 µg/ml). *** indicates $p < 0.001$, * indicates $p < 0.05$, ns indicates not significant ($p > 0.05$).

5.2.2 Comparative 2D-PAGE analysis of *A. fumigatus* ATCC26933 following exposure to a combination of H_2O_2 and gliotoxin

In order to elucidate the mechanisms involved in gliotoxin-mediated relief of H_2O_2-induced stress in *A. fumigatus* ATCC26933, a comparative 2D-PAGE study was undertaken. *A. fumigatus* ATCC26933 was grown in Sabouraud dextrose medium for 24 h prior to addition of one of the four treatments outlined in Table 5.1. Mycelia (n = 5/treatment) were harvested after 4 h and protein was extracted as described in Section 2.2.2.2. TCA/acetone precipitation was carried out on protein lysates prior to resuspension of protein in IEF buffer (Section 2.1.6.2). Protein was separated on pH 4 - 7 IEF strips, followed by resolution by SDS-PAGE (Section 2.2.4.3). Colloidal Coomassie staining was carried out on gels, with subsequent protein spot analysis using Progenesis™ SameSpot software (Section 2.2.4.4). Gels from all four treatments were aligned (n = 20; 5 gels/treatment) and subsets of treatments were compared as outlined in Figure 5.3.

Table 5.1: Treatments carried out on *A. fumigatus* ATCC26933, with addition of gliotoxin, H_2O_2 and/or methanol indicated.

Treatment	**Gliotoxin (µg/ml)[1]**	H_2O_2 **(mM)[2]**	**Methanol[3]**
Solvent Control	-	-	✓
Gliotoxin alone	10	-	-
H_2O_2 alone	-	2	✓
Gliotoxin and H_2O_2 (Co-addition)	10	2	-

[1]Gliotoxin stock (500 µl) (Table 2.1) added per 50 ml culture. [2] H_2O_2 stock (100 µl) (Table 2.1) added per 50 ml culture. [3]Methanol (500 µl) added per 50 ml culture as a solvent control for gliotoxin.

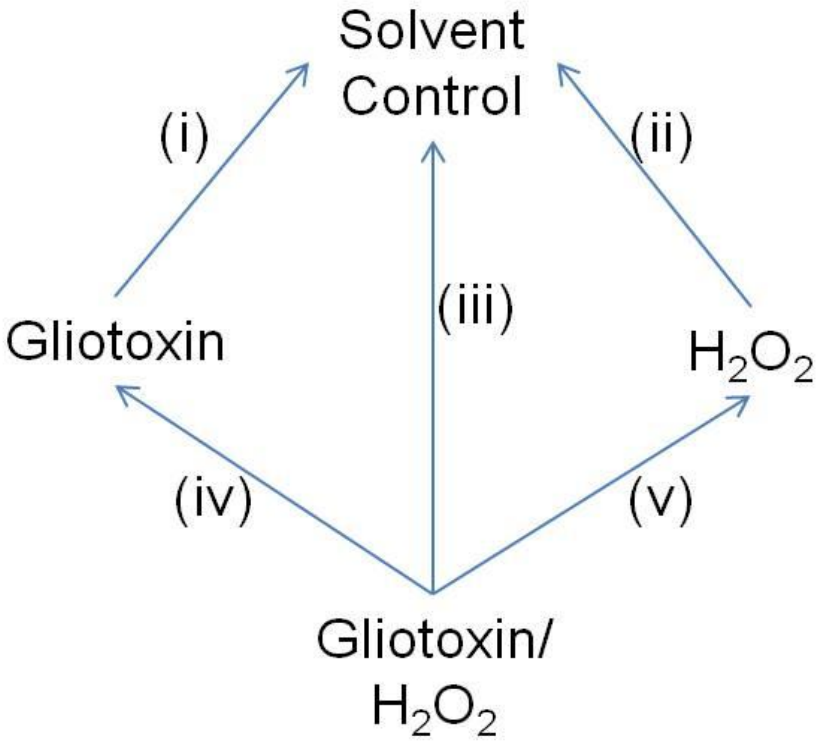

Figure 5.3: Comparison sets used for analysis of 2D-PAGE of *A. fumigatus* ATCC26933 following gliotoxin and H_2O_2 exposure, individually and combined. Arrows point to control gels in each comparison set. Comparison sets include (i) Gliotoxin alone v Solvent Control, (ii) H_2O_2 alone v Solvent control, (iii) Co-addition v Solvent control, (iv) Co-addition v Gliotoxin alone, (v) Co-addition v H_2O_2 alone.

Proteins spots (n = 29) were found to be significantly differentially expressed ($p < 0.05$) under these conditions (Figure 5.4). Three of these proteins spots had a fold increase ≥ 1.5 fold ($p < 0.05$) and two had a fold decrease ≥ 1.5 fold ($p < 0.05$), following exposure to gliotoxin alone relative to the solvent control (Comparison (i)). Six proteins spots exhibited a fold increase ≥ 1.5 fold ($p < 0.05$), following exposure to H_2O_2 alone relative to the solvent control (Comparison (ii)). Nine of these proteins spots had a fold increase ≥ 1.5 fold ($p < 0.05$) and three showed a fold decrease ≥ 1.5 fold ($p < 0.05$), under gliotoxin/H_2O_2 co-addition relative to the solvent control (Comparison (iii)). Nine proteins spots presented with a fold increase ≥ 1.5 fold ($p < 0.05$) and one had a fold decrease ≥ 1.5 fold ($p < 0.05$), in the co-addition relative to exposure to gliotoxin alone (Comparison (iv)). Seven proteins spots yielded a fold increase ≥ 1.5 fold ($p < 0.05$) and six had a fold decrease ≥ 1.5 fold ($p < 0.05$), in the co-addition relative to H_2O_2 alone (Comparison (v)). Redundancy was noted, with some protein spots included in multiple comparison sets, resulting in the differential expression of 29 unique protein spots. These protein spots were excised and subjected to in-gel trypsin digestion (Section 2.2.6.1), followed by LC-MS/MS analysis for protein identification (Section 2.2.6.3).

a.

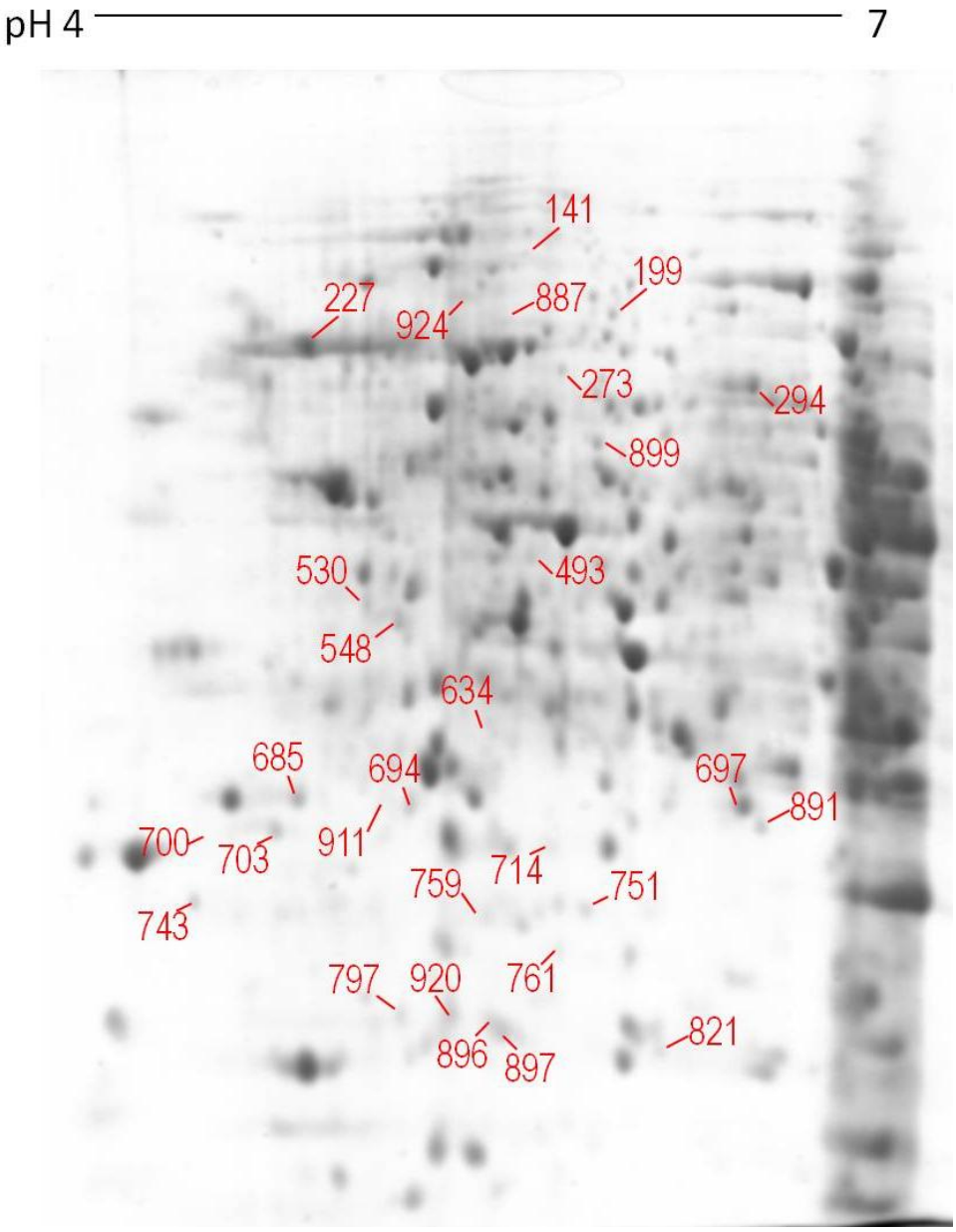

Colloidal Coomassie stained 2D-PAGE gel
of *A. fumigatus* mycelial proteins;
Solvent control

b.

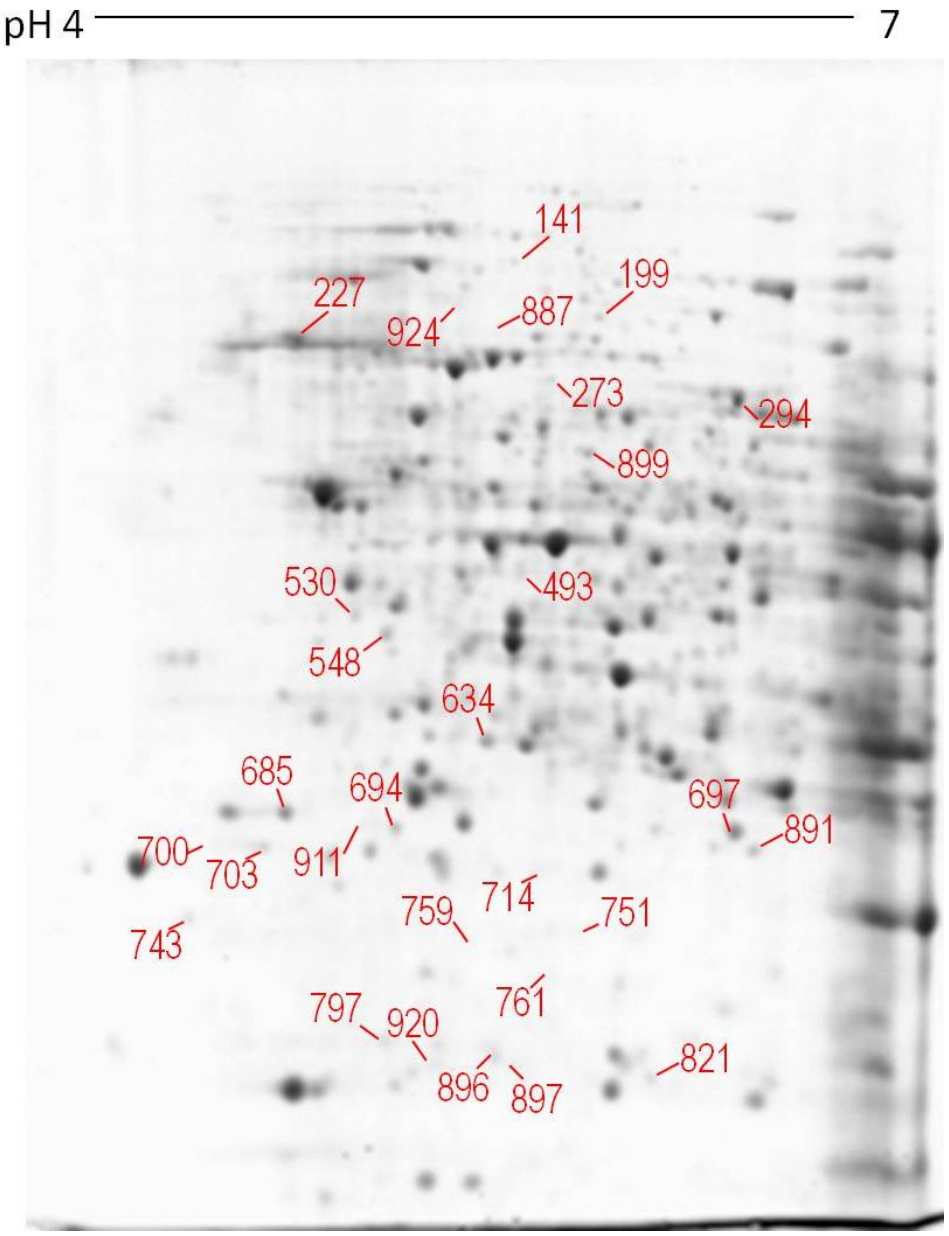

Colloidal Coomassie stained 2D-PAGE gel
of *A. fumigatus* mycelial proteins;
Gliotoxin alone

c.

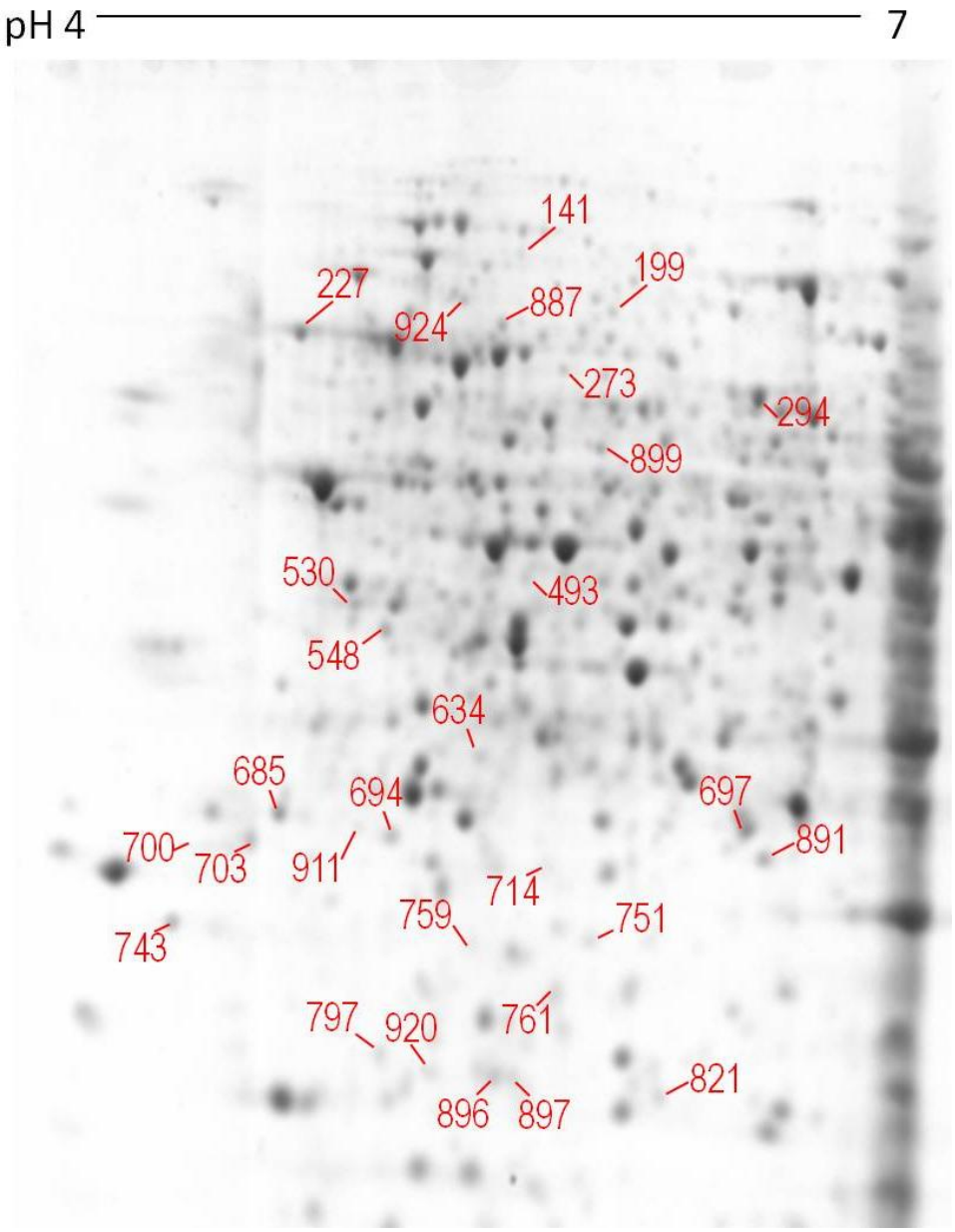

Colloidal Coomassie stained 2D-PAGE gel
of *A. fumigatus* mycelial proteins;
H_2O_2 alone

d.

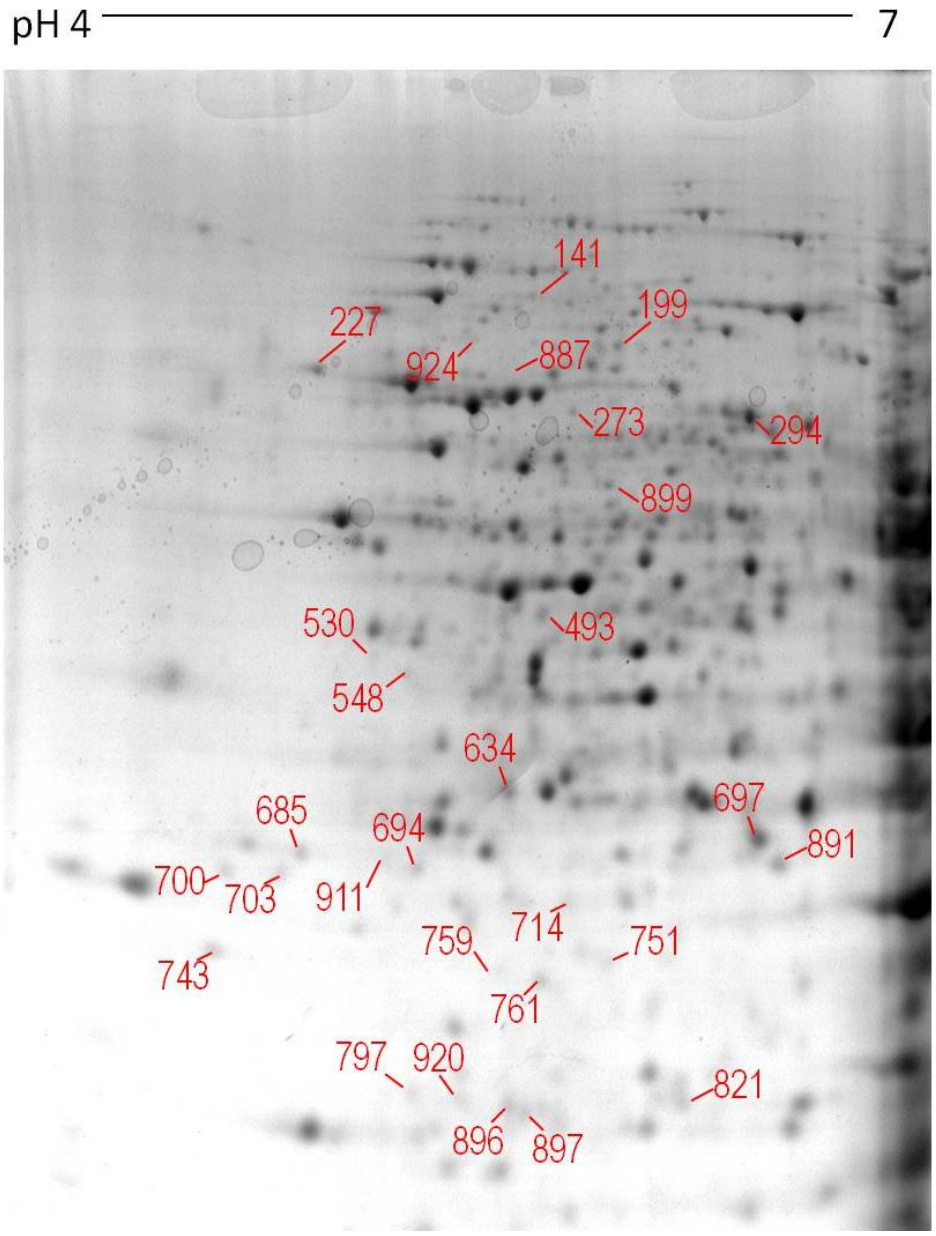

Colloidal Coomassie stained 2D-PAGE gel
of *A. fumigatus* mycelial proteins;
Gliotoxin and H_2O_2 combined

Figure 5.4: 2D-PAGE analysis of *A. fumigatus* ATCC26933 (a) solvent control, (b) following exposure to gliotoxin (10 µg/ml) for 4 h, (c) following exposure to 2 mM H_2O_2 for 4 h, (d) following exposure to a combination of gliotoxin (10 µg/ml) and H_2O_2 (2 mM) for 4 h. The proteins were first separated on pH 4 – 7 strips followed by SDS-PAGE. Proteins found to be significantly differentially expressed ($p < 0.05$), after analysis using Progenesis™ SameSpot software, are numbered.

5.2.3 Identification of differentially expressed proteins by LC-MS/MS

LC-MS/MS analysis was used to identify the 29 protein spots differentially expressed following challenges with gliotoxin and H_2O_2, individually or in combination (Tables 5.2 and 5.3). Protein expression was assessed for all conditions relative to the solvent control (Table 5.2) The expression of proteins after gliotoxin/ H_2O_2 co-exposure was also assessed relative to the individual treatments of gliotoxin alone or H_2O_2 alone (Table 5.3). In total, 28 unique proteins were identified by LC-MS/MS, from 29 excised protein spots. Molecular chaperone and allergen Mod-E/Hsp90/Hsp1 (termed Hsp90) (AFUA_5G04170) was identified from two distinct spots (Spots 743 and 924; Figure 5.4). The positions of these protein spots indicate proteins with low and high molecular masses, respectively, and may be indicative of protein degradation or cleavage.

Proteins (n = 13) were significantly altered in expression following co-addition relative to H_2O_2 alone ($p < 0.05$) (Table 5.3, Comparison set (v)). Proteins up-regulated in the co-addition included those with oxidation-reduction activity. GliT, a gliotoxin oxidoreductase (Scharf *et al.*, 2010; Schrettl *et al.*, 2010), was up-regulated in the co-additive condition relative to H_2O_2 alone (5.0 fold) but was not induced by H_2O_2 alone (Figure 5.5, Tables 5.2 and 5.3). A decrease in expression of proteins associated with response to stress was observed following gliotoxin/ H_2O_2 co-exposure, relative to H_2O_2 alone. Hsp90 and the oxidative stress protein Svf1 were down-regulated in the co-addition (2.1 and 1.7 fold, respectively), reflective of the relief of H_2O_2-induced stress (Table 5.3, Comparison set (v)). An increase in expression of the Ran-specific GTPase and the proliferating cell nuclear antigen (PCNA), involved in cell-cycle regulation and DNA-repair (Baumer *et al.*, 2000; Burkovics *et al.*, 2009), respectively, was also observed in the co-addition analysis (Table 5.3). The class V chitinase, associated with cell autolysis (Yamazaki *et al.*, 2007), was expressed at a significantly lower level in the

co-addition relative to H_2O_2 alone ($p < 0.05$) (Table 5.3, Comparison set (v)). Two hydrolases, isochorismate family hydrolase and the HAD family hydrolase, were up-regulated when both gliotoxin and H_2O_2 were present (Table 5.3). Proteins involved in amino acid and nucleic acid metabolism (Valerius *et al.*, 2001; Sieńko *et al.*, 2007), glutamine amidotransferase:cyclase and methylenetetrahydrofolate reductase, were also differentially expressed (Table 5.3). Additionally an unknown function protein (AFUA_6G03460) was detected, which underwent a 2.7 fold decrease in expression in the co-addition scenario, relative to H_2O_2 alone (Table 5.3).

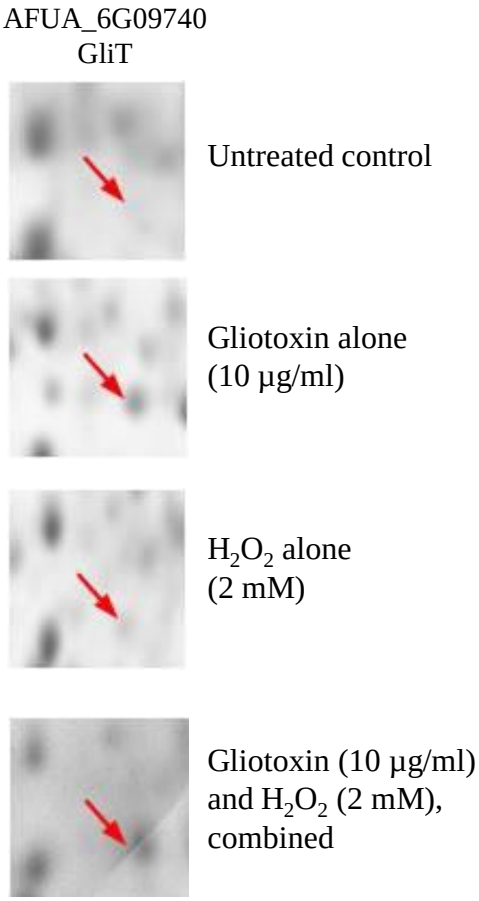

Figure 5.5: Increased expression of the gliotoxin oxidoreductase GliT in response to gliotoxin but not H_2O_2. GliT expression was increased following exposure to exogenous gliotoxin alone (4.6 fold) and in combination with H_2O_2 (4.7 fold), relative to the solvent control. No significant difference in expression of GliT was detected upon exposure of *A. fumigatus* to H_2O_2 alone, relative to the control ($p > 0.05$), indicating GliT expression is mediated by gliotoxin only.

Table 5.2: Proteins undergoing significant differential expression[1] in *A. fumigatus* ATCC26933 following exposure to gliotoxin and H_2O_2, separately or combined, relative to the solvent control. Protein identification was achieved by 2D-PAGE and LC-MS/MS.

Protein name	**Gliotoxin v Control[2] (i)**	**H_2O_2 v Control[2] (ii)**	**Co-addition v Control[2] (iii)**	**Sequence coverage %**	**tM_r (Da)**	**CADRE ID. (AFUA_)**	**Spot No.**
14-3-3 family protein ArtA	-	↑ 1.9	↑ 2.1	46	29102	2G03290	703
ATP synthase gamma chain, mitochondrial precursor, putative	-	↑ 1.6	↑ 1.9	38	31547	1G03510	891
Molecular chaperone and allergen Mod-E/Hsp90/Hsp1	-	↑ 2.0	-	8	80640	5G04170	743
Unknown function protein	-	↑ 2.3	-	10	63462	6G03460	887
14-3-3 family protein	-	↑ 1.9	-	38	30104	6G06750	685
Thioredoxin reductase Trr1/Trr2	-	↑ 1.6	-	18	42190	4G12990	493
Thioredoxin reductase GliT	↑ 4.6	-	↑ 4.7	16	36004	6G09740	634
Proteasome component Pre8	↓ 1.8	-		27	30463	7G05870	761
Succinate dehydrogenase subunit Sdh1	↑ 1.5	-		18	71148	3G07810	294
Translation elongation factor EF2 subunit	↑ 1.6	-		9	93198	2G13530	697
Bifunctional purine biosynthetic protein Ade1	↓ 1.7	-		9	86419	6G04730	141

Protein name	**Gliotoxin v Control[2] (i)**	**H_2O_2 v Control[2] (ii)**	**Co-addition v Control[2] (iii)**	**Sequence coverage %**	**tM_r (Da)**	**CADRE ID. (AFUA_)**	**Spot No.**
Proliferating cell nuclear antigen (PCNA)	-	-	↑ 7.5	8	24034	1G04900	700
Glycyl-tRNA synthetase	-	-	↓ 1.9	4	79100	5G05920	199
Cytochrome c peroxidase Ccp1	-	-	↑ 1.8	14	40379	4G09110	714
Unknown function protein	-	-	↑ 1.9	26	27921	3G00730	797
Isochorismatase family hydrolase	-	-	↑ 1.6	31	20904	6G12220	821
NADH-ubiquinone dehydrogenase 24 kDa subunit	-	-	↑ 1.8	12	29771	2G09130	897
Xanthine-guanine phosphoribosyl transferase Xpt1, putative	-	-	↑ 1.9	28	19505	4G04550	896
Methylenetetrahydrofolate reductase (MTHFR)	-	-	↓ 1.6	10	69279	2G11300	273
Glutamine amidotransferase:cyclase	-	-	↓ 2.0	27	60190	2G06230	899

[1]$p< 0.05$; [2]Fold increase (↑) or decrease (↓) of protein upon exposure of *A. fumigatus* ATCC26933 to gliotoxin alone, H_2O_2 alone or the co-addition, relative to control. CADRE ID., *A. fumigatus* gene annotation nomenclature according to Nierman *et al.* (2005) and Mabey *et al.* (2004); tM_r, theoretical molecular mass; Spot No, according to Figure 5.4; Co-addition: incubation with gliotoxin and H_2O_2 in combination.(i, ii, iii) indicates comparison sets as described in Figure 5.3.

Table 5.3: Proteins undergoing significant differential expression[1] in *A. fumigatus* ATCC26933 following exposure to a combination of gliotoxin and H_2O_2 (co-addition), relative to the control, gliotoxin alone or H_2O_2 alone. Protein identification was achieved by 2D-PAGE and LC-MS/MS.

Protein Name	**Co-addition v Control[2] (iii)**	**Co-addition v Gliotoxin[2] (iv)**	**Co-addition v H_2O_2[2] (v)**	**Sequence coverage %**	**tM_r (Da)**	**CADRE ID. (AFUA_)**	**Spot No.**
Proteasome component Pre8	-	↑ 2.6	-	27	30463	7G05870	761
HAD superfamily hydrolase	-	↑ 2.4	↑ 1.6	22	27360	5G08270	911
Hsp70 chaperone BiP/Kar2	-	↓ 1.6	-	24	73385	2G04620	227
Proliferating cell nuclear antigen (PCNA)	↑ 7.5	↑ 7.9	↑ 2.3	8	24034	1G04900	700
F-actin capping protein alpha subunit	-	↑ 1.8	-	18	30422	6G10060	694
ATP synthase gamma chain, mitochondrial precursor, putative	↑ 1.9	↑ 1.7	-	38	31547	1G03510	891
Glucosamine-6-phosphate isomerase/6-phosphogluconolactonase family	-	↑ 2.1	-	3	93269	1G02980	751
Isochorismatase family hydrolase	↑ 1.6	↑ 1.7	↑ 1.5	31	20904	6G12220	821
NADH-ubiquinone dehydrogenase 24 kDa subunit	↑ 1.8	↑ 1.8	↑ 1.5	12	29771	2G09130	897
Xanthine-guanine phosphoribosyl transferase Xpt1, putative	↑ 1.9	↑ 1.7	-	28	19505	4G04550	896
Thioredoxin reductase GliT	↑ 4.7	-	↑ 5.0	16	36004	6G09740	634

Protein Name	**Co-addition v Control[2] (iii)**	**Co-addition v Gliotoxin[2] (iv)**	**Co-addition v H_2O_2[2] (v)**	**Sequence coverage %**	**tM_r (Da)**	**CADRE ID. (AFUA_)**	**Spot No.**
Class V chitinase	-	-	↓ 1.5	24	43638	3G11280	548
Unknown function protein	-	-	↓ 2.7	10	63462	6G03460	887
NADH-quinone oxidoreductase, 23 kDa subunit	-	-	↑ 1.8	12	25752	1G06610	920
Molecular chaperone and allergen Mod-E/Hsp90/Hsp1	-	-	↓ 2.1	6	80640	5G04170	924
Glutamine amidotransferase:cyclase	↓ 2.0	-	↓ 1.6	27	60190	2G06230	899
Methylenetetrahydrofolate reductase (MTHFR)	↓ 1.6	-	↓ 1.6	10	69279	2G11300	273
Ran-specific GTPase-activating protein 1	-	-	↑ 2.0	13	27644	5G12180	759
Oxidative stress protein Svf1	-	-	↓ 1.7	9	43421	5G11820	530
14-3-3 family protein ArtA	↑ 2.1	-	-	46	29102	2G03290	703
Glycyl-tRNA synthetase	↓ 1.9	-	-	4	79100	5G05920	199
Cytochrome c peroxidase Ccp1	↑ 1.8	-	-	14	40379	4G09110	714
Unknown function protein	↑ 1.9	-	-	26	27921	3G00730	797

[1] $p < 0.05$; [2]Fold increase (↑) or decrease (↓) of protein in the co-addition, relative to the solvent control, gliotoxin alone or H_2O_2 alone. CADRE ID., *A. fumigatus* gene annotation nomenclature according to Nierman *et al.* (2005) and Mabey *et al.* (2004); tM_r, theoretical molecular mass; Spot No, according to Figure 5.4; Co-addition: incubation with both gliotoxin and H_2O_2. (i, ii, iii) indicates comparison sets as described in Figure 5.3. Data from comparison set (iii) (Co-addition v Control) from Table 5.2 is included for ease of analysis.

5.2.4 Comparative 2D-PAGE analysis of *A. fumigatus* Δ*gliK* following exposure to gliotoxin

Following the observation in Section 5.2.1 that *A. fumigatus* Δ*gliK* exhibited increased sensitivity to exogenous gliotoxin, 2D-PAGE was carried out to investigate the proteome changes associated with this phenotype. *A. fumigatus* Δ*gliK* was cultured in Sabouraud dextrose broth for 24 h before addition of gliotoxin (10 µg/ml) or the equivalent volume of methanol as a control (n = 5, respectively). After 4 h, mycelia were harvested and protein was extracted as described in Section 2.2.2.2. Protein lysates were subjected to TCA/acetone precipitation before resuspension in IEF buffer (Section 2.1.6.2) and separation on pH 4 - 7 strips (Section 2.2.4.3). Following separation of proteins by SDS-PAGE, Colloidal Coomassie staining was carried out to visualise total proteins on the gels (Section 2.2.4.4). Progenesis™ SameSpot software was subsequently used to analyse the stained gels, and protein spots demonstrating significant differential expression were located (Figure 5.6).

Protein spots (n = 33) were found to be differentially expressed in *A. fumigatus* Δ*gliK* upon exposure to gliotoxin (10 µg/ml) for 4 h. Nineteen of these proteins spots had a fold increase ≥ 1.5 ($p < 0.05$), while the remaining fourteen protein spots exhibited a fold decrease ≥ 1.5 ($p < 0.05$) in response to gliotoxin. These protein spots were excised from the gels and subjected to trypsin digestion as described in Section 2.2.6.1. LC-MS/MS analysis was carried out to ascertain the identity of these proteins (Section 2.2.6.3).

a.

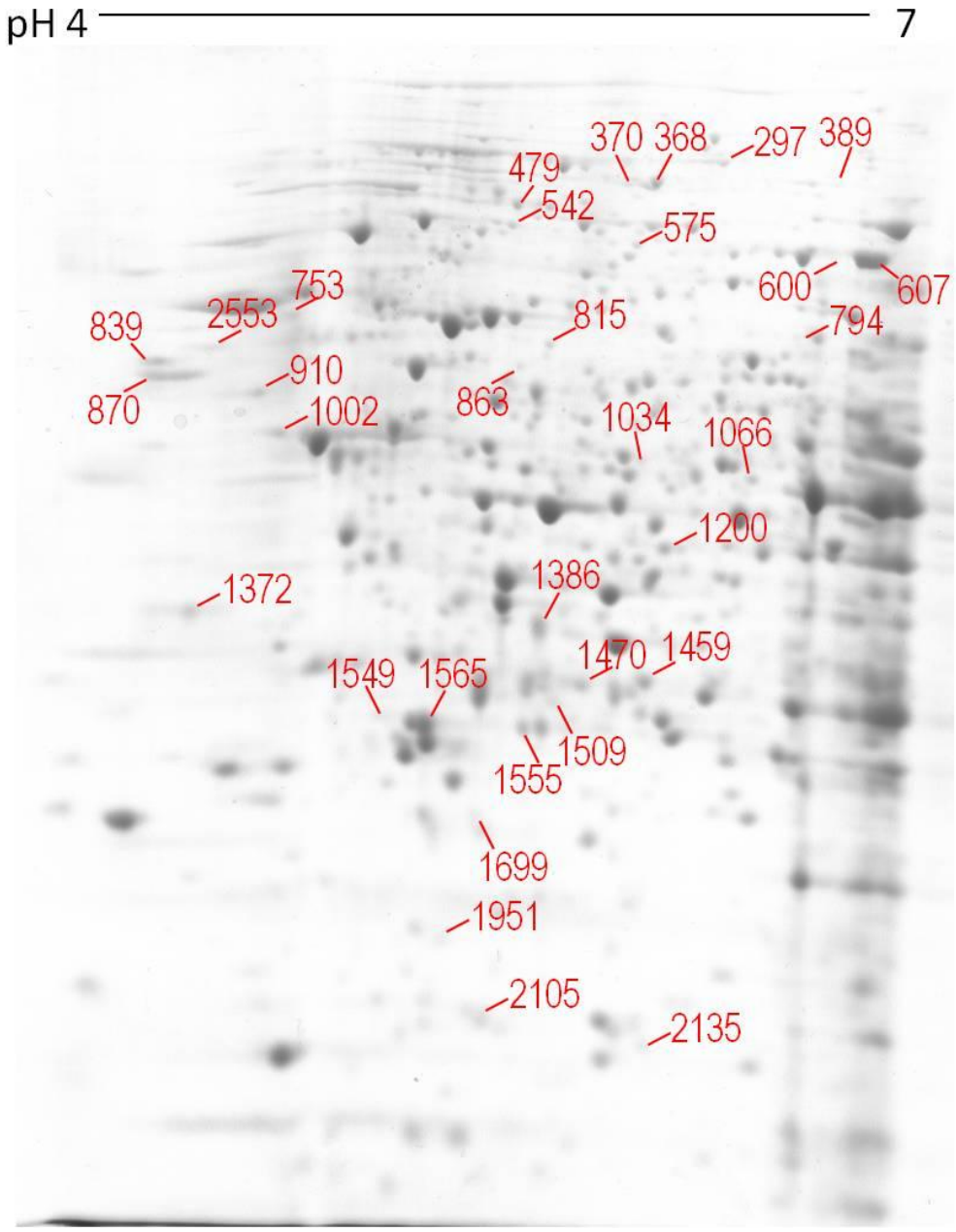

Colloidal Coomassie stained 2D-PAGE gel
of *A. fumigatus* Δ*gliK* mycelial proteins;
Solvent control

b.

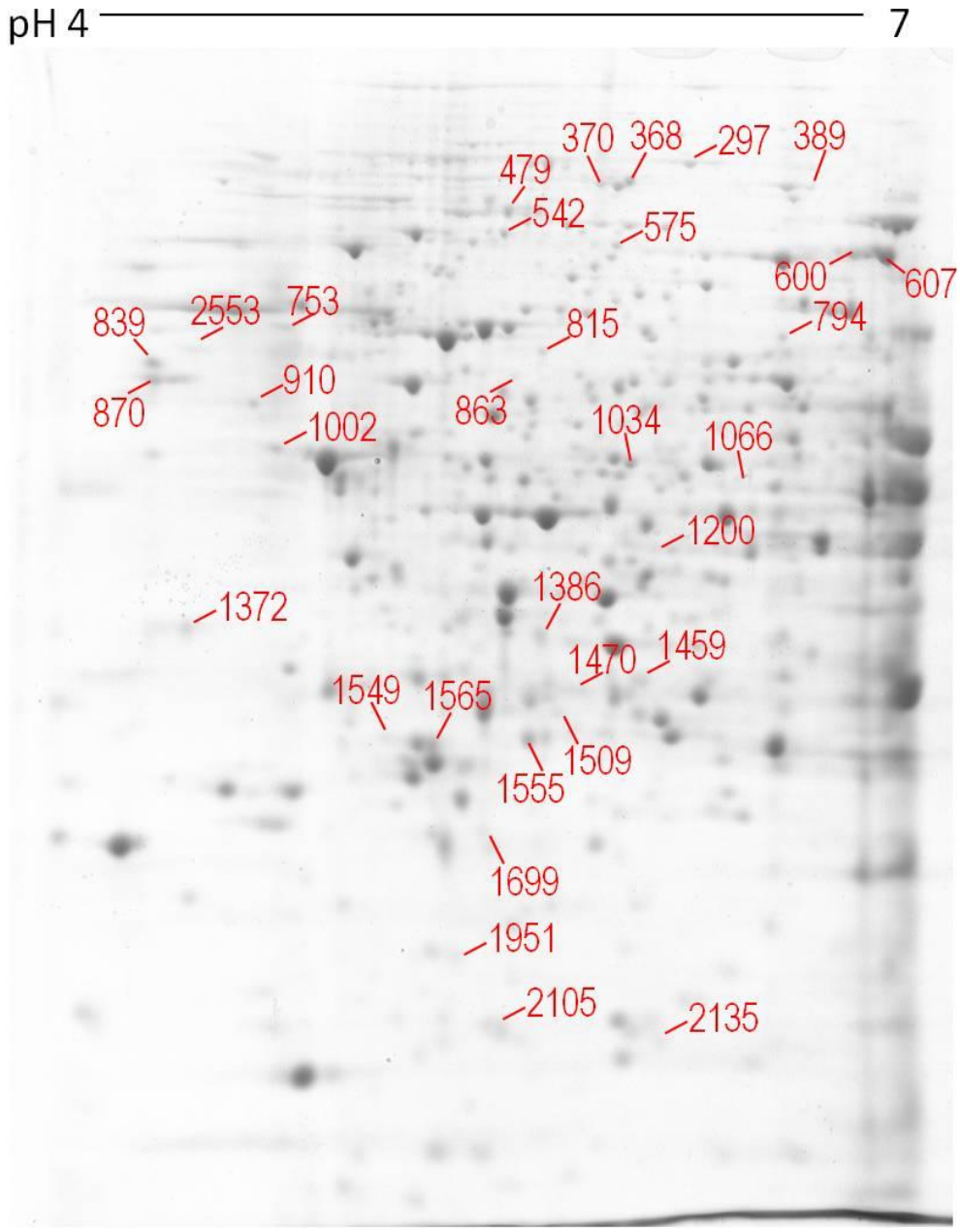

Colloidal Coomassie stained 2D-PAGE gel
of *A. fumigatus* Δ*gliK* mycelial proteins;
Gliotoxin (10 µg/ml)

Figure 5.6: 2D-PAGE analysis of *A. fumigatus* Δ*gliK* (a) control, (b) following exposure to gliotoxin (10 µg/ml) for 4 h. The proteins were first separated on pH 4 – 7 strips followed by SDS-PAGE. Proteins found to be significantly differentially expressed ($p < 0.05$), after analysis using Progenesis™ SameSpot software, are numbered.

5.2.5 LC-MS/MS identification of differentially expressed proteins

Proteins (n = 30) were identified by LC-MS/MS, from the 31 protein spots differentially regulated in *A. fumigatus* Δ*gliK*, following exposure to gliotoxin for 4 h (Table 5.4). Translation elongation factor eEF-3 (AFUA_7G05660; Spot 297; Figure 5.6) showed the largest fold increase in response to exogenous gliotoxin, while pyruvate dehydrogenase E1 component alpha subunit (AFUA_1G06960; Spot 1200; Figure 5.6) displayed the largest decrease.

Up-regulation of eighteen protein spots, corresponding to seventeen distinct *A. fumigatus* proteins, was observed in Δ*gliK* in response to gliotoxin (Table 5.4). A decrease in expression of thirteen distinct *A. fumigatus* proteins was detected in gliotoxin-exposed Δ*gliK* (Table 5.4). Cobalamin-independent methionine synthase MetH/D (AFUA_4G07360) was identified from two independent spots positioned alongside each other on the gel (Spots 600 and 607, Figure 5.6) and was up-regulated 1.9 and 2.2 fold respectively, following gliotoxin exposure. The positions of these protein spots indicated that the proteins had the same molecular mass but differed slightly in p*I*. These slight changes in p*I* may be a result of post-translational modification of the protein. Down-regulation of thirteen proteins was observed in *A. fumigatus* Δ*gliK* upon exposure to gliotoxin (Table 5.4). Two isoforms of the thiazole biosynthesis enzyme, encoded by the pyrithiamine resistance gene (*ptrA*) from *A. oryzae* were also identified. This gene was used as a selection marker in the generation of the *gliK* deletion strain.

Proteins undergoing significant differential expression in *A. fumigatus* Δ*gliK* following exposure to gliotoxin include those involved in translation, amino acid metabolism, those exhibiting regulatory roles and endoplasmic reticulum (ER)

associated proteins. The translation initiation factor EifCb, translation elongation factors EF3, eEF3 and G1 and the alanyl-tRNA synthetase are involved in translation (Triana-Alonso *et al.*, 1995; Kapp and Lorsch, 2004; Towpik, 2005; Jackson *et al.*, 2010). A number of proteins are involved in the processes surrounding amino acid metabolism. Specifically, cobalamin-independent methionine synthase MetH/D and the methylenetetrahydrofolate reductase are associated with methionine biosynthesis (Sieńko *et al.*, 2007; Suliman *et al.*, 2007). Diphthamide synthase is involved in histidine modification (Liu *et al.*, 2004), while glycine dehydrogenase and alanine aminotransferase catalyse the reversible catabolism of glycine and alanine, respectively (Piper *et al.*, 2002; Garcia-Campusano *et al.*, 2009). Homogentisate 1,2-dioxygenase is associated with tyrosine and phenylalanine degradation (Schmaler-Ripcke *et al.*, 2009). Regulatory proteins identified here include a subunit of protein phosphatase 2A (PP2A) and the zinc finger protein ZPR1, which each have distinct roles in the control of transcription and translation (Mishra *et al.*, 2007; Kaul *et al.*, 2011). Protein disulphide isomerise Pdi1 also exhibits a regulatory role and is associated with the ER-unfolded protein response (Gauss *et al.*, 2011). Several other ER-associated proteins were identified, including CRAL/TRIO domain protein, aspartic endopeptidase Pep2 and the vesicular fusion protein Sec17 (Schnabl *et al.*, 2003; Parr *et al.*, 2007; Perry *et al.*, 2009)

Table 5.4: Proteins undergoing a significant change in expression[1] in *A. fumigatus* Δ*gliK* following exposure to gliotoxin (10 µg/ml), relative to the solvent control. Protein identification was achieved by 2D-PAGE and LC-MS/MS.

Protein name	**Fold Change[2]**	**Sequence coverage %**	**tM_r (Da)**	**CADRE ID. (AFUA_)**	**Spot No.**
Proteins Upregulated following Gliotoxin Addition:					
Translation elongation factor eEF-3	↑ 5.6	8	117768.4	7G05660	297
Alanyl-tRNA synthetase	↑ 3.0	4	113714.5	8G03880	368
Eukaryotic translation initiation factor 3 subunit EifCb	↑ 2.7	5	85065.4	1G02030	542
Translation elongation factor G1	↑ 2.5	19	87877.7	4G08110	575
Heat shock protein Hsp98/Hsp104/ClpA	↑ 2.2	13	111096.9	1G15270	370
Glycine dehydrogenase	↑ 2.2	18	115203.5	4G03760	389
Cobalamin-independent methionine synthase MetH/D	↑ 2.2	5	87736.8	4G07360	607
Vesicular-fusion protein Sec17	↑ 2.0	31	32840.9	2G12870	1699
CTP synthase	↑ 2.0	27	64869.3	7G05210	794
Cobalamin-independent methionine synthase MetH/D	↑ 1.9	14	87736.8	4G07360	600
Aminopeptidase	↑ 1.9	35	106227.3	4G09030	479

Protein name	Fold Change[2]	Sequence coverage %	tM_r (Da)	CADRE ID. (AFUA_)	Spot No.
Alanine aminotransferase	↑ 1.9	31	55135.5	6G07770	1034
Methylenetetrahydrofolate reductase (MTHFR)	↑ 1.8	39	69278.9	2G11300	815
Mitochondrial processing peptidase alpha subunit, putative	↑ 1.7	8	63997	1G11870	863
Xanthine-guanine phosphoribosyl transferase Xpt1, putative	↑ 1.7	29	19505.5	4G04550	2105
Isochorismatase family hydrolase	↑ 1.7	26	20904.6	6G12220	2135
Pyruvate dehydrogenase complex component Pdx1	↑ 1.5	27	35523.1	3G08270	1509
GNAT family acetyltransferase	↑ 1.5	39	29061.1	5G00720	1951
Proteins Downregulated following Gliotoxin Addition:					
Pyruvate dehydrogenase E1 component alpha subunit, putative	↓ 2.8	47	41709.5	1G06960	1200
Ran gtpase activating protein 1 (RNA1 protein)	↓ 2.4	8	46228.2	3G07680	1002
Protein phosphatase 2a 65kDa regulatory subunit	↓ 2.3	7	69220	1G05610	753
Diphthine synthase	↓ 2.1	24	31492.2	1G14020	1549
Homogentisate 1,2-dioxygenase (HmgA)	↓ 2.1	26	50255.6	2G04220	1066
Aspartic endopeptidase Pep2	↓ 2.1	20	43355.1	3G11400	1372
Zinc finger protein ZPR1	↓ 2.1	23	53620	6G10470	2553

Protein name	**Fold Change[2]**	**Sequence coverage %**	**tM_r (Da)**	**CADRE ID. (AFUA_)**	**Spot No.**
CRAL/TRIO domain protein	↓ 2.0	27	46169.8	5G03690	910
Translation elongation factor EF2 subunit	↓ 1.9	11	93428.8	2G13530	1459
Thiamine biosynthesis protein (Nmt1)	↓ 1.9	38	38323	5G02470	1470
Oxidoreductase, 2OG-Fe(II) oxygenase family	↓ 1.8	13	43013.2	1G01000	1386
Nucleosome assembly protein Nap1	↓ 1.8	28	48336.4	5G05540	839
Protein disulfide isomerase Pdi1	↓ 1.6	31	56187.2	2G06150	870

[1] $p < 0.05$; [2]Fold increase (↑) or decrease (↓) of protein upon exposure to gliotoxin (10 µg/ml), relative to the solvent control. CADRE ID., *A. fumigatus* gene annotation nomenclature according to Nierman *et al.* (2005) and Mabey *et al.* (2004); tM_r, theoretical molecular mass; Spot No, according to Figure 5.5.

5.3 Discussion

Exposure of mammalian cells to gliotoxin has been shown to increase the production of ROS, while H_2O_2 induces oxidative stress (Pardo *et al.*, 2006). Both conditions also result in numerous alterations to the proteome of *A. fumigatus* (Lessing *et al.*, 2007; Schrettl *et al.*, 2010; Carberry *et al.*, 2012). Co-addition of gliotoxin and H_2O_2 to *A. fumigatus* was expected to result in an additive or synergistic effect, due to the combination of two inducers of oxidative stress. Paradoxically, phenotypic analysis described in this Chapter revealed an alternate effect of the co-exposure of *A. fumigatus* ATCC26933 and Δ*gliK* to gliotoxin and H_2O_2. While *A. fumigatus* Δ*gliK* exhibited significant growth inhibition upon exposure to gliotoxin or H_2O_2 individually, gliotoxin was observed to relieve H_2O_2-induced inhibition in a concentration-dependent manner. This relief of H_2O_2-induced stress was also observed in *A. fumigatus* ATCC26933 indicating that the mechanism involved was not dependent on the disruption of the *gliK* gene. Comparative 2D-PAGE identified changes in protein expression associated with gliotoxin-mediated relief of H_2O_2-induced stress. Differential expression of 29 protein spots was observed, upon comparison of the conditions tested (Figure 5.3), corresponding to 28 unique *A. fumigatus* proteins (Tables 5.2 and 5.3). Proteins (n = 13) were differentially regulated following exposure to a combination of H_2O_2 (2 mM) and gliotoxin (10 µg/ml), relative to H_2O_2 (2 mM) alone, and may aid in the elucidation of the mechanisms involved in gliotoxin-mediated relief of H_2O_2-induced stress. These proteins (n = 13) were extracted from Table 5.3 and presented in Table 5.5 for clarity (Comparison set (v)). Of these, seven proteins showed increased expression and six showed decreased expression in response to the co-addition of gliotoxin and H_2O_2, relative to H_2O_2 alone. The increased expression of proteins with predicted or demonstrated oxidoreductase activity in response to gliotoxin and H_2O_2 in combination, relative to H_2O_2 alone, was observed. These proteins included the gliotoxin

oxidoreductase GliT, NADH-quinone oxidoreductase (23 kDa subunit) and NADH-ubiquinone dehydrogenase (24 kDa subunit), with 5.0, 1.8 and 1.5 fold increase in expression, respectively. Proteins exhibiting a decrease in expression included the stress-response proteins, Hsp90 and oxidative stress protein Svf1. Proteins (n = 30) differentially expressed in *A. fumigatus* Δ*gliK* following exposure to gliotoxin were identified, in an effort to characterise the increased sensitivity of the deletion strain to gliotoxin. Increased expression of 17 unique proteins and decreased expression of 13 proteins was observed in *A. fumigatus* Δ*gliK* following incubation with gliotoxin (10 µg/ml) for 4 h (Table 5.4).

The combined effects of gliotoxin and H_2O_2 were investigated to determine the effects of co-addition on *A. fumigatus*. Phenotypic analysis of *A. fumigatus* ATCC26933 and Δ*gliK*, grown in the presence of gliotoxin (0 - 10 µg/ml) and H_2O_2 (0 - 1 mM), was carried out. While at 1 mM H_2O_2, growth of *A. fumigatus* ATCC26933 and Δ*gliK* were both significantly inhibited ($p < 0.001$, respectively), relief of this inhibition was observed upon growth on a combination of gliotoxin and H_2O_2. Relief of H_2O_2-mediated stress was achieved by gliotoxin in a concentration-dependent manner, with growth on gliotoxin (10 µg/ml) plus H_2O_2 (1 mM) exhibiting no significant difference to growth on gliotoxin (10 µg/ml) alone (Figures 5.1c and 5.2c and d). Choi *et al.* (2007) noted that gliotoxin catalysed H_2O_2 reduction, mediated by the thioredoxin redox system. The authors proposed that gliotoxin replaces 2-cys peroxiredoxin as an electron acceptor, in the reduction of H_2O_2 to H_2O in mammalian cells (Figure 5.7). The inhibition by gliotoxin of H_2O_2-induced human umbilical vein endothelial cell (HUVEC) angiogenesis, in a dose-dependent manner, was also observed (Choi *et al.*, 2007).

Figure 5.7: Schematic representation of thioredoxin-dependent H_2O_2-reducing activity of gliotoxin. Gliotoxin disulfide can be reduced by thioredoxin-SH groups. From Choi *et al.* (2007).

Alterations in protein expression after exposure of *A. fumigatus* ATCC26933 to a combination of gliotoxin (10 µg/ml) and H_2O_2 (2 mM) were investigated, relative to exposure to H_2O_2 (2 mM) alone (Figure 5.8). The increase in expression of three proteins involved in oxido-reduction processes was noted, with a fold increase of 5.0, 1.5 and 1.8 observed for the gliotoxin oxidoreductase GliT (AFUA_6G09740), NADH-ubiquinone dehydrogenase (24 kDa subunit) (AFUA_2G09130) and NADH-quinone oxidoreductase (23 kDa subunit) (AFUA_1G06610), respectively. The gliotoxin oxidoreductase GliT is encoded by a member of the gliotoxin biosynthetic cluster (*gli*) (Gardiner and Howlett, 2005) and is responsible for the oxidation and reduction of the disulphide bridge of gliotoxin (Scharf *et al.*, 2010; Schrettl *et al.*, 2010). In addition to a key role in the gliotoxin biosynthetic process, this action also mediates self-protection against the harmful effects of gliotoxin (Scharf *et al.*, 2010; Schrettl *et al.*, 2010). Expression of GliT is induced by the presence of exogenous gliotoxin (Schrettl *et al.*, 2010; Carberry *et al.*, 2012) and this induction was also observed in this study (Tables 5.2 and 5.3). Increased expression of GliT was detected following exposure to gliotoxin alone (4.6 fold) and combined with H_2O_2 (4.7 fold) relative to the solvent control (Figure 5.4 and 5.5). There was no significant alteration to expression of GliT in response to H_2O_2 alone ($p > 0.05$) and this demonstrates that GliT expression is not regulated by H_2O_2 and up-regulation in the co-addition condition is solely a result of gliotoxin presence. GliT may be involved in the protection of *A. fumigatus* against H_2O_2-induced stress, as induction of expression by gliotoxin, correlates with relief of H_2O_2 sensitivity (Figure 5.10). While *A. fumigatus* Δ*gliT* is not significantly sensitive to H_2O_2, relative to the parent strain (Schrettl *et al.*, 2010), the substantial increase in GliT expression, as induced by exogenous gliotoxin, may provide a protective mechanism against H_2O_2.

Table 5.5: Proteins (*n* = 13) exhibiting significant differential expression[1] in *A. fumigatus* ATCC26933 following the co-addition of gliotoxin and H_2O_2, relative to H_2O_2 alone. Data extracted from Table 5.3 and re-charted for clarity.

Protein Name	Co-addition v Control (iii)	Co-addition v Gliotoxin (iv)	Co-addition v H_2O_2 (v)	CADRE ID. (AFUA_)	Spot No.
Proteins Up-regulated in Co-addition v H_2O_2					
Thioredoxin reductase GliT	↑ 4.7	-	↑ 5.0	6G09740	634
Proliferating cell nuclear antigen (PCNA)	↑ 7.5	↑ 7.9	↑ 2.3	1G04900	700
Ran-specific GTPase-activating protein 1	-	-	↑ 2.0	5G12180	759
NADH-quinone oxidoreductase (23 kDa subunit)	-	-	↑ 1.8	1G06610	920
HAD superfamily hydrolase	-	↑ 2.4	↑ 1.6	5G08270	911
Isochorismatase family hydrolase	↑ 1.6	↑ 1.7	↑ 1.5	6G12220	821
NADH-ubiquinone dehydrogenase (24 kDa subunit)	↑ 1.8	↑ 1.8	↑ 1.5	2G09130	897
Proteins Down-regulated in Co-addition v H_2O_2					
Unknown function protein	-	-	↓ 2.7	6G03460	887
Molecular chaperone and allergen Mod-E/Hsp90/Hsp1	-	-	↓ 2.1	5G04170	924
Oxidative stress protein Svf1	-	-	↓ 1.7	5G11820	530
Glutamine amidotransferase:cyclase	↓ 2.0	-	↓ 1.6	2G06230	899
Methylenetetrahydrofolate reductase	↓ 1.6	-	↓ 1.6	2G11300	273
Class V chitinase	-	-	↓ 1.5	3G11280	548

[1]$p < 0.05$; Fold increase (↑) or decrease (↓) of protein in the co-additive condition, relative to the solvent control, gliotoxin alone or H_2O_2 alone. Co-addition: incubation with both gliotoxin and H_2O_2. CADRE ID., *A. fumigatus* gene annotation nomenclature according to Nierman *et al.* (2005) and Mabey *et al.* (2004); Spot No, according to Figure 5.4. Red border indicates proteins (n = 13) differentially regulated in the co-addition, relative to H_2O_2 alone.

The expression of two additional proteins, involved in the oxidation-reduction process, was increased in the combined treatment of gliotoxin and H_2O_2, relative to H_2O_2 alone. The NADH ubiquinone dehydrogenase (24 kDa subunit) displayed an increase in expression during H_2O_2 and gliotoxin co-addition, relative to the solvent control (1.8 fold), gliotoxin alone (1.8 fold) and H_2O_2 alone (1.5 fold) (Table 5.5). This indicates that expression of this protein is affected by the combination of gliotoxin and H_2O_2, but not by the individual treatments. Increased expression of NADH-quinone oxidoreductase (23 kDa subunit) was also observed following exposure of *A. fumigatus* to a combination of gliotoxin and H_2O_2, relative to H_2O_2 alone (1.8 fold). Up-regulation of transcripts of both of these proteins has previously been demonstrated in *A. fumigatus* in response to the anti-malarial agent, artemisinin (Gautam *et al.*, 2011). Artemisinins contain an endoperoxide bridge, essential for mediation of anti-malarial activity (O'Neill *et al.*, 2010). These up-regulated proteins form part of complex I of the mitochondrially-located electron transport chain (ETC) and are involved in the oxidation of NADH from the citric acid cycle to NAD^+ (Lin and Guarente, 2003). Although complex I is actually a source of ROS in the electron transport chain (Voulgaris *et al.*, 2012), components of the ETP, including the alternative oxidase AoxA, are involved in fungal resistance to oxidative stress (Grahl *et al.*, 2012). Additionally, generation of low-levels of ROS can elicit a signalling mechanism that promotes survival (Trachootham *et al.*, 2008). Alternatively, increased expression of components of the ETC could be indicative of increased energy requirement due to recovery of growth in the co-exposure condition (Figure 5.10).

The proliferating cell nuclear antigen (PCNA) exhibited a 2.3 fold increase in expression following incubation with a combination of gliotoxin and H_2O_2, relative to H_2O_2 alone. Moreover, expression of this protein was also dramatically up-regulated in the co-addition condition, relative to gliotoxin alone (7.9 fold) and the solvent control

(7.5 fold) (Figure 5.8, Table 5.5). This suggests that PCNA is induced by H_2O_2 (approximately 5 fold) and not by exposure to gliotoxin alone. Clearly, a combination of H_2O_2 with gliotoxin leads to further induction of this protein. The PCNA protein forms a complex around the DNA strand and has a role in the regulation of DNA replication and repair. Indeed, PCNA is involved in the process of DNA-repair following H_2O_2-mediated damage (Burkovics *et al.*, 2009) and acts as an anchor to the DNA template for binding partners (Zamir *et al.*, 2012). The increase in PCNA expression observed in response to H_2O_2, alone or coupled with gliotoxin, may therefore be indicative of H_2O_2-induced DNA damage in these conditions. Furthermore, additional induction of PCNA expression in the co-addition condition relative to H_2O_2, alone, may account for the recovery of growth, due to enhanced DNA repair capacity (Figure 5.10). Detection of DNA damage in each of the conditions tested could deduce whether further induction of this repair mechanism contributes to the gliotoxin mediated recovery from H_2O_2-induced growth inhibition.

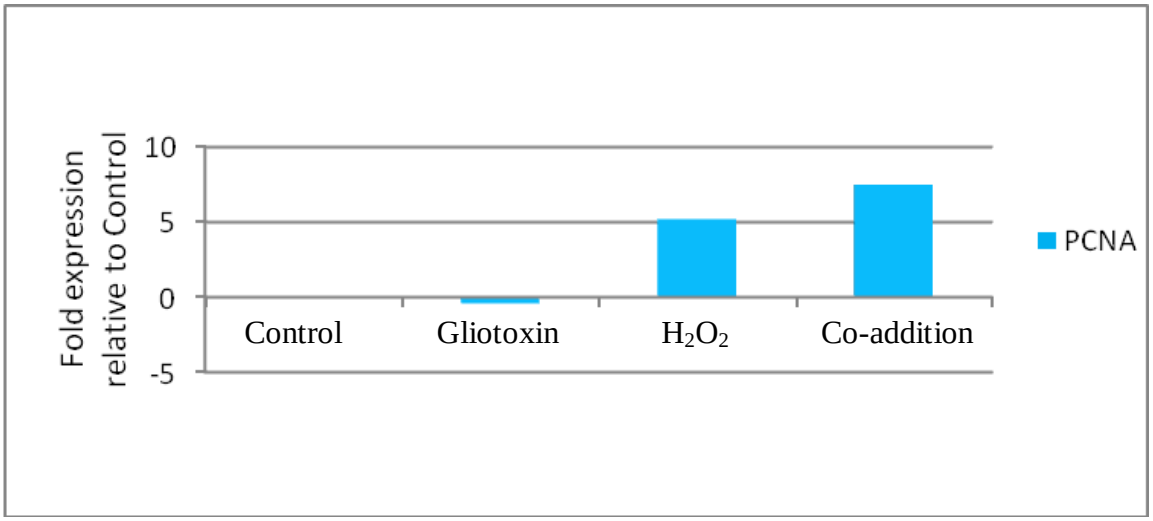

Figure 5.8: Fold expression of the proliferating cell nuclear antigen (PCNA) upon exposure to gliotoxin alone, H_2O_2 alone and co-addition of gliotoxin and H_2O_2, relative to the control.

The Ran-specific GTPase-activating protein 1 (AFUA_5G12180) is also significantly induced by growth in gliotoxin combined with H_2O_2, relative to H_2O_2 alone (2.0 fold, $p < 0.05$). This protein did not demonstrate any differential regulation relative to either the solvent control or gliotoxin treatment alone which may indicate that expression of this protein is down-regulated in the presence of H_2O_2 alone, and expression returns to a basal level upon co-addition of gliotoxin. The Ran-specific GTPase-activating-protein 1 is involved in the up-regulation of protein degradation through ubiquitination and also functions in the regulation of nuclear import/export (Baumer *et al.*, 2000). Depletion of the *S. cerevisiae* ortholog of this protein, Yrb1, correlates with cell-cycle arrest, underlining the importance of this protein during mitosis (Baumer *et al.*, 2000). The level of Ran GTPase-activating protein 1 may account for the growth inhibition observed in the presence of H_2O_2 alone, relative to a combination of gliotoxin and H_2O_2 (Figure 5.1). The subsequent increase in expression of this protein upon incubation with gliotoxin and H_2O_2 in combination coincides with the recovery from H_2O_2-induced stress. Thus, the control of factors involved in cell-cycle regulation may be critical in the gliotoxin-mediated relief of H_2O_2-induced growth inhibition.

The increased expression of two hydrolases was also observed in the presence of gliotoxin and H_2O_2, relative to H_2O_2 alone. The isochorismatase family hydrolase was observed to increase 1.5 fold and the HAD superfamily hydrolase increased 1.6 fold in this comparison. Additionally, the HAD superfamily hydrolase exhibited increased expression in the co-addition condition, relative to gliotoxin alone (2.4 fold) (Table 5.5), indicating that regulation of expression of this protein is affected by both gliotoxin and H_2O_2. Isochorismatase family hydrolase catalyses the production of pyruvate and 2,3-dihydroxybenzoate from isochorismate (Soanes *et al.*, 2008), and orthologs of this protein were up-regulated in *A. niger* in response to DTT and in *A. oryzae* and *A.*

nidulans in response to hypoxia (Guillemette *et al.*, 2007; Terabayashi *et al.*, 2012). Conversely, the HAD superfamily hydrolase is observed to be down-regulated in *A. fumigatus* in response to hypoxic conditions (Vödisch *et al.*, 2011). While no defined metabolic role has been determined for the HAD superfamily hydrolase in *Aspergillus* species, an orthologous protein in *Penicillium brasiliensis* is necessary for adherence to host cells and the transcript was up-regulated in the transition from conidia to mycelial growth phases (Hernández *et al.*, 2010; Ndez *et al.*, 2012). The up-regulation of these hydrolases, in addition to the other proteins discussed, may mediate the relief of H_2O_2-induced stress, and could be further investigated by targeted deletion of the respective genes.

Proteins involved in the response to cellular stress were observed to undergo a decrease in expression in the co-addition condition, relative to H_2O_2 alone. A decrease in expression of Hsp90 (2.1 fold) and the oxidative stress protein Svf1 (1.7 fold) was noted. Hsp90 displayed up-regulation in the presence of H_2O_2 alone, relative to the solvent control (2.0 fold), with this response reversing upon co-incubation with gliotoxin. In line with these observations at the proteomic level, the transcript of Hsp90 was also reported to be up-regulated in *A. fumigatus* in response to exogenous H_2O_2 (Fraczek *et al.*, 2010). Hsp90 is a stress-induced protein involved in the refolding of denatured proteins and signal transduction (Fraczek *et al.*, 2010; Franzosa *et al.*, 2011). The decrease in expression of the Hsp90 may be a result of a decrease in oxidative stress, correlating with the relief of growth inhibition observed. However Hsp90 transcripts were also noted to decrease during *A. fumigatus* biofilm growth in a time-dependent manner (Bruns *et al.*, 2010b). This decrease in expression coincided with an increase in gliotoxin production by the biofilm and may point to Hsp90 regulation directly by gliotoxin itself. Quantitative RT-PCR or western blot analysis could be employed, respectively, to determine if expression or translation of Hsp90, are regulated

by gliotoxin. The decreased expression of the Svf1 protein, with a nuclear localisation and a role in the response to oxidative stress (Brace *et al.*, 2005; Teutschbein *et al.*, 2010), is also indicative of the attenuation of oxidative stress in the co-addition condition relative to H_2O_2 alone (Figure 5.10).

A decrease in expression of the class V chitinase in the presence of a combination of gliotoxin and H_2O_2 (1.5 fold) was observed, relative H_2O_2 alone. This protein belongs to subgroup A of fungal/bacterial chitinases which are associated with fungal growth and autolysis (Alcazar-Fuoli *et al.*, 2011; Hartl *et al.*, 2012). The orthologous *A. nidulans* protein, ChiB, has demonstrated involvement in the autolysis of the fungal mycelia in response to stress (Yamazaki *et al.*, 2007). A higher level of expression of this protein, in the presence of H_2O_2 alone, may indicate the occurrence of mycelial autolysis, which could have been stimulated by the presence of oxidative stress. This autolysis could also account for the growth-inhibited phenotype observed in the presence of H_2O_2 alone (Figure 5.1).

Proteins involved in amino acid and nucleotide metabolism underwent a decrease in expression in the presence of gliotoxin and H_2O_2 combined, relative to H_2O_2 alone. Glutamine amidotransferase:cyclase and methylenetetrahydrofolate reductase both underwent a 1.6 fold decrease in expression, relative to H_2O_2 alone. Additionally, expression of these proteins were down-regulated, 2.0 fold and 1.6 fold respectively, in the co-addition condition, relative to the solvent control. Considering these observations, H_2O_2 does not appear to be involved in the regulation of these proteins. Instead, gliotoxin, either independently or in combination with H_2O_2, is responsible for the decrease in expression of these proteins. Glutamine amidotransferase:cyclase catalyses two steps in the biosynthesis of histidine, producing both a histidine precursor and 5-aminoimidazole-4-carboxamide ribonucleotide (AICAR), an intermediate of the purine biosynthetic process, thus linking these pathways (Valerius *et al.*, 2001).

Interestingly, a bifunctional purine biosynthetic protein Ade1 was observed to be down-regulated in the presence of gliotoxin relative to the solvent control (1.7 fold) (Figure 5.9). Conversely, xanthine-guanine phosphoribosyl transferase Xpt1, was observed to be up-regulated in the presence of gliotoxin and H_2O_2 combined, relative to the solvent control (1.9 fold) and gliotoxin alone (1.7 fold), indicating expression of this protein is influenced by H_2O_2. Indeed, Lessing *et al.* (2007) observed an increase in expression of this protein following exposure to H_2O_2 for 45 min. The Xpt1 protein is involved in the salvage pathway of purine nucleotide biosynthesis, whereby XMP and GMP are formed from their precursors, xanthine and guanine, respectively (Guetsova *et al.*, 1999) (Figure 5.9). Additionally, Carberry *et al.* (2012) noted the up-regulation of another component of the purine salvage pathway, adenine phosphoribosyltransferase, in response to exogenous gliotoxin. These observations indicate that *de novo* purine biosynthesis is down-regulated in the presence of gliotoxin and the alternative salvage pathway is utilised in its place (Figure 5.9). Methylenetetrahydrofolate reductase forms part of the methionine biosynthesis pathway, and catalyses the conversion of 5,10-methylenetetrahydrofolate (THF) to 5,-methylTHF (Sieńko *et al.*, 2007). This provides a co-substrate for the production of methionine from homocysteine. Together, these observations underline the influence of gliotoxin and H_2O_2, either alone or in combination, on amino acid and nucleotide biosynthesis in *A. fumigatus*. Furthermore, while no definitive functions have been demonstrated for the unknown function protein (AFUA_6G03460), computational analysis has assigned the function of D-alanine-D-alanine ligase to this protein (www.*Aspergillus*genome.org). This protein is observed to be up-regulated in the presence of H_2O_2 (2.3 fold), relative to the solvent control, with expression returned to basal level upon the co-addition of gliotoxin. This extends the influence of gliotoxin and H_2O_2 to include alanine metabolism.

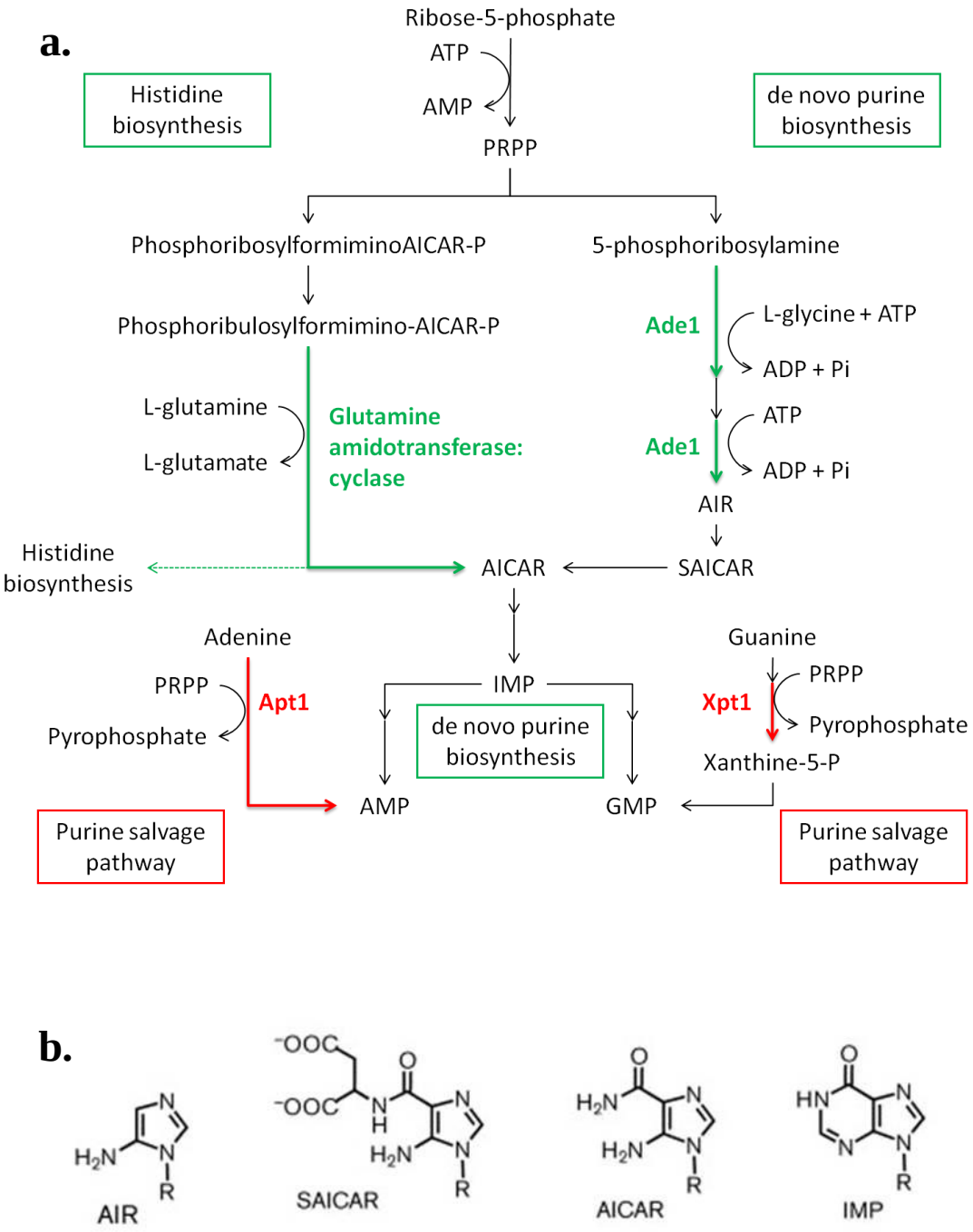

Figure 5.9: (a) Overview of the regulation of the purine metabolic pathway by gliotoxin and H_2O_2, either alone or in combination. Enzymes and pathways undergoing an increase in expression, relative to the solvent control, are indicated in red and decreased expression is indicated in green. Metabolites are indicated in black. Ade1, bifunctional purine biosynthetic protein; Xpt1, xanthine-guanine phosphoribosyltransferase; Apt1, adenine phosphoribosyltransferase. Enzymes of the histidine and *de novo* purine

biosythesis converging pathways, glutamine amidotransferase:cyclase and Ade1, are down-regulated in response to gliotoxin. Expression of enzymes involved in the purine salvage pathways, Xpt1 and Apt1, is up-regulated in the presence of H_2O_2 and gliotoxin, repsectively, relative to a solvent control (Lessing *et al.*, 2007; Carberry *et al.*, 2012). Figure adapted from pathway.yeastgenome.org. (b) Structures of intermediate molecules in the purine and histidine biosynthesis pathway; 5-aminoimidazole ribonucleotide (AIR), *N*-succinyl-5-aminoimidazole-4-carboxamide ribonucleotide (SAICAR), 5-aminoimidazole-4-carboxamide ribonucleotide (AICAR) and inosine monophosphate (IMP).

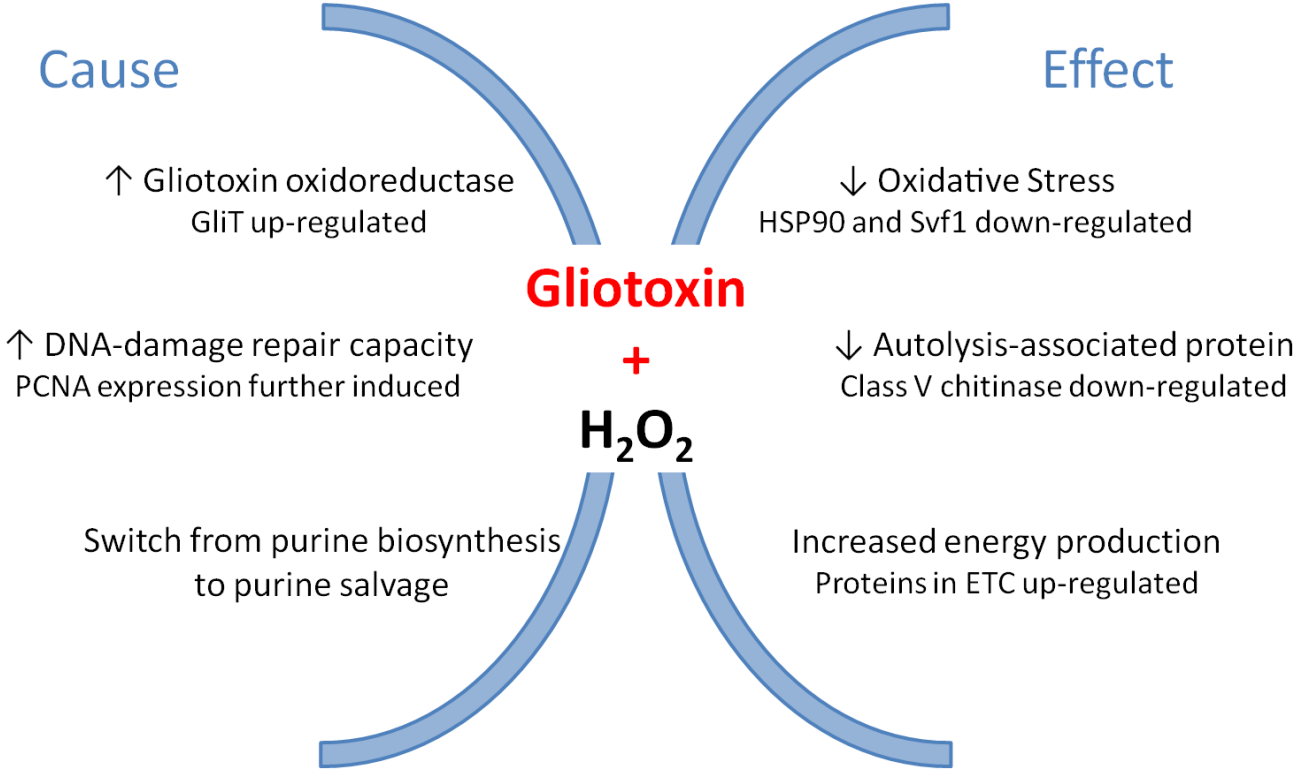

Figure 5.10: Outline of factors possibly contributing to the relief of H_2O_2-induced stress by gliotoxin (cause) and proteins differentially regulated which reflect the associated relief of stress (effect).

Gliotoxin (1-10 µg/ml) significantly inhibited the growth of *A. fumigatus* Δ*gliK*, relative to ATCC26933 wild-type ($p < 0.001$) (Figures 5.1a and 5.2a). As a member of the gliotoxin biosynthetic cluster on Chromosome 6 (Gardiner and Howlett, 2005), the function of the *gliK*-encoded protein has not yet been definitively reported. Results that will be discussed in Chapter 6 reveal GliK to be essential for the production of gliotoxin and disruption of this gene results in impaired efflux of exogenously applied gliotoxin (Gallagher, 2010; Gallagher *et al.*, 2012). The changes in protein expression in *A. fumigatus* Δ*gliK*, exposed to gliotoxin (10 µg/ml), relative to a solvent control, were analysed (Table 5.4). Proteins ($n = 30$) were differentially expressed in *A. fumigatus* Δ*gliK* following incubation with gliotoxin for 4 h. Expression of proteins involved in translation and amino acid metabolism were altered in the presence of exogenous gliotoxin, in addition to proteins associated with the endoplasmic reticulum. Regulatory proteins also displayed significant changes in expression in *A. fumigatus* Δ*gliK* following exposure to gliotoxin, relative to the solvent control ($p < 0.05$).

Cellular translation appears to be significantly affected by the application of exogenous gliotoxin to *A. fumigatus* Δ*gliK*. The translation elongation factors eEF3 and G1 displayed a 5.6 and 2.5 fold increase in expression, respectively, following exposure to gliotoxin, along with the eukaryotic translation initiation factor 3 subunit EifCb (2.7 fold increase). Conversely, the translation elongation factor EF2 subunit was observed to decrease in expression (1.9 fold), relative to the control. This is an opposing effect to that observed in the wild-type strain, whereby application of exogenous gliotoxin resulted in a 1.6 fold increase in expression of EF2, relative to the solvent control. The contrasting regulation of EF2 in response to exogenous gliotoxin could account for the differences in sensitivity observed between the growth of *A. fumigatus* wild-type and Δ*gliK* (Figure 5.1). The process of eukaryotic translation begins with the formation of the 80S ribosome complex at the start codon of mRNA and requires a number of

translation initiation factors (Jackson *et al.*, 2010). EifCb is a subunit of eIF3, which in co-ordination with eIF1, eIF1A and eIF3j, mediates the dissociation of ribosome complexes following termination of translation. This allows the ribosome subunits to be recycled for future translation events. The 40S ribosomal subunit retains the bound initiation factors and forms the 43S pre-initiation complex, which can attach to mRNA and commence scanning for the start codon (Jackson *et al.*, 2010). This protein is essential for translation and upon disruption of the ortholog in *A. nidulans*, *sgdA*, germination was impaired (Osherov and May, 2000). The initiation stage of translation is believed to be the rate-limiting step of the entire process due to its complexity (Arava *et al.*, 2003). Consequently, the up-regulation of the EifCb protein is indicative of the escalation of protein synthesis in *A. fumigatus* Δ*gliK* in response to exogenous gliotoxin.

Following translation initiation, aminoacyl-tRNAs (aa-tRNA) are recruited to the mRNA:80S ribosome complex and the polypeptide chain is extended. The cytosolic eukaryotic translation elongation factors eEF3 and EF2 were observed to be alternatively regulated in *A. fumigatus* Δ*gliK* in the presence of exogenous gliotoxin, with a 5.6 fold increase and 1.9 fold decrease in expression noted respectively. The eEF3 protein is a fungal-specific member of the tranlation elongation process and is required for the binding of aa-tRNA to the A site and detachment of deacetylated-tRNA from the E site of ribosomes (Triana-Alonso *et al.*, 1995; Kapp and Lorsch, 2004). This action is mediated through an interaction with the aa-tRNA transporter, eEF1A, at the ribosome A site, and ATP hydrolysis activity for the reciprocal control of the E site (Anand *et al.*, 2003). As eEF1A also exhibits a role in actin binding and bundling, up-regulation of the eEF3 protein may promote the protein synthesis activity of eEF1A, in lieu of cytosketeton assembly (Gross and Kinzy, 2005; Anand *et al.*, 2006). While eEF1A was not observed to be differentially expressed in *A. fumigatus* Δ*gliK* following

exposure to gliotoxin, a zinc finger protein ZPR1 underwent a decrease in expression (2.1 fold). The ZPR1 protein binds to eEF1A and regulates transcription and the cell cycle (Yanaka *et al.*, 2009). ZPR1 competes with eEF1Bα for binding to eEF1A and can consequently regulate translation elongation in response to growth stimuli (Mishra *et al.*, 2007). Interestingly, expression of eEF1B is induced in *A. fumigatus* ATCC26933 in response to exogenous gliotoxin (Carberry *et al.*, 2012). Reduction in the levels of ZPR1 in mammalian cells has been shown to negatively affect DNA replication and transcription, and ultimately leads to cell-cycle arrest (Gangwani, 2006). The ZPR1 transcript is highly induced during *A. fumigatus* conidial germination (Lamarre *et al.*, 2008) and down-regulation of this protein may account for the significant growth inhibition observed in the Δ*gliK* strain in response to gliotoxin.

Contrary to the up-regulation of eEF3 in response to gliotoxin, a second elongation factor EF2 was down-regulated in this condition (1.9 fold). EF2 facilitates the translocation of the tRNA-mRNA complex from the ribosomal A to the P-site and the P to the E-site, through GTP hydrolysis (Taylor *et al.*, 2007). This action allows incoming cognate aa-tRNA to occupy the A-site and the process repeats to extend the polypeptide chain (Figure 5.11). The EF2 transcript has been reported to be down-regulated during biofilm growth, in a time-dependent manner and correlating with an increase in gliotoxin production (Bruns *et al.*, 2010b). This may be indicative of the regulation, either directly or indirectly, by gliotoxin of EF2 expression. The observed decrease in EF2 expression in gliotoxin exposed-Δ*gliK* may correlate with a reduced rate of translation due to disruption of the polypeptide elongation process. Correspondingly, the down-regulation of two EF2-associated proteins, diphthine synthase (2.1 fold) and protein phosphatase 2a (PP2A) (65kDa regulatory subunit) (2.3 fold), was also observed in *A. fumigatus* Δ*gliK* in the presence of exogenous gliotoxin. EF2 possesses a unique post-translationally modified histidine residue, diphthamide,

which has been shown to be the target of the diphtheria toxin in inactivating eukaryotic EF2 (Liu *et al.*, 2004). While diphthamide modification of EF2 is not essential for translational elongation, disruption of this residue has been linked to an increase in frame-shifting and so is important in maintaining translational fidelity (Ortiz *et al.*, 2006). The observed reduction in expression of diphthine synthase may be a direct result of the down-regulation of EF2 as diphthamide is a post-translational modification (PTM) exclusively found on the EF2 protein (Greganova *et al.*, 2011). A subunit of the PP2A protein, involved in regulation of EF2 activity was also down-regulated in *A. fumigatus* Δ*gliK* in the presence of gliotoxin. Regulation of EF2 activity is achieved through phosphorylation, a process mediated by the EF2 kinase and PP2A. Phosphorylation of EF2 by EF2 kinase results in inactivation of the elogation factor, while de-phosphorylation, and consequently re-activation, is achieved through the action of PP2A (Kaul *et al.*, 2011). The presence of PP2A has been demonstrated previously to be important in *S. cerevisiae* for resistance to the reducing agent, DTT, with a null mutant exhibiting increased sensitivity to the dithiol-containing agent (Rand and Grant, 2006). Decrease in the the amount of PP2A in gliotoxin-treated Δ*gliK* may result in negative regulation of EF2 activity and subsequently, a reduction in the rate of translational elongation. Despite up-regulation of other members of the translational machinery, decreased copy numbers, activity and fidelity of the EF2 protein could reduce the overall rate of translation through disruption of the elongation stage. No such inhibition of translation was noted in the wild-type upon exposure to gliotoxin (Table 5.3) (Carberry *et al.*, 2012), and in fact, up-regulation of EF2 was noted instead. This may account for the significant growth inhibition noted in *A. fumigatus* Δ*gliK* relative to the wild-type, following exposure to gliotoxin. (Figures 5.1 and 5.2).

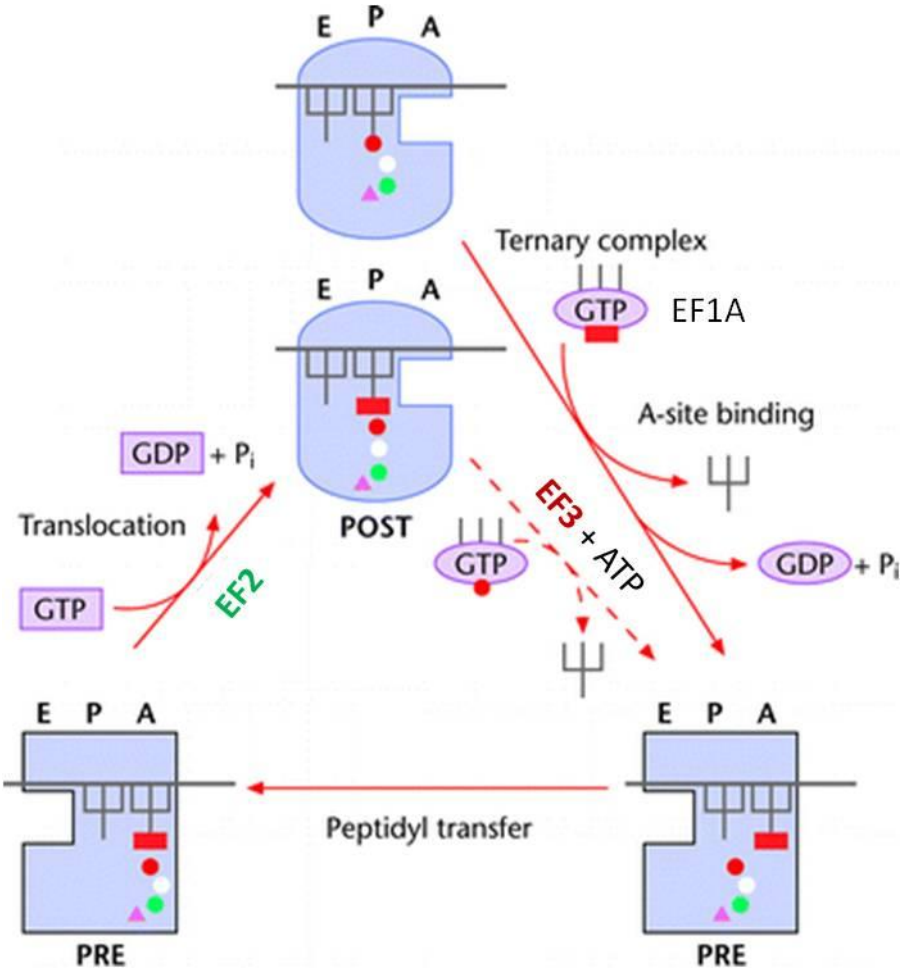

Figure 5.11: Overview of fungal translation elongation. EF1A and EF3 interact to deliver aa-tRNA to the A-site of the ribosome and subsequently remove deacetylated-tRNA from the E-site. Translocation of tRNA-mRNA complexes, from the A and P sites to the P and E sites respectively, is mediated by EF2. Proteins up-regulated in *A. fumigatus* Δ*gliK* in response to gliotoxin are shown in red, with down-regulated proteins shown in green. Adapted from Chakraburtty (2001).

In addition to translation factors, enzymes involved in the wider protein synthesis and processing mechanisms were also differentially regulated in *A. fumigatus* Δ*gliK* upon exposure to gliotoxin. An increase in the presence of two independant protein spots, both identified as cobalamin-independent methionine synthase MetH/D, was noted (1.9 and 2.2 fold, respectively). MetH/D has been shown to be a target of the transcriptional activator *yap1* in *A. fumigatus* and expression of this protein is induced in the presence of oxidative stress (Lessing *et al.*, 2007). In fungi, the production of methionine from homocysteine is catalysed by MetH/D and in *C. albicans* this enzyme has been shown to be essential for cell viability (Suliman *et al.*, 2007). Homocysteine induces up-regulation of *A. nidulans* methionine synthase (Kacprzak *et al.*, 2003), in addition to positive regulation of methylenetetrahydrofolate reductase expression (MTHFR) (Sieńko *et al.*, 2007). Additionally, significantly increased expression of MTHFR was observed in gliotoxin-exposed Δ*gliK* (1.8 fold; $p < 0.05$) (Figure 5.12). This is a contrasting scenario to that observed in *A. fumigatus* wild-type, whereby down-regulation of MTHFR was noted in response to gliotoxin and H_2O_2 combined, relative to the solvent control. These observations may be indicative of elevated homocysteine levels in *A. fumigatus* Δ*gliK*, but not in the wild-type, following exposure to gliotoxin. High levels of homocysteine can be toxic to the cell, and must be metabolised to either methionine or cysteine to prevent its detrimental effects (Kacprzak *et al.*, 2003).

Methionine produced from homocysteine can either be used in protein synthesis or alternatively enter the methionine cycle, whereby it is metabolised to form S-adenosylmethionine (SAM) (Suliman *et al.*, 2007). SAM is a ubiquitous cellular methyl donor and is utilised by methyltransferases for DNA, protein and metabolite methylation reactions (Grillo and Colombatto, 2008). Indeed, as discussed earlier, SAM is required for the production of diphthamide though utilisation by diphthine synthase.

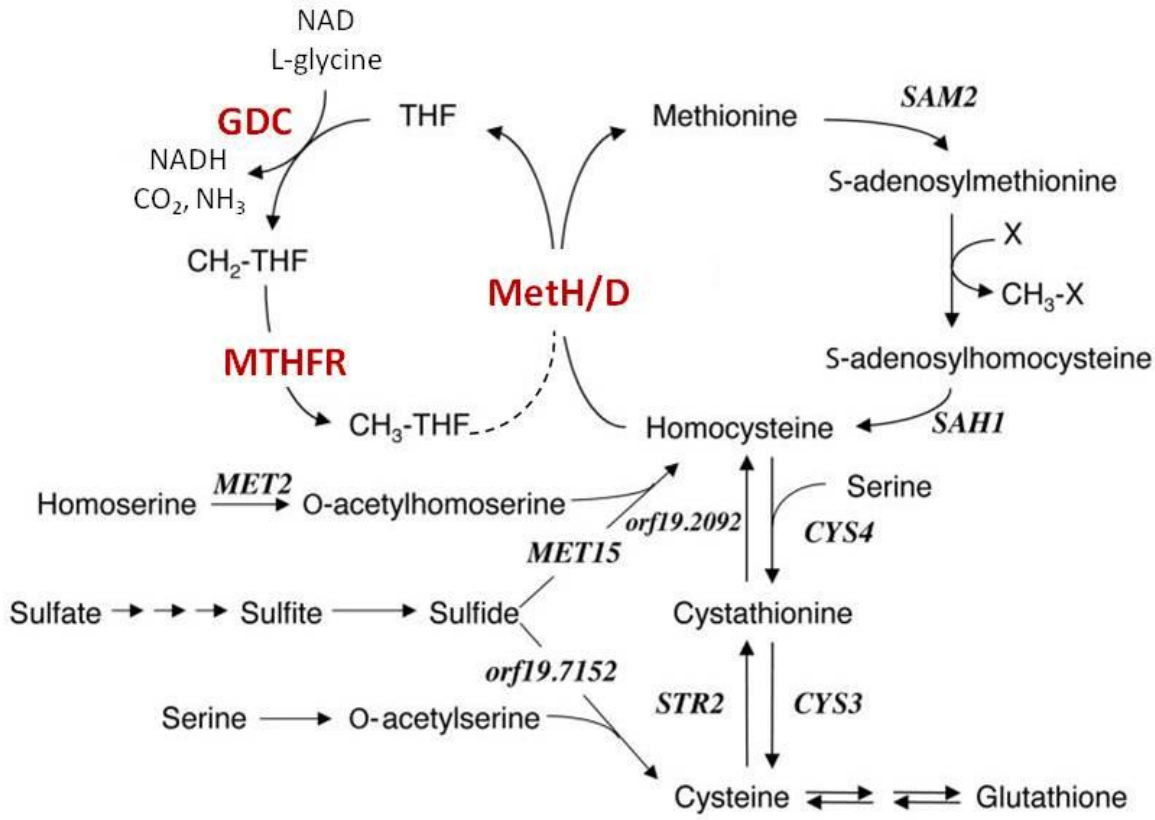

Figure 5.12: Overview of methionine biosynthesis, coupled with the methyl cycle, in fungi. Proteins increased in expression in gliotoxin-exposed *A. fumigatus* Δ*gliK* are denoted in red font. GDC, glycine decarboxylase complex; THF, tetrahydrofolate; CH_2-THF, 5,10-methyleneTHF; CH_3-THF, 5-methylTHF; MTHFR, methylenetetrahydrofolate reductase; MetH/D, cobalamin-independent methionine synthase. Adapted from Suliman *et al.* (2007).

Methionine synthase couples the methyl cycle and the methionine biosynthesis cycle through the methylation of homocysteine and the subsequent regeneration of tetrahydrofolate (THF) (Figure 5.12). An additional step in the methyl cycle, involving the conversion of THF to 5,10-methyleneTHF, is usually catalysed by serine hydroxymethyltransferase, with the simultaneous metabolism of serine and formation of glycine (MacFarlane *et al.*, 2008). However, in the presence of excess glycine or a limited pool of 5,10-methyleneTHF, this step can be catalysed by the mitochondrial glycine decarboxylase complex (GDC) (Piper *et al.*, 2000). A subunit of this complex, glycine dehydrogenase, was also noted to increase in expression in *A. fumigatus* Δ*gliK* following incubation with gliotoxin (2.2 fold) and suggests the overall up-regulation of the methyl cycle in this condition (Figure 5.12).

Alanine aminotransferase catalyses the conversion of pyruvate and L-glutamate to 2-oxoglutarate and L-alanine in a reversible reaction (Garcia-Campusano *et al.*, 2009). Subsequently, alanine is ligated to tRNA by alanyl-tRNA synthetase, for use in translation. Both alanine aminotransferase and alanyl-tRNA synthetase were increased in expression in *A. fumigatus* Δ*gliK* following exposure to gliotoxin (1.9 and 3.0 fold, respectively), further demonstrating the influence of exogenous gliotoxin on protein synthesis in *A. fumigatus* Δ*gliK*.

Proteins involved in response to stress induced by disulphide bond reducing agents were also differentially expressed in *A. fumigatus* Δ*gliK* following incubation with gliotoxin. Protein disulphide isomerase Pdi1 and protein phosphatase PP2A undergo a decrease in expression in *A. fumigatus* Δ*gliK* upon exposure to gliotoxin, 1.6 fold and 2.3 fold, respectively. Isochorismatase family hydrolase, also associated with reductive stress, increased in expression (1.7 fold), in gliotoxin-exposed *A. fumigatus* Δ*gliK*. The reducing agent, dithiothreitol (DTT) efficiently reduces target disulphide bonds, with the concurrent formation of a stable internal disulphide bond. DTT is often

utilised to induce endoplasmic reticulum (ER)-stress in *in vitro* studies as it elicits the unfolded protein response (UPR) (Perrone *et al.*, 2005; Rand and Grant, 2006; Guillemette *et al.*, 2007). Expression of protein disulphide isomerase Pdi1 and isochorismatase family hydrolase has previously been shown to be increased in *A. niger* in the presence of DTT (Guillemette *et al.*, 2007). Additionally, the presence of a point mutation in the *pdi1* gene in *S.cerevisiae* correlated with a decrease in resistance to DTT, demonstrating the involvement of Pdi1 in the protection against redox stress (Gauss *et al.*, 2011). PP2A also has a role in protection against-DTT induced stress as disruption of the orthologous gene in *S. cerevisiae* resulted in increased DTT sensitivity (Rand and Grant, 2006). The regulatory role of PP2A was discussed earlier with regard to elongation factor 2 EF2. An additional target of PP2A is the anti-apoptotic BCL-2 protein located in the endoplasmic reticulum. Phosphorylated BCL-2 is targeted for degradation and lower levels of the BCL-2 protein correlate with an increase in apoptosis associated with ER-stress (Lin *et al.*, 2006) (Figure 5.13a). PP2A regulates the anti-apoptotic activity of BCL-2 by dephosphorylating it and thus preventing targeted degradation of this protein (Lin *et al.*, 2006) (Figure 5.13a). These authors also demonstrated an increase in H_2O_2-induced apoptosis following disruption of PP2A expression, and down-regulation of this protein may explain the increased H_2O_2 sensitivity observed in *A. fumigatus* Δ*gliK*. As discussed in Chapter 1, a pro-apoptotic member of the Bcl-2 family, Bak, is involved in gliotoxin mediated apoptosis of mammalian cells (Figure 1.8) (Pardo *et al.*, 2006), and points to further involvement of this group of apoptosis regulators in gliotoxin sensitivity. Protein disulphide isomerase Pdi1 is associated with the endoplasmic reticulum (ER) and functions in reduction, oxidation or disulphide-dithiol interchange (Stolf *et al.*, 2011) (Figure 5.13b). Through these functions, Pdi1 acts as a molecular chaperone and executes the re-folding of mispaired disulphide containing proteins, forming an integral part of the unfolded

protein response (UPR) to ER-stress (Xiao *et al.*, 2004). Consequently, down-regulation of the Pdi1 and PP2A proteins in gliotoxin-exposed Δ*gliK* may account for the observed increase in sensitivity to the redox molecule due to ineffective activation of the UPR. The UPR is a signalling pathway that is activated upon the detection of an accumulation of misfolded proteins in the ER, which may elicit toxic effects if not removed (Richie *et al.*, 2009). A transmembrane protein Ire1p, is responsible for triggering the translation of a transcription factor Hac1 that regulates the expression of UPR-related genes involved in folding and secretion (Back *et al.*, 2005). Interestingly, the Ran GTPase activating protein 1 RNA1 is required for the Ire1p nuclear import and subsequent Hac1 translation (Goffin *et al.*, 2006). The RNA1 protein was reduced in expression in gliotoxin exposed- Δ*gliK* which could result in an attenuated UPR in response to ER-stress.

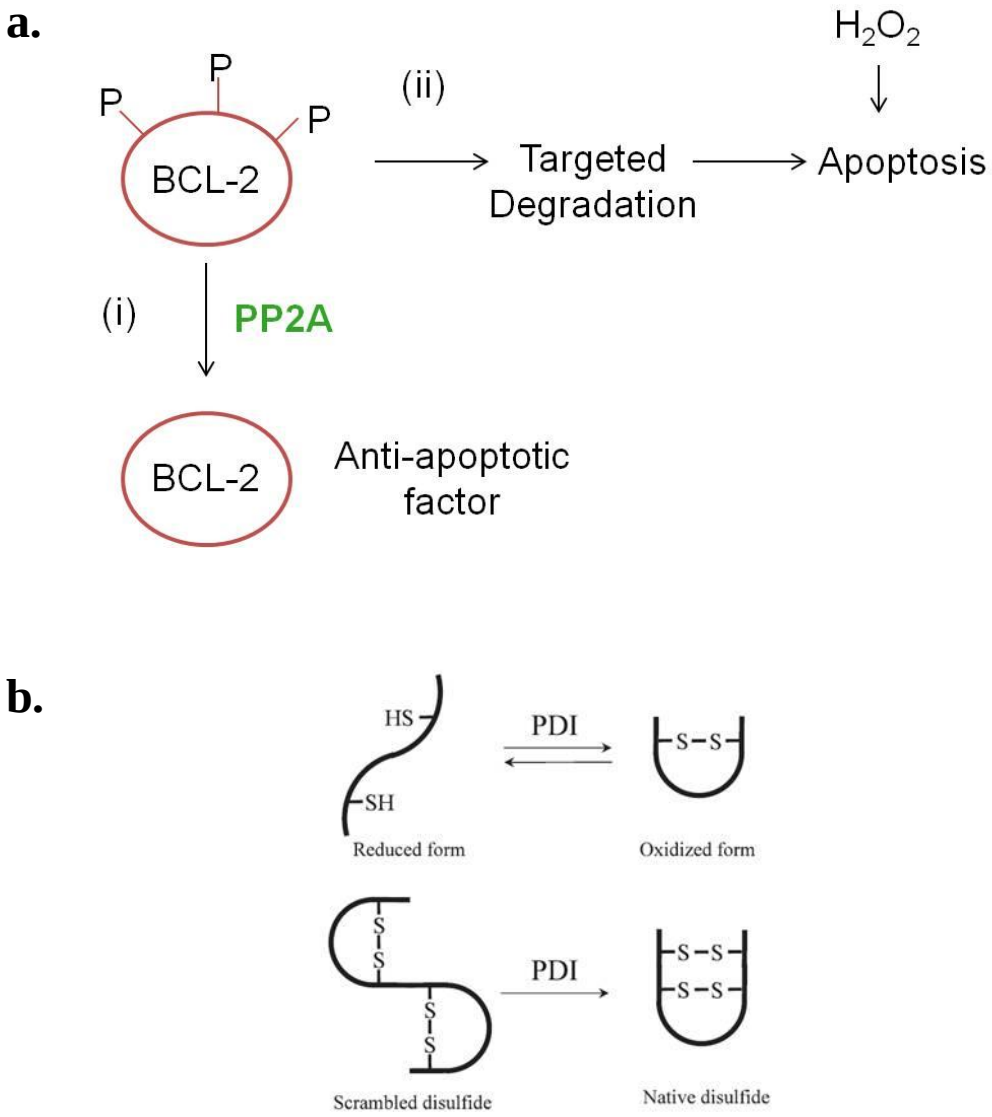

Figure 5.13: Proteins involved in response to ER-stress, downregulated in *A. fumigatus* Δ*gliK* upon exposure to gliotoxin. (a) BCL-2 can be dephosphorylated by PP2A (green) in the ER and provides anti-apoptotic activity (i). Loss of PP2A activity results in degradation of phosphorylated BCL-2 (ii) and an associated increase in apoptosis susceptibility in the presence of death stimuli (e.g. H_2O_2). (b) Protein disulphide isomerase (PDI) carries out oxidation, reduction and isomerase reactions to facilitate correct folding of proteins containing free sulphydrals in the ER. Downregulation of both PP2A and protein disulphide isomerase is observed in *A. fumigatus* Δ*gliK* following incubation with gliotoxin. Image from Okada *et al.* (2010).

Differential regulation of other ER associated proteins was detected in *A. fumigatus* Δ*gliK* following incubation with gliotoxin. This includes CRAL/TRIO domain protein and aspartic endopeptidase Pep2, which are down-regulated, and the vesicular-fusion protein Sec17, which is up-regulated in *A. fumigatus* Δ*gliK* in response to gliotoxin. The CRAL/TRIO domain protein exhibits homology with the *S. cerevisiae* Sfh5 protein, which is involved in phosphatidyinositol transfer and is localised in the peripheral endoplasmic reticulum (Schnabl *et al.*, 2003). Aspartic endopeptidase Pep2 is enriched in the conidia of *A. fumigatus* and expression of this protein is further induced in response to hypoxia and neutrophil exposure (Asif *et al.*, 2006; Sugui *et al.*, 2008; Teutschbein *et al.*, 2010; Vödisch *et al.*, 2011). The orthologous protein in *S.cerevisiae*, Pep4, is processed through the ER and Golgi before maturation and localisation in the vacuole, where it elicits the maturation of various other hydrolases (Parr *et al.*, 2007). *S.cerevisiae* Pep4 is involved in protein degradation following stress and is important for protein turnover after oxidative damage (Marques *et al.*, 2006). Mutants deficient in this protein exhibit an increase in ROS accumulation correlating with a higher rate of apoptosis, underlining the significance of this protein for the maintenance of cellular homeostasis following the induction of stress (Carmona-Gutiérrez *et al.*, 2011). Accordingly, the reduction in Pep2 expression, as observed in gliotoxin-exposed Δ*gliK*, may potentiate the harmful effects of exogenous gliotoxin. The vesicular fusion protein Sec17, involved in vesicle-mediated protein transport between the ER and Golgi (Perry *et al.*, 2009), was up-regulated in *A. fumigatus* Δ*gliK* in the presence of gliotoxin. This may be suggestive of additional protein trafficking, either within the cell or for secretion, following *A. fumigatus* Δ*gliK* exposure to gliotoxin. Overall, these observations point to the altered systems biology within the ER in *A. fumigatus* Δ*gliK*, following gliotoxin-induced stress. Interestingly, Carberry *et al.* (2012) noted the up-regulation of the Cu, Zn superoxide dismutase SOD1, in *A. fumigatus* in response to

exogenous gliotoxin. In yeast, *sod1* expression is induced in response to ER stress and, along with maintenance of NADP(H) levels, is critical for cell survival in this condition (Tan *et al.*, 2009). No differential expression of SOD1 was noted in gliotoxin-treated Δ*gliK* and, in the presence of ER-stress, might be required to reduce levels of superoxide anions. Elevated superoxide anions, in the absence of SOD1, negatively affect UPR induction and exacerbate ER-stress (Tan *et al.*, 2009).

A subset of proteins demonstrated altered expression in both *A. fumigatus* wild-type and Δ*gliK*, in response to gliotoxin. Isochorismatase family hydrolase and the aminopeptidase (AFUA_4G09030) were both observed to undergo an increase in expression in *A. fumigatus* wild-type and Δ*gliK*, exposed to gliotoxin (Tables 5.2 and 5.4) (Carberry *et al.*, 2012). Additionally Carberry *et al.* (2012) noted the up-regulation of the β subunit of the mitochondrial processing peptidase (MPP) in gliotoxin-exposed *A. fumigatus* wild-type, while increased expression of the MPP α subunit was observed following *A. fumigatus* Δ*gliK* incubation with gliotoxin. Due to the analogous regulation of these proteins in both wild-type and Δ*gliK*, in response to gliotoxin, it is unlikely that they contribute to the change in gliotoxin-sensitivity. Interestingly, some proteins detected in both *A. fumigatus* wild-type and Δ*gliK* following gliotoxin exposure, were regulated in opposite directions. Differential regulation of these proteins may account for the altered gliotoxin-sensitivity observed between the wild-type and Δ*gliK* strains of *A. fumigatus*. Methylenetetrahydrofolate reductase (MTHFR), thiamine biosynthesis protein Nmt1 and elongation factor 2 EF2 displayed differential regulation in *A. fumigatus* wild-type compared to Δ*gliK* in response to gliotoxin. As discussed earlier expression of MTHFR, involved in the methyl cycle, can be regulated by homocysteine (Sieńko *et al.*, 2007) and this may suggest higher levels of homocysteine in *A. fumigatus* Δ*gliK* relative to wild-type following exposure to gliotoxin. The activity of EF2 can be controlled by PP2A, whereby lower levels of this regulatory protein in

gliotoxin-exposed Δ*gliK* could result in a higher amount of phosphorylated, and so inactive, EF2 (Kaul *et al.*, 2011). In contrast expression of EF2 is increased in *A. fumigatus* wild-type in response to gliotoxin. Disruption of translation elongation in gliotoxin exposed-Δ*gliK* could explain the respective growth inhibition, relative to the wild-type. The thiamine biosynthesis protein Nmt1 was up-regulated in *A. fumigatus* ATCC26933 in response to gliotoxin (Carberry *et al.*, 2012), while it was down-regulated in this condition in Δ*gliK*. Thiamine biosynthesis is self-regulating, with the presence of excess thiamine eliciting the activation of a riboswitch and consequently inhibiting the translation of the biosynthesis enzyme (Wachter, 2010). The differential regulation of this gene in *A. fumigatus* wild-type compared to Δ*gliK*, could be an indirect result of the presence of the pyrithiamine resistance gene (*ptrA*) in Δ*gliK*, incorporated as a selection marker during the generation of the mutant strain (Gallagher, 2010). The *ptrA* gene codes for an enzyme involved in thiamine biosynthesis, with a riboswitch that is resistant to the antagonist action of pyrithiamine (Kubodera *et al.*, 2000). As a result, differential regulation of this protein may result from the transformation process instead of *gliK* loss.

Finally, expression of the gliotoxin oxidoreductase GliT was not detected by comparative 2D-PAGE to be differentially regulated in *A. fumigatus* Δ*gliK* in the presence of gliotoxin. As discussed previously, GliT is involved in protection from exogenous gliotoxin and the expression of this protein is induced in the presence of the toxin (Figure 5.4) (Schrettl *et al.*, 2010; Carberry *et al.*, 2012). Furthermore, an increase in the expression of the *gliT* transcript was observed in *A. fumigatus* Δ*gliK* following gliotoxin exposure, as was observed for the wild-type strain (Dr. Grainne O' Keeffe, personal communication). While transcriptional up-regulation of a gene does not always correlate with translation, we postulate that this is not the case here. Absence of GliT in *A. fumigatus* ATCC26933 has been shown to result in complete growth inhibition in the

presence of exogenous gliotoxin (10 µg/ml) (Schrettl *et al.*, 2010). While exogenous gliotoxin (10 µg/ml) also significantly inhibited the growth of *A. fumigatus* Δ*gliK* ($p < 0.001$), growth was still evident at 63.3 ± 1.67 % ($n = 3$) of the control. Considering this, the enhanced sensitivity of *A. fumigatus* Δ*gliK* to gliotoxin does not appear to be caused by the absence of GliT protein. Alternatively, we propose that GliT may be secreted from the cell in gliotoxin-exposed Δ*gliK*. Numerous studies, mainly immunological in nature, have detected GliT in the culture supernatants of *A. fumigatus* and antibodies directed against GliT have been proposed for use as an immunological biomarker of *A. fumigatus* infection (Kumar *et al.*, 2011; Shi *et al.*, 2012a, 2012b). In fact, an increase in expression of the vesicular-fusion protein Sec17, in gliotoxin-treated Δ*gliK*, could be indictive of this altered secretion. Enhanced secretion of GliT from *A. fumigatus* Δ*gliK* could also account for the observed increase in sensitivity of the *A. fumigatus gliK* deletion strain to gliotoxin. Exogenous gliotoxin could be reduced externally by secreted GliT and mediate some protection from the oxidised molecule. With lower concentrations of internal GliT than the wild-type, *A. fumigatus* Δ*gliK* would be more susceptible to the cytotoxic effects of any gliotoxin that may be taken up by the cell. While further analysis on the secretome of *A. fumigatus* Δ*gliK* would be required to prove this hypothesis definitively, this nevertheless represents a positive step in the characterisation of gliotoxin-induced sensitivity in the *gliK* mutant.

In summary, the work described in this Chapter illustrates the alteration of *A. fumigatus* wild-type and Δ*gliK* growth in response to the combined stresses of gliotoxin and H_2O_2, with the complementary analysis of the resultant proteomic changes. Gliotoxin was observed to relieve H_2O_2-induced growth inhibition in both *A. fumigatus* wild-type and Δ*gliK*, in a dose-dependent manner, suggesting a common relief mechanism in both strains. Comparative proteomic analysis of *A. fumigatus* wild-type revealed the up-regulation ($n = 7$) and down-regulation ($n = 6$) of proteins upon co-

addition of gliotoxin and H_2O_2, relative to growth on H_2O_2 alone (≥ 1.5 fold difference, $p < 0.05$). Additionally, proteomic analysis of *A. fumigatus* Δ*gliK* revealed proteins undergoing an increase ($n = 17$) or a decrease ($n = 13$) in expression upon exposure to gliotoxin (≥ 1.5 fold difference, $p < 0.05$). Proteins involved in oxidation-reduction, DNA repair and cell-cycle regulation were expressed at a higher level in *A. fumigatus* wild-type under co-addition conditions, compared to growth in the presence of H_2O_2 alone. Down-regulated proteins included those typically induced in response to oxidative stress and an autolysis-associated protein. An increase in selected oxidoreductase expression in response to gliotoxin, including GliT, may account for the relief of H_2O_2-associated oxidative stress. In turn, the observed decrease in stress-induced proteins is reflective of the absence of oxidative stress in the co-addition condition. The proteomic response of *A. fumigatus* Δ*gliK* following gliotoxin exposure, revealed the perturbation of translation, amino acid metabolism and proteins associated with the endoplasmic reticulum (ER). This points to the induction of ER-stress by gliotoxin in the absence of GliK.

Overall, these proteomic profiles provide an insight into the pathways and mechanisms involved in the interaction of *A. fumigatus* with gliotoxin. The systems altered in response to a combination of gliotoxin and H_2O_2 have been identified and this can be utilised to direct future investigations. Targeted gene deletion could elucidate whether the proteins identified in this study were essential for the gliotoxin-mediated relief of H_2O_2-induced growth inhibition (cause), or if their differential regulation was a down-stream effect of growth recovery (effect). Additionally, the unknown function protein GliK, has been explored for its role in the interaction of gliotoxin with *A. fumigatus*. Mechanisms altered in reposnse to exogenous gliotoxin were identified in the gliotoxin-sensitive mutant Δ*gliK*, and may point to the mode of action of gliotoxin in cells lacking the gliotoxin biosynthetic cluster or GliK orthologs. In Chapter 6, the

contribution of GliK to gliotoxin biosynthesis will be investigated and the effect that deletion of *gliK* has on the metabolome of *A. fumigatus* will be determined.

CHAPTER 6

Metabolomic investigation of

A. fumigatus Δ*gliK*

6 Chapter 6

6.1 Introduction

Subsequent to proteomic characterisation of *A. fumigatus*, comparative profiling of low molecular mass metabolites can also be used in functional analyses to elucidate the impact of gene deletion from an organism. As discussed in Chapter 5, deletion of *gliK* from *A. fumigatus* results in increased sensitivity to exogenous gliotoxin and to H_2O_2. In order to determine the effect of GliK absence on the metabolite profile, namely gliotoxin production, a comparative metabolite investigation was carried out. Utilising RP-HPLC, MALDI-ToF, LC-MS/MS analysis, in addition to chemical modification of metabolites for enhanced detection and functional group identification, the metabolite profiles of *A. fumigatus* ATCC26933 and Δ*gliK* were analysed and compared.

Culture conditions and sample preparation utilised for metabolite analysis present a wide opportunity for differential expression and profiling of compounds. Optimisation of culture media, incubation time, temperature and level of culture agitation can be used for efficient targeted production of specific metabolites or alternatively, to profile a range of compounds simultaneously (Dombrink-Kmizman and Blackburn, 2005; Atalla *et al.*, 2008). A number of groups have optimised production of secondary metabolites (SM), including mycotoxins and pharmaceutical compounds, from microorganisms (Feng and Leonard, 1998; Casas López *et al.*, 2003; Dombrink-Kmizman and Blackburn, 2005; Atalla *et al.*, 2008). Mevinolin and lovastatin, utilised as competitive inhibitors of cholesterol biosynthetic enzymes, have been effectively isolated from *A. terreus*, through selection of appropriate carbon and nitrogen sources (Casas López *et al.*, 2003; Atalla *et al.*, 2008). The mycotoxin patulin was most efficiently produced from *Penicillium* species when cultured in potato dextrose broth (PDB) supplemented with manganese (Dombrink-Kmizman and Blackburn, 2005). The

production of sterigmatocystin by *A. nidulans* is supported on nitrate as a nitrogen source while these conditions repress aflatoxin production in *A. parasiticus* (Feng and Leonard, 1998; Price *et al.*, 2005), highlighting the importance of culture condition optimisation for SM analysis. Similarly, sample preparation prior to analysis can also affect the range of metabolites characterised. Aqueous or organic extractions can target compounds with varying polarity. While methanol-water mixtures can be utilised for the extraction of polar compounds, chloroform partitions non-polar (hydrophobic) compounds for subsequent analysis (Villas-Bôas *et al.*, 2005).

Metabolite analysis methods include RP-HPLC, MS-based methods and thin-layer chromatography (TLC) (Kosalec *et al.*, 2005; Dettmer *et al.*, 2007; Lee *et al.*, 2009a; Davis *et al.*, 2011a; Willmann *et al.*, 2011). TLC was traditionally utilised for separation of metabolites from a range of organisms and can be used analytically or preparatively, as a purification technique for additional targeted analysis (Frisvad *et al.*, 2008). RP-HPLC is the favoured chromatography practice for metabolite analysis and can be used independently or coupled with MS for characterisation of compounds (Lei *et al.*, 2011). RP-HPLC involves separation of compounds based on their relative partitioning between a stationary phase (e.g. C_{18}) and a mobile phase (Kazakevich and LoBrutto, 2007). Optimisation of separation gradients can enable efficient resolution of multiple metabolites using a single analysis (Sulyok *et al.*, 2007). Bouligand *et al.* (2006) utilised an optimised RP-HPLC gradient program for the separation of glutathione and the main associated precursor molecules, with subsequent confirmation of identity by MS/MS analysis. MS analysis can be conducted in positive ion or negative ion mode, with use of both amenable to extended metabolite identification (Lei *et al.*, 2011). Ion-trap instruments are capable of performing multiple rounds of MS on selected precursor ions to generate fragmentation patterns, in addition to measuring the

mass of the relevant molecule (Dettmer *et al.*, 2007). Neutral losses from the precursor ions provide information about putative functional groups and may allude to the identity of the ion (Dettmer *et al.*, 2007). Interpretation of the mass of molecules of interest can be complicated by the presence of adducts of the ion. Common adducts detected include H^+, Na^+, K^+ and H_2O, which alter the observed mass of the molecular ion by a value of 1.003, 21.982, 37.957. or 18.01, respectively (Brown *et al.*, 2009b). Additionally, the presence of isotopes of elements can augment the observed size of the molecular ion and correct identification of the monoisotopic peak is essential for accurate mass determination (Varghese *et al.*, 2012). Another factor for consideration in molecular ion mass determination is the presence of multiply charged species. Mass spectrometry measures the mass-to-charge ratio (*m/z*), and multiplicity of charge can be determined by analysing the corresponding isotopic peaks. For example, presence of a C_{13} isotope in a singly charged molecule will result in an isotopic peak of M + 1, whereas the same peak on a doubly charged molecule will give M + 0.5 (Brown *et al.*, 2009b). The phenomenon of dimer formation $(2M+H)^+$ can also result during MS analysis, which can aid in the validation of correct mass assignment to the molecular ion (Muschik and Veenstra, 2009). Once a molecular mass has been deduced for the metabolite of interest, the respective fragmentation pattern generated during electrospray ionisation (ESI) can be used as a fingerprint for future comparisons with a standard to confirm the assigned identification (Brown *et al.*, 2009b).

Chemical derivatisation can be used to enhance the characterisation of the metabolome. Methods utilised include metabolic labelling (e.g., feeding experiments with labelled precursor metabolites) or chemical labelling (e.g., conjugation of fluorescent compound) (Halket *et al.*, 2005; Feldberg *et al.*, 2009). Chemical labelling of the ETP-type toxin, gliotoxin, carried out by Davis *et al.* (2011b) enabled accurate

identification of gliotoxin by RP-HPLC and MS, with increased sensitivity. Reduction of the disulphide bond of gliotoxin, followed by alkylation of the free sulphydral groups using 5'-iodoacetamidofluorescein (5'-IAF), produced a di-acetamidofluorescein derivative (GT-$(AF)_2$) (Davis *et al.*, 2011b) (Figure 6.1). This strategy also effectively labelled another ETP, sporidesmin A, and resulted in an increase sensitivity of detection by RP-HPLC, in addition to confirmation of identity through MALDI-ToF analysis. Additionally, chemical labelling of metabolites can alter the hydrophobicity of compounds, consequently modifying their retention profile on RP-HPLC analysis. This process can enable the characterisation and purification of hydrophilic molecules that are incompatible with RP-HPLC in their native state (Ruhaak *et al.*, 2010).

To date, elucidation of the gliotoxin biosynthetic mechanism has involved the use of functional genomics, whereby effects of disruption of genes in the *gli* cluster have been monitored (Balibar and Walsh, 2006; Bok *et al.*, 2006; Kupfahl *et al.*, 2006; Scharf *et al.*, 2010, 2011; Schrettl *et al.*, 2010; Davis *et al.*, 2011a). Deletion of a gene involved in secondary metabolite (SM) biosynthesis could result in accumulation of intermediates and offer insight into the role of the respective protein in the biosynthetic pathway (Sanchez *et al.*, 2012). Disruption of the *gliG* gene, encoding a glutathione-S-transferase (GST) in *A. fumigatus*, resulted in the loss of gliotoxin production and the coincident appearance of an alternative metabolite with *m/z* 263 (Davis *et al.*, 2011a; Scharf *et al.*, 2011). These authors independently verified this molecule as an off-pathway shunt metabolite and identified GliG as the enzyme responsible for thiolation of the gliotoxin precursor. Similarly, following the deletion of *gliT*, absence of gliotoxin production was noted, with the appearance of a molecule corresponding to the *m/z* of a monothiol form gliotoxin (Schrettl *et al.*, 2010).

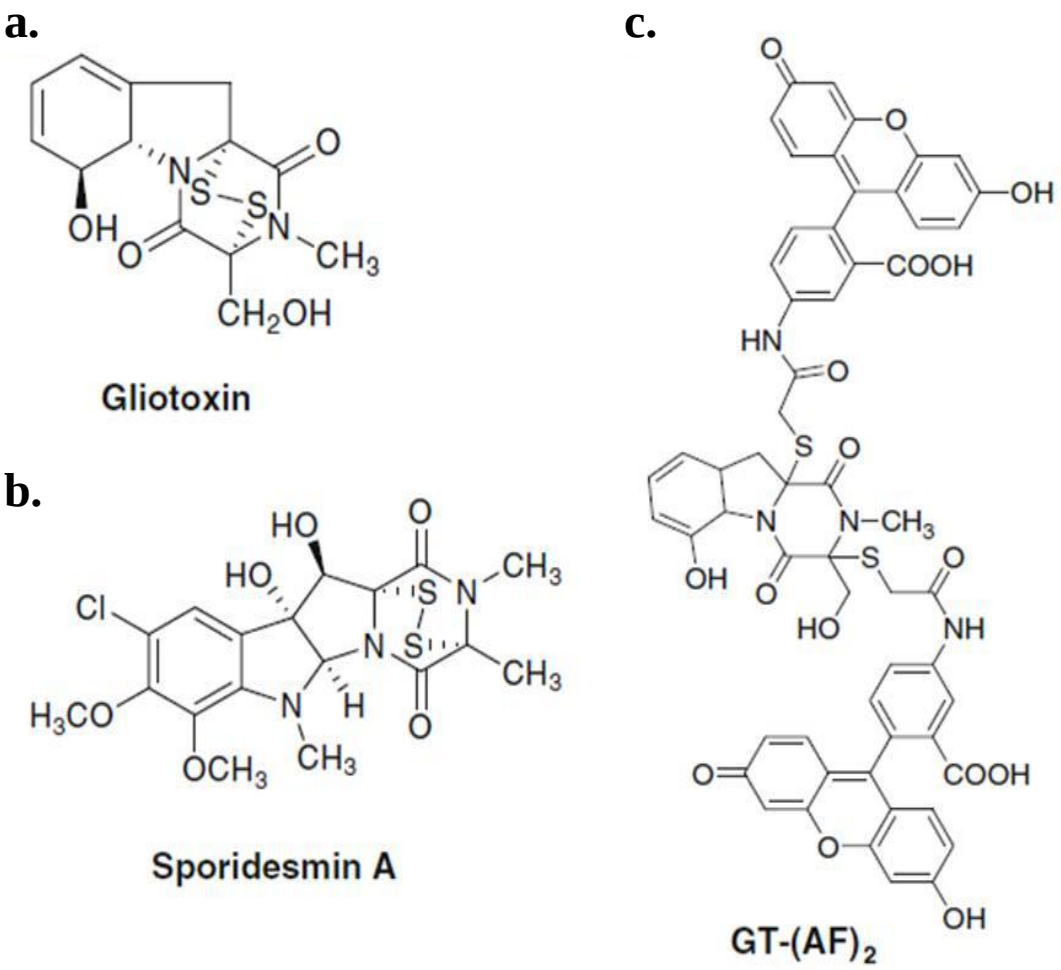

Figure 6.1: Chemical structures of (a) gliotoxin, (b) sporidesmin A and (c) proposed structure of di-acetamidofluorescein gliotoxin (GT-$(AF)_2$).

Forseth *et al.* (2011) subsequently performed comparative metabolomic profiling of *A. fumigatus* following the deletion of the transcriptional regulator *gliZ*, with the identification of 19 *gliZ*-dependent metabolites (Figure 6.2). Identification of *gliZ*-dependent compounds with varying structural motifs, revealed the extent to which the *gli* cluster contributes to the metabolome of *A. fumigatus* (Figure 6.2).

Our hypothesis was that investigation of the metabolome of the *gliK* deletion strain may reveal whether GliK has a role in gliotoxin biosynthesis. Additionally, alterations to the metabolite profile following deletion of *gliK* may allude to the mechanisms associated with the altered phenotypes observed in *A. fumigatus* Δ*gliK* relative to the wild-type. Consequently, the aims of the work presented in this Chapter were (i) to identify optimal culture conditions for gliotoxin production in *A. fumigatus* ATCC26933, (ii) to determine the effect of *gliK* deletion on gliotoxin production, (iii) to characterise changes to the intracellular and extracellular metabolome of *A. fumigatus* ATCC26933 following deletion of *gliK*.

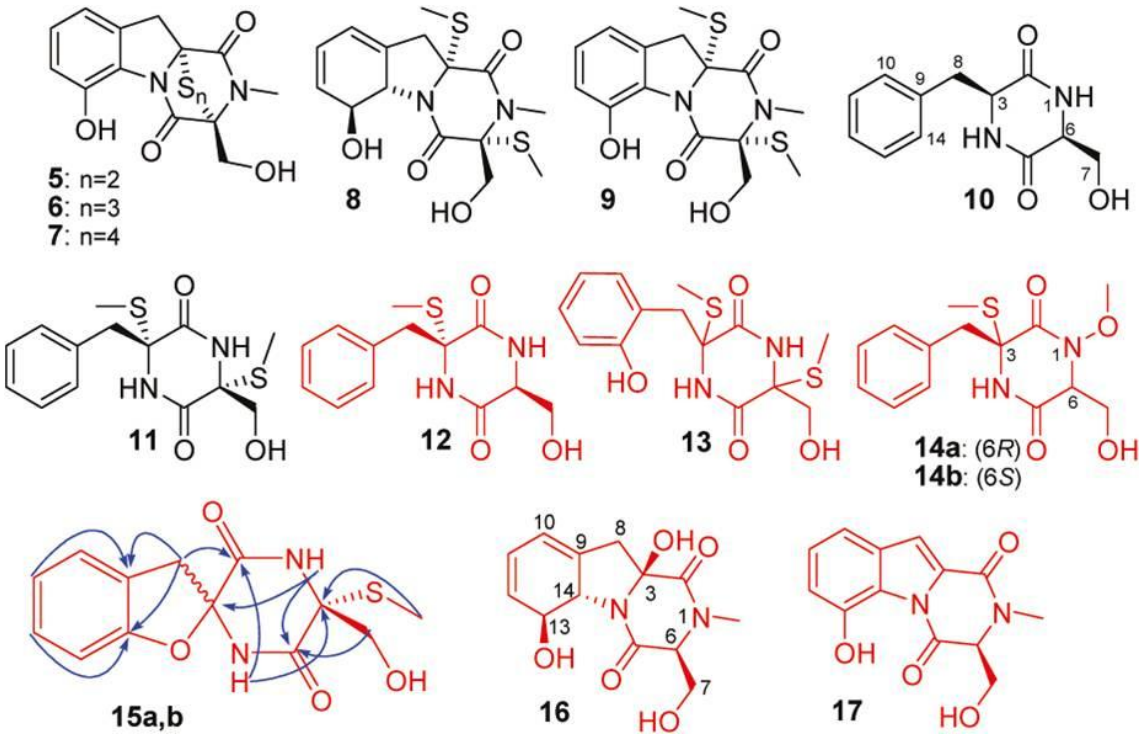

Figure 6.2: GliZ-dependent metabolites identified from *A. fumigatus*, demonstrating intermediate polarity. Novel metabolites are indicated in red. From Forseth *et al.* (2011).

6.2 Results

6.2.1 Identification of Culture Conditions for Enhanced Gliotoxin Production by *A. fumigatus* ATCC26933

In order to comprehensively characterise the effect of deletion of *gliK* on gliotoxin production in *A. fumigatus*, optimal conditions for gliotoxin production were investigated using *A. fumigatus* ATCC26933 (wild-type). *A. fumigatus* wild-type was inoculated into each of the following media (i - iv) and incubated at 37 °C in the dark at 200 rpm:

(i) YES (Section 2.1.5.11)

(ii) RPMI (Section 2.1.5.12)

(iii) AMM (Section 2.1.5.5)

(iv) Czapek-Dox Broth (Section 2.1.5.9)

Culture supernatants were harvested at 48 and 72 h, and chloroform was used to perform organic extractions on the supernatants (Section 2.2.4.11). The dried organic extracts (Section 2.2.4.12) were resuspended in a minimal volume of HPLC-grade methanol and analysed by RP-HPLC using a 5 to 95 % acetonitrile gradient (Section 2.2.5.1; Table 2.7, Gradient 1). A reference standard of commercially produced gliotoxin was analysed in tandem.

Gliotoxin was observed to be optimally produced in Czapek-Dox medium following a culture time of 72 h. Standard gliotoxin was detected at a retention time (R_T) of 13.390 min by RP-HPLC analysis (Figure 6.3a). Equivalent peaks, at retention times of 13.424 and 13.404 min, were detected from the organic extracts of culture supernatants collected from Czapek-Dox cultures at 48 h and 72 h respectively (Figure 6.3, b and c). This equates to gliotoxin concentration levels of 5.61 and 11.20 µg/ml, in culture supernatants collected from Czapek-Dox cultures at 48 h and 72 h respectively.

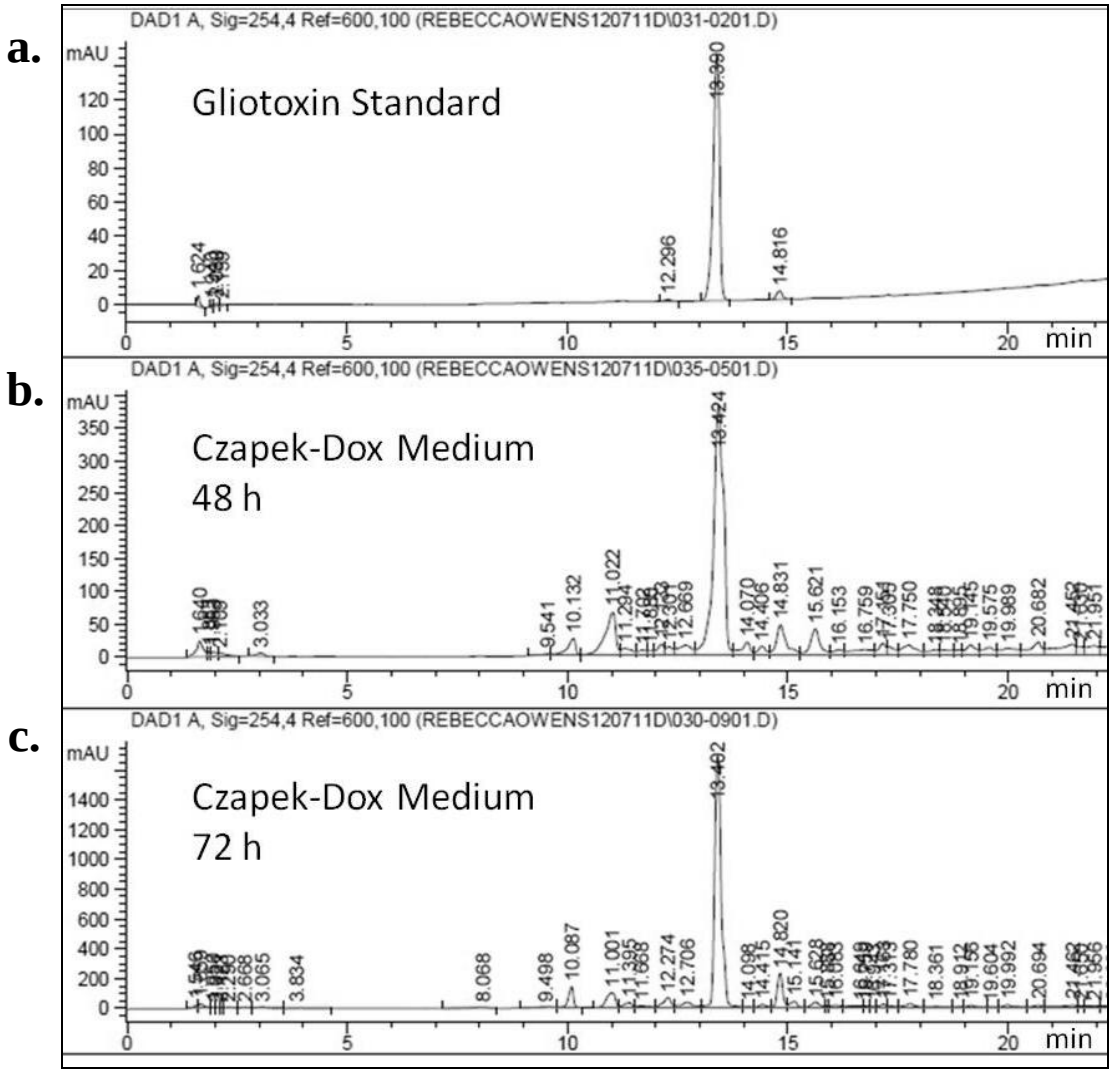

Figure 6.3: RP-HPLC analysis of gliotoxin production by *A. fumigatus* wild-type in Czapek-Dox medium. Organic extracts of culture supernatants (48 h and 72 h; 37 °C) were subjected to RP-HPLC analysis and absorbance was monitored at 254 nm. (a) Gliotoxin standard (2 µg) elutes at R_T = 13.390 min. (b*) A. fumigatus* ATCC26933 wild-type strain at 48 h secreted gliotoxin (R_T = 13.424 min). (c) *A. fumigatus* ATCC26933 wild-type strain at 72 h secreted gliotoxin (R_T = 13.402 min).

6.2.2 Comparative analysis of *A. fumigatus* ATCC26933, wild-type and Δ*gliK*, extracellular metabolites

Organic extracts from *A. fumigatus* ATCC26933, wild-type and Δ*gliK*, culture supernatants were compared by RP-HPLC, MALDI-ToF MS and LC-MS/MS to determine whether deletion of *gliK* resulted in an alteration of the extracellular metabolome. The culture conditions identified in Section 6.2.1, as optimal for gliotoxin production, were used for extracellular metabolite comparisons.

6.2.2.1 RP-HPLC analysis of organic extracts from *A. fumigatus* ATCC26933, wild-type and Δ*gliK*, culture supernatants

Comparative RP-HPLC analyses were performed on organic extracts from *A. fumigatus* ATCC26933, wild-type and Δ*gliK*, culture supernatants (37 °C; 72 h; Czapek-Dox broth). Gliotoxin standards (2 µg; 20 µl) were analysed alongside these samples and absorbance was monitored at 254 nm (Figure 6.4).

Gliotoxin standard eluted at a retention time of 13.516 min with a peak area of 1423.42. Organic extracts from wild-type supernatants yielded an absorbance (R_T = 13.50 ± 0.0044 min) with peak area range of 6433 ± 119.7. This correlated with the retention time of gliotoxin as deduced by comparison with the commercial standard. Gliotoxin was not detectable in organic extracts from *A. fumigatus* Δ*gliK* culture supernatants by RP-HPLC (Figure 6.4). A number of peaks were observed to increase in intensity in culture supernatants from Δ*gliK*, relative to the wild-type (R_T = 13.236, 14.257, 15.207 and 15.676 min) (Figure 6.4). Further analyses were required to characterise these differentially produced compounds and to confirm the absence of gliotoxin from Δ*gliK* culure supernatants.

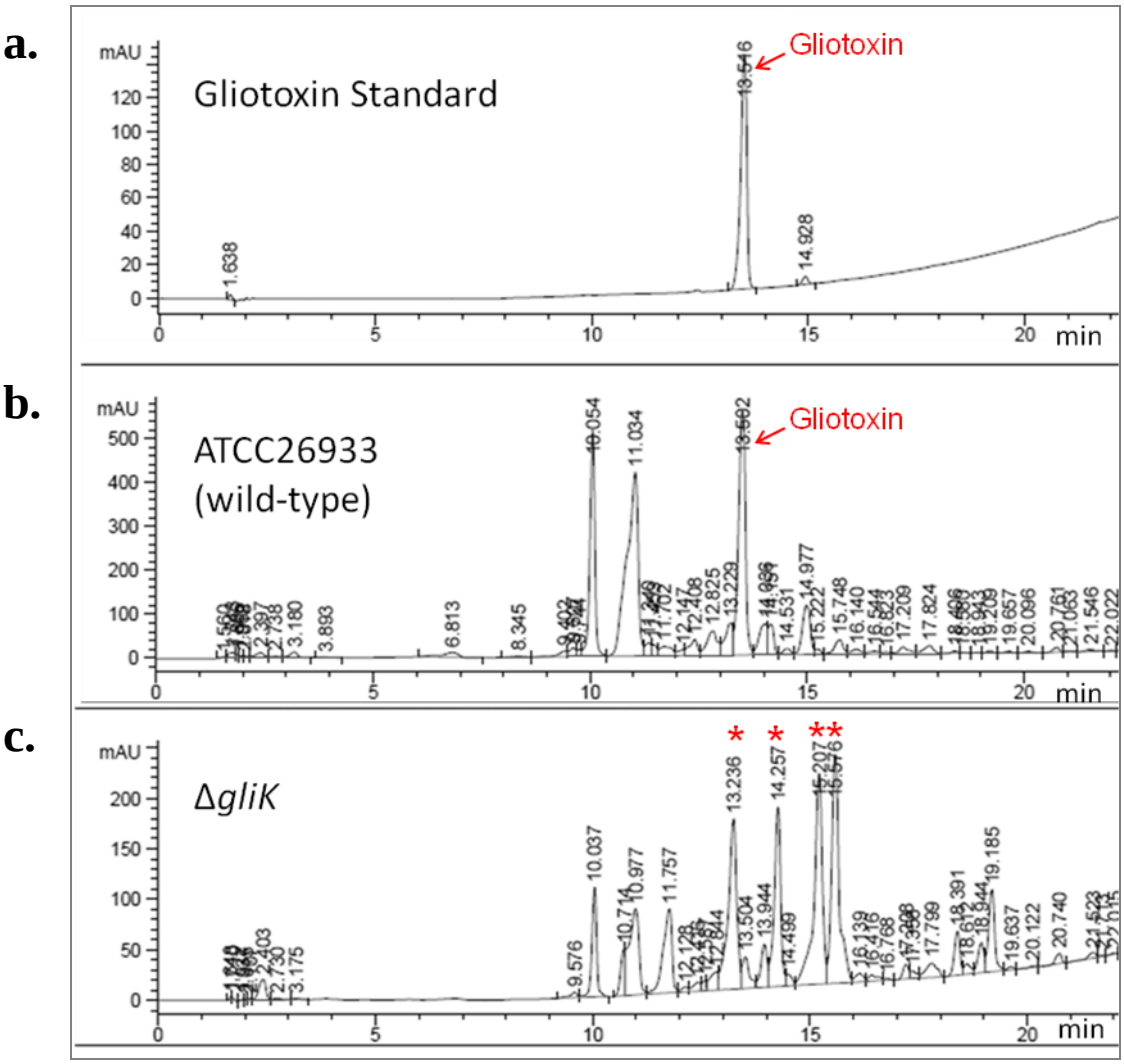

Figure 6.4: Comparative RP-HPLC analysis of organic extracts from *A. fumigatus* ATCC26933 wild-type and Δ*gliK* culture supernatants. Organic extracts of culture supernatants (72 h; 37 °C, Czapek-Dox broth) were subjected to RP-HPLC analysis and absorbance was monitored at 254 nm. (a) Gliotoxin standard (2 µg) elutes at R_T = 13.516 min with a peak area of 1423.42. (b) *A. fumigatus* ATCC26933 wild-type strain secretes gliotoxin with a peak area of 6433 ± 119.7 (R_T = 13.502 min). (c) Gliotoxin is not detectable in culture supernatants of *A. fumigatus* Δ*gliK*. An increase in the presence and intensity of a number of peaks is evident in *A. fumigatus* Δ*gliK* (indicated by red asterix), relative to wild-type.

6.2.2.2 Reduction and alkylation of organic extracts from *A. fumigatus*, wild-type and Δ*gliK*, culture supernatants

Further investigation was carried out to determine if gliotoxin was produced by Δ*gliK*. Reduction of the disulphide bond of gliotoxin and subsequent alkylation of the thiol groups with 5'-IAF results in formation of diacetamidofluorescein-gliotoxin (GT-$(AF)_2$) (Figure 6.1) (Davis *et al.*, 2011b). This compound exhibits a shift in retention time upon analysis by RP-HPLC, in addition to an increased molar absorptivity relative to gliotoxin. Reduction of organic extracts of *A. fumigatus* ATCC26933, wild-type and Δ*gliK*, culture supernatants (37 °C; 72 h; Czapek-Dox broth) was carried out using sodium borohydride ($NaBH_4$) as described in Section 2.2.5.2. Control samples were prepared in tandem, which omitted the $NaBH_4$-mediated reduction of gliotoxin (non-reduced (NR) + 5'-IAF). Following 5'-IAF labelling, RP-HPLC analysis was carried out for the detection of GT-$(AF)_2$ using gradient 2 (Table 2.8) (Figure 6.5).

Gliotoxin displayed an additional peak at retention time of 5.261 min following $NaBH_4$ reduction and 5'-IAF alkylation (R + 5'-IAF). This represents diacetamidofluorescein-gliotoxin (GT-$(AF)_2$). An equivalent labelled species was observed in organic extracts from wild-type culture supernatants (R_T = 5.134 ± 0.01325 min) indicating the presence of GT-$(AF)_2$ following reduction and alkylation. No GT-$(AF)_2$ peak was detected in organic extracts from Δ*gliK* culture supernatants following reduction and alkylation, further confirming the absence of gliotoxin from *A. fumigatus* Δ*gliK*.

In addition to RP-HPLC analysis, MALDI-ToF MS was used to determine if GT-$(AF)_2$ was present in Δ*gliK* samples (Section 2.2.5.4). MALDI-ToF MS detected a compound with a molecular mass of 1102.9 Da ($(M + H)^+$), equating to the molecular mass of GT-$(AF)_2$, in organic extracts from wild-type culture supernatants (Figure

6.6a). No equivalent compound was detected in organic extracts from Δ*gliK* culture supernatants using this method (Figure 6.6b). Based on RP-HPLC and MALDI-ToF MS analysis, GT-$(AF)_2$ was not detectable in organic extracts from Δ*gliK* culture supernatants, leading to the conclusion that gliotoxin biosynthesis is abolished following deletion of *gliK*.

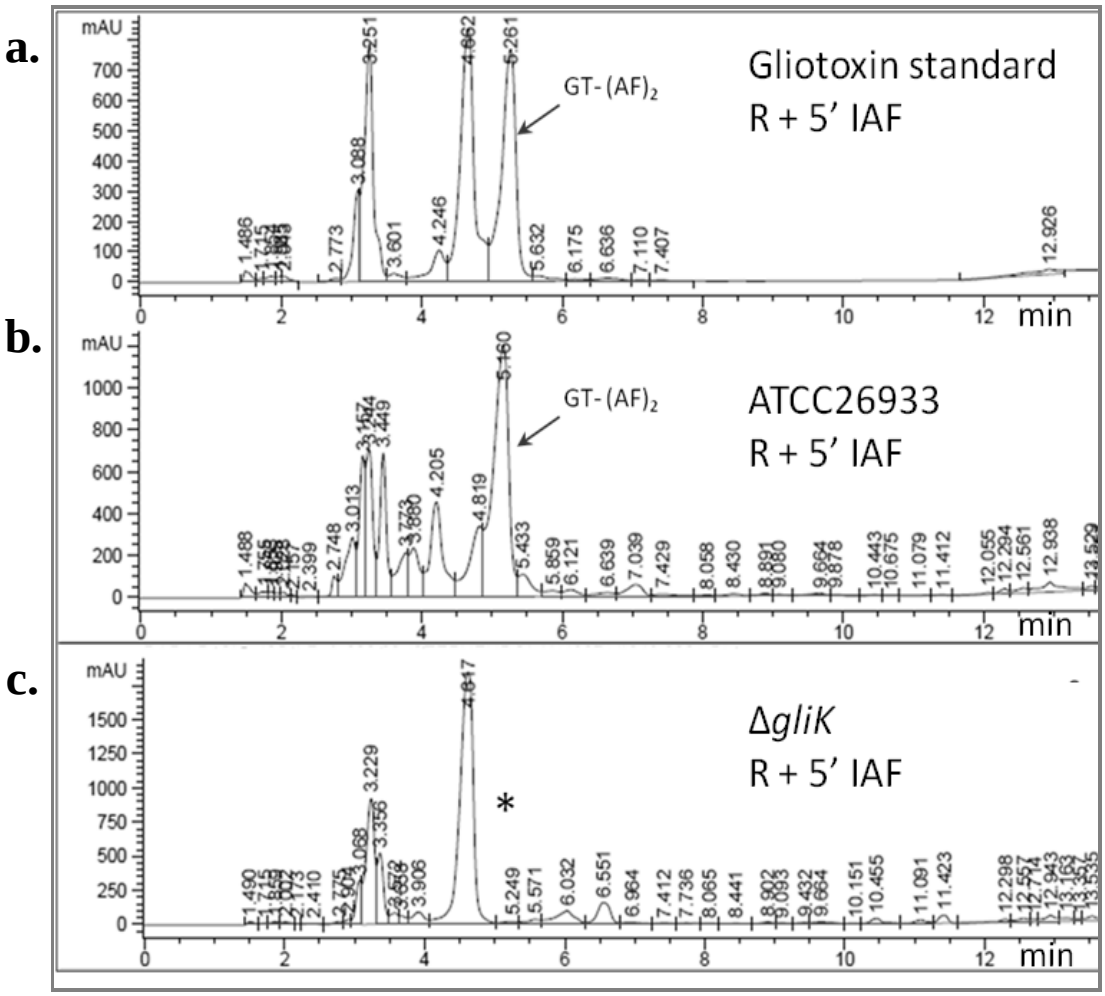

Figure 6.5: RP-HPLC analysis of reduced and alkylated organic extracts of *A. fumigatus* ATCC26933, wild-type and Δ*gliK*, culture supernatants. Absorbance detection at 254 nm is shown for all samples. (a) Gliotoxin standard (2 µg). GT-$(AF)_2$ was detected at R_T = 5.261 min. (b) *A. fumigatus* wild-type. GT-$(AF)_2$ was detected at R_T = 5.160 min. (c) *A. fumigatus* Δ*gliK*. No GT-$(AF)_2$ was detected (indicated by the asterix). R + 5'-IAF, Reduced with $NaBH_4$ and alkylated with 5'-IAF; NR + 5'-IAF, non-reduced and alkylated with 5'-IAF.

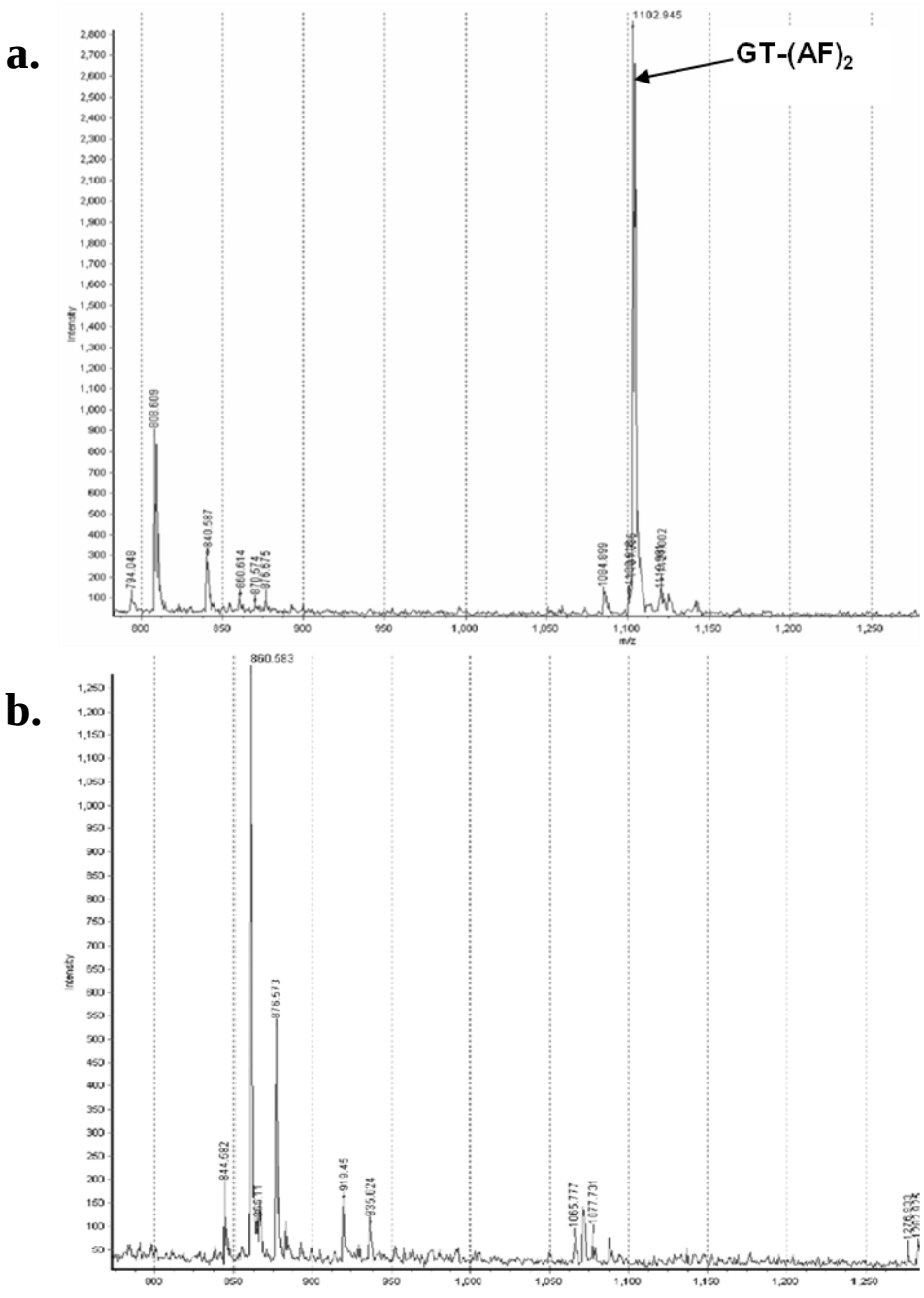

Figure 6.6: (a) MALDI-ToF analysis reveals diacetamidofluorescein-gliotoxin (GT-$(AF)_2$) (*m/z* 1102.9) (Davis *et al.*, 2011b) following reduction and alkylation of organic extracts from *A. fumigatus* ATCC26933 wild-type (b) GT-$(AF)_2$ is not present in organic extracts of *A. fumigatus* Δ*gliK*.

6.2.2.3 Analysis of *A. fumigatus* ATCC26933, wild-type and Δ*gliK*, metabolite profiles by LC-MS/MS

Comparative analyses of organic extracts from *A. fumigatus* ATCC26933, wild-type and Δ*gliK*, culture supernatants were carried out by LC-MS/MS (Section 2.2.6.4). Alignment of total ion chromatographs (TIC) of wild-type and Δ*gliK* organic extracts was performed (Figure 6.7) and revealed distinct differences in the relevant metabolite profiles.

Singly charged ions were not excluded from ESI LC-MS/MS analyses. Organic extracts of *A. fumigatus* wild-type and Δ*gliK* culture supernatants yielded two distinct spectra on LC-MS/MS analysis (Figure 6.7). Wild-type extracts produced spectra with dominant peaks between retention times 6.7 and 6.9 min. These peaks are attributable to the elution of gliotoxin, confirmed by the presence of the precursor ion ($(M + H)^+$ = 327.2) and characteristic product ions ($(M + H)^+$ = 263, 245, 227) (Figure 6.8b) (Schrettl *et al.*, 2010). LC-MS/MS analysis confirmed the absence of gliotoxin production, and revealed the presence of metabolites, of $(M+H)^+$ = 394 and 396, which were significantly more abundant in culture supernatants of *A. fumigatus* Δ*gliK* (p = 0.0024, fold difference = 24.1; p = 0.0003, fold difference = 9.6, respectively). These species ($(M+H)^+$ = 394 and 396) were targeted for MS^2 (Figure 6.8, c and d) and appear to be related compounds that differ by 2 Da. This relationship is evident by the same difference between their relative product ion base peaks ($(M + H)^+$ = 338 and 340, respectively). The presence of dimers of these compounds is also noted ($(2M + H)^+$ = 787 and 791 respectively. These ions are all singly charged as deduced by interrogating the isotopic peaks of each compound. This analysis confirms the abolition of gliotoxin biosynthesis in *A. fumigatus* following deletion of *gliK*, and coincides with the substantial increase in production of two extracellular compounds with $(M+H)^+$ = 394

and 396. These compounds may represent stable intermediates of the gliotoxin biosynthetic process, which accumulate consequent to *gliK* deletion. Alternatively, these molecules may be shunt metabolites, formed as a result of the relative instability of on-pathway intermediates as observed in *A. fumigatus* Δ*gliG* (Davis *et al.*, 2011a).

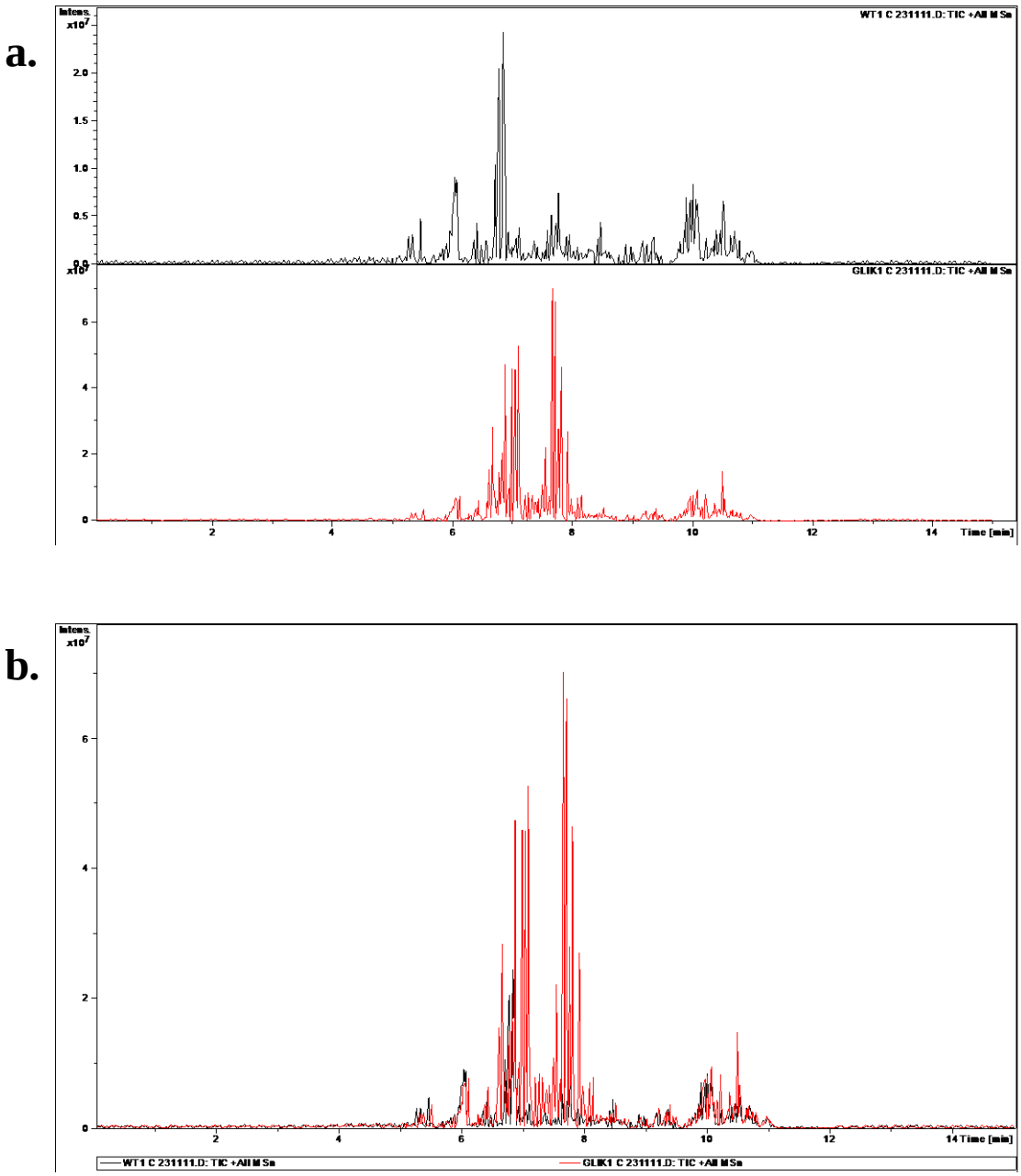

Figure 6.7: Total ion chromatographs (TIC) of organic extracts from culture supernatants of *A. fumigatus* wild type (black) and Δ*gliK* (red) cultures as analysed by LC-MS/MS, (a) in list view and (b) overlaid.

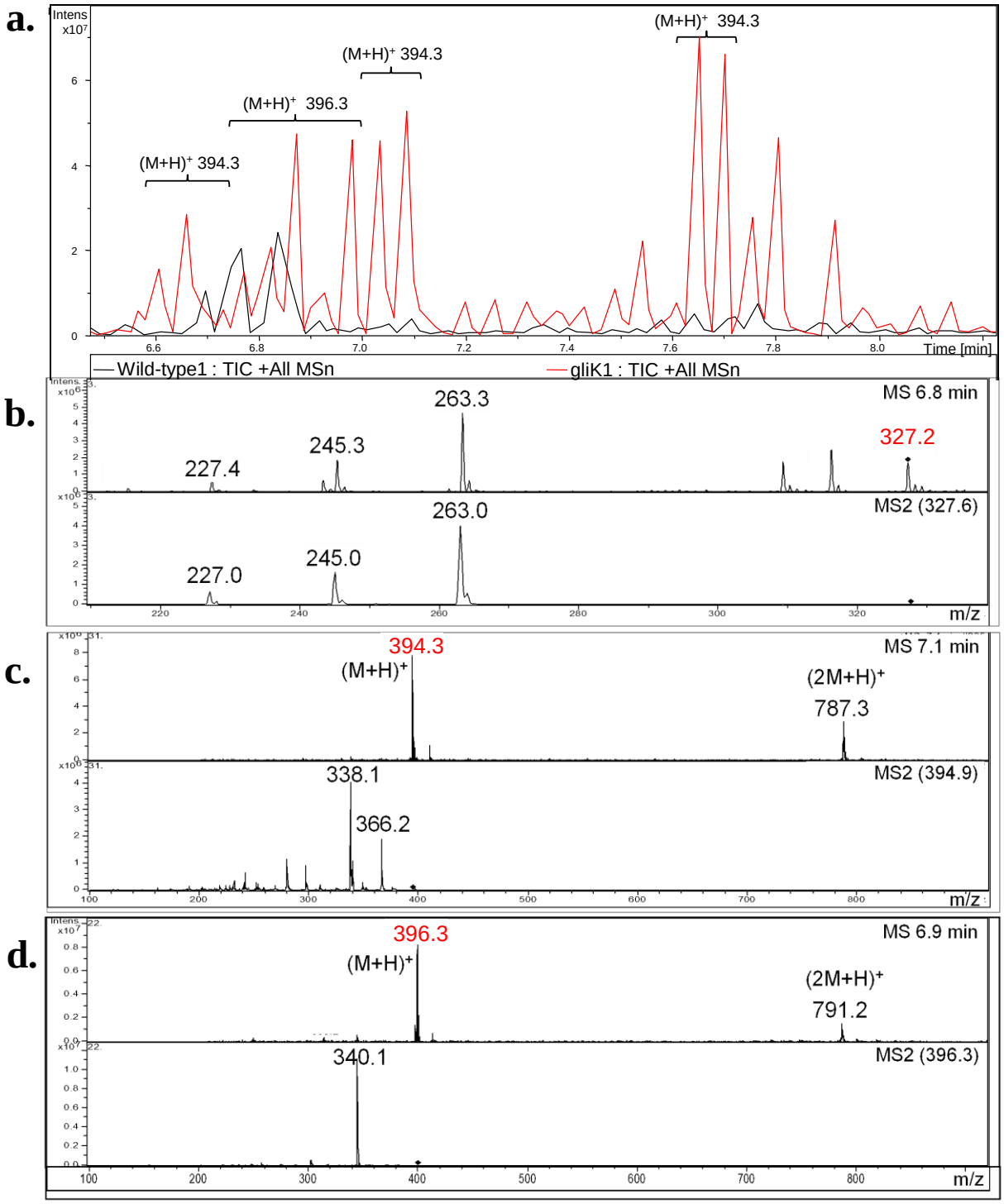

Figure 6.8: (a) Total ion chromatograph (TIC) of organic extracts from wild-type (black) and Δ*gliK* (red) culture supernatants, overlaid. (b) Gliotoxin (*m/z* = 327.2) was identified in the mass spectra from the wild-type culture supernatant but was not found in the Δ*gliK* culture supernatants. Comparative profiling identified compounds (*m/z* = 394.3; 396.3) that were present at higher amounts in organic extracts of Δ*gliK*, relative

to wild-type culture supernatants. Mass spectra from the molecular species (c) *m/z* = 394.3 and (d) *m/z* = 396.3 are shown. Selected precursor ions from MS are indicated in red text, with resultant MS^2 spectra included directly below.

6.2.3 Comparative analysis of *A. fumigatus* ATCC26933, wild-type and Δ*gliK*, intracellular metabolites

Following on from the observation in Section 6.2.2, that deletion of *gliK* results in the loss of gliotoxin production from *A. fumigatus*, comparative analysis of the intracellular metabolome was undertaken. Lysates from *A. fumigatus* ATCC26933, wild-type and Δ*gliK* mycelia were analysed by RP-HPLC and LC-MS/MS to determine whether Δ*gliK* exhibited an altered intracellular metabolome. The culture conditions identified in Section 6.2.1, as optimal for gliotoxin production, were used for extracellular metabolite comparisons.

6.2.3.1 Analysis of intracellular *A. fumigatus* ATCC26933, wild-type and Δ*gliK*' metabolite profiles by RP-HPLC

Mycelia from *A. fumigatus* ATCC26933, wild-type and Δ*gliK*, were harvested at 72 h, following growth in Czapek-Dox broth at 37 °C (Section 2.1.5.9). Protein extracts were prepared using non-reducing lysis buffer (Section 2.1.5.18, 2.2.2.1). Small-scale organic extractions were performed in the protein lysates and comparative RP-HPLC analyses were carried out on the resultant organic extracts from *A. fumigatus* ATCC26933 and Δ*gliK* (Figure 6.9). RP-HPLC analysis revealed no substantial differences between the metabolic profile of the organic extracts from wild-type and Δ*gliK* mycelial lysates (Figure 6.9). Consequently, additional investigation was required to determine any differences between the intracellular metabolome of Δ*gliK* relative to wild-type.

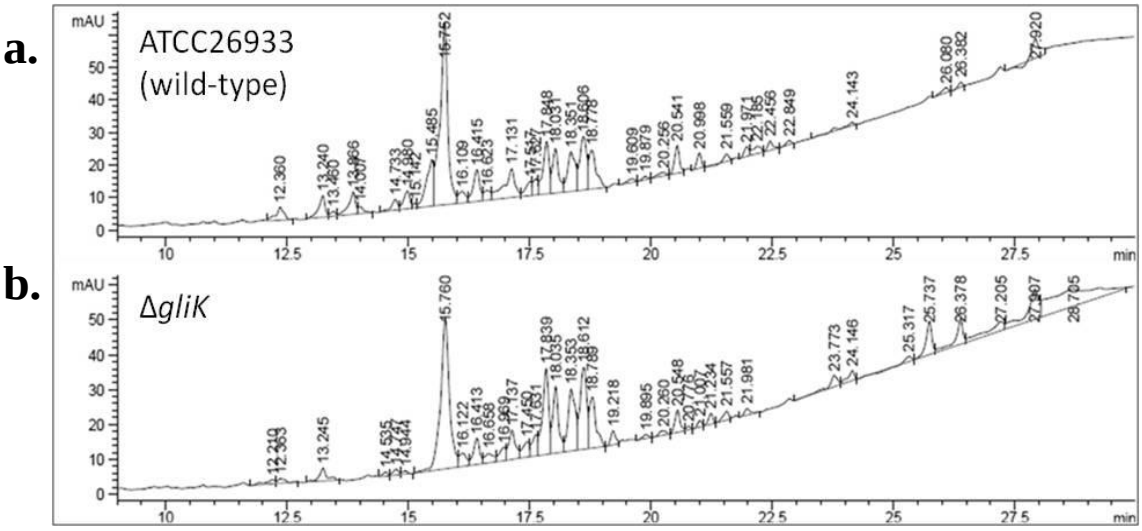

Figure 6.9: Comparative RP-HPLC analysis of organic extracts from *A. fumigatus* ATCC26933 (a) wild-type and (b) Δ*gliK* mycelial lysates. Absorbance was monitored at 254 nm.

6.2.3.2 Quantitation of free sulphydrals present in lysates from *A. fumigatus*, wild-type and Δ*gliK*, mycelia

The quantity of free sulphydral groups present in mycelial lysates of *A. fumigatus* wild-type and Δ*gliK*, was measured using an Aldithiol-4® titration (Section 2.2.5.4). Aldithiol-4® measures the concentration of free thiols in a sample, but does not distinguish between thiols from proteins or small molecular mass metabolites. Control samples, consisting of the non-reducing lysis buffer (Section 2.1.5.18) were subjected to titration with Aldrithiol-4®, and used to determine baseline absorbance changes. The concentration of total free sulphydrals (of proteinaceous or non-proteinaceous origin) per mg of protein was significantly higher in the *A. fumigatus* Δ*gliK* lysates compared to the wild-type (p = 0.0028; n = 3; fold difference = 2.2) (Figure 6.10). This result signifies the presence of elevated intracellular thiols in Δ*gliK*, which may be related GliK absence.

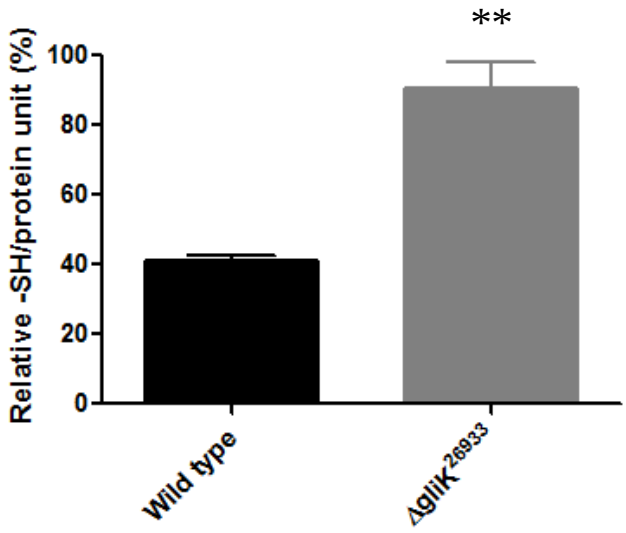

Figure 6.10: Relative concentration of free sulphydral groups per unit of protein (SH/mg protein). Concentration of free sulphydral groups, relative to protein concentration, in lysates of *A. fumigatus* Δ*gliK* (grey) is significantly higher than wild-type (black) (p = 0.0028; n = 3; fold difference = 2.2).

6.2.3.3 Alkylation of lysates from *A. fumigatus*, wild-type and Δ*gliK*, mycelia

Based on the observation of a significantly higher concentration of sulphydrals in mycelial lysates of *A. fumigatus* Δ*gliK*, relative to wild-type, further investigation was carried out. Mycelial lysates, were examined for the presence of free sulphydrals or disulphide bonds, using reduction and alkylation as described in Section 2.2.5.2 (Davis *et al.*, 2011b). Non-reduced samples were prepared concurrently, without $NaBH_4$-mediated reduction prior to alkylation with 5'-IAF (NR + 5'-IAF). RP-HPLC analysis was carried out to assess any differential alkylation that occurs as a result of the deletion of *gliK*.

Reduction and subsequent alkylation of protein lysates with 5'-IAF (R + 5'-IAF), revealed two peaks in each sample at R_T = 12.07 ± 0.001732 (n = 3) and 14.07 ± 0.002186 (n = 3) min (Figure 6.11). These peaks were attributable to un-reacted 5'-IAF, as deduced by comparison with the control sample. An additional peak, not present in the control sample, was detected in both wild-type and Δ*gliK* at R_T = 11.71 ± 0.003 min (n = 6) and was indicative of a 5'-IAF labelled compound (Figure 6.11). An equivalent absorbance was observed in the non-reduced *A. fumigatus* lysates, following 5'-IAF labelling (NR + 5'-IAF) at R_T = 11.72 ± 0.0115 min (n = 6) (Figure 6.12). This signifies that the 5'-IAF labelled compound contains at least one free sulphydral group as reduction was not required prior to alkylation with 5'-IAF. This 5'-IAF labelled intracellular compound, termed AF11.7, was present at significantly higher levels in Δ*gliK* compared to wild-type (p = 0.0343; n = 6; 5.7 fold difference) based on the relative peak areas from RP-HPLC analysis. An increase in the intracellular concentration of this sulphydral containing metabolite in Δ*gliK*, correlates with the observations from Aldrithiol-4® titrations (Section 6.2.3.2). Fractionation was utilised

to purify the 5'-IAF labelled compound, from both wild-type and Δ*gliK* for further characterisation by LC-MS/MS.

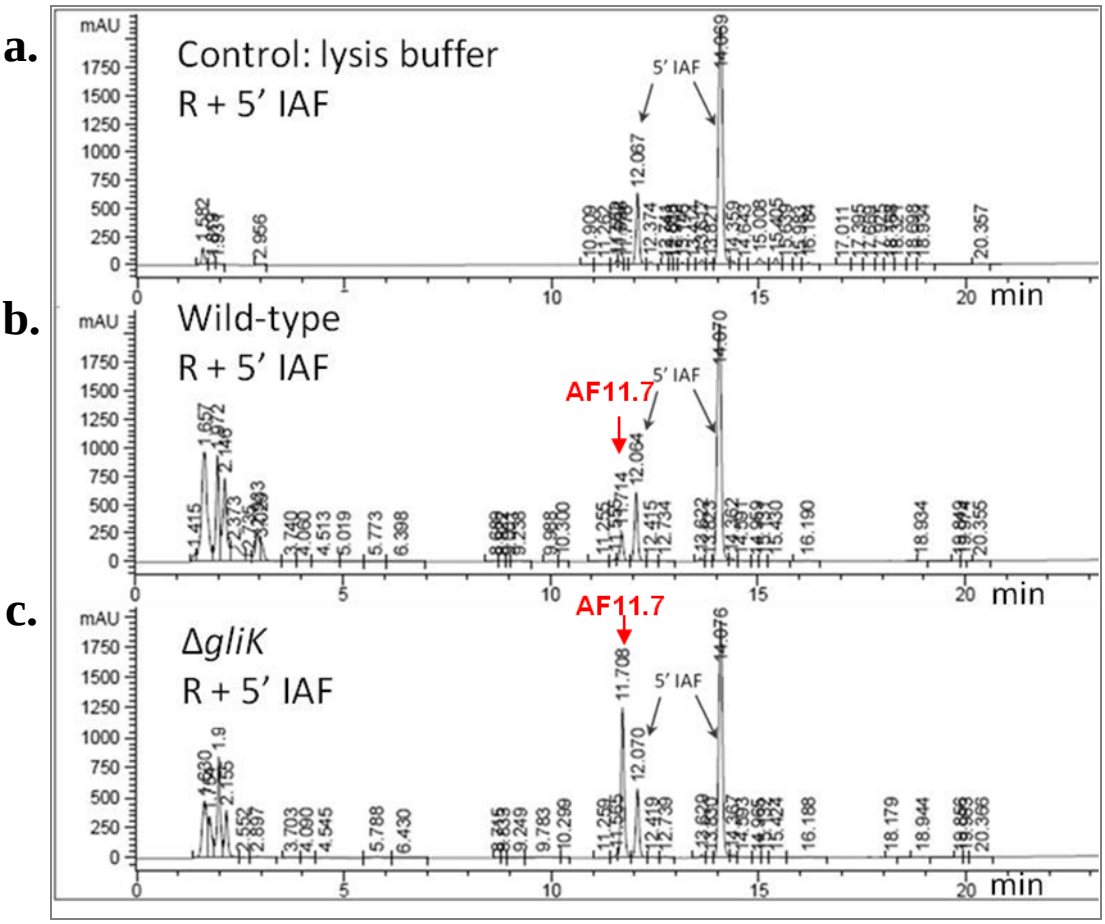

Figure 6.11: RP-HPLC analysis of *A. fumigatus* ATCC26933, wild-type and Δ*gliK*, mycelial lysates, with $NaBH_4$-mediated reduction prior to 5'-IAF labelling (R + 5'-IAF). Absorbance detection at 254 nm is shown for all samples. (a) Lysis buffer control R + 5'-IAF. Unreacted 5'-IAF was detected at R_T = 12.067; 14.069 min. (b) *A. fumigatus* wild-type R + 5'-IAF. A 5'-IAF labelled metabolite (AF11.7) eluted at R_T = 11.714 min (red arrow). (c) *A. fumigatus* Δ*gliK* R + 5'-IAF. A 5'-IAF labelled metabolite (AF11.7) eluted at R_T = 11.708 min (red arrow), with a substantially higher intensity than observed in wild-type. R + 5'-IAF, Reduced with $NaBH_4$ and alkylated with 5'-IAF.

a.

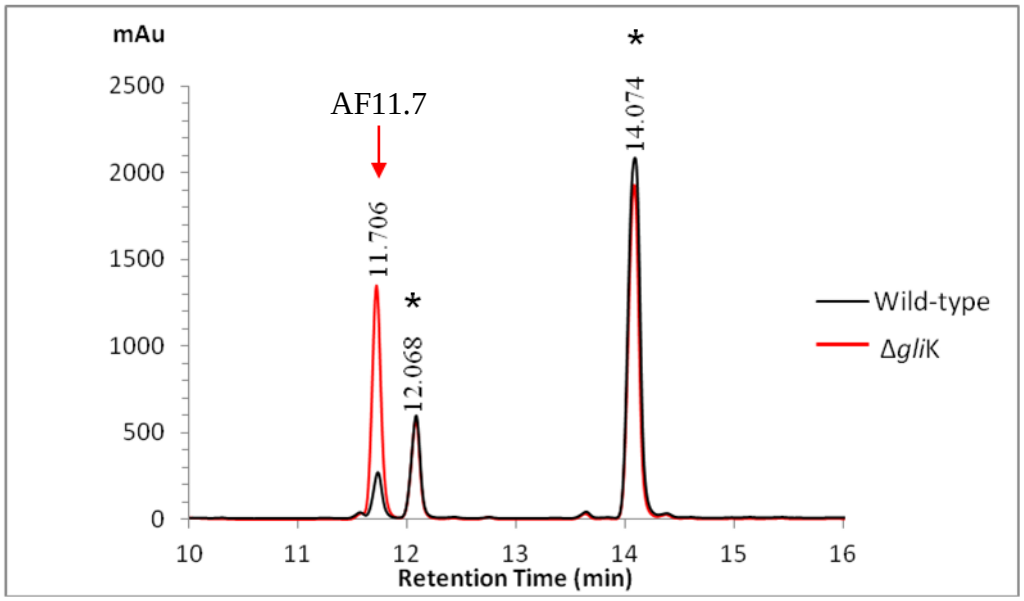

Figure 6.12: Overlaid RP-HPLC analysis of *A. fumigatus* ATCC26933 wild-type (black) and Δ*gliK* (red) mycelial lysates, with no reduction prior to 5'-IAF labeling (NR + 5'-IAF). A 5'-IAF labelled metabolite, eluted at R_T = 11.706 min (AF11.7; red arrow), and was present at significantly higher amounts in *A. fumigatus* Δ*gliK* than in wild-type (p = 0.0343). Unreacted 5'-IAF was detected at R_T = 12.068; 14.074 min (indicated by asterix). Absorbance detection is shown at 254 nm. NR + 5'-IAF; non-reduced and alkylated with 5'-IAF.

6.2.3.4 LC-MS/MS analysis of 5'-IAF labelled intracellular metabolite

In order to ascertain the molecular mass of the 5'-IAF labelled metabolite purified from *A. fumigatus* wild-type and Δ*gliK* mycelial lysates in Section 6.2.3.3, LC-MS/MS was carried out. To facilitate LC-MS/MS analysis, fractions corresponding to AF11.7 were collected following RP-HPLC of alkylated mycelial lysates (Section 6.2.3.3). Fractions were dried to completion and resuspended in 10 % (v/v) methanol, 0.1 % (v/v) formic acid (Section 2.1.3.9). A control sample, consisting of the equivalent fraction from alkylation of the lysis buffer was also analysed. The ubiquitous monothiol, glutathione (GSH), was also subjected to alkylation with 5'-IAF and the resultant labelled molecule was also fractionated and analysed by LC-MS/MS.

Total ion current (TIC) chromatographs of the fractions from wild-type and Δ*gliK* 5'-IAF labelled lysates, each display two peaks at retention times between 5.9 and 6.0 min (Figure 6.13a). These peaks are both attributable to a compound with $(M+H)^+$ = 617.3 (Figure 6.13b). This compound is present at significantly higher levels in the Δ*gliK* (NR + 5'-IAF) relative to the wild-type lysates ($p < 0.001$; $n = 6$; fold difference = 4.96), as observed previously by RP-HPLC (Figure 6.12). No equivalent compound was detected in the control samples. A number of doubly charged molecular species were detected ($(M+2H)^{2+}$ = 309.2, 287.2), formed as a result of double protonation of the molecular ion ($(M+H)^+$ = 617. 3) or of product ions ($(M+H)^+$ = 573.3) respectively (Figure 6.13b). MS^2 fragmentation of selected precursor ions is shown (Figure 6.13c). Notably, alkylation of GSH with 5'-IAF produces a compound with $(M+H)^+$ = 695.3 (Figure 6.13d), as would be predicted based on the theoretical molecular mass of acetamidofluorescein-glutathione (GS-AF). Importantly, this excludes GSH as a candidate for the elevated, monothiol, intracellular metabolite.

a.

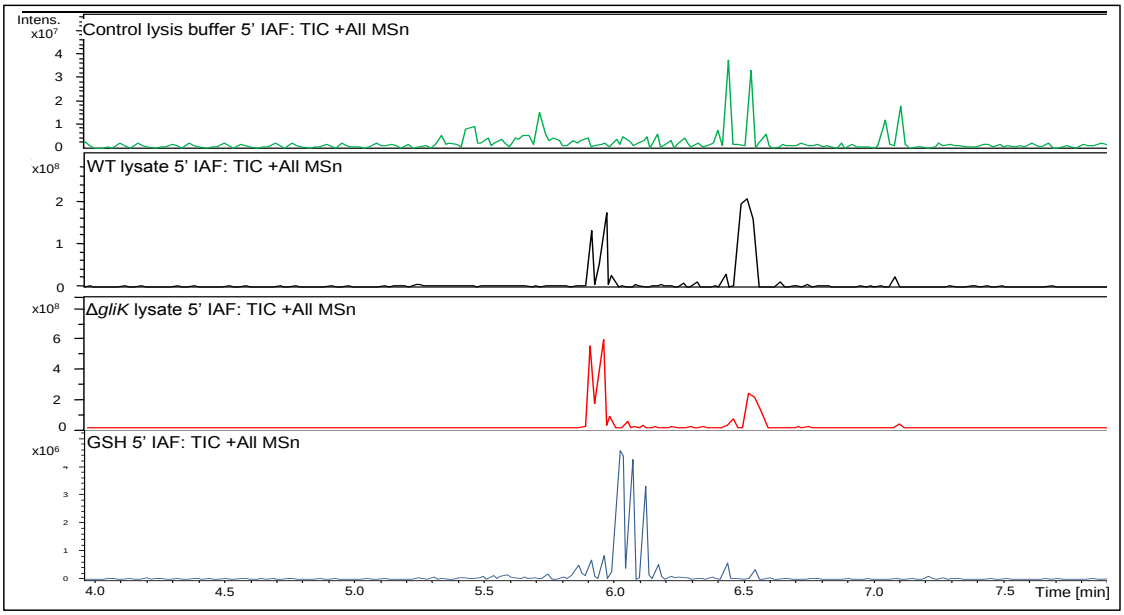
Intens.
Control lysis buffer 5' IAF: TIC +All MSn
WT lysate 5' IAF: TIC +All MSn
ΔgliK lysate 5' IAF: TIC +All MSn
GSH 5' IAF: TIC +All MSn
Time [min]

b.

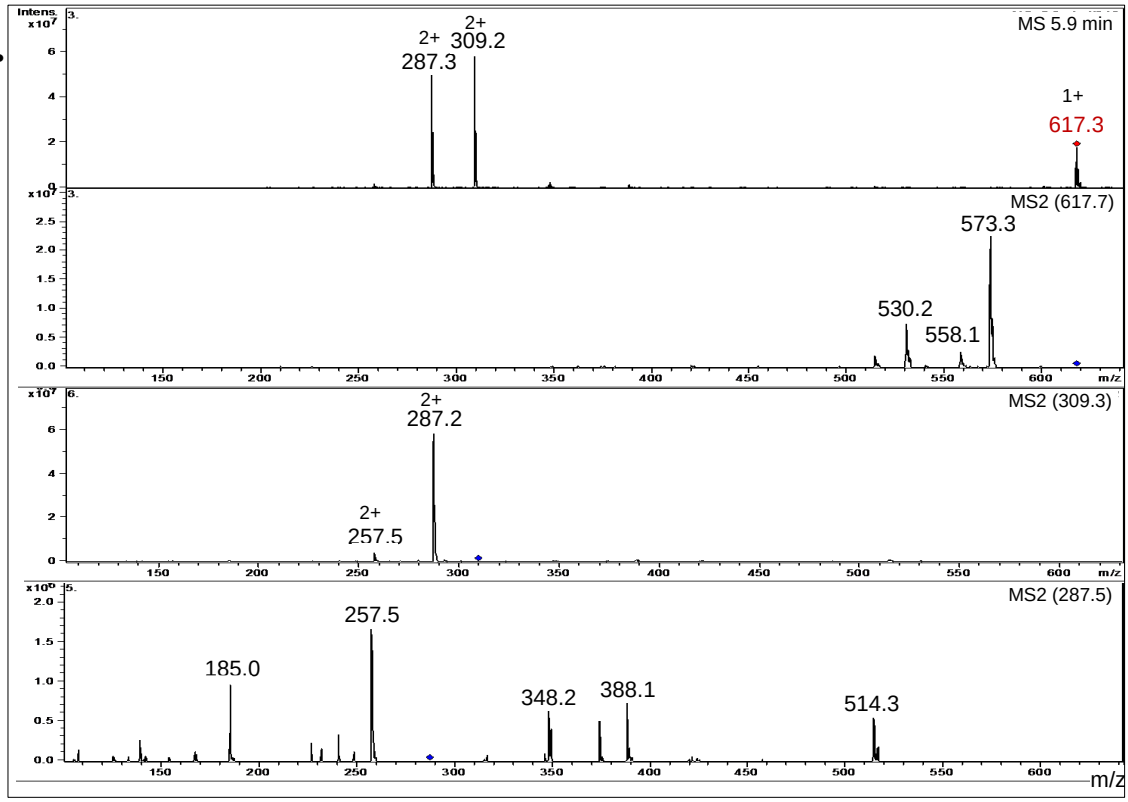
MS 5.9 min
2+ 287.3
2+ 309.2
1+ 617.3

c.

MS2 (617.7)
573.3
530.2
558.1
MS2 (309.3)
2+ 287.2
2+ 257.5
MS2 (287.5)
257.5
185.0
348.2
388.1
514.3
m/z

d.

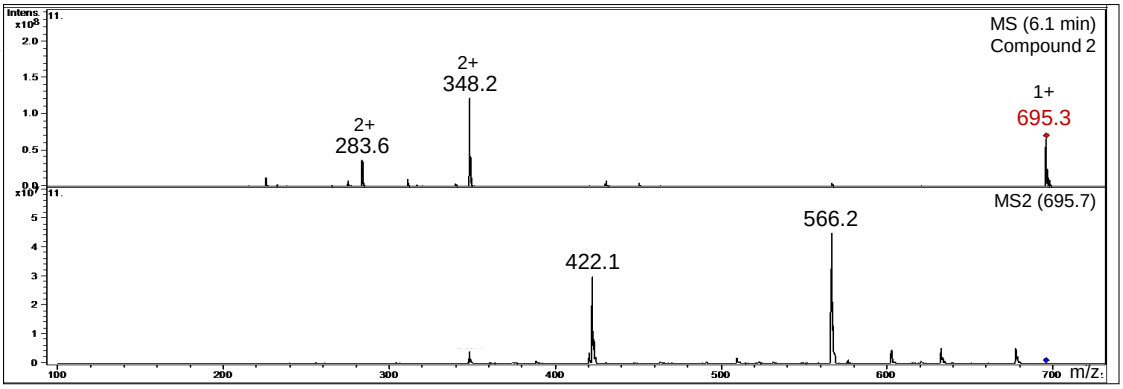
MS (6.1 min)
Compound 2
2+ 348.2
2+ 283.6
1+ 695.3
MS2 (695.7)
566.2
422.1
m/z

Figure 6.13: (a) Total ion chromatograph (TIC) of the 11-12 min fraction from RP-HPLC analyses of 5'-IAF labelled mycelia lysates of *A. fumigatus* ATCC26933 wild-type (black) and Δ*gliK* (red). The equivalent fraction from 5'-IAF labelling of GSH (blue) and lysate buffer (green), are also shown. (b) Mass spectra of the compounds observed at retention times of 5.9-6.0 min, from each of the *A. fumigatus* samples, revealed a singly charged molecule with $(M+H)^+$ = 617.3 along with two doubly charged molecules with *m/z* = 309.2 and 287.3 respectively. These compounds were not found in the mass spectra of the 5'-IAF labelled buffer control or GSH. (c) MS^2 analyses of each of these three ions was carried out. (d) Mass spectra of the compound observed at retention times of 6.0-6.2 min in the 5'-IAF labelled GSH samples revealed a singly charged molecule with $(M+H)^+$ = 695.3, correlating to acetamidofluorescein-glutathione, along with two doubly charged molecules with *m/z* = 348.2 and 283.6.

The mass of the 5'IAF labelled precursor ion ($(M + H)^+$ = 617.3; M = 616.3) is partially attributable to the conjugated fluorophore and this was deducted to determine the mass of the original metabolite. The molecular mass of the labelled molecule (*m/z* 617.3) indicates that the metabolite contains a single free thiol group, as each acetamidofluorescein moiety contributes 388.3 Da to the overall mass. Alkylation with 5'-IAF (M_r = 515.2 Da), results in derivatisation of a thiol group (-SH) with acetamidofluorescein, and the concurrent loss of hydrogen iodide (HI; M_r = 127.9 Da). The mass of the intracellular, monothiol metabolite was 229 Da (M229), as deduced by subtracting the acetamidofluorescein moiety from the precursor mass (616.3 - (515.2 - 127.9)).

The mass of this metabolite, combined with the presence of a single thiol, did not correlate with any metabolites characterised from *A. fumigatus* and also did not yield an identification from any well cited or extensively studied fungal metabolites. This lack of prior identification in *A. fumigatus* may have stemmed from the difficulty associated with purification of the native metabolite due to the hydrophilic nature of the molecule. Chemical derivatisation of M229 with 5'-IAF was required in order to impart hydrophobicity to the compound and enable subsequent purification and characterisation using RP-HPLC. The fragmentation pattern observed for the 5'-IAF labelled metabolite (AF11.7) included a neutral loss of 44 (617.3 - 573.3), a neutral loss of 59 (573.3 - 514.3) and a neutral loss of 126.2 (514.3-388.1) (Figure 6.13). Extensive analysis of the literature lead to the identification of a selenium (Se) -containing compound, selenoneine, with a *m/z* of 278 (Yamashita and Yamashita, 2010). Selenoneine is a selenium analogue of a sulphur-containing molecule, ergothioneine (EGT). Ergothioneine ($C_9H_{15}N_3O_2S$) is a hydrophilic molecule which possesses a molecular mass of 229 Da, and exists as a tautomer of a thiol and thione form (Figure

6.14). Additionally, the fragmentation pattern observed for AF11.7 corresponds with that reported for ergothioneine, upon deduction of the mass of the acetamidofluorescein moiety (Nikodemus *et al.*, 2011; Tepwong *et al.*, 2012). The identified neutral loss of 44 (617.3 - 573.3) corresponded to the loss of COO^-, neutral loss of 59 (573.3 - 514.3) corresponded to $N(CH_3)_3^+$ and a neutral loss of 126.2 (514.3-388.1) corresponded to $C_5N_2H_6S$ (Figure 6.14). The identification of the 5'-IAF labelled metabolite as ergothioneine was thus confirmed based on: (i) agreement between predicted molecular mass of 5'-IAF labelled metabolite and ergothioneine (both 229 Da), (ii) presence of a single thiol group, (iii) hydrophilic nature and (iv) fragmentation pattern evidence (Yamashita and Yamashita, 2010). To my knowledge this is the first identification of ergothioneine in *A. fumigatus*. This analysis confirmed the presence of elevated levels of ergothioneine in *A. fumigatus* ATCC26933 following deletion of *gliK*.

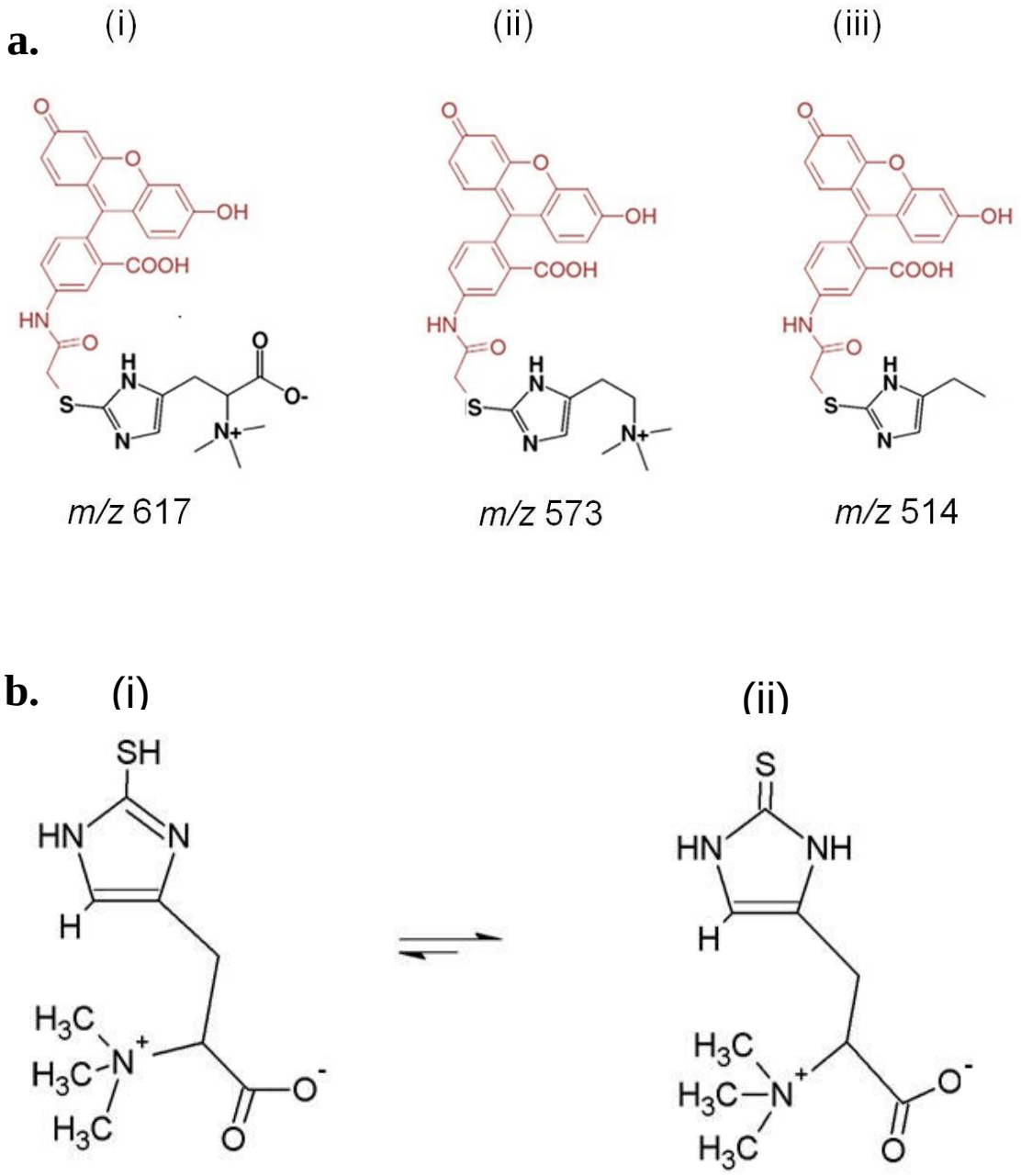

Figure 6.14: (a) Chemical structure of (i) acetamidofluorescein ergothioneine (ERG-AF), and two of the product ions generated fom MS/MS (ii, iii). The acetamidofluorescein moiety is indicated in red. (b) The thiol (i) and thione (ii) tautomers of ergothioneine. Image from (Gallagher *et al.*, 2012).

6.3 Discussion

The work presented in this Chapter involved the characterisation of the metabolome of *A. fumigatus* following deletion of *gliK* from the *gli* cluster (Gardiner and Howlett, 2005; Gallagher *et al.*, 2012). Most significantly, deletion of *gliK* resulted in the abolition of gliotoxin production. Absence of gliotoxin in Δ*gliK* coincided with the significantly elevated levels of two metabolites ($(M + H)^+$ = 394 and 396), which contained no detectable free sulphydrals or disulphide bonds. These compounds may represent shunt metabolites or intermediates from the gliotoxin biosynthetic pathway. Intracellular free sulphydral levels were significantly higher in *A. fumigatus* Δ*gliK*, relative to wild-type. This was attributable to the significantly increased concentration of intracellular ergothioneine (EGT; $C_9H_{15}N_3O_2S$) in *A. fumigatus* Δ*gliK*, relative to the parent strain, and represents the first identification of ergothioneine in *A. fumigatus*. Alteration in the intracellular ergothioneine levels may provide insight into the role of GliK in *A. fumigatus*.

To date, the function of GliK in gliotoxin biosynthesis is unknown. Deletion of *gliP*, *gliZ*, *gliI*, *gliG* and *gliT*, corresponding to an NRPS, a transcription factor, a carbon-sulphur lyase, a glutathione-S-transferase and a gliotoxin oxidoreductase respectively, has resulted in the abrogation of gliotoxin production (Bok *et al.*, 2006; Cramer *et al.*, 2006; Kupfahl *et al.*, 2006; Scharf *et al.*, 2010, 2011, 2012a; Schrettl *et al.*, 2010; Davis *et al.*, 2011a; Forseth *et al.*, 2011). In order to accurately distinguish between gliotoxin production in *A. fumigatus* ATCC26933, wild-type and Δ*gliK*, conditions were identified for optimal gliotoxin production in ATCC26933. Culture in Czapek-Dox broth resulted in high gliotoxin yields at 48 h, with further increase in gliotoxin detected at 72 h. Gliotoxin, detected by RP-HPLC, was present in 48 h culture supernatants of ATCC26933 wild-type at a concentration of 5.61 µg/ml and this rose to

11.20 µg/ml at 72 h. Based on these observations, gliotoxin production in Δ*gliK* was analysed relative to wild-type following culture in Czapek-Dox for 72 h. RP-HPLC of organic extracts from culture supernatants revealed a dramatically altered metabolite profile in Δ*gliK*, compared to wild-type. This profile indicated the absence of gliotoxin in Δ*gliK* and also revealed the coincident increase in intensity of a number of other peaks. Reduction and alkylation with 5'-IAF was employed to increase the sensitivity of gliotoxin detection by RP-HPLC and MALDI-ToF (Davis *et al.*, 2011b). Overall, no 5'-IAF labelled gliotoxin (GT-$(AF)_2$) was detected by RP-HPLC or MALDI-ToF in Δ*gliK*, while this compound was identified from wild-type (Figures 6.5 and 6.6). Further confirmation of gliotoxin absence from culture supernatants of Δ*gliK*, was provided by LC-MS/MS. Abolition of gliotoxin production following deletion of *gliK*, implies a role for GliK in the gliotoxin biosynthesis pathway (Gallagher *et al.*, 2012).

In the absence of gliotoxin production in Δ*gliK*, two hydrophobic metabolites were detected by LC-MS/MS with $(M + H)^+$ = 394 and 396. While low levels of these compounds were detectable in culture supernatants from *A. fumigatus* wild-type, significantly higher levels were present in Δ*gliK* (p = 0.0024, fold difference = 24.1; p = 0.0003, fold difference = 9.6, respectively). These compounds appeared to be related, based on analogous fragmentation patterns, producing product ions with $(M + H)^+$ = 338 and 340, respectively. This 2 Da difference in compounds can sometimes be attributable to the presence of an oxidised (S-S) or reduced ($(-SH)_2$) disulphide bond. However, reduction and alkylation of these samples did not detect the presence of a disulphide bond or free sulphydrals. Interestingly, organic extracts from Δ*gliK* culture supernatants produce no growth inhibitory effects on *A. fumigatus* wild-type, while wild-type extracts significantly inhibited radial growth of Δ*gliK* (Gallagher *et al.*, 2012). The growth inhibition associated with wild-type extracts, correlates with the enhanced

sensitivity of Δ*gliK* to gliotoxin. The elevated levels of the *m/z* 394 and 396 extracellular metabolites in Δ*gliK* did not produce growth inhibitory effects in *A. fumigatus* wild-type, indicating these compounds are not auto-toxic. These extracellular compounds, possessing higher molecular mass(es) than gliotoxin, could represent off-pathway shunt metabolites of gliotoxin production. Deletion of *gliG* from *A. fumigatus* has been shown to abolish gliotoxin biosynthesis, with the coincident production of a shunt metabolite, 6-benzyl-6-hydroxy-1-methoxy-3-methylene-piperazine-2,5-dione (Davis *et al.*, 2011a). Interestingly, these external metabolites (*m/z* 394-396) were absent from the culture supernatants of Δ*gliG,* indicating that production of *m/z* 394-396 is GliG-dependant (Gallagher *et al.*, 2012). This is indicative of GliK functionality occurring after GliG in the gliotoxin biosynthetic pathway as evidenced by the accumulation of these GliG-dependent products in the *gliK* deletion strain (Figure 6.15). In order to ascertain whether these extracellular metabolites were shunt metabolites or on-pathway biosynthetic intermediates, preliminary feeding experiments were carried out. These consisted of the addition of Δ*gliK* metabolites (*m/z* 394-396) to wild-type lysates, however no conversion of the extracellular metabolites to gliotoxin was detected. Interestingly, these compounds (*m/z* 394-396) did not correlate to any of the masses attributable to *gliZ* dependent metabolites identified by Forseth *et al.* (2011).

Differential profiling of the intracellular metabolome of *A. fumigatus* ATCC26933, wild-type and Δ*gliK*¸ was carried out to characterise changes resulting from the deletion of *gliK*. Initially, examination of organic extracts from mycelial lysates presented no substantial changes to the internal metabolite profile, as determined by RP-HPLC (Figure 6.9). As this analysis was limited to non-polar intracellular compounds, further investigation was performed using aqueous mycelial extracts of wild-type and Δ*gliK*.

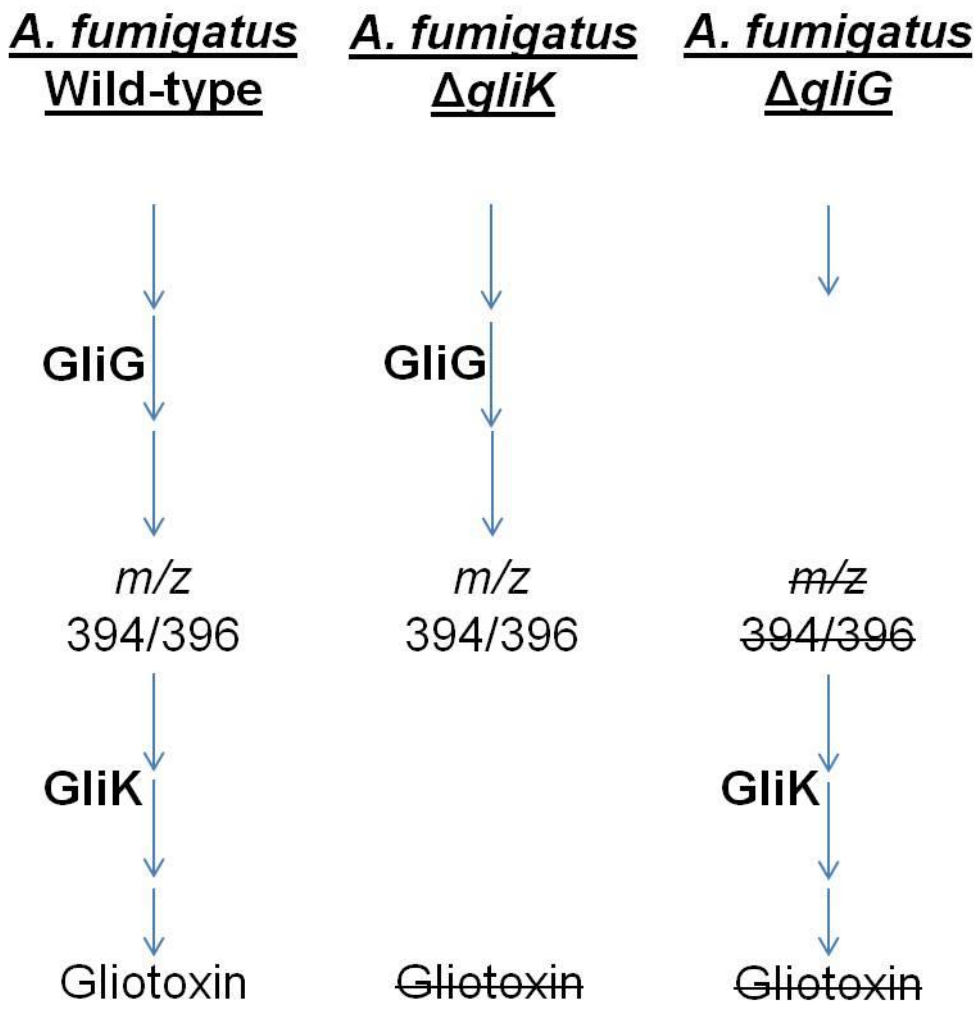

Figure 6.15: Schematic of the mechanistic positioning of GliG preceding GliK in the gliotoxin biosynthetic pathway. In *A. fumigatus* wild-type, the presence of both GliG and GliK results in the production of gliotoxin. Gliotoxin production is abolished in Δ*gliK*, with the concurrent accumulation of *m/z* 394/396. Deletion of *gliG* also results in the loss of gliotoxin production, in addition to the loss of *m/z* 394/396. This indicates that the production of *m/z* 394/396 is dependent on the presence of GliG. It is yet unclear whether *m/z* 394/396 are on-pathway intermediates of the gliotoxin biosynthetic process or shunt metabolites.

Aldrithiol-4® titrations, to detect total free thiols, revealed a significant increase in the concentration of free sulphydral groups in mycelial lysates of Δ*gliK* compared to wild-type (p = 0.0028) (Figure 6.10). A fold increase of 2.2 was observed in the total free sulphydral concentration, relative to protein, in *A. fumigatus* Δ*gliK*. The consequences of elevated levels of free sulphydrals in Δ*gliK* may alter the cellular redox potential (Murray *et al.*, 2011). The converse may also be true, with a perturbation in the redox status of Δ*gliK*, resulting in the increase in intracellular free thiols. This disturbance could affect processes such as transcriptional regulation (Murray *et al.*, 2011), and may account for the distinct proteomic profiles of *A. fumigatus* wild-type and Δ*gliK* following gliotoxin treatment (Chapter 5).

Comparative RP-HPLC analysis of aqueous mycelial extracts from *A. fumigatus* wild-type and Δ*gliK* did not reveal any detectable differences due to relatively large proportion of hydrophilic compounds present. These hydrophilic molecules were not retained by the C_{18} column and eluted prior to the gradient. In order to investigate the observed variance in sulphydral content between wild-type and Δ*gliK* mycelial extracts, alkylation with 5'-IAF was utilised (Davis *et al.*, 2011b). This strategy ultimately revealed significantly elevated levels of ergothioneine in *A. fumigatus* Δ*gliK* (p = 0.0343; n = 6; fold difference = 5.7). The identification of ergothioneine was supported by multiple factors, outlined in Table 6.1. Significantly, this represents the first identification of ergothioneine in *A. fumigatus*.

Table 6.1: Factors contributing to the identification of 5'-IAF labelled metabolite (AF11.7) as ergothioneine

	5'-IAF labelled metabolite	**Ergothioneine**
Molecular mass:	229 Da	229 Da
Number of free thiol groups	1	1 Exists as a thione-thiol tautomer
Physical properties	Hydrophilic	Hydrophilic
MS fragmentation pattern:	Neutral loss: 44 (COO^-)	Neutral loss: 43.9862 (COO^-)
	Neutral loss: 59 ($C(NH_3)_3$)	Neutral loss: 59.0733 ($C(NH_3)_3$)
	Neutral loss: 126 ($C_5N_2H_6S$)	Neutral loss: 126.03 ($C_5N_2H_6S$)

Fragmentation pattern of ergothioneine taken from Tepwong *et al.* (2012).

Ergothioneine is a sulphur-containing derivative of histidine, produced by fungi and mycobacteria (Figure 6.14) (Paul and Snyder, 2010; Seebeck, 2010; Bello *et al.*, 2012). Ergothioneine is a tautomer and predominantly exists in the thione at physiological pH rather than the thiol form (Figure 6.14) (Hand *et al.*, 2005; Paul and Snyder, 2010). The existence of ergothioneine as a thione imparts additional stability to the metabolite (Jayaram *et al.*, 2008). Consequently, ergothioneine has a higher redox potential than glutathione (GSH) and so is less susceptible to oxidation into the disulphide form (Carlsson *et al.*, 1974; Jayaram *et al.*, 2008). The anti-oxidant properties of ergothioneine were demonstrated to be more potent than uric acid, GSH or Trolox® (a water-soluble derivative of Vitamin E), with regard to scavanging capacity for peroxynitrates, hydroxyl and peroxyl radicals *in vitro* (Franzoni *et al.*, 2006). Additionally inhibition of ergothioneine biosynthesis correlates with increased sensitivity of conidia to peroxides, but not superoxide, in the ascomycete *Neurospora crassa* (Bello *et al.*, 2012).

The mechanisms of ergothioneine biosynthesis have been investigated in mycobacteria with the identification of a cluster of genes involved in production of the molecule (Figure 6.16a) (Seebeck, 2010). Mycobacterial ergothionine biosynthesis involves tri-methylation of the histidine via EgtD, with S-adenosylmethionine (SAM) as the methyl donor. Interestingly, enzymes involved in the biosynthesis of SAM and modification of histidine were differentially regulated in *A. fumigatus* Δ*gliK* in response to gliotoxin (Chapter 5) and this will be discussed in more detail in Chapter 7. Incorporation of the sulphydral group into ergothioneine is through conjugation with γ-glutamyl cysteine and is mediated by EgtB in an iron-dependent manner. Subsequent cleavage of the glutamate group by EgtC and loss of pyruvate result in the formation of ergothioneine (Seebeck, 2010). A fungal ergothioneine biosynthesis gene, *NcEgt-1*, was

also identified in the ascomycete *Neurospora crassa*, with domains analogous to both EgtB and EgtD (Bello *et al.*, 2012). The ortholog of this gene in *A. fumigatus* is DUF323 domain protein (AFUA_2G15650) with 47 % identity and 61 % sequence similarity to NcEgt-1 (http://blast.ncbi.nlm.nih.gov/Blast.cgi). This may represent a fusion protein, containing a domain with homology to SAM-dependent methyltransferases, in addition to a split domain with homology to formylglycine-generating sulfatase enzyme (Figure 6.16b) (Seebeck, 2010; Bello *et al.*, 2012).

Ergothioneine biosynthesis has been shown to be up-regulated significantly in the mushroom *Ganoderma neo-japonicum* following addition of methionine to the media (Lee *et al.*, 2009b). This may result from conversion of methionine to SAM, which is subsequently utilised for methylation of histidine in the initial step of ergothioneine biosynthesis (Figure 6.16). Interestingly, ergothioneine production was observed to increase upon disruption of mycothiol production in *Mycobacterium smegmatis* (Ta *et al.*, 2011). This may indicate cross-talk between secondary metabolite biosynthesis pathways and may account for the similiar observation in *A. fumigatus* upon abrogation of gliotoxin biosynthesis. These authors noted that elevated ergothioneine did not compensate for the loss of mycothiol with regard to cumene hydroperoxide (CuOOH) resistance, indicating the redox role of ergothioneine may be more limited than previously noted.

Ergothioneine, while not synthesised by mammals, is absorbed in the diet and concentrated in specific tissues in the body via the action of an ergothioneine transporter (ETT) (Gründemann *et al.*, 2005; Gründemann, 2012). Ergothioneine has been noted to accumulate in tissues associated with oxidative stress exposure including the kidneys, liver, erythrocytes, ocular lens and seminal fluid (Hand and Honek, 2005). Paul and Snyder (2010) demonstrated, using RNAi, that ETT-depleted HeLa cells were more

sensitive to oxidative stress and ergothioneine could prevent H_2O_2-induced apoptosis. These authors also verified that ergothioneine directly scavenges hydroxyl radicals and superoxide, protecting proteins from H_2O_2-induced oxidation and blocking DNA damage in HeLa cells. Protection against H_2O_2-induced DNA damage by ergothioneine was also noted in PC12 neuronal cells (Colognato *et al.*, 2006). Ergothioneine was found to inhibit the TNF-α or H_2O_2 -mediated transcription and release of IL-8 and the transactivation of NFκB in A549 alveolar epithelial cells (Rahman *et al.*, 2003). Ergothioneine was also observed to indirectly protect against GSH depletion, through inhibition of NFκB activation (Rahman *et al.*, 2003).

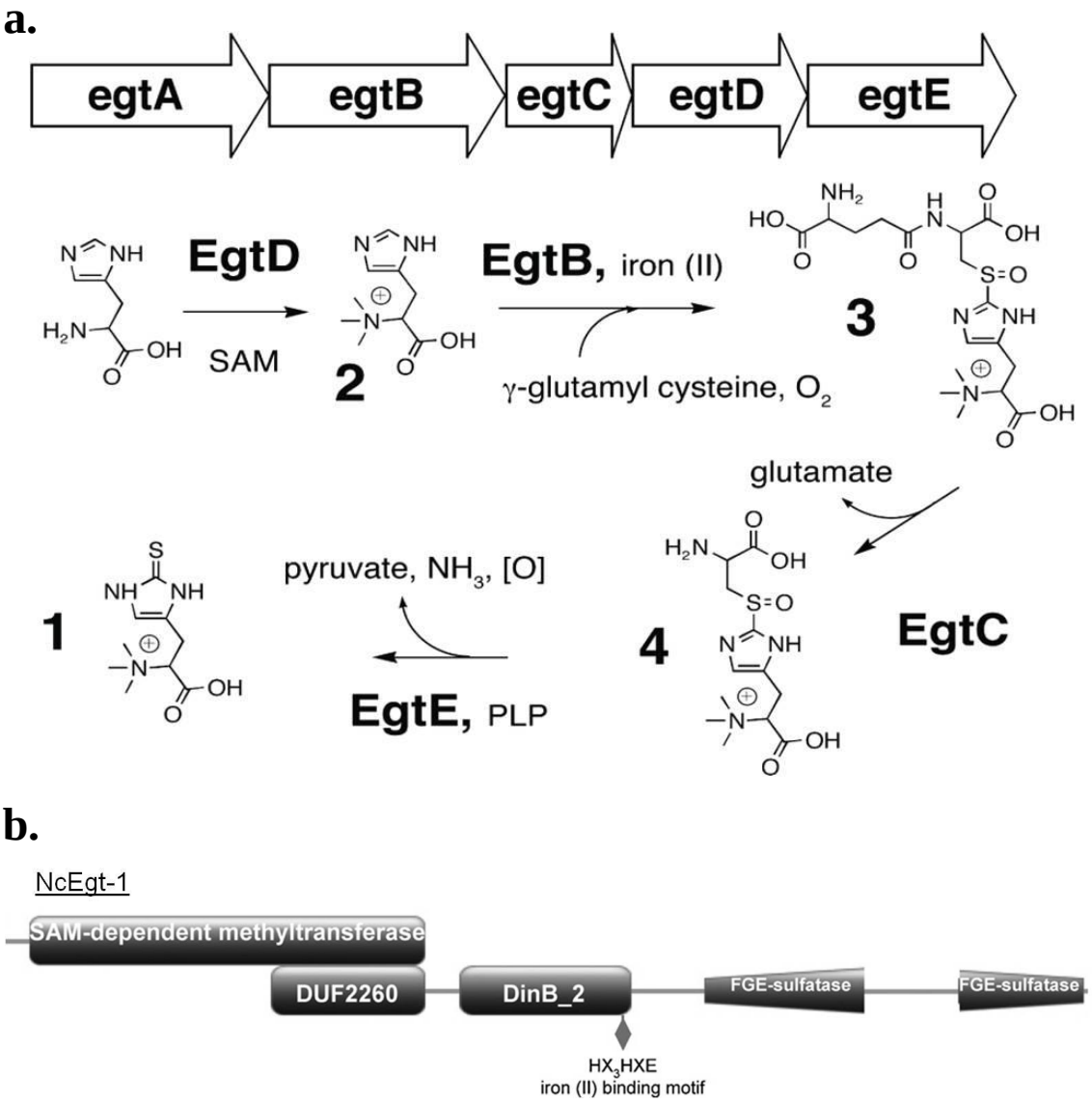

Figure 6.16: (a) Biosynthesis of ergothioneine in mycobacteria. The cluster codes for a γ-glutamyl cysteine synthetase (EgtA), an FGE-like protein (EgtB), a glutamine amidotransferase (EgtC), a SAM-dependent methyltransferase (EgtD) and a PLP-binding protein (EgtE). Adapted from Seebeck (2010). (b) Annotation of multiple conserved domains in *N. crassa* NcEgt-1, indicating a possible fusion protein that is essential for ergothioneine production in *N. crassa*. From Bello *et al.* (2012).

Interestingly sulphurisation of the methylated precursor of ergothionine involves γ-glutamyl cysteine, while GSH provides the sulphur moieties in gliotoxin biosynthesis (Figures 6.16 and 6.17b) (Seebeck, 2010; Davis *et al.*, 2011a; Scharf *et al.*, 2011). This observation may help explain the increased ergothionine levels in *A. fumigatus* following deletion of *gliK*. The GliK protein contains a conserved γ-glutamyl cyclotransferase (GGCT) -like domain, as determined by blastp analysis of the protein sequence (http://blast.ncbi.nlm.nih.gov/Blast.cgi). Proteins with GGCT activity catalyse the production of pyroglutamic acid (5-oxoproline) from γ-glutamyl containing dipeptides. This enzyme forms part of the γ-glutamyl cycle and is involved in the catabolism of glutathione (L-γ-glutamyl-L-cysteinyl-glycine; GSH) (Oakley *et al.*, 2010) (Figure 6.17a). This putative function of GliK is supported by the observation of elevated ergothioneine levels in Δ*gliK* compared to wild-type. Expression of a GGCT-like protein would result in cleavage of γ-glutamyl dipeptides, including γ-glutamyl cysteine. This enzymatic catabolism of γ-glutamyl cysteine could reduce the amount of substrate (i.e. γ-glutamyl cysteine) available for sulphurisation of the ergothionine precursor. Accordingly, absence of the GliK protein, with a GGCT-like domain, could result in increased availability of γ-glutamyl cysteine leading to enhanced ergothioneine biosynthesis. While the role of GliK in gliotoxin biosynthesis is yet unclear, GliK may catalyse the removal of one or both L-glutamate moieties from the di-glutathionylated product of GliG (Figure 6.17b). This function has putatively been assigned to the dipeptidase GliJ (Gardiner and Howlett, 2005), however no functional genomic or biochemical analysis has been performed to confirm this. Alternatively, there may be a link between the γ-glutamyl cycle and gliotoxin production. As glutathione is essential in the gliotoxin biosynthetic process (Davis *et al.*, 2011a; Scharf *et al.*, 2011) (Figure 6.17b), disruption of the γ-glutamyl cycle, by deletion of a putative GGCT, may contribute to the loss of gliotoxin production in Δ*gliK*.

a.

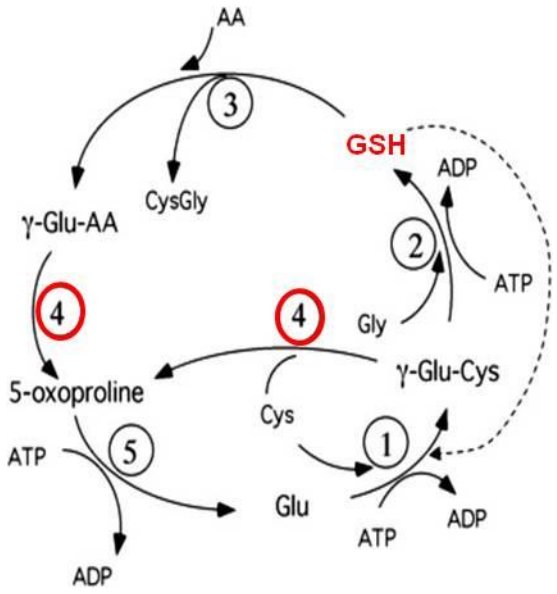

γ-glutamyl cycle

b.

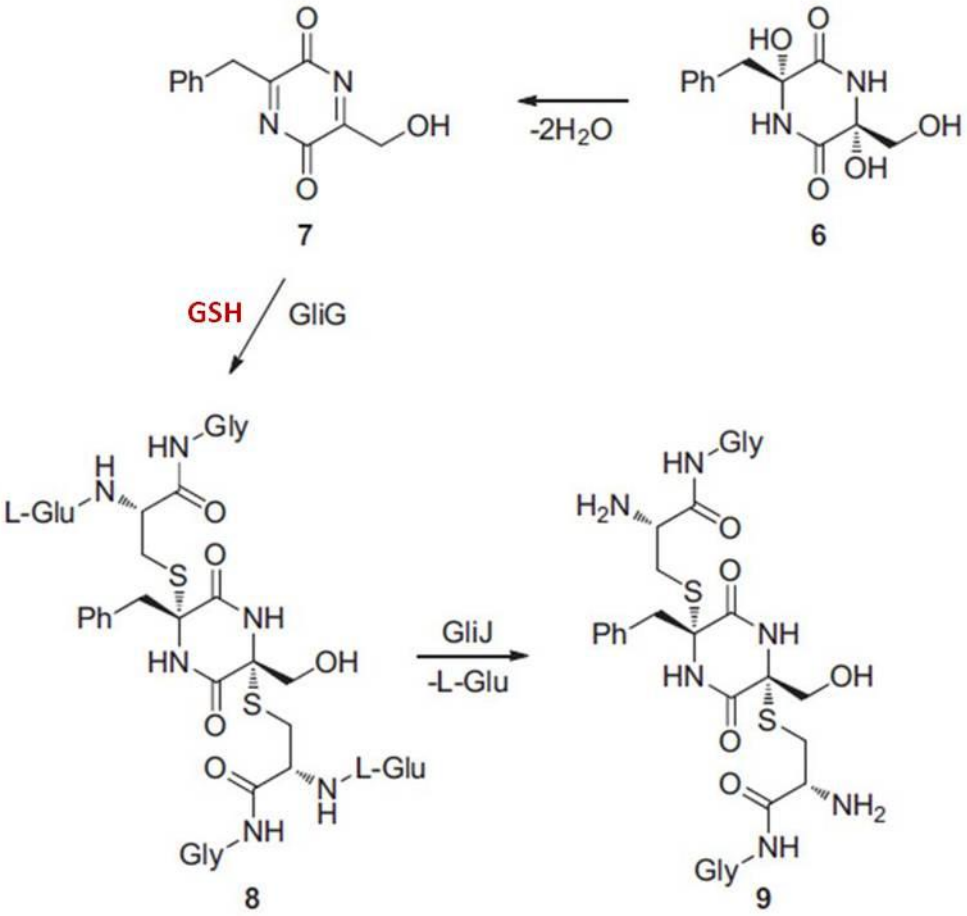

Gliotoxin biosynthesis:
GSH incorporation

Figure 6.17: (a) Outline of the γ-glutamyl cycle. 1, γ-glutamyl cysteine synthetase; 2, glutathione synthetase; 3, γ-glutamyl transpeptidase; 4, γ-glutamylcyclotransferase (GGCT) 5, 5-oxoprolinase. GGCT (red circle) is involved in the catabolism of glutathione (GSH). Adapted from Oakley *et al.* (2008) (b) Sub-section of the proposed gliotoxin biosynthetic pathway, demonstrating the incorporation of GSH molecules into the gliotoxin precursor molecule. This thiolation step is catalysed by the glutathione-S-transferase, GliG. Adapted from Davis *et al.* (2011a).

In summary, RP-HPLC, MALDI-ToF, LC-MS/MS and selective chemical modification were utilised to comparatively characterise the intracellular and extracellular metabolome of *A. fumigatus* ATCC26933 following deletion of *gliK*. Analysis of culture supernatants revealed the absence of gliotoxin production in *A. fumigatus* Δ*gliK*, demonstrating for the first time that GliK is essential for gliotoxin biosynthesis in *A. fumigatus*. The absence of gliotoxin in *A. fumigatus* Δ*gliK* coincided with significantly increased levels of extracellular metabolites, with *m/z* 394-396, relative to the parent strain. These extracellular metabolites (*m/z* 394-396), may represent on-pathway intermediates or shunt metabolites of gliotoxin biosynthesis, accumulating in the absence of GliK. Future work required to characterise these metabolites will be described in Chapter 7. Investigation of the intracellular metabolome revealed significantly elevated levels of free thiols in *A. fumigatus* Δ*gliK* compared to wild-type. This phenomenon was attributable to the significant increase in levels of a monothiol-containing metabolite in *A. fumigatus* Δ*gliK*. This metabolite was subsequently identified as ergothioneine and the work described in this Chapter represents the first detection of this metabolite in *A. fumigatus*. The presence of elevated levels of ergothioneine in Δ*gliK*, may support the putative function of GliK as a γ-glutamyl cyclotransferase. Overall, the results presented in this Chapter represent a progression in the characterisation of an unknown function protein, GliK, highlighting it as an essential protein in the gliotoxin biosynthetic process, after the GliG step. Metabolomic profiling, coupled with comparative proteomics analysis carried out in Chapter 5, provides further insight into the cellular mechanisms affected by deletion of *gliK* and these will be discussed in more detail in Chapter 7.

CHAPTER 7

Final Discussion

7 Chapter 7: Discussion

7.1 Overview

This discussion will (i) consider the implications of the expansion of the *A. fumigatus* proteome and immunoproteome achieved by the present effort and (ii) contextualise the global effects of gliotoxin-associated biochemistry in *A. fumigatus*.

The epoch of genome sequencing has facilitated substantial progress in the characterisation of the transcriptome and proteome of *A. fumigatus* and related species (Carberry *et al.*, 2006; Jørgensen *et al.*, 2009; Vödisch *et al.*, 2009; Albrecht *et al.*, 2011; Pusztahelyi *et al.*, 2011). While technologies utilised for transcriptomics enable global analysis on a genome-wide scale, proteomics of *A. fumigatus* is still in its formative years (Kniemeyer, 2011). Furthermore, despite the advanced capabilities of *in silico* genome annotation, the function of many genes, and their resultant products, remains undetermined (Teutschbein *et al.*, 2010). Targeted gene deletion and comparative profiling have been employed to determine gene function and to identify the systems influenced by the presence of the respective protein (Hortschansky *et al.*, 2007; Lessing *et al.*, 2007; Doyle, 2011b; O'Hanlon *et al.*, 2011; Hagag *et al.*, 2012). The status of *A. fumigatus* as the second leading cause of invasive fungal infection necessitates comprehensive proteomic profiling of this organism, which may facilitate the identification of mechanisms contributing to pathogenicity (Thornton, 2008; Kniemeyer, 2011). To this end, the focus of the work presented in this thesis has been the progression of proteomic and immunoproteomic analysis of *A. fumigatus*, in addition to the use of comparative proteomic and metabolic profiling to identify the biological networks affected by gliotoxin in *A. fumigatus*. Resultant data has revealed insights into the phenomenon of gliotoxin-mediated recovery from H_2O_2-induced growth inhibition, and use of a gliotoxin sensitive mutant of *A. fumigatus*, Δ*gliK*, has

identified putative mechanisms by which gliotoxin toxicity is elicited. Furthermore, the influence of a protein of unknown function, GliK, on the metabolite profile of *A. fumigatus* was demonstrated for the first time (Gallagher *et al.*, 2012). Coupled with comparative proteomic profiling, this presents a multi-dimensional view of the systems influenced following deletion of *gliK* from *A. fumigatus*.

7.2 Global Proteomic and Immunoproteomic Characterisation of *A. fumigatus*

Implementation of an MS-based proteomics approach lead to the identification of 427 non-redundant proteins from the mycelia and supernatant of *A. fumigatus*. Through use of gel-free preparations, proteins identified spanned a wide molecular mass and p*I* range, and included proteins containing multiple transmembrane regions, as well as hydrophobic proteins. Proteins identified extended from 9 to 434 kDa, with multiple proteins (n = 10) possessing a molecular mass ≥ 142 kDa. Computational prediction of the number of transmembrane (TM) regions revealed the identification of proteins with up to 14 TM helices in addition to detection of hydrophobic proteins. These capabilities superseded those attainable using the traditional 2D-PAGE approach of proteome mapping (Carberry *et al.*, 2006; Vödisch *et al.*, 2009; Teutschbein *et al.*, 2010).

Large-scale gel-free proteomics identified a number of proteins (n = 20) encoded by genomic clusters, with predicted or proven roles in secondary metabolite biosynthesis. Proteins (n = 14) which form part of a 'supercluster' on Chromosome 8 were identified, including proteins involved in the production of pseurotin A (Maiya *et al.*, 2007) and fumitremorgin B (Grundmann and Li, 2005; Maiya *et al.*, 2006) metabolism. An additional nine proteins were detected from this 'supercluster', which are predicted to be involved in the biosynthesis of an unidentified metabolite. Detection of protein expression of multiple members of this predicted secondary metabolite cluster strongly indicates that this cluster is active under the growth conditions

employed. This information may prove essential in prospective studies for identification of this uncharacterised metabolite. Identification of the gliotoxin oxidoreductase GliT, a member of the gliotoxin biosynthetic cluster, was achieved using MS-based proteomics (Gardiner and Howlett, 2005; Scharf *et al.*, 2010; Schrettl *et al.*, 2010). Gliotoxin production was detected in these conditions following extracellular metabolite analysis, thus confirming that detection of this protein, GliT, correlated with cluster activity and metabolite biosynthesis. A putative Zn-dependent hydrolase/oxidoreductase family protein was also detected from the second ETP cluster in *A. fumigatus*. This cluster is positioned on Chromosome 3 (AFUA_3G12870 - AFUA_3G13010) and contains a partial number of ETP biosynthesis genes relative to the gliotoxin cluster (Patron *et al.*, 2007). Cross-talk may be essential between these two ETP clusters in order to complete biosynthesis of distinct products, and co-expression of proteins from both clusters may support this theory. All cluster proteins identified in this condition are either partially or fully regulated by the transcription factor LaeA, a global regulator of secondary metabolism (Bok and Keller, 2004; Bok *et al.*, 2005; Perrin *et al.*, 2007). Thus, LaeA activity was indirectly determined through a global proteomics investigation.

Methods to reduce sample complexity will continue to expand proteome characterisation (Millioni *et al.*, 2011; Zhang *et al.*, 2011). Coupling of MS-based shotgun proteomics with pre-fractionation based on protein size facilitated the identification of an additional 17 proteins that were not detected using the direct method. Ion exchange chromatography (SCX) is regularly utilised in MS-based proteomics, for pre-fractionation of peptides prior to LC-MS/MS, in a bid to expand the capacity for protein identification (Washburn *et al.*, 2001; Ouyang *et al.*, 2010). Pre-incubation with gold nanoparticles (AuNPs) represents an alternative, efficient manner by which to fractionate complex lysates (Cedervall *et al.*, 2007; Keidel *et al.*, 2010). *A.*

fumigatus proteins adhering to the surface of 30 nm AuNPs were predominantly categorised as proteins with binding function or co-factor requirement according to FunCat annotation (Ruepp *et al.*, 2004). Compilation of proteomic data from *A. fumigatus* studies revealed that this functional category has the highest representation from all proteins identified (Kniemeyer *et al.*, 2011). Consequently, the ability to partition, and remove, these proteins could enrich low abundance proteins.

Characterisation of the secretome of *A. fumigatus* was undertaken and yielded successful identification of 42 unique proteins. This study on the extracellular fraction of *A. fumigatus* expands the number of currently reported secreted proteins, with cross-validation of the *in silico* annotation methods, SignalP and SecretomeP. A number of unknown function proteins (n = 7), were identified from culture supernatants and knowledge of their secretion could contribute to the functional annotation of these proteins in future studies. Secreted proteins have long been investigated for their potential use as biomarkers of infection or as putative virulence factors (Wartenberg *et al.*, 2011). Thus, extensive characterisation of the secretome of *A. fumigatus* may contribute to understanding mechanisms of pathogenicity, or alternatively, identify enzymes with potential biotechnological applications (Ferreira de Oliveira and De Graaff, 2011; Kniemeyer, 2011).

The secretome of *A. fumigatus* has been extensively targeted for the identification of antigenic and allergenic proteins (Gautam *et al.*, 2007; Singh *et al.*, 2010a; Shi *et al.*, 2012a, 2012b). Intracellular proteins also represent potential targets of the immune system, and recent studies have identified immunogenic proteins from conidia or early germlings of *A. fumigatus* (Asif *et al.*, 2010; Singh *et al.*, 2010b). Classically, mycelial lysates were used to identify immunoreactive proteins from *A. fumigatus* (Latge, 1999), however, no analogous studies have been completed since the

sequencing of the genome. *A. fumigatus*-related disease is not required for the development of antibodies, and anti-*A. fumigatus* antibodies are present in most healthy individuals, albeit at low levels, as a consequence of routine environmental exposure (Latge, 1999). Indeed, utilising sera pools from healthy individuals, immunoreactivity was observed against *A. fumigatus* mycelial lysates in 93 % of the human sera tested. The mycelial targets of anti-*A. fumigatus* IgG (n = 25) were identified following 2D-PAGE separation and immunoblotting with human sera pools. Antigens identified included previously characterised immunogenic *A. fumigatus* proteins (n = 12), including the molecular chaperones Hsp70, Hsp88 and Hsp90 (Singh *et al.*, 2010b), providing validation of the detection and identification strategies employed. Furthermore, expansion of the immunome of *A. fumigatus* was achieved, by identification of thirteen additional immunoreactive proteins, with previously unidentified antigenicity. These included two carboxypeptidases (AFUA_5G07330 and AFUA_8G04120), 1,3-β-glucanosyltransferase Gel4 (AFUA_2G05340) and a putative aminopeptidase (AFUA_2G00220). As these aforementioned proteins have not been detected in either secretome or conidial/early germling proteome maps to date (Gautam *et al.*, 2007; Neustadt *et al.*, 2009; Singh *et al.*, 2010a, 2010b; Teutschbein *et al.*, 2010; Cagas *et al.*, 2011b; Wartenberg *et al.*, 2011; Suh *et al.*, 2012), their immunodetection may have been hampered in previous studies by their localisation exclusively in mycelia. Thus, targeting mycelial lysates for identification of *A. fumigatus* antigens represents a significant development in immunome characterisation.

Identification of antigenic proteins not only serves to present new vaccine targets or diagnostic markers of infection, but may also provide insight into the mechanisms of pathogenicity and the *in vivo* conditions experienced by *A. fumigatus* in the host (Tjalsma *et al.*, 2008; Doyle, 2011b; Thornton *et al.*, 2012). The majority of the

proteins identified as antigenic in this study have previously demonstrated increased expression in response to various forms of stress (n = 19/25). These stresses, including heat shock, hypoxia, oxidative stress and exposure to host cells, are likely encountered by *A. fumigatus* in the human lung (Figure 7.1) (Lessing *et al.*, 2007; Sugui *et al.*, 2008; Albrecht *et al.*, 2010; Morton *et al.*, 2011; Oosthuizen *et al.*, 2011; Vödisch *et al.*, 2011). Heat-shock was observed to result in up-regulation of seven of the antigens herein identified, with eleven hypoxia-induced proteins identified as immunogenic (Figure 7.1). Through H_2O_2-induced oxidative stress, increased expression of multiple antigenic and allergic proteins is noted, including Hsp88, Hsp90 and cobalamin-independent methionine synthase MetH/D. Oxidative stress reflects the exposure of inhaled conidia and mycelia to ROS generated by macrophages and neutrophils in the lung (Philippe *et al.*, 2003; Brown *et al.*, 2009a). Furthermore, incubation of *A. fumigatus* with neutrophils, airway epithelial cells, dendritic cells and host-associated factors similarly induces proteins identified here as antigenic (Figure 7.1) (Shen *et al.*, 2004; Sugui *et al.*, 2008; Morton *et al.*, 2011; Oosthuizen *et al.*, 2011). We postulate that increased expression of these proteins, following exposure to the host environment, could indicate a role for these proteins in the pathobiology of *A. fumigatus*. In addition, enhanced expression of these proteins could increase the opportunity for presentation to the immune system and consequently account for development of immunoreactivity. Based on these observations of stress-induced antigen expression, it is clear that *in vitro* conditions that mimic host environments, possibly through combination of stresses, could enable further characterisation of immunome of *A. fumigatus*. Moreover the observation of ubiquitous, low-level immunoreactivity against *A. fumigatus* antigens presents the opportunity for purification of anti-*Aspergillus* antibodies from healthy individuals which may contribute to diagnostic tool development.

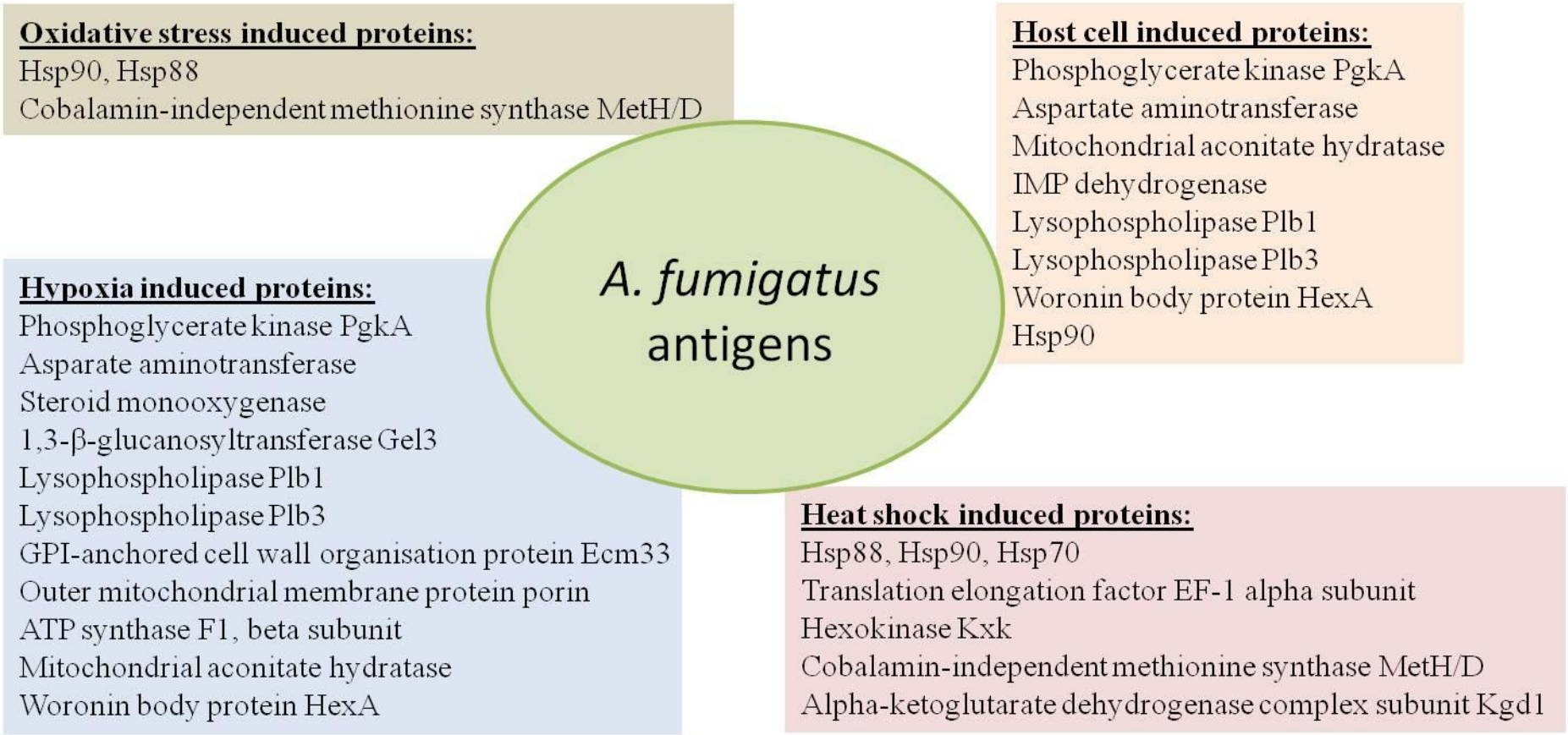

Figure 7.1: Summary of proteins, identified in this thesis as antigenic, that have previously been shown to undergo increased expression in response to various forms of host-associated stress.

7.3 Gliotoxin-associated mechanisms in *A. fumigatus*

Combinatorial stress induction in *A. fumigatus* was investigated using H_2O_2 and gliotoxin, in a bid to uncover any synergistic or additive phenotypic response. In an unexpected phenomenon, H_2O_2-induced growth inhibition of *A. fumigatus* ATCC26933 was actually relieved by gliotoxin, in a dose-dependent manner (0 - 10 µg/ml). This antagonistic effect was similarly noted using the gliotoxin and H_2O_2-sensitive mutant *A. fumigatus* Δ*gliK*. Choi *et al.* (2007) identified gliotoxin as a small molecule targeting the mammalian thioredoxin redox system, with the concurrent oxidation of NADPH and reduction of H_2O_2. These authors postulated that gliotoxin replaced 2-cys-peroxiredoxin (Prx) as an electron acceptor, consequently eliciting an anti-oxidant function through elimination of H_2O_2. Gliotoxin was demonstrated to execute this function *in vitro* and additionally was observed to suppress H_2O_2-induced angiogenesis in a dose-dependent manner (Choi *et al.*, 2007). We posit that an analogous scenario may occur in *A. fumigatus*, whereby gliotoxin redox cycling may serve to reduce H_2O_2 (Figure 7.2). This redox cycling may be mediated by the thioredoxin redox system, as observed in the mammalian model, or alternatively may be facilitated by the gliotoxin oxidoreductase GliT (Figure 7.2). GliT was observed to be significantly up-regulated in the co-addition scenario relative to the presence of H_2O_2 alone (5.0 fold, $p < 0.05$), with exogenous gliotoxin exclusively responsible for the induction of expression. Schrettl *et al.* (2010) demonstrated that GliT exhibits NADPH-dependent gliotoxin reductase activity and proposed that gliotoxin may form part of an anti-oxidant defence system within *A. fumigatus*. Interestingly, intracellular GliT was not observed to undergo significant induction in *A. fumigatus* Δ*gliK* following exposure to gliotoxin, and this may account partly for the significantly enhanced sensitivity of this mutant to gliotoxin.

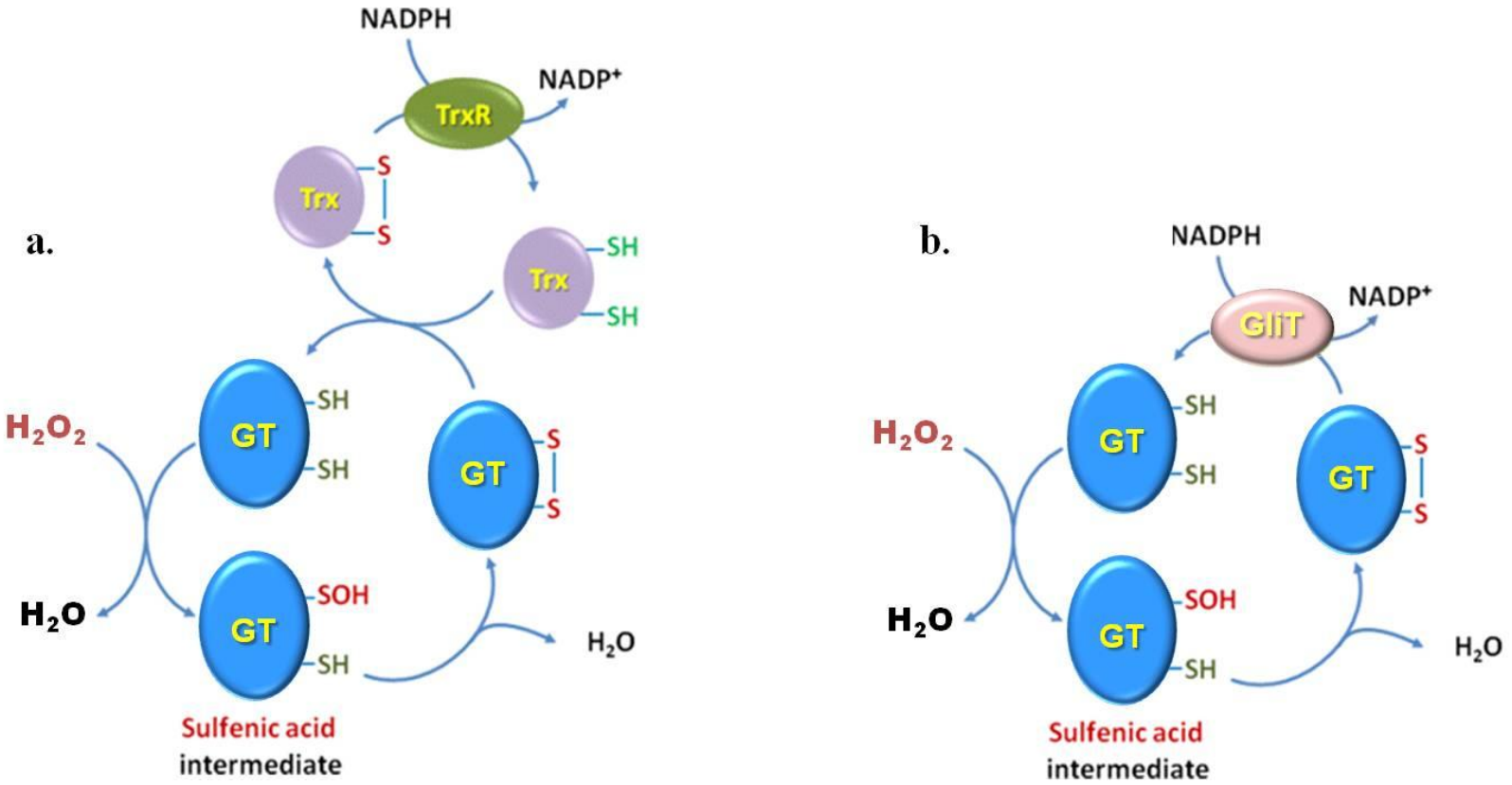

Figure 7.2: Model of gliotoxin (GT) replacing 2-cys peroxiredoxin in (a) the thioredoxin redox system, with the reduction of H_2O_2 and the oxidation of NADPH or (b) putative model of NADPH-dependent reduction of gliotoxin by the gliotoxin oxidoreductase GliT. Adapted from Zhu *et al.* (2012). TrxR, thioredoxin reductase; Trx, thioredoxin.

For the proposed model of GliT-gliotoxin mediated reduction of H_2O_2 to hold true, basal intracellular levels or extracellular GliT would have to be sufficient to perform gliotoxin, and consequently H_2O_2, reduction. *In vitro* analysis to confirm this model is required. Many of the proteins undergoing significant differential expression in the response to co-addition of gliotoxin and H_2O_2, relative to H_2O_2 alone, appear to reflect the relief of both stress and growth inhibition associated with the former condition. These proteins include Hsp90 and the oxidative stress protein Svf1, which decreased in expression, coincident with gliotoxin-mediated relief of H_2O_2-induced growth inhibition. This indicates the reduction in oxidative stress caused by H_2O_2 upon co-application of gliotoxin. The class V chitinase, associated with autolysis in response to stress (Yamazaki *et al.*, 2007), was observed to decrease in expression in the co-addition condition. Higher relative levels of this protein, expressed in the presence of H_2O_2, may account for the growth inhibition observed, due to elevation of H_2O_2-induced cell lysis. Decrease of expression of this chitinase, consequent to gliotoxin co-addition, may lead to reduction in autolysis, possibly due to relief of the triggering stress. Similarly the Ran-specific GTPase activating protein 1, involved in cell cycle regulation (Baumer *et al.*, 2000), is differentially regulated in the co-addition scenario relative to H_2O_2 alone. Decreased levels of this protein, as observed in the presence of H_2O_2 alone, are associated with cell cycle arrest. An increase in the Ran-specific GTPase activating protein 1 upon co-addition of gliotoxin and H_2O_2, correlates with recovery of growth inhibition and again may be reflective of the relief of H_2O_2-induced stress. Increased expression of proteins from the electron transport chain (ETC), namely NADH quinone oxidoreductase and NADH ubiquinone dehydrogenase, in the co-addition condition may also be attributable to the relief of growth inhibition, and indicate an associated increase in cellular energy requirement to support growth (Fernie *et al.*, 2004). Altogether, these proteins appear to reflect the growth recovery associated

with co-addition of gliotoxin and H_2O_2, and may represent the 'effect' rather than the 'cause' of this relief.

As discussed previously, GliT may contribute to the gliotoxin-mediated reversal of H_2O_2-induced growth inhibition, representing a possible candidate for the 'cause' of this relief. The proliferating cell nuclear antigen PCNA may represent another possible contributor to this growth recovery. The role of PCNA in DNA replication and repair has been demonstrated, and this protein is involved in the response to H_2O_2-induced DNA damage (Burkovics *et al.*, 2009). While PCNA increases in expression in response to H_2O_2 alone, further induction is observed upon co-addition of gliotoxin (2.3 fold, $p < 0.05$). This may increase the capacity for repair of DNA damage caused by H_2O_2 and contribute to the growth recovery associated with the co-addition condition. Up-regulation of purine salvage was also noted in the combinatorial condition, and this may further support the increase in DNA repair in this condition with the elevation in nucleotide recycling. Down-regulation of *de novo* purine biosynthesis is elicited by gliotoxin in the co-addition scenario, as indicated by decreased expression of glutamine amidotransferase:cyclase and the bifunctional purine biosynthetic protein Ade1. Up-regulation of the purine salvage pathway is demonstrated through increased expression of adenine and xanthine-guanine phosphoribosyltransferases, Apt1 and Xpt1, respectively. Combined, these proteomic alterations indicate that gliotoxin-mediated relief of H_2O_2-induced growth inhibition may be facilitated by redox cycling of gliotoxin, possibly involving GliT, and the elevated capacity for DNA damage repair. Further targeted investigation of these mechanisms, involving *in vitro* biochemical analysis and measurement of relative DNA damage, would confirm the hypotheses revealed by comparative proteomics.

The mechanisms of gliotoxin-mediated toxicity were probed using a gliotoxin-sensitive mutant of *A. fumigatus*, Δ*gliK*. Deletion of *gliK* resulted in the abrogation of gliotoxin biosynthesis and led to a significant increase in sensitivity to exogenous gliotoxin, relative to the parent strain (Gallagher *et al.*, 2012). Biological systems affected by gliotoxin application to *A. fumigatus* Δ*gliK* included protein synthesis, the methyl cycle, regulatory systems (e.g. apoptosis and cell-cycle regulation) and mechanisms associated with endoplasmic reticulum (ER) stress.

Dysregulation of proteins/enzymes involved in translation was observed in *A. fumigatus* Δ*gliK* upon exposure to gliotoxin, which may have contributed to the observed growth inhibition associated with this treatment (Figure 7.3). A number of proteins involved in translation initiation and elongation were observed to increase in expression, including the translation initiation factor 3 subunit EifCb (2.7 fold), and the translation elongation factors eEF3 and G1 (5.6 and 2.5 fold, respectively). EifCb is essential for translation and initiation is deemed as the rate-determining step in this process (Osherov and May, 2000; Arava *et al.*, 2003). While this observation appears to indicate that translation is up-regulated in gliotoxin-exposed *A. fumigatus* Δ*gliK*, differential regulation of other translation-associated factors is concurrently observed. The translation elongation factor EF2 undergoes a decrease in expression (1.6 fold) in addition to down-regulation of proteins involved in post-translational modification (PTM) and regulation of EF2, namely diphthine synthase and protein phosphatase 2a (PP2A), respectively. Diphthine synthase is involved in the incorporation of an EF2 exclusive PTM, consisting of a modified histidine residue (Liu *et al.*, 2004), while PP2A dephosphorylates EF2, thus re-activating the elongation factor (Kaul *et al.*, 2011). Decreased levels of EF2, coupled with reduction of EF2 activity may result in disruption of translation in *A. fumigatus* Δ*gliK*, following gliotoxin addition.

Conversely, EF2 expression is induced in *A. fumigatus* ATCC26933 in response to gliotoxin (Carberry *et al.*, 2012), and this differential expression may account for the significant growth inhibition associated with gliotoxin-exposed *A. fumigatus* Δ*gliK*, relative to the parent strain.

Gliotoxin was observed to elicit an effect on a number of components of the ER in *A. fumigatus* Δ*gliK*, and this may be suggestive of ER-associated stress as a mechanism for gliotoxin toxicity (Figure 7.3). Decreased expression of protein disulphide isomerise Pdi1, with an integral role in the unfolded protein response (UPR) to ER-stress (Xiao *et al.*, 2004), was observed in *A. fumigatus* Δ*gliK* following gliotoxin exposure. Pdi1 acts as a chaperone and is involved in the oxidation, reduction and reorganisation of incorrectly paired protein disulphides. Gliotoxin can form mixed disulphides with proteins, and through redox cycling can mediate mispairing of protein disulphides (Bertling *et al.*, 2010). Therefore, lower expression of Pdi1 in *A. fumigatus* Δ*gliK* in the presence of gliotoxin could result in an accumulation of misfolded proteins, and subsequently elicit toxic effects (Richie *et al.*, 2009). In addition to a role in translation, PP2A also executes a regulatory function in the ER, through de-phosphorylation of the anti-apoptotic factor BCL-2, thus preserving BCL-2 from degradation (Lin *et al.*, 2006). Reduction in PP2A levels in gliotoxin-treated *A. fumigatus* Δ*gliK* could correspond with an increase in apoptosis, mediated by BCL-2 degradation. This observation is echoed in the mammalian model, whereby the Bcl-2 family member, Bak, is central to gliotoxin-induced apoptosis (Pardo *et al.*, 2006). Regulation of the UPR is further affected in *A. fumigatus* Δ*gliK* by decreased expression of the Ran GTPase activating proteins RNA1 in response to gliotoxin. RNA1 is indirectly required for induction of UPR-related gene expression, by facilitating Ire1p transport into the nucleus (Back *et al.*, 2005; Goffin *et al.*, 2006). Further observation of

differential regulation of ER-associated proteins (CRAL/TRIO protein, aspartic endopeptidase Pep2 and vesicular fusion protein Sec17) supports the hypothesis that gliotoxin-mediated toxicity in sensitive organisms involves ER-stress and possibly the coincident induction of apoptosis. Moreover, attenuation of protein synthesis is induced by the UPR (Lai *et al.*, 2007), and this may account for the dysregulation of translation observed in gliotoxin-exposed *A. fumigatus* Δ*gliK*.

Expression of enzymes involved in the methyl cycle of *A. fumigatus* Δ*gliK* was also observed to undergo significant induction in the presence of gliotoxin (Figure 7.3). Increased expression of cobalamin-independent methionine synthase in this condition is indicative of enhanced methionine production, which may lead to elevated levels of S-adenosylmethionine (SAM) (Barak *et al.*, 2003). SAM, formed by the adenosylation of methionine, is a major source of methyl groups for a range of biomolecules including proteins, nucleic acids and secondary metabolites (Kanai *et al.*, 2012). SAM-mediated methylation of the sulphydral groups of gliotoxin may represent a potential defence mechanism against the toxin, as di-methylated gliotoxin does not undergo redox cycling, and thus exhibits abated activity (Nishida *et al.*, 2005). This may account for the multiple S-methylated GliZ-dependent molecules, potentially generated via the gliotoxin biosynthetic process (Forseth *et al.*, 2011).

Observation of significantly elevated levels of ergothioneine in *A. fumigatus* Δ*gliK* may also result from increased availability of methionine and SAM. Biosynthesis of ergothioneine is intrinsically linked to the methionine biosynthetic cycle, with SAM responsible for providing the three methyl groups on the α-amino group of the precursor, histidine (Seebeck, 2010). This relationship is re-inforced by the observation that supplementation of growth media with methionine, results in the increased production of ergothioneine in several mushroom species (Lee *et al.*, 2009b, 2009c).

Thus, increased synthesis of methionine, and consequently SAM, may account for the increased levels of ergothioneine in *A. fumigatus* Δ*gliK*. Differential regulation of methylenetetrahydrofolate reductase (MTHFR) in gliotoxin exposed-*A. fumigatus* wild-type and Δ*gliK* could be a consequence of the sensitive phenotype noted in the latter. Specifically, while MTHFR expression decreases in gliotoxin-exposed *A. fumigatus* wild-type, an increase in expression in noted upon exposure of *A. fumigatus* Δ*gliK* to gliotoxin. Indeed, MTHFR transcription and translation is induced by ER-stress (Leclerc and Rozen, 2008), further underlining the prediction of ER-associated stress in the gliotoxin sensitive mutant *A. fumigatus* Δ*gliK*. This presents a mechanism by which gliotoxin mediates toxicity in sensitive organisms and further investigation to confirm the induction of ER-stress by gliotoxin could confirm whether this effect is specific to *A. fumigatus* Δ*gliK* or a universal mode of action.

Deletion of *gliK* resulted in significantly altered phenotypic and proteomic responses to gliotoxin, and consequently metabolome analysis of Δ*gliK* revealed substantial modification of the intra and extracellular metabolome of *A. fumigatus*. The previously uncharacterised protein, GliK, was demonstrated to be essential for gliotoxin biosynthesis in *A. fumigatus*. Loss of gliotoxin production in Δ*gliK* correlated with a significant increase in levels of extracellular hydrophobic metabolites (*m/z* 394-396), representing putative intermediates or shunt metabolites of the gliotoxin biosynthetic pathway. Absence of these metabolites in *A. fumigatus* Δ*gliG* indicates the production of these molecules is GliG-dependent, and accumulation of *m/z* 394-396 in Δ*gliK* supports the hypothesis that the biological activity of GliG precedes that of GliK in gliotoxin biosynthesis.

a.

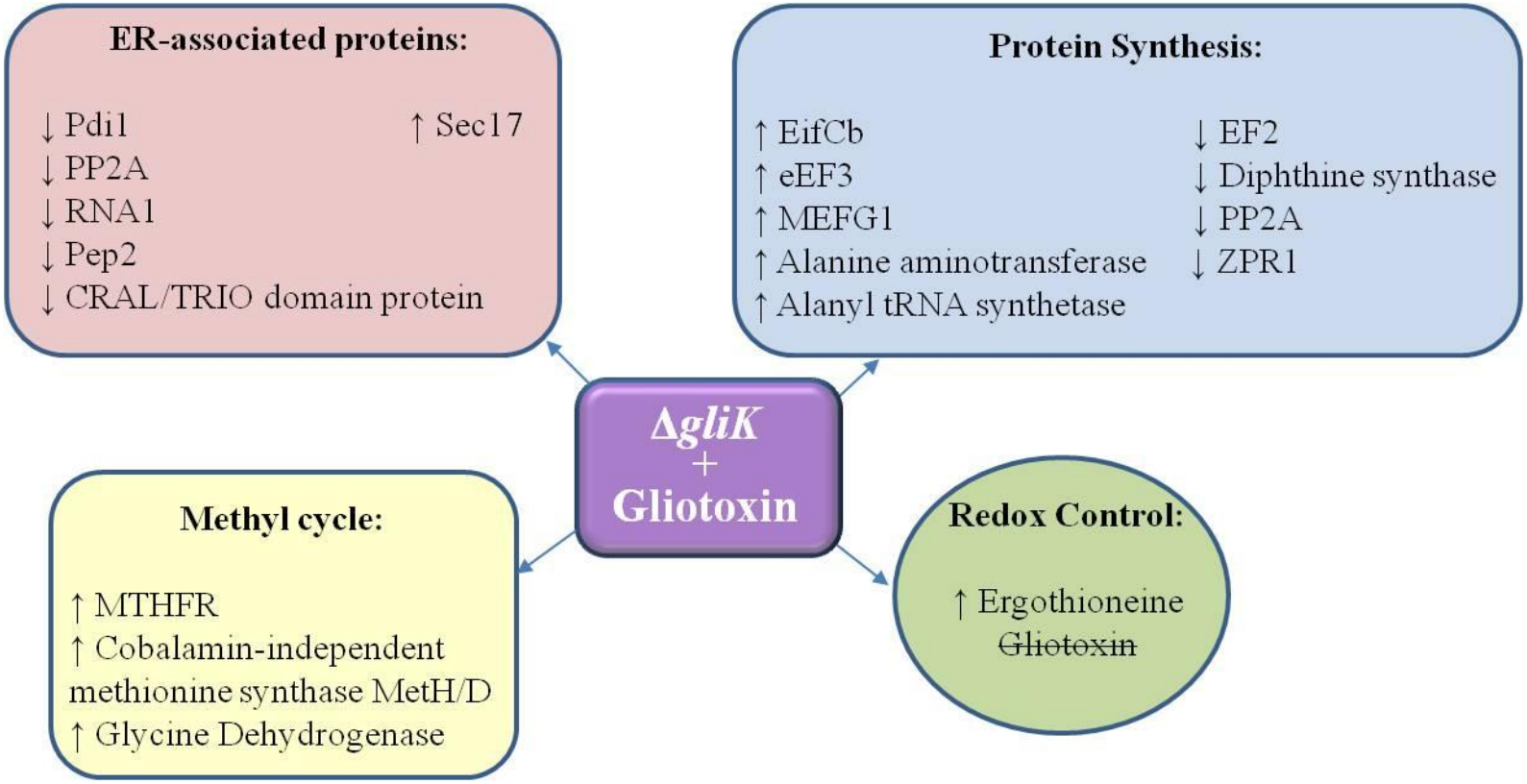
ER-associated proteins:
↓ Pdi1
↓ PP2A
↓ RNA1
↓ Pep2
↓ CRAL/TRIO domain protein
↑ Sec17
Protein Synthesis:
↑ EifCb
↑ eEF3
↑ MEFG1
↑ Alanine aminotransferase
↑ Alanyl tRNA synthetase
↓ EF2
↓ Diphthine synthase
↓ PP2A
↓ ZPR1
ΔgliK + Gliotoxin
Methyl cycle:
↑ MTHFR
↑ Cobalamin-independent methionine synthase MetH/D
↑ Glycine Dehydrogenase
Redox Control:
↑ Ergothioneine
~~Gliotoxin~~

b.

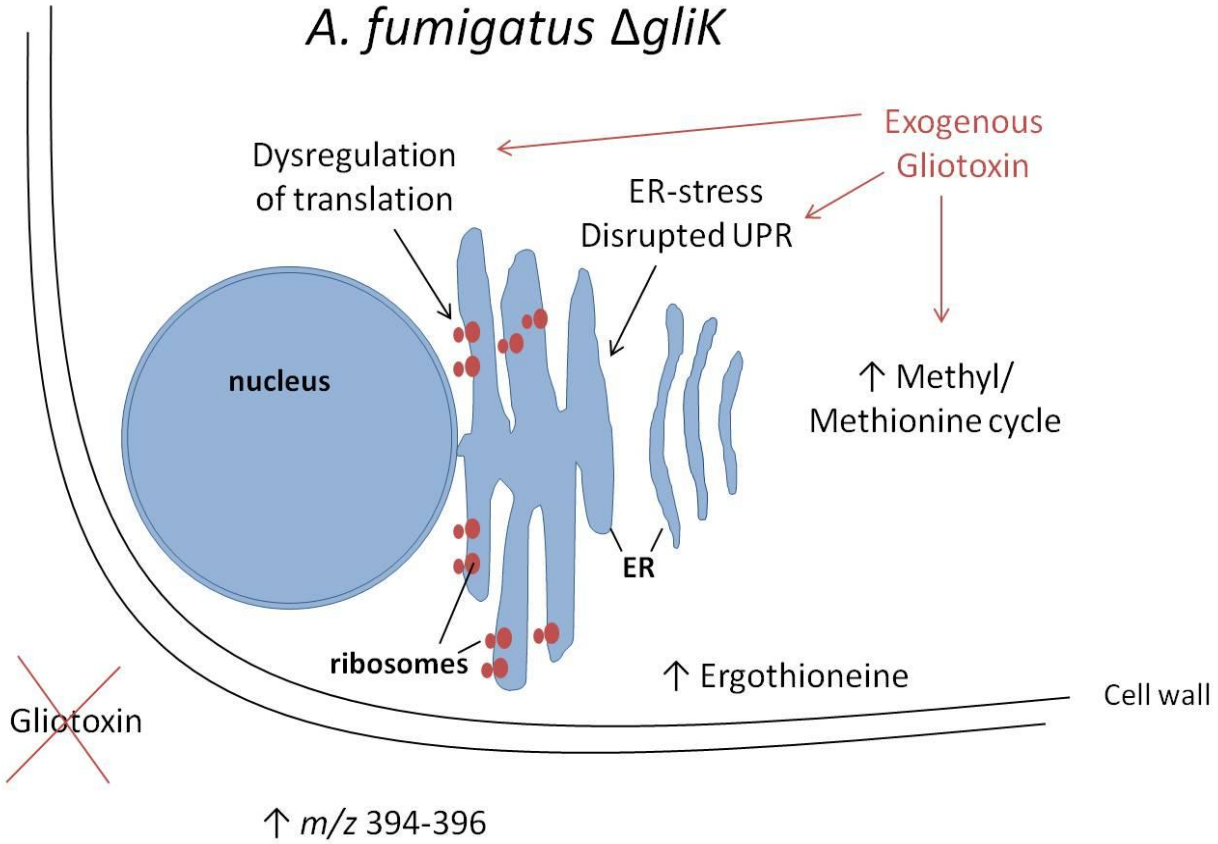

Figure 7.3: (a) Summary and (b) schematic representation of cellular functions and biosynthetic processes altered in *A. fumigatus* Δ*gliK*.

Purification and identification of these metabolites (*m/z* 394-396) would further inform the model of gliotoxin biosynthesis and could elucidate the specific role played by GliK in the pathway. This strategy was implemented previously to determine the roles of GliI and GliG in gliotoxin biosynthesis (Davis *et al.*, 2011a; Scharf *et al.*, 2012a).

Significantly, this thesis describes the first reported detection of ergothioneine in *A. fumigatus* (Gallagher *et al.*, 2012), and GliK absence resulted in significantly elevated levels of this poorly characterised, but ubiquitous, thione-thiol tautomer. A conserved gamma-glutamyl cyclotransferase (GGCT)-like domain was recently annotated in GliK, indicating the function of this protein may be connected to the cleavage of γ-glutamyl groups from dipeptides. This putative function could point to the role of GliK in gliotoxin biosynthesis, through removal of one or both γ-glutamyl moieties from the di-glutathionylated gliotoxin precursor (Figure 1.7). Furthermore, GGCT activity may explicate the elevation in ergothioneine levels in *A. fumigatus* Δ*gliK*, as the biosynthesis of ergothioneine involves incorporation of a γ-glutamyl dipeptide (γ-glutamyl cysteine), as deduced in *Mycobacterium* (Seebeck, 2010). Therefore, absence of GliK could lead to reduced catabolism of the substrate of ergothioneine biosynthesis. Biochemical confirmation of GGCT activity in GliK may aid in the elucidation of the specific role of this protein in gliotoxin biosynthesis. As ergothioneine has not been examined in *A. fumigatus* to date, the role of this molecule in the redox environment has not been taken into consideration. Ergothioneine, could potentially contribute to the enhanced sensitivity of *A. fumigatus* Δ*gliK* to gliotoxin, through reduction of gliotoxin and consequent disruption of gliotoxin efflux (Gallagher *et al.*, 2012). Further investigation of this molecule is required to determine the contribution of ergothioneine levels to the redox status of *A. fumigatus* and other

filamentous fungi. In this regard, it is recommended that determination of ergothioneine levels should be incorporated into future functional investigations of oxidative stress.

To conclude, this study expands the proteomic characterisation of *A. fumigatus* and contributes to the expansion of the immunome. Additionally, mechanisms affected by gliotoxin in *A. fumigatus* have been extrapolated, and inform the role of gliotoxin as both a toxin, in sensitive organisms, and a potential anti-oxidant in *A. fumigatus*. Finally cross-talk between the gliotoxin and ergothioneine biosynthesis was identified, extending our comprehension of the fungal metabolome. Altogether, this study contributes to the global and targeted characterisation of protein and metabolite systems operating in *A. fumigatus*, while revealing many interesting avenues for future investigations.

CHAPTER 8

Bibliography

8 Bibliography

Abad, A., Fernández-Molina, J.V., Bikandi, J., Ramírez, A., Margareto, J., Sendino, J., Luis Hernando, F., Pontón, J., Garaizar, J. and Rementeria, A. (2010). What makes *Aspergillus fumigatus* a successful pathogen? Genes and molecules involved in invasive aspergillosis. *Rev. Iberoam. Micol.* **27**: 155–182.

Adav, S.S., Li, A.A., Manavalan, A., Punt, P. and Sze, S.K. (2010). Quantitative iTRAQ Secretome Analysis of *Aspergillus niger* Reveals Novel Hydrolytic Enzymes. *J. Proteome Res.* **9**: 3932–3940.

Aebersold, R. and Mann, M. (2003). Mass spectrometry-based proteomics. *Nature* **422**: 198–207.

Agarwal, R. (2011). Allergic bronchopulmonary aspergillosis: Lessons for the busy radiologist. *World J. Radiol.* **3**: 178–181.

Agarwal, R., Hazarika, B., Gupta, D., Aggarwal, A.N., Chakrabarti, A. and Jindal, S.K. (2010). *Aspergillus* hypersensitivity in patients with chronic obstructive pulmonary disease: COPD as a risk factor for ABPA? *Med. Mycol.* **48**: 988–994.

Aguirre, J., Hansberg, W. and Navarro, R. (2006). Fungal responses to reactive oxygen species. *Med. Mycol.* **44**: 101–107.

Aimanianda, V., Bayry, J., Bozza, S., Kniemeyer, O., Perruccio, K., Elluru, S.R., Clavaud, C., Paris, S., Brakhage, A.A., Kaveri, S. V, Romani, L. and Latgé, J.-P. (2009). Surface hydrophobin prevents immune recognition of airborne fungal spores. *Nature* **460**: 1117–1121.

Albrecht, D., Guthke, R., Brakhage, A.A. and Kniemeyer, O. (2010). Integrative analysis of the heat shock response in *Aspergillus fumigatus*. *BMC Genomics* **11**: 32.

Albrecht, D., Kniemeyer, O., Mech, F., Gunzer, M., Brakhage, A.A. and Guthke, R. (2011). On the way toward systems biology of *Aspergillus fumigatus* infection. *International Journal of Medical Microbiology* **301**: 453–459.

Albrethsen, J. (2007). Reproducibility in protein profiling by MALDI-TOF mass spectrometry. *Clinical Chemistry* **53**: 852–858.

Alcazar-Fuoli, L., Clavaud, C., Lamarre, C., Aimanianda, V., Seidl-Seiboth, V., Mellado, E. and Latgé, J.-P. (2011). Functional analysis of the fungal/plant class chitinase family in *Aspergillus fumigatus*. *Fungal Genetics and Biology* **48**: 418–429.

Amitani, R., Taylor, G., Elezis, E., Llewellyn-jones, C., Mitchell, J., Kuze, F., Cole, P.J. and Wilson, R. (1995). Purification and Characterization of Factors Produced by *Aspergillus fumigatus* Which Affect Human Ciliated Respiratory Epithelium. *Infect. Immun.* **63**: 3266–3271.

Anand, M., Balar, B., Ulloque, R., Gross, S.R. and Kinzy, T.G. (2006). Domain and nucleotide dependence of the interaction between *Saccharomyces cerevisiae* translation elongation factors 3 and 1A. *The Journal of Biological Chemistry* **281**: 32318–32326.

Anand, M., Chakraburtty, K., Marton, M.J., Hinnebusch, A.G. and Kinzy, T.G. (2003). Functional interactions between yeast translation eukaryotic elongation factor (eEF) 1A and eEF3. *The Journal of Biological Chemistry* **278**: 6985–6991.

Andersen, M.R., Nielsen, M.L. and Nielsen, J. (2008). Metabolic model integration of the bibliome, genome, metabolome and reactome of *Aspergillus niger*. *Molecular Systems Biology* **4**: 178.

Antinori, S., Nebuloni, M., Magni, C., Fasan, M., Adorni, F., Viola, A., Corbellino, M., Galli, M., Vago, G., Parravicini, C. and Ridolfo, A.L. (2009). Trends in the postmortem diagnosis of opportunistic invasive fungal infections in patients with AIDS: a retrospective study of 1,630 autopsies performed between 1984 and 2002. *Am. J. Clin. Pathol.* **132**: 221–227.

Anzai, K., Mayuzumi, S., Nakashima, T., Sato, H., Inaba, S., Park, J.-Y., Kuwahara, N., Suzuki, R., Utsumi, N., Yokoyama, F., Ohfuku, Y. and Ando, K. (2008). Comparison of Groupings among Members of the Genus *Aspergillus* Based on Phylogeny and Production of Bioactive Compounds. *Biosci. Biotechnol. Biochem.* **72**: 2199–2202.

Arava, Y., Wang, Y., Storey, J.D., Liu, C.L., Brown, P.O. and Herschlag, D. (2003). Genome-wide analysis of mRNA translation profiles in *Saccharomyces cerevisiae*. *Proc. Natl. Acad. Sci. U. S. A.* **100**: 3889–3894.

Ashburner, M., Ball, C.A., Blake, J.A., Botstein, D., Butler, H., Cherry, J.M., Davis, A.P., Dolinski, K., Dwight, S.S., Eppig, J.T., Harris, M.A., Hill, D.P., Issel-tarver, L., Kasarskis, A., Lewis, S., Matese, J.C., Richardson, J.E., Rubin, G.M. and Sherlock, G. (2000). Gene Ontology : tool for the unification of biology. *Nat. Genet.* **25**: 25–29.

Asif, A.R., Oellerich, M., Amstrong, V.W., Gross, U. and Reichard, U. (2010). Analysis of the cellular *Aspergillus fumigatus* proteome that reacts with sera from rabbits developing an acquired immunity after experimental aspergillosis. *Electrophoresis* **31**: 1947–1958.

Asif, A.R., Oellerich, M., Amstrong, V.W., Riemenschneider, B., Monod, M. and Reichard, U. (2006). Proteome of Conidial Surface Associated Proteins of *Aspergillus fumigatus* Reflecting Potential Vaccine Candidates and Allergens. *J. Proteome Res.* **5**: 954–962.

Atalla, M.M., Hamed, E.R. and El-Shami, A.R. (2008). Optimization of a culture medium for increased mevinolin production by *Aspergillus terreus* strain. *Malaysian Journal of Microbiology* **4**: 6–10.

Azie, N., Neofytos, D., Pfaller, M., Meier-Kriesche, H.-U., Quan, S.-P. and Horn, D. (2012). The PATH (Prospective Antifungal Therapy) Alliance® registry and invasive fungal infections: update 2012. *Diagn. Microbiol. Infect. Dis.* **73**: 293–300.

Back, S.H., Schröder, M., Lee, K., Zhang, K. and Kaufman, R.J. (2005). ER stress signaling by regulated splicing: IRE1/HAC1/XBP1. *Methods* **35**: 395–416.

Balibar, C.J. and Walsh, C.T. (2006). GliP, a multimodular nonribosomal peptide synthetase in *Aspergillus fumigatus*, makes the diketopiperazine scaffold of gliotoxin. *Biochemistry* **45**: 15029–15038.

Balloy, V., Huerre, M., Latgé, J. and Chignard, M. (2005). Differences in Patterns of Infection and Inflammation for Corticosteroid Treatment and Chemotherapy in Experimental Invasive Pulmonary Aspergillosis. *Infect. Immun.* **73**: 494–503.

Barak, A.J., Beckenhauer, H.C., Mailliard, M.E., Kharbanda, K.K. and Tuma, D.J. (2003). Betaine Lowers Elevated S- Adenosylhomocysteine Levels in Hepatocytes from Ethanol-Fed Rats. *The Journal of Nutrition* **133**: 2845–2848.

Barker, B.M., Kroll, K., Vödisch, M., Mazurie, A., Kniemeyer, O. and Cramer, R.A. (2012). Transcriptomic and proteomic analyses of the *Aspergillus fumigatus* hypoxia response using an oxygen-controlled fermenter. *BMC Genomics* **13**: 62.

Baumer, M., Kunzler, M., Steigemann, P., Braus, G.H. and Irniger, S. (2000). Yeast Ran-binding Protein Yrb1p Is Required for Efficient Proteolysis of Cell Cycle Regulatory Proteins Pds1p and Sic1p. *The Journal of Biological Chemistry* **275**: 38929–38937.

Bayram, Ö., Krappmann, S., Ni, M., Bok, J.W., Helmstaedt, K., Yu, J. and Braus, G.H. (2008). VelB/VeA/LaeA Complex Coordinates Light Signal with Fungal Development and Secondary Metabolism. *Science* **320**: 1504–1506.

Beauvais, A. and Latgé, J.P. (2001). Membrane and cell wall targets in *Aspergillus fumigatus*. *Drug Resist. Updates* **4**: 38–49.

Bello, M.H., Barrera-Perez, V., Morin, D. and Epstein, L. (2012). The *Neurospora crassa* mutant NcΔEgt-1 identifies an ergothioneine biosynthetic gene and demonstrates that ergothioneine enhances conidial survival and protects against peroxide toxicity during conidial germination. *Fungal Genetics and Biology* **49**: 160–172.

Ben-Ami, R., Lewis, R.E. and Kontoyiannis, D.P. (2010). Enemy of the (immunosuppressed) state: an update on the pathogenesis of Aspergillus fumigatus infection. *Br. J. Haematol.* **150**: 406–417.

Ben-Ami, R., Lewis, R.E., Leventakos, K. and Kontoyiannis, D.P. (2009). *Aspergillus fumigatus* inhibits angiogenesis through the production of gliotoxin and other secondary metabolites. *Blood* **114**: 5393–5399.

Bendtsen, J.D., Jensen, L.J., Blom, N., Von Heijne, G. and Brunak, S. (2004). Feature-based prediction of non-classical and leaderless protein secretion. *Protein Engineering, Design & Selection* **17**: 349–356.

Bendtsen, J.D., Kiemer, L., Fausbøll, A. and Brunak, S. (2005). Non-classical protein secretion in bacteria. *BMC Microbiology* **5**: 58.

Berger, A.C., Vanderford, T.H., Gernert, K.M., Nichols, W., Faundez, V., Corbett, A.H. and Nichols, J.W. (2005). Saccharomyces cerevisiae Npc2p Is a Functionally Conserved Homologue of the Human Niemann-Pick Disease Type C 2 Protein, hNPC2. *Eukaryot. Cell* **4**: 1851–1862.

Bergmann, A., Hartmann, T., Cairns, T., Bignell, E.M. and Krappmann, S. (2009). A regulator of *Aspergillus fumigatus* extracellular proteolytic activity is dispensable for virulence. *Infect. Immun.* **77**: 4041–4050.

Bernardo, P.H., Brasch, N., Chai, C.L.L. and Waring, P. (2003). A Novel Redox Mechanism for the Glutathione-dependent Reversible Uptake of a Fungal Toxin in Cells. *J. Biol. Chem.* **278**: 46549–46555.

Bertling, A., Niemann, S., Uekötter, A., Fegeler, W., Lass-Flörl, C., Von Eiff, C. and Kehrel, B.E. (2010). *Candida albicans* and its metabolite gliotoxin inhibit platelet function via interaction with thiols. *Thrombosis and Haemostasis* **104**: 270–278.

Bhabhra, R. and Askew, D.S. (2005). Thermotolerance and virulence of *Aspergillus fumigatus* : role of the fungal nucleolus. *Med. Mycol.* **43**: 87–93.

Bhabhra, R., Miley, M.D., Mylonakis, E., Boettner, D., Fortwendel, J., Panepinto, J.C., Postow, M., Rhodes, J.C. and Askew, D.S. (2004). Disruption of the *Aspergillus fumigatus* Gene Encoding Nucleolar Protein CgrA Impairs Thermotolerant Growth and Reduces Virulence. *Infect. Immun.* **72**: 4731–4740.

Bhatia, S., Fei, M., Yarlagadda, M., Qi, Z., Akira, S., Saijo, S., Iwakura, Y., Van Rooijen, N., Gibson, G.A., St Croix, C.M., Ray, A. and Ray, P. (2011). Rapid host defense against *Aspergillus fumigatus* involves alveolar macrophages with a predominance of alternatively activated phenotype. *PloS One* **6**: e15943.

Bok, J.W., Balajee, S.A., Marr, K.A., Andes, D., Nielsen, K.F., Frisvad, J.C. and Keller, N.P. (2005). LaeA , a Regulator of Morphogenetic Fungal Virulence Factors. *Eukaryot. Cell* **4**: 1574–1582.

Bok, J.W., Chung, D., Balajee, S.A., Marr, K.A., Andes, D., Nielsen, K.F., Frisvad, J.C., Kirby, K.A. and Keller, N.P. (2006). GliZ, a transcriptional regulator of gliotoxin biosynthesis, contributes to *Aspergillus fumigatus* virulence. *Infect. Immun.* **74**: 6761–6768.

Bok, J.W. and Keller, N.P. (2004). LaeA , a Regulator of Secondary Metabolism in *Aspergillus* spp . *Eukaryot. Cell* **3**: 527–535.

Bonnett, C.R., Cornish, E.J., Harmsen, A.G. and Burritt, J.B. (2006). Early neutrophil recruitment and aggregation in the murine lung inhibit germination of *Aspergillus fumigatus* Conidia. *Infect. Immun.* **74**: 6528–6539.

Bouligand, J., Deroussent, A., Paci, A., Morizet, J. and Vassal, G. (2006). Liquid chromatography-tandem mass spectrometry assay of reduced and oxidized glutathione and main precursors in mice liver. *Journal of Chromatography B* **832**: 67–74.

Boutboul, F., Alberti, C., Leblanc, T., Sulahian, A., Gluckman, E., Derouin, F. and Ribaud, P. (2002). Invasive Aspergillosis in Allogeneic Stem Cell Transplant Recipients : Increasing Antigenemia Is Associated with Progressive Disease. *Clin. Infect. Dis.* **34**: 939–943.

Brace, J.L., Vanderweele, D.J. and Rudin, C.M. (2005). Svf1 inhibits reactive oxygen species generation and promotes survival under conditions of oxidative stress in *Saccharomyces cerevisiae*. *Yeast* **22**: 641–652.

Brachat, S., Dietrich, F.S., Voegeli, S., Zhang, Z., Stuart, L., Lerch, A., Gates, K., Gaffney, T. and Philippsen, P. (2003). Reinvestigation of the *Saccharomyces cerevisiae* genome annotation by comparison to the genome of a related fungus: *Ashbya gossypii*. *Genome Biology* **4**: R45.

Brakhage, A.A. and Langfelder, K. (2002). Menacing mold: the molecular biology of *Aspergillus fumigatus*. *Annu. Rev. Microbiol.* **56**: 433–455.

Brakhage, A.A. and Liebmann, B. (2005). *Aspergillus fumigatus* conidial pigment and cAMP signal transduction: significance for virulence. *Med. Mycol.* **43**: 75–82.

Brik, A., Salem, A.M., Kamal, A.R., Abdel-Sadek, M., Essa, M., El Sharawy, M., Deebes, A. and Bary, K.A. (2008). Surgical outcome of pulmonary aspergilloma. *Eur. J. Cardiothorac. Surg.* **34**: 882–885.

Brouard, J., Knauer, N., Boelle, P.-Y., Corvol, H., Henrion-Caude, A., Flamant, C., Bremont, F., Delaisi, B., Duhamel, J.-F., Marguet, C., Roussey, M., Miesch, M.-C., Chadelat, K., Boule, M., Fauroux, B., Ratjen, F., Grasemann, H. and Clement, A. (2005). Influence of interleukin-10 on *Aspergillus fumigatus* infection in patients with cystic fibrosis. *J. Infect. Dis.* **191**: 1988–1991.

Brown, A.J.P., Haynes, K. and Quinn, J. (2009a). Nitrosative and oxidative stress responses in fungal pathogenicity. *Curr. Opin. Microbiol.* **12**: 384–391.

Brown, M., Dunn, W.B., Dobson, P., Patel, Y., Winder, C.L., Francis-McIntyre, S., Begley, P., Carroll, K., Broadhurst, D., Tseng, a, Swainston, N., Spasic, I., Goodacre, R. and Kell, D.B. (2009b). Mass spectrometry tools and metabolite-specific databases for molecular identification in metabolomics. *The Analyst* **134**: 1322–1332.

Bruneau, J.M., Magnin, T., Tagat, E., Legrand, R., Bernard, M., Diaquin, M., Fudali, C. and Latgé, J.P. (2001). Proteome analysis of *Aspergillus fumigatus* identifies

glycosylphosphatidylinositol-anchored proteins associated to the cell wall biosynthesis. *Electrophoresis* **22**: 2812–2823.

Bruns, S., Kniemeyer, O., Hasenberg, M., Aimanianda, V., Nietzsche, S., Thywissen, A., Jeron, A., Latgé, J.-P., Brakhage, A.A. and Gunzer, M. (2010a). Production of extracellular traps against *Aspergillus fumigatus* in vitro and in infected lung tissue is dependent on invading neutrophils and influenced by hydrophobin RodA. *PLoS Pathogens* **6**: e1000873.

Bruns, S., Seidler, M., Albrecht, D., Salvenmoser, S., Remme, N., Hertweck, C., Brakhage, A.A., Kniemeyer, O. and Müller, F.-M.C. (2010b). Functional genomic profiling of *Aspergillus fumigatus* biofilm reveals enhanced production of the mycotoxin gliotoxin. *Proteomics* **10**: 3097–3107.

Burkovics, P., Hajdú, I., Szukacsov, V., Unk, I. and Haracska, L. (2009). Role of PCNA-dependent stimulation of 3'-phosphodiesterase and 3'-5' exonuclease activities of human Ape2 in repair of oxidative DNA damage. *Nucleic Acids Research* **37**: 4247–4255.

Cagas, S.E., Jain, M.R., Li, H. and Perlin, D.S. (2011a). Profiling the *Aspergillus fumigatus* proteome in response to caspofungin. *Antimicrob. Agents Chemother.* **55**: 146–154.

Cagas, S.E., Jain, M.R., Li, H. and Perlin, D.S. (2011b). The Proteomic Signature of *Aspergillus fumigatus* During Early Development. *Molecular & Cellular Proteomics* **10**: M111.010108.

Calvo, A.M., Wilson, R.A., Bok, J.W. and Keller, N.P. (2002). Relationship between Secondary Metabolism and Fungal Development Fungal Development. *Microbiol. Mol. Biol. Rev.* **66**: 447–459.

Camps, S.M.T., Van der Linden, J.W.M., Li, Y., Kuijper, E.J., Van Dissel, J.T., Verweij, P.E. and Melchers, W.J.G. (2012). Rapid induction of multiple resistance mechanisms in *Aspergillus fumigatus* during azole therapy: a case study and review of the literature. *Antimicrob. Agents Chemother.* **56**: 10–16.

Carberry, S., Molloy, E., Hammel, S., O'Keeffe, G., Jones, G.W., Kavanagh, K. and Doyle, S. (2012). Gliotoxin effects on fungal growth: Mechanisms and exploitation. *Fungal Genet. Biol.* **49**: 302–312.

Carberry, S., Neville, C.M., Kavanagh, K. and Doyle, S. (2006). Analysis of major intracellular proteins of *Aspergillus fumigatus* by MALDI mass spectrometry: identification and characterisation of an elongation factor 1B protein with glutathione transferase activity. *Biochemical and Biophysical Research Communications* **341**: 1096–1104.

Carlsson, J., Kierstant, M.P.J. and Brocklehurst, K. (1974). Reactions of L-Ergothioneine and Some Other Aminothiones with 2,2'- and 4,4'-Dipyridyl Disulphides and of L-Ergothioneine with Iodoacetamide. *Biochem. J.* **139**: 221–235.

Carmona-Gutiérrez, D., Bauer, M.A., Ring, J., Knauer, H., Eisenberg, T., Büttner, S., Ruckenstuhl, C., Reisenbichler, A., Magnes, C., Rechberger, G.N., Birner-Gruenberger, R., Jungwirth, H., Fröhlich, K.-U., Sinner, F., Kroemer, G. and Madeo, F. (2011). The propeptide of yeast cathepsin D inhibits programmed necrosis. *Cell Death & Disease* **2**: e161.

Carvalho, A., Cunha, C., Bistoni, F. and Romani, L. (2012). Immunotherapy of aspergillosis. *Clin. Microbiol. Infect.* **18**: 120–125.

Casals, E., Pfaller, T., Duschl, A., Oostingh, G.J. and Puntes, V. (2010). Time evolution of the nanoparticle protein corona. *ACS Nano* **4**: 3623–3632.

Casas López, J.L., Sánchez Pérez, J.A., Fernández Sevilla, J.M., Acién Fernández, F.., Molina Grima, E. and Chisti, Y. (2003). Production of lovastatin by *Aspergillus terreus*: effects of the C:N ratio and the principal nutrients on growth and metabolite production. *Enzyme. Microb. Technol.* **33**: 270–277.

Cedervall, T., Lynch, I., Lindman, S., Berggård, T., Thulin, E., Nilsson, H., Dawson, K.A. and Linse, S. (2007). Understanding the nanoparticle-protein corona using methods to quantify exchange rates and affinities of proteins for nanoparticles. *Proc. Natl. Acad. Sci. U. S. A.* **104**: 2050–2055.

Chabane, S., Sarfati, J., Ibrahim-granet, O., Du, C., Schmidt, C., Mouyna, I., Prevost, M., Calderone, R. and Latge, J. (2006). Glycosylphosphatidylinositol-Anchored Ecm33p Influences Conidial Cell Wall Biosynthesis in *Aspergillus fumigatus*. *Applied and Environmental Microbiology* **72**: 3259–3267.

Chai, L.Y.A., Netea, M.G., Sugui, J., Vonk, A.G., Van de Sande, W.J., Warris, A., Kwon-chung, K.J. and Jan, B. (2011a). *Aspergillus fumigatus* Conidial Melanin Modulates Host Cytokine Response. *Immunobiology* **215**: 915–920.

Chai, L.Y.A., Vonk, A.G., Kullberg, B.J., Verweij, P.E., Verschueren, I., Van der Meer, J.W.M., Joosten, L.A.B., Latgé, J.-P. and Netea, M.G. (2011b). *Aspergillus fumigatus* cell wall components differentially modulate host TLR2 and TLR4 responses. *Microbes Infect.* **13**: 151–159.

Chakraburtty, K. (2001). Elongation Factor 3 in Fungal Translation. In eLS, (John Wiley & Sons Ltd.), p. DOI: 10.1038/npg.els.0000686.

Chambers, S.T., Bhandari, S., Scott-Thomas, A. and Syhre, M. (2011). Novel diagnostics: progress toward a breath test for invasive *Aspergillus fumigatus*. *Med. Mycol.* **49 Suppl 1**: S54–61.

Chamilos, G., Luna, M., Lewis, R.E., Bodey, G.P., Chemaly, R., Tarrand, J.J., Safdar, A., Raad, I.I. and Kontoyiannis, D.P. (2006). Invasive fungal infections in patients with hematologic malignancies in a tertiary care cancer center: an autopsy study over a 15-year period (1989-2003). *Haematologica* **91**: 986–989.

Chang, Y.C., Tsai, H.-F., Karos, M. and Kwon-Chung, K.J. (2004). THTA, a thermotolerance gene of *Aspergillus fumigatus*. *Fungal Genet. Biol.* **41**: 888–896.

Chaudhary, N. and Marr, K.A. (2011). Impact of *Aspergillus fumigatus* in allergic airway diseases. *Clin. Transl. Allergy* **1**: 4.

Chiang, L.Y., Sheppard, D.C., Gravelat, F.N., Patterson, T.F. and Filler, S.G. (2008). *Aspergillus fumigatus* stimulates leukocyte adhesion molecules and cytokine production by endothelial cells in vitro and during invasive pulmonary disease. *Infect. Immun.* **76**: 3429–3438.

Choi, H.S., Shim, J.S., Kim, J.-A., Kang, S.W. and Kwon, H.J. (2007). Discovery of gliotoxin as a new small molecule targeting thioredoxin redox system. *Biochem. Biophys. Res. Commun.* **359**: 523–528.

Coleman, J.J., Ghosh, S., Okoli, I. and Mylonakis, E. (2011). Antifungal Activity of Microbial Secondary Metabolites. *PLoS ONE* **6**: e25321.

Colognato, R., Laurenza, I., Fontana, I., Coppedé, F., Siciliano, G., Coecke, S., Aruoma, O.I., Benzi, L. and Migliore, L. (2006). Modulation of hydrogen peroxide-induced DNA damage, MAPKs activation and cell death in PC12 by ergothioneine. *Clinical Nutrition* **25**: 135–145.

Coméra, C., André, K., Laffitte, J., Collet, X., Galtier, P. and Maridonneau-Parini, I. (2007). Gliotoxin from *Aspergillus fumigatus* affects phagocytosis and the organization of the actin cytoskeleton by distinct signalling pathways in human neutrophils. *Microbes Infect.* **9**: 47–54.

Conesa, A., Götz, S., García-Gómez, J.M., Terol, J., Talón, M. and Robles, M. (2005). Blast2GO: a universal tool for annotation, visualization and analysis in functional genomics research. *Bioinformatics* **21**: 3674–3676.

Costanzo, M., Baryshnikova, A., Bellay, J., Kim, Y., Spear, E.D., Sevier, C.S., Ding, H., Koh, J.L.Y., Toufighi, K., Mostafavi, S., Prinz, J., St Onge, R.P., VanderSluis, B., *et al.* (2010). The genetic landscape of a cell. *Science* **327**: 425–431.

Coyle, C.M., Kenaley, S.C., Rittenour, W.R. and Panaccione, D.G. (2007). Association of ergot alkaloids with conidiation in *Aspergillus fumigatus*. *Mycologia* **99**: 804–811.

Cramer, R.A., Gamcsik, M.P., Brooking, R.M., Najvar, L.K., Kirkpatrick, W.R., Patterson, T.F., Balibar, C.J., Graybill, J.R., Perfect, J.R., Abraham, S.N. and Steinbach, W.J. (2006). Disruption of a nonribosomal peptide synthetase in *Aspergillus fumigatus* eliminates gliotoxin production. *Eukaryot. Cell* **5**: 972–980.

Crosdale, D.J., Poulton, K. V, Ollier, W.E., Thomson, W. and Denning, D.W. (2001). Mannose-binding lectin gene polymorphisms as a susceptibility factor for chronic necrotizing pulmonary aspergillosis. *J. Infect. Dis.* **184**: 653–656.

Dagenais, T.R.T., Giles, S.S., Aimanianda, V., Latgé, J.-P., Hull, C.M. and Keller, N.P. (2010). *Aspergillus fumigatus* LaeA-mediated phagocytosis is associated with a decreased hydrophobin layer. *Infect. Immun.* **78**: 823–829.

Dagenais, T.R.T. and Keller, N.P. (2009). Pathogenesis of *Aspergillus fumigatus* in Invasive Aspergillosis. *Clin. Microbiol. Rev.* **22**: 447–465.

Davies, D.H., Liang, X., Hernandez, J.E., Randall, A., Hirst, S., Mu, Y., Romero, K.M., Nguyen, T.T., Kalantari-Dehaghi, M., Crotty, S., Baldi, P., Villarreal, L.P. and Felgner, P.L. (2005). Profiling the humoral immune response to infection by using proteome microarrays: high-throughput vaccine and diagnostic antigen discovery. *Proc. Natl. Acad. Sci. U. S. A.* **102**: 547–552.

Davis, C., Carberry, S., Schrettl, M., Singh, I., Stephens, J.C., Barry, S.M., Kavanagh, K., Challis, G.L., Brougham, D. and Doyle, S. (2011a). The role of glutathione S-transferase GliG in gliotoxin biosynthesis in *Aspergillus fumigatus*. *Chem. Biol.* **18**: 542–552.

Davis, C., Gordon, N., Murphy, S., Singh, I., Kavanagh, K., Carberry, S. and Doyle, S. (2011b). Single-pot derivatisation strategy for enhanced gliotoxin detection by HPLC and MALDI-ToF mass spectrometry. *Analytical and Bioanalytical Chemistry* **401**: 2519–2529.

Denning, D.W. and Hope, W.W. (2010). Therapy for fungal diseases: opportunities and priorities. *Trends Microbiol.* **18**: 195–204.

Dettmer, K., Aronov, P.A. and Hammock, B.D. (2007). Mass Spectrometry-based Metabolomics. *Mass Spectrometry Reviews* **26**: 51–78.

Dewson, G., Kratina, T., Czabotar, P., Day, C.L., Adams, J.M. and Kluck, R.M. (2009). Bak activation for apoptosis involves oligomerization of dimers via their α6 helices. *Mol. Cell* **36**: 696–703.

Dichtl, K., Helmschrott, C., Dirr, F. and Wagener, J. (2012). Deciphering cell wall integrity signalling in *Aspergillus fumigatus*: identification and functional characterization of cell wall stress sensors and relevant Rho GTPases. *Mol. Microbiol.* **83**: 506–519.

Dinamarco, T.M., Almeida, R.S., De Castro, P.A., Brown, N.A., Dos Reis, T.F., Ramalho, L.N.Z., Savoldi, M., Goldman, M.H.S. and Goldman, G.H. (2012). Molecular characterization of the putative transcription factor SebA involved in virulence in *Aspergillus fumigatus*. *Eukaryot. Cell* **11**: 518–531.

Dombrink-Kmizman, M.A. and Blackburn, J.A. (2005). Evaluation of several culture media for production of patulin by *Penicillium* species. *Int. J. Food Microbiol.* **98**: 241–248.

Domingo, M.P., Colmenarejo, C., Martínez-Lostao, L., Müllbacher, A., Jarne, C., Revillo, M.J., Delgado, P., Roc, L., Meis, J.F., Rezusta, A., Pardo, J. and Gálvez, E.M. (2012). Bis (methyl) gliotoxin proves to be a more stable and reliable marker for invasive aspergillosis than gliotoxin and suitable for use in diagnosis. *Diagn. Microbiol. Infect. Dis.* **73**: 57–64.

Doyle, S. (2011a). Fungal Proteomics. In Fungi: Biology and Applications, K. Kavanagh, ed. (Wiley, New York), p. ISBN: 111997769X, 9781119977698.

Doyle, S. (2011b). Fungal proteomics: from identification to function. *FEMS Microbiology Letters* **321**: 1–9.

Du, C., Sarfati, J., Latge, J.-P. and Calderone, R. (2006). The role of the *sakA* (Hog1) and *tcsB* (sln1) genes in the oxidant adaptation of *Aspergillus fumigatus*. *Med. Mycol.* **44**: 211–218.

Dyugovskaya, L., Polyakov, A., Ginsberg, D., Lavie, P. and Lavie, L. (2011). Molecular pathways of spontaneous and TNFalpha-mediated neutrophil apoptosis under intermittent hypoxia. *Am. J. Respir. Cell Mol. Biol.* **45**: 154–162.

Falagas, M.E., Vardakas, K.Z. and Samonis, G. (2008). Decreasing the incidence and impact of infections in neutropenic patients: evidence from meta-analyses of randomized controlled trials. *Curr. Med. Res. Opin.* **24**: 215–235.

Fallon, J.P., Reeves, E.P. and Kavanagh, K. (2010). Inhibition of neutrophil function following exposure to the *Aspergillus fumigatus* toxin fumagillin. *J. Med. Microbiol.* **59**: 625–633.

Fedorova, N.D., Khaldi, N., Joardar, V.S., Maiti, R., Amedeo, P., Anderson, M.J., Crabtree, J., Silva, J.C., Badger, J.H., Albarraq, A., Angiuoli, S., Bussey, H., Bowyer, P., Cotty, P.J., Dyer, P.S., Egan, A., Galens, K., Fraser-Liggett, C.M., Haas, B.J., Inman, J.M., Kent, R., Lemieux, S., Malavazi, I., Orvis, J., Roemer, T., Ronning, C.M., Sundaram, J.P., Sutton, G., Turner, G., Venter, J.C., White, O.R., Whitty, B.R., Youngman, P., Wolfe, K.H., Goldman, G.H., Wortman, J.R., Jiang, B., Denning, D.W. and Nierman, W.C. (2008). Genomic islands in the pathogenic filamentous fungus *Aspergillus fumigatus*. *PLoS Genetics* **4**: e1000046.

Feldberg, L., Venger, I., Malitsky, S., Rogachev, I. and Aharoni, A. (2009). Dual Labeling of Metabolites for Metabolome Analysis (DLEMMA): A New Approach for the Identification and Relative Quantification of Metabolites by Means of Dual Isotope Labeling and Liquid Chromatography-Mass Spectrometry. *Analytical Chemistry* **81**: 9257–9266.

Feldmesser, M. (2006). Role of neutrophils in invasive aspergillosis. *Infect. Immun.* **74**: 6514–6516.

Feng, G.H. and Leonard, T.J. (1998). Culture conditions control expression of the genes for aflatoxin and sterigmatocystin biosynthesis in *Aspergillus parasiticus* and *A. nidulans*. *Applied and Environmental Microbiology* **64**: 2275–2277.

Fenn, J., Mann, M., Meng, C., Wong, S. and Whitehouse, C. (1989). Electrospray ionization for mass spectrometry of large biomolecules. *Science* **246**: 64–71.

Fernie, A.R., Carrari, F. and Sweetlove, L.J. (2004). Respiratory metabolism: glycolysis, the TCA cycle and mitochondrial electron transport. *Current Opinion in Plant Biology* **7**: 254–261.

Ferreira de Oliveira, J.M.P. and De Graaff, L.H. (2011). Proteomics of industrial fungi: trends and insights for biotechnology. *Applied Microbiology and Biotechnology* **89**: 225–237.

Ferreira de Oliveira, J.M.P., Van Passel, M.W.J., Schaap, P.J. and De Graaff, L.H. (2011). Proteomic analysis of the secretory response of *Aspergillus niger* to D-maltose and D-xylose. *PloS One* **6**: e20865.

Finoulst, I., Pinkse, M., Van Dongen, W. and Verhaert, P. (2011). Sample preparation techniques for the untargeted LC-MS-based discovery of peptides in complex biological matrices. *Journal of Biomedicine & Biotechnology* **2011**: 245291.

Forseth, R.R., Fox, E.M., Chung, D., Howlett, B.J., Keller, N.P., Frank, C. and Schroeder, F.C. (2011). Identification of cryptic products of the gliotoxin gene cluster using NMR-based comparative metabolomics and a model for gliotoxin biosynthesis. *J. Am. Chem. Soc.* **133**: 9678–9681.

Fox, E.M. and Howlett, B.J. (2008). Biosynthetic gene clusters for epipolythiodioxopiperazines in filamentous fungi. *Mycol. Res.* **112**: 162–169.

Fraczek, M.G., Rashid, R., Denson, M., Denning, D.W. and Bowyer, P. (2010). *Aspergillus fumigatus* allergen expression is coordinately regulated in response to hydrogen peroxide and cyclic AMP. *Clinical and Molecular Allergy : CMA* **8**: 15.

Franzoni, F., Colognato, R., Galetta, F., Laurenza, I., Barsotti, M., Di Stefano, R., Bocchetti, R., Regoli, F., Carpi, A., Balbarini, A., Migliore, L. and Santoro, G. (2006). An in vitro study on the free radical scavenging capacity of ergothioneine: comparison with reduced glutathione, uric acid and trolox. *Biomedicine & Pharmacotherapy* **60**: 453–457.

Franzosa, E.A., Albanèse, V., Frydman, J., Xia, Y. and McClellan, A.J. (2011). Heterozygous yeast deletion collection screens reveal essential targets of Hsp90. *PloS One* **6**: e28211.

Frisvad, J.C., Andersen, B. and Thrane, U. (2008). The use of secondary metabolite profiling in chemotaxonomy of filamentous fungi. *Mycological Research* **112**: 231–240.

Frisvad, J.C., Rank, C., Nielsen, K.F. and Larsen, T.O. (2009). Metabolomics of *Aspergillus fumigatus*. *Med. Mycol.* **47 Suppl 1**: S53–71.

Furukawa, K., Hoshi, Y., Maeda, T., Nakajima, T. and Abe, K. (2005). *Aspergillus nidulans* HOG pathway is activated only by two-component signalling pathway in response to osmotic stress. *Molecular Microbiology* **56**: 1246–1261.

Galagan, J.E., Calvo, S.E., Cuomo, C., Ma, L.-J., Wortman, J.R., Batzoglou, S., Lee, S.-I., Baştürkmen, M., Spevak, C.C., Clutterbuck, J., Kapitonov, V., Jurka, J., Scazzocchio, C., Farman, M., Butler, J., Purcell, S., Harris, S., Braus, G.H., Draht, O., Busch, S., D'Enfert, C., Bouchier, C., Goldman, G.H., Bell-Pedersen, D., Griffiths-Jones, S., Doonan, J.H., Yu, J., Vienken, K., Pain, A., Freitag, M., Selker, E.U., Archer, D.B., Peñalva, M.A., Oakley, B.R., Momany, M., Tanaka, T., Kumagai, T., Asai, K., Machida, M., Nierman, W.C., Denning, D.W., Caddick, M., Hynes, M., Paoletti, M., Fischer, R., Miller, B., Dyer, P., Sachs, M.S., Osmani, S.A. and Birren, B.W. (2005). Sequencing of *Aspergillus nidulans* and comparative analysis with *A. fumigatus* and *A. oryzae*. *Nature* **438**: 1105–1115.

Gallagher, L. (2010). Functional Genomic Analysis of Natural Product Biosynthesis and Secretion in *Aspergillus fumigatus*.

Gallagher, L., Owens, R.A., O' Keeffe, G., Dolan, S.K., Schrettl, M., Kavanagh, K., Jones, G. and Doyle, S. (2012). The *Aspergillus fumigatus* Protein GliK Protects Against Oxidative Stress and is Essential for Gliotoxin Biosynthesis. *Eukaryot. Cell* **11**: 1226–1238.

Gangneux, J.-P., Camus, C. and Philippe, B. (2010). Epidemiology of invasive aspergillosis and risk factors in non neutropaenic patients. *Rev. Mal. Respir.* **27**: e34–46.

Gangwani, L. (2006). Deficiency of the zinc finger protein ZPR1 causes defects in transcription and cell cycle progression. *The Journal of Biological Chemistry* **281**: 40330–40340.

Garbati, M.A., Alasmari, F.A., Al-Tannir, M.A. and Tleyjeh, I.M. (2012). The role of combination antifungal therapy in the treatment of invasive aspergillosis: a systematic review. *Int. J. Infect. Dis.* **16**: e76–81.

Garcia-Campusano, F., Anaya, V.-H., Robledo-Arratia, L., Quezada, H., Hernandez, H., Riego, L. and Gonzales, A. (2009). ALT1-encoded alanine aminotransferase plays a central role in the metabolism of alanine in *Saccharomyces cerevisiae*. *Can. J. Microbiol.* **374**: 368–374.

Gardiner, D.M. and Howlett, B.J. (2005). Bioinformatic and expression analysis of the putative gliotoxin biosynthetic gene cluster of *Aspergillus fumigatus*. *FEMS Microbiol. Lett.* **248**: 241–248.

Gardiner, D.M., Jarvis, R.S. and Howlett, B.J. (2005a). The ABC transporter gene in the sirodesmin biosynthetic gene cluster of *Leptosphaeria maculans* is not essential for sirodesmin production but facilitates self-protection. *Fungal Genet. Biol.* **42**: 257–263.

Gardiner, D.M., Waring, P. and Howlett, B.J. (2005b). The epipolythiodioxopiperazine (ETP) class of fungal toxins: distribution, mode of action, functions and biosynthesis. *Microbiology* **151**: 1021–1032.

Gastebois, A., Fontaine, T., Latgé, J.-P. and Mouyna, I. (2010a). beta(1-3)Glucanosyltransferase Gel4p is essential for *Aspergillus fumigatus*. *Eukaryot. Cell* **9**: 1294–1298.

Gastebois, A., Mouyna, I., Simenel, C., Clavaud, C., Coddeville, B., Delepierre, M., Latgé, J.-P. and Fontaine, T. (2010b). Characterization of a new beta(1-3)-glucan branching activity of *Aspergillus fumigatus*. *The Journal of Biological Chemistry* **285**: 2386–2396.

Gauss, R., Kanehara, K., Carvalho, P., Ng, D.T.W. and Aebi, M. (2011). A complex of Pdi1p and the mannosidase Htm1p initiates clearance of unfolded glycoproteins from the endoplasmic reticulum. *Molecular Cell* **42**: 782–793.

Gautam, P., Shankar, J., Madan, T., Sirdeshmukh, R., Sundaram, C.S., Gade, W.N., Basir, S.F. and Sarma, P.U. (2008). Proteomic and transcriptomic analysis of *Aspergillus fumigatus* on exposure to amphotericin B. *Antimicrobial Agents and Chemotherapy* **52**: 4220–4227.

Gautam, P., Sundaram, C.S., Madan, T., Gade, W.N., Shah, A., Sirdeshmukh, R. and Sarma, P.U. (2007). Identification of novel allergens of *Aspergillus fumigatus* using immunoproteomics approach. *Clinical and Experimental Allergy : Journal of the British Society for Allergy and Clinical Immunology* **37**: 1239–1249.

Gautam, P., Upadhyay, S.K., Hassan, W., Madan, T., Sirdeshmukh, R., Sundaram, C.S., Gade, W.N., Basir, S.F., Singh, Y. and Sarma, P.U. (2011). Transcriptomic and proteomic profile of *Aspergillus fumigatus* on exposure to artemisinin. *Mycopathologia* **172**: 331–346.

Gauthier, T., Wang, X., Sifuentes Dos Santos, J., Fysikopoulos, A., Tadrist, S., Canlet, C., Artigot, M.P., Loiseau, N., Oswald, I.P. and Puel, O. (2012). Trypacidin, a spore-borne toxin from *Aspergillus fumigatus*, is cytotoxic to lung cells. *PloS One* **7**: e29906.

Goffin, L., Vodala, S., Fraser, C., Ryan, J., Timms, M., Meusburger, S., Catimel, B., Nice, E.C., Silver, P.A., Xiao, C., Jans, D.A. and Gething, M.H. (2006). The Unfolded Protein Response Transducer Ire1p Contains a Nuclear Localization Sequence Recognized by Multiple β Importins. *Mol. Biol. Cell* **17**: 5309–5323.

González-Fernández, R., Prats, E. and Jorrín-Novo, J. V (2010). Proteomics of plant pathogenic fungi. *Journal of Biomedicine & Biotechnology* **2010**: 932527.

Gordon, S.M., Deng, J., Lu, L.J. and Davidson, W.S. (2010). Proteomic Characterization of Human Plasma High Density Lipoprotein Fractionated by Gel Filtration Chromatography. *J. Proteome Res.* **9**: 5239–5249.

Grahl, N., Dinamarco, T.M., Willger, S.D., Goldman, G.H. and Cramer, R.A. (2012). *Aspergillus fumigatus* mitochondrial electron transport chain mediates oxidative stress homeostasis, hypoxia responses and fungal pathogenesis. *Molecular Microbiology* **84**: 383–399.

Graybill, J.R., Bocanegra, R., Najvar, L.K., Loebenberg, D. and Luther, M.F. (1998). Granulocyte colony-stimulating factor and azole antifungal therapy in murine aspergillosis: role of immune suppression. *Antimicrob. Agents Chemother.* **42**: 2467–2473.

Greganova, E., Altmann, M. and Bütikofer, P. (2011). Unique modifications of translation elongation factors. *The FEBS Journal* **278**: 2613–2624.

Griffiths, G.J., Dubrez, L., Morgan, C.P., Jones, N.A., Whitehouse, J., Corfe, B.M., Dive, C. and Hickman, J.A. (1999). Cell damage-induced conformational changes of the pro-apoptotic protein Bak in vivo precede the onset of apoptosis. *J. Cell Biol.* **144**: 903–914.

Griffiths, W.J. and Wang, Y. (2009). Mass spectrometry: from proteomics to metabolomics and lipidomics. *Chem. Soc. Rev.* **38**: 1882–1896.

Grillo, M.A. and Colombatto, S. (2008). S-adenosylmethionine and its products. *Amino Acids* **34**: 187–193.

Gross, S.R. and Kinzy, T.G. (2005). Translation elongation factor 1A is essential for regulation of the actin cytoskeleton and cell morphology. *Nature Structural and Molecular Biology* **12**: 772–778.

Grundmann, A. and Li, S.-M. (2005). Overproduction, purification and characterization of FtmPT1, a brevianamide F prenyltransferase from *Aspergillus fumigatus*. *Microbiology* **151**: 2199–2207.

Gründemann, D. (2012). The ergothioneine transporter controls and indicates ergothioneine activity--a review. *Preventive Medicine* **54 Suppl**: S71–4.

Gründemann, D., Harlfinger, S., Golz, S., Geerts, A., Lazar, A., Berkels, R., Jung, N., Rubbert, A. and Schömig, E. (2005). Discovery of the ergothioneine transporter. *Proc. Natl. Acad. Sci. U. S. A.* **102**: 5256–5261.

Gstaiger, M. and Aebersold, R. (2009). Applying mass spectrometry-based proteomics to genetics, genomics and network biology. *Nature Reviews. Genetics* **10**: 617–627.

Guetsova, M.L., Crother, T.R., Taylor, M.W. and Daignan-Fornier, B. (1999). Isolation and Characterization of the *Saccharomyces cerevisiae* XPT1 Gene Encoding Xanthine Phosphoribosyl Transferase. *Journal of Bacteriology* **181**: 2984.

Guillemette, T., Peij, N.N.M.E. Van, Goosen, T., Lanthaler, K., Robson, G.D., Van den Hondel, C.A., Stam, H. and Archer, D.B. (2007). Genomic analysis of the secretion stress response in the enzyme-producing cell factory *Aspergillus niger*. *BMC Genomics* **8**: 158–175.

Guthke, R., Möller, U., Hoffmann, M., Thies, F. and Töpfer, S. (2005). Dynamic network reconstruction from gene expression data applied to immune response during bacterial infection. *Bioinformatics* **21**: 1626–1634.

Haas, H. (2012). Iron - A Key Nexus in the Virulence of Aspergillus fumigatus. *Front. Microbiol.* **3**: 28.

Hafen, G.M., Hartl, D., Regamey, N., Casaulta, C. and Latzin, P. (2009). Allergic bronchopulmonary aspergillosis: the hunt for a diagnostic serological marker in cystic fibrosis patients. *Expert Review of Molecular Diagnostics* **9**: 157–164.

Hagag, S., Kubitschek-Barreira, P., Neves, G.W.P., Amar, D., Nierman, W., Shalit, I., Shamir, R., Lopes-Bezerra, L. and Osherov, N. (2012). Transcriptional and Proteomic Analysis of the *Aspergillus fumigatus* Δ*prtT* Protease-Deficient Mutant. *PLoS ONE* **7**: e33604.

Halket, J.M., Waterman, D., Przyborowska, A.M., Patel, R.K.P., Fraser, P.D. and Bramley, P.M. (2005). Chemical derivatization and mass spectral libraries in metabolic profiling by GC/MS and LC/MS/MS. *Journal of Experimental Botany* **56**: 219–243.

Hall, T.A. (1999). BioEdit: a user-friendly biological sequence alignment editor and analysis program for Windows 95/98/NT. *Nucleic Acids Symposium Series* **41**: 95–98.

Han, X., Gross, R.W., Introduction, I. and Marzo, D. (2005). Shotgun Lipidomics : Electrospray Ionization Mass Spectrometric Analysis and Quantitation of Cellular Lipidomes Direactly From Crude Extracts of Biological Samples. *Mass Spectrometry Reviews* **24**: 367–412.

Hand, C.E. and Honek, J.F. (2005). Biological chemistry of naturally occurring thiols of microbial and marine origin. *Journal of Natural Products* **68**: 293–308.

Hand, C.E., Taylor, N.J. and Honek, J.F. (2005). Ab initio studies of the properties of intracellular thiols ergothioneine and ovothiol. *Bioorganic & Medicinal Chemistry Letters* **15**: 1357–1360.

Hao, W., Pan, Y.-X., Ding, Y.-Q., Xiao, S., Yin, K., Wang, Y.-D., Qiu, L.-W., Zhang, Q.-L., Woo, P.C.Y., Lau, S.K.P., Yuen, K.-Y. and Che, X.-Y. (2008). Well-characterized monoclonal antibodies against cell wall antigen of *Aspergillus* species improve immunoassay specificity and sensitivity. *CVI* **15**: 194–202.

Harder, A., Wildgruber, R., Nawrocki, A., Fey, S.J., Larsen, P.M. and Görg, A. (1999). Comparison of yeast cell protein solubilization procedures for two-dimensional electrophoresis. *Electrophoresis* **20**: 826–829.

Hartl, L., Zach, S. and Seidl-Seiboth, V. (2012). Fungal chitinases: diversity, mechanistic properties and biotechnological potential. *Applied Microbiology and Biotechnology* **93**: 533–543.

Hartmann, T., Cairns, T.C., Olbermann, P., Morschhäuser, J., Bignell, E.M. and Krappmann, S. (2011). Oligopeptide transport and regulation of extracellular proteolysis are required for growth of *Aspergillus fumigatus* on complex substrates but not for virulence. *Molecular Microbiology* **82**: 917–935.

Henriet, S.S. V, Verweij, P.E. and Warris, A. (2012). *Aspergillus nidulans* and Chronic Granulomatous Disease: A Unique Host-Pathogen Interaction. *J. Infect. Dis.* **206**: 1128–1137.

Herbrecht, R., Denning, D.W., Patterson, T.F., Bennett, J.E., Greene, R.E., Oestmann, J.-W., Kern, W. V, Marr, K.A., Ribaud, P., Lortholary, O., Sylvester, R., Rubin, R.H., Wingard, J.R., Stark, P., Durand, C., Caillot, D., Thiel, E., Chandrasekar, P.H., Hodges, M.R., Schlamm, H.T., Troke, P.F. and De Pauw, B. (2002). Voriconazole versus Amphotericin B for Primary Therapy of Invasive Aspergillosis. *N. Engl. J. Med.* **347**: 408–415.

Herbrecht, R., Maertens, J., Baila, L., Aoun, M., Heinz, W., Martino, R., Schwartz, S., Ullmann, a J., Meert, L., Paesmans, M., Marchetti, O., Akan, H., Ameye, L., Shivaprakash, M. and Viscoli, C. (2010). Caspofungin first-line therapy for invasive aspergillosis in allogeneic hematopoietic stem cell transplant patients: an European Organisation for Research and Treatment of Cancer study. *Bone Marrow. Transplant.* **45**: 1227–1233.

Hercus, T.R., Broughton, S.E., Ekert, P.G., Ramshaw, H.S., Perugini, M., Grimbaldeston, M., Woodcock, J.M., Thomas, D., Pitson, S., Hughes, T., D'Andrea, R.J., Parker, M.W. and Lopez, A.F. (2012). The GM-CSF receptor family: mechanism of activation and implications for disease. *Growth Factors* **30**: 63–75.

Hernández, O., Almeida, A.J., Gonzalez, A., Garcia, A.M., Tamayo, D., Cano, L.E., Mcewen, J.G., Herna, O. and Restrepo, A. (2010). A 32-Kilodalton Hydrolase Plays an Important Role in *Paracoccidioides brasiliensis* Adherence to Host Cells and Influences Pathogenicity. *Infect. Immun.* **78**: 5280–5286.

Hohl, T.M., Van Epps, H.L., Rivera, A., Morgan, L. a, Chen, P.L., Feldmesser, M. and Pamer, E.G. (2005). *Aspergillus fumigatus* triggers inflammatory responses by stage-specific beta-glucan display. *PLoS Pathogens* **1**: e30.

Hope, W.W., Walsh, T.J. and Denning, D.W. (2005). Laboratory diagnosis of invasive aspergillosis. *Lancet Infect. Dis.* **5**: 609–622.

Horn, F., Heinekamp, T., Kniemeyer, O., Pollmächer, J., Valiante, V. and Brakhage, A.A. (2012). Systems biology of fungal infection. *Frontiers in Microbiology* **3**: 108.

Hortschansky, P., Eisendle, M., Al-Abdallah, Q., Schmidt, A.D., Bergmann, S., Thön, M., Kniemeyer, O., Abt, B., Seeber, B., Werner, E.R., Kato, M., Brakhage, A.A. and Haas, H. (2007). Interaction of HapX with the CCAAT-binding complex--a novel mechanism of gene regulation by iron. *The EMBO Journal* **26**: 3157–3168.

Howard, S.J., Webster, I., Moore, C.B., Gardiner, R.E., Park, S., Perlin, D.S. and Denning, D.W. (2006). Multi-azole resistance in *Aspergillus fumigatus*. *Int. J. Antimicrob. Agents* **28**: 450–453.

Hurne, A.M., Chai, C.L.L. and Waring, P. (2000). Inactivation of Rabbit Muscle Creatine Kinase by Reversible Formation of an Internal Disulfide Bond Induced by the Fungal Toxin Gliotoxin. *J. Biol. Chem.* **275**: 25202–25206.

Ibrahim-Granet, O., Philippe, B., Boleti, H., Boisvieux-Ulrich, E., Grenet, D., Stern, M. and Latge, J.P. (2003). Phagocytosis and Intracellular Fate of *Aspergillus fumigatus* Conidia in Alveolar Macrophages. *Infect. Immun.* **71**: 891–903.

Ishikawa, M., Ninomiya, T., Akabane, H., Kushida, N., Tsujiuchi, G., Ohyama, M., Gomi, S., Shito, K. and Murata, T. (2009). Pseurotin A and its analogues as inhibitors of immunoglobulin E production. *Bioorg. Med. Chem. Lett.* **19**: 1457–1460.

Jackson, R.J., Hellen, C.U.T. and Pestova, T. V (2010). The mechanism of eukaryotic translation initiation and principles of its regulation. *Nature Reviews. Molecular Cell Biology* **11**: 113–127.

Jain, R., Valiante, V., Remme, N., Docimo, T., Heinekamp, T., Hertweck, C., Gershenzon, J., Haas, H. and Brakhage, A.A. (2011). The MAP kinase MpkA controls cell wall integrity, oxidative stress response, gliotoxin production and iron adaptation in Aspergillus fumigatus. *Mol. Microbiol.* **82**: 39–53.

Jarque, I., Tormo, M., Bello, J.L., Rovira, M., Batlle, M., Julia, A., Tabares, S., Rivas, C., Capote, F.J. and Sanz, M.A. (2012). Caspofungin for the treatment of invasive fungal disease in hematological patients (ProCAS Study). *Med. Mycol.* 1–5.

Jayaram, P.N., Roy, G. and Mugesh, G. (2008). Effect of thione—thiol tautomerism on the inhibition of lactoperoxidase by anti-thyroid drugs and their analogues. *Journal of Chemical Sciences* **120**: 143–154.

Jeans, A.R., Howard, S.J., Al-Nakeeb, Z., Goodwin, J., Gregson, L., Warn, P. a and Hope, W.W. (2012). Combination of voriconazole and anidulafungin for the treatment of triazole resistant *Aspergillus fumigatus* in an in vitro model of invasive pulmonary aspergillosis. *Antimicrob. Agents Chemother.* **56**: 5180–5185.

Jegorov, A., Hajduch, M., Sulc, M. and Havlicek, V. (2006). Nonribosomal cyclic peptides : specific markers of fungal infections. *J. Mass Spectrom.* **41**: 563–576.

Johnson, G.L., Bibby, D.F., Wong, S., Agrawal, S.G. and Bustin, S.A. (2012). A MIQE-Compliant Real-Time PCR Assay for Aspergillus Detection. *PLoS ONE* **7**: e40022.

Johnson, L.B. and Kauffman, C.A. (2003). Voriconazole: a new triazole antifungal agent. *Clin. Infect. Dis.* **36**: 630–637.

Jørgensen, T.R., Goosen, T., Van den Hondel, C.A., Ram, A.F.J. and Iversen, J.J.L. (2009). Transcriptomic comparison of *Aspergillus niger* growing on two different sugars reveals coordinated regulation of the secretory pathway. *BMC Genomics* **10**: 44.

Kacprzak, M.M., Lewandowska, I., Matthews, R.G. and Paszewski, A. (2003). Transcriptional regulation of methionine synthase by homocysteine and choline in *Aspergillus nidulans*. *The Biochemical Journal* **376**: 517–524.

Kall, L., Krogh, A. and Sonnhammer, E.L.L. (2004). A Combined Transmembrane Topology and Signal Peptide Prediction Method. *J. Mol. Biol.* **338**: 1027–1036.

Kaloriti, D., Tillmann, A., Cook, E., Jacobsen, M., You, T., Lenardon, M., Ames, L., Barahona, M., Chandrasekaran, K., Coghill, G., Goodman, D., Gow, N.A.R., Grebogi, C., Ho, H.-L., Ingram, P., McDonagh, A., Moura, A.P.S. De, Pang, W., Puttnam, M., Radmaneshfar, E., Romano, M.C., Silk, D., Stark, J., Stumpf, M., Thiel, M., Thorne, T., Usher, J., Yin, Z., Haynes, K. and Brown, A.J.P. (2012). Combinatorial stresses kill pathogenic *Candida* species. *Medical Mycology* **50**: 699–709.

Kanai, M., Masuda, M., Takaoka, Y., Ikeda, H., Masaki, K., Fujii, T. and Iefuji, H. (2012). Adenosine kinase-deficient mutant of *Saccharomyces cerevisiae* accumulates S-adenosylmethionine because of an enhanced methionine biosynthesis pathway. *Appl. Microbiol. Biotechnol.* 1–8.

Kanehisa, M., Goto, S., Sato, Y., Furumichi, M. and Tanabe, M. (2012). KEGG for intergration and interpretation of large-scale molecular data sets. *Nucleic Acids Research* **40**: D109–D114.

Kapp, L.D. and Lorsch, J.R. (2004). The molecular mechanics of eukaryotic translation. *Annual Review of Biochemistry* **73**: 657–704.

Karas, M., Gluckmann, M. and Schafer, J. (2000). Ionization in matrix-assisted laser desorption / ionization : singly charged molecular ions are the lucky survivors. *J. Mass Spectrom.* **35**: 1–12.

Karas, M. and Hillenkamp, F. (1988). Laser Desorption Ionization of Proteins with Molecular Masses Exceeding 10 000 Daltons. *Analytical Chemistry* **60**: 2299–2301.

Kartsonis, N.A., Saah, A.J., Joy Lipka, C., Taylor, A.F. and Sable, C. a (2005). Salvage therapy with caspofungin for invasive aspergillosis: results from the caspofungin compassionate use study. *J. Infect.* **50**: 196–205.

Kato, N., Suzuki, H., Takagi, H., Uramoto, M., Takahashi, S. and Osada, H. (2011). Gene disruption and biochemical characterization of verruculogen synthase of *Aspergillus fumigatus*. *Chembiochem* **12**: 711–714.

Kaul, G., Pattan, G. and Rafeequi, T. (2011). Eukaryotic elongation factor-2 (eEF2): its regulation and peptide chain elongation. *Cell Biochemistry and Function* **29**: 227–234.

Kawamura, S., Maesaki, S., Tomono, K., Tashiro, T. and Kohno, S. (2000). Clinical evaluation of 61 patients with pulmonary aspergilloma. *Internal Medicine* **39**: 209–212.

Kazakevich, Y. V. and LoBrutto, R. (2007). HPLC for Pharmaceutical Scientists (Wiley).

Keidel, E.-M., Ribitsch, D. and Lottspeich, F. (2010). Equalizer technology--Equal rights for disparate beads. *Proteomics* **10**: 2089–2098.

Keller, N., Bok, J., Chung, D., Perrin, R.M. and Keats Shwab, E. (2006). LaeA, a global regulator of *Aspergillus* toxins. *Med. Mycol.* **44**: 83–85.

Keller, N.P., Turner, G. and Bennett, J.W. (2005). Fungal secondary metabolism - from biochemistry to genomics. *Nat. Rev. Microbiol.* **3**: 937–947.

Khaldi, N., Seifuddin, F.T., Turner, G., Haft, D., Nierman, W.C., Wolfe, K.H. and Fedorova, N.D. (2010). SMURF: genomic mapping of fungal secondary metabolite clusters. *Fungal Genet. Biol.* **47**: 736–741.

Khoufache, K., Puel, O., Loiseau, N., Delaforge, M., Rivollet, D., Coste, A., Cordonnier, C., Escudier, E., Botterel, F. and Bretagne, S. (2007). Verruculogen associated with *Aspergillus fumigatus* hyphae and conidia modifies the electrophysiological properties of human nasal epithelial cells. *BMC Microbiology* **7**: 5.

Kikuchi, K. and Kakeya, H. (2006). A bridge between chemistry and biology. *Nature Chemical Biology* **2**: 392–394.

Kim, Y., Nandakumar, M.P. and Marten, M.R. (2007). Proteomics of filamentous fungi. *Trends in Biotechnology* **25**: 395–400.

Kleijn, R.J., Van Winden, W. a, Van Gulik, W.M. and Heijnen, J.J. (2005). Revisiting the ^{13}C-label distribution of the non-oxidative branch of the pentose phosphate pathway based upon kinetic and genetic evidence. *The FEBS Journal* **272**: 4970–4982.

Kleinberg, M. (2006). What is the current and future status of conventional amphotericin B? *Int. J. Antimicrob. Agents* **27 Suppl 1**: 12–16.

Kniemeyer, O. (2011). Proteomics of eukaryotic microorganisms: The medically and biotechnologically important fungal genus *Aspergillus*. *Proteomics* **11**: 1–12.

Kniemeyer, O., Lessing, F., Scheibner, O., Hertweck, C. and Brakhage, A.A. (2006). Optimisation of a 2-D gel electrophoresis protocol for the human-pathogenic fungus *Aspergillus fumigatus*. *Current Genetics* **49**: 178–189.

Kniemeyer, O., Schmidt, A.D., Vödisch, M., Wartenberg, D. and Brakhage, A.A. (2011). Identification of virulence determinants of the human pathogenic fungi Aspergillus fumigatus and Candida albicans by proteomics. *International Journal of Medical Microbiology* **301**: 368–377.

Knutsen, A.P. (2006). Genetic and respiratory tract risk factors for aspergillosis: ABPA and asthma with fungal sensitization. *Med. Mycol.* **44**: 61–70.

Knutsen, A.P. and Slavin, R.G. (2011). Allergic bronchopulmonary aspergillosis in asthma and cystic fibrosis. *Clinical and Developmental Immunology* **2011**: 843763.

Kontoyiannis, D.P. (2012). Invasive mycoses: strategies for effective management. *Am. J. Med.* **125**: S25–38.

Kosalec, I., Pepeljnjak, S. and Jandrlic, M. (2005). Influence of Media and Temperature on Gliotoxin Production in *Aspergillus fumigatus* Strains. *Arhiv Za Higijenu Rada I Toksikologiju* **56**: 269–273.

Kradin, R.L. and Mark, E.J. (2008). The pathology of pulmonary disorders due to *Aspergillus* spp. *Arch. Pathol. Lab. Med.* **132**: 606–614.

Kraemer, R., Deloséa, N., Ballinari, P., Gallati, S. and Crameri, R. (2006). Effect of allergic bronchopulmonary aspergillosis on lung function in children with cystic fibrosis. *Am. J. Respir. Crit. Care. Med.* **174**: 1211–1220.

Krah, A. and Jungblut, P.R. (2004). Immunoproteomics. In Molecular Diagnosis of Infectious Diseases, J. Decker, and U. Reischl, eds. (Springer), pp. 19–33 ISBN: 1592596797, 9781592596799.

Kremer, A., Westrich, L. and Li, S.-M. (2007). A 7-dimethylallyltryptophan synthase from *Aspergillus fumigatus*: overproduction, purification and biochemical characterization. *Microbiology* **153**: 3409–3416.

Ku, N.S., Han, S.H., Choi, J.Y., Kim, S.B., Kim, H.-W., Jeong, S.J., Kim, C.O., Song, Y.G. and Kim, J.M. (2012). Diagnostic value of the serum galactomannan assay for invasive aspergillosis: It is less useful in non-haematological patients. *Scand. J. Infect. Dis.* **44**: 600–604.

Kubodera, T., Yamashita, N. and Nishimura, A. (2000). Pyrithiamine Resistance Gene (*ptrA*) of *Aspergillus oryzae*: Cloning, Characterization and Application as a Dominant Selectable Marker for Transformation. *Bioscience, Biotechnology, and Biochemistry* **64**: 1416.

Kuge, S., Jones, N. and Nomoto, a (1997). Regulation of yAP-1 nuclear localization in response to oxidative stress. *The EMBO Journal* **16**: 1710–1720.

Kumar, A., Ahmed, R., Singh, P.K. and Shukla, P.K. (2011). Identification of virulence factors and diagnostic markers using immunosecretome of Aspergillus fumigatus. *J. Protemics* **74**: 1104–1112.

Kupfahl, C., Heinekamp, T., Geginat, G., Ruppert, T., Härtl, A., Hof, H. and Brakhage, A.A. (2006). Deletion of the gliP gene of *Aspergillus fumigatus* results in loss of gliotoxin production but has no effect on virulence of the fungus in a low-dose mouse infection model. *Mol. Microbiol.* **62**: 292–302.

Kurup, V.P., Knutsen, A.P., Moss, R.B. and Bansal, N.K. (2006). Specific antibodies to recombinant allergens of *Aspergillus fumigatus* in cystic fibrosis patients with ABPA. *Clinical and Molecular Allergy : CMA* **4**: 11.

Kwon-Chung, K.J. and Sugui, J.A. (2009). What do we know about the role of gliotoxin in the pathobiology of *Aspergillus fumigatus*? *Med. Mycol.* **47**: 1–12.

Lai, E., Teodoro, T. and Volchuk, A. (2007). Endoplasmic reticulum stress: signaling the unfolded protein response. *Physiology* **22**: 193–201.

Lamarre, C., Sokol, S., Debeaupuis, J.-P., Henry, C., Lacroix, C., Glaser, P., Coppée, J.-Y., François, J.-M. and Latgé, J.-P. (2008). Transcriptomic analysis of the exit from dormancy of *Aspergillus fumigatus* conidia. *BMC Genomics* **9**: 417.

Lara-Rojas, F., Sánchez, O., Kawasaki, L. and Aguirre, J. (2011). *Aspergillus nidulans* transcription factor AtfA interacts with the MAPK SakA to regulate general stress responses, development and spore functions. *Mol. Microbiol.* **80**: 436–454.

Latge, J. (1999). *Aspergillus fumigatus* and Aspergillosis. *Clin. Microbiol. Rev.* **12**: 310–350.

Latgé, J.P., Kobayashi, H., Debeaupuis, J.P., Diaquin, M., Sarfati, J., Wieruszeski, J.M., Parra, E., Bouchara, J.P. and Fournet, B. (1994). Chemical and immunological characterization of the extracellular galactomannan of *Aspergillus fumigatus*. *Infect. Immun.* **62**: 5424–5433.

Leclerc, D. and Rozen, R. (2008). Endoplasmic reticulum stress increases the expression of methylenetetrahydrofolate reductase through the IRE1 transducer. *The Journal of Biological Chemistry* **283**: 3151–3160.

Lee, I., Oh, J., Shwab, E.K., Dagenais, T.R.T., Andes, D. and Keller, N.P. (2009a). HdaA, a class 2 histone deacetylase of *Aspergillus fumigatus*, affects germination and secondary metabolite production. *Fungal Genet. Biol.* **46**: 782–790.

Lee, W.Y., Park, E.-J. and Ahn, J.K. (2009b). Supplementation of methionine enhanced the ergothioneine accumulation in the *Ganoderma neo-japonicum* mycelia. *Applied Biochemistry and Biotechnology* **158**: 213–221.

Lee, W.Y., Park, E.-J., Ahn, J.K. and Ka, K.-H. (2009c). Ergothioneine Contents in Fruiting Bodies and Their Enhancement in Mycelial Cultures by the Addition of Methionine. *Mycobiology* **37**: 43.

Lehrnbecher, T., Tramsen, L., Koehl, U., Schmidt, S., Bochennek, K. and Klingebiel, T. (2011). Immunotherapy against invasive fungal diseases in stem cell transplant recipients. *Immunol. Investig.* **40**: 839–852.

Lei, Z., Huhman, D. V and Sumner, L.W. (2011). Mass spectrometry strategies in metabolomics. *The Journal of Biological Chemistry* **286**: 25435–25442.

Lemke, A., Kiderlen, A.F. and Kayser, O. (2005). Amphotericin B. *Appl. Microbiol. Biotechnol.* **68**: 151–162.

Lessing, F., Kniemeyer, O., Wozniok, I., Loeffler, J., Kurzai, O., Haertl, A. and Brakhage, A.A. (2007). The *Aspergillus fumigatus* transcriptional regulator AfYap1 represents the major regulator for defense against reactive oxygen intermediates but is dispensable for pathogenicity in an intranasal mouse infection model. *Eukaryot. Cell* **6**: 2290–2302.

Letscher-Bru, V. (2003). Caspofungin: the first representative of a new antifungal class. *J. Antimicrob. Chemother.* **51**: 513–521.

Levitz, S.M. and Farrell, T.P. (1990). Human neutrophil degranulation stimulated by *Aspergillus fumigatus*. *J. Leukoc. Biol.* **47**: 170–175.

Li, B. and Walsh, C.T. (2011). Streptomyces clavuligerus HlmI is an intramolecular disulfide- forming dithiol oxidase in holomycin biosynthesis. *Biochemistry* **50**: 4615–4622.

Ligr, M., Velten, I., Fröhlich, E., Madeo, F., Ledig, M., Fröhlich, K.U., Wolf, D.H. and Hilt, W. (2001). The proteasomal substrate Stm1 participates in apoptosis-like cell death in yeast. *Molecular Biology of the Cell* **12**: 2422–2432.

Lin, S.-J. and Guarente, L. (2003). Nicotinamide adenine dinucleotide, a metabolic regulator of transcription, longevity and disease. *Curr. Opin. Cell Biol.* **15**: 241–246.

Lin, S.S., Bassik, M.C., Suh, H., Nishino, M., Arroyo, J.D., Hahn, W.C., Korsmeyer, S.J. and Roberts, T.M. (2006). PP2A regulates BCL-2 phosphorylation and proteasome-mediated degradation at the endoplasmic reticulum. *The Journal of Biological Chemistry* **281**: 23003–23012.

Link, A.J., Eng, J., Schieltz, D.M., Carmack, E., Mize, G.J., Morris, D.R., Garvik, B.M. and Yates, J.R. (1999). Direct analysis of protein complexes using mass spectrometry. *Nature Biotechnology* **17**: 676–682.

Liu, S., Milne, G.T., Kuremsky, J.G., Fink, G.R. and Leppla, S.H. (2004). Identification of the Proteins Required for Biosynthesis of Diphthamide , the Target of Bacterial ADP-Ribosylating Toxins on Translation Elongation Factor 2 †. *Mol. Cell. Biol.* **24**: 9487–9497.

Lodeiro, S., Xiong, Q., Wilson, W.K., Ivanova, Y., Smith, M.L., May, G.S. and Matsuda, S.P.T. (2009). Protostadienol biosynthesis and metabolism in the pathogenic fungus *Aspergillus fumigatus*. *Org. Lett.* **11**: 1241–1244.

Losada, L., Ajayi, O., Frisvad, J.C., Yu, J. and Nierman, W.C. (2009). Effect of competition on the production and activity of secondary metabolites in *Aspergillus species*. *Med. Mycol.* **47 Suppl 1**: S88–96.

Lu, X., Sun, J., Nimtz, M., Wissing, J., Zeng, A.-P. and Rinas, U. (2010). The intra- and extracellular proteome of *Aspergillus niger* growing on defined medium with xylose or maltose as carbon substrate. *Microbial Cell Factories* **9**: 23.

Lubec, G., Afjehi-Sadat, L., Yang, J.-W. and John, J.P.P. (2005). Searching for hypothetical proteins: theory and practice based upon original data and literature. *Progress in Neurobiology* **77**: 90–127.

Lundqvist, M., Stigler, J., Elia, G., Lynch, I., Cedervall, T. and Dawson, K.A. (2008). Nanoparticle size and surface properties determine the protein corona with possible implications for biological impacts. *Proc. Natl. Acad. Sci. U. S. A.* **105**: 14265–14270.

Ma, J.E., Yun, E.Y., Kim, Y.E., Lee, G.D., Cho, Y.J., Jeong, Y.Y., Jeon, K.-N., Jang, I.S., Kim, H.C., Lee, J.D. and Hwang, Y.S. (2011). Endobronchial aspergilloma: report of 10 cases and literature review. *Yonsei Medical Journal* **52**: 787–792.

Maaheimo, H., Fiaux, J., Cakar, P., Bailey, J.E., Sauer, U. and Szyperski, T. (2001). Central carbon metabolism of *Saccharomyces cerevisiae* explored by biosyntheric fractional ^{13}C labeling of common amino acids. *European Journal of Biochemistry / FEBSr* **268**: 2464–2479.

Mabey, J.E., Anderson, M.J., Giles, P.F., Miller, C.J., Attwood, T.K., Paton, N.W., Bornberg-Bauer, E., Robson, G.D., Oliver, S.G. and Denning, D.W. (2004). CADRE: the Central *Aspergillus* Data REpository. *Nucleic Acids Research* **32**: D401–5.

MacFarlane, A.J., Liu, X., Perry, C.A., Flodby, P., Allen, R.H., Stabler, S.P. and Stover, P.J. (2008). Cytoplasmic Serine Hydroxymethyltransferase Regulates the Metabolic Partitioning of Methylenetetrahydrofolate but Is Not Essential in Mice. *J. Biol. Chem.* **283**: 25846–25853.

Machida, M., Asai, K., Sano, M., Tanaka, T., Kumagai, T., Terai, G., Kusumoto, K.-I., Arima, T., Akita, O., Kashiwagi, Y., Abe, K., Gomi, K., Horiuchi, H., *et al.* (2005). Genome sequencing and analysis of *Aspergillus oryzae*. *Nature* **438**: 1157–1161.

Maertens, J., Egerer, G., Shin, W.S., Reichert, D., Stek, M., Chandwani, S., Shivaprakash, M. and Viscoli, C. (2010). Caspofungin use in daily clinical practice for treatment of invasive aspergillosis: results of a prospective observational registry. *BMC Infect. Dis.* **10**: 182.

Maertens, J., Raad, I., Petrikkos, G., Boogaerts, M., Selleslag, D., Petersen, F.B., Sable, C.A., Kartsonis, N.A., Ngai, A., Taylor, A., Patterson, T.F., Denning, D.W. and Walsh, T.J. (2004). Efficacy and safety of caspofungin for treatment of invasive aspergillosis in patients refractory to or intolerant of conventional antifungal therapy. *Clin. Infect. Dis.* **39**: 1563–1571.

Maertens, J., Theunissen, K. and Boogaerts, M. (2002). Invasive Aspergillosis : Focus on New Approaches and New Therapeutic Agents. *Curr. Med. Chem.* **1**: 65–81.

Maertens, J., Theunissen, K., Lodewyck, T., Lagrou, K. and Van Eldere, J. (2007). Advances in the serological diagnosis of invasive *Aspergillus infections* in patients with haematological disorders. *Mycoses* **50 Suppl 1**: 2–17.

Maiya, S., Grundmann, A., Li, S.-M. and Turner, G. (2006). The fumitremorgin gene cluster of *Aspergillus fumigatus*: identification of a gene encoding brevianamide F synthetase. *Chembiochem : a European Journal of Chemical Biology* **7**: 1062–1069.

Maiya, S., Grundmann, A., Li, X., Li, S.-M. and Turner, G. (2007). Identification of a hybrid PKS/NRPS required for pseurotin A biosynthesis in the human pathogen *Aspergillus fumigatus*. *Chembiochem* **8**: 1736–1743.

Marques, M., Mojzita, D., Amorim, M.A., Almeida, T., Hohmann, S., Moradas-Ferreira, P. and Costa, V. (2006). The Pep4p vacuolar proteinase contributes to the turnover of oxidized proteins but PEP4 overexpression is not sufficient to increase chronological lifespan in *Saccharomyces cerevisiae*. *Microbiology* **152**: 3595–3605.

Marr, K. a, Laverdiere, M., Gugel, A. and Leisenring, W. (2005). Antifungal therapy decreases sensitivity of the *Aspergillus* galactomannan enzyme immunoassay. *Clin. Infect. Dis.* **40**: 1762–1769.

Mazandu, G.K. and Mulder, N.J. (2012). Function Prediction and Analysis of *Mycobacterium tuberculosis* Hypothetical Proteins. *International Journal of Molecular Sciences* **13**: 7283–7302.

McCormick, A., Loeffler, J. and Ebel, F. (2010). *Aspergillus fumigatus*: contours of an opportunistic human pathogen. *Cell. Microbiol.* **12**: 1535–1543.

McDonagh, A., Fedorova, N.D., Crabtree, J., Yu, Y., Kim, S., Chen, D., Loss, O., Cairns, T., Goldman, G., Armstrong-James, D., Haynes, K., Haas, H., Schrettl, M.,

May, G., Nierman, W.C. and Bignell, E. (2008). Sub-telomere directed gene expression during initiation of invasive aspergillosis. *PLoS Pathogens* **4**: e1000154.

Mennink-Kersten, M.A.S.H., Ruegebrink, D., Klont, R.R., Warris, A., Blijlevens, N.M.A., Donnelly, J.P. and Verweij, P.E. (2008). Improved detection of circulating *Aspergillus* antigen by use of a modified pretreatment procedure. *Journal of Clinical Microbiology* **46**: 1391–1397.

Millioni, R., Tolin, S., Puricelli, L., Sbrignadello, S., Fadini, G.P., Tessari, P. and Arrigoni, G. (2011). High abundance proteins depletion vs low abundance proteins enrichment: comparison of methods to reduce the plasma proteome complexity. *PloS One* **6**: e19603.

Mishra, A.K., Gangwani, L., Davis, R.J. and Lambright, D.G. (2007). Structural insights into the interaction of the evolutionarily conserved ZPR1 domain tandem with eukaryotic EF1A, receptors, and SMN complexes. *Proc. Natl. Acad. Sci. U. S. A.* **104**: 13930–13935.

Mitsuguchi, H., Seshime, Y., Fujii, I., Shibuya, M., Ebizuka, Y. and Kushiro, T. (2009). Biosynthesis of steroidal antibiotic fusidanes: functional analysis of oxidosqualene cyclase and subsequent tailoring enzymes from *Aspergillus fumigatus*. *J. Am. Chem. Soc.* **131**: 6402–6411.

Morton, C.O., Varga, J.J., Hornbach, A., Mezger, M., Sennefelder, H., Kneitz, S., Kurzai, O., Krappmann, S., Einsele, H., Nierman, W.C., Rogers, T.R. and Loeffler, J. (2011). The Temporal Dynamics of Differential Gene Expression in *Aspergillus fumigatus* Interacting with Human Immature Dendritic Cells In Vitro. *PLoS ONE* **6**: e16016.

Murdock, B.J., Shreiner, A.B., McDonald, R. a, Osterholzer, J.J., White, E.S., Toews, G.B. and Huffnagle, G.B. (2011). Coevolution of TH1, TH2, and TH17 responses during repeated pulmonary exposure to *Aspergillus fumigatus* conidia. *Infect. Immun.* **79**: 125–135.

Murray, D.B., Haynes, K. and Tomita, M. (2011). Redox regulation in respiring *Saccharomyces cerevisiae*. *BBA - General Subjects* **1810**: 945–958.

Muschik, G.M. and Veenstra, T.D. (2009). Analytical and statistical approaches to metabolomics research. *Journal of Separation Science* **32**: 2183–2199.

Ndez, O.H.Á., Almeida, A.J., Tamayo, D., Torres, I., Garcia, A.N.A.M., Pez, A.L.Ó., Restrepo, A. and Ewen, J.G.M.C. (2012). The hydrolase PbHAD32 participates in the adherence of *Paracoccidioides brasiliensis* conidia to epithelial lung cells. *Med. Mycol.* **50**: 533–537.

Neustadt, M., Costina, V., Kupfahl, C., Buchheidt, D., Eckerskorn, C., Neumaier, M. and Findeisen, P. (2009). Characterization and identification of proteases secreted by

Aspergillus fumigatus using free flow electrophoresis and MS. *Electrophoresis* **30**: 2142–2150.

Nierman, W.C., Pain, A., Anderson, M.J., Wortman, J.R., Kim, H.S., Arroyo, J., Berriman, M., Abe, K., Archer, D.B., Bermejo, C., Bennett, J., Bowyer, P., Chen, D., *et al.* (2005). Genomic sequence of the pathogenic and allergenic filamentous fungus *Aspergillus fumigatus*. *Nature* **438**: 1151–1156.

Nikodemus, D., Lazic, D., Bach, M., Bauer, T., Pfeiffer, C., Wiltzer, L., Lain, E., Schomig, E. and Grundmann, D. (2011). Paramount Levels of Ergothioneine Transporter SLC22A4 mRNA in Boar Seminal Vesicles and Cross-Species Analysis of Ergothioneine and Glutathione in Seminal Plasma. *J. Physiol. Pharmacol.* **62**: 411–419.

Nishida, S., Yoshida, L.S., Shimoyama, T., Nunoi, H., Kobayashi, T. and Tsunawaki, S. (2005). Fungal Metabolite Gliotoxin Targets Flavocytochrome b 558 in the Activation of the Human Neutrophil NADPH Oxidase. *Infect. Immun.* **73**: 235–244.

Nivoix, Y., Velten, M., Letscher-Bru, V., Moghaddam, A., Natarajan-Amé, S., Fohrer, C., Lioure, B., Bilger, K., Lutun, P., Marcellin, L., Launoy, A., Freys, G., Bergerat, J.-P. and Herbrecht, R. (2008). Factors associated with overall and attributable mortality in invasive aspergillosis. *Clin. Infect. Dis.* **47**: 1176–1184.

Nosanchuk, J.D. and Casadevall, A. (2006). Impact of melanin on microbial virulence and clinical resistance to antimicrobial compounds. *Antimicrob. Agents Chemother.* **50**: 3519–3528.

Oakley, A.J., Coggan, M. and Board, P.G. (2010). Identification and characterization of gamma-glutamylamine cyclotransferase, an enzyme responsible for gamma-glutamyl-epsilon-lysine catabolism. *The Journal of Biological Chemistry* **285**: 9642–9648.

Oakley, A.J., Yamada, T., Liu, D., Coggan, M., Clark, A.G. and Board, P.G. (2008). The identification and structural characterization of C7orf24 as gamma-glutamyl cyclotransferase. An essential enzyme in the gamma-glutamyl cycle. *The Journal of Biological Chemistry* **283**: 22031–22042.

Okada, K., Hashimoto, S. and Imaoka, S. (2010). Biological Functions of Protein Disulfide Isomerase as a Target of Phenolic Endocrine-disrupting Chemicals. *J. Health Sci.* **56**: 1–13.

Old, W.M., Meyer-Arendt, K., Aveline-Wolf, L., Pierce, K.G., Mendoza, A., Sevinsky, J.R., Resing, K. a and Ahn, N.G. (2005). Comparison of label-free methods for quantifying human proteins by shotgun proteomics. *Molecular & Cellular Proteomics* **4**: 1487–1502.

Ong, S.-E., Blagoev, B., Kratchmarova, I., Kristensen, D.B., Steen, H., Pandey, A. and Mann, M. (2002). Stable Isotope Labeling by Amino Acids in Cell Culture, SILAC, as a Simple and Accurate Approach to Expression Proteomics. *Mol. Cell. Proteomics* **1**: 376–386.

Oosthuizen, J.L., Gomez, P., Ruan, J., Hackett, T.L., Moore, M.M., Knight, D.A. and Tebbutt, S.J. (2011). Dual Organism Transcriptomics of Airway Epithelial Cells Interacting with Conidia of *Aspergillus fumigatus*. *PLoS ONE* **6**: e20527.

Orciuolo, E., Stanzani, M., Canestraro, M., Galimberti, S., Carulli, G., Lewis, R., Petrini, M. and Komanduri, K. V (2007). Effects of *Aspergillus fumigatus* gliotoxin and methylprednisolone on human neutrophils: implications for the pathogenesis of invasive aspergillosis. *J. Leukoc. Biol.* **82**: 839–848.

Ortiz, P.A., Ulloque, R., Kihara, G.K., Zheng, H. and Kinzy, T.G. (2006). Translation elongation factor 2 anticodon mimicry domain mutants affect fidelity and diphtheria toxin resistance. *The Journal of Biological Chemistry* **281**: 32639–32648.

Osherov, N. and May, G. (2000). Conidial germination in *Aspergillus nidulans* requires RAS signaling and protein synthesis. *Genetics* **155**: 647–656.

Ouyang, H., Luo, Y., Zhang, L., Li, Y. and Jin, C. (2010). Proteome analysis of *Aspergillus fumigatus* total membrane proteins identifies proteins associated with the glycoconjugates and cell wall biosynthesis using 2D LC-MS/MS. *Molecular Biotechnology* **44**: 177–189.

O'Brian, G.R., Georgianna, D.R., Wilkinson, J.R., Yu, J., Abbas, H.K., Bhatnagar, D., Cleveland, T.E., Nierman, W. and Payne, G.A. (2007). The effect of elevated temperature on gene transcription and aflatoxin biosynthesis. *Mycologia* **99**: 232–239.

O'Gorman, C.M., Fuller, H.T. and Dyer, P.S. (2009). Discovery of a sexual cycle in the opportunistic fungal pathogen *Aspergillus fumigatus*. *Nature* **457**: 471–474.

O'Hanlon, K.A., Cairns, T., Stack, D., Schrettl, M., Bignell, E.M., Kavanagh, K., Miggin, S.M., O'Keeffe, G., Larsen, T.O. and Doyle, S. (2011). Targeted Disruption of Nonribosomal Peptide Synthetase *pes3* Augments the Virulence of *Aspergillus fumigatus*. *Infect. Immun.* **79**: 3978–3992.

O'Hanlon, K.A., Gallagher, L., Schrettl, M., Jöchl, C., Kavanagh, K., Larsen, T.O., Doyle, S. and O' Hanlon, K.A. (2012). Nonribosomal Peptide Synthetase Genes *pesL* and *pes1* Are Essential for Fumigaclavine C Production in *Aspergillus fumigatus*. *Appl. Environ. Microbiol.* **78**: 3166–3176.

O'Neill, P.M., Barton, V.E. and Ward, S. a (2010). The molecular mechanism of action of artemisinin--the debate continues. *Molecules* **15**: 1705–1721.

Pagano, L., Caira, M., Candoni, A., Offidani, M., Martino, B., Specchia, G., Pastore, D., Stanzani, M., Cattaneo, C., Fanci, R., Caramatti, C., Rossini, F., Luppi, M., Potenza, L., Ferrara, F., Mitra, M.E., Fadda, R.M., Invernizzi, R., Aloisi, T., Picardi, M., Bonini, A., Vacca, A., Chierichini, A., Melillo, L., De Waure, C., Fianchi, L., Riva, M., Leone, G., Aversa, F. and Nosari, A. (2010). Invasive aspergillosis in patients with acute myeloid leukemia: a SEIFEM-2008 registry study. *Haematologica* **95**: 644–650.

Paoletti, M., Rydholm, C., Schwier, E.U., Anderson, M.J., Szakacs, G., Lutzoni, F., Debeaupuis, J.-P., Latgé, J.-P., Denning, D.W. and Dyer, P.S. (2005). Evidence for sexuality in the opportunistic fungal pathogen *Aspergillus fumigatus*. *Curr. Biol.* **15**: 1242–1248.

Pardo, J., Urban, C., Galvez, E.M., Ekert, P.G., Müller, U., Kwon-Chung, J., Lobigs, M., Müllbacher, A., Wallich, R., Borner, C. and Simon, M.M. (2006). The mitochondrial protein Bak is pivotal for gliotoxin-induced apoptosis and a critical host factor of *Aspergillus fumigatus* virulence in mice. *J. Cell Biol.* **174**: 509–519.

Park, H.-S., Bayram, Ö., Braus, G.H., Kim, S.C. and Yu, J.-H. (2012). Characterization of the velvet regulators in *Aspergillus fumigatus*. *Mol. Microbiol.* **86**: 937–953.

Parr, C.L., Keates, R.A.B., Bryksa, B.C., Ogawa, M. and Yada, R.Y. (2007). The structure and function of *Saccharomyces cerevisiae* proteinase A. *Yeast* **24**: 467–480.

Patron, N.J., Waller, R.F., Cozijnsen, A.J., Straney, D.C., Gardiner, D.M., Nierman, W.C. and Howlett, B.J. (2007). Origin and distribution of epipolythiodioxopiperazine (ETP) gene clusters in filamentous ascomycetes. *BMC Evol. Biol.* **7**: 174.

Patterson, K. and Strek, M.E. (2010). Allergic bronchopulmonary aspergillosis. *Proc. Am. Thorac. Soc.* **7**: 237–244.

Paul, B.D. and Snyder, S.H. (2010). The unusual amino acid L-ergothioneine is a physiologic cytoprotectant. *Cell Death and Differentiation* **17**: 1134–1140.

De Pauw, B., Walsh, T.J., Donnelly, J.P., Stevens, D.A., Edwards, J.E., Calandra, T., Pappas, P.G., Maertens, J., Lortholary, O., Kauffman, C.A., Denning, D.W., Patterson, T.F., Maschmeyer, G., Bille, J., Dismukes, W.E., Herbrecht, R., Hope, W.W., Kibbler, C.C., Kullberg, B.J., Marr, K.A., Muñoz, P., Odds, F.C., Perfect, J.R., Restrepo, A., Ruhnke, M., Segal, B.H., Sobel, J.D., Sorrell, T.C., Viscoli, C., Wingard, J.R., Zaoutis, T. and Bennett, J.E. (2008). Revised Definitions of Invasive Fungal Disease from the European Organization for Research and Treatment of Cancer/Invasive Fungal Infections Cooperative Group and the National Institute of Allergy and Infectious Diseases Mycoses Study Group (EORTC/ MSG). *Clin. Infect. Dis.* **46**: 1813–1821.

Pel, H.J., De Winde, J.H., Archer, D.B., Dyer, P.S., Hofmann, G., Schaap, P.J., Turner, G., De Vries, R.P., Albang, R., Albermann, K., Andersen, M.R., Bendtsen, J.D., Benen, J.A.E., *et al.* (2007). Genome sequencing and analysis of the versatile cell factory *Aspergillus niger* CBS 513.88. *Nature Biotechnology* **25**: 221–231.

Pernemalm, M., Lewensohn, R. and Lehtiö, J. (2009). Affinity prefractionation for MS-based plasma proteomics. *Proteomics* **9**: 1420–1427.

Perrin, R.M., Fedorova, N.D., Bok, J.W., Cramer, R.A., Wortman, J.R., Kim, H.S., Nierman, W.C. and Keller, N.P. (2007). Transcriptional regulation of chemical diversity in *Aspergillus fumigatus* by LaeA. *PLoS Pathogens* **3**: e50.

Perrone, G.G., Grant, C.M. and Dawes, I.W. (2005). Glutathione Homeostasis in *Saccharomyces cerevisiae*. *Molecular Biology of the Cell* **16**: 218–230.

Perry, R.J., Mast, F.D. and Rachubinski, R. a (2009). Endoplasmic reticulum-associated secretory proteins Sec20p, Sec39p, and Dsl1p are involved in peroxisome biogenesis. *Eukaryot. Cell* **8**: 830–843.

Petersen, T.N., Brunak, S., Von Heijne, G. and Nielsen, H. (2011). SignalP 4.0: discriminating signal peptides from transmembrane regions. *Nat. Meth.* **8**: 785–786.

Petrik, M., Haas, H., Dobrozemsky, G., Lass-Flörl, C., Helbok, A., Blatzer, M., Dietrich, H. and Decristoforo, C. (2010). 68Ga-siderophores for PET imaging of invasive pulmonary aspergillosis: proof of principle. *J. Nucl. Med.* **51**: 639–645.

Pfeiffer, C.D., Fine, J.P. and Safdar, N. (2006). Diagnosis of invasive aspergillosis using a galactomannan assay: a meta-analysis. *Clin. Infect. Dis.* **42**: 1417–1427.

Philippe, B., Ibrahim-Granet, O., Prevost, M.C., Gougerot-Pocidalo, M.A., Sanchez Perez, M., Van Der Meeren, A. and Latge, J.P. (2003). Killing of *Aspergillus fumigatus* by Alveolar Macrophages Is Mediated by Reactive Oxidant Intermediates. *Infect. Immun.* **71**: 3034–3042.

Pihet, M., Carrere, J., Cimon, B., Chabasse, D., Delhaes, L., Symoens, F. and Bouchara, J.-P. (2009). Occurrence and relevance of filamentous fungi in respiratory secretions of patients with cystic fibrosis--a review. *Med. Mycol.* **47**: 387–397.

Piper, M.D., Hong, S.P., Ball, G.E. and Dawes, I.W. (2000). Regulation of the balance of one-carbon metabolism in *Saccharomyces cerevisiae*. *The Journal of Biological Chemistry* **275**: 30987–30995.

Piper, M.D.W., Hong, S.P., Eissing, T., Sealey, P. and Dawes, I.W. (2002). Regulation of the yeast glycine cleavage genes is responsive to the availability of multiple nutrients. *FEMS Yeast Research* **2**: 59–71.

Pitarch, A., Abian, J., Carrascal, M., Sánchez, M., Nombela, C. and Gil, C. (2004). Proteomics-based identification of novel *Candida albicans* antigens for diagnosis of systemic candidiasis in patients with underlying hematological malignancies. *Proteomics* **4**: 3084–3106.

Price, M.S., Conners, S.B., Tachdjian, S., Kelly, R.M. and Payne, G.A. (2005). Aflatoxin conducive and non-conducive growth conditions reveal new gene associations with aflatoxin production. *Fungal Genetics and Biology* **42**: 506–518.

Priebe, S., Linde, J., Albrecht, D., Guthke, R. and Brakhage, A.A. (2011). FungiFun: A web-based application for functional categorization of fungal genes and proteins. *Fungal Genet. Biol.* **48**: 353–358.

Pusztahelyi, T., Klement, E., Szajli, E., Klem, J., Miskei, M., Karányi, Z., Emri, T., Kovács, S., Orosz, G., Kovács, K.L., Medzihradszky, K.F., Prade, R. a and Pócsi, I. (2011). Comparison of transcriptional and translational changes caused by long-term menadione exposure in *Aspergillus nidulans*. *Fungal Genetics and Biology* **48**: 92–103.

Rabilloud, T. (2009). Membrane proteins and proteomics: love is possible, but so difficult. *Electrophoresis* **30 Suppl 1**: S174–80.

Rabilloud, T., Chevallet, M., Luche, S. and Lelong, C. (2010). Two-dimensional gel electrophoresis in proteomics: Past, present and future. *Journal of Proteomics* **73**: 2064–2077.

Rahman, I., Gilmour, P.S., Jimenez, L. a, Biswas, S.K., Antonicelli, F. and Aruoma, O.I. (2003). Ergothioneine inhibits oxidative stress- and TNF-alpha-induced NF-kB activation and interleukin-8 release in alveolar epithelial cells. *Biochem. Biophys. Res. Commun.* **302**: 860–864.

Rand, J.D. and Grant, C.M. (2006). The Thioredoxin System Protects Ribosomes against Stress-induced Aggregation. *Molecular Biology of the Cell* **17**: 387–401.

Reeves, E.P., Reiber, K., Neville, C., Scheibner, O., Kavanagh, K. and Doyle, S. (2006). A nonribosomal peptide synthetase (Pes1) confers protection against oxidative stress in *Aspergillus fumigatus*. *The FEBS Journal* **273**: 3038–3053.

Reid, K.B., Madan, T., Eggleton, P., Kishore, U., Strong, P., Aggrawal, S.S., Sarma, P.U. and Reid, K.B.M. (1997). Binding of pulmonary surfactant proteins A and D to *Aspergillus fumigatus* conidia enhances phagocytosis and killing by human neutrophils and alveolar macrophages. *Infect. Immun.* **65**: 3171.

Reverberi, M., Ricelli, A., Zjalic, S., Fabbri, A.A. and Fanelli, C. (2010). Natural functions of mycotoxins and control of their biosynthesis in fungi. *Appl. Microbiol. Biotechnol.* **87**: 899–911.

Richie, D.L., Hartl, L., Aimanianda, V., Winters, M.S., Fuller, K.K., Miley, M.D., White, S., McCarthy, J.W., Latgé, J.-P., Feldmesser, M., Rhodes, J.C. and Askew, D.S. (2009). A role for the unfolded protein response (UPR) in virulence and antifungal susceptibility in Aspergillus fumigatus. *PLoS Pathogens* **5**: e1000258.

Rizzetto, L. and Cavalieri, D. (2011). Friend or foe: using systems biology to elucidate interactions between fungi and their hosts. *Trends in Microbiology* **19**: 509–515.

Rochfort, S. (2005). Metabolomics Reviewed: A New "Omics" Platform Technology for Systems Biology and Implications for Natural Products Research. *Journal of Natural Products* **68**: 1813–1820.

Ross, P.L., Huang, Y.N., Marchese, J.N., Williamson, B., Parker, K., Hattan, S., Khainovski, N., Pillai, S., Dey, S., Daniels, S., Purkayastha, S., Juhasz, P., Martin, S., Bartlet-Jones, M., He, F., Jacobson, A. and Pappin, D.J. (2004). Multiplexed protein

quantitation in *Saccharomyces cerevisiae* using amine-reactive isobaric tagging reagents. *Molecular & Cellular Proteomics* **3**: 1154–1169.

Ruepp, A., Zollner, A., Maier, D., Albermann, K., Hani, J., Mokrejs, M., Tetko, I., Güldener, U., Mannhaupt, G., Münsterkötter, M. and Mewes, H.W. (2004). The FunCat, a functional annotation scheme for systematic classification of proteins from whole genomes. *Nucleic Acids Research* **32**: 5539–5545.

Ruhaak, L.R., Zauner, G., Huhn, C., Bruggink, C., Deelder, A.M. and Wuhrer, M. (2010). Glycan labeling strategies and their use in identification and quantification. *Analytical and Bioanalytical Chemistry* **397**: 3457–3481.

Rundberget, T. and Wilkins, A.L. (2002). Determination of *Penicillium* mycotoxins in foods and feeds using liquid chromatography – mass spectrometry. *J. Chromatogr. A* **964**: 189–197.

Sagan, D. and Goździuk, K. (2010). Surgery for pulmonary aspergilloma in immunocompetent patients: no benefit from adjuvant antifungal pharmacotherapy. *Ann. Thorac. Surg.* **89**: 1603–1610.

Sainz, J., Hassan, L., Perez, E., Romero, A., Moratalla, A., López-Fernández, E., Oyonarte, S. and Jurado, M. (2007). Interleukin-10 promoter polymorphism as risk factor to develop invasive pulmonary aspergillosis. *Immunol. Lett.* **109**: 76–82.

Sanchez, J.F., Somoza, A.D., Keller, N.P. and Wang, C.C.C. (2012). Advances in *Aspergillus* secondary metabolite research in the post-genomic era. *Nat. Prod. Rep.* **29**: 351–371.

Santamaría, R., Rizzetto, L., Bromley, M., Zelante, T., Lee, W., Cavalieri, D., Romani, L., Miller, B., Gut, I., Santos, M., Pierre, P., Bowyer, P. and Kapushesky, M. (2011). Systems biology of infectious diseases: a focus on fungal infections. *Immunobiology* **216**: 1212–1227.

Sarikaya Bayram, O., Bayram, O., Valerius, O., Park, H.S., Irniger, S., Gerke, J., Ni, M., Han, K.-H., Yu, J.-H. and Braus, G.H. (2010). LaeA control of velvet family regulatory proteins for light-dependent development and fungal cell-type specificity. *PLoS Genetics* **6**: e1001226.

Sato, I., Shimizu, M., Hoshino, T. and Takaya, N. (2009). The glutathione system of *Aspergillus nidulans* involves a fungus-specific glutathione S-transferase. *The Journal of Biological Chemistry* **284**: 8042–8053.

Schaaff, I., Hohmann, S. and Zimmermann, F.K. (1990). Molecular analysis of the structural gene for yeast transaldolase. *European Journal of Biochemistry / FEBS* **188**: 597–603.

Scharf, D.H., Chankhamjon, P., Schlerlach, K., Heinekamp, T., Roth, M., Brakhage, A.A. and Hertweck, C. (2012a). Epidithiol Formation by an Unprecedented Twin

Carbon-Sulfur Lyase in the Gliotoxin Pathway. *Agnew. Chem. Int. Edit.* **51**: 10064–10068.

Scharf, D.H., Heinekamp, T., Remme, N., Hortschansky, P., Brakhage, A.A. and Hertweck, C. (2012b). Biosynthesis and function of gliotoxin in *Aspergillus fumigatus*. *Applied Microbiology and Biotechnology* **93**: 467–472.

Scharf, D.H., Remme, N., Habel, A., Chankhamjon, P., Scherlach, K., Heinekamp, T., Hortschansky, P., Brakhage, A.A. and Hertweck, C. (2011). A dedicated glutathione S-transferase mediates carbon-sulfur bond formation in gliotoxin biosynthesis. *J. Am. Chem. Soc.* **133**: 12322–12325.

Scharf, D.H., Remme, N., Heinekamp, T., Hortschansky, P., Brakhage, A.A. and Hertweck, C. (2010). Transannular Disulfide Formation in Gliotoxin Biosynthesis and Its Role in Self-Resistance of the Human Pathogen *Aspergillus fumigatus*. *J. Am. Chem. Soc.* **132**: 10136–10141.

Schmaler-Ripcke, J., Sugareva, V., Gebhardt, P., Winkler, R., Kniemeyer, O., Heinekamp, T. and Brakhage, A.A. (2009). Production of pyomelanin, a second type of melanin, via the tyrosine degradation pathway in *Aspergillus fumigatus*. *Appl. Environ. Microbiol.* **75**: 493–503.

Schnabl, M., Oskolkova, O. V, Holic, R., Brezna, B., Pichler, H., Zagorsek, M., Kohlwein, S.D., Paltauf, F., Daum, G. and Griac, P. (2003). Subcellular localization of yeast Sec14 homologues and their involvement in regulation of phospholipid turnover. *Eur. J. Biochem.* **270**: 3133–3145.

Schrettl, M., Bignell, E., Kragl, C., Joechl, C., Rogers, T., Arst, H.N., Haynes, K. and Haas, H. (2004). Siderophore biosynthesis but not reductive iron assimilation is essential for *Aspergillus fumigatus* virulence. *J. Exp. Med.* **200**: 1213–1219.

Schrettl, M., Bignell, E., Kragl, C., Sabiha, Y., Loss, O., Eisendle, M., Wallner, A., Arst, H.N., Haynes, K. and Haas, H. (2007). Distinct roles for Intra- and Extracellular Siderophores during *Aspergillus fumigatus* Infection. *PLoS Pathogens* **3**: 1195–1207.

Schrettl, M., Carberry, S., Kavanagh, K., Haas, H., Jones, G.W., O'Brien, J., Nolan, A., Stephens, J., Fenelon, O. and Doyle, S. (2010). Self-protection against gliotoxin-a component of the gliotoxin biosynthetic cluster, GliT, completely protects *Aspergillus fumigatus* against exogenous gliotoxin. *PLoS Pathogens* **6**: e1000952.

Seebeck, F.P. (2010). In vitro reconstitution of Mycobacterial ergothioneine biosynthesis. *J. Am. Chem. Soc.* **132**: 6632–6633.

Segal, B.H. and Romani, L.R. (2009). Invasive aspergillosis in chronic granulomatous disease. *Med. Mycol.* **47 Suppl 1**: S282–90.

Segal, B.H. and Walsh, T.J. (2006). Current approaches to diagnosis and treatment of invasive aspergillosis. *Am. J. Respir. Crit. Care. Med.* **173**: 707–717.

Sharon, H., Hagag, S. and Osherov, N. (2009). Transcription factor PrtT controls expression of multiple secreted proteases in the human pathogenic mold *Aspergillus fumigatus*. *Infect. Immun.* **77**: 4051–4060.

Shen, D.-K., Noodeh, A.D., Kazemi, A., Grillot, R., Robson, G. and Brugère, J.-F. (2004). Characterisation and expression of phospholipases B from the opportunistic fungus *Aspergillus fumigatus*. *FEMS Microbiology Letters* **239**: 87–93.

Sheppard, D.C., Doedt, T., Chiang, L.Y., Kim, H.S., Chen, D., Nierman, W.C. and Filler, S.G. (2005). The *Aspergillus fumigatus* StuA Protein Governs the Up- Regulation of a Discrete Transcriptional Program during the Acquisition of Developmental Competence. *Molecular Biology of the Cell* **16**: 5866–5879.

Shevchenko, A., Tomas, H., Havlis, J., Olsen, J. V and Mann, M. (2007). In-gel digestion for mass spectrometric characterization of proteins and proteomes. *Nature Protocols* **1**: 2856–2860.

Shi, L., Li, F., Huang, M., Lu, J., Kong, X., Wang, S. and Shao, H. (2012a). Immunoproteomics based identification of thioredoxin reductase GliT and novel *Aspergillus fumigatus* antigens for serologic diagnosis of invasive aspergillosis. *BMC Microbiology* **12**: 11.

Shi, L.-N., Li, F.-Q., Lu, J.-F., Kong, X.-X., Wang, S.-Q., Huang, M., Shao, H.-F. and Shao, S.-H. (2012b). Antibody specific to thioredoxin reductase as a new biomarker for serodiagnosis of invasive aspergillosis in non-neutropenic patients. *Clin. Chim. Acta* **413**: 938–943.

Shimizu, M., Fujii, T., Masuo, S., Fujita, K. and Takaya, N. (2009). Proteomic analysis of *Aspergillus nidulans* cultured under hypoxic conditions. *Proteomics* **9**: 7–19.

Sieńko, M., Natorff, R., Zieliński, Z., Hejduk, A. and Paszewski, A. (2007). Two *Aspergillus nidulans* genes encoding methylenetetrahydrofolate reductases are up-regulated by homocysteine. *Fungal Genetics and Biology* **44**: 691–700.

Da Silva Ferreira, M.E., Malavazi, I., Savoldi, M., Brakhage, A.A., Goldman, M.H.S., Kim, H.S., Nierman, W.C. and Goldman, G.H. (2006). Transcriptome analysis of *Aspergillus fumigatus* exposed to voriconazole. *Current Genetics* **50**: 32–44.

Silvestris, N., Del Re, M., Azzariti, A., Maiello, E., Lombardi, L., Cinieri, S., Guarini, A., Brunetti, A.E., Delcuratolo, S., De Vita, F., Pisconti, S., Danesi, R. and Colucci, G. (2012). Optimized granulocyte colony-stimulating factor prophylaxis in adult cancer patients: from biological principles to clinical guidelines. *Expert Opin. Ther. Targets* **16 Suppl 2**: S111–7.

Singh, B., Oellerich, M., Kumar, R., Kumar, M., Bhadoria, D.P., Reichard, U., Gupta, V.K., Sharma, G.L. and Asif, A.R. (2010a). Immuno-reactive molecules identified from the secreted proteome of *Aspergillus fumigatus*. *J. Proteome Res.* **9**: 5517–5529.

Singh, B., Sharma, G.L., Oellerich, M., Kumar, R., Singh, S., Bhadoria, D.P., Katyal, A., Reichard, U. and Asif, A.R. (2010b). Novel cytosolic allergens of *Aspergillus fumigatus* identified from germinating conidia. *Journal of Proteome Research* **9**: 5530–5541.

Singh, S., Gupta, S., Singh, B., Sharma, S.K., Gupta, V.K. and Sharma, G.L. (2012). Proteomic Characterization of *Aspergillus fumigatus* Treated with an Antifungal Coumarin for Identification of Novel Target Molecules of Key Pathways. *Journal of Proteome Research* **11**: 3259–3268.

Sixto, M.L.J., Vareechon, C., Cowden, S., Cobb, B.A., Latgé, J., Momany, M., Pearlman, E. and Leal, M.S.J. (2012). Fungal antioxidant pathways promote survival against neutrophils during infection. *The Journal of Clinical Investigation* **122**: 2482–2498.

Soanes, D.M., Alam, I., Cornell, M., Wong, H.M., Hedeler, C., Norman, W., Rattray, M., Hubbard, S.J., Oliver, S.G. and Talbot, N.J. (2008). Comparative Genome Analysis of Filamentous Fungi Reveals Gene Family Expansions Associated with Fungal Pathogenesis. *PLoS ONE* **3**: e2300.

Spikes, S., Xu, R., Nguyen, C.K., Chamilos, G., Kontoyiannis, D.P., Jacobson, R.H., Ejzykowicz, D.E., Chiang, L.Y., Filler, S.G. and May, G.S. (2008). Gliotoxin production in *Aspergillus fumigatus* contributes to host-specific differences in virulence. *J. Infect. Dis.* **197**: 479–486.

Srinivasan, U., Bala, A., Jao, S., Starke, D.W., Jordan, T.W. and Mieyal, J.J. (2006). Selective Inactivation of Glutaredoxin by Sporidesmin and Other Epidithiopiperazinediones. *Biochemistry* **45**: 8978–8987.

Stanimirovic, Z., Stevanovic, J., Bajic, V. and Radovic, I. (2007). Evaluation of genotoxic effects of fumagillin by cytogenetic tests in vivo. *Mutat. Res.* **628**: 1–10.

Stanzani, M., Orciuolo, E., Lewis, R., Kontoyiannis, D.P., Martins, S.L.R., St John, L.S. and Komanduri, K. V (2005). *Aspergillus fumigatus* suppresses the human cellular immune response via gliotoxin-mediated apoptosis of monocytes. *Blood* **105**: 2258–2265.

Steele, C., Rapaka, R.R., Metz, A., Pop, S.M., Williams, D.L., Gordon, S., Kolls, J.K. and Brown, G.D. (2005). The beta-glucan receptor dectin-1 recognizes specific morphologies of *Aspergillus fumigatus*. *PLoS Pathogens* **1**: e42.

Steffan, N., Grundmann, A., Afiyatullov, S., Ruan, H. and Li, S. (2009). FtmOx1, a non-heme Fe(II) and alpha-ketoglutarate-dependent dioxygenase, catalyses the endoperoxide formation of verruculogen in *Aspergillus fumigatus*. *Organic and Biomolecular Chemistry* **7**: 4082–4087.

Stincone, A., Daudi, N., Rahman, A.S., Antczak, P., Henderson, I., Cole, J., Johnson, M.D., Lund, P. and Falciani, F. (2011). A systems biology approach sheds new light on *Escherichia coli* acid resistance. *Nucleic Acids Research* **39**: 7512–7528.

Stolf, B.S., Smyrnias, I., Lopes, L.R., Vendramin, A., Goto, H., Laurindo, F.R.M., Shah, A.M. and Santos, C.X.C. (2011). Protein disulfide isomerase and host-pathogen interaction. *TheScientificWorldJournal* **11**: 1749–1761.

Sugui, J. a, Pardo, J., Chang, Y.C., Müllbacher, A., Zarember, K. a, Galvez, E.M., Brinster, L., Zerfas, P., Gallin, J.I., Simon, M.M. and Kwon-Chung, K.J. (2007a). Role of *laeA* in the Regulation of *alb1*, *gliP*, Conidial Morphology, and Virulence in *Aspergillus fumigatus*. *Eukaryot. Cell* **6**: 1552–1561.

Sugui, J.A., Kim, H.S., Zarember, K.A., Chang, Y.C., Gallin, J.I., Nierman, W.C. and Kwon-Chung, K.J. (2008). Genes differentially expressed in conidia and hyphae of *Aspergillus fumigatus* upon exposure to human neutrophils. *PloS One* **3**: e2655.

Sugui, J.A., Pardo, J., Chang, Y.C., Zarember, K.A., Nardone, G., Galvez, E.M., Müllbacher, A., Gallin, J.I., Simon, M.M. and Kwon-Chung, K.J. (2007b). Gliotoxin is a virulence factor of *Aspergillus fumigatus*: *gliP* deletion attenuates virulence in mice immunosuppressed with hydrocortisone. *Eukaryot. Cell* **6**: 1562–1569.

Suh, M.-J., Fedorova, N.D., Cagas, S.E., Hastings, S., Fleischmann, R.D., Peterson, S.N., Perlin, D.S., Nierman, W.C., Pieper, R. and Momany, M. (2012). Development stage-specific proteomic profiling uncovers small, lineage specific proteins most abundant in the *Aspergillus fumigatus* conidial proteome. *Proteome Science* **10**: 30.

Suhadolnik, R.J. and Chenowath, R.G. (1958). Biosynthesis of Gliotoxin. 1. Incorporation of Phenylalanine-1- and -2-C^{14}. *J. Am. Chem. Soc.* **80**: 4391–4392.

Suliman, H.S., Appling, D.R. and Robertus, J.D. (2007). The Gene for Cobalamin-independent Methionine Synthase is Essential in *Candida albicans*: A Potential Antifungal Target. *Archives of Biochemistry and Biophysics* **467**: 218–226.

Sulyok, M., Krska, R. and Schuhmacher, R. (2007). A liquid chromatography/tandem mass spectrometric multi-mycotoxin method for the quantification of 87 analytes and its application to semi-quantitative screening of moldy food samples. *Analytical and Bioanalytical Chemistry* **389**: 1505–1523.

Ta, P., Buchmeier, N., Newton, G.L., Rawat, M. and Fahey, R.C. (2011). Organic hydroperoxide resistance protein and ergothioneine compensate for loss of mycothiol in *Mycobacterium smegmatis* mutants. *Journal of Bacteriology* **193**: 1981–1990.

Tan, S., Teo, M., Lam, Y.T., Dawes, I.W. and Perrone, G.G. (2009). Cu, Zn Superoxide Dismutase and NADP(H) Homeostasis Are Required for Tolerance of Endoplasmic Reticulum Stress in *Saccharomyces cerevisiae*. *The American Society for Cell Biology* **20**: 1493–1508.

Taylor, D.J., Nilsson, J., Merrill, a R., Andersen, G.R., Nissen, P. and Frank, J. (2007). Structures of modified eEF2 80S ribosome complexes reveal the role of GTP hydrolysis in translocation. *The EMBO Journal* **26**: 2421–2431.

Tepwong, P., Giri, A., Sasaki, F., Fukui, R. and Ohshima, T. (2012). Mycobial enhancement of ergothioneine by submerged cultivation of edible mushroom mycelia and its application as an antioxidative compound. *Food Chem.* **131**: 247–258.

Terabayashi, Y., Shimizu, M., Kitazume, T., Masuo, S., Fujii, T. and Takaya, N. (2012). Conserved and specific responses to hypoxia in *Aspergillus oryzae* and *Aspergillus nidulans* determined by comparative transcriptomics. *Applied Microbiology and Biotechnology* **93**: 305–317.

Teutschbein, J., Albrecht, D., Po, M., Guthke, R., Aimanianda, V., Latge, J. and Brakhage, A.A. (2010). Proteome Profiling and Functional Classification of Intracellular Proteins from Conidia of the Human-Pathogenic Mold *Aspergillus fumigatus* research articles. *J. Proteome Res.* **9**: 3427–3442.

Thomas, B., Rutman, A., Hirst, R.A., Haldar, P., Wardlaw, A.J., Bankart, J., Brightling, C.E. and O'Callaghan, C. (2010). Ciliary dysfunction and ultrastructural abnormalities are features of severe asthma. *J. Allergy Clin. Immunol.* **126**: 722–729.e2.

Thompson, G.R. and Patterson, T.F. (2008). Pulmonary aspergillosis. *Sem. Resp. Crit. Care. M.* **29**: 103–110.

Thornton, C., Johnson, G. and Agrawal, S. (2012). Detection of invasive pulmonary aspergillosis in haematological malignancy patients by using lateral-flow technology. *JoVE* e3721.

Thornton, C.R. (2008). Development of an immunochromatographic lateral-flow device for rapid serodiagnosis of invasive aspergillosis. *CVI* **15**: 1095–1105.

Thornton, C.R. (2010). Detection of invasive aspergillosis. *Adv. Appl. Microbiol.* **70**: 187–216.

Thulasiraman, V., Lin, S., Gheorghiu, L., Lathrop, J., Lomas, L., Hammond, D. and Boschetti, E. (2005). Reduction of the concentration difference of proteins in biological liquids using a library of combinatorial ligands. *Electrophoresis* **26**: 3561–3571.

Thywißen, A., Heinekamp, T., Dahse, H.-M., Schmaler-Ripcke, J., Nietzsche, S., Zipfel, P.F. and Brakhage, A.A. (2011). Conidial Dihydroxynaphthalene Melanin of the Human Pathogenic Fungus *Aspergillus fumigatus* Interferes with the Host Endocytosis Pathway. *Front. Microbiol.* **2**: 96.

Thön, M., Al-Abdallah, Q., Hortschansky, P. and Brakhage, A.A. (2007). The thioredoxin system of the filamentous fungus *Aspergillus nidulans*: impact on development and oxidative stress response. *The Journal of Biological Chemistry* **282**: 27259–27269.

Tierney, L., Linde, J., Müller, S., Brunke, S., Molina, J.C., Hube, B., Schöck, U., Guthke, R. and Kuchler, K. (2012). An Interspecies Regulatory Network Inferred from Simultaneous RNA-seq of *Candida albicans* Invading Innate Immune Cells. *Frontiers in Microbiology* **3**: 85.

Tillie-Leblond, I. and Tonnel, a-B. (2005). Allergic bronchopulmonary aspergillosis. *Allergy* **60**: 1004–1013.

Tjalsma, H., Schaeps, R.M.J. and Swinkels, D.W. (2008). Immunoproteomics: From biomarker discovery to diagnostic applications. *Proteomics. Clinical Applications* **2**: 167–180.

Towpik, J. (2005). Regulation of Mitochondrial Translation in Yeast. *Cell. Mol. Biol. Lett.* **10**: 571–594.

Trachootham, D., Lu, W., Ogasawara, M. a, Nilsa, R.-D.V. and Huang, P. (2008). Redox regulation of cell survival. *Antioxidants & Redox Signaling* **10**: 1343–1374.

Traunmüller, F., Popovic, M., Konz, K.-H., Smolle-Jüttner, F.-M. and Joukhadar, C. (2011). Efficacy and safety of current drug therapies for invasive aspergillosis. *Pharmacology* **88**: 213–224.

Triana-Alonso, F.J., Chakraburtty, K. and Nierhaus, K.H. (1995). The Elongation Factor 3 Unique in Higher Fungi and Essential for Protein Biosynthesis Is an E Site Factor. *The Journal of Biological Chemistry* **270**: 20473–20478.

Trof, R.J., Beishuizen, A., Debets-Ossenkopp, Y.J., Girbes, A.R.J. and Groeneveld, A.B.J. (2007). Management of invasive pulmonary aspergillosis in non-neutropenic critically ill patients. *Intensive Car Med.* **33**: 1694–1703.

Tsai, H.F., Chang, Y.C., Washburn, R.G., Wheeler, M.H. and Kwon-Chung, K.J. (1998). The developmentally regulated *alb1* gene of *Aspergillus fumigatus*: its role in modulation of conidial morphology and virulence. *J. Bacteriol.* **180**: 3031–3038.

Tsai, H.F., Wheeler, M.H., Chang, Y.C. and Kwon-Chung, K.J. (1999). A developmentally regulated gene cluster involved in conidial pigment biosynthesis in *Aspergillus fumigatus*. *J. Bacteriol.* **181**: 6469–6477.

Tsunawaki, S., Yoshida, L.S., Nishida, S., Kobayashi, T. and Shimoyama, T. (2004). Fungal Metabolite Gliotoxin Inhibits Assembly of the Human Respiratory Burst NADPH Oxidase. *Infect. Immun.* **72**: 3373–3382.

Tunger, O., Bayram, H., Degerli, K., Dinc, G. and Cetin, B.C. (2008). Comparison of the efficacy of combination and monotherapy with caspofungin and liposomal amphotericin B against invasive candidiasis. *Saudi Med. J.* **29**: 728–733.

Twumasi-Boateng, K., Yu, Y., Chen, D., Gravelat, F.N., Nierman, W.C. and Sheppard, D.C. (2009). Transcriptional profiling identifies a role for BrlA in the response to

nitrogen depletion and for StuA in the regulation of secondary metabolite clusters in *Aspergillus fumigatus*. *Eukaryot. Cell* **8**: 104–115.

Ullmann, A.J., Sanz, M.A., Tramarin, A., Barnes, R.A., Wu, W., Gerlach, B. a, Krobot, K.J. and Gerth, W.C. (2006). Prospective study of amphotericin B formulations in immunocompromised patients in 4 European countries. *Clin. Infect. Dis.* **43**: e29–38.

Upadhyay, S.K., Gautam, P., Pandit, H., Singh, Y., Basir, S.F. and Madan, T. (2012). Identification of fibrinogen-binding proteins of *Aspergillus fumigatus* using proteomic approach. *Mycopathologia* **173**: 73–82.

Ushio-Fukai, M. and Alexander, R.W. (2004). Reactive oxygen species as mediators of angiogenesis Signaling Role of NAD(P)H oxidase. *Mol. Cell. Biochem.* **264**: 85–97.

Valerius, O., Draht, O., Kübler, E., Adler, K., Hoffmann, B. and Braus, G.H. (2001). Regulation of *hisHF* transcription of *Aspergillus nidulans* by adenine and amino acid limitation. *Fungal Genetics and Biology* **32**: 21–31.

Valiante, V., Heinekamp, T., Jain, R., Härtl, A. and Brakhage, A.A. (2008). The mitogen-activated protein kinase MpkA of *Aspergillus fumigatus* regulates cell wall signaling and oxidative stress response. *Fungal Genet. Biol.* **45**: 618–627.

Vandeputte, P., Ferrari, S. and Coste, A.T. (2012). Antifungal resistance and new strategies to control fungal infections. *Int. J. Microbiol.* **2012**: 713687.

Varghese, R.S., Zhou, B., Nezami Ranjbar, M.R., Zhao, Y. and Ressom, H.W. (2012). Ion annotation-assisted analysis of LC-MS based metabolomic experiment. *Proteome Science* **10 Suppl 1**: S8.

Villas-Bôas, S.G., Mas, S., Akesson, M., Smedsgaard, J. and Nielsen, J. (2005). Mass spectrometry in metabolome analysis. *Mass Spectrometry Reviews* **24**: 613–646.

Volling, K., Thywissen, A., Brakhage, A.A. and Saluz, H.P. (2011). Phagocytosis of melanized Aspergillus conidia by macrophages exerts cytoprotective effects by sustained PI3K/Akt signalling. *Cell. Microbiol.* **13**: 1130–1148.

Volpi, I., Perruccio, K., Tosti, A., Capanni, M., Ruggeri, L., Posati, S., Aversa, F., Tabilio, A., Romani, L., Martelli, M.F. and Verlardi, A. (2001). Postgrafting administration of granulocyte colony-stimulating factor impairs functional immune recovery in recipients of human leukocyte antigen haplotype-mismatched hematopoietic transplants. *Blood* **97**: 2514–2521.

Voulgaris, I., O'Donnell, A., Harvey, L.M. and McNeil, B. (2012). Inactivating alternative NADH dehydrogenases: enhancing fungal bioprocesses by improving growth and biomass yield? *Scientific Reports* **2**: 322.

De Vrankrijker, A.M.M., Van der Ent, C.K., Van Berkhout, F.T., Stellato, R.K., Willems, R.J.L., Bonten, M.J.M. and Wolfs, T.F.W. (2011). *Aspergillus fumigatus*

colonization in cystic fibrosis: implications for lung function? *Clin. Microbiol. Infect.* **17**: 1381–1386.

Vödisch, M., Albrecht, D., Lessing, F., Schmidt, A.D., Winkler, R., Guthke, R., Brakhage, A.A. and Kniemeyer, O. (2009). Two-dimensional proteome reference maps for the human pathogenic filamentous fungus *Aspergillus fumigatus*. *Proteomics* **9**: 1407–1415.

Vödisch, M., Scherlach, K., Winkler, R., Hertweck, C., Braun, H.-P., Roth, M., Haas, H., Werner, E.R., Brakhage, A.A. and Kniemeyer, O. (2011). Analysis of the *Aspergillus fumigatus* proteome reveals metabolic changes and the activation of the pseurotin A biosynthesis gene cluster in response to hypoxia. *J. Proteome Res.* **10**: 2508–2524.

Wachter, A. (2010). Riboswitch-mediated control of gene expression in eukaryotes. *RNA Biology* **7**: 67–76.

Wagener, J., Echtenacher, B., Rohde, M., Kotz, A., Krappmann, S., Heesemann, J. and Ebel, F. (2008). The putative alpha-1,2-mannosyltransferase AfMnt1 of the opportunistic fungal pathogen *Aspergillus fumigatus* is required for cell wall stability and full virulence. *Eukaryot. Cell* **7**: 1661–1673.

Ward, O.P., Qin, W.M., Dhanjoon, J., Ye, J. and Singh, A. (2005). Physiology and Biotechnology of *Aspergillus*. *Adv. Appl. Microbiol.* **58C**: 1–75.

Waring, P., Sjaarda, A. and Lin, Q.H. (1995). Gliotoxin Inactivates Alcohol Dehydrogenase by either Covalent Modification or Free Radical Damage Mediated by Redox Cycling. *Biochem. Pharmacol.* **49**: 1195–1201.

Warner, J.R. (1999). The economics of ribosome biosynthesis in yeast. *Trends in Biochemical Sciences* **24**: 437–440.

Wartenberg, D., Lapp, K., Jacobsen, I.D., Dahse, H.-M., Kniemeyer, O., Heinekamp, T. and Brakhage, A.A. (2011). Secretome analysis of *Aspergillus fumigatus* reveals Asp-hemolysin as a major secreted protein. *Journal of Clinical Microbiology* **301**: 602–611.

Wartha, F., Beiter, K., Normark, S. and Henriques-Normark, B. (2007). Neutrophil extracellular traps: casting the NET over pathogenesis. *Curr. Opin. Microbiol.* **10**: 52–56.

Washburn, M.P., Wolters, D. and Yates, J.R. (2001). Large-scale analysis of the yeast proteome by multidimensional protein identification technology. *Nature Biotechnology* **19**: 242–247.

White, P.L., Bretagne, S., Klingspor, L., Melchers, W.J.G., McCulloch, E., Schulz, B., Finnstrom, N., Mengoli, C., Barnes, R. a, Donnelly, J.P. and Loeffler, J. (2010). *Aspergillus* PCR: one step closer to standardization. *Journal of Clinical Microbiology* **48**: 1231–1240.

White, P.L., Mengoli, C., Bretagne, S., Cuenca-Estrella, M., Finnstrom, N., Klingspor, L., Melchers, W.J.G., McCulloch, E., Barnes, R. a, Donnelly, J.P. and Loeffler, J. (2011). Evaluation of *Aspergillus* PCR protocols for testing serum specimens. *J. Clin. Microbiol.* **49**: 3842–3848.

Wiedner, S.D., Burnum, K.E., Pederson, L.M., Anderson, L.N., Fortuin, S., Chauvigné-Hines, L.M., Shukla, A.K., Ansong, C., Panisko, E. a, Smith, R.D. and Wright, A.T. (2012). Multiplexed activity-based protein profiling of the human pathogen *Aspergillus fumigatus* reveals large functional changes upon exposure to human serum. *J. Biol. Chem.* 10.1074/jbc.M112.394106.

Willger, S.D., Grahl, N. and Cramer Jr, R.A. (2009). *Aspergillus fumigatus* metabolism: Clues to mechanisms of in vivo fungal growth and virulence. *Med. Mycol.* **47**: S72–79.

Willger, S.D., Puttikamonkul, S., Kim, K.-H., Burritt, J.B., Grahl, N., Metzler, L.J., Barbuch, R., Bard, M., Lawrence, C.B. and Cramer, R.A. (2008). A Sterol-Regulatory Element Binding Protein Is Required for Cell Polarity, Hypoxia Adaptation, Azole Drug Resistance, and Virulence in Aspergillus fumigatus. *PLoS Pathogens* **4**: e1000200.

Willmann, J., Thiele, H. and Leibfritz, D. (2011). Combined reversed phase HPLC, mass spectrometry, and NMR spectroscopy for a fast separation and efficient identification of phosphatidylcholines. *Journal of Biomedicine & Biotechnology* **2011**:

Wingard, J.R., Kubilis, P., Lee, L., Yee, G., White, M., Walshe, L., Bowden, R., Anaissie, E., Hiemenz, J. and Lister, J. (1999). Clinical significance of nephrotoxicity in patients treated with amphotericin B for suspected or proven aspergillosis. *Clin. Infect. Dis.* **29**: 1402–1407.

Winstead, J.A. and Suhadolnik, R.J. (1960). Biosynthesis of Gliotoxin . II . Further Studies on the Incorporation of Carbon-14 and Tritium-labeled Precursors. *J. Am. Chem. Soc.* **82**: 1644–1647.

Xiao, R., Wilkinson, B., Solovyov, A., Winther, J.R., Holmgren, A., Lundström-Ljung, J. and Gilbert, H.F. (2004). The contributions of protein disulfide isomerase and its homologues to oxidative protein folding in the yeast endoplasmic reticulum. *The Journal of Biological Chemistry* **279**: 49780–49786.

Yamada, A., Kataoka, T. and Nagai, K. (2000). The fungal metabolite gliotoxin : immunosuppressive activity on CTL-mediated cytotoxicity. *Immunol. Lett.* **71**: 27–32.

Yamashita, Y. and Yamashita, M. (2010). Identification of a novel selenium-containing compound, selenoneine, as the predominant chemical form of organic selenium in the blood of bluefin tuna. *The Journal of Biological Chemistry* **285**: 18134–18138.

Yamazaki, H., Yamazaki, D., Takaya, N., Takagi, M. and Ohta, A. (2007). A chitinase gene, *chiB* ,involved in the autolytic process of Aspergillus nidulans. *Current Genetics* **51**: 89–91.

Yanaka, N., Kaseda, Y., Tanaka, A., Nogusa, Y., Sumiyoshi, N. and Kato, N. (2009). Generation of a Zinc Finger Protein ZPR1 Mutant That Constitutively Interacted with Translation Elongation Factor 1α. *Bioscience, Biotechnology, and Biochemistry* **73**: 2809–2811.

Yoshida, S., Ono, M., Shono, T., Izumi, H., Ishibashi, T., Suzuki, H. and Kuwano, M. (1997). Involvement of Interleukin-8, Vascular Endothelial Growth Factor, and Basic Fibroblast Growth Factor in Tumor Necrosis Factor Alpha-Dependent Angiogenesis. *Mol. Cell. Biol.* **17**: 4015–4023.

Zaas, A.K., Liao, G., Chien, J.W., Weinberg, C., Shore, D., Giles, S.S., Marr, K. a, Usuka, J., Burch, L.H., Perera, L., Perfect, J.R., Peltz, G. and Schwartz, D. a (2008). Plasminogen alleles influence susceptibility to invasive aspergillosis. *PLoS Genetics* **4**: e1000101.

Zamir, L., Zaretsky, M., Fridman, Y., Ner-Gaon, H., Rubin, E. and Aharoni, A. (2012). Tight coevolution of proliferating cell nuclear antigen (PCNA)-partner interaction networks in fungi leads to interspecies network incompatibility. *Proc. Natl. Acad. Sci. U. S. A.* **109**: E406–14.

Zhang, L., Feng, D., Fang, W., Ouyang, H., Luo, Y., Du, T. and Jin, C. (2009). Comparative proteomic analysis of an *Aspergillus fumigatus* mutant deficient in glucosidase I (AfCwh41). *Microbiology* **155**: 2157–2167.

Zhang, Q., Faca, V. and Hanash, S. (2011). Mining the plasma proteome for disease applications across seven logs of protein abundance. *Journal of Proteome Research* **10**: 46–50.

Zhao, Y., Liu, J., Wang, J., Wang, L., Yin, H., Tan, R. and Xu, Q. (2004). Fumigaclavine C improves concanavalin A-induced liver injury in mice mainly via inhibiting TNF-alpha production and lymphocyte adhesion to extracellular matrices. *J. Pharm. Pharmacol.* **56**: 775–782.

Zhou, H., Hu, H., Zhang, L., Li, R., Ouyang, H., Ming, J. and Jin, C. (2007). O-Mannosyltransferase 1 in *Aspergillus fumigatus* (AfPmt1p) is crucial for cell wall integrity and conidium morphology, especially at an elevated temperature. *Eukaryot. Cell* **6**: 2260–2268.

Zhu, H., Santo, A. and Li, Y. (2012). The antioxidant enzyme peroxiredoxin and its protective role in neurological disorders. *Experimental Biology and Medicine* **237**: 143–149.

Zmeili, O.S. and Soubani, A.O. (2007). Pulmonary aspergillosis: a clinical update. *QJM* **100**: 317–334.

CHAPTER 9

Appendix I

9 Appendix I

Table: *A. fumigatus* mycelial proteins (*n* = 370) identified by shotgun mass spectrometry, described in Section 3.2.1, arranged in order of increasing CADRE ID.

CADRE ID. (AFUA_)	Protein name	tp*I*	tM_r	GRAVY score	TM	Coverage (%)	Unique peptides	SM Score
1G00420[a]	Carboxypeptidase S1, putative (EC 3.4.16.-)	5.29	60133.23	-0.36148	0	14	6	89.07
1G00990[a]	Short chain dehydrogenase/reductase family protein (EC 1.-.-)	10.08	29491.36	-0.43065	0	28	6	100.04
1G01000[a]	Oxidoreductase, 2OG-Fe(II) oxygenase family	5.33	42635.58	-0.27273	0	32	9	162.75
1G01010	Polyketide synthase, putative	5.52	231309.97	-0.18823	0	1	2	24.62
1G02070	Cytochrome C1/Cyt1, putative (EC 1.10.2.2)	8.29	35125.88	-0.34796	1	16	3	53.62
1G02290	Unknown function protein	4.37	11774.74	-0.46981	0	29	2	41.04
1G02550[a]	Tubulin alpha-1 subunit	4.98	50025.27	-0.32098	0	40	12	200.92
1G02980	6-phosphogluconolactonase, putative (EC 3.1.1.31)	8.59	93269.00	-0.46791	0	3	2	32.51
1G03100	ATP synthase delta chain, mitochondrial, putative (EC 3.6.3.14)	5.27	17640.15	0.007273	0	12	2	26.07
1G03390[a]	60S ribosomal protein L12	9.36	25728.56	-0.28312	0	31	4	68.2
1G03510[a]	ATP synthase gamma chain	7.64	31546.83	-0.22276	0	31	5	97.15
1G03610	Unknown function protein	6.93	32100.69	-0.36879	0	11	3	45.96
1G03720	UPF0136 domain protein	10.22	16880.62	0.322785	4	15	1	20.49
1G04070[a]	Eukaryotic translation initiation factor eIF-5A	5.58	21164.02	-0.41146	0	28	4	72.6
1G04150	Tartrate dehydrogenase, putative (EC 1.1.1.93)	6.91	24077.71	-0.23721	0	18	4	55.45

CADRE ID. (AFUA_)	Protein name	tp*I*	tM_r	GRAVY score	TM	Coverage (%)	Unique peptides	SM Score
1G04190[a]	Polyadenylate-binding protein, cytoplasmic and nuclear (PABP) (Poly(A)-binding protein) (Polyadenylate tail-binding protein)	5.74	81445.19	-0.72019	0	1	1	18.95
1G04320	40S ribosomal protein S8	6.85	40561.75	0.017507	0	26	4	66.26
1G04530	Ribosomal L18ae protein family	10.69	17403.46	-0.5	0	16	2	39.67
1G04540[a]	NADH-cytochrome b5 reductase 2 (EC 1.6.2.2) (Mitochondrial cytochrome b reductase)	5.55	39791.00	-0.35472	0	24	6	107.14
1G04660	Ribosomal protein L15	11.5	27762.26	-0.89698	0	9	2	27.34
1G04850	Dynein light chain type 1, putative	7.83	14884.96	-0.54453	0	17	1	19.98
1G04940	Small COPII coat GTPase sar1 (EC 3.6.5.-)	5.96	21431.73	-0.13333	0	7	1	21.65
1G05080[a]	60S ribosomal protein P0	5.11	33495.33	-0.02173	0	39	7	129.44
1G05340	40S ribosomal protein S19	9.56	24835.26	-0.50045	0	6	2	31.56
1G05390[a]	Mitochondrial ADP,ATP carrier protein (Ant), putative	9.97	33321.49	0.046429	2	25	9	158.7
1G05500[a]	40S ribosomal protein S12	5.33	33444.95	-0.39795	0	17	2	34.27
1G05630[a]	40S ribosomal protein S3, putative	9.18	29201.46	-0.31053	0	31	7	120.51
1G06210	N-acetylglucosamine-phosphate mutase (EC 5.4.2.3)	5.79	61515.88	-0.19541	0	3	1	19.19
1G06300	Proteasome regulatory particle subunit (RpnF), putative	5.71	52886.47	-0.21359	0	3	1	22.03
1G06390[a]	Translation elongation factor EF-1 alpha subunit	9.12	50019.60	-0.29565	0	34	12	216.04
1G06580[a]	High expression lethality protein Hel10	6.36	21808.80	-1.35072	0	17	2	34.1
1G06770[a]	40S ribosomal protein S26	10.88	13468.86	-0.7563	0	12	1	19.76
1G06790	Importin beta-3 subunit, putative	4.66	121431.97	-0.13169	0	2	1	21.57

CADRE ID. (AFUA_)	Protein name	tp*I*	tM_r	GRAVY score	TM	Coverage (%)	Unique peptides	SM Score
1G06830[a]	60S acidic ribosomal protein P1 (AfP1)	4.1	11128.40	0.096396	0	47	3	53.65
1G06960	Pyruvate dehydrogenase E1 component alpha subunit, putative (EC 1.2.4.1)	6.36	41479.04	-0.46432	0	16	5	79.12
1G07380	Glutamate synthase Glt1, putative (EC 1.4.1.13)	5.98	234290.73	-0.28923	0	1	2	27.65
1G07440[a]	Molecular chaperone Hsp70	5.09	69660.29	-0.4105	0	47	21	372.95
1G08810	Glycerol-3-phosphate dehydrogenase, mitochondrial (EC 1.1.99.5)	6.71	76830.19	-0.27745	1	6	3	36.25
1G09100[a]	60S ribosomal protein L9, putative	9.67	21843.17	-0.31875	0	36	7	111.78
1G09130	Unknown function protein	8.56	76550.12	-0.48047	0	2	1	22.2
1G09330	Eukaryotic translation initiation factor 3 subunit F (eIF3f)	4.81	37198.51	-0.26203	0	6	2	35.8
1G09440	40S ribosomal protein S23	10.46	15900.70	-0.52414	0	18	1	19.9
1G09660	Mitochondrial 2-oxodicarboxylate carrier protein, putative	9.82	33200.53	0.034098	2	6	1	20.8
1G09970	Eukaryotic translation initiation factor 3 subunit H (eIF3h)	5.96	41014.53	-0.36603	0	5	1	19.02
1G10130[a]	Adenosylhomocysteinase (EC 3.3.1.1)	5.82	48490.04	0.060538	0	22	7	121.07
1G10350[a]	Phosphoglycerate kinase (EC 2.7.2.3)	6.31	44761.47	-0.21487	0	44	16	255.96
1G10630[a]	S-adenosylmethionine synthase (EC 2.5.1.6)	5.66	42195.98	-0.21318	0	46	11	180.66
1G10910[a]	Tubulin beta, putative	4.79	51794.00	-0.37876	0	41	11	191.9
1G11120[a]	Unknown function protein	4.47	34722.07	-0.52277	0	6	1	21.39
1G11130	60S ribosomal protein L6	10.15	22453.03	-0.635	0	19	3	47.34
1G11190[a]	Eukaryotic translation elongation factor 1 subunit Eef1-beta, putative	4.54	30142.49	-0.76353	0	22	4	82.16

CADRE ID. (AFUA_)	Protein name	tp*I*	tM_r	GRAVY score	TM	Coverage (%)	Unique peptides	SM Score
1G11710[a]	Ribosomal protein	9.88	24252.58	-0.31751	0	12	2	39.81
1G11730	ADP-ribosylation factor, putative	5.54	21003.07	-0.27596	0	24	3	48.95
1G12070	Glycine cleavage system H protein	4.75	18626.88	-0.11886	0	18	2	31.79
1G12170[a]	Elongation factor Tu	6.69	48285.99	-0.32227	0	19	5	86.05
1G12610	Heat shock protein Hsp88, putative (Hsp70 chaperone Hsp88)	5.08	80044.81	-0.53796	0	12	6	99.11
1G12800	Isocitrate dehydrogenase, NAD-dependent (EC 1.1.1.41)	8.72	41727.08	-0.12234	0	17	6	81.92
1G12890[a]	60S ribosomal protein L5, putative	8.59	35482.98	-0.83734	0	41	9	175.12
1G13090	Anthranilate synthase component ii, putative (EC 4.1.1.48) (EC 4.1.3.27) (EC 5.3.1.24) (Anthranilate synthase multifunctional protein TrpC, putative) (EC 4.1.3.27)	5.93	82231.73	-0.10157	0	4	2	33.66
1G13140	G-protein complex alpha subunit GpaA/FadA	5.04	40769.47	-0.38895	0	12	3	39.34
1G13470	Prohibitin complex subunit Phb1, putative	9	31024.45	-0.21357	0	10	2	24.57
1G13490[a]	Spermidine synthase (EC 2.5.1.16)	5.24	15674.03	-0.12222	0	7	2	34.27
1G13500[a]	Transketolase TktA (EC 2.2.1.1)	6.13	74827.91	-0.2076	0	22	9	166.75
1G14200[a]	Mitochondrial processing peptidase beta subunit, putative (EC 3.4.24.64)	5.9	53269.94	-0.32401	0	15	7	100.66
1G14220	Fibrillarin (Fibrillarin, putative) (Nucleolar protein NopA)	10.29	32572.25	-0.34872	0	6	1	18.36
1G14330	ABC transporter, putative	6.82	168183.61	-0.10995	12	2	3	38.31
1G14410[a]	60S ribosomal protein L17	10.64	21666.02	-0.53041	0	24	5	85.68
1G14550[a]	Superoxide dismutase [Mn], mitochondrial (EC 1.15.1.1) (allergen Asp f 6)	7.13	23390.47	-0.49333	0	6	1	19.78

CADRE ID. (AFUA_)	Protein name	tp*I*	tM_r	GRAVY score	TM	Coverage (%)	Unique peptides	SM Score
1G14570	Phosphoribosyl-AMP cyclohydrolase, putative (EC 1.1.1.23)	5.46	92881.52	-0.05883	0	8	3	40.59
1G14780	BAP31 domain protein, putative	9.05	24133.35	0.058019	3	11	2	28.76
1G15020[a]	40S ribosomal protein S5, putative	6.92	37605.90	-0.11257	0	18	3	68.43
1G15140	Mitochondrial phosphate carrier protein (Mir1), putative	9.38	33849.07	0.263777	0	41	8	145.07
1G15730[a]	40S ribosomal protein S22	9.67	14674.04	-0.18231	0	26	2	40.26
1G16190	Probable glycosidase crf1 (EC 3.2.-.-) (Crh-like protein 1) (allergen Asp f 9)	4.6	40283.87	-0.26076	0	6	2	37.68
1G16840[a]	Translationally-controlled tumor protein homolog (TCTP)	11.17	22811.93	-0.89602	0	26	4	64.98
2G02100[a]	Dihydrolipoyl dehydrogenase (EC 1.8.1.4)	8.32	54971.13	-0.13762	0	21	7	113.06
2G02490	Unknown function protein	9.6	42498.89	-0.2381	0	3	1	18.45
2G03010	Cytochrome c subunit Vb, putative	5.28	23916.77	-0.57905	0	12	2	29.4
2G03120	Probable glycosidase crf2 (EC 3.2.-.-) (Crh-like protein 2)	4.67	46710.32	-0.37133	1	5	2	31.92
2G03290[a]	14-3-3 family protein ArtA, putative	4.79	29101.64	-0.43563	0	49	12	216.68
2G03380	Alkaline serine protease	9.72	13437.77	0.007087	0	28	2	38.99
2G03510[a]	Carboxypeptidase 5 (Pheromone processing carboxypeptidase (Sxa2), putative) (EC 3.4.16.-)	6.4	40908.96	0.067588	0	14	6	105.6
2G03720[a]	Peptidyl-prolyl cis-trans isomerase (EC 5.2.1.8)	8.76	22290.17	-0.24634	0	28	5	74.93
2G03870	FK506-binding protein 2 (EC 5.2.1.8) (Peptidyl-prolyl cis-trans isomerase) (PPIase) (Rotamase)	5.35	14637.79	-0.11269	0	11	1	20.69
2G04310	Argininosuccinate synthase (EC 6.3.4.5)	5.49	41670.35	-0.22989	0	8	3	39.2

CADRE ID. (AFUA_)	Protein name	tp*I*	tM_r	GRAVY score	TM	Coverage (%)	Unique peptides	SM Score
2G04620[a]	Hsp70 chaperone BiP/Kar2, putative	4.91	73384.68	-0.37485	0	7	5	77.06
2G04710[a]	Cytochrome b5, putative	5.35	23911.94	-0.23134	2	9	2	32.82
2G04980	Tyrosine decarboxylase, putative (EC 4.1.1.-)	5.58	55059.10	-0.10613	0	2	1	23.71
2G05910[a]	Hexokinase Kxk, putative (EC 2.7.1.1)	5.06	54209.22	-0.22347	0	10	3	52.73
2G06150[a]	Protein disulfide isomerase Pdi1, putative (EC 5.3.4.1)	4.58	56186.92	-0.32998	0	16	5	93.39
2G07380	Ribosomal protein L18	11.81	20853.36	-0.49402	0	25	4	71.97
2G07420	Actin-bundling protein Sac6, putative	5.78	72478.63	-0.31502	0	4	2	37.25
2G07970	60S ribosomal protein L19	11.46	24785.90	-1.01611	0	26	6	84.04
2G08370[a]	Glutathione S-transferase, putative (EC 2.5.1.-)	9.32	16074.71	0.250345	3	15	2	35.13
2G09210	60S ribosomal protein L10	8.96	55206.83	-0.32926	0	23	4	66.97
2G09290[a]	Antigenic mitochondrial protein HSP60, putative	5.53	61949.95	-0.09949	0	25	10	141.07
2G09650[a]	Aspartate transaminase, putative (EC 2.6.1.1)	8.6	51182.79	-0.23262	0	9	3	50.57
2G09790	Glucose-6-phosphate isomerase (EC 5.3.1.9)	5.91	61315.46	-0.26148	0	5	2	41.54
2G09850[a]	Oxidoreductase, 2-nitropropane dioxygenase family, putative (EC 1.-.-.-)	6.52	37702.48	-0.02873	0	8	2	36.28
2G09960[a]	Mitochondrial Hsp70 chaperone (Ssc70), putative	6.02	74465.27	-0.38219	0	18	9	129.38
2G10070	Carbamoyl-phosphate synthase, large subunit (EC 6.3.5.5)	5.87	129214.48	-0.16009	0	7	5	80.49
2G10090	40S ribosomal protein S15, putative	10.38	19849.10	-0.72706	0	20	2	46.39
2G10100[a]	60S acidic ribosomal protein P2 (AfP2) (allergen Asp f 8)	4.29	11141.34	-0.11712	0	23	2	40.76

CADRE ID. (AFUA_)	Protein name	tp*I*	tM_r	GRAVY score	TM	Coverage (%)	Unique peptides	SM Score
2G10440	40S ribosomal protein S11	8.42	45746.17	-0.3055	0	36	4	59.86
2G10500	40S ribosomal protein Rps16, putative	10.19	15971.55	-0.39231	0	29	5	73.33
2G11060[a]	Acyl CoA binding protein family	5.72	17309.63	-0.29051	0	25	2	38.68
2G11150	Secretory pathway gdp dissociation inhibitor	5.33	52280.27	-0.38803	0	9	3	41.5
2G11260	3-isopropylmalate dehydratase (EC 4.2.1.33) (Alpha-IPM isomerase) (Isopropylmalate isomerase)	5.62	84076.50	-0.23629	0	3	2	26.4
2G11850[a]	60S ribosomal protein L3 (allergen Asp f 23)	10.18	44444.67	-0.62959	0	5	2	30.87
2G11940	Adenylosuccinate lyase Ade13, putative (EC 4.3.2.2)	6.22	54739.59	-0.29979	0	3	1	18.15
2G12400	ATP synthase oligomycin sensitivity conferral protein, putative (EC 3.6.3.14)	9.65	24389.11	-0.1674	0	26	6	87.02
2G12870	Vesicular-fusion protein sec17	5.32	32840.78	-0.54589	0	4	1	18.24
2G13110	Cytochrome c	10.06	26271.16	-0.47191	0	10	2	26.5
2G13240	V-type ATPase, B subunit, putative (EC 3.6.3.14)	5.73	56418.17	-0.32411	0	15	5	91.8
2G13290	GYF domain protein	6.7	214986.29	-0.54821	0	1	2	22.08
2G13530[a]	Translation elongation factor EF-2 subunit, putative	6.51	93198.10	-0.23468	0	34	22	400.25
2G13680	Calcium/calmodulin-dependent protein kinase, putative (EC 2.7.11.17)	6.09	48721.50	-0.4341	0	8	2	27.83
2G13860	Histone H4	11.36	11386.34	-0.54369	0	28	3	56.87
2G14990	Tubulin subunit TubB	5.03	50441.50	-0.33659	0	15	5	73.82
2G15240	Small oligopeptide transporter, OPT family	7.64	89268.85	0.276263	14	5	3	46.54

CADRE ID. (AFUA_)	Protein name	tp*I*	tM_r	GRAVY score	TM	Coverage (%)	Unique peptides	SM Score
2G15290[a]	DUF636 domain protein	6.27	14849.09	-0.24338	0	17	1	23.17
2G15760	Ubiquitin-activating enzyme E1	5.11	114685.85	-0.36089	0	1	1	20.67
2G16010[a]	Prolyl-tRNA synthetase (EC 6.1.1.15)	6.23	71010.65	-0.51177	0	3	1	18.01
2G16090	Karyopherin alpha subunit, putative	4.97	60683.84	-0.27917	0	2	1	23.31
2G16200	Uracil phosphoribosyltransferase (EC 2.4.2.9)	5.53	24357.12	0.139648	0	5	1	18.17
2G16370	60S ribosomal protein L32	11.28	14966.79	-0.61374	0	9	1	22.29
2G17000[a]	PT repeat family protein	10.84	27279.81	-0.88819	1	3	4	59.45
2G17110[a]	Cdc48p (Cell division control protein Cdc48) (EC 3.6.1.-)	5.09	90218.23	-0.35946	0	21	13	212.67
3G00270[a]	Probable glucan endo-1,3-beta-glucosidase eglC (EC 3.2.1.39) (Endo-1,3-beta-glucanase eglC) (Laminarinase eglC)	4.9	44651.21	0.064126	1	24	8	167.1
3G00730[a]	Unknown function protein	5.11	27920.69	-0.27903	0	12	2	40.86
3G00880	UPF0619 GPI-anchored membrane protein	4.68	21605.40	-0.09589	0	11	2	26.79
3G04170	Pyruvate dehydrogenase E1 beta subunit PdbA, putative (EC 1.2.4.1)	5.59	48427.44	-0.33393	0	12	4	66.35
3G04210	Fatty acid synthase alpha subunit FasA	6.09	204599.82	-0.32649	0	2	2	42.03
3G05350[a]	Histone H2B	10.12	14955.22	-0.68	0	10	1	20.61
3G05370[a]	Dihydrolipoamide succinyltransferase, putative (EC 2.3.1.61)	10.33	25586.74	-0.53722	0	9	4	66.76
3G05450	Glutamate carboxypeptidase, putative (EC 3.-.-.-)	5.47	53015.24	-0.32824	0	8	2	31.97
3G05600	60S ribosomal protein L27a, putative	10.44	16761.31	-0.6349	0	26	3	43.92
3G06140	Cytoskeleton assembly control protein Sla2, putative	5.46	118383.10	-0.6418	0	3	2	29.48

CADRE ID. (AFUA_)	Protein name	tp*I*	tM_r	GRAVY score	TM	Coverage (%)	Unique peptides	SM Score
3G06460[a]	Conserved hypothetical protein	9.46	18915.55	-0.61796	1	13	1	22.18
3G06530	Sulfate adenylyltransferase (EC 2.7.7.4) (ATP-sulfurylase) (Sulfate adenylate transferase) (SAT)	6.57	64333.17	-0.40488	0	9	3	47.43
3G06610	Proteasome regulatory particle subunit (RpnE), putative	6.76	58444.39	-0.41319	1	5	2	25.69
3G06840[a]	40S ribosomal protein S4, putative	4.77	59751.47	-0.21517	0	28	6	101.54
3G06960	60S ribosomal protein L21, putative	10.23	17980.83	-0.56266	0	14	1	18.16
3G06970	40S ribosomal protein S9	5.56	44846.27	-0.48014	0	14	4	53.53
3G07430[a]	Peptidyl-prolyl cis-trans isomerase (EC 5.2.1.8)	7.75	17741.20	-0.25031	0	39	5	87.1
3G07640[a]	Plasma membrane H+-ATPase Pma1 (EC 3.6.3.6)	5.22	108992.15	0.042206	10	31	26	445.15
3G07810	Succinate dehydrogenase subunit Sdh1, putative	6.5	71148.03	-0.41314	0	10	5	68.73
3G08160[a]	ATP-dependent RNA helicase eIF4A (EC 3.6.4.13) (Eukaryotic initiation factor 4A)(Translation initiation factor1)	5.46	27670.46	-0.26532	0	15	6	120.92
3G08380[a]	Inorganic diphosphatase, putative (EC 3.6.1.1)	7.62	43623.57	-0.42096	0	39	9	154.09
3G08430	Mitochondrial phosphate carrier protein, putative	9.55	44335.33	-0.11216	2	7	3	38.42
3G08440	Unknown function protein	9.43	14742.25	-1.18175	0	21	2	28.49
3G08580	Glycine-rich RNA-binding protein, putative	5.7	12809.85	-0.91356	0	31	2	29.99
3G08660[a]	Isocitrate dehydrogenase [NADP] (EC 1.1.1.42)	5.61	45768.89	-0.13597	0	7	3	44.53
3G08980	Threonine synthase Thr4, putative (EC 4.2.3.1)	8.18	56129.61	-0.26897	0	6	2	26.51
3G09030[a]	Regulatory protein SUAPRGA1	4.88	40094.88	-0.4661	0	10	2	25.95

CADRE ID. (AFUA_)	Protein name	tp*I*	tM_r	GRAVY score	TM	Coverage (%)	Unique peptides	SM Score
3G09290[a]	Phosphoglycerate mutase, 2,3-bisphosphoglycerate-independent (EC 5.4.2.1)	5.44	57454.24	-0.41615	0	4	2	39.75
3G09320[a]	Serine hydroxymethyltransferase (EC 2.1.2.1)	7.63	51873.35	-0.28025	0	27	10	162.27
3G10730[a]	40S ribosomal protein S7e	10.15	22844.25	-0.54677	0	27	3	53.93
3G11070	Pyruvate decarboxylase (EC 4.1.1.1)	4.83	25438.58	-0.3	0	13	4	63.92
3G11400[a]	Vacuolar protease A (EC 3.4.23.25) (Aspartic endopeptidase pep2) (Aspartic protease pep2)	4.81	43354.87	-0.13894	0	18	4	69.34
3G11610	Non-histone chromosomal protein 6	9.07	12078.37	-1.63173	0	14	2	27.52
3G11690[a]	Fructose-bisphosphate aldolase, class II (EC 4.1.2.13)	6.59	58385.12	-0.25275	0	24	6	107.19
3G11830	Phosphoglucomutase (PGM) (EC 5.4.2.2) (Glucose phosphomutase)	6.29	60501.49	-0.24973	0	6	3	49.52
3G12270[a]	Glutathione peroxidase	9.3	25755.79	-0.22596	0	34	7	98.64
3G12300	60S ribosomal protein L22, putative	5.74	13422.22	-0.41453	0	27	2	36.86
3G12800	Clathrin-coated vesicle protein (Bud7), putative	5.23	80264.62	-0.33792	0	2	1	21.03
3G13010	Zn-dependent hydrolase/oxidoreductase family protein, putative	6.79	46099.30	-0.55553	0	3	1	19.51
3G13320[a]	40S ribosomal protein S0	4.81	32122.23	-0.16498	0	17	3	55.11
3G13390	Vacuolar ATP synthase subunit d, putative (EC 3.6.3.14)	4.87	40937.45	-0.19146	0	7	1	19.46
3G13400	Nucleolar protein 58	7.13	64562.60	-0.58613	0	6	2	36.06
3G13910	NADH-ubiquinone oxidoreductase B18 subunit, putative	8.38	10797.27	-0.80968	0	10	1	20.14
3G14490[a]	Ketol-acid reductoisomerase (EC 1.1.1.86)	9.32	56353.31	-0.29764	0	22	8	128.12

CADRE ID. (AFUA_)	Protein name	tp*I*	tM_r	GRAVY score	TM	Coverage (%)	Unique peptides	SM Score
3G14665	Unknown function protein	4.26	14579.46	-0.01136	0	11	1	18.24
3G14680[a]	Lysophospholipase 3 (EC 3.1.1.5) (Phospholipase B 3)	5.39	67416.54	-0.12889	1	17	8	146.88
4G00960	6-phosphofructokinase (EC 2.7.1.11) (6PF-1-K) (Phosphohexokinase)	6.68	88713.03	-0.25111	0	2	2	30.97
4G02790	Carbon-nitrogen family hydrolase, putative	7.04	33796.57	-0.09	0	14	2	32.14
4G03050[a]	Profilin	5.87	14491.32	-0.12574	0	14	1	20.15
4G03320[a]	Membrane bound cation transporter, putative	6.67	110475.71	-0.46454	11	2	2	34
4G03760	Glycine dehydrogenase (EC 1.4.4.2)	6.71	115202.81	-0.1834	0	3	3	32.7
4G03860	Eukaryotic translation initiation factor 3 subunit C (eIF3c)	5.05	97508.60	-0.5884	0	3	2	33.19
4G03880	60S ribosomal protein L7	9.7	34252.62	-0.56869	0	12	3	59.3
4G04460	60S ribosomal protein L13	10.58	24826.73	-0.77078	0	22	5	69.08
4G04520[a]	Succinyl-CoA synthetase beta subunit, putative (EC 6.2.1.4)	6.2	28538.34	-0.17778	0	15	6	99.82
4G04810	Rab GTPase SrgA, putative	6.43	22787.78	-0.28689	0	22	3	41.34
4G05830	Translation initiation factor, putative	5.92	41590.56	0.024031	0	7	2	33.74
4G06620[a]	Glutamate/Leucine/Phenylalanine/Valine dehydrogenase, putative (EC 1.4.1.4)	5.79	49367.83	-0.17598	0	41	13	218.46
4G06820[a]	Protein ecm33	4.8	41505.47	-0.00879	0	9	3	49.56
4G06910[a]	Outer mitochondrial membrane protein porin	5.51	48017.08	-0.03423	0	17	6	99.11
4G07360[a]	Cobalamin-independent methionine synthase MetH/D (EC 2.1.1.14)	6.33	86894.57	-0.30646	0	28	17	311.27
4G07580	Translation initiation factor EF-2 gamma subunit, putative	6.87	55187.76	-0.15306	0	6	2	25.55

CADRE ID. (AFUA_)	Protein name	tp*I*	tM_r	GRAVY score	TM	Coverage (%)	Unique peptides	SM Score
4G07690	Phosphoribosylaminoimidazolecarboxamide formyltransferase/IMP cyclohydrolase	6.39	65027.90	-0.24303	0	5	2	28.8
4G07700	Clathrin heavy chain	5.29	192938.13	-0.26255	0	5	5	82.63
4G07710	Pyruvate carboxylase, putative (EC 6.4.1.1)	6.23	131272.97	-0.19899	0	14	12	196.8
4G07730[a]	60S ribosomal protein L11	10.04	20113.24	-0.6375	0	15	2	38.45
4G08040	RAB GTPase Ypt5, putative	8.72	23729.95	-0.28853	0	10	2	26.02
4G08580[a]	Mitochondrial peroxiredoxin Prx1, putative (EC 1.11.1.7)	5.38	23392.65	-0.20657	0	36	5	81.74
4G08600	Aldehyde dehydrogenase, putative (EC 1.2.1.3)	6.48	60059.63	-0.11127	0	8	3	52.76
4G08720	Lysophospholipase 1 (EC 3.1.1.5) (Phospholipase B 1)	9.75	17880.81	-0.39758	1	7	4	67.87
4G09030	Aminopeptidase (EC 3.4.11.7)	6.31	106226.77	-0.27671	0	2	1	24.11
4G09110	Cytochrome c peroxidase, mitochondrial (CCP) (EC 1.11.1.5)	8.64	40379.25	-0.4571	1	8	2	34.07
4G10050	Calmodulin	4.69	26660.78	-0.60302	0	12	2	26.98
4G10350[a]	Polyubiquitin UbiD/Ubi4, putative	6.48	35199.24	-0.47866	0	7	2	41.19
4G10410	Aspartate aminotransferase, putative (EC 2.6.1.1)	8.94	47892.64	-0.24783	0	19	6	92.91
4G10770	Fatty acid oxygenase PpoA, putative (EC 1.-.-.-)	6.15	121250.04	-0.32243	0	8	7	104.15
4G10800	40S ribosomal protein S6	10.72	15832.19	-0.38667	0	19	4	59.56
4G11050	NADH-ubiquinone oxidoreductase, subunit F, putative (EC 1.6.5.3)	8.44	54560.20	-0.37681	0	6	2	28.74
4G11250	Carbonic anhydrase (EC 4.2.1.1)	8.62	30827.50	-0.04355	0	4	1	21.11
4G11340	Saccharopine dehydrogenase Lys9, putative (EC 1.5.1.7)	5.91	49449.90	-0.14222	0	10	3	49.58

CADRE ID. (AFUA_)	Protein name	tp*I*	tM_r	GRAVY score	TM	Coverage (%)	Unique peptides	SM Score
4G11580	Superoxide dismutase (EC 1.15.1.1)	8.96	25153.31	-0.40568	0	6	1	19.86
4G11650	Alpha-ketoglutarate dehydrogenase complex subunit Kgd1, putative (EC 1.2.4.2)	3.96	222643.84	-0.66931	0	6	4	59.3
4G11730	Glycerol dehydrogenase (GldB), putative (EC 1.1.1.72)	5.97	36827.82	-0.44923	0	11	2	25.32
4G11980	Anthranilate phosphoribosyltransferase, putative (EC 2.4.2.18)	5.5	45969.53	-0.06014	1	4	1	20.31
4G12450[a]	Conserved lysine-rich protein, putative	5.03	57003.08	-0.78983	0	21	10	156.23
4G12870	Methylmalonate-semialdehyde dehydrogenase, putative (EC 1.2.1.27)	8.27	63864.67	-0.05698	0	5	2	29.36
4G13120[a]	Glutamine synthetase (EC 6.3.1.2)	5.13	35803.15	-0.22048	0	10	4	59.09
4G13170[a]	G-protein comlpex beta subunit CpcB	6.06	34979.37	-0.2943	0	27	7	108.29
4G13500	Aldehyde dehydrogenase, putative (EC 1.2.1.5)	8.44	56426.99	-0.12237	0	4	1	19.53
4G14000	Tripeptidyl-peptidase sed4 (EC 3.4.14.-) (Sedolisin-D)	4.88	63944.64	-0.15202	0	7	2	42.73
4G14380	Glutathione S-transferase, putative	7.69	30012.21	-0.24248	0	10	2	35.69
5G00720	GNAT family acetyltransferase, putative	5.23	29060.93	-0.54395	0	6	1	18.61
5G01030[a]	Glyceraldehyde-3-phosphate dehydrogenase (EC 1.2.1.12)	6.17	36140.02	-0.16837	0	34	10	171.11
5G01440	Allergen, putative (EC 1.-.-.-)	8.44	21950.18	-0.04505	0	19	3	54.01
5G01860	ARP2/3 complex subunit Arc18, putative	6.31	21149.31	-0.19521	0	7	1	20.65
5G01970[a]	Glyceraldehyde-3-phosphate dehydrogenase (EC 1.2.1.12)	6.96	36314.28	-0.11124	0	55	14	246.3
5G02370	Vacuolar ATP synthase catalytic subunit A, putative (EC 3.6.3.14)	5.83	74912.38	-0.25729	0	9	4	80.82
5G02470[a]	Thiamine biosynthesis protein (Nmt1), putative)	6.03	38322.82	-0.27193	0	34	7	113.35

CADRE ID. (AFUA_)	Protein name	tp*I*	tM_r	GRAVY score	TM	Coverage (%)	Unique peptides	SM Score
5G02640	O-methyltransferase, putative (EC 2.1.1.-)	4.95	47749.73	-0.1065	0	20	5	84.57
5G02750[a]	Cytochrome c oxidase subunit Va, putative	5.62	17991.28	-0.41076	0	34	5	80.84
5G03020[a]	60S ribosomal protein L4, putative	10.96	40503.89	-0.36166	0	31	10	171.21
5G03080	Septin	8.8	44414.55	-0.70286	0	6	2	25.3
5G03490[a]	Nucleoside diphosphate kinase (NDK) (NDP kinase) (EC 2.7.4.6)	7.76	16932.49	-0.14444	0	54	7	112.28
5G03560	Glutamyl-tRNA synthetase (EC 6.1.1.17)	7.17	81424.25	-0.42965	0	6	2	25.37
5G03690	Phosphatidylinositol transfer protein sfh5 (PITP sfh5)	4.79	46169.61	-0.54198	1	5	2	32.95
5G03990	Vacuolar aspartyl aminopeptidase Lap4, putative	6.61	56024.37	-0.2031	0	2	1	19.59
5G04170[a]	Heat shock protein 90 (65 kDa IgE-binding protein) (Heat shock protein hsp1) (allergen Asp f 12)	4.95	80639.96	-0.62861	0	29	17	281.97
5G04210[a]	Ubiquinol-cytochrome C reductase complex core protein 2, putative (EC 1.10.2.2)	9.47	36893.97	-0.14029	0	17	6	97.05
5G04220	Mitochondrial DNA replication protein (Yhm2), putative	9.86	32080.36	-0.0396	0	14	2	37.84
5G04230[a]	Citrate synthase	8.69	52111.79	-0.2346	0	23	9	149.08
5G04320	Secretion related GTPase SrgB/Ypt1	6.59	17608.94	-0.40189	0	16	2	29.37
5G04370[a]	NADH-ubiquinone oxidoreductase, subunit G, putative (EC 1.6.5.3)	5.8	73371.09	-0.37988	0	20	9	143.19
5G05450	40S ribosomal protein S1	10.05	29200.85	-0.59258	0	15	3	43.67
5G05500	D-3-phosphoglycerate dehydrogenase (EC 1.1.1.95)	5.98	51483.73	-0.07627	0	2	1	18.34
5G05540[a]	Nucleosome assembly protein Nap1, putative	4.43	48336.20	-0.84374	0	6	2	29.43
5G05630	60S ribosomal protein L23	10.26	16125.92	-0.42083	0	18	2	35.28

CADRE ID. (AFUA_)	Protein name	tp*I*	tM_r	GRAVY score	TM	Coverage (%)	Unique peptides	SM Score
5G06060	E3 ubiquitin ligase complex SCF subunit sconC (Sulfur controller C) (Sulfur metabolite repression control protein C)	4.35	18141.24	-0.65443	0	15	1	23.91
5G06070	ABC multidrug transporter Mdr1 (EC 3.6.3.-)	6.68	147784.44	0.023573	12	2	2	47.39
5G06130	Succinyl-CoA synthetase alpha subunit, putative (EC 6.2.1.5)	8.83	34573.54	0.000604	0	4	1	19.76
5G06360[a]	60S ribosomal protein L8, putative	10.97	27485.65	-0.53976	0	14	2	35.87
5G06390	Adenosine kinase, putative (EC 2.7.1.20)	5.02	36858.82	-0.18491	0	6	2	28.88
5G06680	4-aminobutyrate transaminase GatA (EC 2.6.1.19)	4.59	68143.67	-0.16904	0	12	4	67.74
5G06710	DUF89 domain protein	5.13	54146.46	-0.38583	0	7	2	31.79
5G06780	Carbamoyl-phosphate synthase arginine-specific small chain (CPS-A) (EC 6.3.5.5)	6.65	49336.79	-0.15298	0	3	1	19.87
5G07120[a]	RNP domain protein	9.15	37138.34	-0.79034	0	20	4	74.99
5G07780	Squalene epoxidase-like protein (Squalene monooxygenase Erg1)	8.93	52682.51	0.138462	3	19	5	93.4
5G07890[a]	SsDNA binding protein, putative	10.43	20526.29	-0.3871	0	8	1	18.68
5G08090	Pyridoxine biosynthesis protein	6.04	32736.71	-0.00617	0	4	1	19.42
5G08130	Protein transport protein Sec61 alpha subunit, putative	8.41	52221.60	0.482845	10	4	1	20.06
5G08810	Epoxide hydrolase, putative (EC 3.3.2.9)	5.67	44118.91	-0.22525	0	5	1	18.58
5G08830[a]	Woronin body protein HexA, putative	6.56	49836.57	-0.8046	0	29	8	134.44
5G09210[a]	Autophagic serine protease Alp2 (EC 3.4.21.48)	5.57	41139.99	-0.16676	0	18	6	95.94
5G09230[a]	Transaldolase (EC 2.2.1.2)	6.04	35448.58	-0.13488	0	34	10	166.3
5G09330[a]	CipC-like antibiotic response protein, putative	5.84	15052.55	-1.13462	0	35	5	85.84

CADRE ID. (AFUA_)	Protein name	tp*I*	tM_r	GRAVY score	TM	Coverage (%)	Unique peptides	SM Score
5G10370	Iron-sulfur protein subunit of succinate dehydrogenase Sdh2, putative (EC 1.3.99.1)	9.15	33915.92	-0.5689	0	7	2	29.61
5G10550[a]	ATP synthase subunit beta (EC 3.6.3.14)	5.3	55620.38	-0.07881	0	62	21	415.78
5G10560	Cytochrome c oxidase subunit V	9.96	22199.62	-0.5398	1	14	3	45.2
5G10570	Cofilin	5.47	17028.14	-0.4474	0	17	2	39.96
5G10610	Ubiquinol-cytochrome c reductase iron-sulfur subunit (EC 1.10.2.2)	9.2	32609.47	-0.18154	0	21	4	82.06
5G10640	Tyrosyl-tRNA synthetase (EC 6.1.1.1)	6.18	43615.23	-0.36113	0	5	1	20.06
5G11230	RAS protein (RAS small monomeric GTPase RasA) (Ras GTPase)	4.97	23901.11	-0.35352	0	11	2	41.52
5G11240[a]	Oxidoreductase, short chain dehydrogenase/reductase family	9.51	29575.22	-0.08022	0	7	1	21.27
5G12180[a]	Ran-specific GTPase-activating protein 1, putative	4.93	27643.55	-1.02955	0	24	5	88.44
5G12260[a]	Disulfide isomerase (TigA), putative (EC 5.3.4.1)	6.12	40253.93	-0.31304	0	14	3	47.75
5G12780	Kelch repeat protein	6.47	118900.04	-0.50643	0	13	4	59.13
5G13450[a]	Triosephosphate isomerase (EC 5.3.1.1)	5.87	28068.18	-0.12266	0	29	4	76.01
5G14680	Unknown function protein	4.82	20247.02	-0.55084	0	24	4	64.68
6G02090[a]	ATP synthase subunit E, putative (EC 3.6.3.14)	8.6	26216.90	-0.51293	0	9	2	26.36
6G02280[a]	Putative peroxiredoxin pmp20 (EC 1.11.1.15) (Peroxisomal membrane protein pmp20) (Thioredoxin reductase) (allergen Asp f	5.36	18452.98	-0.11607	0	53	9	151.47
6G02470	Fumarate hydratase, putative (EC 4.2.1.2)	9.1	63159.39	-0.21117	0	16	6	87.93
6G02630	ATP-dependent RNA helicase sub2 (EC 3.6.4.13)	5.85	50320.48	-0.33482	0	7	2	31
6G02750[a]	Nascent polypeptide-associated complex subunit beta (NAC-beta)	5.32	20546.17	-0.51183	0	9	1	20.87

CADRE ID. (AFUA_)	Protein name	tp*I*	tM_r	GRAVY score	TM	Coverage (%)	Unique peptides	SM Score
6G03730	2-methylcitrate dehydratase, putative (EC 4.2.1.79)	8.62	62104.99	-0.27437	0	2	1	18.49
6G03810[a]	ATP synthase D chain, mitochondrial, putative (EC 3.6.3.14)	9.11	28696.01	-0.19961	0	23	3	55.59
6G03820[a]	Nascent polypeptide-associated complex subunit alpha (NAC-alpha)	4.85	21972.24	-0.70392	0	13	2	39.35
6G03830	Ribosomal protein L14	9.95	15885.71	-0.3	0	8	1	21.28
6G04570[a]	Translation elongation factor eEF-1 subunit gamma, putative	7.18	54182.67	-0.35602	0	17	8	142.13
6G04620	NADH-ubiquinone oxidoreductase B14 subunit, putative (EC 1.6.5.3)	8.07	9756.14	-0.54878	0	11	1	19.49
6G04740[a]	Actin Act1	5.87	43893.19	-0.20356	0	33	10	177.3
6G04920	NAD-dependent formate dehydrogenase AciA/Fdh (EC 1.2.1.2)	6.08	62998.59	-0.20351	0	13	4	61.19
6G04970	Phosphoserine aminotransferase (EC 2.6.1.52)	6.36	46893.41	-0.19907	0	7	2	27.15
6G05110	Mitochondrial import receptor subunit (Tom40), putative	5.65	38216.49	-0.02394	0	8	2	24.91
6G05210[a]	Malate dehydrogenase, NAD-dependent (EC 1.1.1.37)	6.77	34810.15	0.062121	0	62	12	217.09
6G06340	Glucosamine-fructose-6-phosphate aminotransferase	6.24	77286.83	-0.14813	0	12	6	94.66
6G06370	NAD(+)-isocitrate dehydrogenase subunit I (EC 1.1.1.41)	8.42	49745.35	-0.06505	0	16	5	69.05
6G06690	CFEM domain protein, putative	5.07	19453.62	0.122222	0	8	1	18.03
6G06750[a]	14-3-3 family protein	4.74	30103.50	-0.53838	0	37	10	159.51
6G06770[a]	Enolase (EC 4.2.1.11) (2-phospho-D-glycerate hydro-lyase) (2-phosphoglycerate dehydratase) (allergen Asp f 22)	5.39	47305.37	-0.31598	0	49	15	280.25
6G06780	Proteasome regulatory particle subunit Rpt4, putative (EC 3.4.25.1)	5.67	44112.90	-0.34504	0	3	1	18.82

CADRE ID. (AFUA_)	Protein name	tp*I*	tM_r	GRAVY score	TM	Coverage (%)	Unique peptides	SM Score
6G06870	Casein kinase I homolog, putative	9.62	58779.24	-0.77533	0	4	2	26.48
6G06900	GTPase Rho1 (Rho GTPase Rho1)	6.09	22530.06	-0.1685	0	17	2	36.01
6G07430[a]	Pyruvate kinase (EC 2.7.1.40)	5.06	45778.53	-0.20222	0	17	6	113.47
6G07620	GDP-mannose pyrophosphorylase A (EC 2.7.7.13)	5.92	58445.43	0.000763	0	2	1	18.14
6G07770	Alanine aminotransferase, putative (EC 2.6.1.-)	5.71	55135.21	-0.13653	0	16	5	93.83
6G08050[a]	6-phosphogluconate dehydrogenase, decarboxylating (EC 1.1.1.44)	5.86	55799.67	-0.16988	0	36	13	240.2
6G08660[a]	M protein repeat protein	5.04	131895.88	-0.63293	0	3	2	39.36
6G08720	5'-methylthioadenosine phosphorylase (Meu1), putative (EC 2.4.2.28)	9.95	26670.60	-0.54768	0	16	4	47.34
6G08810	NADH-ubiquinone oxidoreductase 304 kDa subunit (EC 1.6.5.3)	9.28	38191.46	-0.47395	0	11	3	48.73
6G09740	GliT (Thioredoxin reductase GliT) (EC 1.-.-.-)	5.44	36003.77	-0.10808	0	12	2	42.69
6G10450	Unknown function protein	9.32	26688.25	-0.43952	0	12	2	29.74
6G10650	ATP citrate lyase, subunit 1, putative (EC 2.3.3.8)	8.66	78829.14	-0.06146	0	19	10	163.14
6G10660	ATP citrate lyase subunit (Acl), putatibe (EC 6.2.1.5)	5.88	52917.75	-0.07119	0	16	5	85
6G10700	Chaperonin, putative	7.89	13385.50	0.014754	0	18	2	24.68
6G10990	NADPH cytochrome P450 reductase (CprA), putative (EC 1.6.2.4)	5.38	76782.85	-0.29856	1	5	2	31.2
6G11850[a]	Unknown function protein	8.68	44191.40	-0.29118	0	18	5	81.19
6G12170[a]	FK506-binding protein 1A (FKBP) (EC 5.2.1.8) (Peptidyl-prolyl cis-trans isomerase) (PPIase) (Rapamycin-binding protein)	6.57	12129.74	-0.38929	0	41	3	49.35
6G12280	NADH-ubiquinone oxidoreductase 213 kDa subunit	9.1	21172.84	-0.27056	0	26	3	49.47

CADRE ID. (AFUA_)	Protein name	tp*I*	tM_r	GRAVY score	TM	Coverage (%)	Unique peptides	SM Score
6G12300	RNP domain protein	9.63	51992.12	-0.81333	0	5	2	29.27
6G12580	Anthranilate synthase component I, putative (EC 4.1.3.27)	5.7	57019.42	-0.16015	0	8	2	34.41
6G12660	40S ribosomal protein S10b	9.74	17860.29	-0.96968	0	13	2	29.04
6G12740[a]	Dienelactone hydrolase family protein (EC 3.1.1.-)	6.16	26942.80	-0.10694	0	28	6	89.17
6G12830	Protein transport protein sec24	6.15	99701.96	-0.14984	3	3	2	24.84
6G12930[a]	Mitochondrial aconitate hydratase, putative (EC 4.2.1.3)	6.26	85529.08	-0.35578	0	21	12	187.53
6G12990	Cytosolic large ribosomal subunit protein L7A	10.21	28877.91	-0.48898	0	18	4	74.86
6G13250	60S ribosomal protein L31e	10.49	14007.26	-0.68293	0	16	2	22.65
6G13300	GTP-binding nuclear protein Ran, putative	5.6	46047.01	-0.37651	0	30	4	55.85
6G13490	Glutamate decarboxylase (EC 4.1.1.15)	5.85	58918.15	-0.40447	0	4	2	29.76
6G13540	Carboxypeptidase 3 (Carboxypeptidase CpyA/Prc1, putative) (EC 3.4.16.5)	5.5	60916.78	-0.39134	0	6	2	29
6G13550	Ribosomal protein S13p/S18e	10.58	14674.93	-0.86457	0	27	3	44.74
6G14090	CFEM domain protein	4.09	26811.00	-0.08984	1	3	1	19.49
7G01460[a]	Ribosomal protein S5	10.54	28304.88	-0.39807	0	27	5	96.66
7G01830	Pyrophosphorylase (UTP-glucose-1-phosphate uridylyltransferase Ugp1, putative)	6.41	56925.01	-0.25616	0	16	5	83.03
7G02230[a]	MRNA binding post-transcriptional regulator (Csx1), putative	5.55	39564.22	-0.01456	0	9	4	53.55
7G02340	L-PSP endoribonuclease family protein (Hmf1), putative	9.08	18015.73	0.017857	0	6	1	18.29

CADRE ID. (AFUA_)	Protein name	tp*I*	tM_r	GRAVY score	TM	Coverage (%)	Unique peptides	SM Score
7G03740	14-alpha sterol demethylase (14-alpha sterol demethylase Cyp51B) (EC 1.14.13.-)	7.64	58930.86	-0.12538	1	2	1	21.25
7G04070	Phospho-2-dehydro-3-deoxyheptonate aldolase (EC 2.5.1.54)	6.28	40071.54	-0.31816	0	7	1	19.3
7G04190	Cyclopropane-fatty-acyl-phospholipid synthase, putative (EC 2.1.1.79)	6.4	58957.04	-0.25819	2	9	2	32.5
7G04210[a]	Tropomyosin, putative	4.91	17867.72	-1.18182	0	8	1	25.13
7G04290[a]	Amino acid permease (Gap1), putative	8.47	63262.49	0.415437	12	9	5	74.21
7G05220	Mitochondrial carrier protein, putative	9.06	78228.66	-0.26356	1	10	3	52.38
7G05290[a]	40S ribosomal protein S13	10.35	16501.34	-0.25946	0	14	2	26.75
7G05370	Septin AspB	5.91	59344.75	-0.68349	0	4	2	23.33
7G05450	SUN domain protein (Uth1), putative (EC 3.2.1.-)	5.24	43504.21	-0.29686	0	6	1	23.16
7G05660[a]	Translation elongation factor eEF-3, putative (EC 3.6.3.-)	5.84	117767.79	-0.2939	0	28	19	313.16
7G05720[a]	Pyruvate dehydrogenase complex, dihydrolipoamide acetyltransferase component, putative (EC 2.3.1.12)	6.26	52031.59	-0.23711	0	20	8	106.84
7G05740[a]	Malate dehydrogenase (EC 1.1.1.37)	9.08	35898.07	-0.06676	0	40	8	154.27
7G06810	L-amino acid oxidase LaoA (EC 1.4.3.2)	6.04	78562.68	-0.3901	0	9	5	73.45
8G00230	Phytanoyl-CoA dioxygenase family protein FtmF	5.55	32666.51	-0.23093	0	14	3	40.88
8G00370	Polyketide synthase, putative	6.36	266597.78	-0.13712	0	10	12	208.22
8G00380[a]	DltD N-terminal domain protein	4.92	32697.21	-0.19555	0	27	5	96.87
8G00390[a]	O-methyltransferase, putative	5.39	63680.47	0.059578	0	33	6	95.06

CADRE ID. (AFUA_)	Protein name	tp*I*	tM_r	GRAVY score	TM	Coverage (%)	Unique peptides	SM Score
8G00400[a]	Unknown function protein	5.67	16054.54	-0.19167	0	21	2	35.11
8G00430[a]	Unknown function protein	5.13	18142.28	-0.58089	0	62	7	121.78
8G00440[a]	Steroid monooxygenase, putative (EC 1.-.-.-)	5.48	101032.18	-0.30508	0	32	20	363.59
8G00480[a]	Phytanoyl-CoA dioxygenase family protein	8.89	48089.24	-0.02565	0	20	6	95.95
8G00500	Acetate-CoA ligase, putative (EC 6.2.1.1)	6.74	79469.45	-0.21248	0	9	3	55.1
8G00510[a]	Cytochrome P450 oxidoreductase OrdA-like, putative	8.37	60965.12	-0.27481	1	27	11	194.75
8G00530[a]	Alpha/beta hydrolase, putative	5.57	49101.87	-0.18225	0	32	11	183.05
8G00540[a]	Hybrid PKS-NRPS enzyme, putative	5.7	434005.61	-0.11183	2	28	73	1266.12
8G00550[a]	Methyltransferase SirN-like, putative	5.21	29553.68	-0.33395	0	43	11	203.84
8G00580[a]	Glutathione S-transferase, putative	5.17	26804.76	-0.17511	0	17	5	75.65
8G01160[a]	Tartrate dehydrogenase, putative (EC 1.1.1.-)	5.41	39695.25	-0.15328	0	17	4	75.02
8G03880	Alanyl-tRNA synthetase, putative (EC 6.1.1.7)	6.04	113713.99	-0.51147	0	4	3	43.39
8G03930[a]	Hsp70 chaperone (HscA), putative	5.3	66972.99	-0.31564	0	37	14	254.68
8G04000[a]	Acetyl-CoA acetyltransferase, putative (EC 2.3.1.9)	9.09	36173.73	-0.46192	0	26	6	105.74
8G04890	Unknown function protein	4.8	18592.70	-0.08807	1	14	2	41.89
8G05320[a]	ATP synthase subunit alpha	9.14	59932.73	-0.12824	0	33	17	293.44
8G05440	Mitochondrial ATPase subunit ATP4, putative (EC 3.6.3.14)	9.36	29727.04	-0.09562	0	24	5	90.29
8G05580	Acetyl-coA hydrolase Ach1, putative (EC 2.8.3.8)	6.29	58145.20	-0.31543	0	4	1	20.82

CADRE ID. (AFUA_)	Protein name	tp*I*	tM_r	GRAVY score	TM	Coverage (%)	Unique peptides	SM Score
8G05600[a]	Unknown function protein	9.97	9288.14	-0.89157	0	27	2	32.42
8G05610[a]	Probable beta-glucosidase btgE (EC 3.2.1.21) (Beta-D-glucoside glucohydrolase btgE) (Cellobiase btgE) (Gentiobiase btgE)	5.81	52639.98	-0.20162	0	12	6	95.11
8G07210	Hydroxymethylglutaryl-CoA synthase, putative (EC 2.3.3.10)	8.85	55774.49	-0.35788	0	10	3	44.53

CADRE ID., *A. fumigatus* gene annotation nomenclature according to Nierman *et al.* (2005) and Mabey *et al.* (2004); tp*I*, theoretical isoelectric point; tM_r, theoretical molecular mass; TM, number of transmembrane regions; GRAVY score, grand average of hydropathy; SM score, Spectrum Mill protein score. [a]Protein was also identified by gel filtration coupled shotgun mass spectrometry as outlined in Section 3.2.2.